SHORTER CONTRIBUTIONS TO ISOTOPE RESEARCH

U.S. GEOLOGICAL SURVEY BULLETIN 1622

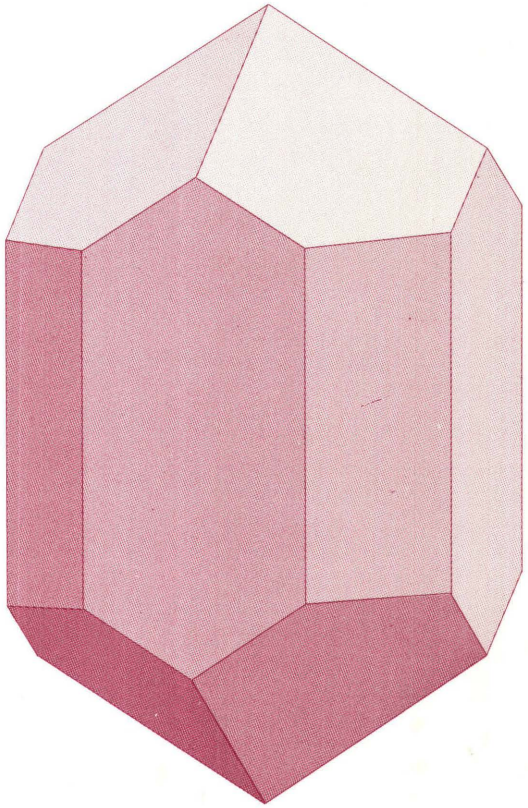

The cover depicts a crystal of the mineral zircon ($ZrSiO_4$), which is contained by most igneous rocks in small amounts (usually less than 0.1 percent). Because of its refractory nature and relatively high concentrations of uranium and thorium, zircon is commonly used for isotopic dating.

Artwork by Arthur L. Isom

SHORTER CONTRIBUTIONS TO ISOTOPE RESEARCH

Edited by Zell E. Peterman and Diane C. Schnabel

Topical reports on
geochronology and
isotope geochemistry

U.S. GEOLOGICAL SURVEY BULLETIN 1622

DEPARTMENT OF THE INTERIOR
DONALD PAUL HODEL, *Secretary*

U.S. GEOLOGICAL SURVEY
Dallas L. Peck, Director

UNITED STATES GOVERNMENT PRINTING OFFICE, WASHINGTON: 1986

For sale by the Branch of Distribution
Books and Open-File Reports Section
U.S. Geological Survey
Federal Center
Box 25425
Denver, CO 80225

Library of Congress Cataloging in Publication Data

Shorter contributions to isotope research.
(Geological Survey Bulletin ; 1622)
Includes bibliographies.
Supt. of Docs. no.: I 19.3:1622–A
1. Geological time—Addresses, essays, lectures. 2. Isotope geology—United States—Addresses, essays, lectures. 3. Geology—United States—Addresses, essays, lectures. I. Peterman, Zell E. II. Schnabel, Diane C. III. Series: U.S. Geological Survey Bulletin ; 1622.
QE75.B9 no. 1622 557.3s [551.7'01] 84–600171 [QE508]

SHORTER CONTRIBUTIONS TO ISOTOPE RESEARCH

CONTENTS

[For convenience in cross-referencing, each chapter of this publication has a letter designation]

1986

U.S. GEOLOGICAL SURVEY BULLETIN 1622

SHORTER CONTRIBUTIONS TO ISOTOPE RESEARCH

GEOCHRONOLOGY OF PRECAMBRIAN AND TERTIARY ROCKS IN THE MINERAL MOUNTAINS, SOUTH-CENTRAL UTAH

Chapter A

By JOHN N. ALEINIKOFF, DENNIS L. NIELSON[1], CARL E. HEDGE, and STANLEY H. EVANS, JR.[1]

CONTENTS

[1]University of Utah Research Insitute, University of Utah, Salt Lake City, Utah.

Abstract

Uranium-thorium-lead and rubidium-strontium studies of two metamorphic units from the Mineral Mountains, Utah, document the existence of Early Proterozoic rocks in south-central Utah. A paragneiss and an orthogneiss are about 1,720 million years old; both units are highly deformed and are in fault-bounded slices. The gneisses are intruded by foliated hornblende granodiorite previously thought to be also of Precambrian age. The granodiorite has been dated using zircon, sphene, and thorite, as about 25 million years old, which makes it an early phase of the intrusive complex of the Mineral Mountains. Potassium-argon determinations for hornblende and biotite from all three units show that mid-Tertiary to Quaternary thermal activity affected the rocks. Data for zircons from the hornblende granodiorite suggest a complex, multistage history involving inherited Proterozoic source material and magmatic zircon, both of which may have two-stage histories.

INTRODUCTION

The Mineral Mountains in south-central Utah are made up mostly of an intrusive complex, with minor associated sedimentary, extrusive, and metamorphic units (fig. A1). The intrusive complex is of Tertiary age, and is the largest body of plutonic rocks exposed in the state of Utah.

Previous geologic mapping in the area not specifically related to this study includes the work of Liese (1957), Earll (1957), Condie (1960), Petersen (1975), Evans (1975), and Lipman and others (1978). More recently, the central and northern parts of the Mineral Mountains have been mapped at a scale of 1:24,000 by Nielson and others (1978) and Sibbett and Nielson (1980a). These results also have been summarized in Sibbett and Nielson (1980b) and the present study is an outgrowth of this work. Studies centered on the Roosevelt Hot Springs geothermal system, which is on the central western margin of the range, have created an abundant and diverse geoscience data base for the Mineral Mountains area, and some of the results have been summarized in McKinney (1978) and Ward and others (1978).

ACKNOWLEDGMENTS

This work was partially supported by contract No. DE-AC07–80ID12079 from the Division of Geothermal Energy of the U.S. Department of Energy to the University of Utah Research Institute. We thank R. Hopper, G. Cebula and J. Groen for mineral separations, and L. Fischer and L. Kwak for chemical processing. Identification of thorite by E. E. Foord is gratefully acknowledged. This manuscript was reviewed and thereby substantially improved by J. S. Stuckless and T. A. Steven.

GEOLOGY

A generalized map of the central part of the Mineral Mountains is shown in figure A1. The reader is referred to the more complete studies of Nielson and others (1978), and Sibbett and Nielson (1980a), for details of the geology of the range.

The oldest rocks exposed in the Mineral Mountains are gneisses that were assigned a Precambrian age on the basis of lithologic character and regional relationships. These rocks crop out along the west-central margin of the range. The Precambrian units vary widely in lithology and consist largely of granitic gneiss, banded gneiss, schist, and migmatite, with small included lenses of quartzite (Nielson and others, 1978; Sibbett and Nielson, 1980a). Outcrops have a number of penetrative deformational features. Schistosity is well developed, and small-scale isoclinal folding has produced strong northeast-plunging lineations on schistosity planes. A few widely scattered outcrops show gentle cylindrical refolding of the isoclinal folds along flat-lying east-west axes.

In hand specimen, the banded gneiss is typically fine to medium grained and equigranular, and consists of biotite, hornblende, potassium-feldspar, plagioclase, and quartz in highly variable proportions. Preferentially oriented biotite books and stressed and elongate quartz grains mark the schistosity. Dark layers are predominantly plagioclase, biotite, and hornblende with lesser amounts of quartz and potassium-feldspar. Light-colored layers consisting mostly of potassium-feldspar and quartz are typically coarser grained and locally contain small amounts of muscovite. In both light and dark layers, biotite flakes commonly rim potassium-feldspar grains. Zircon is a common accessory mineral and is especially abundant as inclusions within biotite. Apatite also is an abundant accessory mineral, but sphene generally is uncommon. In addition to this typical mineralogy, a 2- to 3-m-thick layer of distinctive sillimanite-cordierite-corundum-biotite schist is exposed in one small outcrop just south of Wild Horse Canyon. This layer demonstrates both a compositional variability within the banded gneiss and a lack of diffusion within the metamorphic system, suggesting that the banding within much of the gneiss represents original sedimentary layering.

Granitic gneiss occurs as a pink, medium-grained, equigranular, and well-foliated rock that consists of quartz, potassium-feldspar, plagioclase, biotite, and muscovite, with accessory zircon, apatite, and sphene. In marked contrast to the layered paragneiss, this unit has

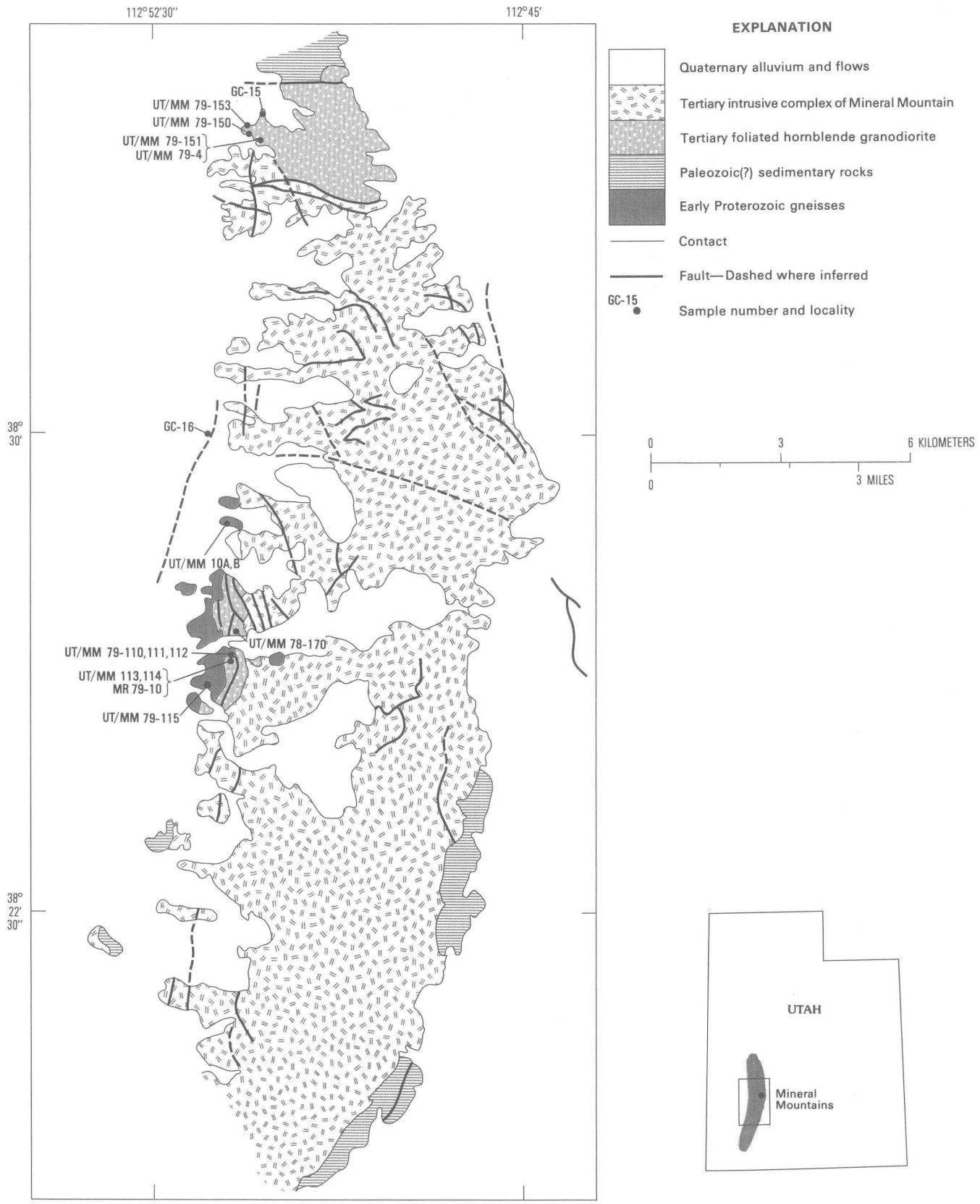

Figure A1. Generalized geologic map of the central part of the Mineral Mountains, Utah (simplified from Sibbett and Nielson, 1980a).

Table A1. Chemical analyses of Precambrian rocks from the Mineral Mountains, Utah

[J. Mason and F. H. Brown, analysts. Sample UT/MM 79–115 is orthogneiss; all other samples are paragneiss. LOI, loss on ignition; NA, not analyzed for]

Sample No.----	UT/MM-79-10A	UT/MM-79-10B	UT/MM-79-110	UT/MM-79-111[1]	UT/MM-79-112	UT/MM-79-115[1]
	Oxide, in weight percent					
SiO_2	77.84	72.52	73.61	78.01	75.31	73.30
TiO_2	0.08	0.68	0.35	0.14	0.12	0.20
Al_2O_3	12.34	11.52	14.73	14.43	14.21	14.10
^2FeO	0.94	5.11	2.84	1.10	1.09	1.86
MnO	0.01	0.04	0.04	0.03	0.03	0.03
MgO	0.29	1.30	1.11	0.75	0.68	0.42
CaO	0.93	1.46	4.60	3.22	0.91	1.28
K_2O	3.29	2.13	2.79	3.76	3.40	3.13
Na_2O	4.35	3.34	0.79	1.31	5.10	5.28
P_2O_5	0.01	0.05	0.11	0.07	0.06	0.06
LOI	0.57	0.70	0.50	0.46	0.42	0.40
Sum----------	100.76	99.42	101.47	103.28	101.33	100.06
	Trace element, in parts per million					
Nb	10	20	10	10	5	20
Zr	160	465	140	155	105	160
Y	35	125	15	10	15	30
Sr	85	70	295	235	125	100
Rb	85	105	30	35	100	230
Th	15	25	15	25	20	45
Pb	10	15	5	15	30	45
Ba	600	550	NA	NA	690	680

[1]Dated by U-Pb zircon method

[2]Total iron calculated as FeO.

a uniform composition, at least on outcrop scale, and probably represents a metaigneous rock.

Chemical analyses of six samples are listed in table A1. These samples of both paragneiss and orthogneiss were collected from the more quartzofeldspathic layers in the gneisses.

Foliated hornblende granodiorite to quartz monzonite intrudes the Precambrian rocks just described. The foliation in this rock is nearly parallel to that in the Precambrian gneiss, and therefore Nielson and others (1978) proposed that it also was of Precambrian age. Essentially identical rocks later were found to be intrusive into Cambrian marbles in the northern part of the range, at which locality the foliation is nearly parallel to the contact with the marbles and is considered to be a flow structure. Correlation of the two bodies of foliated hornblende granodiorite is supported not only by their similar appearance in the field, but also by the similarities in chemical composition (table A2) and identical morphologies of the zircons separated from both of them.

ANALYTICAL PROCEDURES

The paragneiss (sample UT/MM 79–111), orthogneiss (sample UT/MM 79–115), and a flow-foliated

Table A2. Chemical analyses of Tertiary foliated hornblende granodiorite samples from the Mineral Mountains, Utah

[J. Mason and F. H. Brown, analysts. LOI, loss on ignition; NA, not applicable]

Sample No.----	UT/MM-78-170	UT/MM-79-113[1]	UT/MM-79-114	UT/MM-79-150	UT/MM-79-151	UT/MM-79-153
	Oxide, in weight percent					
SiO_2	63.52	59.88	67.83	72.08	63.57	65.69
TiO_2	0.60	0.63	0.43	0.26	0.71	0.57
Al_2O_3	15.92	16.60	15.92	14.40	15.89	14.99
^2FeO	4.57	5.33	2.89	1.88	5.04	4.29
MnO	0.09	0.11	0.06	0.04	0.09	0.08
MgO	2.40	2.96	1.45	0.44	2.32	1.95
CaO	4.32	5.00	2.71	1.63	4.50	3.76
K_2O	3.33	4.30	3.42	3.74	3.82	3.52
Na_2O	3.86	2.75	4.96	4.48	3.19	3.74
P_2O_5	0.19	0.27	0.14	0.07	0.26	0.20
LOI	0.75	0.36	0.55	0.85	0.86	0.77
Sum----------	99.55	98.19	100.36	99.87	100.25	99.56
	Trace element, in parts per million					
Nb	15	10	15	10	10	10
Zr	130	105	170	120	140	150
Y	20	15	30	10	15	15
Sr	785	850	550	445	870	685
Rb	70	90	120	125	85	90
Th	5	15	30	25	25	10
Pb	15	15	30	25	15	15
^3U	2	NA	NA	3	<2	<2
Ba	925	980	1200	910	980	855

[1]Hornblende granodiorite, dated by U-Th-Pb zircon method.

[2]Total Fe calculated as FeO.

[3]Uranium determined fluorimetrically.

hornblende granodiorite (samples UT/MM 79–113 and UT/MM 80–4) were dated by the U-Th-Pb (uranium-thorium-lead) method. Zircons were separated from about 50 kg (kilograms) of rock, using a crusher, pulverizer, Wilfley[2] table, and heavy liquids. The heavy-mineral separates were at least 99 percent pure zircon. Size and magnetic fractions were separated and were upgraded by hand-picking out impurities to ensure nearly absolute purity.

Uranium, thorium, and lead were extracted from zircon, sphene, and thorite. Size and magnetic fractions of zircon and sphene were leached in separate solutions of warm 7N HNO_3 and warm 6.5N HCl. About 10–20 mg (milligrams) of zircon were dissolved in ultrapure 48-percent HF (2 mL (milliliters)) and 16N HNO_3 (1 mL) in a teflon bomb assembly at 210°C in an oven. Dissolution took three days or more. Samples for which thorium concentrations were determined were evaporated to dryness with ^{235}U and ^{230}Th spike and redissolved in 1N HNO_3. Overnight equilibration in the oven at 210°C was followed by liquid-aliquoting portions for lead composition and concentration. Samples that were not analyzed for thorium were not equilibrated in 1N HNO_3 and were spiked for uranium, liquid-aliquoted, and spiked for lead after dissolution.

[2]Use of trade and company names is for descriptive purposes only and does not imply endorsement by the U.S. Geological Survey.

Sphene was immersed in ultrapure 70-percent $HClO_4$ (0.50 mL) and 6.5N HCl (4 mL) in a teflon bomb assembly in an oven (210°C) overnight. The next day, 48–percent HF (1 mL) and 16N HCl (2 mL) were added and the sample was dissolved overnight. The sample was spiked and aliquoted for uranium, thorium, and lead after complete dissolution.

Thorite was immersed in 48-percent HF (0.50 mL) and 6.5N HCl (1 mL) in a screwtop teflon beaker and heated on a hotplate at 200°C overnight. After evaporation to dryness, 70-percent $HClO_4$ (0.50 mL) and 16N HNO_3 (1 mL) were added. The sample dissolved after three days of boiling. After 3 mL of 6.5N HCl were added, the solution was ready for aliquoting.

Lead was concentrated on a bromide-form ion-exchange column (modified from Krogh, 1973) and was analyzed using the single-Re-filament, H_3PO_4/silica gel technique. Uranium and thorium were extracted on nitrate-form ion-exchange columns and were analyzed using a triple-Re-filament assembly. All isotopes were analyzed on a 30.5-cm-radius, 90°-sector, single-focusing mass spectrometer with digital data collection.

Uranium, thorium, and lead concentrations were determined by isotope dilution and are believed to be accurate to at least 1 percent. Lead isotopic compositions are believed accurate to at least 0.1 percent, except where the $^{206}Pb/^{204}Pb$ is greater than 5000, as it is in samples UT/MM 79–111 and UT/MM 79–115. The errors for atomic ratios may be as high as 5–10 percent in these analyses but the atomic percent of ^{204}Pb is so small that these large errors have no significant effect on the age calculations. Laboratory blanks, usually less than 1 ng (nanogram), determined during the course of the study, were of the composition

$$^{204}PB:^{206}PB:^{207}Pb:^{208}PB = 1:18.7:15.6:38.2$$

and were subtracted from the analyses. Common lead was assumed to have the composition

1:15.7:15.3:35.3

(estimated from Stacey and Kramers, 1975) for the metamorphic rocks and

1:18.24:15.57:38.37,

as determined by analysis of a potassium-feldspar, for the hornblende granodiorite.

Age calculations used decay and isotopic constants of Steiger and Jäger (1977). Regression analysis followed the algorithm of Ludwig (1980). Analytical procedures for K-Ar (potassium-argon) determinations are similar to those reported in Evernden and Curtis (1965) and Dalrymple and Lanphere (1969).

GEOCHRONOLOGY

Previous radiometric dating of units of the intrusive complex of the Mineral Mountains have been published by Park (1968), Liese (1957), Armstrong (1970), Bowers (1978), and Lipman and others (1978), but no ages are available for the Precambrian rocks or for the foliated hornblende granodiorite. Stacey and others (1968) measured common lead isotope ratios in galenas and feldspars from mining districts throughout Utah, including the Milford district just to the west of the Mineral Mountains, and concluded that the lead was derived from an Early Proterozoic source rock.

Metamorphic Rocks

Two size fractions of zircon from each metamorphic rock were analyzed. Zircons in the paragneiss (UT/MM 79–111) are euhedral and some are slightly rounded (fig. A2*A*). They are blocky in morphology, with length-to-width ratios of about 2 or 3 to 1 and contain abundant opaque and clear inclusions. They do not appear to be detrital (that is, they are not rounded or frosted) and on the basis of their morphology and the compositions of the paragneiss, we conclude that the rock sampled is volcanic in origin. Zircons in the orthogneiss (UT/MM 79–115) are also euhedral (fig. A2*B*). They are more prismatic than the zircons from the paragneiss, having length-to-width ratios of about 4 or 5 to 1, and contain few inclusions. Their general morphology is typical of plutonic zircons and the rock in which they occur is interpreted to be a metaquartz monzonite.

Isotopic data for the gneisses are presented in table A3 and are plotted in figure A3. The $^{207}Pb/^{206}Pb$ ages range from 1,723 to 1,708 Ma (million years) and the U-Pb ages range from 1,482 to 662 Ma. As shown in figure A3, a best-fit line through the four data points has concordia intercept-ages of $1,716 \pm 31$ and 7 ± 93 Ma (95–percent confidence limits). Three of the four points are about 33 percent discordant, whereas the fourth sample plots about 67 percent down the discordia. A reasonable explanation for this array is suggested by the uranium concentration data. The three least discordant zircons have concentrations that range from 1,371 to 2,193 ppm (parts per million) uranium, whereas the most discordant size fraction contains 3,736 ppm uranium. Thus, a Cenozoic event that caused lead loss from the zircons would have had a significantly greater effect on the most uranium-rich (and thereby most radiation-damaged) sample.

We interpret the data to indicate an age of about 1,720 Ma for both metamorphic units. Specifically, the orthogneiss was intruded at this time, during regional metamorphism of the paragneiss inasmuch as there is no evidence in the U-Th-Pb systematics for a younger metamorphic event. Plutonic rocks of similar age in Colorado (such as the Boulder Creek Granite) also are interpreted as being syntectonic in origin (Tweto, 1977). Igneous rocks in the next youngest age group in Colorado, about 1,400 Ma (Tweto, 1977) generally are not foliated and are considered to be post-tectonic.

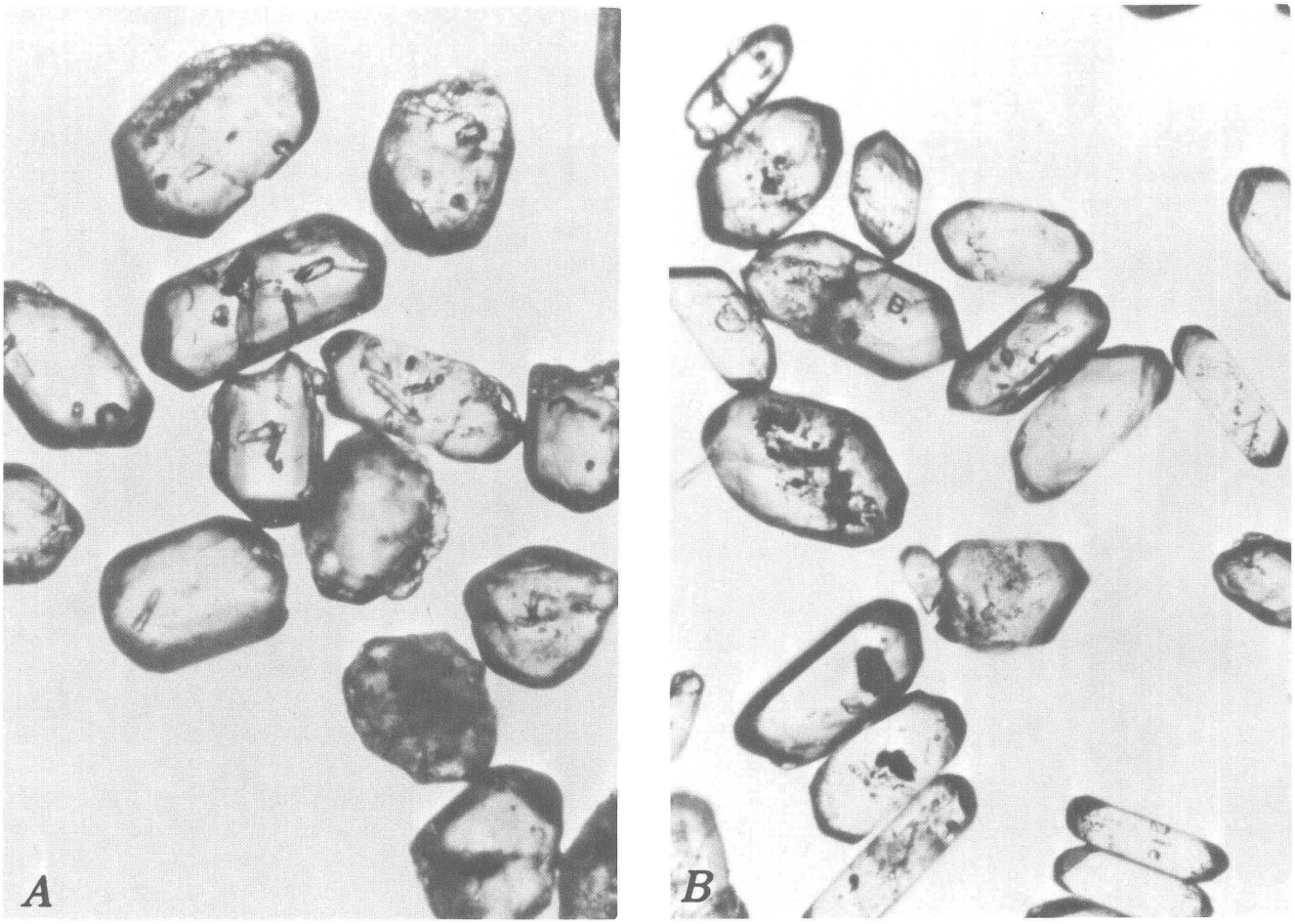

Figure A2. Photomicrographs of zircons from metamorphic rocks of the Mineral Mountains, Utah. *A*, Zircons from paragneiss sample UT/MM 79–111 (size fraction, +150 mesh); *B*, Zircons from orthogneiss sample UT/MM 79–115 (size fraction, +150 mesh). Grains in both *A* and *B* are about 170 μm long.

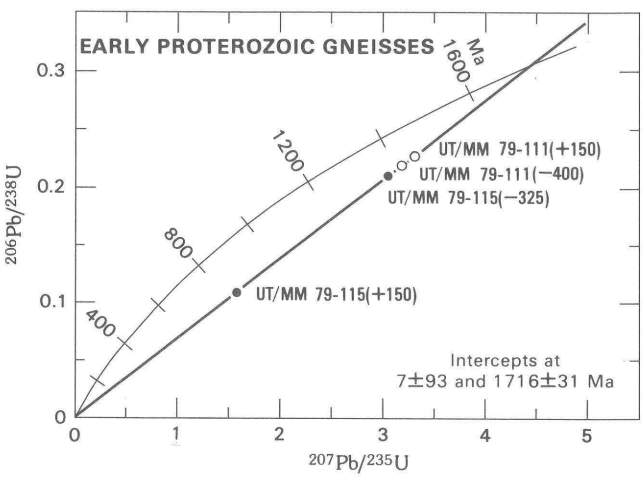

Figure A3. Uranium-lead concordia plot of zircons from metamorphic rocks from the Mineral Mountains, Utah. Sample UT/MM 79–11 (open circles) is a paragneiss; sample UT/MM 79–115 (solid circles) is an orthogneiss.

Zircons in the paragneiss may be volcanic in origin or they may have formed during regional metamorphism and intrusion of the orthogneiss protolith. There is no evidence in the zircon data for the age of a parent rock of the paragneiss. This lack of evidence may be explained by: (1) the absence of detrital zircons from the precursor sedimentary pile, or (2) the precursor volcanic(?) rocks were formed only shortly before burial and metamorphism and thus the slight age difference of the protolith and metamorphic rock cannot be resolved. The lower intercept of the discordia corresponds to a Cenozoic age and could have been caused by Quaternary dilatancy (Goldich and Mudrey, 1972) or, more likely, by intermittent igneous activity in this area since early Miocene time. Evans and Steven (1982) reported an age of about 9 Ma for emplacement of rhyolite domes and flows a few kilometers east of the Mineral Mountains.

Rubidium-strontium (Rb-Sr) data for the orthogneiss and paragneiss are listed in table A4. Three paragneiss samples show scatter well beyond the limits of analytical error (see fig. A4). This scatter presumably is due to

Table A3. Uranium-thorium-lead data for zircon, thorite, and sphene from the Mineral Mountains, Utah
[Leaders (---) indicate no Th concentration determined and thus no $^{208}Pb/^{232}Th$ age calculated; NM, nonmagnetic; VM, very magnetic]

Mineral: (size fraction)	Concentration (ppm)			Atomic percent				Age (million years)			
	U	Th	Pb	^{204}Pb	^{206}Pb	^{207}Pb	^{208}Pb	$^{206}Pb/^{238}U$	$^{207}Pb/^{235}U$	$^{207}Pb/^{206}Pb$	$^{208}Pb/^{232}Th$
Sample UT/MM 79-111 (paragneiss)											
Zircon: (+150)	1370.5	---	308.25	0.0025	86.93	9.204	3.864	1320	1482	1723	---
(-400)	1957.3	---	429.48	0.0012	86.17	9.056	4.774	1281	1452	1712	---
Sample UT/MM 79-115 (orthogneiss)											
Zircon: (+150)	3736.3	---	415.9	0.0010	84.53	8.879	6.593	669	963	1712	---
(-325)	2192.6	---	458.2	0.0007	86.83	9.092	4.082	1234	1419	1708	---
Sample UT/MM 79-113 (hornblende granodiorite)											
Zircon: (+100)VM	338.2	---	2.05	0.4299	64.69	9.401	25.48	25.8	26.4	82.8	---
(+100)	363.0	162.5	1.72	0.1866	75.16	6.297	18.36	25.4	25.8	62.8	26.9
(-100+150)	375.5	189.5	1.91	0.2046	73.41	6.536	19.85	26.5	27.4	103.7	27.5
(-325+400)	531.0	---	2.69	0.1130	70.19	5.086	24.61	25.8	27.0	139.1	---
(-400)	1122.9	---	7.21	0.1670	47.06	4.842	47.94	21.1	23.1	238.6	---
Sample UT/MM 4-80 (hornblende granodiorite)											
Zircon: (+150)NM	512.0	---	4.74	0.0537	81.65	7.008	11.29	55.7	88.9	1108	---
Sphene----------	308.5	384.2	3.07	0.8148	42.82	13.974	42.39	20.7	20.7	20.7	20.1
	Concentration										
	U (weight percent)	Th	Pb (ppm)								
Thorite----------	12.1	58.7	666.30	0.0069	38.48	1.892	59.62	15.6	15.7	24.7	15.2

Table A4. Rubidium-strontium data for rocks from the Mineral Mountains, Utah

Sample No.	Rb (parts per million)	Sr (parts per million)	$^{87}Rb/^{86}Sr$	$^{87}Sr/^{86}Sr$
		Paragneiss		
UT/MM 79-110	28.8	269	0.3092	0.7177
UT/MM 79-111	49.9	225	0.6429	0.7282
UT/MM 79-112	89.4	108	2.404	0.7621
		Orthogneiss		
UT/MM 79-115	216	94.1	6.743	0.8717
		Granodiorite		
UT/MM 79-113	96.6	857	0.3262	0.70560

heterogeneous initial $^{87}Sr/^{86}Sr$. One orthogneiss sample also was analyzed. The relatively high $^{87}Rb/^{86}Sr$ of 6.743 allows calculation of an apparent age of 1,750 Ma if an initial $^{87}Sr/^{86}Sr$ of 0.702 is assumed. This isochron also passes through one of the paragneiss data points. This Rb-Sr age is in satisfactory agreement with the zircon age data, considering that the assumption of initial $^{87}Sr/^{86}Sr$ may not be quite accurate.

Potassium-argon data of biotites from three samples of the banded gneiss are listed in table A5. Sample GC–16

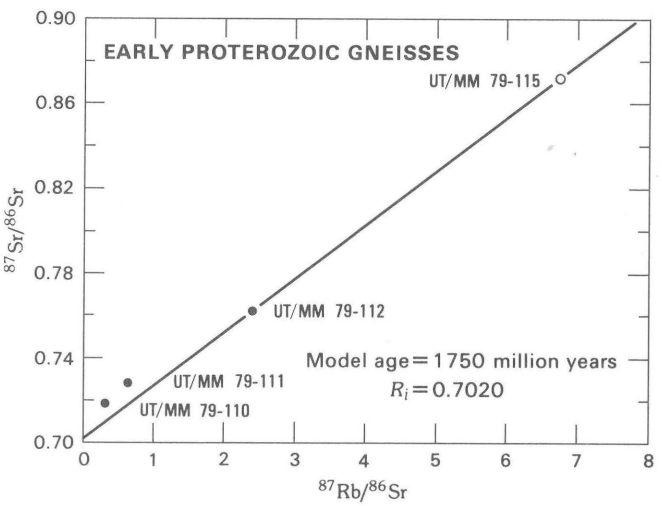

Figure A4. Rubidium-strontium isochron plot of metamorphic rocks from the Mineral Mountains, Utah. Errors (2σ) are 0.035 percent and 1.7 percent for $^{87}Sr/^{86}Sr$ and $^{87}Rb/^{86}Sr$, respectively. Open circle is orthogeniss; solid circles are paragneiss. The line is a model isochron calculated through the orthogneiss data point assuming an initial $^{87}Sr/^{86}Sr$ (R_i) of 0.702.

Table A5. Potassium-argon data for rocks from the Mineral Mountains, Utah

Sample No.	Mineral	Weight (grams)	K (percent)	Moles/gram Ar^{40} ($x10^{-11}$)	Percent Ar^{40} (atmospheric)	Age (million years)	Reference
			Gneiss				
GC-16	Biotite------	0.45942	7.505	14.009	63.7	10.7±0.2	Bowers (1978).
GC-15	--do.--------	2.56070	6.323	13.797	27.8	12.5±0.1	Do.
UT/MM 79-10	--do.--------	0.77447	7.60	13.016	47	9.85±0.37	
			Hornblende granodiorite				
MR 79-10	Biotite------	0.56814	7.49	13.448	72	10.3±0.6	
	Hornblende---	2.50659	0.75	5.284	39	40.3±1.4	
UT/MM 78-170	Biotite------	0.79213	7.40	12.666	50	9.86±0.37	
UT/MM 79-150	--do.--------	0.52549	7.89	18.362	27	13.4±0.5	
UT/MM 79-151	Biotite------	0.60145	7.77	26.392	34	19.5±0.7	
	Hornblende---	2.53078	0.67	4.503	59	38.4±1.6	
UT/MM 79-153	Biotite------	0.50100	7.40	17.473	57	13.6±0.6	
	Hornblende---	2.50158	0.79	3.744	33	27.2±0.9	

(Bowers, 1978) was collected from an outcrop in Negro Mag Wash. The outcrop is along a major fault zone and within 50 m of an active fumarole. Sample GC–15 was collected from an outcrop of gneiss that presently is interpreted as a xenolith (about 400 m^2 in area) within some of the more felsic phases of the intrusive complex of the Mineral Mountains. A cataclasite found in the same outcrop indicates that the sample is near a fault zone. Sample UT/MM 79–10 was collected from an outcrop which is on the eastern margin of the Roosevelt Hot Springs geothermal field. This sample also was collected within about 100 m of a principal range-front fault. The average of the three K-Ar dates is about 11 Ma. This age is near that of 9 Ma reported by Evans and Steven (1982) for rhyolite lavas just east of the Mineral Mountains and indicates, in light of the Rb-Sr and U-Pb data, extensive resetting of the K-Ar system.

Hornblende Granodiorite

Three accessory minerals (zircon, sphene, and thorite) from the hornblende granodiorite were analyzed for U-Th-Pb isotopes. The zircons are distinctly bright pink and have virtually no evidence, such as dark core material, for an inherited component. The crystals are euhedral and nearly equant with length-to-width ratios ranging from about 1 to 4 (fig. A5*A*). The sphene is anhedral, coarse grained, and bright yellow. Thorite is subhedral to euhedral, forming prisms similar in shape to zircons (fig. A5*B*), from which it can be distinguished by its olive- to emerald-green. Several grams of each accessory mineral were extracted from about 50 kg of rock. The thorite was identified by Eugene E. Foord, U.S. Geological Survey, using X-ray diffraction of preheated crystals and X-ray fluorescence (EDS).

Isotopic data for two samples of hornblende granodiorite are listed in table A2 and plotted on figure A6. The zircon data from sample UT/MM 79–113 do not form a linear pattern and so a complicated multistage history must be invoked to explain the data array. The $^{207}Pb/^{206}Pb$ ages range with decreasing grain size from 63 Ma (+100 mesh) to 239 Ma (–400 mesh). All U-Pb and Th-Pb ages cluster around 25 Ma ± about 4 Ma In an attempt to determine more definitely the intrusive age of the granodiorite, another sample (UT/MM 4–80) from a more northerly locality in the Mineral Mountains was collected. Based on the data from UT/MM 79–113, we thought that the coarsest and least magnetic size fraction would yield the youngest $^{207}Pb/^{206}Pb$ ages. As can be seen in table A2 and figure A6, the $^{207}Pb/^{206}Pb$ age of UT/MM 4–80 (+150)NM is far older (1,108 Ma) than any of the other size fractions. We attribute the older Pb/Pb ages to inheritance of old radiogenic lead, derived from magmatic source regions, in young (~25-Ma-old) granodiorite zircons.

Given an age of 25 m.y., sample UT/MM 79–113 has a calculated initial $^{87}Sr/^{86}Sr$ of 0.70548. Such ratios are typical of andesitic volcanic rocks erupted at about this same time about 24 km to the east in the Marysvale volcanic field (C. E. Hedge, unpub. data).

Potassium-argon ages for samples of foliated hornblende quartz monzonite and hornblende granodiorite are listed in table A5. There is considerably more scatter in the dates on these intrusive units than in the dates for

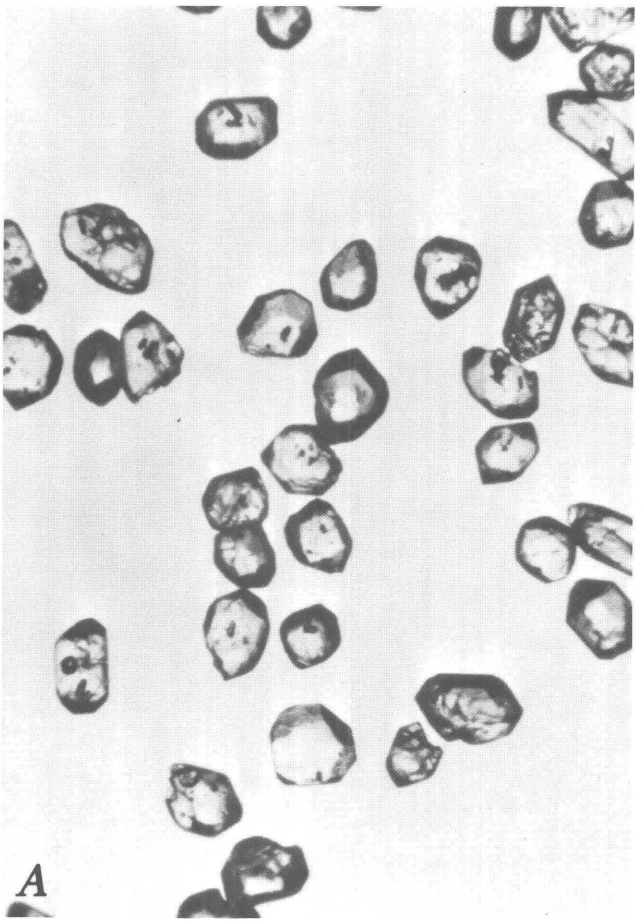

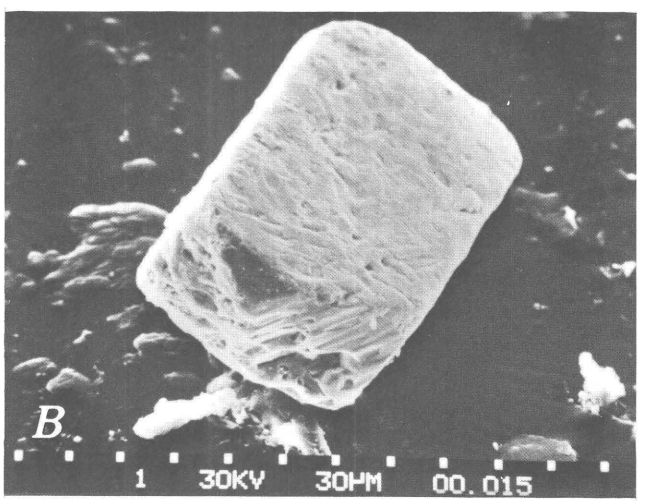

Figure A5. Photomicrographs of uraniferous minerals from Tertiary granodiorite, Mineral Mountains, Utah. *A*, Zircons from granodiorite sample UT/MM 79–113 (size fraction, +100 mesh). Grains are about 200 μm long. *B*, Scanning electron microscope photograph of thorite from granodiorite sample UT/MM 79–113. Grain is about 200 μm long.

the Early Proterozoic gneisses. The biotite ages vary by a factor of two and the hornblende ages are markedly different from the biotite ages from the same samples. In comparing the biotite ages with the U-Pb ages, clearly the biotites all have been reset. The hornblende ages are more problematical. One date of 27 Ma is concordant with the U-Pb ages. The other hornblende ages are somewhat older and excess argon is the likely cause of the anomalously old ages. Note that the ages of biotites from the granodiorite in the northern part of the range are older than those from the central part of the range. This geographic distribution of ages may represent a greater distance from the perturbing younger thermal center for these samples.

Sphene and thorite samples from the granodiorite were analyzed also. As shown in table A3, the sphene yields a concordant age of about 21 Ma, younger than any of the zircons. Thorite has a $^{207}Pb/^{206}Pb$ age of about 25 Ma and U-Pb and Th-Pb ages are about 15 Ma. Elsewhere, U-Th-Pb ages on sphene have been shown (Hanson and other, 1971) to have been reset by contact metamorphism. Such ages are thought to be more resistant to resetting than K-Ar hornblende ages, but less resistant than U-Pb zircon ages (Hanson and others, 1971). Thus, the igneous acitvity in this area appears to have prevented final closing of the U-Th-Pb system in the sphene until 21 m.y. ago. The thorite $^{207}Pb/^{206}Pb$ date of 25 Ma is interpreted as the age of intrusion. Subsequently, lead was lost, changing U-Pb and Th-Pb ratios to reflect a younger age. Because of the short time span and the uncertainty in the crystallization age, we cannot determine precisely when in the last 25 m.y. this lead was lost, although Quaternary lead loss due to dilatancy (Goldich and Mudrey, 1972) or loss during any of the several Miocene to Quaternary episodes of igneous activity known to have occurred in this area seems likely.

DISCUSSION

In the simple two-stage example where the lead isotopic composition of a zircon is a function only of the age of crystallization and the age of the inherited material, a linear array is formed. The location of a data point along this "inheritance line" (in our study between 25 and 1,720 Ma) is determined by the amount of each lead isotope contributed by the two end-member sources. For the intercepts to yield geologically reasonable dates, no lead may have been lost from either end member prior to or subsequent to the mixing. In the Mineral Mountains, the hornblende grandiorite shows isotopic evidence for disturbance to the U-Pb system after crystallization of the zircons 25 Ma ago. The fine-grained size fractions, (–325+400 mesh) and (–400 mesh), have moved down towards the present (O Ma). The concentrations of uranium in the fine-grained zircons are considerably higher

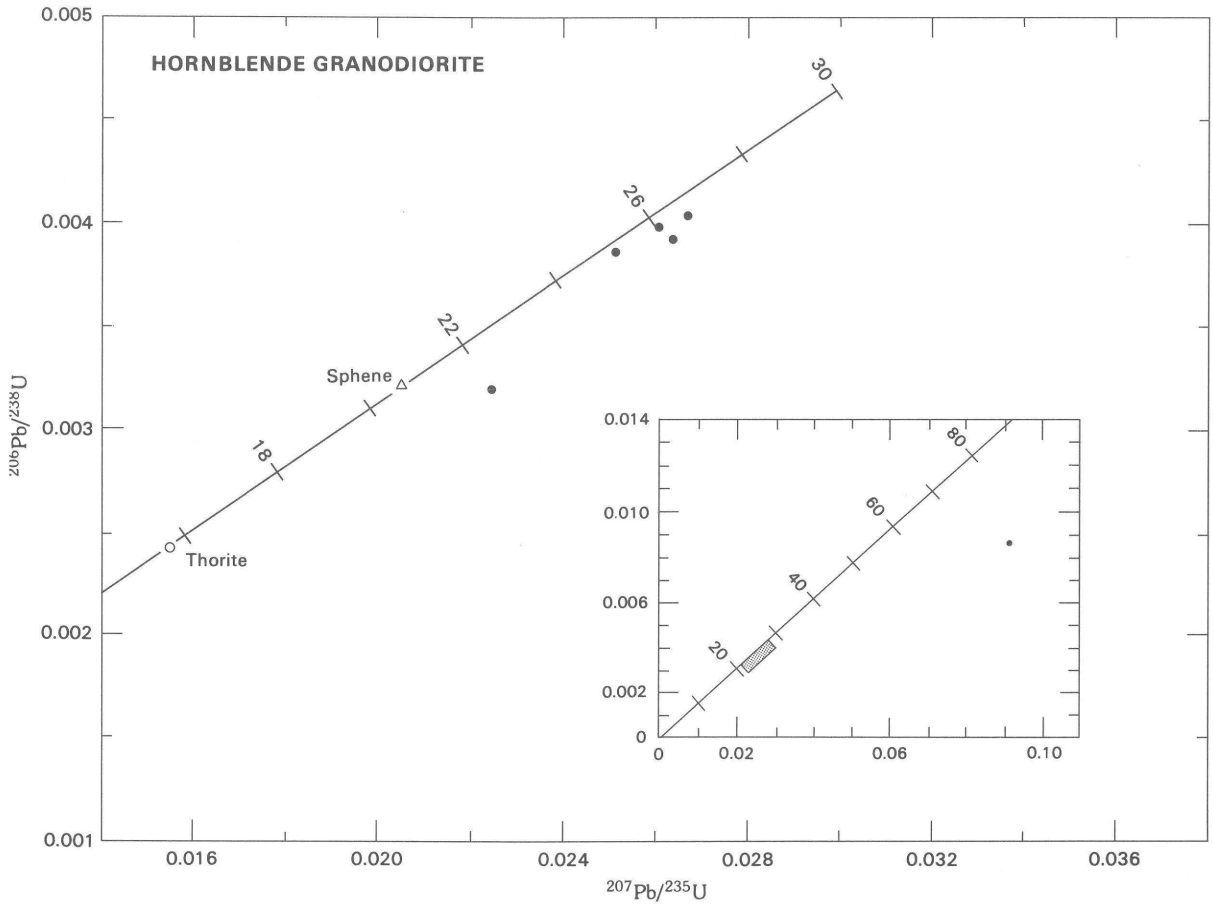

Figure A6. Uranium-lead concordia plot of zircons, sphene, and thorite from hornblende granodiorite from the Mineral Mountains, Utah. Solid circles, zircon fractions from UT/MM 79–113. Solid circle in inset shows location of UT/MM 4–80 (size fraction, +150 mesh NM); shaded area contains hornblende granodiorite data points from UT/MM 79–113.

(between 531 and 1,123 ppm, respectively) than in the coarser grains (between 338 and 376 ppm). Therefore, the fine-grained zircons probably accumulated more radiation damage and were more susceptible to lead loss caused by either local thermal activity or dilatancy. This area of Utah is known for its repeated episodes of intrusion and volcanism during the past 25 Ma and is, in fact, an active geothermal area today. Therefore, the U-Th-Pb data from the coarser zircon grains indicate an intrusive age of about 25 Ma ago and suggest derivation from much older (Proterozoic) rock.

A likely parent for the hornblende granodiorite, as indicated by the U-Pb isotopic data, is a unit of Early Proterozoic age. However, based on whole-rock chemistry and strontium isotope data, the paragneiss and orthogneiss analyzed in this study cannot have been the parent material. A more likely source rock would be lower crustal material, which should have been more mafic in composition and should have had lower $^{87}Sr/^{86}Sr$. If only modern lead loss has occurred since intrusion of the granodiorite, then the data points for the granodiorite should fall on or below an "inheritance chord" between 25 Ma and 1,720 Ma. As previously discussed, the two fine-grained fractions of sample UT/MM 79–113 plot below this line, due, at least in part, to recent lead loss. However, sample UT/MM 4–80 (+150) which has a $^{207}Pb/^{206}Pb$ age of 1,108 Ma, plots slightly above the "inheritance chord". We explain this plot position by invoking a small amount of lead loss from the Proterozoic zircons probably about 1,400 million years ago, caused by the thermal event responsible for the intrusion of Middle Proterozoic anorogenic plutonic rocks. Another possible cause for the observed scatter is that the lower crustal source material is slightly younger than the Proterozoic material dated in this study.

The possible multistage history of the hornblende granodiorite is shown graphically in figure A7. A point (*X*) would move some unknown distance (assumed to be a maximum of about 30 percent) from point *A* towards point *B*. About 1,400 million years later, during anatexis, partially resorbed zircons were incorporated into Tertiary magmas, to serve as nuclei for new zircons crystallizing

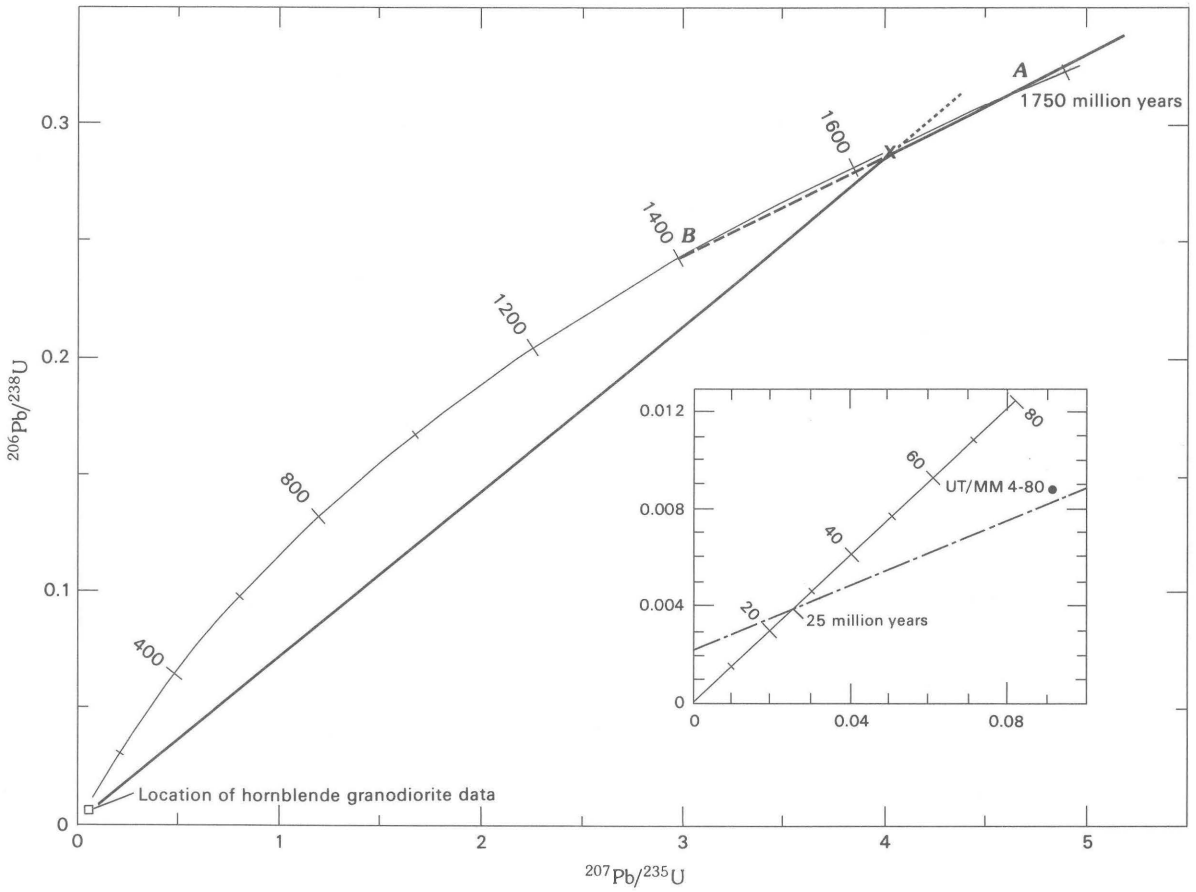

Figure A7. Model U-Pb concordia plot showing possible multistage history for zircons in granodiorite sample UT/MM 79–113, Mineral Mountains, Utah. Zircons in Precambrian rocks shift from point A towards point B to a position near point X on chord *A–B*. These discordant zircons were nuclei around which 25–m.y.–old zircon grew when the hornblende granodiorite magma crystallized. Inset shows the present location of sample UT/MM 4–80 (+150)NM with respect to a dash-dot reference line between 25 and 1750 m.y. Note that a line constructed from 25 m.y. through X would yield an erroneously young parent age. Another possibility is that the chord from 25 m.y. through X might accurately date the source rock at a slightly younger age than the Precambrian rocks dated in this study.

in the hornblende granodiorite magma. Thus, a chord constructed from the probable age of intrusion (25 Ma) through the value for sample UT/MM 4–80 (+150)NM would give an erroneously young upper intercept. Note that modern lead loss in UT/MM 4–80 (+150)NM might have fortuitously moved the data point down towards the present so that it plotted on the "inheritance chord" between 25 Ma and 1,720 Ma. Thus, what in reality might be a complicated four-stage history would appear to be a simple two-stage history.

In conclusion, the orthogneisses and paragneisses of the Mineral Mountains are about 1,720 Ma. Evidence for rocks of this age was found by Stacey and others (1968), based on common-lead data from galenas from the Milford district. Our study confirms their conclusions and identifies a possible source rock for the lead in the galenas from south-central Utah.

The foliated hornblende granodiorite previously mapped as Precambrian is shown to be about 25 Ma, based on data from zircons. Ages of sphene and thorite, which occur in minor and trace amounts, respectively, confirm the zircon-age data. Zircons also show that the granodiorite probably was derived from Early Proterozoic material, although a likely parent material has not been found in the area.

REFERENCES CITED

Armstrong, R. L., 1970, Geochronology of Tertiary igneous rocks, eastern Basin and Range Province, western Utah, eastern Nevada and vicinity, U.S.A.: Geochimica et Cosmochimica Acta, v. 34, p. 203–232.

Bowers, D., 1978, Potassium-argon dating and petrology of the Mineral Mountains pluton, Utah: University of Utah M.S. thesis, 76 p.

Condie, K. C., 1960, Petrogenesis of the Mineral Range pluton, southwestern Utah: University of Utah M.S. thesis, 92 p.

Dalrymple, G. B., and Lanphere, M. A., 1969, Potassium-argon dating: San Francisco, W. H. Freeman and Co., 250 p.

Earll, F. N., 1957, Geology of the central Mineral Range, Beaver County, Utah: University of Utah Ph. D. thesis, 112 p.

Evans, S. H., Jr., 1975, Geology of the central and northern Mineral Mountains, Utah: University of Utah, Dept. of Geology and Geophysics, Topical Report 77–7, 1 p.

Evans, S. H., Jr., and Steven, T. A., 1982, Rhyolites in the Gillies Hill-Woodtick Hill area, Beaver County, Utah: Geological Society of America Bulletin, v. 93, no. 11, p. 1131–1141.

Evernden, J. F., and Curtis, G. H., 1965, The potassium-argon dating of Late Cenozoic rocks in east Africa and Italy: Current Anthropology, v. 6, p. 343–385.

Goldich, S. S., and Mudrey, M. G., 1972, Dilatancy model for discordant U-Pb ages, *in* Tugarinov, A. (ed.), Contributions to recent geochemistry and analytical chemistry, (A. P. Vinogradov Volume), Moscow, USSR, NAUKA Publ. Office, p. 415–418.

Hanson, G. N., Catanzaro, E. J., and Anderson, D. H., 1971, U-Pb ages for sphene in a contact metamorphic zone: Earth and Planetary Science Letters, v. 12, p. 231–237.

Krogh, T. E., 1973, A low-contamination method for hydrothermal decomposition of zircon and extraction of U and Pb for isotopic age determinations: Geochimica et Cosmochimica Acta, v. 37, p. 485–494.

Liese, H. C., 1957, Geology of the northern Mineral Range, Millard and Beaver Counties, Utah: University of Utah M.S. thesis, 88 p.

Lipman, P. W., Rowley, P. D., Mehnert, H. H., Evans, S. H., Nash, W. P.,and Brown, F.H., 1978, Pleistocene rhyolite of the Mineral Mountains, Utah—Geothermal and archeological significance: U.S. Geological Survey Journal of Research, v. 6, no. 1, p. 133–147.

Ludwig, K. R., 1980, Calculation of uncertainties of U-Pb isotope data: Earth and Planetary Science Letters, v. 46, p. 212–220.

McKinney, D. B., 1978, Annotated bibliography of the geology of Roosevelt Hot Springs Known Geothermal Resource Area and the adjacent Mineral Mountains, March 1978: University of Utah Research Institute, Earth Science Laboratory Report, U.S. Department of Energy contract EG–78–C–07–1701.

Nielson, D. L., Sibbett, B. S., McKinney, D. B., Hulen, J. B., Moore, J. N., and Sainberg, S. M., 1978, Geology of the Roosevelt Hot Springs KGRA, Beaver County, Utah: University of Utah Research Institute, Earth Science Laboratory Report 12, 121 p.

Park, G. M., 1968, Some geochemical and geochronologic studies of the beryllium deposits in western Utah: University of Utah M.S. thesis, 104 p.

Petersen, C. A., 1975, Geology of the Roosevelt Hot Springs area, Beaver County, Utah: Utah Geology, v. 2, p. 109–116.

Sibbett, B. S., and Nielson, 1980a, Geology of the central Mineral Mountains, Beaver County, Utah: University of Utah Research Institute, Earth Science Laboratory Report 33, 42 p.

———1980b, The Mineral Mountains intrusive complex, Utah [abs.]: Geological Society of America Abstracts with Programs, Rocky Mountain Section, v. 12, p. 305.

Stacey, J. S., Zartman, R. E., and Nkomo, I. T., 1968, A lead isotope study of galenas and selected feldspars from mining districts in Utah: Economic Geology, v. 63, p. 796–814.

Stacey, J. S., and Kramers, J. D., 1975, Approximation of terrestrial lead isotope evolution by a two-stage model: Earth and Planetary Science Letters, v. 26, p. 207–221.

Steiger, R. H. and Jäger, E., 1977, Subcommission on geochronology; Convention on the use of decay constants in geo- and cosmochronology: Earth and Planetary Science Letters, v. 36, p. 359–362.

Tweto, Ogden, 1977, Nomenclature of Precambrian rocks in Colorado: U.S. Geological Survey Bulletin 1422–D, 22 p.

Ward, S. H., Parry, W. T., Nash, W. P., Sill, W. R., Cook, K. L., Smith, R. B., Chapman, D. S., Brown, F. H., Whelan, J. A., and Bowman, J. R., 1978, A summary of the geology, geochemistry, and geophysics of the Roosevelt Hot Springs thermal area, Utah: Geophysics, v. 43, p. 1515–1542.

1986

U.S. GEOLOGICAL SURVEY BULLETIN 1622

SHORTER CONTRIBUTIONS TO ISOTOPE RESEARCH

URANIUM-LEAD ZIRCON AGES AND COMMON LEAD MEASUREMENTS FOR THE ARCHEAN GNEISSES OF THE GRANITE MOUNTAINS, WYOMING

Chapter B

By LYNN B. FISCHER and JOHN S. STACEY

CONTENTS

FIGURES

TABLES

Abstract

Zircons from the metamorphic complex of the Granite Mountains, Wyoming, yield uranium-lead concordia ages of 2,880 Ma (10^6 years) for the massive augen gneisses and 3,230 Ma for the layered gneisses. This older 3,200–Ma event, predicted by Z. E. Peterman and R. A. Hildreth from the high initial $^{87}Sr/^{86}Sr$ value, is supported further by common lead measurements and by the $^{177}Hf/^{176}Hf$ chondrite model ages of 3,200 Ma. However, such measurements do not preclude a period of crustal residence for the precursors of the layered gneisses prior to 3,200 Ma.

INTRODUCTION

The Granite Mountains of Wyoming are part of an extensive Archean terrane, the Wyoming age province, which includes Montana, Wyoming, and adjacent parts of Idaho and Utah. The Precambrian basement of the Granite Mountains was uplifted during the Laramide orogeny, exposing Archean metamorphic and igneous rocks. This paper presents U-Pb (uranium-lead) zircon age determinations and U-Th-Pb (uranium-thorium-lead) data for feldspars from these metamorphic rocks. Zircon and feldspar were concentrated from samples collected for an earlier study by Peterman and Hildreth (1978) who, primarily on the basis of Rb-Sr (rubidium-strontium) analyses, concluded that the Archean gneisses were involved in a high-grade metamorphism 2,860±60 Ma ago. Uranium-lead analyses of zircon from granite of Lankin Dome and Long Creek Mountain confirmed a younger event that has concordia ages of approximately 2,600 Ma (Ludwig and Stuckless, 1978).

On the basis of Rb-Sr data and geologic evidence, Peterman and Hildreth (1978) observed two separate groups of Archean gneisses. The relatively high $^{87}Sr/^{86}Sr$ initial ratio of 0.7048 ± 0.0012 that they obtained on one group of gneisses suggested that the precursors had a crustal history several hundred million years prior to metamorphism. This present U-Pb study of the ancient gneisses was undertaken on Peterman's samples not only to confirm the regional metamorphic event, but also to investigate the pre-metamorphic history of these rocks.

ACKNOWLEDGMENTS

We are indebted to our colleagues Z. E. Peterman, S. S. Goldich, and J. N. Rosholt for helpful discussions in reviewing this manuscript. Thanks are due also to Peterman for supplying the mineral separates. Becky Hopper separated the zircons and helped with the chemical procedures. Loretta Kwak analyzed zircon fractions 1 and 3.

GEOLOGY

The Precambrian geology of the Granite Mountains is complex, and, as Peterman and Hildreth (1978) noted, there is a lack of detailed mapping and laboratory studies. The generalized geologic map showing sample localities (fig. B1) and the abbreviated summary that follows are based on the work of Peterman and Hildreth (1978) to which the reader is referred. Peterman and Hildreth (1978) noted three principal rock groups: gneiss, granite, and diabase dikes. The granitic gneisses that contain the oldest Precambrian rocks show considerable variety in texture, structure, and composition. The two types with which we are concerned were designated layered gneiss and augen gneiss by Peterman and Hildreth (1978). The compositionally layered quartz-feldspathic gneiss generally is granodioritic in composition. The foliated, but not layered, biotite-quartz-plagioclase augen gneiss is tonalitic and is called "massive" gneiss to distinguish it from the layered rock. Most of the gneisses in the two categories likely were derived from igneous precursors. Peterman and Hildreth (1978), however, concluded that some of the biotite-rich gneisses and schists, as well as some of the amphibolitic rocks, probably were derived from sedimentary precursors. They proposed that an original sedimentary-volcanic sequence, similar to the sedimentary-volcanic sequence in the southwestern Wind River Range northwest of the Granite Mountains, was metamorphosed at 2,860 Ma and later was intruded by granite.

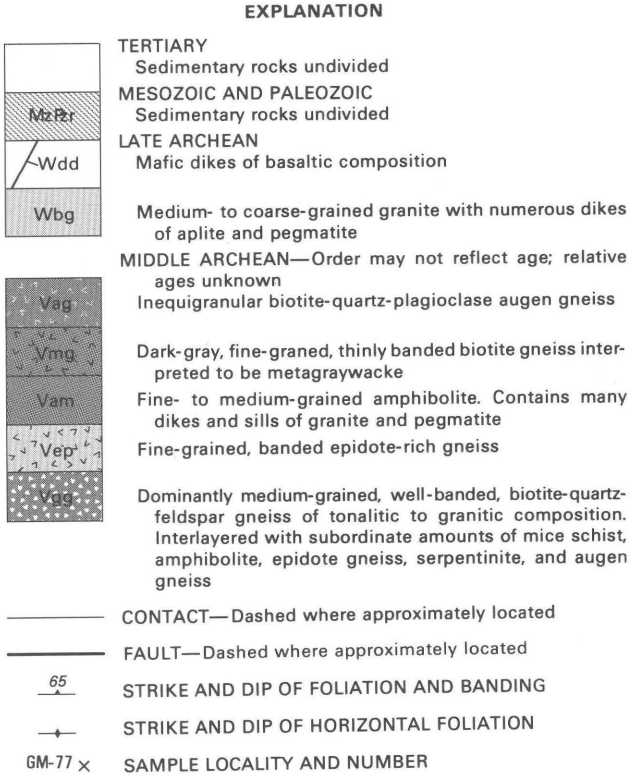

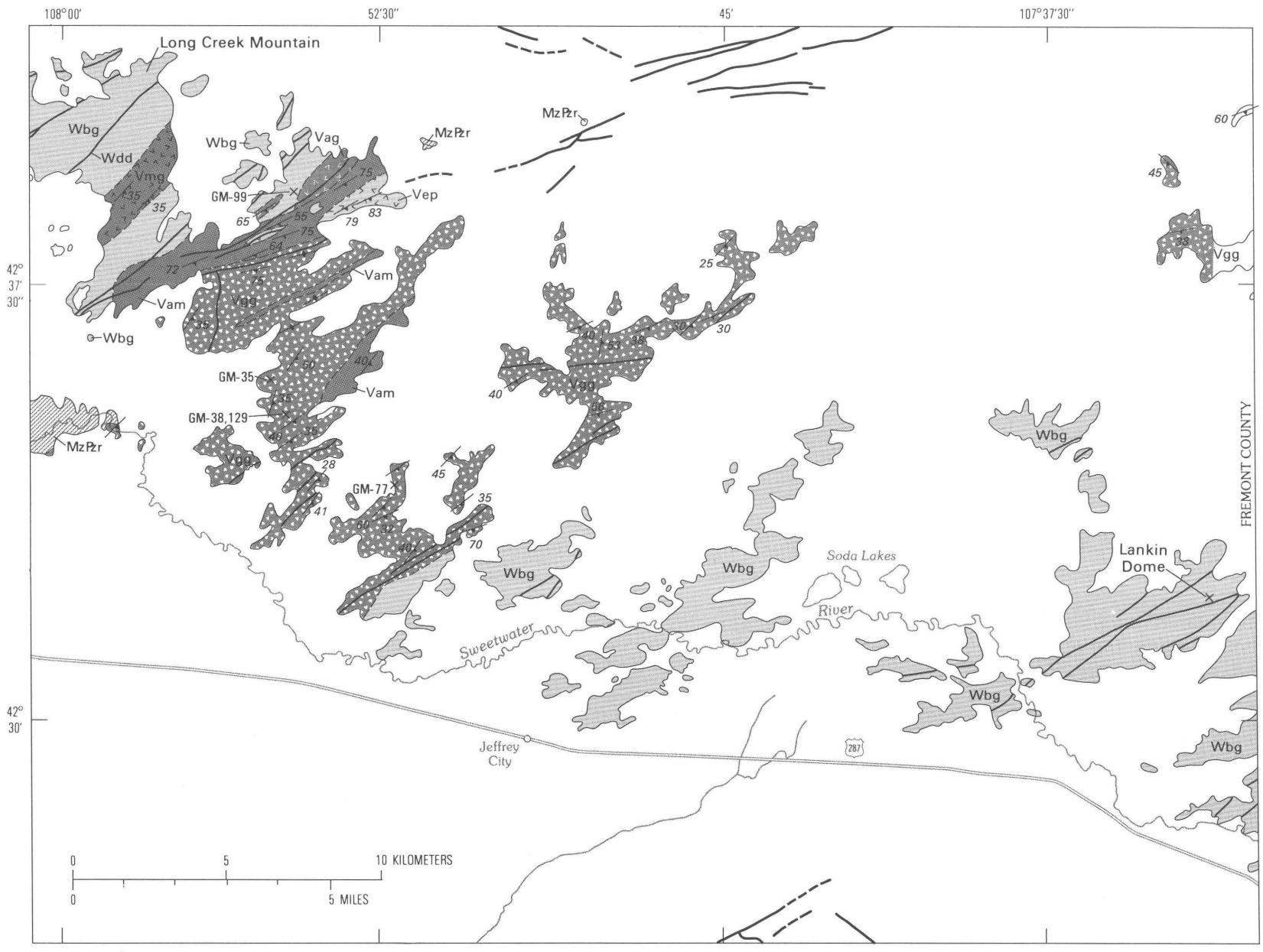

Figure B1 (above and facing page). Map of the geology of the Precambrian of the Granite Mountains, Wyo. Shown are localities of samples analyzed in this study. Map is modified from Peterman and Hildreth (1978).

Table B1. Description of samples from the Granite Mountains included in this study
[Modified from Peterman and Hildreth (1978)]

Sample No.	Latitude, longitude	Description
		Layered gneisses
GM-35-68	42°34′21" N., 108°55′37" W.	Light-gray, fine- to medium-grained, xenoblastic inequigranular granodioritic gneiss. Leucocratic bands alternate with more biotite-rich bands. Plagioclase moderately sericitized.
GM-38-68	42°35′04" N., 107°54′55" W.	Medium-gray, fine- to medium-grained, xenoblastic inequigranular tonalitic gneiss. Alternating light-dark bands. Plagioclase only slightly sericitized.
GM-77-68	42°33′58" N., 107°52′18" W.	Dark-gray, fine- to medium-grained, xenoblastic, inequigranular granodioritic gneiss with thin discontinuous leucocratic layers alternating with thicker mafic layers.
GM-129-77	42°35′04" N., 107°54′55" W.	New sample collected by Z. E. Peterman from outcrop of GM-38-68.
W2-CR5	42°40′13" N., 107°32′46" W.	Medium-grained biotite gneiss and schist. Drill core, 153-ft depth.
		Massive gneisses
GM-98-68	42°32′38" N., 108°12′40" W.	Medium-gray, medium-grained, xenoblastic, inequigranular tonalitic gneiss. Well-developed foliation, but is not banded.
GM-99-68	42°38′59" N., 107°54′18" W.	Medium- to coarse-grained biotite augen gneiss. Augens have been highly sheared locally into leucocratic streaks.

The granitic rocks form a major part of the uplifted Precambrian block of the Granite Mountains. These granites that were intruded into the gneisses are massive to foliated, light-gray to reddish-gray biotite granite. The fine- to medium-grained diabase dikes, according to Peterman and Hildreth (1978), generally are fresh or are relatively unaltered. Potassium-argon data indicated that the dikes were intruded into the gneisses and granite about 2,600 Ma, shortly after granitic plutonism.

SAMPLES

Four samples of layered gneiss and two of the more massive gneiss are described briefly in table B1. Sample W2–CR5 is core from a drill hole; the others are surface samples collected by Peterman. The zircon concentrates were split into two or more fractions by sieving, and for easy reference the analyzed fractions are numbered from 1 to 15. The morphology of the zircon is varied; some of the grains are rounded, but most are well-formed crystals ranging from stubby to long, slender prismatic forms that have dipyramidal terminations. Color ranges from clear or pale yellow to dark reddish brown. In general, the dark-brown crystals have a relatively higher uranium content than the lighter colored grains, but this relationship is not constant.

ANALYTICAL PROCEDURES

Preparation of feldspar samples for isotope analysis consisted of washing the concentrates with 7N HNO_3 and 6N HCl followed by leaching with warm 5-percent HF (Ludwig and Silver, 1977). Feldspars were then dissolved in a solution of 48-percent HF, 15N HNO_3 and 50-percent $HClO_4$ by heating in a teflon digestion container at 160°C. Zircon samples were split into size and magnetic fractions and washed with warm 7N HNO_3 and 6N HCl. Samples were then dissolved in a solution of 48-percent HF and 15N HNO_3 in a teflon bomb assembly at 208°C (Krogh, 1973). Lead was extracted using a bromide-form, anion-exchange resin column, and was analyzed on a mass spectrometer using the single rhenium filament silica-gel technique (Cameron and others, 1969). Uranium was extracted on a nitrate-form, ion-exchange resin column and was analyzed as a metal on a triple rhenium filament assembly.

Isotopic ratios were measured using a 30-cm-radius 90°-sector mass spectrometer, and corrections for Pb fractionation were determined from analysis of National Bureau of Standards sample SRM–981. Analytical precision of isotopic ratios within 95-percent confidence limits are ±0.12 percent for lead ratios, and ±1 percent for zircon U/Pb. Uranium and lead concentrations determined by isotopic dilution are ±1 percent for zircon samples and ±3 percent for feldspar samples.

RESULTS

Uranium-Lead Zircon Data

The analytical data and the apparent ages for the 15 zircon fractions are reported in table B2. Most of the fractions have highly discordant apparent ages, indicating considerable lead loss from the zircon at some time in its past history, although uranium gain may have been a contributing factor. The layered gneiss samples give quite different apparent ages (table B2). The fractions from sample GM–77 give nearly concordant ages of about 2,600 Ma, but the fractions from samples GM–129 and

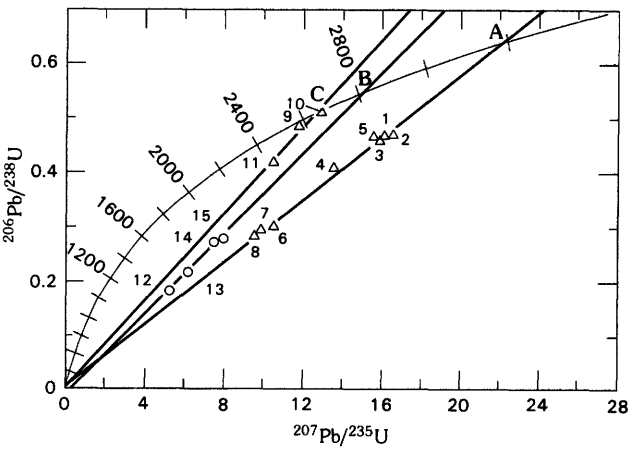

Figure B2. Uranium-lead concordia diagram. The intercepts are 32±290 and 3,187±162 Ma (point A); −96±660 and 2,819±30 Ma (point B); and 21 and 2,654 Ma (point C). Data are from table B2 for the 15 zircon fractions.

Table B2. Lead-uranium data for zircons from the Archean gneisses, Granite Mountains, Wyo.
[Numbers in parentheses are mesh sizes of zircon separates. Suffix letters refer to magnetic (M), nonmagnetic (NM), abraded (A). Atomic ratios are corrected for laboratory blank]

Fraction No.	Sample No. (fraction)	Concentration (parts per million) U	Pb	Atomic ratio $^{206}Pb/^{204}Pb$	$^{206}Pb/^{238}U$	$^{207}Pb/^{235}U$	$^{207}Pb/^{206}Pb$	Age, Ma $^{206}Pb/^{238}U$	$^{207}Pb/^{235}U$	$^{207}Pb/^{206}Pb$
				Layered gneisses						
	GM-129-77:									
1.	(50-100)	1047	584	1633	0.4631	16.011	0.2511	3453	2877	3191
2.	(50-100)A	1130	630	1470	0.4608	16.248	0.2557	2443	2891	3220
3.	(100-150)	1008	554	1658	0.4561	15.846	0.2523	2422	2868	3200
4.	(200-325)M	937	487	702	0.4058	13.580	0.2427	2196	2721	3138
5.	(-325)NM	950	528	1406	0.4629	15.572	0.2443	2452	2851	3148
	W2-CR5:									
6.	(+150)	570	233	293	0.3006	10.566	0.2550	1694	2486	3216
7.	(150-200)	952	392	395	0.2917	9.958	0.1476	1650	2431	3169
8.	(-200)	660	252	368	0.2822	9.618	0.2472	1602	2399	3167
	GM-77-68:									
9.	(+100)	494	348	417	0.4850	11.803	0.1765	2549	2589	2620
10.	(100-325)	484	350	328	0.5123	12.878	0.1823	2666	2671	2674
11.	(-325)	550	322	341	0.4179	10.458	0.1815	2251	2476	2667
				Massive gneisses						
	GM-98-68:									
12.	(+150)	1804	695	614	0.2732	7.491	0.1989	1557	2172	2817
13.	(-150)	1967	765	1722	0.2793	7.961	0.2067	1588	2227	2880
	GM-99-68:									
14.	(+100)	1835	456	695	0.1836	5.262	0.2079	1086	1863	2890
15.	(100-150)	1718	518	630	0.2180	6.175	0.2054	1271	2001	2870

W2–CR5 give minimum ages greater than 3,100 Ma. The fractions from the massive gneiss (samples GM–98 and GM–99) give sharply discordant ages, but the $^{207}Pb/^{206}Pb$ values are in a narrow range from 2,817 to 2,890 Ma.

The U-Pb data plotted in a concordia diagram (fig. B2) show three groups of apparent ages. Linear regressions of the data give intercepts on the concordia curve of 3,190 Ma, 2,820 Ma, and 2,650 Ma (fig. B2, lines A, B, and C). The points for zircon fractions 9, 10, and 11 of the layered gneiss sample GM–77 plot near the concordia curve, but fractions (12–15) from the massive gneiss (samples GM–98 and GM–99) with marked age discordance plot along line B well below concordia. Similarly, fractions 6, 7, and 8 of layered gneiss W2–CR5 plot along line A well below the concordia curve. Their positions can be explained by lead losses on the order of 50 percent, providing their true or original age was 3,190 Ma. The scatter of the data points about lines A and C (fig. B2), however, is significantly greater than the analytical error, and a complicated geologic history is indicated.

Figure B3 is a concordia diagram in which the U-Pb data are interpreted with the following assumptions:

1. The $^{207}Pb/^{206}Pb$ ages (table B2) give only a minimum age for the layered gneisses (fig. B3, line A).
2. The zircon data for the massive augen gneiss mark a distinct event that may be related to the major regional metamorphism dated by the Rb-Sr isochron age of 2,860 ± 80 Ma by Peterman and Hildreth (1978).
3. The nearly concordant ages of zircon fractions 9–11 from layered gneiss sample GM–77 are metamorphic ages; that is, the U-Pb isotopic systems were reset at the time of emplacement of granite magma at about 2,600 Ma.
4. The age discordance, in large part, resulted from lead loss during the Laramide orogeny about 60 Ma.

With these assumptions, line A (fig. B3) gives a minimum age of 3,230 Ma for the layered gneiss, line B gives an apparent age of 2,880 ± 90 Ma for the massive gneiss, and line C is the time of emplacement of granitic magma at 2,600 Ma. The lower intercepts for lines A, B, and C have been constrained at 60 Ma, the approximate time of the Laramide orogeny. Some of the supporting data for the assumptions and some implications of the interpretive diagram for the past geologic history are considered in the discussion that follows.

Ludwig and Stuckless (1978) analyzed zircon from the granite of Long Creek Mountain, about 6 km west of sample GM–99 (fig. B1), and zircon from granite similar to that of Lankin Dome. Ages derived by the concordia-diagram technique were 2,640 ± 20 Ma and 2,595 ± 40 Ma for granite types from the Long Creek Mountain and Lankin Dome, respectively. The lower intercepts on concordia were 50 ± 40 Ma and 100 ± 75 Ma, respectively. The lower intercepts are imprecise, but Ludwig and Stuckless (1978) concluded that the zircon crystallized about 2,600 Ma and lost lead during the Laramide uplift. The two ages differ by more than analytical error and suggest that granitic magmatic activity was not a single episode sharply limited in time. For the purpose of this discussion, the U-Pb zircon ages of Ludwig and Stuckless (1978) and the Rb-Sr isochron age of 2,550 ± 60 Ma for the granite (Peterman and Hildreth, 1978) are the basis for line C in figure B3. We conclude that the apparent ages for zircon fractions 9, 10, and 11 from layered gneiss sample GM–77–68 are indeed metamorphic ages for the gneiss, which at this locality is in close proximity with the larger granitic masses of the Granite Mountains.

The conclusion that the data points (9, 10, 11, fig. B3) for zircon from layered gneiss sample GM–77–68 represent metamorphic alteration of the U-Pb systems also is supported by the scatter of the points. The broader implication, however, is that points 9, 10, 11 moved along a chord that, for the present, is anchored by point A (fig. B3). Whether or not this age discordance was produced solely by the 2,600-Ma event, or in part by intervening geologic events is uncertain. Clearly, however, some age discordance was produced since the 2,600-Ma event, and this secondary discordance is attributed to relatively recent lead loss for which the Laramide orogeny, about 60 Ma, is a logical assignment. A major age discordance, however, is apparent in comparing sample GM–77 with samples GM–129 and W2–CR5 (figs. B2 and B3), and the chord A–C (fig. B3) is a requirement, although its upper intercept may be questioned as is considered.

The zircon fractions 1–5 of sample GM–129 and fractions 6–8 of sample W2–CR5 define line A in figure B2, but the deviation of the data points from line A is well outside analytical error. A possibility may be that

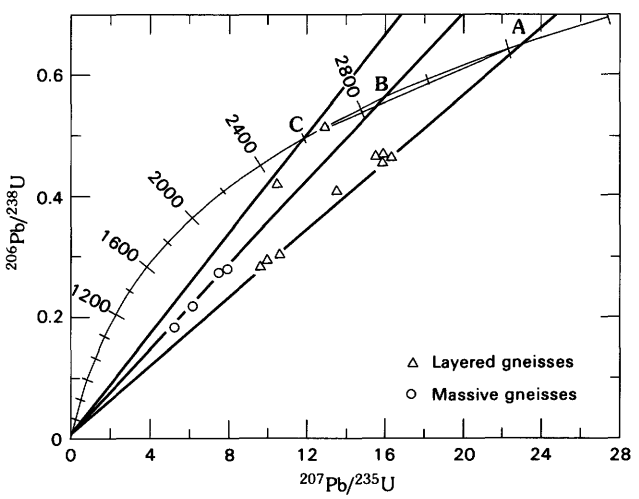

Figure B3. Interpretive uranium-lead concordia diagram. All lines are regressed thru a lower intercept of 60 Ma (point D). Upper intercepts are 3,230 Ma (point A); 2,880 Ma (point B); and 2,600 Ma (point C).

the original time of formation falls within the analytical error, suggesting a maximum age of 3,250 Ma; however, our interpretation (fig. B3, line A) gives a minimum age of 3,230 Ma for the precursor of the layered gneiss. Zircon samples along line A have complicated patterns of age discordance. Fractions 6–8 from sample W2–CR5 have uranium contents ranging from 570 to 660 ppm, not much greater than the uranium concentration in fractions 9–11 that are nearly concordant. A possible explanation is that the latter zircons were recrystallized or the surfaces were annealed during the 2,600-Ma event so that lead losses during the Laramide event were relatively small. Compared with the zircon fractions 1–5 of sample GM–129, the marked age discordance of fractions 6–8 of sample W2–CR5 cannot be explained on the basis of uranium content. Fractions 1–5 range from 937 to 1047 ppm uranium. The largest size fraction, 1 (−50+100 mesh), has the highest content of 1,047 ppm uranium, and gives an apparent $^{207}Pb/^{206}Pb$ age of 3,191 Ma. The crystal corners and edges of a part of fraction 1 were abraded in an air-driven, diamond-studded cell, leaving more or less spherical-shaped grains. The abraded fraction (2) has a somewhat larger content of 1,130 ppm uranium, compared with 1,047 ppm of uranium in the original euhedral crystal. The $^{207}Pb/^{206}Pb$ age of the abraded zircon is 3,220 Ma compared with 3,191 Ma for the original zircon. Although the difference is relatively small (1 percent), it is considered to be real. Abrasion experiments could not be continued because of a lack of sample, but the data (table B2, figs. B2 and B3) indicate that 3,200 Ma cannot be accepted as the unquestioned age of the precursor of the layered gneiss.

The U-Pb data for zircon fractions 12 and 13 from sample GM–99 and for fractions 14 and 15 from sample GM–98 contrast sharply with the data from the layered gneiss and constitute a third group with an apparent age of 2,820–2,880 Ma (figs. B2 and B3). These zircon ages bracket the Rb-Sr isochron age of 2,860 Ma that Peterman and Hildreth (1978) attributed to a major metamorphism. The possibility exists that the massive augen gneiss is of different origin from that of the layered gneiss. Support for this concept is found in the Rb-Sr data for sample GM–98, which plot below the 2,860 Ma isochron. From the data of Peterman and Hildreth (1978, table 3, p. 11) the Rb-Sr age for sample GM–98, using the isochron initial $^{87}Sr/^{86}Sr$ of 0.7048, is 2,640 Ma, and for biotite from the rock the age is 2,440 Ma. These data suggest the possibility that the precursor of the massive augen gneiss was a granitic intrusion emplaced in the layered gneiss 2,880 Ma and metamorphosed during the 2,600-Ma event.

Lutetium-Hafnium Data

In a hafnium (Hf) study of continental evolution, John Patchett (Patchett and others, 1981) analyzed the least discordant fraction of sample GM–129 zircon. In addition, for our study he analyzed zircon from the massive augen gneiss GM–99. Both sets of data are in table B3. Using the present-day $^{177}Lu/^{176}Hf$, the $^{177}Hf/^{176}Hf$ correct back to chondrite model ages of about 3,200 Ma. These model Lu-Hf ages on zircon from the augen gneiss and layered gneiss are similar and support the concept that both gneiss types were formed at least 3,200 Ma, and that a more complicated geologic history is indicated for the massive augen gneiss than was suggested by the apparent U-Pb zircon age.

Common Lead Feldspar Data

Results of feldspar analyses for U and Pb concentrations and Pb isotope ratios are given in table B4. Initial lead isotope ratios are in some instances less radiogenic than were reported previously for the same samples by Nkomo and Rosholt (1972). This difference probably is due to our leaching the feldspar crystals with dilute HF before digestion, a procedure later initiated by Ludwig and Silver (1977) to remove surficial lead.

In both plots of figure B4, all points are well above the model average growth curve. On the $^{207}Pb/^{204}Pb$-$^{206}Pb/^{204}Pb$ plot (fig. B4), the measured data are scattered, but because the uranium and thorium contents are significant, each must contain a fraction of radiogenic lead

Table B3. Lutetium-hafnium data for zircons from two gneiss samples from the Granite Mountains

[Analyzed by John Patchett. T_{ch} is the chondrite model age]

Sample No.	Concentration (parts per million) Lu	Hf	$\frac{^{176}Lu}{^{177}Hf}$	$\frac{^{176}Hf}{^{177}Hf}$	$\frac{^{176}Hf}{^{177}Hf_{ch}}$	T_{ch}, in Ma
[1]GM-129-77	17.1	12,090	0.000200	0.280714	0.280702	3,200
GM-99-68	113.8	12,527	0.001288	0.28077	0.280690	3,200

[1]Data for GM-129-77 is from Patchett and others (1981).

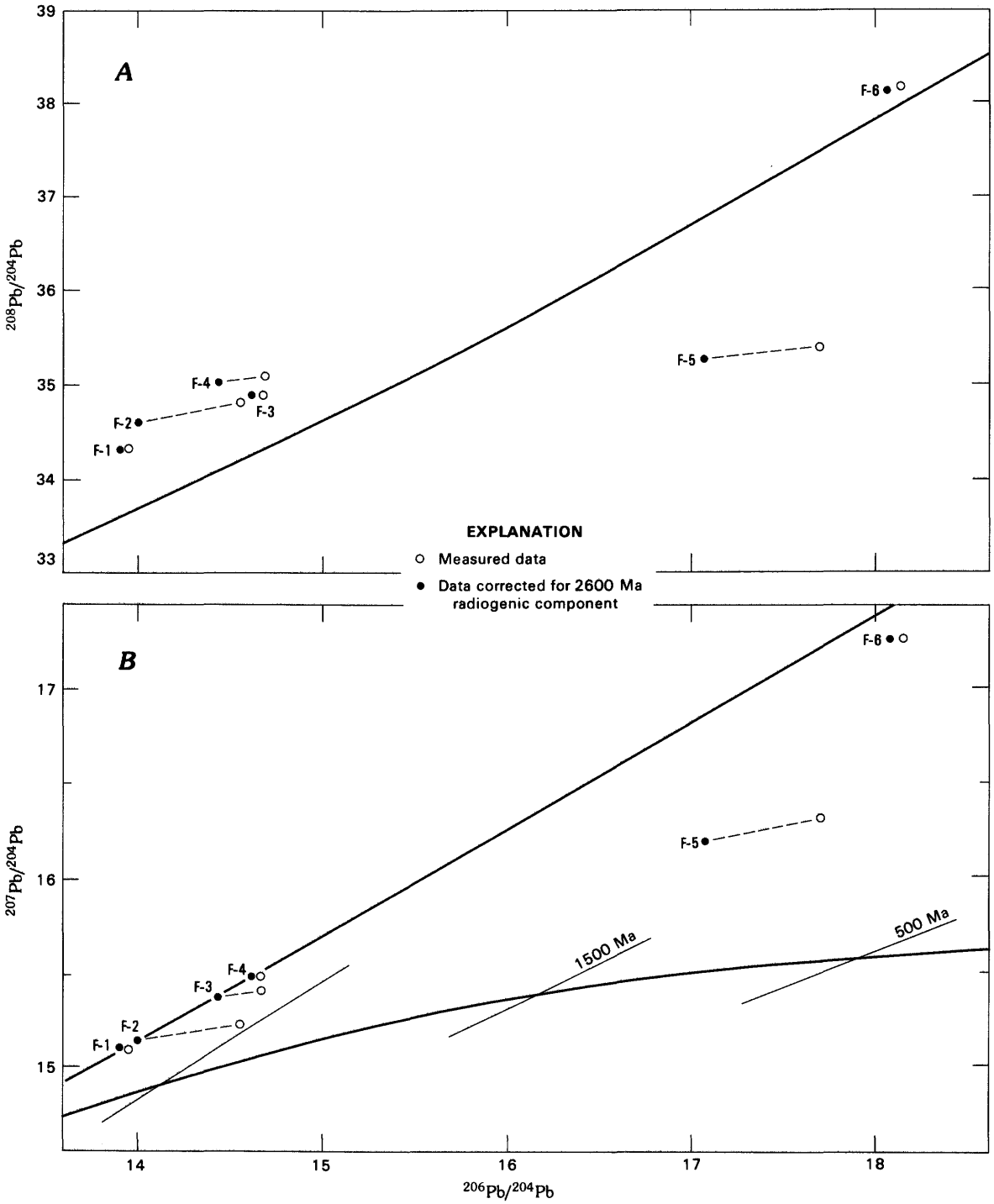

Figure B4. Common lead isochron plots. *A*, Lead isotopic data for the feldspars of the samples analyzed for this study. Measured ratios are plotted together with those corrected for 2,600 Ma. *B*, Corrected data for the layered gneisses form a secondary isochron that has a slope of 0.557 ± 0.013 indicating a common age of formation of 3,300 Ma. Average growth curves are from Stacey and Kramers (1975). Samples are identified by laboratory number.

formed since the rocks were last metamorphosed, probably by emplacement of the granites 2,600 Ma. This event was sufficiently intense to almost completely reset the zircons of sample GM–77, and therefore may have redistributed lead into the feldspars at that time. Therefore, in figure B4 the feldspar lead data all are plotted with corrections for radiogenic growth in the last 2,600 Ma. A linear array is formed by the corrected layered gneiss data, the

Table B4. Lead-uranium-thorium data for some HF-leached feldspars from the Archean gneisses of the Granite Mountains, Wyo

Sample No.		Measured ratios			Concentration (parts per million)		
Lab.	Field	$^{206}Pb/^{204}Pb$	$^{207}Pb/^{204}Pb$	$^{208}Pb/^{204}Pb$	Pb	U	Th
		Layered gneisses					
F-1	GM-35-68	13.951	15.096	34.340	37.4	0.04	0.04
F-2	GM-38-68	14.572	15.232	34.825	10.9	0.21	0.19
F-3	GM-77-68	14.676	15.493	34.896	14.2	0.02	0.01
F-4	W2-CR-5	14.688	15.416	35.083	42.2	0.36	0.3
		Massive gneisses					
F-5	GM-98-68	17.702	16.302	35.374	15.16	0.30	0.17
F-6	GM-99-68	18.167	17.259	38.152	55.3	0.12	0.36

trend of which almost incorporates the data point for the massive augen gneiss (sample GM–99). The data point for the other massive gneiss (sample GM–98) is quite different and is not included.

If the linear array is not fortuitous, then it could be regarded as a secondary isochron that would imply a single initial lead isotopic composition at a common time of formation for all the samples. The slope of the isochron is a function of two times, t_1 and t_2. If t_2 is 2,600 Ma, the time of lead redistribution into the feldspars, then the source age of t_1 can be computed from the equation:

$$R = \frac{(e^{\lambda' t}1 - e^{\lambda' t}2)}{137.88(e^{\lambda t}1 - e^{\lambda t}2)}$$

where λ' is the decay constant for ^{235}U and λ is the decay constant for ^{238}U.

Using the layered gneiss data only, the slope R is 0.557 ± 0.013, and t_1 is $3{,}360 \pm 50$ Ma. Great precision cannot be expected from feldspar data because of their susceptibility to disturbance during such vast periods of time. This calculation is presented to show that the data are consistent with the proposed minimum age of ~3,200 Ma for all the layered gneiss samples analyzed. We also note that the whole-rock U-Pb systems must have been effectively closed between that time and 2,600 Ma; otherwise linearity of the data, as seen in figure B4, would have been disturbed.

As previously noted, the isochron determined by the layered gneiss samples nearly incorporates one of the massive gneisses (GM–99). If the GM–99 point is included in the array, then $R = 0.515 \pm 0.0046$ and $t_1 = 3{,}190$ Ma. The data suggest the possibility that sample GM–99 also may be derived from a 3,200-Ma precursor, as was indicated by the Lu-Hf data, and that GM–99 later was metamorphosed severely at 2,860 Ma. Feldspar data from the other massive gneiss (sample GM–98) are quite different and may have been affected by one of the later Proterozoic events in the region (Peterman and Hildreth, 1978). The locality of GM–98, which should be noted, is more than 25 km west of the vicinity of all other samples (fig. B1). These facts may indicate that this gneiss is of a different origin and that 2,880 Ma is the minimum age of formation of GM–98.

In figure B5, the feldspar line is extended back to intersect at point M, an isochron drawn through troilite lead 0 that has a slope corresponding to lead evolution between 4,570 and 3,200 Ma. Point M then corresponds to a growth in the mantle with a quite reasonable value of 8.3 for μ. Point M is also the initial lead isotopic composition of the gneisses when they were formed ~3,200 Ma, shortly after separation from the mantle. Subsequently, lead evolved in these crustal rocks with higher μ values, ranging from 10.3 to 15.6 for the layered gneisses, and to 41.3 for the highly radiogenic augen gneiss (sample GM–99). Metamorphism associated with the granitic plutonism in the region equilibrated the lead within the rocks and preserved in their feldspars the lead isotopic compositions of the rocks at that time. Measurements made by Nkomo and Rosholt (1972) showed that the layered gneisses subsequently have lost much of their uranium.

The high $^{208}Pb/^{204}Pb$ and $^{207}Pb/^{204}Pb$, all of which are above the average growth curves in figure B4, are evidence that thorium and uranium were both differen-

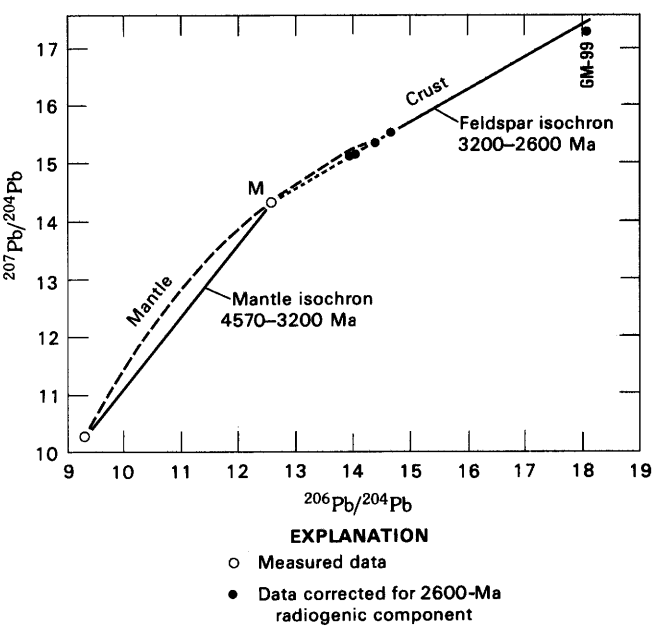

Figure B5. Common lead evolution diagram. Proposed model for formation of feldspar lead in the layered gneisses: Lead formed in the mantle from troilite composition 4,570 to ~3,200 Ma with a μ~8.3. Gneisses were formed from mantle-derived material at 3,200 Ma and their feldspar lead had the composition M. Final metamorphism at 2,600 Ma introduced different amounts of radiogenic lead to each feldspar sample to form the data line shown.

tiated into the crust preferentially with respect to lead. The ability to account for these high ratios in such ancient rocks is an attractive feature of the comparatively simple model outlined herein.

Worth noting is that data with similarly high $^{207}Pb/^{204}Pb$ and $^{208}Pb/^{204}Pb$ are characteristic of Archean environments around the world. For instance, they are found in feldspar lead from the Sacred Heart granite in the Minnesota River Valley (Doe and Delevaux, 1980), in ore leads from Que Que, Zimbabwe (Robertson, 1973) and in ores from Pilbara in Western Australia (Richards and others, 1981).

SUMMARY OF EVENTS IN THE ARCHEAN

2600-Ma granitic plutonism.—Previous studies by Ludwig and Stuckless (1978) and Stuckless and Nkomo (1978) have determined the age of granitic plutonism at 2,600 Ma. This event is represented in our data by the layered gneiss (sample GM–77) in which the zircons were reset along a chord anchored at 2,600 Ma. Feldspar common lead data for most of the gneiss samples also show the effects of the plutonism because lead in these minerals was redistributed during this time.

2860- to 2880-Ma regional metamorphism.—The two massive gneiss samples, GM–98 and GM–99, both yield rather discordant U-Pb zircon data giving an age of about 2,880 Ma. Although possibly these data could indicate modern lead loss from a 2,6000- to 3,200-Ma chord on the concordia diagram, our preferred interpretation is that at 2,880–2,860 Ma there was a significant metamorphic event as proposed by Peterman and Hildreth (1978) in their Rb-Sr study.

3200-Ma gneiss formation.—Uranium-lead zircon data give an upper intercept concordia age of $3,170 \pm 50$ Ma if lead loss is assumed to have been due to uplift in the Laramide. The scattering of data points suggests that a better estimate for the minimum age of formation can be obtained from the two fractions with the highest $^{207}Pb/^{206}Pb$. This upper intercept age is 3,230 Ma for a lower intercept of 60 Ma. The Lu-Hf data from the layered gneiss sample GM–129 and the massive gneiss sample GM–99 yield chondrite model ages of 3,200 Ma.

When corrected for in-place decay of uranium, the least radiogenic lead from feldspars in the layered gneisses has a Stacey and Kramers (1975) model age of 3,000 Ma. Because of the complex history of the region, this age must be regarded as a minimum age estimate. The isotopic composition of the feldspar leads yields a secondary $^{207}Pb/^{206}Pb$ isochron (fig. B5), the slope of which is consistent with 3,200–Ma time of origin.

Crustal history prior to 3,200 Ma.—The data presented in this study suggest 3,200 Ma as a minimum age of formation of the layered gneisses and possibly of one of the massive augen gneisses. The scatter of data on the U-Pb concordia diagram and the slightly older $^{207}Pb/^{206}Pb$ age from the abraded zircon suggest an event prior to 3,200 Ma. The Lu-Hf data shows that Hf fractionation from the mantle was limited to 100–200 Ma prior to 3,200 Ma, even if the early mantle was more heterogeneous than is indicated by the work of Patchett and others (1981). However, the considerable U-Pb age discordance suggests possible disturbance of the Lu-Hf system. Analyses of our fairly discordant zircons then may yield younger ages. The lead evolution model, previously discussed and presented in figure B5, indicates that our feldspar data are consistent with separation from the mantle and formation of the layered gneisses about 3,200–3,300 Ma. However, the feldspar data, in addition to the zircon U-Pb and Lu-Hf data, do not preclude a previous crustal history for these Archean gneisses.

REFERENCES CITED

Cameron, A. E., Smith, D. H., and Walker, R. L., 1969, Mass spectrometry of nanogram size samples of lead: Analytical Chemistry, v. 41, p. 525–526.

Doe, B. R., and Delevaux, M. H., 1980, Lead isotope investigations in the Minnesota River Valley—Late-tectonic and post-tectonic granites: Geological Society of America Special Paper 182, p. 105–112.

Krogh, T. E., 1973, A low-contamination method for hydrothermal decomposition of zircon and extraction of U and Pb for isotopic age determinations: Geochimica et Cosmochimica Acta, v. 37, p. 485–494.

Ludwig, K. R., and Silver, L. T., 1977, Lead-isotope inhomogeneity in Precambrian igneous K-feldspars: Geochimica et Cosmochimica Acta, v. 41, p. 1457–1471.

Ludwig, K. R., and Stuckless, J. S.,, 1978, Uranium-lead isotope systematics and apparent ages of zircons and other minerals in Precambrian granitic rocks, Granite Mountains, Wyoming: Contributions to Mineralogy and Petrology, v. 65, p. 243–254.

Nkomo, I. T., and Rosholt, J. N., 1972, A lead-isotope age and U-Pb discordance of Precambrian gneiss from Granite Mountains, Wyoming, *in* Geological Survey research, 1972: U.S. Geological Survey Professional Paper 800–C, p. C169–C177.

Patchett, P. J., Kuovo, O., Hedge, C. E., and Tatsumoto, M., 1981, Evolution of continental crust and mantle heterogeneity—Evidence from Hf isotopes: Contributions to Mineralogy and Petrology, v. 78, p. 279–297.

Peterman, Z. E., and Hildreth, R. A., 1978, Reconnaissance geology and geochronology of the Precambrian of the Granite Mountains, Wyoming: U.S. Geological Survey Professional Paper 1055, 22 p.

Richards, J. R., Fletcher, L. J., and Blockley, J. G., 1981, Pilbara galenas; Precise isotopic assay of the oldest Australian leads—Model ages and growth-curve implications: Mineralium Deposita, v. 16, p. 7–30.

Robertson, D. K., 1973, A model discussing the early history of the Earth based on a study of lead isotope ratios from veins in some Archean cratons of Africa: Geochimica et Cosmochimica Acta, v. 37, p. 2099–2124.

Stacey, J. S., and Kramers, J. D., 1975, Approximation of terrestrial lead isotope evolution by a two-stage model: Earth and Planetary Science Letters, v. 26, p. 207–221.

Stuckless, J. S., and Nkomo, I. T., 1978, Uranium-lead isotope systematics in uraniferous alkali-rich granites from the Granite Mountains, Wyoming; Implications for uranium source rocks: Economic Geology, v. 73, p. 427–441.

Tatsumoto, M., Knight, R. J., and Allegre, C. J., 1973, Time differences in the formation of meteorites as determined from the ratio of lead–207 to lead–206: Science, v. 180, p. 1279–1283.

1986

U.S. GEOLOGICAL SURVEY BULLETIN 1622

SHORTER CONTRIBUTIONS TO ISOTOPE RESEARCH

FISSION-TRACK AGES OF AIR-FALL TUFFS IN MIOCENE SEDIMENTARY ROCKS OF THE ESPAÑOLA BASIN, SANTA FE COUNTY, NEW MEXICO

Chapter C

By GLEN A. IZETT and C. W. NAESER

CONTENTS

FIGURE

TABLE

Abstract

Zircon fission-track ages of two air-fall tuffs in the middle part of the Miocene Skull Ridge Member of Galusha and Blick (1971) of the Tesuque Formation of the Santa Fe Group range in age from 14.6 to 12.7 million years. These ages place estimated limits of about 16–13 million years for the age range of the 220-meter-thick member. The dated tuffs are stratigraphically near fossil-mammal quarries of the American Museum of Natural History and provide age control for the correlation of these fossils with those of the Lower Snake Creek quarries in the Sheep Creek Formation in Nebraska and with fossil mammals in the upper one-third of the Troublesome Formation in Middle Park, Colo.

Zircon fission-track ages of two air-fall tuffs of the overlying Pojoaque Member of Galusha and Blick (1971) of the Tesuque Formation are 11.4 and 9.4 million years and date the middle part of the 500–meter-thick Pojoaque Member. These dated tuffs are stratigraphically near fossil-mammal assemblages in the member that correlate with fossil-mammal assemblages in the Miocene Valentine Formation of the Ogallala Group of Galusha and Blick, 1971, in central Nebraska. A tuff stratigraphically near the Burge fossil-mammal quarry has a fission-track age of about 10 million years.

INTRODUCTION

An unusually large number of prominent, thick air-fall tuffs are interlayered in the continental Miocene sedimentary rocks of the Santa Fe Group in the Española basin of north-central New Mexico. The names for the Miocene rocks of the Santa Fe Group used in this report are those advocated by Galusha and Blick (1971), although many of these names have not been, and are not herein, formally adopted by the U.S. Geological Survey. Miocene time as used in this report ranges from about 24 to 5 m. y. (million years).

At least 37 superposed air-fall tuff beds, as thick as 2 m (meters), occur in a nearly continuous stratigraphic succession in the Skull Ridge Member of the Tesuque Formation of the Santa Fe Group (Galusha and Blick, 1971, figs. 17 and 23), and these tuffs have the potential for establishing the isotopic age range of the upper Cenozoic rocks of the area. Large numbers of fossil land mammals have been collected in the last 100 years in the Española basin, and many of the collections are related stratigraphically to the tuff bed succession (Galusha and Blick, 1971). Reliable isotopic ages of the tuffs would aid in establishing the age of fossil-mammal collections from elsewhere in the western United States. Moreover, isotopic ages of the tuff marker beds could set limits on the rates of evolution of the different land-mammal groups.

The paleomagnetic stratigraphy of the upper part of the Santa Fe Group rocks was studied by McFadden (1977), and a lower part of the Santa Fe currently is being studied by S. F. Barghoorn of Columbia University. Reliable isotopic ages are needed to calibrate the paleomagnetic-reversal sequence in the Española basin. Isotopic ages also are required to date the times of deformation of the Miocene rocks of the basin. For the above-mentioned reasons, several of the thickest, purest-looking tuffs were collected for fission-track dating.

FISSION-TRACK DATING

The fission-track method of dating volcanic ashes and tuffs has proved to be a generally much more accurate method than the potassium-argon method because of the problem of contamination of the ashes and tuffs with much older detrital minerals of the enclosing sediments incorporated into the tuffs during deposition. These older, spurious minerals (potassium-bearing minerals in particular) are difficult to remove from the mineralogically similar primary-bearing minerals of the tuffs necessary for potassium-argon dating. These older potassium-bearing minerals supply a disproportionate amount of ^{40}Ar to the total ^{40}Ar extracted from the minerals in the laboratory. Accordingly, anomalously old ages result. In the early 1970's, Henry Faul and his coworkers at the University of Pennsylvania attempted to date, by the K-Ar (potassium-argon) method, certain of the upper Cenozoic tuffs in the Española basin and hoped to circumvent the contamination problem by using careful collection techniques and by rejecting those tuffs that appeared to be contaminated with detrital sediments. However, the results of their work were disappointing in that unrealistically old ages were determined in most instances (H. Faul, oral commun., 1979). On the other hand, the fission-track method allows a geochronologist the opportunity to date only glass-mantled microphenocrysts separated from ashes or tuffs, or to date only those microphenocrysts that clearly belong to a pyrogenic population of primary microphenocrysts. For example, zircon crystals of Precambrian age incorporated in a tuff during deposition can be recognized by their extremely high fossil fission-track densities (coupled with normal uranium concentrations) and their metamict character, and therefore they would not be included in the fission-track count.

The samples used for the fission-track dating of the Santa Fe Group tuffs were collected by G. A. Izett in 1974 in company with Ted Galusha (now deceased), at that time with the American Museum of Natural History. Nearly all the individual tuffs of the Miocene and Pliocene sequence were collected with the hope that many of the

beds could be dated. Galusha invited Izett to collect and date the tuffs inasmuch as Galusha recognized the potential they have as stratigraphic markers and the potential they have as targets for isotopic age analyses. Unfortunately, many of the tuffs proved not to be suitable for dating because not enough pyrogenic zircons could be obtained from many of the pervasively contaminated tuffs.

We dated two prominent marker tuffs of the Skull Ridge Member in its type area: the No. 2 and No. 4 white ash beds. These two thick tuffs were dated because they can be traced throughout much of the area and because they are related stratigraphically to fossil-mammal quarries of the American Museum of Natural History. The No. 2 white ash bed, which is about 1.5 m thick, is about 40 m above the base of the Skull Ridge Member, and the No. 4 white ash bed, which is about 1.5 m thick, is about 145 m above the base of the member. The Skull Ridge Member, which overlies the Nambe Member (fig. C1), is about 220 m thick according to Galusha and Blick (1971).

The other two tuff beds in the overlying Pojoaque Member of the Tesuque Formation of Galusha and Blick (1971) were dated also: an unnamed ash bed not shown on the diagrams of Galusha and Blick (1971, fig. 23) and an overlying tuff called the blue-gray ash. These two tuffs are separated by about 60 m of orange-gray silty sandstone. The Pojoaque Member is about 500 m thick according to the diagrams presented by Galusha and Blick (1971). The two tuffs were collected in the Pojoaque Bluffs area, which is the area from which most of the fossil-vertebrate collections were made and studied by Cope (1877), and from which many collections of fossil vertebrates were made by Galusha.

METHODS AND RESULTS

Zircon microphenocrysts were separated from about 5-kilogram samples of the tuffs by conventional mineral-separation techniques, and the zircons were dated using fission-track dating methods described by Naeser (1969). The dosimeter used to measure the neutron flux at the time the samples were irradiated in the reactor was a National Bureau of Standards (NBS) standard glass No. 962 originally irradiated by B. S. Carpenter of the National Bureau of Standards in the NBS reactor along with copper and gold foils. The decay constant used to calculate the fission-track ages is $\lambda_f = 7.03 \times 10^{-17} yr^{-1}$. In addition, pure glass-shard fractions of the two gray ash beds (samples 74G326 and 74G327) were dated by the fission-track method, and the results are given in table C1.

The fission-track ages of the glass shards are systematically younger than are the zircon fission-track ages from the same tuffs. The tendency for fission-track glass ages to be younger than zircon ages from the same tuffs results from track fading or annealing at ambient temperatures in the glass shards over time (Naeser and others, 1980).

On the basis of fission-track ages reported here, the Skull Ridge Member probably ranges from about 16 to 13 m.y., and the age of the middle part of the Pojoaque Member ranges from about 12 to 9 m.y. According to Galusha and Blick (1971, p. 110), the fossil mammals of the Skull Ridge Member are Barstovian in terms of North American land mammal ages and most closely match fossil mammals of the Lower Snake Creek quarries excavated in the Sheep Creek Formation in Nebraska. Fossil mammals collected from the upper third of the Troublesome Formation (Miocene) in Middle Park, Colo., are also about the same age as those in the Lower Snake Creek quarries (Izett, 1968, p. 45). The fossils in the Troublesome are stratigraphically near the level of a tuff fission-track dated at about 14 m.y. (Izett and Barclay, 1973). Fossil mammals of the Pojoaque Member most closely match fossil mammals of the Valentine Formation (Miocene) as used by Galusha and Blick (1971, p. 64) of the Valentine, Neb., area. In terms of North American land mammal ages, the rocks were assigned a Valentinian to Clarendonian age by Galusha and Blick (1971, p. 12 and 64). A tuff stratigraphically just above the Burge fossil quarry in the Ash Hollow Formation of the Ogallala Group in the Valentine, Neb., area was dated by the fission-track zircon method at about 10 m.y. (Izett, 1975). This age of 10 m.y. falls within the age range of the Pojoaque Member as determined by our fission-track ages.

Zircon fission-track ages of 12.7 ± 1.8 and 10.8 ± 1.6 were reported by Manley and Naeser (1977), for two air-fall tuffs in Miocene rocks in the northeast part of the Española basin. These tuffs were thought by Manley and Naeser (1977) to be in the Tesuque Formation and fall within the age range of the uppermost part of the Skull Ridge Member and the lower part of the Pojoaque Member as determined in the present paper.

Fission-track zircon ages reported here for the tuffs in the Pojoaque Member (samples 74G326 and 74G327 of table C1) previously were reported by Naeser and others (1980, table 5, p. 26–27, entries 5 and 8). Unfortunately, the age data and the descriptions were incorrectly published. In table 4 of Naeser and others (1980), entries 5 and 8 were switched; entry 5 should have read entry 8, and entry 8 should have read entry 5. Entry 5 of table 5 was incorrectly given to be in sec. 31, T. 20 N., R. 9; it should have been listed in the SE¼ sec. 36, T. 20 N., R. 8 E. In addition, entry 5 of table 5 should have been assigned sample number 74G326 rather than 74G327, and entry 8 should have been assigned sample number 74G327 rather than 74G326.

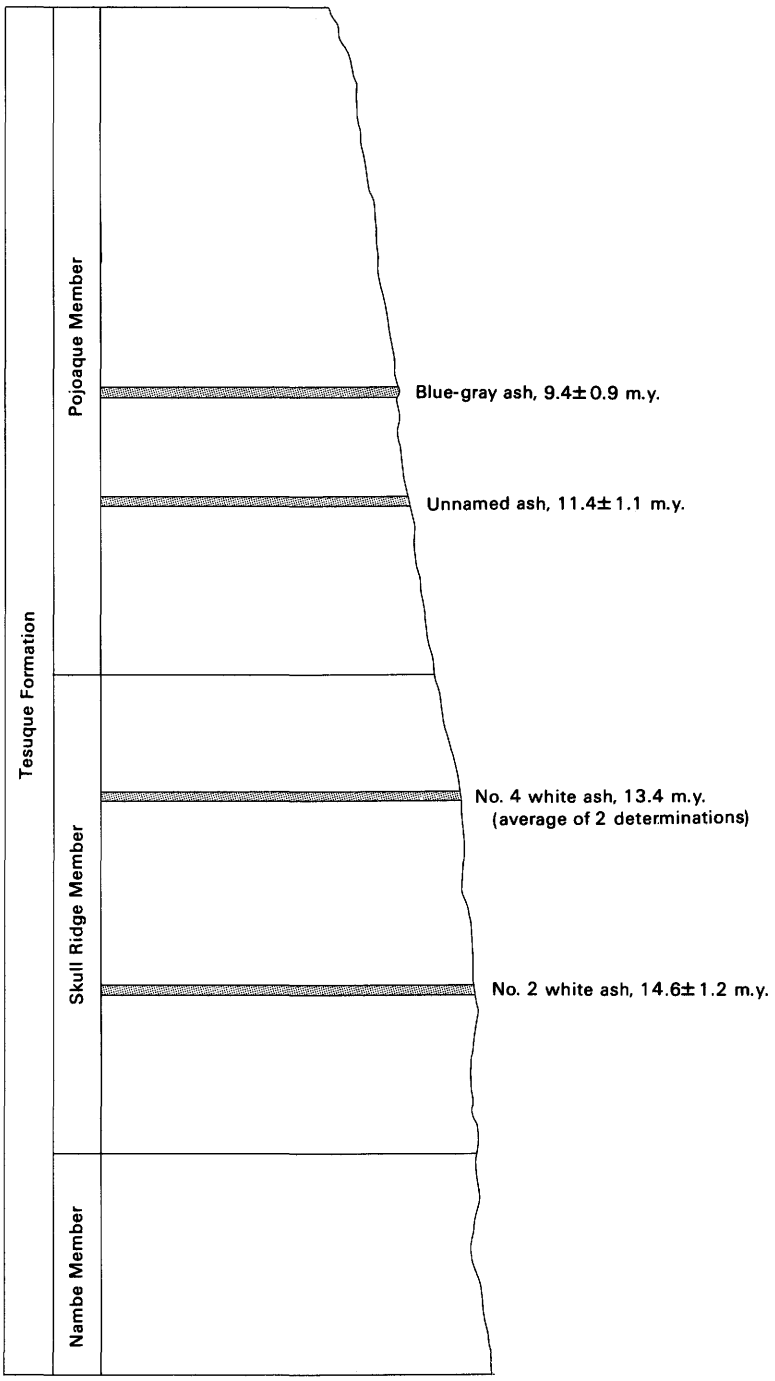

Figure C1. Generalized stratigraphic diagram showing the relationships among certain air-fall tuffs of the Skull Ridge and Pojoaque Members of the Tesuque Formation (Santa Fe Group) of Miocene age of Galusha and Blick (1971). Modified from diagrams of Galusha and Blick (1971, figs. 17 and 23).

Table C1. Fission-track ages of zircon microphenocrysts and glass shards separated from volcanic ash beds in the Tesuque Formation of Galusha and Blick (1971) in the Española basin, Santa Fe County, N. Mex.

[F, neutron fluence; P_s, spontaneous track density; P_i, induced track density; cm^2, square centimeters; ± is 2 sigma; numbers in parentheses are the number of tracks counted]

Sample No.	Description and locality	Material dated	F neutrons/cm^2	P_s tracks/cm^2 x10^{15}	P_i tracks/cm^2 x10^6	Age x10^6
74G327	Blue-gray volcanic ash in the Pojoaque Member of the Tesuque Formation of Galusha and Blick (1971, p. 62); SW1/4SE1/4 sec. 36, T. 20 N., R. 8 E., Espanola 7-1/2 minute quadrangle, Santa Fe County, N. Mex.	Zircon-----	1.10	1.35 (153)	9.47 (493)	9.4±0.9
		Glass------	1.78	0.0149 (157)	0.253 (347)	6.3±1.2
74G326	Volcanic ash in the Pojoaque Member of the Tesuque Formation of Galusha and Blick (1971); about 60 m below blue-gray ash 74G327; this ash bed not shown on diagram by Galusha and Blick (1971, p. 62); SW1/4 SE1/4 sec. 36, T. 20 N., R. 8 E., Espanola 7-1/2-minute quadrangle, Santa Fe County, N. Mex.	Zircon-----	1.10	1.19 (132)	6.88 (382)	11.4±1.1
		Glass------	2.09	0.0212 (55)	0.331 (228)	8.0±2.4
74G314	Volcanic ash in the Skull Ridge Member of the Tesuque Formation of Galusha and Blick (1971); No. 4 white ash bed of Galusha and Blick (1971, p. 31); center sec. 14, T. 20 N., R. 9 E., Cundiyo 7-1/2-minute quadrangle, Santa Fe County, N. Mex.	Zircon-----	1.21	1.51 (251)	7.76 (647)	14.1±1.1
		--do.------	0.784	2.12 (491)	7.81 (904)	12.7±1.4
74G317	Volcanic ash in the Skull Ridge Member of the Tesuque Formation of Galusha and Blick (1971); No. 2 white ash bed of Galusha and Blick (1971, p. 31); center sec. 15, T. 20 N., R. 9 E., Cundiyo 7-1/2-minute quadrangle, Santa Fe County, N. Mex.	Zircon-----	0.780	2.50 (255)	7.99 (40)	14.6±1.2

REFERENCES CITED

Cope, E. D., 1877, Report upon the extinct Vertebrata obtained in New Mexico by parties of the expedition of 1874, *in* Wheeler, G. M., Report upon United States geographical surveys west of the 100th meridian: Washington D.C., v. 4, pt. 2, p. 1–370.

Galusha, Ted, and Blick, J. C., 1971, Stratigraphy of the Santa Fe Group, New Mexico: American Museum of Natural History Bulletin, v. 144, no. 1, 127 p.

Izett, G. A., 1968, Geology of the Hot Sulphur Springs quadrangle, Grand County, Colorado: U.S. Geological Survey Professional Paper 586, 79 p.

———1975, Late Cenozoic sedimentation and deformation in northern Colorado and adjoining areas, *in* Curtis, Bruce, ed., Cenozoic history of the Southern Rocky Mountains: Geological Society of America Memoir 144, p. 179–209.

Izett, G. A., and Barclay, C.S.V., 1973, Geologic map of the Kremmling 15–minute quadrangle, Grand County, Colorado: U.S. Geological Survey Geologic Quadrangle Map GQ–1115, scale 1:62,500.

Manley, Kim, and Naeser, C. W., 1977, Fission-track ages for tephra layers in upper Cenozoic rocks, Española Basin, New Mexico: Isochron/West, no. 18, p. 13–14.

McFadden, B. J., 1977, Magnetic polarity stratigraphy of the Chamita Formation stratotype (Mio-Pliocene) of north-central New Mexico: American Journal of Science, v. 277, p. 769–800.

Naeser, C. W., 1969, Etching fission tracks in zircons: Science, v. 165, no. 3891, p. 388.

Naeser, C. W., Izett, G. A., and Obradovich, J. D., 1980, Fission-track and K-Ar ages of natural glasses: U.S. Geological Survey Bulletin 1489, 31 p.

1986

U.S. GEOLOGICAL SURVEY BULLETIN 1622

SHORTER CONTRIBUTIONS TO ISOTOPE RESEARCH

MUSCOVITE-PHENOCRYSTIC TWO-MICA GRANITES OF NORTHEASTERN NEVADA ARE LATE CRETACEOUS IN AGE

Chapter D

By DONALD E. LEE, JOHN S. STACEY, and LYNN B. FISCHER

CONTENTS

FIGURES

TABLES

Abstract

Three representatives of a unique ("muscovite-phenocrystic") type of two-mica granite are exposed along a north-south trend about 225 kilometers long in northeastern Nevada. This type of two-mica granite is distinguished in part by the presence of large phenocrysts of muscovite, and practically all the biotite in the rock is present as euhedra within this muscovite. Chemical, mineralogical, and isotopic data suggest that the muscovite-phenocrystic two-mica granites crystallized from anatectic magmas formed from upper Precambrian and Lower Cambrian pelitic sediments, along a trend that corresponds to the westward disappearance of a continental basement.

Near the southern part of the trend just described are exposed three examples of a more common ("equigranular") type of two-mica granite, in which muscovite and biotite are present as discrete crystals. The equigranular-type two-mica granites also may have evolved through anatexis of the pelitic sediments.

For various reasons potassium-argon and rubidium-strontium radiometric dating methods have been of limited usefulness in our efforts to investigate possible age differences between the two types of two-mica granites. Moreover free (that is, not included in apatite) zircon crystals are so sparse in the muscovite-phenocrystic type that to recover a workable amount of zircon from any one of these three plutons has heretofore been impossible.

This paper presents radiometric ages for zircon recovered from the muscovite-phenocrystic two-mica granite of the Kern Mountains, White Pine County, Nev. Together with previously reported potassium-argon and rubidium-strontium age data, this new information suggests that all three of the muscovite-phenocrystic two-mica granites probably crystallized during Late Cretaceous time. The equigranular two-mica granites appear to range in age from Jurassic to Cretaceous, and possibly to Tertiary.

This paper also presents radiometric age data for zircons from the Osceola stock of the southern Snake Range, Nevada, and from the Notch Peak pluton of the House Range, western Utah. Both of these calc-alkalic intrusives are Jurassic in age. The Jurassic igneous event was rather widespread in the region.

INTRODUCTION

During 1969–1976, one of us (Lee) visited more than 160 plutons while systematically sampling granitoid rocks in the Basin and Range Province of Nevada, Utah, California, and Arizona. Among these 160 plutons, three are two-mica granites that resemble each other and are unlike any of the other plutons observed during this study. To our knowledge, they also are unlike any plutonic rocks described in the literature.

The unusual two-mica granites are along a north-south trend about 225 km (kilometers) in northeastern Nevada (fig. D1) and are distinguished in part by the presence of large phenocrysts of muscovite, most of which contain small inclusions of euhedral biotite. These three muscovite-phenocrystic (Lee, Kistler, Friedman, and Van Loenen, 1981) two-mica granites are present in the Pole Canyon-Can Young Canyon area of the southern Snake Range, in the Kern Mountains (sample 244–MW–6) and in the Toana Range (sample 415). Chemical analyses, accessory mineral contents, oxygen isotope data and initial $^{87}Sr/^{86}Sr$ ratios indicate that these unusual granites crystal-

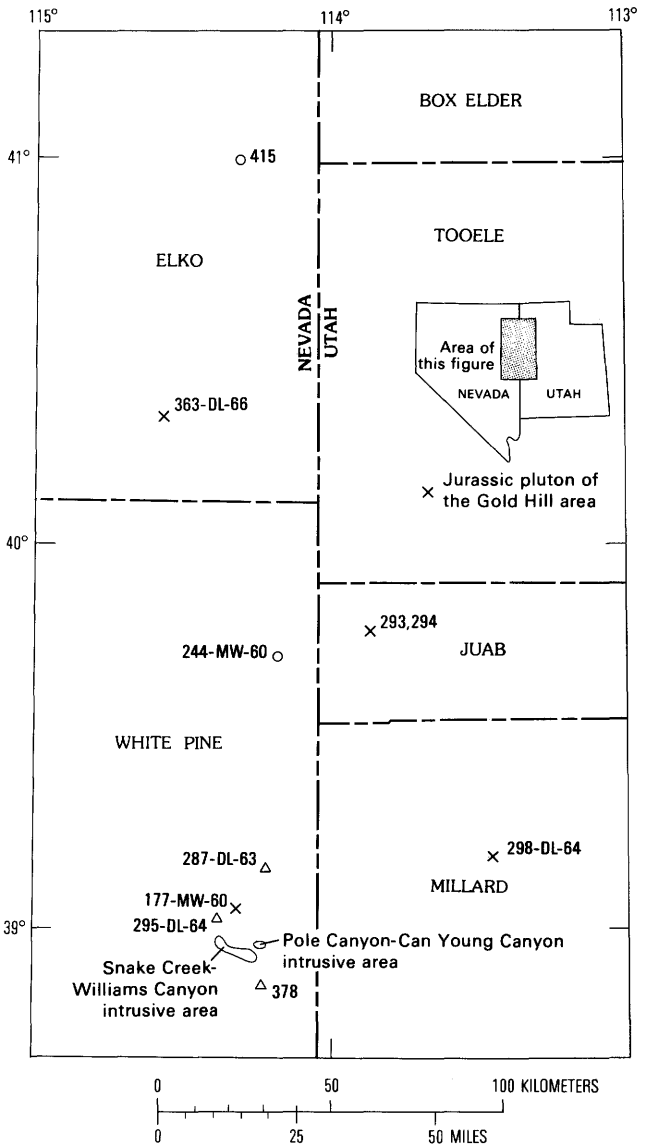

Figure D1. Northeastern Nevada and northwestern Utah, showing locations of muscovite-phenocrystic two-mica granites (open circles), equigranular two-mica granites (open triangles), and calc-alkalic rocks (X's). Numbers are those assigned to samples. The Pole Canyon-Can Young Canyon and the Snake Creek-Williams Canyon intrusive areas are outlined.

lized from evolved (S-type) magmas, and Lee, Kistler, Friedman, and Van Loenen (1981) have suggested that they may have resulted from anatexis of upper Precambrian-Lower Cambrian clastic sediments near the westward disappearance of a continental basement delineated on the basis of lead isotope data by Stacey and Zartman (1978).

Three additional two-mica granites, with muscovite and biotite in separate grains, are present in the southern part of the 225-km-long north-south trend just mentioned. These are the equigranular-type two-mica granites of Lee, Kistler, Friedman, and Van Loenen (1981), samples 287–DL–63, 295–DL–64, and 378 (fig. D1). The equigranular-type two-mica granites also might have evolved from anatexis of upper Precambrian-Lower Cambrian clastic sediments. Lee, Kistler, Friedman, and Van Loenen (1981) suggested that there may be systematic age differences between the muscovite-phenocrystic and equigranular types of two-mica granites, but data have been too few to check this possibility. The purpose of the present paper is to present new information on the ages of the two-mica granite types just described. We also present new information to show that calc-alkalic intrusives of Jurassic age are rather widespread in the region.

ANALYTICAL METHODS

Zircon was recovered from crushed materials using the Frantz[1] isodynamic separator and the heavy liquids bromoform and methylene iodide. The special procedure required for zircon sample 244–MW–60 is described separately later in this report.

Clerici solution was used for final cleanup of some samples. After sizing, the crystals were heated gently in nitric acid to remove all traces of lead remaining from the Clerici solution. Chemical separation of lead and uranium followed the ion-exchange procedures of Krogh (1973) with minor modifications. Mass spectrometry was carried out on a 30-cm-radius, 90°-sector instrument, using the silica-gel single filament method of Cameron and others (1969) for lead, and triple filament for uranium. Analytical precision of feldspar lead-isotope ratios is ± 0.12 percent (95-percent confidence limits). Uncertainties in zircon uranium-lead ratios are about ± 1 percent.

Laboratory blank corrections averaged 0.5 nanograms for lead isotopic analyses. Common lead corrections for each zircon fraction were made using the isotopic composition of feldspar lead from sample 244–MW–60 reported in this manuscript.

[1]Trade and company names are used for descriptive purposes only and do not imply endorsement by the U.S. Geological Survey.

Constants used in the calculation are:

$$\lambda^{238}U = 0.155125;\ ^{235}U = 0.98485;\ \lambda^{238}U/^{235}U = 137.88$$

MUSCOVITE-PHENOCRYSTIC TWO-MICA GRANITES

The Age Dating Problem

Obtaining radiometric dates of emplacement for the muscovite-phenocrystic two-mica granites has been difficult for these reasons:

1. All three of the plutons are exposed beneath regional thrust faults, and K-Ar (potassium-argon) ages determined may not be emplacement ages because they may have been reset by heat and stress related to later movement on these thrust faults (Lee and others, 1970, 1980).

2. Whole-rock Rb-Sr (rubidium-strontium) data for the muscovite-phenocrystic two-mica granite of the Kern Mountains failed to yield a well-defined isochron (Best and others, 1974), because of scatter much larger than possible experimental errors. This type of scatter is not unusual for muscovite granites derived by anatexis in an upper crustal environment (R. W. Kistler, written commun.) We will consider in a later section the recently obtained (chap. P, this volume) Rb-Sr age of 79 Ma for the muscovite-phenocrystic two-mica granite of the Pole Canyon-Can Young Canyon area.

3. Almost all of the zircon in the muscovite-phenocrystic two-mica granites of the Pole Canyon-Can Young Canyon (Lee and Van Loenen, 1971, p. 5, 39) and Kern Mountains (Lee and others, 1973, p. 267) areas is present as tiny acicular inclusions in large, equant, rather poorly formed, and sparsely distributed apatite crystals (fig. D2). The muscovite-phenocrystic two-mica granite of the Toana Range contains discrete crystals of stubby zircon, but these are very sparse (<0.02 weight percent of the rock) and tiny (<0.08 mm (millimeters) long). Thus, until now we have been discouraged in our attempts to recover enough zircon from any one of these unusual granites for uranium-thorium-lead isotopic age determinations.

Kern Mountain Pluton

In addition to the zircons included in apatite (fig. D2), a few scattered grains of free zircon are present in the muscovite-phenocrystic granites of the southern Snake Range and the Kern Mountains. Most of the free zircon grains are about 0.2 mm long and 0.06 mm wide. In order to recover a concentrate of this zircon, a 10-kg (kilogram) sample (244–MW–60) of the Kern Mountains

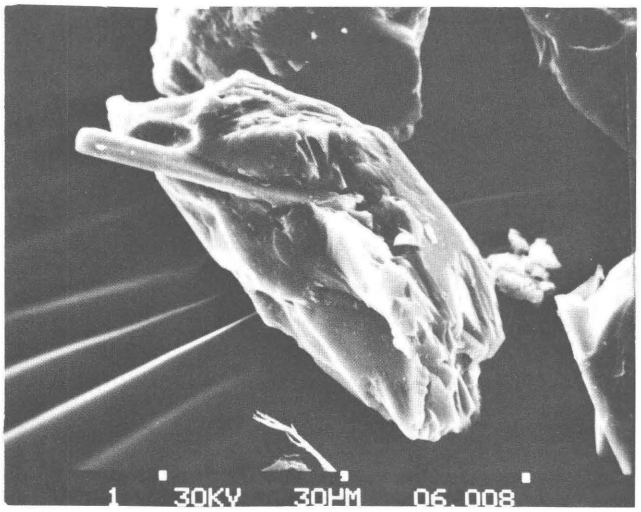

Figure D2. Scanning electron micrograph of zircon in apatite. The columnar zircon crystal is about 5 micrometers (0.005 mm) wide and 50 micrometers (0.05 mm) long. Sample 135–DL–62, from the Pole Canyon-Can Young Canyon area of the southern Snake Range. Scanning electron micrograph by A. J. Gude, 3d.

pluton granite was collected at lat 39°35′55″ N., long 114°07′55″ W. This sample was crushed to –35 mesh and run over a Wilfley table to obtain about 5 kg of heavy concentrate, which was further refined in bromoform by means of a separatory funnel. The bromoform heavies were centrifuged in methylene iodide and run through a Frantz isodynamic separator to obtain a final zircon concentrate of about 70 mg (milligrams). Assuming a 50-percent recovery, the results of this tedious procedure indicate that sample 244–MW–60 contains about 0.0007 weight percent free zircon.

Zircon data (table D1) for the Kern Mountains samples are shown on a concordia plot (fig. D3). Aplite sample 245–MW–60 was collected less than 3-m (meters) from two-mica granite sample 244–MW–60. Data for these two samples define a cord that has a lower intercept age of 75±9 m.y. (95-percent confidence limits). The upper intercept of 1970±330 m.y. shows that sample 244–MW–60 contains a considerable amount of inherited zircon of Early Proterozoic age. This observation is direct evidence that this Late Cretaceous granite was derived at least in part from Early Proterozoic material. Lead from the potassium feldspar of sample 244–MW–60 also has been analyzed and its isotopic composition is:

$$^{206}Pb/^{204}Pb = 18.968;\ ^{207}Pb/^{204}Pb = 15.761;$$
$$^{208}Pb/^{204}Pb = 39.991.$$

These data are transitional between area I and area II types of lead as defined by Zartman (1974). Such a composition reflects derivation from the Proterozoic basement of Utah, with addition of radiogenic lead from continental sediments in this region, and is consistent with our proposed origin for this granite. For a discussion of lead isotopic characteristics on the Nevada-Utah State line, the reader is referred to the study of the Gold Hill mining district by Stacey and Zartman (1978).

Whole-rock rubidium and strontium data were obtained for samples 244–MW–60 and 245–MW–60 by Zell Peterman and listed by Lee and others (1980, p. 22). A two-point isochron based on these data gives an initial $^{87}Sr/^{86}Sr$ of 0.719 at an age of 71.6 Ma. This age agrees with the zircon results just discussed. Best and others (1974) found similarly high $^{87}Sr/^{86}Sr$ for this granite.

Muscovite samples 244–MW–60 and 245–MW–60 gave K-Ar ages of 50.9 and 47.9 Ma, respectively, (Lee and others, 1980, p. 18), results that presumably reflect partial degassing of these muscovites by heating resulting from recent movement on an overlying thrust fault. About 10 km northwest of these samples, where the muscovites were less completely degassed, the apparent K-Ar ages increase to as much as 69.2 Ma (Lee and others, 1980). Best and others (1974) listed K-Ar ages of 63.9 and 47.1 Ma for the two-mica granite of the Kern Mountains.

From their studies, Best and others (1974) and Lee and others (1980) postulated minimum ages of 60 and 70 Ma, respectively, for the main Kern Mountains intrusive event. Although the zircon data presented here confirm the general validity of these earlier estimates, the results of all these studies taken together testify to the complexity of the magmatic and metamorphic history of the Kern Mountains.

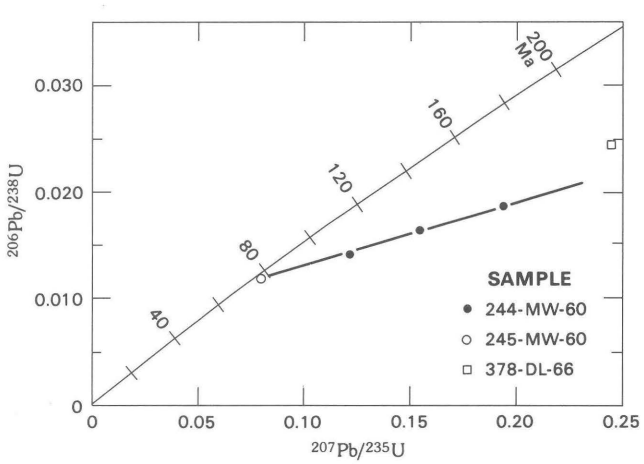

Figure D3. Uranium-lead zircon data from Cretaceous samples studied in this paper. The regression line for three fractions from sample 244–MW–60 and one from the aplite phase 245–MW–60 has a lower intercept of 75±9 Ma. The upper intercept of 1970±330 Ma shows inheritance of zircon from the Early Proterozoic material. The single data point from sample 378–DL–66 also shown inheritance of older lead, and its position indicates a Cretaceous rather than a Jurassic age.

Table D1. Uranium-lead data for zircon fractions from two-mica granites and calc-alkalic rocks discussed in this paper

Sample Number (mesh size)	Concentration (parts per million) Pb	U	Atomic ratios $\frac{^{206}Pb}{^{238}U}$	$\frac{^{207}Pb}{^{235}U}$	$\frac{^{207}Pb}{^{206}Pb}$	Age, million years $\frac{^{206}Pb}{^{238}U}$	$\frac{^{207}Pb}{^{235}U}$	$\frac{^{207}Pb}{^{206}Pb}$	Blank corrected $\frac{^{206}Pb}{^{204}Pb}$
Kern Mountains--Two-mica granite phase									
244-MW-60:									
(+200)-------	51.2	2866	0.01853	0.1930	0.07551	118	179	1082	9302
(-200 +400)--	51.0	3278	0.01633	0.1547	0.06873	104	146	890	11467
(-400)-------	47.0	3447	0.01406	0.1218	0.06284	90	117	703	3426
Kern Mountains--aplite phase									
245-MW-60:									
All sizes----	92.8	7475	0.01196	0.07949	0.04819	76	78	109	1361
Lexington Creek stock									
378-DL-66:									
All sizes----	37.9	1509	0.02466	0.2449	0.07201	157	222	986	2642
Osceola stock									
177-MW-60:									
(+250)NM[1]---	37.2	1319	0.02548	0.1804	0.05134	162	168	256	2389
(+250)NM-A[2]-	36.5	1314	0.02592	0.1933	0.05409	165	179	375	3155
(-250)NM-----	48.1	1825	0.02042	0.1418	0.05037	130	135	212	2388
Notch Peak pluton--main intrusive phase									
298-DL-64:									
(+150)NM-----	47.9	1696	0.02377	0.1620	0.04945	151	152	169	392
(-400)-------	83.5	2777	0.02237	0.1524	0.04942	143	144	167	221
Notch Peak pluton--xenolith									
299-DL-64:									
(+200)NM-----	64.8	2589	0.02171	0.1479	0.04941	138	140	167	1769

[1]NM, nonmagnetic.

[2]Abraded.

Southern Snake Range Pluton

Data for a muscovite, an aplite, and four samples of muscovite-phenocrystic two-mica granite from the Pole Canyon-Can Young Canyon pluton of the southern Snake Range give an initial $^{87}Sr/^{86}Sr$ of 0.7165 at an age of about 79 Ma (chap. P, this volume). As noted earlier, Rb-Sr data for a sample of the muscovite-phenocrystic two-mica granite of the Kern Mountains and a related aplite give a two-point isochron showing an initial $^{87}Sr/^{86}Sr$ of 0.719 at an age of 71 ± 6 Ma. Thus, results of Rb-Sr studies, as well as the chemical, petrological, and mineralogical data presented by Lee, Kistler, Friedman, and Van Loenen (1981), serve to emphasize the great similarities between these two unusual granites that appear in outcrop about 83 km apart (fig. D1).

Potassium-argon ages for six micas recovered from the muscovite-phenocrystic two-mica granite of the Pole Canyon-Can Young Canyon area range from 30.8 ± 2.1 to 77.7 ± 2.2 Ma (Lee and others, 1970). The younger ages result from partial degassing of the micas by thermal stresses resulting from recent (17–18 Ma) movement on the overlying Snake Range dècollement. The oldest age (77.7 ± 2.2 Ma) is in good agreement with the Rb-Sr age (79 Ma) just noted, and it was obtained for a muscovite recovered from the sample exposed farthest below the Snake Range décollement (Lee and others, 1970, table 1, fig. 2).

Table D2. Summary of radiometric age data for muscovite-phenocrystic two-mica granites of northeastern Nevada

Age	Southern Snake Range pluton	Kern Mountains pluton	Toana Range pluton
Muscovite:			
K-Ar age[1]-------	77.7±2.2 Ma	69.2±1.6 Ma	71.2±2.0 Ma.
Rb-Sr age-------	About 79 Ma (initial $^{87}Sr/^{86}Sr$=0.7165).	71±6 Ma (initial $^{87}Sr/^{86}Sr$=0.719).	Not determined.
Isotopic age of zircon-------	Not determined--------	75±9 Ma[2]	Do.

[1]Only maximum K-Ar ages are listed. The younger K-Ar ages noted in the text presumably result from degassing due to heat stress related to late movement on overlying thrust faults.

[2]Age obtained for the source rock is 1970±330 Ma.

Toana Range Pluton

Only K-Ar radiometric ages are available presently for the muscovite-phenocrystic two-mica granite of the Toana Range. The muscovite and biotite recovered from sample 415 (fig. D1) gave markedly discordant K-Ar ages of 71.2±2.0 and 15.4±0.5 Ma, respectively (Lee and Marvin, 1981). Muscovite from sample 415 is phengitic, similar to muscovites recovered from other two-mica granites in northeastern Nevada. However, biotite from sample 415 is distinct chemically from other biotites recovered from these two-mica granites in that it is a hydrobiotite, with H_3O^+ substituting for K^+ in the interlayer X-group. These characteristics have led Lee, Kistler, Friedman, and Van Loenen (1981) to suggest that the composition of this biotite was altered by postmagmatic processes. Such an alteration also would account for the low K-Ar age (15.4±0.5 Ma) obtained for this biotite.

About 1 km northeast of sample 415, at lat 41°0′55″ N., long 114°17′30″ W., the Cambrian part of the Prospect Mountain Quartzite is exposed in intrusive contact with the granite. Two samples of metamorphic muscovite recovered from this quartzite gave K-Ar ages of 72.5±2.0 and 75.6±2.1 Ma (Lee and others, 1980), in good agreement with the K-Ar age (71.2±2.0 Ma) determined for muscovite from sample 415, recovered from the granite itself.

The map of Stewart and Carlson (1978) shows the two-mica granite represented by sample 415 as a Tertiary-Jurassic pluton intruding the Cambrian part of the Prospect Mountain Quartzite, with Cambrian carbonate thrust over the quartzite. In view of these field relations, the most obvious interpretation of these K-Ar ages might seem to be that the 71.2±2.0 age determined for igneous muscovite from sample 415 actually represents the time of crystallization. The metamorphic muscovite ages (72.5±2.0 and 75.6±2.1 Ma) might then represent degassing resulting from thermal contact action on the quartzite, and the degassing and chemical alteration of biotite from sample 415 may have resulted from postmagmatic stress related to late movement on the overlying thrust fault. However, the possibility exists that the K-Ar ages of the muscovites themselves may have been modified by stresses related to later movement on the thrust fault, as has been found in southern Snake Range (Lee and others, 1970) and elsewhere (Lee and others, 1980) in eastern White Pine County, Nev.

From the radiometric age data for the muscovite-phenocrystic two-mica granites summarized in table D2, clearly the Kern Mountains pluton and the Pole Canyon-Can Young Canyon pluton of the southern Snake Range crystallized in Late Cretaceous time. The Toana Range pluton also may be Late Cretaceous in age, but this conclusion must be regarded as tentative pending further study.

EQUIGRANULAR TWO-MICA GRANITES

Lexington Creek Pluton

Sample 378 (fig. D1) is from the equigranular two-mica granite of the Lexington Creek area. (See also chap. P, this volume, fig. P1). Unfortunately insufficient zircon was recovered for more than one analysis, but the data are shown in table D1 and plotted in figure D3. Although no really definitive age estimate is possible because of obvious inheritance, when the data are compared with the others in figures D3 and D4 the lower intercept with concordia seems more to indicate a Cretaceous rather than a Jurassic age. There is no doubt, however, that the sample does contain a high proportion of inherited zircon of Proterozoic age that is consistent with its derivation, at least in part, from a sedimentary source.

Muscovites recovered from three samples of the Lexington Creek pluton gave Late Cretaceous K-Ar age results ranging from 77.9 to 86.3 Ma (Lee and others, 1980). However, the top of this intrusive has been severed by the Snake Range décollement, and the dated muscovites may have been partially degassed as a result of stresses related to movement on the décollement. Thus, the intrusive may be somewhat older than indicated by these K-Ar age data.

Silver Creek Pluton

The equigranular two-mica granite of the Silver Creek area is Tertiary or older. The constituent muscovite and biotite from sample 287–DL–63 gave K-Ar ages of 31.1 ± 1.7 and 25.5 ± 1.3 Ma, respectively (Lee and others, 1970), but again these results probably reflect degassing as a result of late movement along the overlying Snake Range décollement as discussed in the context of many additional K-Ar ages by Lee and others (1980). Uranium-thorium-lead isotopic data show that a metamorphic monazite, possibly related to contact action of this granite on Prospect Mountain Quartzite, apparently crystallized 80–100 Ma ago (Lee, Stern, and Marvin, 1981). Further work will be needed before the significance of these data is fully understood.

Willard Creek Pluton

The two-mica granite of Willard Creek (sample 295–DL–64, fig. D1) has been regarded (Lee, Kistler, Friedman, and Van Loenen, 1981, p. 10,608) as a felsic phase of an intrusive referred to as the Osceola stock by Armstrong (1966). However, recent Rb-Sr work (chap. P, this volume) has shown that the granite of Willard Creek is not comagmatic with the main mass of the Osceola stock that is exposed about 3 km to the northeast of sample 295–DL–64. (See chap. P, this volume, fig. P1). Nonetheless, despite the lack of magmatic affinity between these two intrusive bodies, available radiometric age data indicate that both are Jurassic in age. The muscovite recovered from sample 295–DL–64 gave a K-Ar age of 151 ± 4 m.y. (Lee and others, 1970), probably representing the time of crystallization of this equigranular two-mica granite. The (Jurassic) age of the Osceola stock itself is discussed in the following section.

CALC-ALKALINE ROCKS OF JURASSIC AGE

Osceola Stock

Sample 177–MW–60 is from the Osceola stock. The data in table D1 from the (+250)NM and (–250)NM zircon fractions are plotted in figure D4. If a chord were drawn between these two points, it would have a lower intercept with concordia at 82 Ma. Although this might correspond to the Late Cretaceous event known in the region, the upper intercept would give 348 Ma. This latter seems an unlikely age for a pluton in this part of the continent and so, to investigate further, the (+250)NM fraction was abraded in a sphere-former device adapted for the purpose by S. S. Goldich and J. N. Aleinikoff. The data point (point A in fig. D4) for the abraded fraction has a higher $^{207}Pb/^{206}Pb$ than the unabraded fraction, and a chord through the two (+250)NM fractions has a lower intercept of 160 m.y. (fig. D4). This much more reasonable estimate should be regarded as a minimum age for this zircon because the unabraded fraction may have lost some lead later in its history, just as has the (–250)NM fraction. The $^{207}Pb/^{206}Pb$ age of the (–250)NM fraction is 212 Ma and this higher value probably is due to zircons inherited from the source materials. Whole-rock Rb-Sr work on sample 177–MW–60 and on two other samples from the Osceola stock gives an initial $^{87}Sr/^{86}Sr$ value of 0.7075 at an age of 145 Ma (chap. P, this volume). The lower U-Pb intercept of 160 Ma is in fair agreement with these Rb-Sr results.

Notch Peak Pluton

Finally, we present zircon data for samples collected at lat 39°11′12″ N., long 113°26′30″ W., from the quartz-

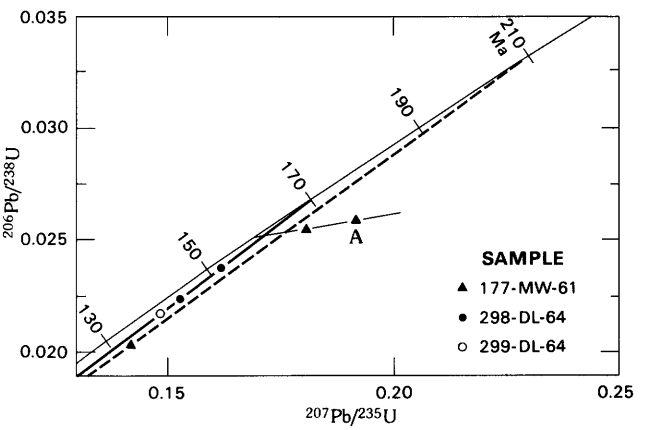

Figure D4. Uranium-lead zircon data from the Jurassic samples studied in this paper. The common age for samples 298–DL–64 and 299–DL–64 is 169 ± 3 Ma, with a lower intercept of 10 ± 11 Ma. Sample 177–MW–61 shows both inheritance and modern lead loss. Abrasion of the (+250)NM fraction produces a chord with lower intercept of ~160 Ma, that is a minimum age. Dotted line shows $^{207}Pb/^{206}Pb$ age of the (–250)NM zircons to be 212 Ma, but this age is artificially high because inherited lead has caused sideways displacement of the point.

monzonite at Notch Peak (Gehman, 1958) of the House Range in western Utah (fig. D1). Two fractions of sample 298–DL–64, from the main intrusive, and one fraction of sample 299–DL–64, a xenolith, give three data points that are on a single cord with a common intercept age of 169 ± 3 Ma (fig. D4). The lower intercept of 10 ± 11 Ma shows recent lead loss that may have taken place during the last uplift of the region.

CONCLUSIONS

Uranium-lead isotopic age results for zircon from sample 244–MW–60 from the muscovite-phenocrystic two-mica granite of the Kern Mountains confirm previously tentative Rb-Sr and K-Ar age data and show that this unusual granite crystallized during Late Cretaceous time. Taken together, these age data for the Kern Mountains intrusive also help to place in perspective Rb-Sr and K-Ar results for the similarly unusual Late Cretaceous muscovite-phenocrystic two-mica granite of the Pole Canyon-Can Young Canyon area, southern Snake Range. Another odd muscovite-phenocrystic two-mica granite, present in the Toana Range of Elko County, also may be Late Cretaceous in age. However, additional work is necessary to check the sparse K-Ar data presently available for this granite. Thus, two and possibly all three of the muscovite-phenocrystic granites of northeastern Nevada (fig. D1) are Late Cretaceous in age.

On the other hand, three examples of equigranular two-mica granites exposed in northeastern Nevada (fig. D1) appear to range in age from Jurassic to Cretaceous, and possibly to Tertiary. The equigranular two-mica granite (sample 295) of the Willard Creek area is shown by K-Ar work to be about 150 Ma old. The equigranular two-mica Lexington Creek intrusive (area of sample 378) is at least as old as Late Cretaceous, as indicated by both U-Pb and K-Ar work. The equigranular two-mica granite of the Silver Creek area, northern Snake Range (sample 287) appears to be middle Tertiary or older, depending upon how much the K-Ar age-dated muscovite and biotite (31 ± 1.7 and 25.5 ± 1.3 Ma, respectively) were degassed as a result of movement on the overlying Snake Range décollement.

The apparent similarity of the ages (Late Cretaceous) of the unusual muscovite-phenocrystic two-mica granites of northeastern Nevada is consistent with the idea that they all evolved in the same way—through anatexis of upper Precambrian-Lower Cambrian argillitic sediments under conditions of relatively low oxygen fugacity, along a line that roughly coincides with the westward disappearance of continental basement. However, we note that the initial Sr isotope values in granitoids of the region suggest that the edge of the continent is farther to the west (R. W. Kistler, oral commun.) than is indicated by the lead isotope data of Stacey and Zartman (1978).

Although one or more of the equigranular two-mica granites of the same general area (fig. D1) also may have evolved through anatexis, the apparent range in age (Jurassic-Tertiary?) of these granites suggests that they are not so closely related genetically. There also are mineralogical differences among these rocks, especially their accessory mineral contents (Lee, Kistler, Friedman, and Van Loenen, 1981).

Although many of the two-mica granites in northeastern Nevada are Late Cretaceous in age, calc-alkalic plutons of Jurassic age also appear to be rather widespread in the eastern Great Basin. In addition to the Osceola stock and Notch Peak pluton discussed in this paper, Jurassic ages have been determined for the Snake Creek-Williams Canyon pluton of the southern Snake Range (Lee and others, 1968; chap. P, this volume), and for the southern part of the Gold Hill stock in western Utah (Stacey and Zartman, 1978).

REFERENCES CITED

Armstrong, R. L., 1966, K-Ar dating using neutron activation for Ar analysis: Geochimica et Cosmochimica Acta, v. 30, no. 5, p. 565–600.

Best, M. G., Armstrong, R. L., Graustein, W. C., Embree, G. F., and Ahlborn, R. C., 1974, Mica granite of the Kern Mountains pluton, eastern White Pine County, Nevada—Mobilized basement of the Cordilleran miogeosyncline?: Geological Society of America Bulletin, v. 85, no. 8, p. 1277–1286.

Cameron, A. E., Smith, D. H., and Walker, R. L., 1969, Mass spectrometry of nanogram size samples of lead: Analytical Chemistry, v. 41, p. 525–526.

Gehman, H. M., Jr., 1958, Notch Peak intrusive, Millard County, Utah—Geology, petrogenesis, and economic deposits: Utah Geological and Mineralogical Survey Bulletin 62, 50 p.

Krogh, T. E., 1973, A low contamination method for hydrothermal decomposition of zircon and extraction of U and Pb for isotopic age determination. Geochimica et Cosmochimica Acta, v. 37, p. 485–494.

Lee, D. E., Brandt, E.L.M., Van Loenen, R. E., and Rose, H. J., Jr., 1973, The chemistry of five accessory rock-forming apatites: U.S. Geological Survey Journal of Research, v. 1, no. 3, p. 267–272.

Lee, D. E., Kistler, R. W., Friedman, I., and Van Loenen, R. E., 1981, Two-mica granites of northeastern Nevada: Journal of Geophysical Research, v, 86, no. B11, p. 10607–10616.

Lee, D. E., and Marvin, R. F., 1981, Markedly discordant K-Ar ages for coexisting biotite and muscovite from a two-mica granite in the Toana Range, Elko County, Nevada: Isochron/West, no. 32, p. 19

Lee, D. E., Marvin, R. F., and Mehnert, H. H., 1980, A radiometric age study of Mesozoic-Cenozoic metamorphism in eastern White Pine County, Nevada, and nearby Utah: U.S. Geological Survey Professional Paper 1158–C, p. 17–28.

Lee, D. E., Marvin, R. F., Stern, T. W., and Peterman, Z. E., 1970, Modification of potassium-argon ages by Tertiary thrusting in the Snake Range, White Pine County, Nevada, *in* Geological Survey research 1970: U.S. Geological Survey Professional Paper 700–D, p. D92–D102.

Lee, D. E., Stern, T. W., and Marvin, R. F., 1981, Uranium-thorium-lead isotopic ages for metamorphic monazite from the northern Snake Range, Nevada: Isochron/West, no. 31, p. 23.

Lee, D. E., Stern, T. W., Mays, R. E., and Van Loenen, R. E., 1968, Accessory zircon from granitoid rocks of the Mount Wheeler mine area, Nevada, *in* Geological Survey research 1968: U.S. Geological Survey Professional Paper 600–D, p. D197–D203.

Lee, D. E., and Van Loenen, R. E., 1971, Hybrid granitoid rocks of the southern Snake Range, Nevada: U.S. Geological Survey Professional Paper 668, 48 p.

Stacey, J. S., and Zartman, R. E., 1978, A lead and strontium isotopic study of igneous rocks and ores from the Gold Hill mining district, Utah: Utah Geology, v. 5, no. 1, p. 1–15.

Stewart, J. H., and Carlson, J. E., 1978, Geologic map of Nevada: U.S. Geological Survey in cooperation with the Nevada Bureau of Mines and Geology.

Zartman, R. E., 1974, Lead isotopic provinces in the Cordillera of the Western United States and their geologic significance: Economic Geology, v. 69, p. 792–805.

1986

U.S. GEOLOGICAL SURVEY BULLETIN 1622

SHORTER CONTRIBUTIONS TO ISOTOPE RESEARCH

GEOCHRONOLOGY OF BASEMENT GRANITE, STEPHENSON COUNTY, ILLINOIS

Chapter E

By ZELL E. PETERMAN, S. S. GOLDICH, LYNN B. FISCHER, and K. FUTA

CONTENTS

FIGURES

TABLES

Abstract

Whole-rock samples of granite from drill holes UPH–1 and UPH–3 in Stephenson County, Ill., define a rubidium-strontium isochron of 1,430±20 million years with an initial $^{87}Sr/^{86}Sr$ of 0.7029±0.0041. Zircons and sphene from the granite define a similar uranium-lead concordia intercept age of 1,454±30 million years. Minor cataclasis and alteration of the granite occurred about 1,200 million years as indicated by rubidium-strontium mineral ages for samples from drill hole UPH–3. This disturbance may be related to stresses imposed on the basement terrane during early phases of Keweenawan rifting to the west or Grenville orogenesis to the east.

INTRODUCTION

Core samples of granite recovered from three deep drill holes in northern Illinois (Hinze and others, 1981) have been made available for scientific purposes and provide an opportunity to study the physical, chemical, and isotopic properties of a Precambrian granite well beneath the effects of near-surface alteration. The present report presents the results of a geochronological study of selected samples from two of these drill holes.

The Precambrian basement in this area (fig. E1) is covered by about 600 m (meters) of lower Paleozoic strata, but fission-track dating of apatite from the IDH (Illinois deep hole) granite suggests that the overlying section was considerably thicker at one time (Zimmerman, 1981). The nearest exposed Precambrian is in central Wisconsin where Archean gneisses and Early and Middle Proterozoic supracrustal rocks, gneisses, and granites crop out.

The IDH granite is one of several Middle Proterozoic anorogenic intrusions in the midcontinent region, the southern Rocky Mountains, and the southwestern United States (Van Schmus and Bickford, 1981; Silver and others, 1977; Emslie, 1978). The composite Wolf River batholith in central Wisconsin is a member of this anorogenic suite of intrusions. Isotopic dating of other

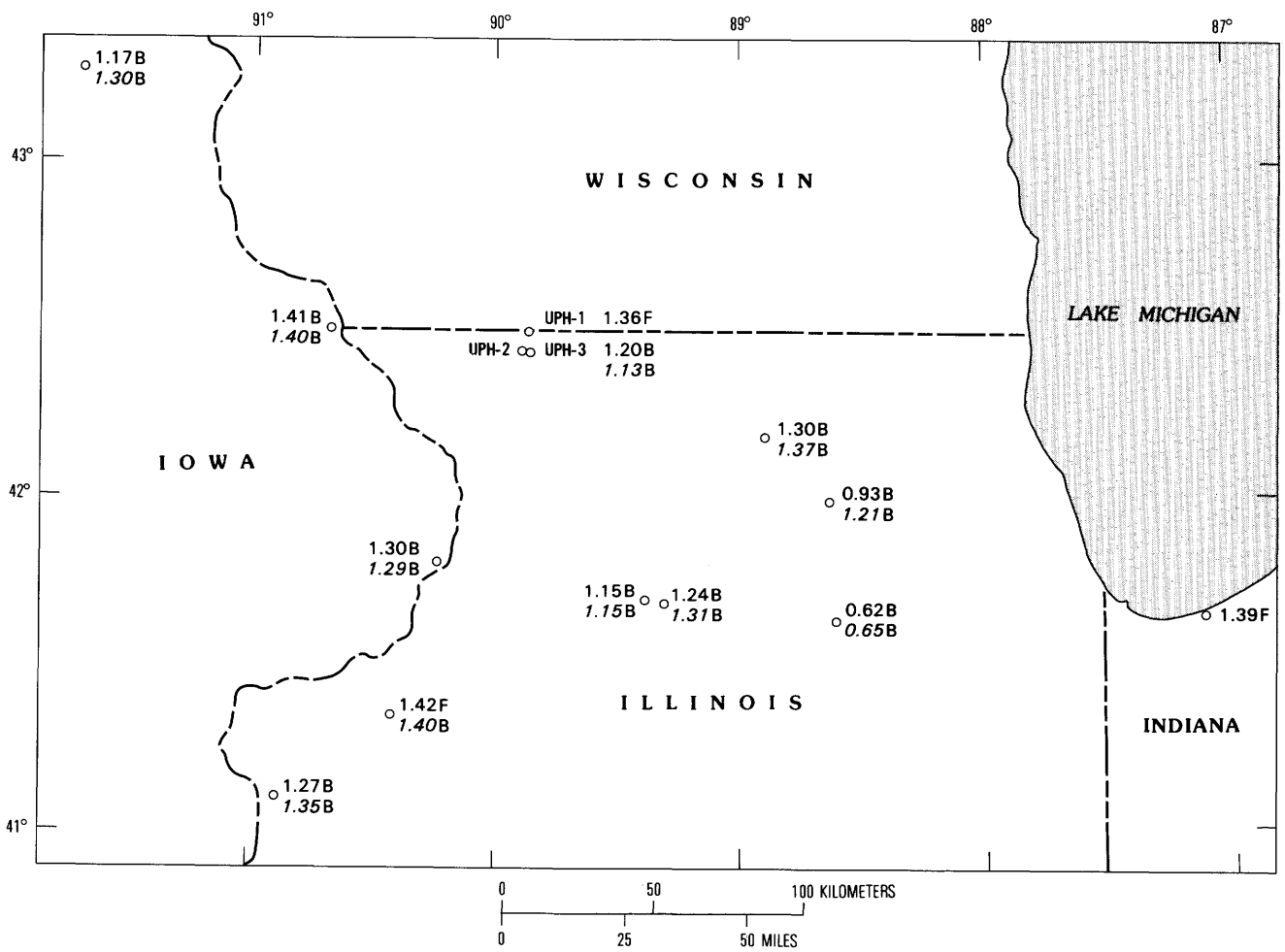

Figure E1. Potassium-argon and rubidium-strontium biotite (Bi) and potassium feldspar (F) ages of Precambrian basement samples obtained from drill holes in northern Illinois and adjacent states. Ages are in millions of years (Ma). Potassium-argon ages are italicized; rubidium-strontium ages are not. Location of drill holes UPH–1, –2, and –3 are shown together with ages from this report. Other ages are from Lidiak and others (1966).

basement samples from eastern Iowa and western Illinois have identified similar Middle Proterozoic granitoids, and aeromagnetic data suggest the presence of a belt of these plutons extending from southeastern Wisconsin to southeastern Iowa (Van Schmus and others, 1981; Hoppe and others, 1983).

ACKNOWLEDGMENTS

We are indebted to H. H. Mehnert for the K-Ar (potassium-argon) determination on biotite from sample 5251, to T. T. Ball for the petrography and modal analyses, and to Linda Martin for sample preparation and mineral separation. We also thank Prof. W. R. Van Schmus for the allocation of samples.

SAMPLES

The drill holes are in Stephenson County in northern Illinois (fig. E1). Coordinates for these holes are as follows: UPH–1, lat 42°30′20″ N., long 89°51′07″ W; UPH–2, lat 42°26′34″ N., long 89°52′01″ W.; and UPH–3, lat 42°26′14″ N., long 89°51′27″ W.

Sample numbers (table E1) are depths in feet; 2031 and 2064 are from drill hole UPH–1, and the others are from UPH–3. Samples 2064, 2209, 3333, 3514, and 5056 were provided by W. R. Van Schmus in the allocation of material for the Illinois drill-hole project. These were whole pieces of core 4.7 cm (centimeters) in diameter and 5–10 cm long. A larger sample of 2031 had been obtained earlier by Goldich from the Illinois Geological Survey, Sample designated 5251 represents the interval from 5245.0 to 5256.8 ft.

PETROGRAPHY

The dated samples (table E1) differ in texture and varietal mineralogy. Samples 2209 and 2290 are fine-grained, biotite-muscovite granites. Sample 3514 is a porphyritic granite that has groundmass texture and mineralogy like those of the fine-grained rocks but with subhedral to euhedral phenocrysts of microcline and plagioclase as much as 1 cm long. The remaining samples—2031, 2064, 5056, and 5251—are coarse-grained, biotite granites. Textures are xenomorphic inequigranular in the fine-grained rocks and hypidiomorphic inequigranular in the coarse-grained granites.

Quartz, perthitic microcline, and albite to sodic oligoclase compose more than 80 percent of all the samples. Quartz is rutilated and contains abundant trails of fluid inclusions. In the fine-grained granites, and to a lesser extent in the coarse-grained rocks, microcline shows a micrographic texture with rounded blebs and rods of quartz. Poikilitic microcline in the coarse-grained granites contains inclusions of quartz, plagioclase, biotite, and accessory minerals. Plagioclase is moderately to severely sericitized to dense patches of very fine grained material,

Table E1. Modal analyses of samples dated, Stephenson County, Ill.
[Modes are based on 1,700 points for sample 2031, 1,000 points for sample 5251, and 600 points for the other samples. Leaders (---) indicate not present; tr, trace]

Drill hole	UPH-1		UPH-3					
Sample No. (also depth, in feet)	2031	2064	2209	2290	3333	3514	5056	5251
Quartz	31	32	40	39	30	35	29	38
Microcline	22	41	30	30	32	35	36	27
Plagioclase	21	15	21	22	26	24	21	23
Muscovite	---	---	6.2	5.2	1.7	2.2	0.2	---
Biotite	6.0	6.7	1.2	3.2	5.5	1.0	7.0	7.7
Hornblende	---	1.0	---	---	---	---	---	.1
Fluorite	.4	.9	.2	1.0	1.3	.7	.3	.5
Monazite	---	---	.2	---	.2	tr	tr	---
Zircon	tr	---	tr	.5	.3	tr	tr	.2
Sphene	.1	---	---	---	---	---	tr	.6
Apatite	.6	.2	---	---	---	---	tr	tr
Opaque minerals	[1]5.4	.7	---	.2	.8	.2	1.0	.5
Allanite	---	---	---	---	---	---	---	.1
Chlorite	1.9	1.0	1.5	.3	.7	1.3	.2	.3
Sericite	10.7	2.7	---	---	.8	.5	5.3	2.2
Carbonate	1.1	---	---	---	.3	---	---	.2

[1]Includes dense iron-oxide staining associated with other alteration minerals generally on plagioclase.

commonly stained with iron oxide, and to discrete, oriented blades of coarser white mica. Biotite ranges from fresh to almost completely altered to chlorite, and commonly is associated with granular sphene. Some biotite grains contain thin lenses of carbonate and a low-birefringent mineral. Hornblende is a trace mineral in two samples. Muscovite is present locally in fibrous intergrowths between biotite and microcline. Fluorite is a ubiquitous accessory mineral and is present as interstitial grains and as inclusions in other minerals. In the coarse-grained granites, biotite is present as clots in association with opaque oxides, sphene, and other accessory minerals. Samples 2031 and 2064 are stained appreciably with iron oxide along fractures and grain boundaries. Thin carbonate veinlets are present in 2031, and sphene is altered locally to an intergrowth of leucoxene and carbonate.

Strain in the samples is present in different degrees. Sample 2209 has well-developed mortar structure, through-going microshear zones, bent and broken plagioclase twins, and mutually sutured grain boundaries. Quartz is highly strained and recrystallized into domains that have sutured boundaries. The other samples show less deformation, but strained quartz and mortar structure around larger grains are common.

CHEMISTRY

Chemical analyses of samples 2031 (hole UPH–1) and 5251 (hole UPH–3) were made by a combination of atomic absorption and conventional chemical methods. These are the large samples from which zircon was concentrated for U-Pb determinations and other minerals for Rb-Sr analyses. The two analyses (table E2) are similar but show greater differences than might be surmised from the modal analyses (table E1), but the coarse-grained rocks are not represented adequately in one or two thin sections. The chemical analyses are similar to published analyses (Van Schmus and others, 1975; Anderson and Cullers, 1978) of granitic rocks from the Wolf River batholith, Wisconsin, about 300 km northeast of the drill holes in Stephenson County, Ill. Samples 2031 and 5251 most closely resemble the Red River adamellite of Anderson and Cullers (1978) for which their average is given in table E2. The low K/Rb and high Ba/Sr and Rb/Sr are distinctive features of both the IDH granite and the granitic phases of the Wolf River batholith. Their potassic character is shown by $K_2O/(K_2O+Na_2O)$ of 0.71 for sample 2031, 0.65 for sample 5251, and 0.61 for the Red River adamellite.

Using GSP–1 as a standard, Rb, Sr, Y, Zr, and Ba were determined by X-ray fluorescence (XRF), for all samples received in the allocation (table E3). Coefficients of variation (1 sigma) are estimated to be ±7 percent for concentrations greater than 100 ppm (parts per million) and about ±15 percent for those less than 100 ppm.

Table E2. Chemical analyses of selected samples, Stephenson County, Ill.
[Leaders (---) indicate not determined]

Drill hole--	UPH-1	UPH-3	
Sample No.--	2031	5251	RR[1]
	Weight percent		
SiO_2--------	71.8	71.32	72.5
Al_2O_3-------	14.1	13.61	13.91
TiO_2--------	.30	.46	.36
Fe_2O_3-------	.39	.75	---
FeO---------	1.08	1.99	[2]2.65
MnO---------	.02	.05	.06
MgO---------	.56	.39	.47
CaO---------	1.37	1.97	1.25
Na_2O--------	2.80	3.00	3.24
K_2O---------	6.82	5.55	5.14
P_2O_5--------	.06	.13	---
H_2O+--------	.29	.13	---
H_2O- -------	.06	.05	---
CO_2---------	.30	.08	---
F----------	.20	---	---
Total---	[3]100.07	99.48	99.59
	Parts per million		
Rb----------	303	302	236
Sr----------	152	132	129
Ba----------	1,150	1,000	705
Y----------	36	71	---
Zr----------	143	254	---
	Weight ratio		
K/Rb--------	187	153	181
K/Sr--------	372	349	330
Rb/Sr-------	1.99	2.29	1.83
Ba/Sr-------	7.56	7.58	5.47
Ba/Rb-------	3.80	3.31	2.99

[1]RR is the average of seven analyses of the Red River adamellite of the Wolf River batholith, Wisconsin (Anderson and Cullers, 1978).

[2]Total Fe reported as FeO.

[3]Total corrected for F.

Except for sample 2185 (table E3), some systematic variations are apparent among these data. Strontium decreases from about 150 to 25 ppm as rubidium increases from about 300 to 650 ppm. The fine-grained granites such as 2209 and 2290 (table E1) are higher in Rb and

Table E3. X-ray fluorescence analyses for Rb, Sr, Y, Zr, and Ba of samples, Stephenson County, Ill.

[Suffix letters B and C and F and G refer to adjacent pieces of core prepared as separate samples]

Sample	Concentration (parts per million)					Weight ratio		
No.	Rb	Sr	Y	Zr	Ba	Rb/Sr	Zr/Y	Ba/Sr
				Drill hole UPH-1				
2004	306	154	71	302	924	1.98	4.2	6.0
2025	301	167	59	305	680	1.80	5.2	4.1
2031	296	149	36	144	956	1.98	4.0	6.4
2064B	299	142	68	285	507	2.10	4.2	3.6
2064C	345	152	43	197	892	2.28	4.6	5.9
2071F	303	137	68	347	568	2.22	5.1	4.1
2071G	299	137	64	236	738	2.19	3.7	5.4
				Drill hole UPH-2				
2185	335	292	75	333	622	1.15	4.4	2.1
2385	318	128	75	317	638	2.48	4.3	5.0
2779	339	130	30	172	873	2.61	5.7	6.7
3194	341	85	40	208	362	4.01	5.2	4.3
3678	371	49	38	71	125	7.57	1.7	2.6
4202	517	50	70	97	243	10.3	1.4	4.9
4405	693	71	73	227	537	9.76	3.1	7.6
4773	435	125	72	278	529	3.48	3.9	4.2
5411	433	90	73	268	480	4.81	3.7	5.3
				Drill hole UPH-3				
2209	621	25	118	212	95	25.1	1.8	3.8
2290	591	34	126	264	55	17.3	2.1	1.6
2397	537	25	104	254	106	21.2	2.4	4.2
2422	524	39	87	174	160	13.3	2.0	4.1
3333	423	68	68	233	226	6.22	2.0	5.0
3514	438	45	101	291	189	9.73	2.9	4.2
3880	392	100	62	246	531	3.92	4.0	5.3
4059	365	103	95	331	541	3.54	3.5	5.3
4609	490	55	82	260	313	8.91	3.2	5.7
4689	423	55	73	225	265	7.69	3.1	4.8
5056	417	96	71	266	520	4.34	3.8	5.4
5251	308	135	71	254	---	2.28	3.8	---

lower in Sr than the coarse-grained rocks. Barium correlates with strontium, and yttrium shows a crude correlation with rubidium.

Anderson and Cullers (1978) concluded that granitic rocks of the Wolf River batholith were anatectic melts of a tonalitic to granodioritic source in the lower to intermediate crust. Fractional crystallization at higher levels produced some of the chemical variations among the different phases. Variations in Rb, Sr, and Ba in the IDH samples (table E3) could be the result of fractional crystallization in which plagioclase was an important precipitate phase.

GEOCHRONOLOGY

Methods

Following ultrasonic cleaning, the samples were crushed, and splits of 30–50 g (grams) were pulverized to –200 mesh in a shaker mill for the whole-rock analyses. Mineral separates were prepared from sized, crushed rock using heavy liquids and magnetic separation.

Samples for Rb and Sr analyses were selected on the basis of XRF determinations to obtain a suitable range in Rb/Sr for the construction of an isochron. Rubidium

Table E4. Rubidium and strontium data for whole-rock samples and minerals, Stephenson Co., Ill.

[Sample numbers are depths in feet. Suffix letters refer to type of sample: WR, whole rock; Ap, apatite; Sp, sphene; Bi, biotite; Pl, Plagioclase; and Mi, microcline. Leaders (---) indicate not determined]

Sample No.	Concentration (parts per million) Rb	Sr	$^{87}Rb/^{86}Sr$	$^{87}Sr/^{86}Sr$[1]
		Drill hole UPH-1		
2031WR	303.0	151.7	5.845	0.82147±3
2031WR	---	151.1	5.867	.82151±2
2031Mi	452.5	162.3	8.193	.86667±3
2031Mi	---	163.3	8.146	.86634±15
2064WR	348.3	149.8	6.816	.83945±4
		Drill hole UPH-3		
2209WR	619.0	29.21	69.87	2.13036±40
2209Mi	1,153	39.60	100.17	2.63314±32
2290WR	560.8	27.75	66.25	2.06461±9
2290Mi	1,181	47.91	82.91	2.36280±18
3333WR	417.4	62.15	20.22	1.11723±30
3514WR	431.7	43.24	30.66	1.33079±23
5056WR	415.2	93.70	13.16	.97585±5
5251WR	302.0	131.9	6.715	.84426±4
5251WR	---	131.5	6.734	.84446±2
5251Ap	12.19	49.41	.7159	.73369±3
5251Sp	13.28	50.27	.7694	.77508±13
5251Pl	85.91	95.95	2.608	.77382±2
5151Pl	---	95.85	2.611	.77384±2
5251Mi	503.8	113.0	13.22	.95922±19
5155Mi	---	112.4	13.29	.95951±3
5251Bi	1,364	22.73	244.8	4.89660±40
5251Bi	---	22.94	242.9	---
		Standard sample GSP-1		
GSP-1	253.3	235.3	3.135	.76888±3

[1]Uncertainties are ±2σ on the mean x 10^5.

and strontium were determined by conventional isotope-dilution methods using enriched ^{87}Rb and ^{84}Sr spikes. Samples were decomposed in HF and H_2SO_4 in covered platinum dishes following spiking, and Sr was purified for isotopic analysis on conventional ion-exchange columns elutriated with HCl.

Analytical uncertainties (1σ) are Rb and Sr, ±0.6 percent; $^{87}Sr/^{86}Sr$, ±0.017 percent. The U.S. Geological Survey rock standard GSP–1 was analyzed in addition to the core samples and the results (table E4) are in agreement with generally accepted values. The average $^{87}Sr/^{86}Sr$ for the E and A standard in this laboratory is 0.70803.

The uncertainties shown for $^{87}Sr/^{86}Sr$ in table E4 are 2σ on the mean determined from the in-run statistics. These uncertainties are 2–20 times lower than the precision determined from replicate analyses of granitic rocks. This difference reflects the difficulty of replicating splits at the 0.1–1 g level of samples in which the constituent minerals differ by nearly an order of magnitude in $^{87}Sr/^{86}Sr$.

Zircon and sphene (table E5) were analyzed following a method modified from that described by Krogh (1973). Analytical uncertainties (1σ) are about ±0.7 percent for parent-daughter ratios and ±0.05 percent for $^{207}Pb/^{206}Pb$.

Isotopic and decay constants recommended by the International Union of Geological Sciences Subcommission on Geochronology (Steiger and Jäger, 1977) were used in calculating the ages. The regressions are calculated using Ludwig's (1982a, b) programs.

Rubidium-Strontium and Potassium-Argon

Rubidium-strontium data for whole-rock samples from drill holes UPH–1 and UPH–3 (table E4) define an isochron (fig. E2) for which the scatter is slightly greater than analytical error. The MSWD (mean square of the weighted deviates) for a model I solution is 3.2. The preferred age of 1,430 ± 20 Ma (million years) is determined from the model III regression which increases the variance in $^{87}Sr/^{86}Sr$ to explain the scatter. Slight variations in initial $^{87}Sr/^{86}Sr$ among the samples would be consistent with a model III solution.

The two fine-grained granites, samples 2209 and 2290, from near the sub-Cambrian unconformity have the highest Rb/Sr. Uranium-lead analyses of these samples indicate loss of lead (Doe and others, 1983; Stuckless and others, 1981), but this disturbance is not evident in the Rb-Sr systems. Exclusion of the two points from the regression yields a model III solution of 1,432 ± 40 Ma and an intercept of 0.7026 ± 0.0069.

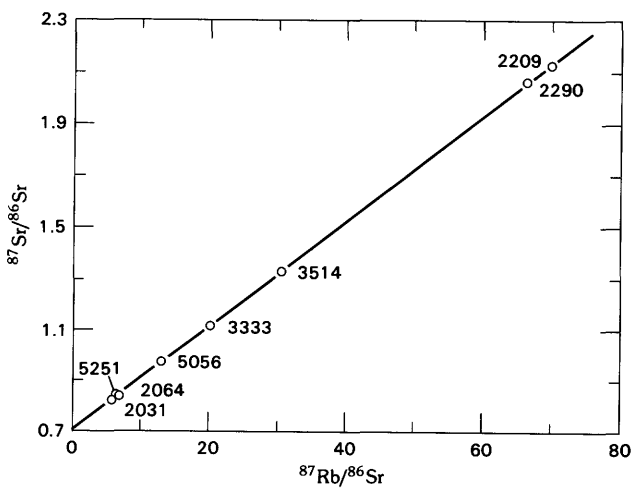

Figure E2. Rubidium-strontium whole-rock isochron for samples from drill holes UPH–1 and UPH–3, Stephenson County, Ill. The slope of the line corresponds to an age of 1,430±20 Ma, and the $^{87}Sr/^{86}Sr$ intercept is 0.7029±0.0041.

Table E5. Uranium, thorium, and lead data for zircons and sphene, Stephenson County, Ill.

[Numbers in parentheses are mesh size of fractions. Isotopic composition of initial lead is assumed to be ^{204}Pb:^{206}Pb:^{207}Pb:^{208}Pb=1:16.27:15.41:35.93. Age in millions of years are given in square brackets below the atom ratio. Leaders (---) indicate not determined]

Sample No. (mesh size)	Material analyzed	Concentration (parts per million)			Isotopic composition of lead (atom percent)[1]				Atom ratio			
		U	Th	Pb	^{204}Pb	^{206}Pb	^{207}Pb	^{208}Pb	$\frac{^{206}Pb}{^{238}U}$	$\frac{^{207}Pb}{^{235}U}$	$\frac{^{207}Pb}{^{206}Pb}$	$\frac{^{208}Pb}{^{232}Th}$
2031:												
(unsized)	Zircon--	768.1	---	131.3	0.078	79.53	8.15	12.24	0.1555	1.9046 [931]	0.0889 [1,083]	--- [1,401]
5251:												
(60-100)	Zircon--	494.8	---	111.8	.118	76.26	8.51	15.12	.1952	2.4205 [1,149]	.0899 [1,249]	--- [1,424]
(60-100)ABR[2]	--do.---	650.2	---	146.4	.090	74.87	7.94	17.10	.1921	2.3684 [1,133]	.0894 [1,233]	--- [1,413]
(100-200)	--do.---	1,100	---	221.9	.161	71.12	8.49	20.22	.1606	1.9401 [960]	.0876 [1,095]	--- [1,375]
(+200)	Sphene--	161.2	129.9	48.1	.082	71.67	7.68	20.57	.2439 [1,407]	3.0682 [1,425]	.0912 [1,452]	0.0735 [1,433]

[1]Corrected for laboratory blank.

[2]Suffix ABR designates abraded sample.

Although the initial $^{87}Sr/^{86}Sr$ intercept is low—0.7029—the large uncertainty of ±0.0041 allows considerable latitude in estimating the Rb/Sr of the source material. At the 95-percent confidence level, the intercept is constrained to a possible range between 0.6988 and 0.7070. The lower limit is impossible, but minimum mantle values can be calculated using the coordinates of the centroid of the whole-rock data as estimates for the average granite. These values are 10.33 for $^{87}Rb/^{86}Sr$ and 0.9149 for $^{87}Sr/^{86}Sr$. Model ages and intercepts, respectively, are 1,431 Ma and 0.7028 in the bulk-earth model of McCulloch and Wasserburg (1978) and 1,434 Ma and 0.7024 in the tonalite-trondhjemite model of Peterman (1979). A bulk-earth value of 0.7028 as the lower limit and 0.7070 as the upper limit for the granite would allow a Rb/Sr between 0.029 and 0.25 for a source of 1.9 Ga. The 0.25 figure commonly is cited as an average Rb/Sr value for the upper crust. An assumed older age for the source would, of course, lower the maximum permissible Rb/Sr. Nonetheless, the possible range in the $^{87}Sr/^{86}Sr$ intercept for the IDH granite allows partial or complete derivation of the granite from older crustal material.

Minerals from four samples were analyzed (table E4) to evaluate the internal isotopic integrity of the granite (fig. E3). Data for whole-rock, plagioclase (about 50 percent quartz), microcline, and biotite from sample 5251 are colinear within analytical error (MSWD=0.99) with an age of 1,201±15 Ma. Exclusion of the biotite from the regression does not change the age significantly (1,211±22 Ma). Data for sphene and apatite (fig. E3) are not colinear with data for the major minerals. This difference probably represents the distribution and association of these minor phases. Sphene occurs mainly with clots of biotite and opaque oxides, and a small amount is related to chloritization of biotite. Thus, sphene could have incorporated a disproportionate amount of radiogenic ^{87}Sr released from the biotite during the disturbance. Some apatite is associated with the mafic clots, but much is distributed throughout the other minerals, such as quartz, where it could not readily accept mobile ^{87}Sr.

Data for whole-rock samples 2209 and 2290 and their constituent microclines (table E4) are colinear within analytical error (fig. E3, inset) and give an age of 1,181±65 Ma (MSWD=0.79). This age is indistinguishable from the mineral isochron for sample 5251. The whole rock and microcline for sample 2031 are on an isochron of 1,357±101 Ma.

A potassium-argon age of biotite from sample 5251 is 1,130±12 Ma. The data are: K_2O, 7.70 percent; ^{40}Ar radiogenic, 2.019×10^{-10} moles/gram; and ^{40}Ar radiogenic/^{40}Ar total, 0.9884.

Uranium-Thorium-Lead

Four samples of zircon and one of sphene were processed and analyzed (table E5). The U-Pb ages for the zircon are appreciably discordant, and the ratios of the $^{207}Pb/^{235}U$ ages to the $^{206}Pb/^{238}U$ ages range from 1.09 to 1.16, but this ratio of the U-Pb ages of the sphene is 1.013. The sphene, therefore, controls the plot for the five samples on a concordia diagram (fig. E4). A regression for the data gives upper and lower intercepts of 1,454±30 Ma and 181±110 Ma, respectively. The concordia age agrees, within analytical error, with the Rb-Sr isochron age of 1,430±20 Ma.

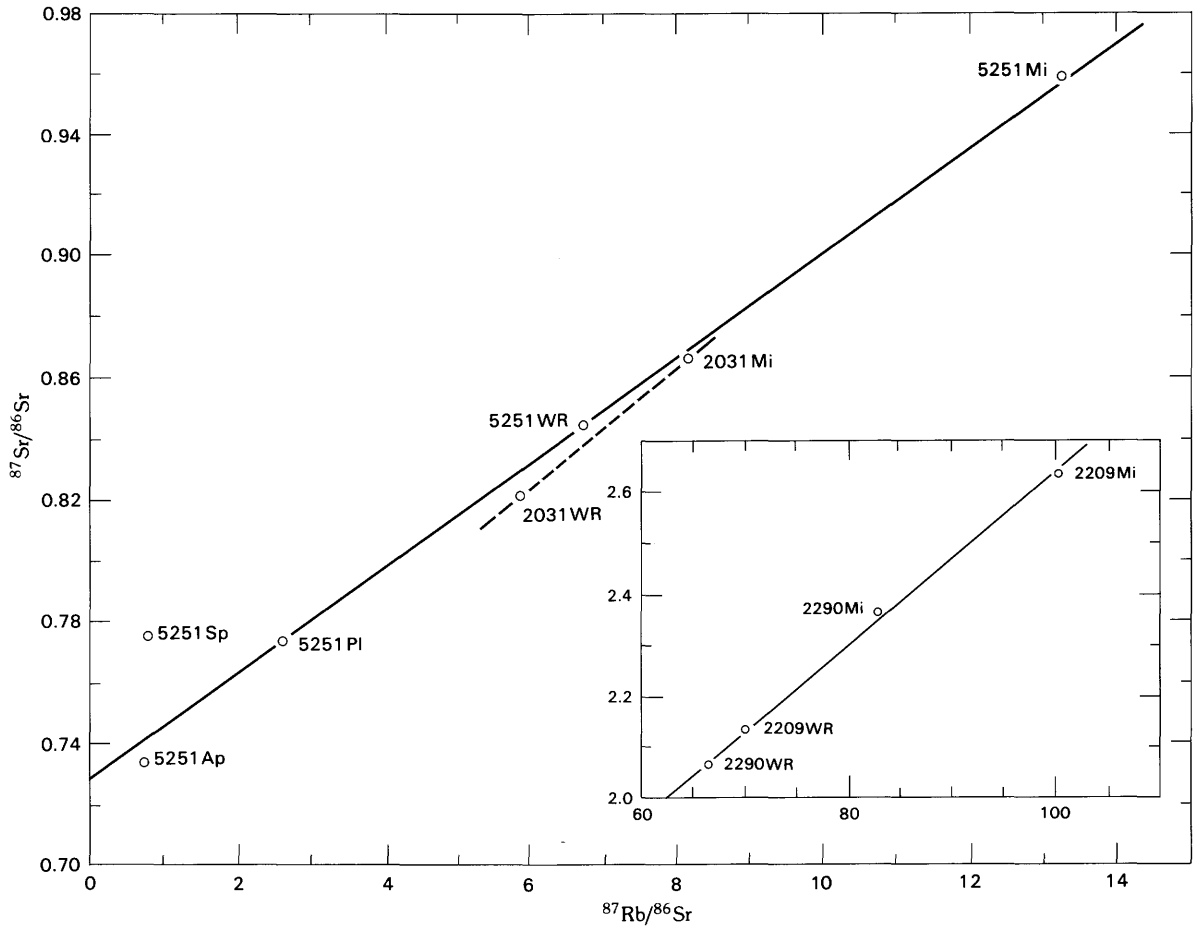

Figure E3. Rubidium-strontium mineral isochrons for samples from Stephenson County, Ill. The isochrons and intercepts, respectively, are 1,201 ± 15 Ma and 0.7290 ± 0.0011 for plagioclase (Pl), whole rock (WR), microcline (Mi), and biotite (Bi)—not shown—for sample 5251 (solid line); 1,357 ± 101 Ma and 0.7076 ± 0.0098 for whole rock and microcline for sample 2031 (dashed line); and 1,181 ± 65 Ma and 0.948 ± 0.073 for whole rocks and microclines for samples 2209 and 2290 (inset). Data points for apatite (Ap) and sphene (Sp) from samples 5251 are excluded from the regression.

A part of sample 5251 (60–100 mesh) was abraded in a sphere-former to see if the zircons were composed of cores and rims of different ages. Although the more resistant material has higher U and Pb contents (table E5), the parent-daughter ratios are not appreciably different than those of the unabraded fraction.

DISCUSSION

The whole-rock Rb-Sr isochron age of 1,430 ± 20 Ma and the U-Pb concordia-intercept age of 1,454 ± 30 Ma agree within experimental error. These ages agree with U-Pb zircon age of 1,461 ± 6 Ma (drill hole UPH–1) and 1,465 ± 8 Ma (drill hole UPH–3), and with a Rb-Sr whole-rock isochron age of 1,404 ± 35 Ma (drill hole UPH–3) reported by Hoppe and others (1983). All the isotopic ages are similar to those of the Wolf River batholith of central Wisconsin (Van Schmus and others, 1975), which, when recalculated for decay constants and regression methods used here, are 1,437 ± 20 Ma (Rb-Sr) and 1,469 ± 28 Ma (U-Pb).

Concordancy of the Rb-Sr mineral ages for samples from drill hole UPH–3 suggests a specific event at about 1,200 Ma. This event is correlated with the deformation and mineralogic alteration of the granite. The greater age of 1,357 ± 101 for microcline from drill hole UPH–1 (sample 2031) may indicate that the disturbance was rather local in extent. Drill hole UPH–1 is about 8 km north of drill hole UPH–3 (fig. E1).

McGinnis and others (1976) interpreted the gravity field of northern Illinois as representing discrete crustal blocks that are fault-bounded. These authors suggested that there was movement along these faults in the Precambrian and the Phanerozoic, and that most of the earthquake epicenters in Illinois are coincident with the inferred fault zones (McGinnis and Ervin, 1974).

Potassium-argon and rubidium-strontium mineral ages of basement samples in this region (fig. E1) probably

represent differential uplift of these domains and (or) localized tectonism at their margins. For example, biotite from a drill hole in northeastern Illinois (fig. E1) has unusually low ages of 620 Ma (Rb-Sr) and 650 Ma (K-Ar). The hole is on or close to the northwest-trending Sandwich fault (McGinnis and others, 1976), and these ages indicate Late Proterozoic movement.

McGinnis and Ervin (1974) suggested that a horizontal stress field imposed on this mosaic of basement domains would produce differential horizontal and vertical movements of these blocks. Activity along the basement faults could be triggered by stresses originating at considerable distances outside the region. Thus, the 1,200-Ma ages recorded by samples from drill hole UPH–3 probably are related to early phases of Keweenawan rifting to the west or to Grenville orogenesis to the east. Depending upon the direction of the stress field, activity may be preferential along certain fault orientations, which would explain the regional pattern of generally concordant age pairs that differ substantially from one area to another (fig. E1). This long history of repeated activity in the basement contrasts with areas in the exposed Canadian shield, such as in the central and western Superior province, where biotite ages are remarkably uniform over broad areas.

The ages reported here and other data indicate disturbances of the IDH granite in the Phanerozoic. Assuming no gain or loss of uranium, the zircon array (fig. E4) could have resulted from loss of 24–40 percent of accumulated radiogenic lead between Late Pennsylvanian and Late Cretaceous time. Whole-rock U-Pb data indicate loss of lead from samples 2209 and 2290 at about this same time (Doe and others, 1983; Stuckless and others, 1981). Fission-track ages of apatite decrease linearly from 130 ± 14 Ma near the sub-Cambrian unconformity to 50 ± 7 Ma at 5400 ft, and Zimmermann (1981) interpreted this pattern as resulting from cooling below the annealing temperature of apatite during the Cretaceous or early Tertiary.

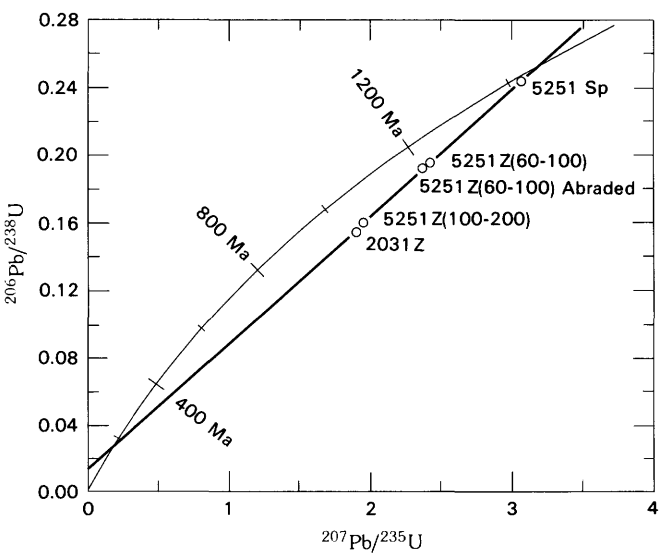

Figure E4. Uranium-lead concordia plot for zircon (Z) and sphene (Sp) (samples from Stephenson County, Ill.). Intercepts are $1,454 \pm 30$ Ma and 181 ± 110 Ma. Size fraction (if any) is shown in parentheses next to sample number.

Correlation of these relatively young disturbances with known geologic events is not clear. The granite was exposed during the Late Proterozoic and Early Cambrian, and it is overlain unconformably by the Upper Cambrian Mount Simon Sandstone. Some disturbance of these sensitive isotopic systems would have been expected at this time. A Bubnoff plot of McGinnis and others (1976) shows a sharp increase in subsidence of the Illinois basin during the Mississippian, and this could have been accompanied by movement along basement faults. The event in the Late Cretaceous to early Tertiary recorded in the fission-track ages is not apparent in the stratigraphic record as it is presently known (Zimmermann, 1981).

SUMMARY

Isotopic dating of samples of basement granite penetrated in the Illinois deep drill holes establishes the time of intrusion, and, together with published ages for this region, records a long and complex tectonic history for the buried basement.

1. The rubidium-strontium whole-rock age of $1,430 \pm 20$ Ma and the zircon-sphene concordia age of $1,454 \pm 30$ Ma agree within analytical error and establish the time of intrusion of this anorogenic granite.

2. The rubidium-strontium mineral ages for samples from drill hole UPH–3 record an event at about 1,200 Ma manifested in the granite by cataclasis and alteration. An age of about 1,360 Ma for microcline from drill hole UPH–1 suggests that this event may have been local in extent.

3. The 1,200-Ma mineral ages for samples from drill hole UPH–3 and several published Rb-Sr and K-Ar biotite ages for basement samples in the region probably are related to differential vertical and horizontal movements of discrete crustal blocks resulting from stresses imposed by early phases of either Keweenawan rifting or Grenville orogenesis. Later activity of this kind also is indicated by published biotite ages.

4. The granite was exposed by Late Cambrian time, but the effects of this uplift and denudation on the isotopic systems, if any, have been obscured by apparent disturbances in middle to late Phanerozoic time.

5. This long-term tectonic history recorded in basement rocks of the region probably is typical of the buried Precambrian basement of the central interior. It

contrasts dramatically with some terranes in the Superior province of the Canadian shield where biotite ages indicate remarkable long-term stability over large areas.

REFERENCES CITED

Anderson, J. L., and Cullers, R. L., 1978, Geochemistry and evolution of the Wolf River batholith, a late Precambrian rapakivi massif in northern Wisconsin, U.S.A.: Precambrian Research, v. 7, p. 287–324.

Doe, B. R., Stuckless, J. S., and Delevaux, M. H., 1983, The possible bearing of the granite of the UPH deep drill holes, northern Illinois, on the origin of Mississippi Valley ore deposits: Journal of Geophysical Research, v. 88, p. 7335–7345..

Emslie, R. F., 1978, Anorthosite massifs, rapakivi granites, and late Proterozoic rifting of North America: Precambrian Research, v. 7, p. 1–98.

Hinze, W. J., Haimson, B. C., and Van Schmus, W. R., 1981, The Illinois deep hole project—An overview [abs.]: EOS, v. 62, no. 17, p. 387.

Hoppe, W. J., Montgomery, C. W., and Van Schmus, W. R., 1983, Age and significance of Precambrian basement samples from northern Illinois and adjacent states: Journal of Geophysical Research, v. 88, p. 7276–7286.

Krogh, T. E., 1973, A low-contamination method for hydrothermal decomposition of zircon and extraction of U and Pb for isotopic determinations: Geochimica et Cosmochimica Acta, v. 37, p. 485–494.

Lidiak, E. G., Marvin, R. F., Thomas, H. H., and Bass, M. N., 1966, Geochronology of the midcontinent region, United States, pt. 4; eastern area: Journal of Geophysical Research, v. 71, p. 5427–5438.

Ludwig, K. R. 1982a, Programs for filing and X-Y plotting of isotopic and other data using an HP–9830 computer and HP–9862 plotter: U.S. Geological Survey Open-File Report OF 82–385, 23 p.

———1982b, Programs for filing and plotting U-Pb isotope data for concordia diagrams, using an HP–9830 computer and HP–9862 plotter: U.S. Geological Survey Open-File Report OF 82–386, 23 p.

McCulloch, M. T., and Wasserburg, G. J., 1978, Sm-Nd and Rb-Sr chronology of continental crust formation: Science, v. 200, p. 1003–1011.

McGinnis, L. D., and Ervin, C. P., 1974, Earthquakes and block tectonics in the Illinois basin: Geology, v. 2, p. 517–519.

McGinnis, L. D., Heigold, P. C., Ervin, C. P., and Heidara, M., 1976, The gravity field and tectonics of Illinois: Illinois State Geological Survey Circular 494, 28 p.

Peterman, Z. E., 1979, Strontium isotope geochemistry of late Archean to late Cretaceous tonalites and trondhjemites, *in* Barker, Fred, ed., Developments in petrology, dacites, trondhjemites, and related rocks: Amsterdam, Elsevier Scientific Publishing Co., p. 133–147.

Silver, L. T., Bickford, M. E., Van Schmus, W. R., Anderson, J. L., Anderson, T. H., Medaris, L. G., Jr., 1977, The 1.4–1.5 b.y. transcontinental anorogenic plutonic perforation of North America [abs.]: Geological Society of America Abstracts with Programs, v. 9, no. 7, p. 1176–1177.

Steiger, R. H., and Jäger, E., 1977, Subcommission on geochronology; convention on the use of decay constants in geo- and cosmochronology: Earth and Planetary Science Letters, v. 36, p. 359–362.

Stuckless, J. S., Doe, B. R., and Delevaux, M., 1981, U-Th-Pb isotope systematics and uranium distribution within granite recovered from drill-hole UPH–3, northern Illinois [abs.]: Geological Society of America Abstracts with Programs, v. 13, n. 7, p. 562.

Van Schmus, W. R., and Bickford, M. E., 1981, Proterozoic chronology and evolution of the midcontinent region, North America, *in* Kroner, A., ed., Precambrian plate tectonics: Amsterdam, Elsevier Scientific Publishing Co., p. 261–296.

Van Schmus, W. R., Hoppe, W. J., and Montgomery, C. W., 1981, Age and geologic significance of Precambrian basement samples from northern Illinois and eastern Iowa [abs.]: Geological Society of America Abstracts with Programs, v. 13, no. 7, p. 572.

Van Schmus, W. R., Medaris, L. G., Jr., and Banks, P. O., 1975, Geology and age of the Wolf River batholith, Wisconsin: Geological Society of America Bulletin, v. 86, p. 907–914.

Zimmermann, R. A., 1981, Where have all the sediments gone?—Fission track dating of the Illinois deep hole core [abs.]: Geological Society of America Abstracts with Programs, v. 13, no. 7, p. 588.

1986

U.S. GEOLOGICAL SURVEY BULLETIN 1622

SHORTER CONTRIBUTIONS TO ISOTOPE RESEARCH

A PROTRACTED ARCHEAN HISTORY IN THE WATERSMEET GNEISS DOME, NORTHERN MICHIGAN

Chapter F

By ZELL E. PETERMAN, R. E. ZARTMAN, and P. K. SIMS

CONTENTS

FIGURES

TABLES

Abstract

Uranium-thorium-lead dating of zircon from biotite gneiss in the Watersmeet dome, northern Michigan, adds to the previous data base for Early Archean core rocks in this structural dome that was rejuvenated late in Early Proterozoic time. The new data, together with previously published data on tonalitic augen gneiss, define a chord with intercepts at 3.56 and 1.25 Ga (10^9 years). Zircon from an amphibolite and gneiss unit are dated at 2.64 Ga, establishing the presence of a volcanic sequence that onlapped the older gneiss terrane during the Late Archean. Consideration of the geologic history and discordia relations for all the zircons suggests that the observed systematics stem from multiple episodes of lead loss. Zircons from Early Archean gneisses are composed of two compositionally distinct domains that are present in oscillatory zones and as chaotic mixtures of the two. One phase is essentially stoichiometric zircon ($ZrSiO_4$), and the other is enriched in CaO, U, and Th and may contain about 10 percent H_2O. Discordance patterns probably are related to differential lead loss from these domains. Spurious Th-Pb ages indicate the presence of phases or inclusions in some of the zircons that have preferentially lost thorium relative to ^{208}Pb.

The geochronologic results emphasize the existence of three major rock-forming and tectonic events in this part of the Great Lakes tectonic zone: (1) formation of Early Archean gneisses—3.5 to 3.6 Ga; (2) accretion of the Late Archean volcanic-plutonic belt—2.6 to 2.8 Ga; and (3) reactivation of the Early Archean basement following blanketing by Early Proterozoic supracrustal rocks—1.7 to 1.8 Ga.

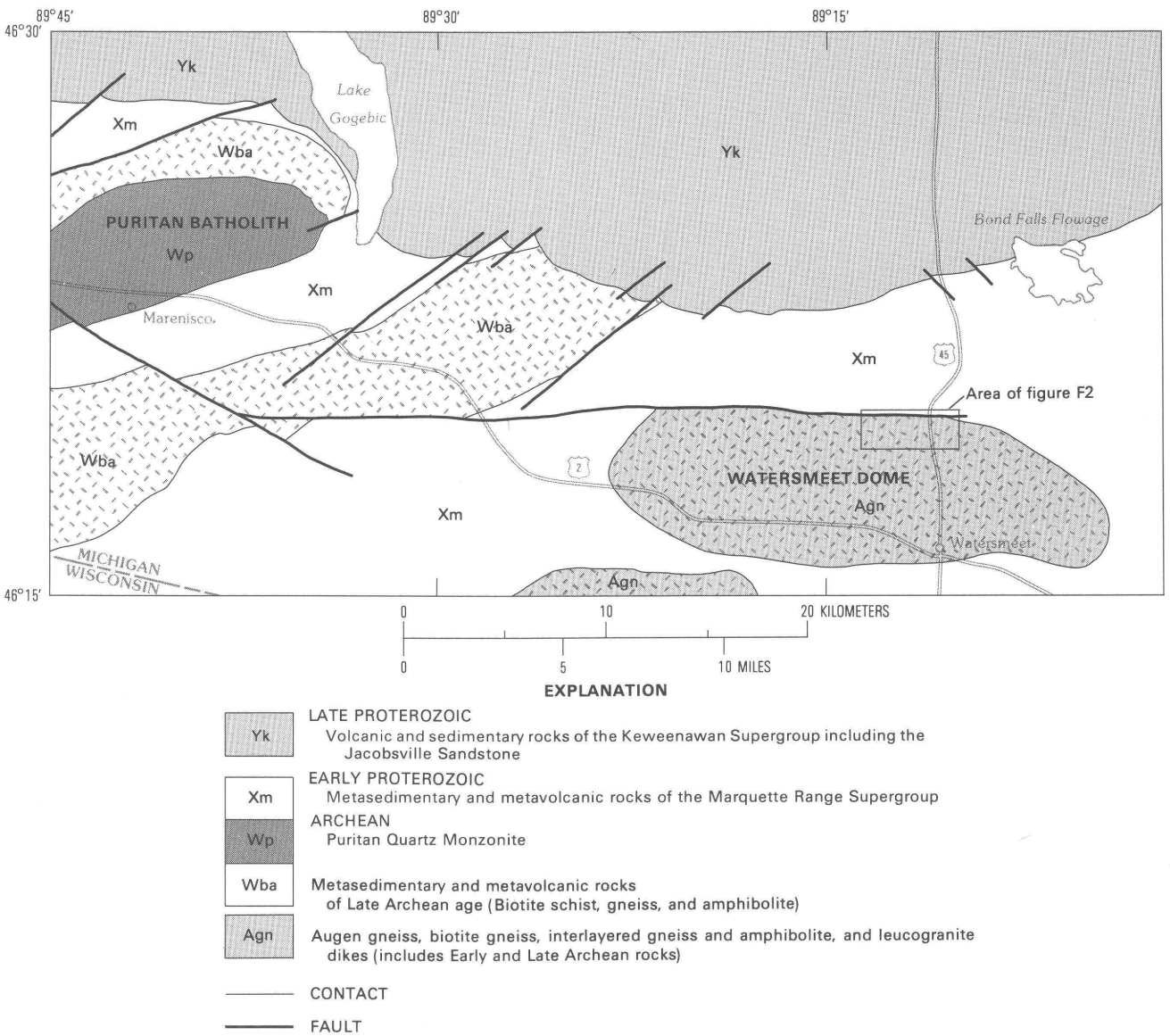

Figure F1. Geologic map of the Marenisco-Watersmeet area, northern Michigan (modified from Sims and others, 1984).

INTRODUCTION

Previous isotopic dating (Peterman and others, 1980) identified an Early Archean gneiss near Watersmeet in the western part of the upper peninsula of Michigan. The gneiss is in the core of a dome that was reactivated during the Penokean orogeny and that is encircled by Early Proterozoic supracrustal rocks—the Marquette Range Supergroup. Late Archean rocks crop out a few kilometers to the northwest of the dome and the intervening area composes the Great Lakes tectonic zone (Sims and others, 1980).

Uraunium-lead (U-Pb) zircon data established a minimum age of 3.4 Ga (3.4×10^9 years) for a polymetamorphosed tonalitic augen gneiss and an age of 2.6 Ga for less deformed leucogranite dikes that intrude the augen gneiss and associated units within the dome (Peterman and others, 1980). The effects of cataclasis and recrystallization that accompanied rejuvenation of the gneiss dome are recorded in Rb-Sr (rubidium-strontium) whole-rock and mineral ages of about 1.75 Ga. Uranium-lead zircon data for the Early Archean gneiss were not readily interpretable in terms of either a single episodic disturbance or continuous diffusion lead-loss model, so that the minimum age of 3.4 Ga was based on the oldest $^{207}Pb/^{206}Pb$ age obtained. Additional isotopic dating of the major units in the Watersmeet dome was undertaken to better understand the discordance patterns exhibited by the U-Pb systems and to explore the possibility of Late Archean depositional overlap on the older gneiss basement during the formation of the Late Archean greenstone-granite belt that is to the northwest.

ACKNOWLEDGMENTS

The following people are gratefully acknowledged: G. T. Cebula for sample preparation, Ralph Christian for the microprobe analyses and back-scatter photographs, S. S. Goldich for abrading the zircon from sample M83, and Loretta Kwak for the analytical work. The technical reviews of John Aleinikoff and Kenneth Ludwig were helpful.

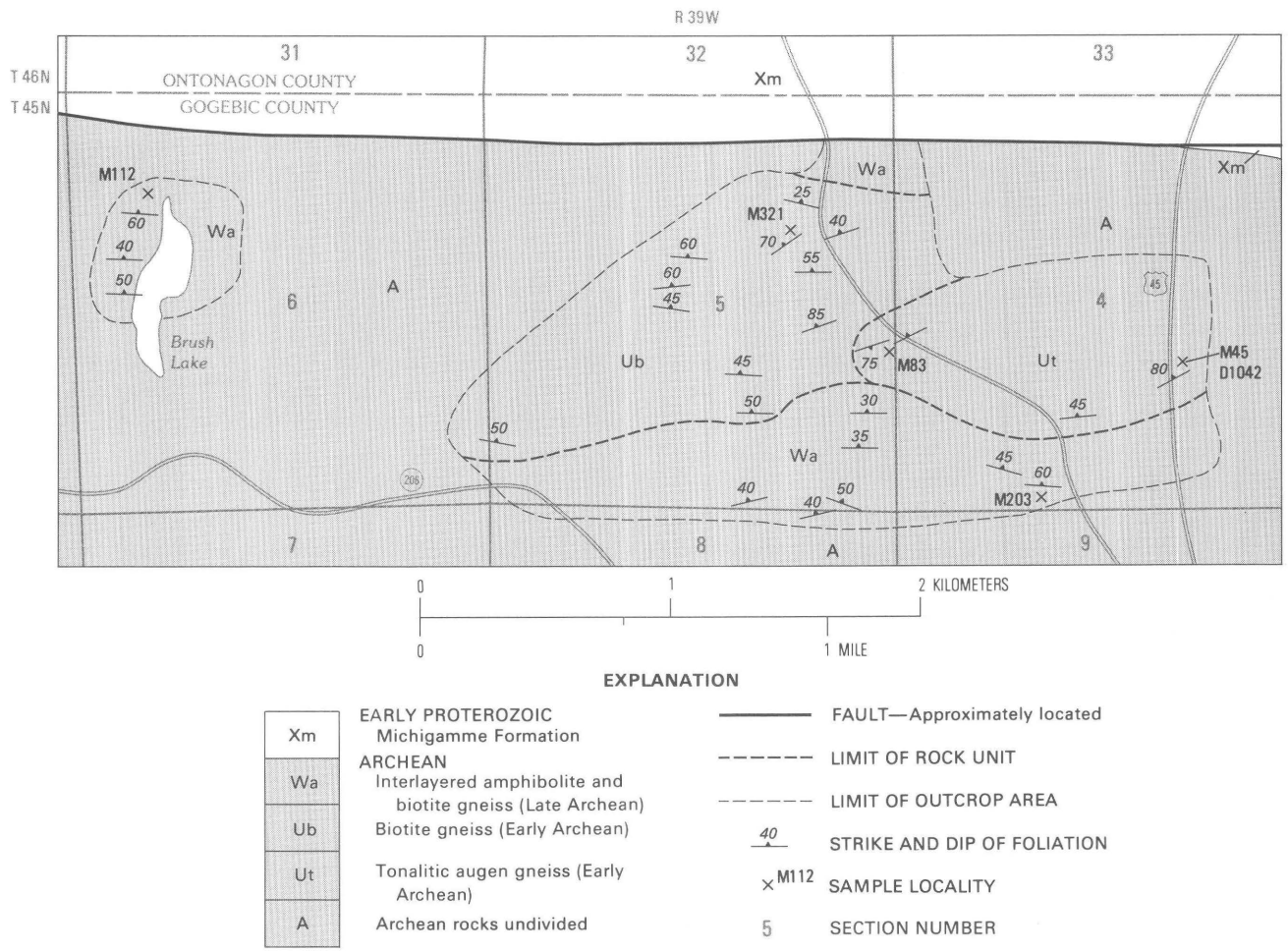

Figure F2. Geologic map of the northern part of the Watersmeet dome showing the distribution of the major lithologic units and the localities of samples (modified from Sims and others, 1984).

GEOLOGIC FRAMEWORK

The geology of the Marenisco-Watersmeet area (fig. F1) represents a remarkably long and complex Archean and Proterozoic history, and coordinated field and laboratory studies have established a chronologic framework of rock-forming, tectonic, and metamorphic events that span at least 2.5 Ga of Precambrian time. Gneiss in the Watersmeet dome is part of an Early Archean sialic crust that is extensive in the Lake Superior region (Sims, 1980). Late Archean greenstone-granite terranes formed marginal to this gneiss terrane in northern Minnesota and northern Michigan about 2.7 Ga. In the Marenisco-Watersmeet area (fig. F1), the Late Archean units are metasedimentary and metavolcanic rocks that are intruded by the 2.65-Ga Puritan Quartz Monzonite (Sims and others, 1977).

In Early Proterozoic time, the composite basement of Early and Late Archean rocks was covered by extensive sedimentary and volcanic strata of the Marquette Range Supergroup, which subsequently were folded and metamorphosed during the Penokean orogeny (about 1.8 Ga). Metamorphism and penetrative deformation during this event increased in intensity from the northwest to the southeast in the area (fig. F1). Locally, the older gneiss basement rose diapirically to penetrate the overlying supracrustal rocks. This deformation also produced two major antiformal folds in the central and northwestern part of the area with cores of Late Archean basement rocks. In Middle Proterozoic time, the region was covered by sedimentary and volcanic rocks of the 1.1–Ga Keweenawan Supergroup.

In this report we are concerned primarily with the Archean units in the Watersmeet dome (fig. F2), and the history of these units during the formation of the Late Archean greenstone-granite belt to the northwest of the dome. Some depositional overlap of Late Archean rocks on the gneiss basement is inferred from field relations (Sims, 1980; Sims and others, 1980). However, much of the evidence of such overlap and of the structural fabric that may have been imposed on the older gneisses during the Late Archean event has been more or less obscured by penetrative deformation and metamorphism that accompanied the Penokean orogeny.

Late Archean igneous activity is known to have extended into the gneiss terrane where it is manifested in the dome by the 2.6-Ga leucogranite dikes. Small bodies of granite northwest of the dome, previously called the granite near Thayer, are now interpreted on the basis of lithologic correlation to be satellite bodies of the main mass of Puritan Quartz Monzonite. Tonalite gneiss originally included with the granite near Thayer and dated at 2.75 Ga (sample M147, Peterman and others, 1980) is interlayered with amphibolite, forming a bimodal suite of gneiss that is thought to be of volcanic origin.

Field studies in the Watersmeet dome (Sims and others, 1984) have delineated two major lithologic units in addition to the augen gneiss and the leucogranite dikes (fig. F2). Biotite gneiss crops out over an area of about one-half square mile just west of the main body of augen gneiss. Foliation and layering in this unit dip moderately to steeply to the north. The unit consists mainly of alternating thinly banded (on a scale of a few millimeters to a few centimeters) and massive biotite gneiss (layers of a meter or more thick). Interlayered amphibolite and biotite gneiss constitute the second unit which crops out to the north and south of the belt of biotite gneiss and augen gneiss and at Brush Lake to the west (fig. F2). A minor but distinctive unit of very fine grained biotite schist is present as thin, elongate but discontinuous, interlayers in the biotite gneiss. All these units are cut by leucogranite dikes.

GEOCHRONOLOGY

Data for uranium-thorium-lead (table F1) were obtained following a method modified from Krogh (1973) of HF dissolution in teflon-lined bombs. Analytical uncertainties (1 sigma) are estimated to be about ± 0.7 percent for parent-daughter ratios and ± 0.05 percent for the measured $^{207}Pb/^{206}Pb$. Isotope ratios and decay constants used in the age calculations are those recommended by the International Union of Geological Sciences Subcommission on Geochronology (Steiger and Jäger, 1977).

Samples and Zircons

Samples of about 15 kg (kilograms) were collected from the biotite gneiss and schist unit and the amphibolite and biotite gneiss unit in the Watersmeet dome (fig. F2). Sample M321 is from an outcrop of thin- to thick-banded biotite gneiss that has interlayers of fine-grained biotite schist. In hand specimen, M321 is strongly banded with thin, discontinuous leucocratic layers alternating with biotite-rich layers that range in width from a few millimeters to a centimeter or more. Sample M203 is from the biotite gneiss component of the amphibolite and biotite gneiss unit. The sample is a medium-grained biotite gneiss but has thin layers of hornblende-rich gneiss.

Zircons were separated using a shaking table, heavy liquids, and a magnetic separator. Concentrates were sized on silk screens and final purification of splits (1–7 mg (milligrams)) for isotopic analyses was done by hand picking. Clerici solution was not used in any of the steps because of the previously observed difficulty of removing this material even by acid leaching from highly fractured zircons.

Table F1. Uranium, thorium, and lead data for zircons

[Numbers in brackets are screen sizes for the fractions. NM, nonmagnetic fractions; ABR, abraded fraction; FLUX indicates sample decomposed by flux technique. Data for sample M83(100–150) are from Peterman and others (1980) and are included here for comparison with data for sample M83(100–150)ABR. Isotopic composition of initial lead (Stacey and Kramers, 1975) is assumed to be $^{204}Pb:^{206}Pb:^{207}Pb:^{208}Pb = 1:11.42:13.25:31.45$ for M83 and M321 series and 1:13.64:14.69:33.37 for M203 series]

	Concentration (parts per million)			Isotopic composition of lead (atom percent)				Atom ratio (age, in 10^6 years)			
Sample No.	U	Th	Pb	^{204}Pb	^{206}Pb	^{207}Pb	^{208}Pb	$\frac{^{206}Pb}{^{233}U}$	$\frac{^{207}Pb}{^{235}U}$	$\frac{^{207}Pb}{^{206}Pb}$	$\frac{^{208}Pb}{^{232}Th}$
M203:											
(100–150)	773.4	215.7	342.0	0.075	74.79	13.58	11.56	0.3790 [2071]	8.8351 [2321]	0.1691 [2549]	0.1614 [3024]
(200–250)	607.5	204.9	303.1	0.044	75.851	13.68	10.43	0.4363 [2334]	10.4233 [2473]	0.1733 [2589]	0.1493 [2812]
(200–250)NM	546.8	189.2	279.1	0.015	77.53	13.86	8.59	0.4588 [2434]	11.1564 [2536]	0.1763 [2619]	0.1343 [2547]
M321:											
(+100)	1680.5	294.7	692.2	0.085	71.10	15.47	13.34	0.3356 [1865]	9.4581 [2384]	0.2044 [2862]	0.2816 [5015]
(200–250)	1289.5	359.3	686.1	0.080	68.50	17.76	13.66	0.4176 [2250]	14.2240 [2765]	0.2470 [3166]	0.2391 [4333]
(200–250)FLUX	1288.7	403.3	692.0	0.091	67.99	17.41	14.51	0.4176 [2249]	13.9310 [2745]	0.2420 [3133]	0.2246 [4095]
(200–250)NM	1162.3	375.2	705.7	0.046	71.46	19.81	8.69	0.5003 [2615]	18.6684 [3025]	0.2706 [3310]	0.1529 [2878]
(–400)	1209.5	544.7	580.7	0.086	69.46	16.09	14.36	0.3818 [2085]	11.4928 [2564]	0.2183 [2968]	0.1396 [2641]
M83:											
(100–150)	520.2	170.2	347.8	0.010	71.06	20.63	8.30	0.5511 [2830]	21.9498 [3182]	0.2889 [3412]	0.1834 [3404]
(100–150)ABR	516.1	203.4	398.2	0.008	70.32	21.04	8.63	0.6294 [3147]	25.8702 [3342]	0.2981 [3460]	0.1844 [3422]

Zircons from sample M321 closely resemble those from the tonalitic augen gneiss (samples D1042 and M83, Peterman and others, 1980) in shape, crystal-face development, internal structure, and color. They are amber to dark brown and have relatively simple prismatic and pyramidal faces. Fine-scale zoning parallels the principal crystal faces. Euhedral apatite inclusions are present, fractures are common, and many grains have zones with disseminated fine opaque inclusions.

A split of the 200–250 mesh fraction of sample M321 was examined under the electron microprobe, revealing the presence of two distinctive phases that are present both as sharply bounded zones and in domains in which the two types form a chaotic microbreccia, usually in the centers of the grains. In back-scatter radiation images, these phases appear as light and dark domains (fig. F3). Microprobe analyses (table F2) indicate that the light phase is uniform in composition, low in trace elements, and is essentially stoichiometric zircon in which the major oxides sum to 100 percent. The dark phase is more complex compositionally and contains an additional 9–10 percent of undetermined elements. Nothing was detected with the energy dispersive system in sufficient concentration to account for this deficit. The proportions of Zr:Hf:Si are nearly the same in both phases, but the dark phase contains appreciable Ca. In this phase, the P_2O_5 content is insufficient to explain the Ca as being contained in apatite inclusions or intergrowths. Thorium and uranium were not detected in the light phase (detection limit is about 0.03 percent UO_2 and 0.07 percent ThO_2). These elements are present in variable amounts in the dark phase, ranging from below the detection limit to 0.48 percent ThO_2 and to 0.33 percent UO_2, with average values of 0.11 and 0.21, respectively. The sharply defined zones of light and dark phases (fig. F3) correspond to the well-developed zoning seen in transmitted

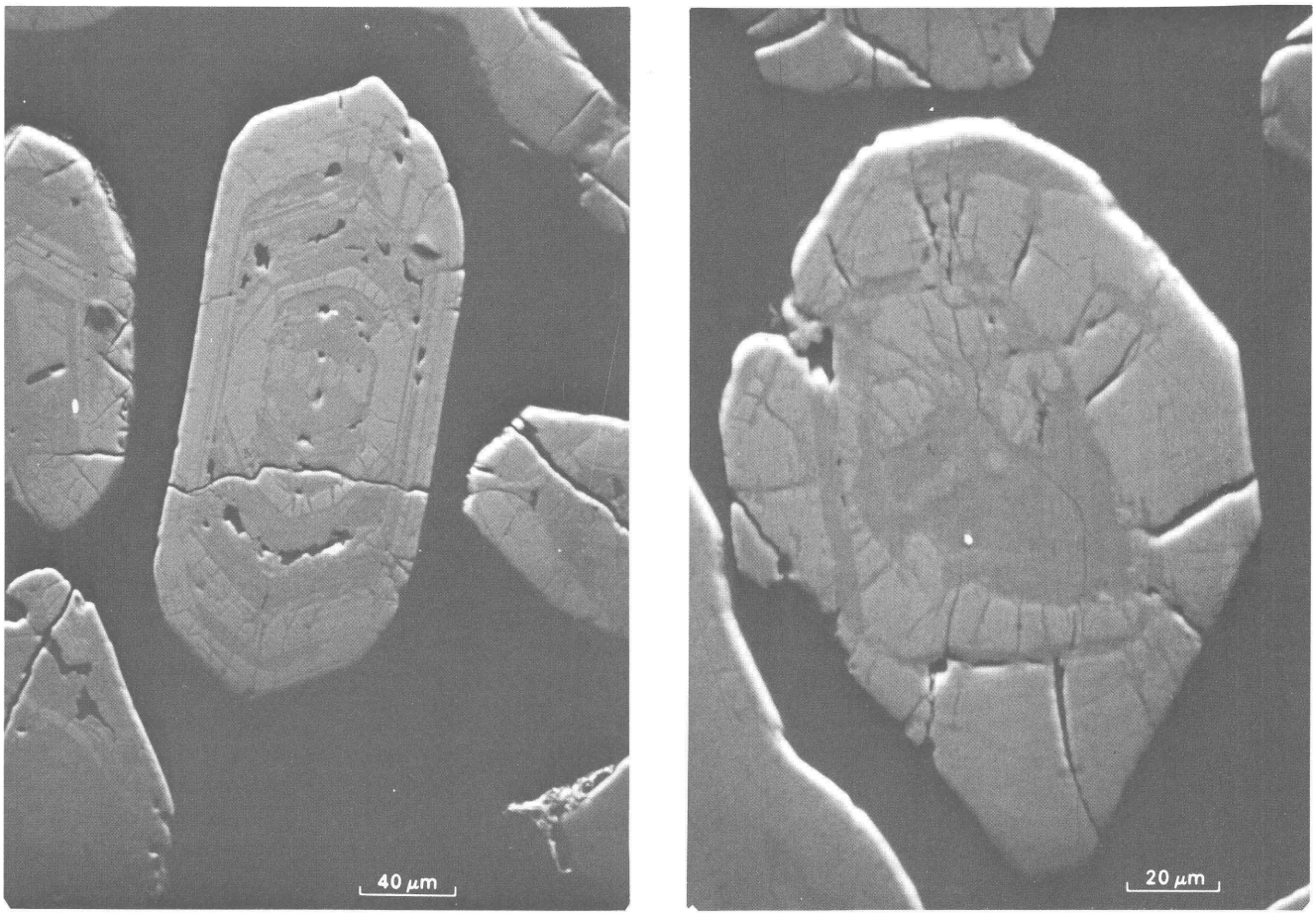

Figure F3. Back-scatter radiation photographs of zircons from sample M321(200–250 mesh fraction). The "light" and "dark" zones correspond to the phases indicated in table F2.

light. The chaotic domains appear as turbid zones in plane light and have uniform but speckled interference colors under crossed nicols.

Some grains from sample M321 show radiating fractures emanating from their cores. Many of these fractures are filled with the dark phase in continuity with the dark phase in the regular zones and in the chaotic milieu. This feature gives the impression of expansion of the dark phase producing fracturing and then infilling of this material in the fractures. The fractures could have resulted from hydration and expansion of the dark phase, which also would account for the missing 9–10 percent in the analyses (table F2). Hydrated phases in zircons are common (see Speer, 1980), and Sommerauer (1979) has observed that the nonstoichiometric phases of complex zircons may contain as much as 10 percent H_2O.

Zircons from sample M203 are lighter in color, optically more uniform, and generally appear to be less degraded than those from sample M321. They show simple prismatic and pyramidal faces but are more elongate, on the average, than the M321 zircons. Fine zoning is present and all the grains have abundant fractures. Back-scatter

Table F2. Microprobe analyses for light and dark phases of zircon from the magnetic 200–250 mesh fraction of sample M321(200–250)M

[Minimum detection limit for minor elements is about 0.05 percent]

Oxide	Light phase (3 analyses)	Dark phase (8 analyses)
SiO_2	32.4	29.0
ZrO_2	66.0	56.5
HfO_2	1.03	1.08
UO_2	0.00	0.21
ThO_2	0.00	0.11
CaO	0.00	1.85
P_2O_5	0.01	0.14
Y_2O_3	0.28	0.79
La_2O_3	0.08	0.08
Ce_2O_3	0.00	0.14
Sum-------	99.8	89.9

radiation images show no evidence of compositional zoning or the presence of distinct domains. In polarized light, the zircons are characterized by uniform high birefringence throughout the grains. Euhedral apatite inclusions are common.

Compositionally distinct domains or zones within zircons are of particular interest because of the implications to the discordance mechanism in the U-Th-Pb systems (see summaries of pertinent literature by Speer, 1980; Gebauer and Grunenfelder, 1979). Generally, the less pure phases are higher in uranium, have greater magnetic susceptibilities, and yield more discordant ages than the stoichiometric phases.

Results

Data for samples M203 and M321 are plotted with data for previously analyzed samples on figures F4 and F5, respectively. Three fractions of M203 are alined along a chord with intercepts at 2.64 and 0.63 Ga. These data clearly place the amphibolite and biotite gneiss unit in the Late Archean with the leucogranite (sample M45) and the bimodal gneisses (sample M147) northwest of the dome. Sample M112 (fig. F4) is also from the amphibolite and biotite gneiss unit (fig. F4), but the data point departs considerably from the chord defined by sample M203. For all three of these arrays, we are omitting the statistical uncertainties derived from the regression calculations. Because of the small sample population and the scatter in excess of analytical error, the statistical uncertainties are magnified to the extent that they have little geologic significance. As will be developed later, the scatter, including the deviation of sample M112, probably is related to the Early Proterozoic event at about 1.8 Ga reflected in the Rb-Sr ages, and, locally, in totally reset zircon ages (Peterman and others, 1980).

Data for size and magnetic fractions of sample M321 (fig. F5) establish the biotite gneiss and schist unit as Early Archean and indistinguishable in age from the tonalitic augen gneiss. Excluding sample M83 (200–270)NM, data for both units define a chord with intercepts at 3.56 ± 0.04 and 1.25 ± 0.09 Ga using Ludwig's (1982) regression program. Excessive scatter of the points is indicated by an MSWD (mean square of the weighted deviates) of 24.

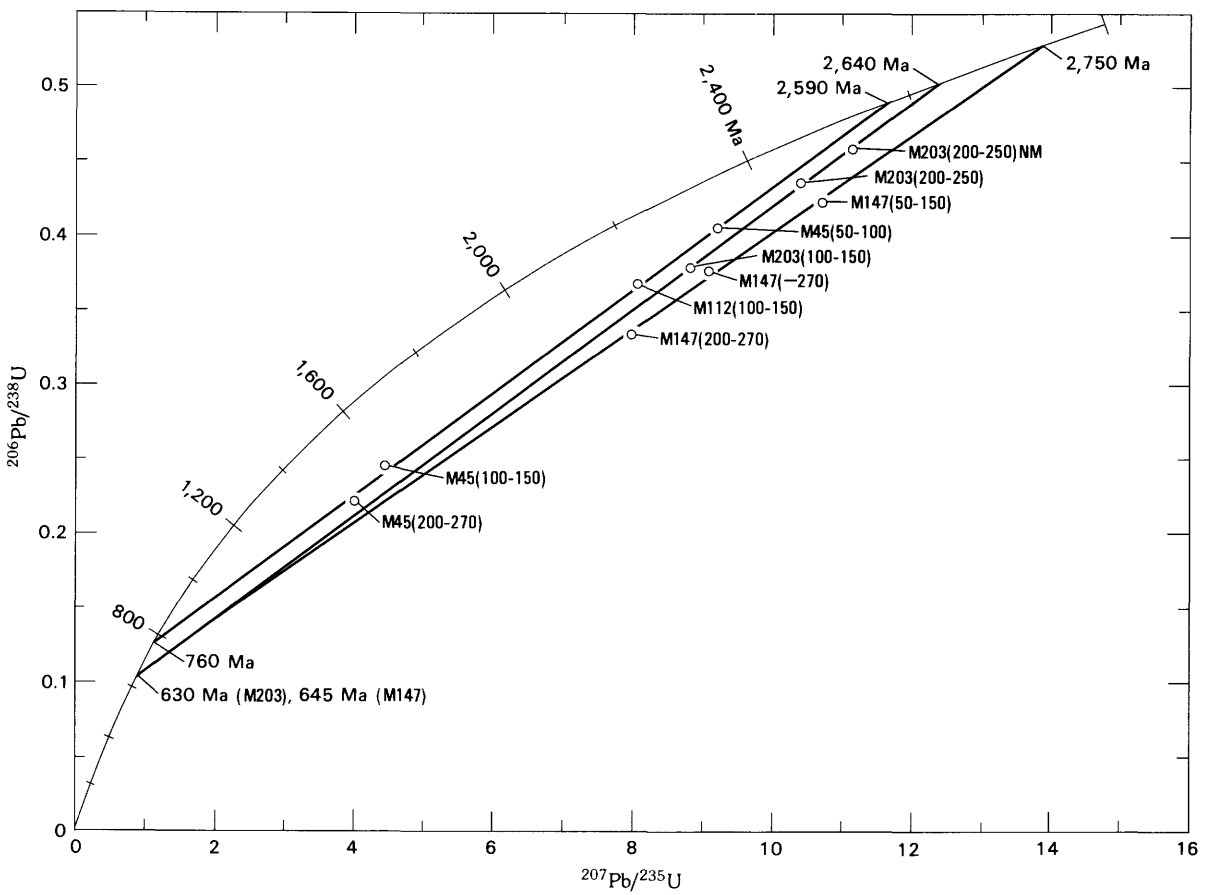

Figure F4. Uranium-lead concordia plot for zircons from Late Archean rocks. Data for samples M45 (leucogranite), M112 (amphibolite and gneiss unit), and M147 (bimodal gneiss unit) are from Peterman and others (1980). Mesh-size fraction of sample is indicated in parentheses. NM, nonmagnetic fraction.

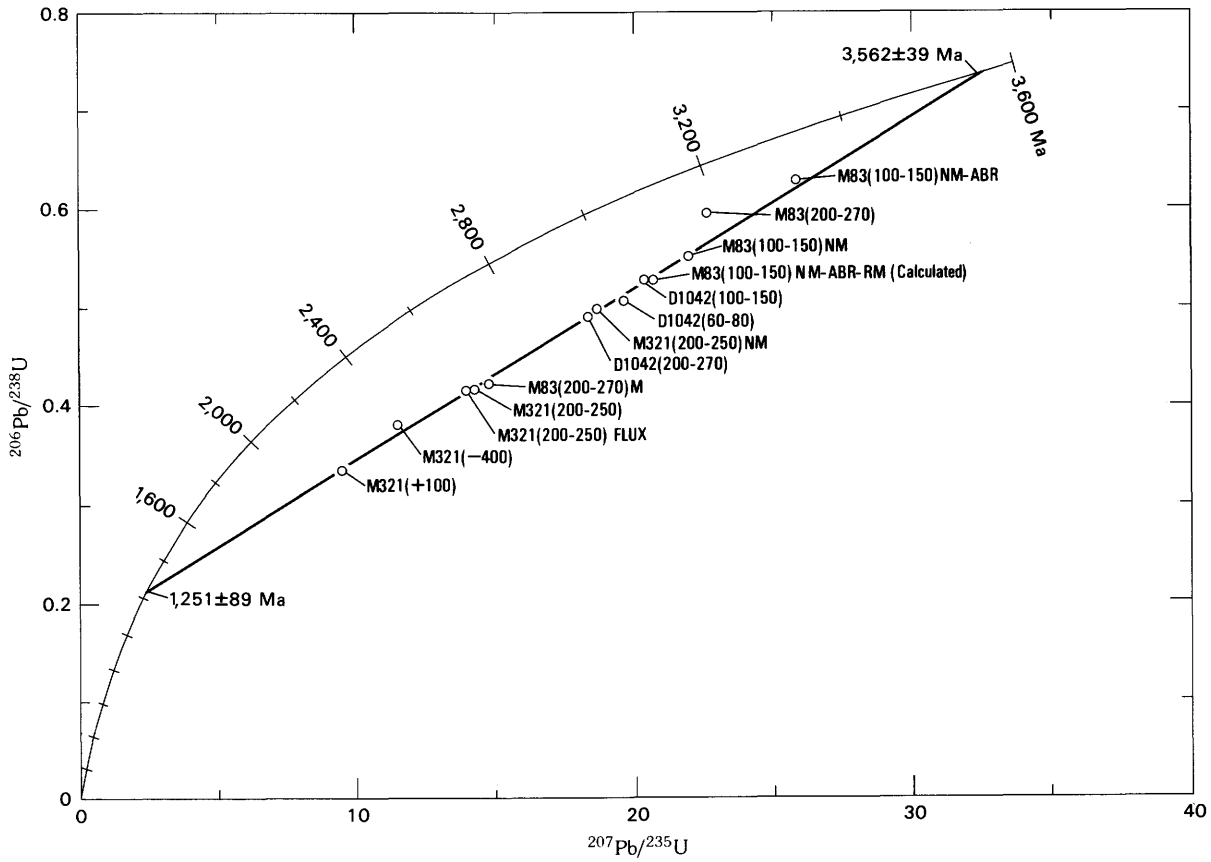

Figure F5. Uranium-lead concordia plot for zircons from Early Archean gneisses of the Watersmeet dome. Sample M321, biotite gneiss; samples M83, D1042, augen gneiss. Except for M83 (100–150)ABR, data are from this paper (table F1) and from Peterman and others (1980). Mesh-size fraction of sample is indicated in parentheses. NM, nomagnetic; ABR, abraded; FLUX, sample decomposed by flux technique.

Sample M83 (100–150)NM-ABR was prepared by mechanically abrading (for example, Krogh, 1982) a split of a previously analyzed sample (table F1) to remove less competent and metamict material or outer zones that may have been enriched in uranium. A 6.7-mg sample was abraded for 20 minutes in a diamond-lined sphere-former, and 1.6 mg of zircon was recovered for analysis. The procedure resulted in fragmentation of most of the crystals and substantial rounding of these fragments. A few survived as whole crystals but these were strongly frosted and corners were rounded.

As shown by the position of the two points on figure F5, the abrading process removed material that was more discordant than the initial fraction. The higher U-Pb ages in the abraded material result from greater amounts of radiogenic ^{206}Pb and ^{207}Pb. The higher ^{208}Pb is compensated by a higher thorium content, with the net result that the Th-Pb ages are nearly the same before and after abrading. The location of the material removed during the abrading is calculated and is shown on figure F5.

These results suggest that the original fraction of sample M83 (100–150)NM contained grains or phases within grains with discrete $^{207}Pb/^{206}Pb$. Insofar as can be determined within the errors, these phases would have been alined along the 3.56- to 1.25-Ga chord. The results of this experiment contrast with those obtained in a leaching study previously done on a split of the same sample (Peterman and others, 1980). The zircons were given a mild wash in HCl and HNO_3 followed by partial dissolution in HF at atmospheric pressure. The radiogenic $^{207}Pb/^{206}Pb$ were found to be little changed in the leachates and residual material although a slight reverse discordance was induced in the residue from HF leaching and the uranium and thorium contents were substantially lower in the residue.

The zircon data for the Early Archean units show the commonly observed relation between discordance and uranium content as illustrated in figure F6. A similar pattern exists for the Late Archean zircons (not shown). Departure of the points from the 3.6–Ga isochron is in the direction of ^{238}U gain or ^{206}Pb loss. The lowest value data point near the isochron is the HF-leached residue of sample M83 (100–150)NM (Peterman and others, 1980). Development of this pattern through gain of ^{238}U

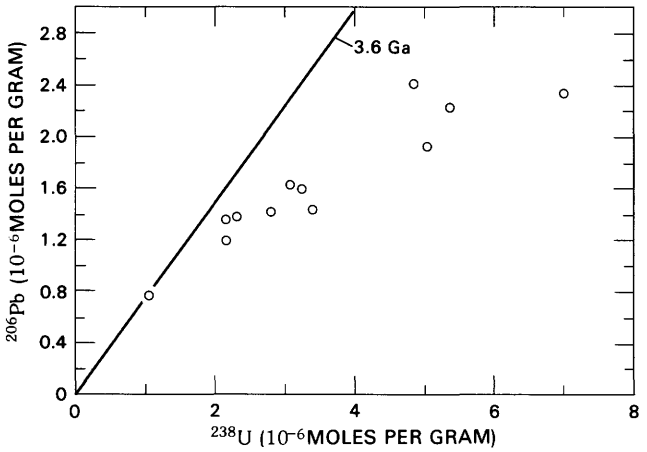

Figure F6. ^{206}Pb versus ^{238}U for zircons from Early Archean gneisses. Data are from this paper (table F1) and from Peterman and others (1980). A 3.6-Ga isochron is shown for reference. The departure of points from the isochron can be explained by loss of ^{206}Pb in approximate proportion to the ^{238}U content.

would require an addition in an amount roughly proportional to that originally present. More likely, the pattern has resulted from loss of ^{206}Pb as a consequence of radiation damage that is proportional to the amount of ^{238}U, although some degree of uranium mobility cannot be ruled out. The general trend of the data array with the nearly condordant value for the HF-leached sample suggests that there may be a "threshold" concentration of uranium of about $1\text{–}2\times10^{-6}$ moles per gram of ^{238}U below which the zircons would have remained closed in spite of multiple thermal events later in their history.

Uranium-Lead Discordance Patterns

The discordance patterns shown by data for the various rock types (figs. F4 and F5) cannot be explained by one-event episodic or continuous diffusion models of lead loss, because all the suites show excessive scatter greater than analytical error and the lower intercepts are not consistent with either of these models. Zircons from the Late Archean units are disposed about chords with lower intercepts in the interval of 0.7 ± 0.1 Ga, whereas the chord for the Early Archean zircons intersects concordia at 1.25 ± 0.09 Ga. The latter age might be attributed to discordance imposed during an early phase of Keweenawan activity, but this is special pleading and does not explain the intercept of the Late Archean arrays. Extrapolation of the near-linear interval of Tilton's (1960) continuous diffusion curve from a primary age of 2.65 Ga would intersect concordia at 0.58 Ga, which is compatible with the value of 0.7 ± 0.1 for the Late Archean arrays. However, extrapolation from a primary age of 3.60 Ga gives a lower intercept of 0.85 Ga, clearly lower than the value for the Early Archean zircons. Extension of radiation-damage dependent curves (Wasserburg, 1963) would intersect concordia at even lower values.

In the ensuing discussion we will consider the effects of discordance produced by multiple disturbances. This will be done in the context of the known geologic framework as deduced from the field relations and the isotopic age data. Systematic lead loss or uranium gain during multiple disturbances can produce spurious chords with upper and lower intercepts that may not correspond to the ages of any of the events (see Gebauer and Grunenfelder, 1979).

All the rock units have had the same post-Archean history except in local zones of high strain. In addition, the Early Archean gneisses were deformed and metamorphosed during the Late Archean event. In considering a multiepisodic model for the Watersmeet zircons, we will set the primary age and the time of disturbances, and consider the effects of varying degrees of discordance imposed during these events. Data other than the upper intercept of the chord (fig. F5) indicate that the Early Archean gneisses are about 3.5–3.6 Ga. A firm minimum age of 3.46 Ga is provided by the least discordant fraction of sample M83 (table F1). Samarium-neodymium model ages, recalculated to revised chondrite constants of Jacobsen and Wasserburg (1980) are as follows: 3.50 Ga for augen gneiss sample D1042 (McCulloch and Wasserburg (1980); and 3.78 Ga for augen gneiss sample M83 and 3.43 for biotite gneiss sample D1395 (Futa, 1981). A lutetium-hafnium model age of 3.51 Ga is reported by Patchett and others (1981) for a fraction of M83 zircon. Collectively, these numbers suggest that the primary age of the gneisses is probably close to the upper concordia intercept of 3.56 Ga (fig. F5).

The Late Archean event corresponds to the formation of the greenstone-granite belt northwest of the dome, intrusion of the Puritan Quartz Monzonite and satellite bodies at about 2.65 Ga, and deformation and metamorphism. Relict mineral assemblages in Late Archean metagraywackes immediately north of the dome indicate that that metamorphic event was at amphibolite grade (Sims and others, 1984). The major thermotectonic event at 1.7–1.8 Ga, attendant with formation of the dome, is recorded in whole-rock and mineral Rb-Sr ages and by concordant zircon of 1.76 Ga from strongly cataclasized gneiss at the western end of the dome (Peterman and others, 1980). This event also was at amphibolite grade. The timing of more recent lead loss, as required by the zircon arrays, is more difficult to establish. The last regional uplift and cooling of the terrane was at about 0.5 Ga as indicated by apatite fission-track ages (R. Zimmermann, oral commun., 1980). We will assume that lead was lost at this time, perhaps related to a dilation process (Goldich and Mudrey, 1972).

The effects of multiepisodic lead loss on zircon arrays are discussed by Wetherill (1956, 1963), Allegre and

others (1974), and Aftalion and van Breeman (1980). If near-linear arrays are produced by multiple events, the discordance imposed on a particular sample during one event must be related in some systematic fashion to that imposed during earlier or later events. Discordancy is expressed by the term $R=(D/P)_a/(D/P)_b$ where D and P refer to daughter and parent isotopes, and a and b refer to immediately after and immediately before the event, respectively. One method of relating R's is $R_1=R_2^x=R_3^y$ . . . where the subscripts, 1, 2, and 3 . . ., are sequential events and x and y are exponents that describe the discordance relations.

In evaluating the multiepisodic model for the Early Archean units, we assign the following values for the primary age and the subsequent events: $T_o=3.60$ Ga, $T_1=2.70$ Ga, $T_2=1.76$ Ga, and $T_3=0.50$ Ga. In estimating relations between R_1, R_2, and R_3, we note the correlation between uranium content and degree of discordance (fig. F6). The time intervals of T_o–T_1 and T_1–T_2 are of nearly the same duration. By assuming similar intensities of events at T_1 and T_2 and by ignoring slightly greater radiation doses in the interval T_o–T_1, we will define the relation of lead loss simply as $R_1=R_2$. To complete the exercise, R_3 is defined in terms of R_1 and R_2 for three different cases:

Case 1: $R_1=R_2=R_3$
Case 2: $R_1=R_2=R_3^2$
Case 3: $R_1=R_2=R_3^{0.5}$

The trajectories for these three cases are shown on figure F7 with the data points for the zircons. Most of the points are in a zone bounded by curves for case 1 and case 2, and, within the range of the data set, the curvatures of these trajectories are relatively slight. Data for the zircons from Late Archean rocks also can be explained by this model for which T_o ranges from 2.60 to 2.80 Ga with T_1 at 1.76 Ga and T_2 at 0.50 Ga. These arrays are best explained by a case 1 calculation in which $R_1=R_2$. Although not constituting proof, these calculations show that the present disposition of zircon data for these rocks is consistent with having evolved through multiple episodes of lead loss in a fairly systematic fashion, and

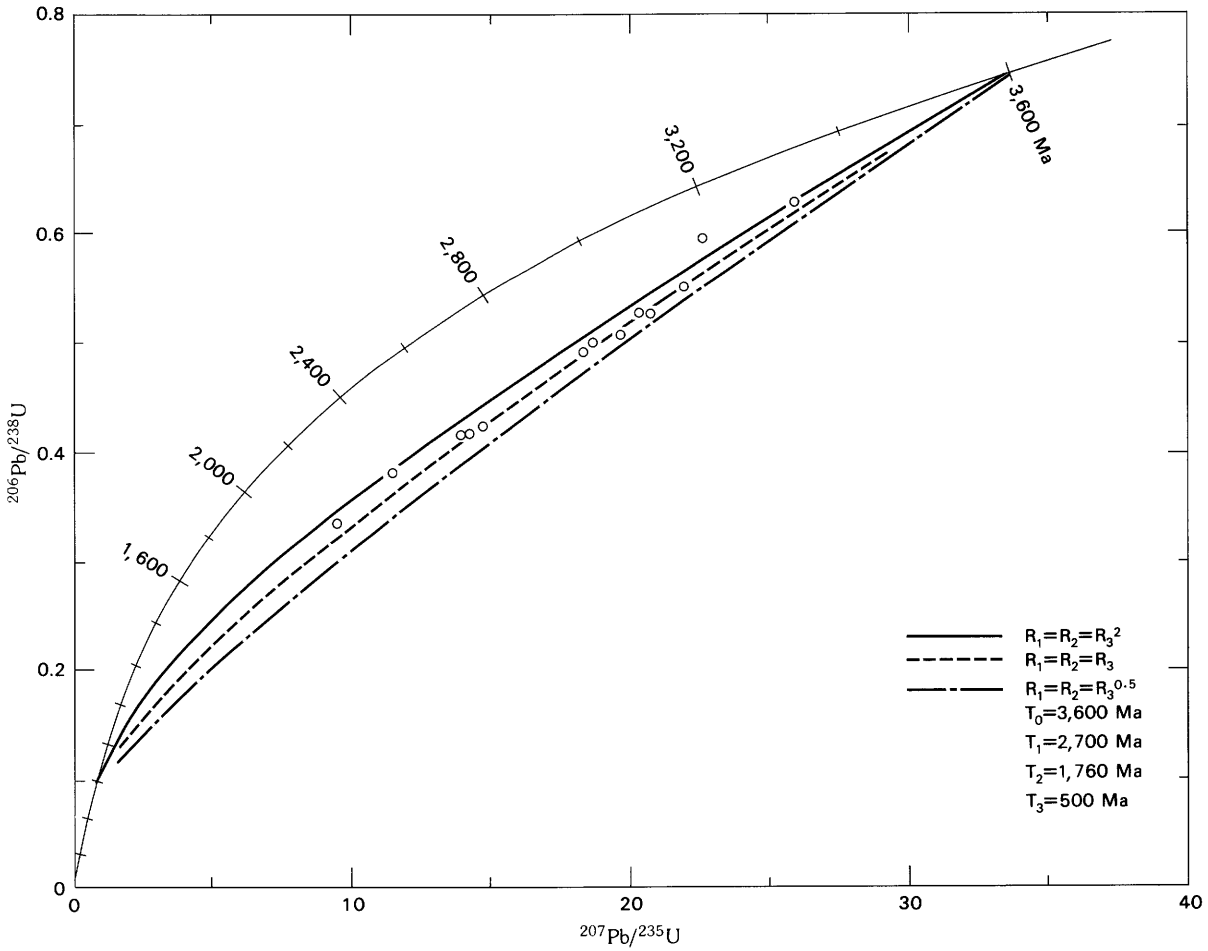

Figure F7. Calculated trajectories for multiepisodic lead loss as discussed in the text.

that the different lower intercepts can be explained by this mechanism.

Thorium-Lead Anomalies

Several Th-Pb ages previously reported (Peterman and others, 1980) are remarkably close to the $^{207}Pb/^{206}Pb$ ages, rather than to the $^{206}Pb/^{238}U$ ages as would be expected by nonfractionating lead loss from one-phase systems (Steiger and Wasserburg, 1966). These ages now appear to represent a general anomaly in the Th-Pb systems further illustrated by spurious ages (impossibly old) for two fractions each of samples M321 and M203 (table F1).

The Th-Pb anomaly was first detected in sample M321 (200–250) which gave an apparent Th-Pb age of 4.33 Ga. A second hand-picked part of this sample was reanalyzed using the older flux method in case some phase was not completely decomposed in the bomb with HF. The uranium and uranogenic-lead contents agree within errors in both splits (table F1). The thorium content of the fluxed sample is higher, but the ^{208}Pb content also is higher, with the net result that the Th-Pb age still is anomalously high although slightly lower, at 4.10 Ga. Because of the small size of the samples used, their exact identity cannot be verified even though the uranium-lead results reproduced adequately. The differences in the thorium-lead results are, therefore, attributed to inhomogeneous distribution of thorium and ^{208}Pb in the two splits, rather than to analytical problems with the bomb decomposition. These anomalous Th-Pb ages prompted the microprobe analyses, described earlier, to search for a thorium-rich phase in the zircons. No thorium "hot spots" were found, although thorium seems to be variably enriched in the nonstoichiometric phase of sample M321 (table F2).

Several lines of evidence indicate that the spurious Th-Pb ages are related to phases or inclusions within the zircons. The presence of discrete grain impurities in the separates is ruled out, as the separates used for analyses were hand-picked, acid-washed, and then checked again for purity. Also, the magnitude of the thorium-age "anomaly" correlates with physical and magnetic properties of the separates. For example, the difference between the Th-Pb and the $^{206}Pb/^{238}U$ ages increases with increasing magnetic susceptibility for samples where such data exist—M83 (200–270), M321 (200–250), and M203 (200–250)—with the Th-Pb age always being the greater of the two. Abrading of sample M83 (100–150)NM significantly reduced the difference in these two ages suggesting that the suspect phase is contained in the physically less-competent material. Leaching of this fraction with HCl and HNO_3 removed unsupported ^{208}Pb, although the total mass removed was quite small (Peterman and others, 1980).

Microcline from sample M321 was analyzed to determine if excess ^{208}Pb may have been present in the rock during the 1.7– to 1.8–Ga metamorphism and recrystallization. The results are:

U (ppm)=0.27 $^{206}Pb/^{204}Pb$=16.947 (16.831)
Th (ppm)=0.86 $^{207}Pb/^{204}Pb$=16.210 (16.198)
Pb (ppm)=44.3 $^{208}Pb/^{204}Pb$=36.485 (36.373)

The numbers in parentheses are the lead-isotope ratios corrected for growth of radiogenic lead since 1.76 Ga, the time of metamorphism indicated by concordant zircon from sample M48 (Peterman and others, 1980). These data show that the lead in the feldspar equilibrated, partially or totally, with the rock-reservoir lead in the Early Proterozoic.

Although the $^{208}Pb/^{204}Pb$ in the feldspar is substantially higher than that assumed (31.45) for making common lead corrections on the zircon data, the effect on the $^{232}Th/^{208}Pb$ ages is relatively small and is insufficient to explain the spurious values by equilibration with a high ^{208}Pb-reservoir at 1.7–1.8 Ga or earlier.

Collectively, these observations suggest that phases or inclusions in the zircons have preferentially lost thorium relative to ^{208}Pb during one or more of the events that disturbed the U-Pb systems. The amount of thorium loss for some samples is considerable. For example, sample M321(+100) with a Th-Pb age of 5.02 Ga, would require 586 ppm thorium, in contrast with the actual content of 295 ppm, to support the ^{208}Pb at an age comparable to the $^{206}Pb/^{238}U$ age. Although of considerable interest, we have not pursued this anomaly further.

GEOCHRONOLOGIC IMPLICATIONS

The new data reported here refine the temporal framework for units and events within this part of the Great Lakes tectonic zone. Isotopic ages cluster in intervals of 1.72–1.82 Ga, 2.60–2.75 Ga, and 3.50–3.60 Ga and record the major rock-forming and tectonic events in this zone (fig. F8).

In northern Michigan and adjacent Wisconsin, Early Archean rocks have been identified thus far only in the Watersmeet dome, although the terrane is undoubtedly much more extensive in the sub-Proterozoic basement. Isotopic resolution at 3.5–3.6 Ga is poor because of the effects of multiple thermal and tectonic overprints as well as the simple time magnification of relatively small analytical uncertainties in the determinations. However, the additional zircon data for the biotite gneiss unit (sample M321) in the Watersmeet dome allows a less ambiguous designation of the primary age than was possible previously (Peterman and others, 1980). Even with the likelihood of discordance imposed by multiple episodes of lead

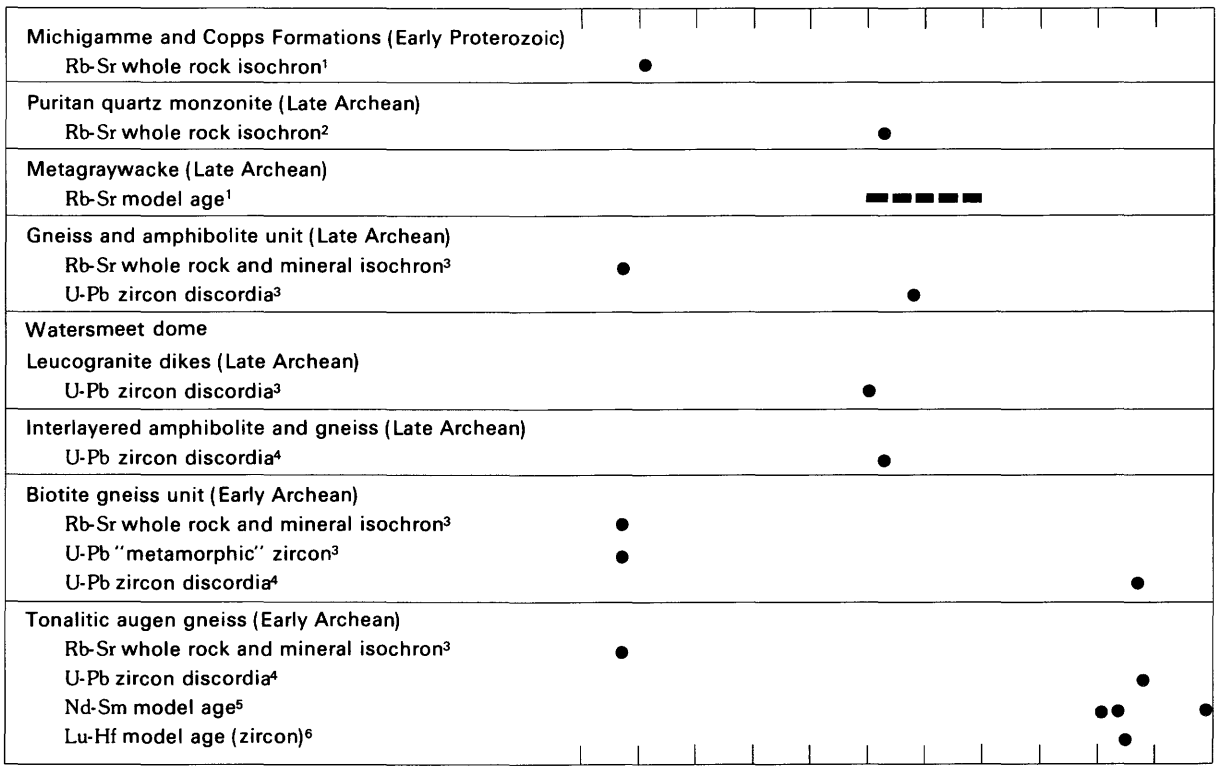

Figure F8. Summary of radiometric ages in the Watersmeet-Marenisco area. The dashed bar indicates the uncertainty in the model age.

loss, as discussed earlier in the paper, we can conclude with some confidence that the age of the augen gneiss and associated biotite gneiss is most likely to be about 3.6 Ga.

Evidence of thermotectonic events in the interval from 3.6 Ga to the Late Archean has not been found. There may have been such events, but their isotopic or lithologic products have been so modified by Late Archean or Early Proterozoic overprinting that they are no longer recognizable, or this Early Archean terrane may indeed have had a long history (about 3.6–2.8 Ga) of thermal and tectonic stability.

The Late Archean event, 2.60–2.75 Ga (fig. F8), was manifested in volcanism, partly submarine, clastic sedimentation in rapidly subsiding troughs, folding and metamorphism, and extensive granitic plutonism. In the Archean rocks southeast of Marenisco (fig. F1), the zircon age of 2.75 Ga represents accumulation of a bimodal sequence of volcanic rocks now metamorphosed to interlayered felsic gneisses and amphibolites. A similar assemblage, but perhaps slightly younger, onlapped the older gneiss terrane, and this unit is dated by zircon from sample M203 at 2.64 Ga. The significance of the apparent age difference between 2.64 and 2.75 Ga depends upon the influence of the 1.76–Ga event on the discordia patterns as previously discussed. Although the apparent concordia-intercept values may be slightly lower than the real ages, the difference between the two rock sequences probably is real. Accumulating data for greenstone belts in the Superior Province indicate protracted volcanic histories in some areas (Davis and others, 1980; Nunes and Pyke, 1980; Nunes and Thurston, 1980; and Nunes and Wood, 1980), although in others extremely thick sequences were erupted over short intervals of time (Nunes and Jensen, 1980). The Puritan Quartz Monzonite, emplaced late in the cycle, is typical of the granitic components of Late Archean greenstone-granite belts. Leucogranite dikes in the Watersmeet dome are considered to be related to this period of granitic plutonism.

The geologic record between the time of stabilization of the composite Archean crust and the inception of deposition of the Marquette Range Supergroup is lacking in this area. By analogy with northern Minnesota (Goldich and others, 1961), the Archean basement probably had stabilized by 2.5 Ga. The depositional interval of the Marquette Range Supergroup is not firmly established, but

an upper age of about 1.9 Ga commonly is accepted based largely on correlative volcanic rocks in Wisconsin (Van Schmus, 1980). In the Marenisco-Watersmeet area, these supracrustal rocks were deformed and metamorphosed during the Penokean orogeny. In the Watersmeet dome, ages between 1.72 and 1.76 Ga (fig. F8) represent diapiric uplift and locally concentrated shearing and cataclasis of the core rocks. Earlier formed structures in the Archean rocks were overprinted and locally obliterated by this tectonism. The 1.72– to 1.76–Ga Rb-Sr whole-rock and mineral ages and U-Pb ages of metamorphic zircon for rocks in the dome are slightly lower than the main phase of the Penokean orogeny as defined in central Wisconsin by the eruption of volcanic rocks and the emplacement of synorogenic intrusions between 1.82 and 1.86 Ga (Van Schmus, 1980). In Minnesota, igneous activity was continuous in the interval of 1.75–1.85 Ga (Goldich, 1981), and in central Wisconsin, late- to post-orogenic granites were emplaced at 1.76 Ga. The penetrative deformation and diapiric uplift of the core of the Watersmeet dome appears to be synchronous with this anorogenic magmatic event. Apparently, Penokean stresses continued to be focused along the Great Lakes tectonic zone 60–100 Ma after synorogenic plutonism had ceased to the south.

CONCLUSIONS

Additional isotopic dating of zircons from gneisses in the core of the Watersmeet dome has refined the temporal framework of events that are recorded in this small inlier of Early and Late Archean rocks:

1. Early Archean rocks in the dome are tonalitic augen gneiss and layered to massive biotite gneiss. Uranium-lead data for zircons from these units define an approximately linear relation on a concordia diagram with intercepts at 1.25 and 3.56 Ga. The upper intercept is thought to be close to the primary age. The near-linear array of points is interpreted to be the result of systematic lead loss in response to events at 2.7 Ga, 1.8 Ga, and during a younger event, perhaps 0.5 Ga. Consequently, the lower intercept of 1.25 Ga has no geologic significance. The zircons from these gneisses are composed of two discrete phases associated in fine zoning and in chaotic mixtures. One phase is stoichiometric zircon, and the other contains appreciable calcium and probably is hydrated. The nonstoichiometric phase has probably lost more radiogenic lead, relative to uranium, than the stoichiometric phase.

2. Uranium-lead data for zircons from an interlayered gneiss and amphibolite unit in the dome establish the age as Late Archean (2.64 Ga) indicating that volcanic rocks were deposited at least locally on the older gneiss basement during the formation of the marginal Late Archean greenstone belt. All units in the dome are cut by leucogranite dikes dated at about 2.6 Ga. The Late Archean zircons also were affected by an event at about 1.8 Ga and at a more recent time. However, the upper intercept ages probably are close to the primary ages of the units.

3. Thorium-lead ages of several fractions of Early and Late Archean zircons are impossibly old. Analytical problems and addition of ^{208}Pb are ruled out as causative factors. More likely, the Th-Pb age anomalies are the result of inclusions or domains in the zircons that have preferentially lost thorium relative to ^{208}Pb during one or more of the events that disturbed the U-Pb systems.

REFERENCES CITED

Aftalion, M., and van Breeman, O., 1980, U-Pb zircon, monazite and Rb-Sr whole rock systematics of granitic gneiss and psammitic semi-pelitic host gneiss from Glenfinnan, northwestern Scotland: Contributions to Mineralogy and Petrology, v. 72, p. 87–98.

Allegre, C. J., Albarede, F., Grunenfelder, M., and Koppel, V., 1974, $^{238}U/^{206}Pb$–$^{235}U/^{207}Pb$–$^{232}Th/^{208}Pb$ zircon geochronology in Alpine and non-Alpine environments: Contributions to Mineralogy and Petrology, v. 43, p. 163–194.

Davis, D. W., Blackburn, C. E., Trowell, N. F., and Edwards, G. R., 1980, Geochronology of the Savant-Crow Lakes area, western Wabigoon subprovince, Districts of Kenora, Rainy River, and Thunder Bay, *in* Pye, E. G., ed., Summary of geochronology studies 1977–1979: Ontario Geological Survey Miscellaneous Paper 92, p. 24–33.

Futa, K., 1981, Sm-Nd systematics of a tonalitic augen gneiss and its constituent minerals from northern Michigan: Geochimica et Cosmochimica Acta, v. 45, p. 1245–1249.

Gebauer, D., and Grunenfelder, M., 1979, U-Th-Pb dating of minerals, *in* Jäger, E., and Hunziker, J. C., eds., Lectures in isotope geology: New York, Springer-Verlag, p. 105–131.

Goldich, S. S., 1981, The Penokean orogeny [abs.]: Institute on Lake Superior Geology, Abstracts and Proceedings, Twenty-seventh annual meeting, East Lansing, Michigan.

Goldich, S. S., and Mudrey, M. G., Jr., 1972, Dilatancy model for discordant U-Pb zircons ages, *in* Tugarinov, A. E., ed., Recent contributions to geochemistry and analytical chemistry: Moscow, Nauka, p. 415–418.

Goldich, S. S., Nier, A. O., Baadsgaard, H., Hoffman, J. H., and Krueger, H. W., 1961, The Precambrian geology and geochronology of Minnesota: Minnesota Geological Survey Bulletin 41, 193 p.

Jacobsen, S. B., and Wasserburg, G. J., 1980, Sm-Nd isotopic evolution of chondrites: Earth and Planetary Science Letters, v. 50, p. 139–155.

Krogh, T. E., 1973, A low-contamination method for hydrothermal decomposition of zircon and extraction of U and Pb for isotopic age determinations: Geochimica et Cosmochimica Acta, v. 37, p. 485–494.

———1982, Improved accuracy of U-Pb zircon ages by the creation of more concordant systems using an air abrasion

technique: Geochimica et Cosmochimica Acta, v. 46, p. 637–649.

Ludwig, K. R., 1982, Programs for filing and plotting U-Pb isotope data for concordia diagrams, using an HP–9830 computer and HP–9862 plotter: U.S. Geological Survey Open-File Report 82–386, 22 p.

McCulloch, M. T., and Wasserburg, G. J., 1980, Sm-Nd model ages from an early Archean tonalitic gneiss, northern Michigan, *in* Morey, G. B., and Hanson, G. N., eds., Selected studies of Archean gneisses and lower Proterozoic rocks, southern Canadian Shield: Geological Society of America Special Paper 182, p. 135–138.

Nunes, P. D., and Jensen, L. S., 1980, Geochronology of the Abitibi metavolcanic belt, Kirkland Lake area—Progress report, *in* Pye, E. G., ed., Summary of geochronology studies 1977–1979: Ontario Geological Survey Miscellaneous Paper 92, p. 40–45.

Nunes, P. D., and Pyke, D. R., 1980, Geochronology of the Abitibi metavolcanic belt, Timmins-Matachewan area—A progress report, *in* Pye, E. G., ed., Summary of geochronology studies 1977–1979: Ontario Geological Survey Miscellaneous Paper 92, p. 34–39.

Nunes, P. D., and Thurston, P. C., 1980, Two hundred and twenty million years of Archean evolution; A zircon U-Pb age stratigraphic study of the Uchi-Confederation Lakes greenstone belt, northwestern Ontario: Canadian Journal of Earth Sciences, v. 17, p. 710–721.

Nunes, P. D., and Wood, J., 1980, Geochronology of the North Spirit Lake area, District of Kenora—Progress report, *in* Pye, E. G., ed., Summary of geochronology studies 1977–1979: Ontario Geological Survey Miscellaneous Paper 92, p. 7–14.

Patchett, P. J., Kouvo, O., Hedge, C. E., and Tatsumoto, M., 1981, Evolution of continental crust and mantle heterogeneity; Evidence from Hf isotopes: Contributions to Mineralogy and Petrology, v. 78, p. 279–297.

Peterman, Z. E., Zartman, R. E., and Sims, P. K., 1980, Tonalitic gneiss of early Archean age from northern Michigan, *in* Morey, G. B., and Hanson, G. N., eds., Selected studies of Archean gneisses and lower Proterozoic rocks, southern Canadian Shield: Geological Society of America Special Paper 182, p. 125–134.

Sims, P. K., 1980, Boundary between Archean greenstone and gneiss terranes in northern Wisconsin and Michigan, *in* Morey, G. B., and Hanson, G. N., eds., Selected studies of Archean gneisses and lower Proterozoic rocks, southern Canadian Shield: Geological Society of America Special Paper 182, p. 113–124.

Sims, P. K., Card, K. D., Morey, G. B., and Peterman, Z. E., 1980, The Great Lakes tectonic zone—A major crustal structure in central North America: Geological Society of America Bulletin, v. 91, p. 690–698.

Sims, P. K., Peterman, Z. E., and Prinz, W. C., 1977, Geology and Rb-Sr age of Precambrian W Puritan Quartz Monzonite, northern Michigan: U.S. Geological Survey Journal of Research, v. 5, p. 185–192.

Sims, P. K., Peterman, Z. E., Prinz, W. C., and Benedict, F. C., 1984, Geology, geochemistry, and age of Archean and early Proterozoic rocks in the Marenisco-Watersmeet area, northern Michigan: U.S. Geological Survey Professional Paper 1292–A, p. A1–A41.

Sommerauer, J., 1979, Physico-chemical stability of zircon and its U-Pb system [abs.]: Geological Society of America Abstracts with Programs, v. 11, no. 7, p. 521.

Speer, J. A., 1980, Zircon, *in* Ribbe, P. H., ed., Reviews in mineralogy, v. 5, Orthosilicates: Mineralogical Society of America, chap. 3, p. 67–112.

Stacey, J. S., and Kramers, J. D., 1975, Approximation of terrestrial lead isotopic evolution by a two-stage model: Earth and Planetary Science Letters, v. 26, p. 207–221.

Steiger, R. H., and Jäger, E., 1977, Subcommission on geochronology: Earth and Planetary Science Letters, v. 36, p. 359–362.

Steiger, R. H., and Wasserburg, G. J., 1966, Systematics in the Pb^{208}–Th^{232}, Pb^{207}–U^{235}, and Pb^{206}–U^{238} systems: Journal of Geophysical Research, v. 71, p. 6065–6090.

Tilton, G. R., 1960, Volume diffusion as a mechanism for discordant lead ages: Journal of Geophysical Research, v. 65, p. 2933–2945.

Wasserburg, G. J., 1963, Diffusion processes in lead-uranium systems: Journal of Geophysical Research, v. 68, p. 4823–4846.

Wetherill, G. S., 1956, Discordant uranium-lead ages, I.: Transactions of the American Geophysical Union, v. 37, p. 320–326.

———1963, Discordant uranium-lead ages—pt. II, Discordant ages resulting from diffusion of lead and uranium: Journal of Geophysical Research, v. 68, p. 2957–2965.

Van Schmus, W. R., 1980, Chronology of igneous rocks associated with the Penokean orogeny in Wisconsin, *in* Morey, G. B., and Hanson, G. N., eds., Selected studies of Archean gneisses and lower Proterozoic rocks, southern Canadian shield: Geological Society of America Special Paper 182, p. 159–168.

1986

U.S. GEOLOGICAL SURVEY BULLETIN 1622

SHORTER CONTRIBUTIONS TO ISOTOPE RESEARCH

AGE OF THE BASEMENT STAUROLITE-BIOTITE SCHIST OF NORTHEASTERN SOUTH DAKOTA

Chapter G

By J. R. RICHARDS,[1] D. M. BARON,[2] and S. S. GOLDICH

CONTENTS

FIGURES

TABLES

[1]Research School of Earth Sciences, Australian National University, Canberra, Australia.
[2]Johnson Division, Universal Oil Products, Inc., St. Paul, Minnesota, U.S.A.

Abstract

Rubidium-strontium analyses of whole-rock samples of staurolite-biotite schist cored in a hole drilled near Bristol, South Dakota, indicate an Archean age (>2,500 million years) for the basement rock. Low-grade metamorphism has altered biotite to chlorite, staurolite to sericite, and garnet to chlorite and sericite. The northeasterly trend of the basement rocks in South Dakota, as determined from geophysical surveys, is alined with the structural trend of the Precambrian basement of Minnesota, and the rubidium-strontium age permits correlation of the staurolite-biotite schist with Archean metasedimentary rocks in northern Minnesota and in the Rainy Lake district of Ontario, Canada. The new data suggest that a regional high-grade (amphibolite facies) metamorphism may have affected the Archean metasedimentary and metavolcanic rocks in a broad belt extending from Ontario southward into northeastern South Dakota. The regional metamorphism was followed by the emplacement of postkinematic granitic rocks that in northern Minnesota and southwestern Ontario have been dated at about 2,650 Ma. Similar 2,600-Ma postkinematic rocks are present in the Minnesota River Valley.

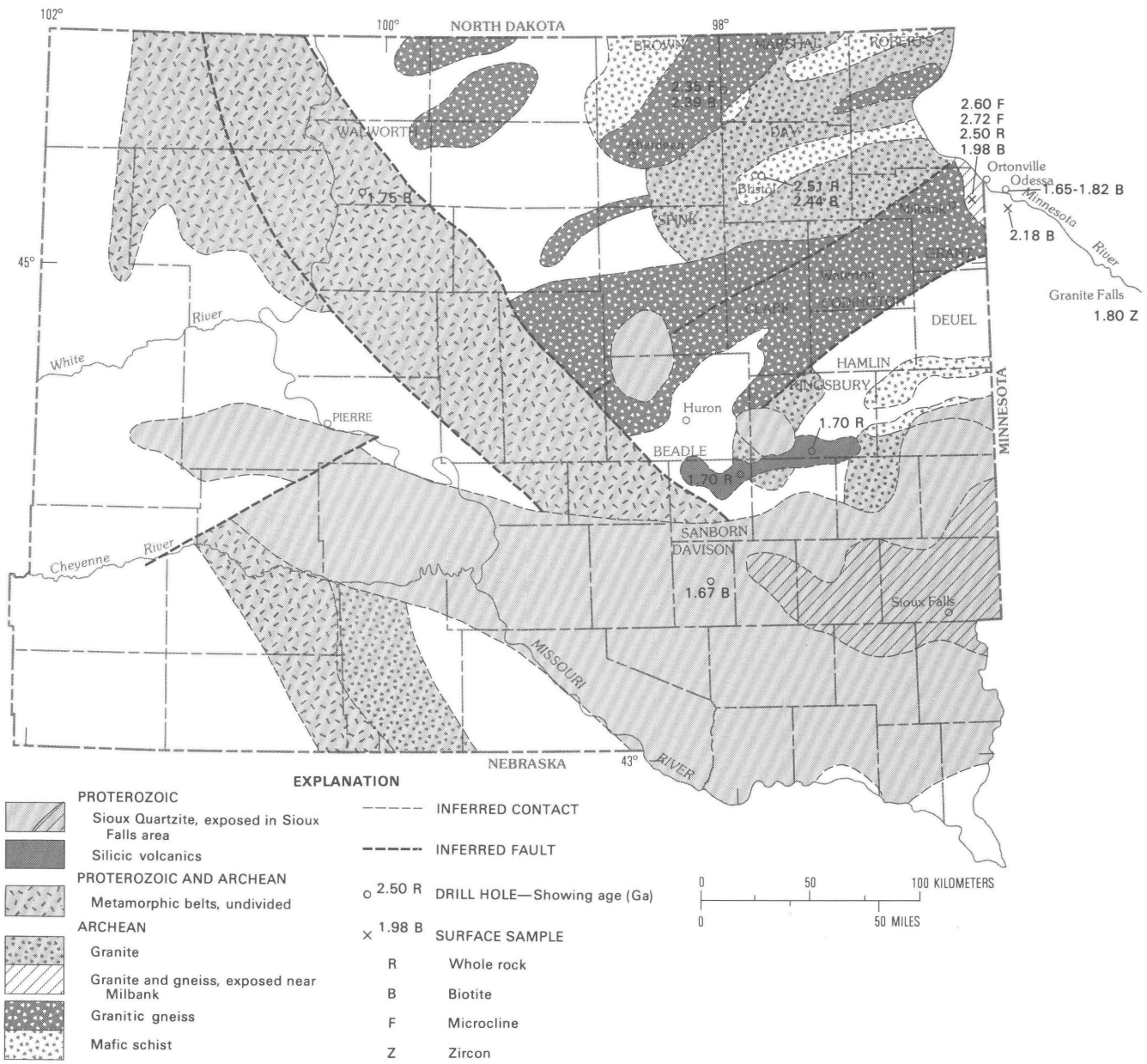

Figure G1. Geologic map of the Precambrian rocks of east-central South Dakota (from Lidiak, 1971) showing location of drill-hole site near Bristol. Isotopic ages are from the present paper and from Goldich and others (1966, 1970).

Table G1. Modal analyses of staurolite-biotite schist

[Modes are volume percentages based on 300 or more points. Leaders (---), not found on point-count traverses; tr, less than 0.3 percent]

Sample No.	1613	1618	1628	1640	1663	1667	1672	1680	1695	1707	1827	1830	1952
Quartz	20	27	29	23	32.4	35	35	40	35	19	21.7	32.3	31.4
Plagioclase	41	10	7	22	18.1	25	17	7	8	15	39.5	42.4	20.4
Biotite	24	12	9	12	20.9	29	13	22	36	18	17.8	22.3	7.4
Chlorite	5	33	31	25	0.5	tr	27	0.2	3	2	0.4	1.5	19.6
Staurolite	---	---	---	---	20.9	5	---	18	5	25	12.3	---	---
Garnet	tr	---	tr	tr	---	0.5	---	2	---	---	1	---	---
Opaque minerals	0.3	6	0.6	7	1.6	3	5	2	---	---	1	1.2	2.6
Sericite	9	5	23	6	5.3	---	1	4	3	13	6	---	16.4
Muscovite	0.4	5	---	2	---	---	---	1	4	2	---	---	---
Potassium-feldspar	---	---	---	---	---	---	---	---	---	---	---	---	1
Tourmaline	0.3	1.5	0.3	3	0.3	2	2	4	3	1	0.4	0.3	1
Zircon	---	0.5	---	---	---	tr	---	---	3	---	---	---	tr

INTRODUCTION

This paper presents the results of Rb-Sr (rubidium-strontium) dating of staurolite-biotite schist and amphibolite cored in a hole drilled about 1 mi (mile) east of Bristol, northeastern South Dakota (fig. G1). A magnetic anomaly found in a vertical-intensity magnetometer survey by the South Dakota Geological Survey (Petsch, 1965, 1967) was investigated by the American Metal Climax Company[3], and two holes were drilled on the anomaly in 1964. One hole penetrated about 1,556 ft (feet) of glacial drift and Mesozoic strata before reaching Precambrian crystalline basement rock, of which 403 ft was cored. On expiration of its lease, the company transferred this core to the South Dakota Geological Survey. The core was studied by Baron (1971), and, during the course of this work, in 1970, he visited the Little Falls area in Minnesota to examine exposures of the Proterozoic staurolite schist that had been dated by the K-Ar (potassium-argon) method at about 1,600 Ma (million years) (Goldich and others, 1961, p. 104). By chance Baron and Goldich met on an outcrop in Little Falls and they agreed that radiometric dating of some samples from the Bristol core would be undertaken at Northern Illinois University in DeKalb, Ill. The work at Northern Illinois University was done by J. R. Richards (J.R.R.) who at the time was Visiting Professor of Geology on leave from the Australian National University. The preliminary age obtained from an isochron of six samples was 2,500 Ma, which indicated that the staurolite-biotite schist basement of northeastern South Dakota is of Archean age and is not correlative with the staurolite schist of the Little Falls area, Minnesota.

Recently, the samples that were originally analyzed at Northern Illinois University and some additional samples, including a biotite concentrate, were analyzed (J.R.R.) in the geochronologic laboratory of the Research School of Earth Sciences, Australian National University. Description of the core, modal analyses, and other mineralogical data are from Baron (1971). The final manuscript was prepared in Denver by S. S. Goldich.

[3]Use of company and trade names is for descriptive purposes only and does not imply endorsement by the U.S. Geological Survey.

ACKNOWLEDGMENTS

We thank W. Compston and I. McDougall for use of facilities at the Australian National University and D. Millar, R. Maier, and Z. Roksandic for assistance with the isotopic analyses. We are indebted to Professor V. J. Ansfield of the University of South Dakota and to the South Dakota Geological Survey for their support. K. R. Ludwig, C. E. Hedge, and Z. E. Peterman of the U.S. Geological Survey assisted materially in discussions and in critical reviews of the manuscript.

LOCATION OF DRILL HOLE SITE AND DESCRIPTION OF CORE

The drill hole 1 mi east of Bristol in Day County, S. Dak. (fig. G1) is situated in the NE¼NE¼SW¼ sec. 29, T. 122 N., R. 57 W. (lat 45°20.9′ N., long 97°42.3′ W.). The basement schist was cored (diameter, ~ 1.5 in.) with approximately 95 percent recovery, and, on the average, about 6 in. (inches) of core was missing from each box that contained 10–ft sections. For this reason, the depth below the surface of the midpoint of each sample taken from the core is given to the nearest foot, and this depth is used as the sample number (table G1, fig. G2).

The Bristol core is a fine-grained porphyroblastic staurolite-biotite-plagioclase-quartz schist with minor amounts of opaque minerals (magnetite-ilmenite), garnet, tourmaline, calcite, and accessory zircon and apatite. The

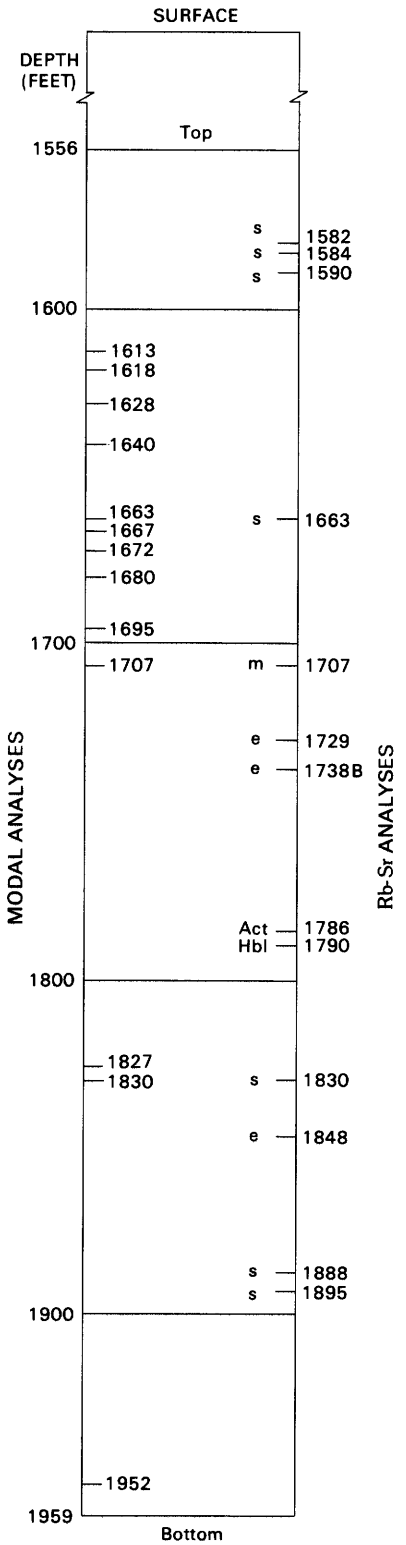

Figure G2. Vertical section of core of staurolite-biotite schist near Bristol, S. Dak. (fig. G1) showing position from which samples were taken. Numbers are those assigned to samples and represent depth, in feet. Degree of alteration of staurolite in rubidium-strontium samples: s <10 percent; m, ~25 percent; e, 70–85 percent. Sample 1738B, biotite concentrate; Act, actinolite schist; Hbl, hornblende schist.

name staurolite-biotite schist is used here for convenience. Throughout the length of the core the staurolite is altered in part or completely to sericite, biotite to chlorite, and garnet to chlorite or to sericite and chlorite. Modal analyses of 300 or more point counts of nine samples from the interval between 1,600 and 1,700 ft (fig. G2) show large differences in mineral composition. Although thin sections were examined, only a few modal analyses (table G1, fig. G2) were made of the core below 1,700 ft. Sampling of the core for Rb-Sr analyses, however, was more evenly distributed over the length of the core (fig. G2).

Table G2. Rubidium-strontium analytical data for whole-rock samples

Sample No.	Concentration (microgram/gram)		Atomic ratio	
	Rb	Sr	$^{87}Rb/^{86}Sr$	$^{87}Sr/^{86}Sr$
1582	94.7	245.5	1.1178	0.7419
1584	92.0	199.3	1.3374	0.7504
1590	92.1	226.0	1.1810	0.7446
1663	96.5	430.4	0.6483	0.7254
1707	100.1	332.4	0.8719	0.7336
1729	96.9	193.7	1.4518	0.7548
1786	127.3	172.2	2.1484	0.7699
1790	73.3	784.7	0.2698	0.7107
1830	90.2	268.9	0.9712	0.7370
1848	88.3	243.2	1.0511	0.7405
1888	86.5	287.4	0.8715	0.7339
1895	91.1	225.7	1.1698	0.7447

Examination with petrographic and binocular microscopes led to the conclusion that all the rock in the core was derived by metamorphism of sedimentary material, probably a graywacke-argillite sequence. The most prominent variations in rock type are a 6-in. layer of quartzite at a depth of 1,612 ft and two thin (less than 1 ft) amphibolitic layers. A thin actinolite-rich layer is at 1,786 ft, and a hornblende-rich layer at 1,790 ft. Some calcite was found in both layers, and they probably were derived from calcareous sediments. The two amphibolitic layers were included in the Rb-Sr sampling (fig. G2).

Biotite and staurolite give the rock a good schistosity, and, if the attitude of the core is taken as vertical from which departures probably were small, the foliation ranges from horizontal to a high dip of about 65°, which is characteristic of the greater part of the core. Porphyroblasts of biotite, as well as of staurolite, continued to grow after the formation of the foliation, and crystals of both minerals are oriented across the metamorphic structure. Kinked biotite also is present and indicates a later period of deformation or shearing prior to the hydrothermal alteration of the biotite to chlorite.

Quartz is always xenoblastic and averages about 0.03 mm (millimeters) in diameter. Some quartzose veins are parallel to the foliation, but many are crosscutting. Like quartz, plagioclase is xenoblastic and averages about 0.03 mm in diameter. The matrix plagioclase nearly always is untwinned. Some larger plagioclase grains in the small quartzose veins, which cut across the foliation, are twinned and these grains range in composition from An_0 to An_{20}. On the average, quartz and sodic plagioclase compose 50 percent of the schist but the range is large (36–75 percent, table G1).

Biotite is an abundant mineral forming porphyroblasts that are subidioblastic and that range in length from 1 to 2.5 mm. The finer grained matrix biotite (0.07–0.15 mm) is xenoblastic. Quartz and zircon are the common inclusions in biotite. Biotite is altered to chlorite, and the abundance of the two minerals is complimentary; an apparent increase in chlorite is accompanied by a decrease in the percentage of biotite.

Staurolite is a conspicuous mineral but ranges considerably in abundance. The porphyroblasts are 4–10 mm long; all show sieve texture (poikiloblastic) with inclusions of quartz, opaque minerals, garnet, and apatite. Commonly the inclusions have helicitic texture. The staurolite commonly is altered partially or completely to sericite. Garnet is present in porphyroblasts from 0.5 to 2 mm in diameter. Like the staurolite, the garnet is poikiloblastic and commonly is helicitic. Partial alteration of garnet to chlorite and sericite is common, but fresh to slightly altered garnet is present in specimens in which the staurolite has been converted completely to sericitic pseudomorphs.

In addition to the abundant fine-grained sericite, muscovite (~0.06 mm in diameter) is present in small amounts that could not be concentrated for purposes of radiometric dating. Potassium-feldspar is absent and could not be detected by staining, except for a small amount in deep sample 1952. Tourmaline is present in trace amounts throughout the core, but is more abundant in quartzose veins, one near the top at a depth of 1,648 ft and another at the bottom at a depth of 1,957 ft.

The staurolite schist represents a terrane that was metamorphosed regionally to the staurolite-almandine amphibolite grade. Subsequent superimposition of low-grade metamorphism resulted in an extensive greenschist-facies mineral assemblage: quartz-albite-biotite-chlorite-sericite. The intensive alteration of staurolite to sericite suggests some mobility of potassium and possibly other elements. Further discussion is deferred to a later section.

ANALYTICAL PROCEDURES

The analytical procedures for the isotopic analyses are similar to those developed over the years in a number of geochronology laboratories. A mixed ^{87}Rb–^{84}Sr spike was used. In the earlier work, some difficulty was experienced in dissolving the staurolite, but two dissolution procedures were found to be effective: prolonged refluxing during several days of a HNO_3–HF mixture, and the teflon pressure assembly (Krogh, 1973). The argon isotopic analyses were made by the method of McDougall (1966). Potassium was determined by flame photometry. The ages were calculated using decay constants and atomic abundance ratios recommended by the International Union of Geological Sciences Subcommission on Geochronology (Steiger and Jäger, 1977).

Linear regressions of the whole-rock Rb-Sr data were made in the U.S. Geological Survey laboratory in Denver using the program of Ludwig (1982). The 2-sigma errors of 1 percent for $^{87}Rb/^{86}Sr$ and 0.02 percent for $^{87}Sr/^{86}Sr$ used in the regressions were supplied by the Australian National University laboratory (J.R.R.).

RESULTS

The Rb-Sr data (table G2) for all the whole-rock samples are plotted in the isochron diagram of figure G3. A regression of the data for 11 samples, excluding sample 1786, gives an age of $2{,}560 \pm 55$ Ma, $R_i = 0.7011 \pm 0.0008$ (model 3). If both amphibolite samples (1786 and 1790) are excluded, the 10 samples of staurolite-biotite schist give an age of $2{,}510 \pm 70$ Ma, $R_i = 0.7020 \pm 0.0011$ (model 3). The difference of 50 m.y. is within the analytical errors of the isochrons (fig. G3, lines A and B). A tie-line connecting the two amphibolite samples gives an approximate age of 2,180 Ma, $R_i = 0.7022$ (fig. G3, line C).

The Rb-Sr and K-Ar apparent ages (table G3) for biotite (sample 1738) are in good agreement at 2,440 Ma. The Rb-Sr age was calculated with $R_i = 0.7020$ from the whole-rock isochron, but a lower value would not appreciably affect the age. The Rb-Sr and K-Ar ages, however, are lower than the isochron ages, and together with the amphibolite data clearly show that both systems (Rb-Sr and K-Ar) have been disturbed.

DISCUSSION

In addition to the metamorphism that produced the staurolite-biotite schist, there is evidence for two successive events. The Rb-Sr and K-Ar biotite ages of 2,440 Ma suggest an event that preceded the low-grade metamorphism. The extensive alteration of staurolite, and, to a lesser extent of garnet, to sericite indicates the mobility of potassium during the low-grade metamorphism. Potassium was released during the alteration of biotite to chlorite, and this process would, of course, also release rubidium, so that the movement of rubidium must be con-

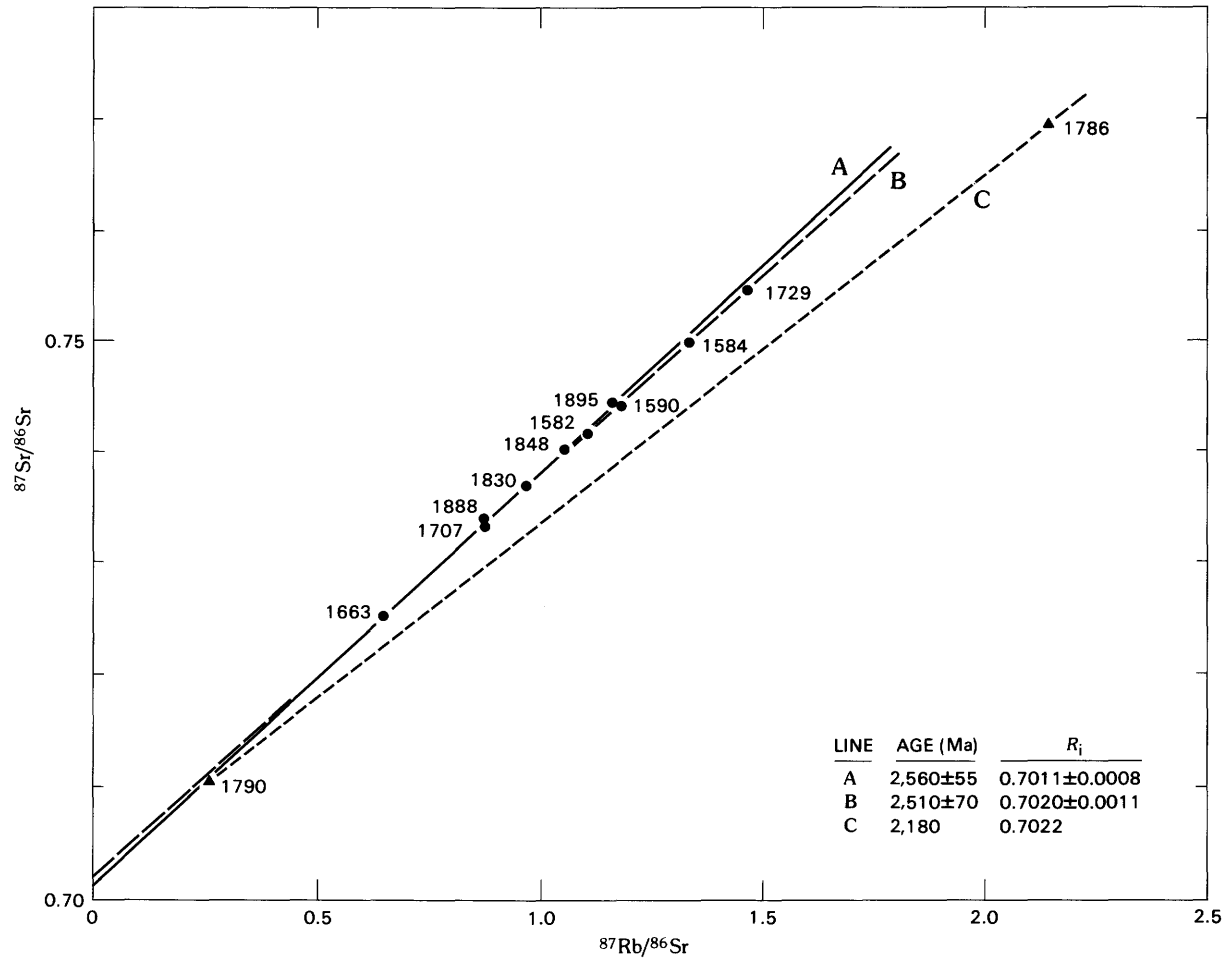

Figure G3. Rubidium-strontium isochron diagram for whole-rock samples of staurolite-biotite schist (solid circles) and amphibolite (triangles). Line A includes all samples except 1786; line B, all samples except 1786 and 1790; line C connects samples 1786 and 1790.

Table G3. Rubidium-strontium and potassium-argon analytical data and ages for biotite from sample 1738
[*Radiogenic $^{+}R_i$=0.7020]

Rubidium-strontium				
Concentration (microgram/gram)		Atomic ratios		
Rb	Sr	$^{87}Sr/^{86}Sr$	$^{87}Sr/^{86}Sr$	Age (Ma)
317.3	11.33	112.1	4.659	$2,443\pm50^{+}$

Potassium-argon			
K (weight percent)	$*^{40}Ar$ (10^{-10} mole/gram)	$*^{40}Ar \times 100$ / Total ^{40}Ar	Age (Ma)
7.350	657.4	99.9	2,438±52
7.332	654.9	100	2,432±46

sidered as a mechanism that could affect the Rb-Sr system. The alteration was not pervasive as can be seen in the plot (fig. G4) of the modal percentages of sericite + muscovite and of chlorite. A similar pattern is noted in the metasomatic replacement of staurolite by sericite (fig. G2). Locally the staurolite is extensively to completely altered, but in adjacent parts of the core it is unaltered. The alteration pattern suggests that the hydrothermal fluids were channeled by porosity that was formed during shearing of the staurolite-biotite schist.

The 10 analyzed staurolite-biotite samples average 93 ppm (parts per million) rubidium and range from 86 to 110 ppm. Strontium ranges from 194 to 430 ppm with an average of 265 ppm. Biotite (sample 1738B) contains 317 ppm rubidium and 11 ppm strontium (table G3). Biotite + chlorite range from 20 to 40 percent in the modes (table G1), and the rubidium in the staurolite-biotite schist can be accounted for almost entirely by the biotite. The samples for Rb-Sr analysis were selected (D. M. Baron) on the basis of the degree of apparent alteration. Seven of the samples show slight (<10 percent) alteration of staurolite to sericite, one has moderate (~25 percent) and two extensive (70–85 percent) alteration (fig. G2). The ages of the whole-rock samples, however, show little ap-

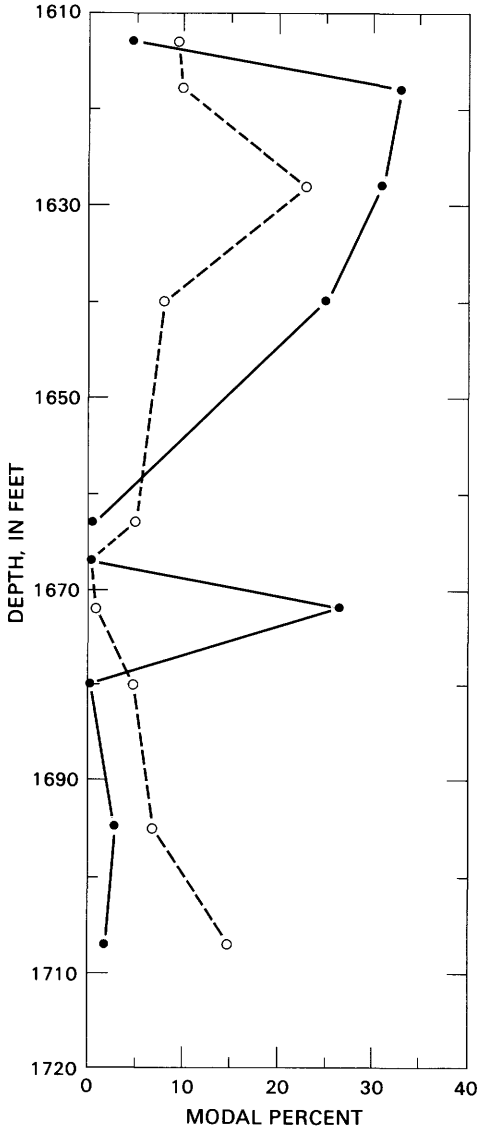

Figure G4. Plot of variations of modal sericite + muscovite (open circles) and of chlorite (solid circles) with depth (data in table G1).

parent variation as is indicated by the close adherence of the data points to the 2,510-Ma isochron (line B, fig. G3). A reasonable conclusion is that in the analyzed samples rubidium and any radiogenic ^{87}Sr that had been formed prior to the time of the low-grade alteration were trapped rather uniformly in the sericite. This conclusion finds some support in the general correlation of the variations of sericite + muscovite and those of chlorite (fig. G4). The low modal percentages of sericite and the much larger amounts of chlorite in parts of the core (see for example sample 1672, table G1, fig. G4), however, are deviations from the pattern and suggest that potassium and rubidium were redistributed within the schist.

Model ages calculated for the actinolite schist (sample 1786) and the hornblende schist (sample 1790), using R_i=0.7020, are 2,190 Ma and 2,240 Ma, respectively. Using R_i=0.7011 (line A, fig. G3) the model ages are 2,220 Ma and 2,460 Ma, respectively. An explanation for the low ages of the amphibolite samples is rubidium gain during the hydrothermal alteration. The net gain in rubidium in the hornblendic layer was relatively small, but it was much larger in the actinolite layer that, on the basis of the common assignment of actinolite to lower grade than hornblende, may have been formed during the alteration. The time of alteration when potassium and rubidium became mobile, however, cannot be stated precisely. The time may have been about 2,250 Ma, or it may be related to a much younger event, in which case the apparent age represents a partial resetting of the Rb-Sr system.

Staurolite schist in the Rice Bay area in the Rainy Lake district, Ontario (fig. G5) has been described by Harris (1974). The staurolite usually is identifiable only by the crystal forms; the white-mica pseudomorphs are from 2 to 10 mm long. Harris (1974) concluded that the staurolite was formed by metamorphism of pelitic rocks to the almandine-amphibolite facies and was altered by retrogressive metamorphism to white mica. Garnet was altered to chlorite. The metasedimentary rocks in the area, the Coutchiching and Seine Series of Lawson (1913), were intruded by postkinematic granite (Algoman of Lawson). The Rb-Sr isochron ages (fig. G6) for the Coutchiching metasedimentary, Keewatin metavolcanics, and Algoman granitic rocks are 2,560 Ma, 2,540 Ma, and 2,485 Ma, respectively, but the U-Pb (uranium-lead) concordia age for zircon from the granite is 2,650 Ma. Rubidium-strontium ages on muscovite from the granite range from 2,545 to 2,700 Ma and support the older U-Pb age. Peterman and others (1972) concluded that the Rb-Sr ages have been affected by younger metamorphic processes. The low Rb-Sr age for the Algoman granite is attributed to low-grade metamorphism.

The Newton Lake Formation (metasedimentary) and the Ely Greenstone (metavolcanic) of northern Minnesota (fig. G5) have been dated by Jahn and Murthy (1975). Postkinematic rocks in the Giants Range Granite have been dated by Catanzaro and Hanson (1971) and Prince and Hanson (1972) and in the Vermilion Granitic Complex by Peterman and others (1972). The Rb-Sr isochron ages for these various lithologic units are shown in figure G6. The Rb-Sr ages are lower than the U-Pb ages.

The postkinematic granitic rocks set a limit on the time of metamorphism of the metasedimentary and metavolcanic rocks in northern Minnesota and in southwestern Ontario. Similar data are not available from northeastern South Dakota, but data are available from the Precambrian rocks in the Minnesota River Valley about 125 mi southeast of Bristol. A major metamorphic event has been dated by Rb-Sr and U-Pb age measurements at 2,600 Ma. Aplite and late postkinematic granite

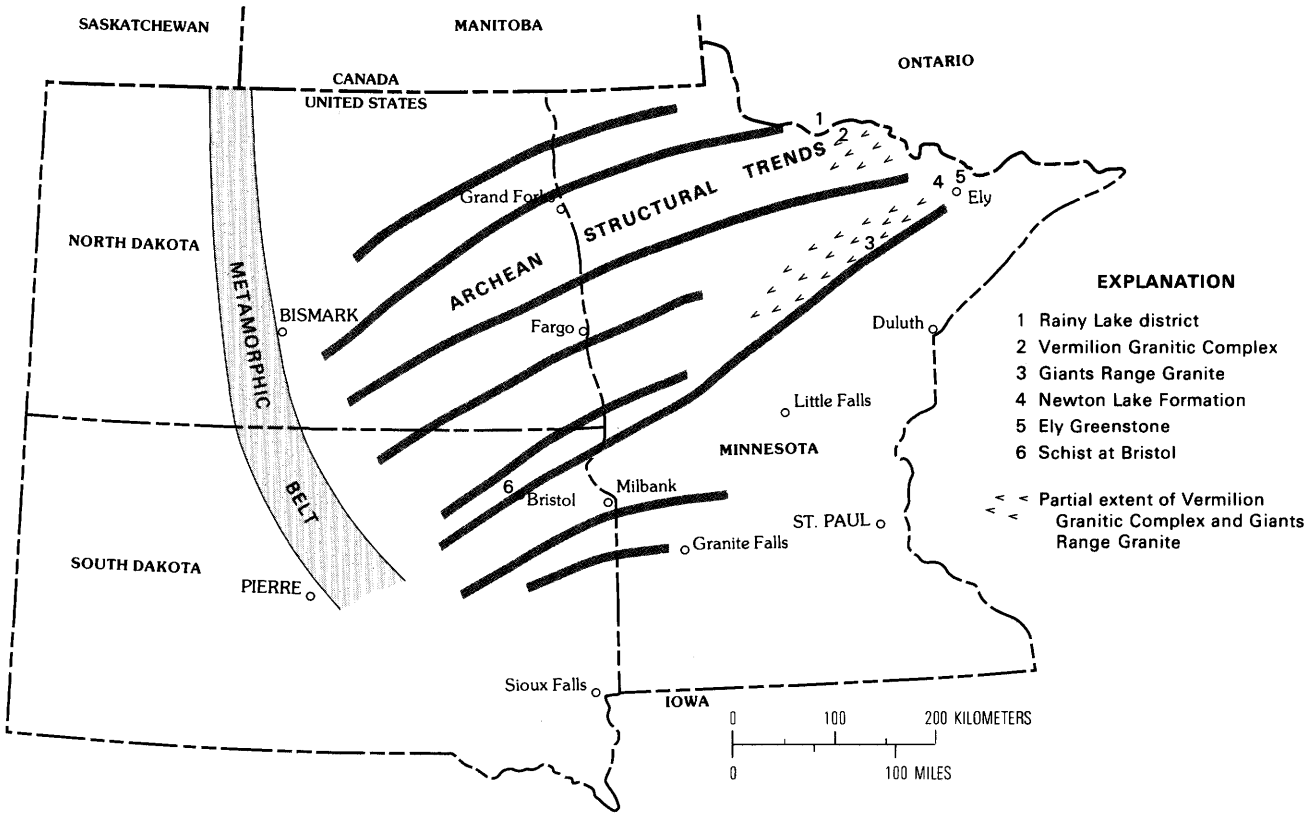

Figure G5. Map showing structural trends of Archean rocks in northeastern South Dakota and adjacent parts of Minnesota and North Dakota. Trend lines are based on figure G1, regional magnetic and gravity trends, and on unpublished data.

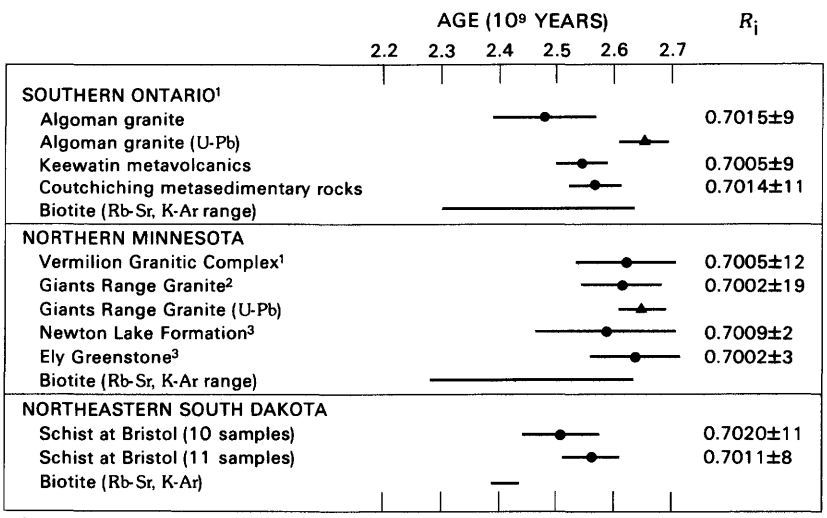

[1] Peterman and others (1972).
[2] Prince and Hanson (1972).
[3] Jahn and Murthy (1975).

Figure G6. Comparative ages determined for Archean metasedimentary, metavolcanic, and postkinematic granitic rocks in the Rainy Lake district, Ontario; northern Minnesota, and core from Bristol, S. Dak. Solid circles, whole-rock rubidium-strontium ages; solid triangles, uranium-lead ages on zircon and sphene; lines give range for rubidium-strontium and potassium-argon ages on biotite.

give a Rb-Sr isochron age of 2,590±40 Ma, R_i=0.7024±0.0011 (Goldich and Wooden, 1981, p. 91). The age determinations from the Minnesota River Valley and those from farther north compiled in figure G6 preclude the acceptance of the Rb-Sr whole-rock age of 2,510 Ma as the time of formation of the staurolite-biotite schist.

A Geologic Model

The apparent contradiction in the radiometric ages and the stratigraphic relations determined geologically (fig. G6) is a well-known basic problem in the radiometric dating of metasedimentary rocks. The factors that controlled or influenced the measured ages are not well known, but considerable progress has been made. An early paper concerned with discordant mineral ages in Australian granites (Arriens and others, 1966) is significant because it cautioned of the possibility of open-rock conditions that might result from the migration of strontium, for example, as a result of "slight earth stress rather than reheating * * * ," incipient weathering, and low-temperature alteration of plagioclase. Peterman and Hildreth (1978) have reviewed some of the problems of interpreting Rb-Sr ages determined on metasedimentary rocks and some of the extensive literature pertaining to the subject. They concluded that relatively low-grade metamorphism may seriously disturb the Rb-Sr system.

An interpretation of the Rb-Sr data based on information derived from previous geochronological studies in the Lake Superior region (see, for example, Goldich, 1968, 1972) is shown in figure G7. Line A (fig. G7) is based on the lower six data points that have $^{87}Rb/^{86}Sr$ of less than 1.0. The approximate age is 2,620 Ma; R_i=0.7006. This age would relate the formation of the staurolite-biotite schist to the 2,600-Ma event, which in

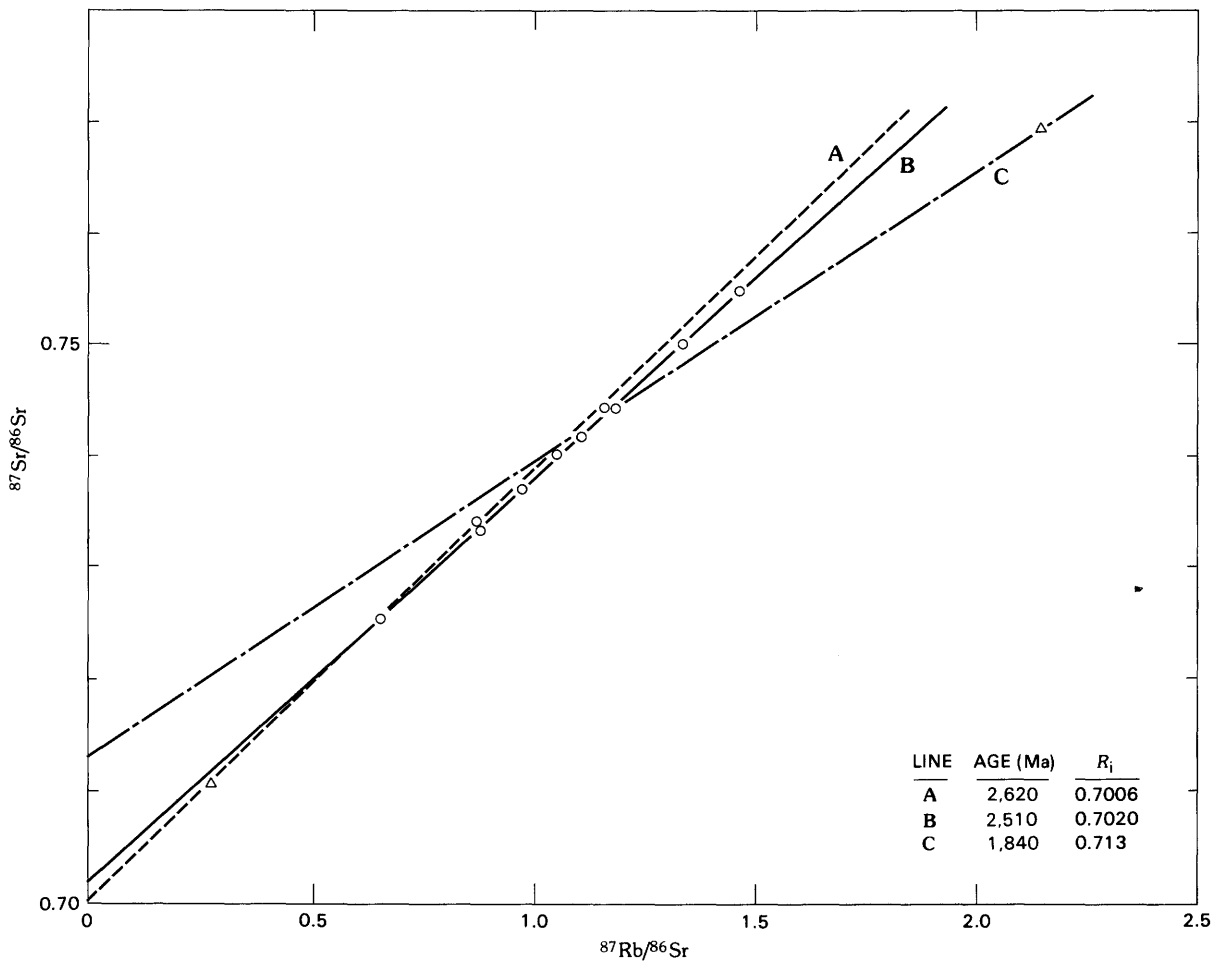

Figure G7. Rubidium-strontium diagram showing a possible geologic interpretation of the analytical data from the Bristol core. Open circles, whole-rock samples of staurolite-biotite schist; open triangles, amphibolite. Line A includes the five lowermost points with $^{87}Rb/^{86}Sr$ of less than 1.0; line B is isochron B in figure G3; line C is a reference line from actinolite schist sample 1786 drawn through the cluster of points for staurolite-biotite schist samples, about at the median for line B.

the Lake Superior region was one of intense deformation, high-grade metamorphism, and magmatic activity. Line B is line B of figure G3, and the 2,510-Ma isochron, then, is a secondary metamorphic age with a higher initial ratio of 0.7020. The whole-rock age is essentially a biotite age and possibly might be related to the uplift and stabilization of the region. Goldich and others (1970) considered this possibility for the Precambrian of the Minnesota River Valley. The K-Ar and Rb-Sr biotite ages of about 2,500 Ma southeast of Granite Falls and ages of about 1,750 Ma at and northwest of Granite Falls may represent the time of stabilization of two Precambrian blocks, explaining the K-Ar and Rb-Sr ages on biotite, but open-system behavior for the staurolite-biotite schist is an inescapable requirement.

Shearing and deformation of the schist during uplift following folding and metamorphism could account for the Rb-Sr whole-rock isochron age of 2,510 Ma. The low-grade alteration of biotite to chlorite, staurolite to sericite, garnet to chlorite and sericite may have been caused by hydrothermal activity that accompanied the shearing; however, if the alteration took place 2,510 Ma ago, the 2,440–Ma age on biotite is difficult to explain, and even more so is the apparent age of about 2,220 Ma for the actinolite schist.

An alternative explanation is that the low-grade alteration was related to the 1,800-Ma (Penokean) event. Line C (fig. G7) from the actinolite schist (sample 1786) was projected through the cluster of points (samples 1582, 1590, 1848, and 1895) and gives an age of 1,840 Ma with an initial ratio of about 0.713. This line, of course, is highly speculative and in no sense an isochron. Goldich and others (1970, p. 3690) pointed out that the 1,800-Ma event in the Minnesota River Valley "should not be equated with the Penokean orogeny to the north and northeast in the sense of a period of folding and metamorphism." A number of small plutons in the Archean of the Minnesota River Valley have been dated at about 1,800 Ma. A U-Pb zircon age of 1,800 Ma was obtained by Catanzaro (1963) for a small adamellite pluton north of Granite Falls, Minn., about 115 mi southeast of Bristol, S. Dak. (fig. G1).

In South Dakota, whole-rock samples of quartz latite cored in a drill hole in Kingsbury County and felsite porphyry from Sanborn County gave Rb-Sr ages of 1,700 Ma (Goldich and others, 1966). The northwest-trending metamorphic belt (figs. G1, G5) was delineated by Lidiak (1971) mainly on magnetic anomalies. He suggested, on the basis of the meager data available, that the belt can be traced by the pattern of gravity highs and lows in the buried basement of North Dakota and onto the shield at the Churchill-Superior boundary and is a Proterozoic deformation. Biotite concentrates from schist cuttings from a well in Walworth County and from granodiorite cored in a hole that penetrated the Sioux Quartzite in Davison County, S. Dak. (fig. G1) gave Penokean ages. The biotite ages, however, do not establish a Proterozoic age for the rocks that may date back to the Archean.

The Bristol drill hole is well within a massive block of Archean rocks (fig. G1). Potassium-argon and rubidium-strontium ages on biotite from the Bristol core are 2,440 Ma, and on biotite from adamellite cored in Marshall County, about 25 mi northwest of Bristol (fig. G1) 2,390 Ma. Biotite near Milbank was dated at 1,980 Ma, and a biotite from metasedimentary rock south of Odessa (fig. G1) gave an age of 2,180 Ma. The progression of numbers suggests the possibility that the biotite ages may have been influenced by the 1,800-Ma event.

SUMMARY

The Rb-Sr isochron age of 2,510 Ma is a minimum value for the time of formation of the staurolite-biotite schist cored near Bristol, S. Dak. The actual time probably was about 2,600 Ma during the major deformation accompanied by magmatic activity that affected the Lake Superior region. The minimum age, however, is significant because it lends considerable support to the concept that a massive block of Archean rocks underlies a large area in northeastern South Dakota.

Structural trends in the basement rocks of northeastern South Dakota, delineated mainly on the basis of magnetic and gravity anomalies, continue in the buried basement rocks of adjacent parts of Minnesota and North Dakota. The radiometric age determinations, however, provide a basis for correlating the staurolite-biotite schist with Archean sequences in northern Minnesota and in southern Ontario. Whole-rock Rb-Sr isochron ages for metasedimentary and metavolcanic rocks both in the Rainy Lake district, Ontario, and in the Vermilion and Giants Range areas of northern Minnesota range from 2,540 to 2,635 Ma, but the U-Pb ages on zircon and sphene date the postkinematic granites emplaced in the metasedimentary and metavolcanic rocks at 2,650 Ma.

Low-grade metamorphism similar to that observed in the Bristol core has affected staurolite-bearing metasedimentary rocks in the Rainy Lake district, Ontario. Staurolite has not been reported from the metasedimentary rocks of the Vermilion Granite Complex and Giants Range Granite of northern Minnesota, but large areas of these rocks have attained amphibolite-facies grade, and high-grade (amphibolite facies) regional metamorphism possibly may have affected a belt of Archean rocks extending from southern Ontario across Minnesota into northeastern South Dakota. A similar regional metamorphism of much younger Early Proterozoic age affected the Thomson Formation of Minnesota, extending from Duluth south into the Mille Lacs Lake area and westward into the Little Falls area where staurolite schist there resembles the staurolite-biotite schist of the Bristol core.

Three samples of the staurolite schist from Little Falls and samples from the Thomson Formation of eastern Minnesota give an isochron age of 1,695 Ma, R_i=0.705 (Keighin and others, 1972).

REFERENCES CITED

Arriens, P. A., Brooks, C., Bofinger, V. M., and Compston, W., 1966, The discordance of mineral ages in granitic rocks resulting from the redistribution of rubidium and strontium: Journal of Geophysical Research, v. 71, p. 4981–4994.

Baron, D. M., 1971, The petrology of a Precambrian schist from Bristol, northeastern South Dakota: Vermillion, S. Dak., University of South Dakota, M.A. Thesis, 59 p.

Catanzaro, E. J., 1963, Zircon ages in southwestern Minnesota: Journal of Geophysical Research, v. 68, p. 2045–2048.

Catanzaro, E. J., and Hanson, G. N., 1971, U-Pb ages for sphene from early Precambrian igneous rocks in northeastern Minnesota-northwestern Ontario: Canadian Journal of Earth Sciences, v. 8, p. 1319–1324.

Goldich, S. S., 1968, Geochronology in the Lake Superior region: Canadian Journal of Earth Sciences, v. 5, p. 715–724.

———1972, Geochronology in Minnesota, *in* Sims, P. K., and Morey, G. B., eds., Geology of Minnesota; A centennial volume: Minnesota Geological Survey, p. 27–37.

Goldich, S. S., Hedge, C. E., and Stern, T. W., 1970, Age of the Morton and Montevideo gneisses and related rocks, southwestern Minnesota: Geological Society of America Bulletin, v. 81, p. 3671–3695.

Goldich, S. S., Lidiak, E. G., Hedge, C. E., and Walthall, F. G., 1966, Geochronology of the midcontinent region, United States—Pt. 2, Northern area: Journal of Geophysical Research, v. 71, p. 5389–5408.

Goldich, S. S., Nier, A. O., Baadsgaard, H., Hoffman, J. H., and Krueger, H. W., 1961, The Precambrian geology and geochronology of Minnesota: Minnesota Geological Survey Bulletin 41, 193 p.

Goldich, S. S., and Wooden, J. L., 1981, Origin of the Morton Gneiss, southwestern Minnesota; Pt. 3, Geochronology, *in* Morey, G. B., and Hanson, G. N., eds., Selected studies of Archean gneisses and lower Proterozoic rocks, southern Canadian shield: Geological Society of America Special Paper 182, p. 77–94.

Harris, F. R., 1974, Geology of the Rainy Lake area, district of Rainy River: Ontario Division of Mines, Geological Report 115, 94 p.

Jahn, Bor-Ming, and Murthy, V. R., 1975, Rb-Sr ages of the Archean rocks from the Vermilion district, northeastern Minnesota: Geochimica et Cosmochimica Acta, v. 39, p. 1679–1689.

Keighin, C. W., Morey, G. B., and Goldich, S., S., 1972, East-central Minnesota, *in* Sims, P. K., and Morey, G. B., eds., Geology of Minnesota; A centennial volume: Minnesota Geological Survey, p. 240–255.

Krogh, T. E., 1973, A low-contamination method for hydrothermal decomposition of zircon and extraction of U and Pb for isotopic determinations: Geochimica et Cosmochimica Acta, v. 37, p. 485–494.

Lawson, A. C., 1913, The Archean geology of Rainy Lake restudied: Geological Survey of Canada Memoir 40, 115 p.

Lidiak, E. G., 1971, Buried Precambrian rocks of South Dakota: Geological Society of America Bulletin, v. 82, p. 1411–1420.

Ludwig, K. R., 1982, Programs for filing and X-Y plotting of isotopic and other data using an HP–9830 computer and HP–9862 plotter: U.S. Geological Survey Open-File Report 82–385, 37 p.

McDougall, I., 1966, Precision methods of potassium-argon isotopic age determinations on young rocks, *in* Methods and techniques in geophysics, v. 2: New York, Interscience, p. 279–304.

Peterman, Z. E., Goldich, S. S., Hedge, C. E., and Yardley, D. H., 1972, Geochronology of the Rainy Lake region, Minnesota–Ontario, *in* Doe, B. R., and Smith, D. K., eds., Studies in mineralogy and Precambrian geology: Geological Society of America Memoir 135, p. 193–215.

Peterman, Z. E., and Hildreth, R. A., 1978, Reconnaissance geology and geochronology of the Precambrian of the Granite Mountains, Wyoming: U.S. Geological Survey Professional Paper 1055, 22 p.

Petsch, B. C., 1965, Significant magnetic anomalies in South Dakota: South Dakota Academy of Science Proceedings, 1965, v. 44, p. 52–62.

Petsch, B. C., compiler, 1967, Vertical-intensity magnetic map of South Dakota—Ground magnetometers survey: South Dakota Geological Survey Mineral Resources Investigation Map 4, scale about 1 in.=12 mi.

Prince, L. A., and Hanson, G. N., 1972, Rb-Sr isochron ages for the Giants Range Granite, northeastern Minnesota, *in* Doe, B. R., and Smith, D. K., eds., Studies in mineralogy and Precambrian geology: Geological Society of America Memoir 135, p. 217–224.

Steiger, R. H., and Jäger, E., 1977, Subcommision on geochronology; convention on the use of decay constants in geo- and cosmochronology: Earth and Planetary Science Letters, v. 36, p. 359–362.

1986

U.S. GEOLOGICAL SURVEY BULLETIN 1622

SHORTER CONTRIBUTIONS TO ISOTOPE RESEARCH

APATITE FISSION-TRACK AGE FOR THE BULL DOMINGO BOULDER PIPE, CUSTER COUNTY, COLORADO

Chapter H

By W. N. SHARP and C. W. NAESER

CONTENTS

FIGURE

TABLE

Abstract

Fission-track ages of apatites from Precambrian gneissic boulders in the Bull Domingo pipe in Custer County, Colorado, confirm an Oligocene age for the pipe. Although S. F. Emmons, as early as 1896, had related formation of the highly mineralized structure to Tertiary volcanism at Silver Cliff, the geologic setting of the pipe—entirely enclosed within Precambrian rocks, and lack of Tertiary clast in the pipe—as well as isotopic data for Cambrian or Precambrian leads in the pipe, had left an uncertainty regarding its age.

DISCUSSION

Fission-track counts of apatites were used to settle the age uncertainty regarding a small, richly mineralized, breccia pipe, the Bull Domingo, that is associated closely with the eruptive centers at Silver Cliff and Rosita, Colo. (Sharp, 1978). The Bull Domingo mineralized pipe is totally within the Precambrian terrane of the south slope of the Wet Mountains, about 3 miles north of the towns of Silver Cliff and Westcliffe, and a mile or so from the limits of the Tertiary eruptive center at Silver Cliff (fig.

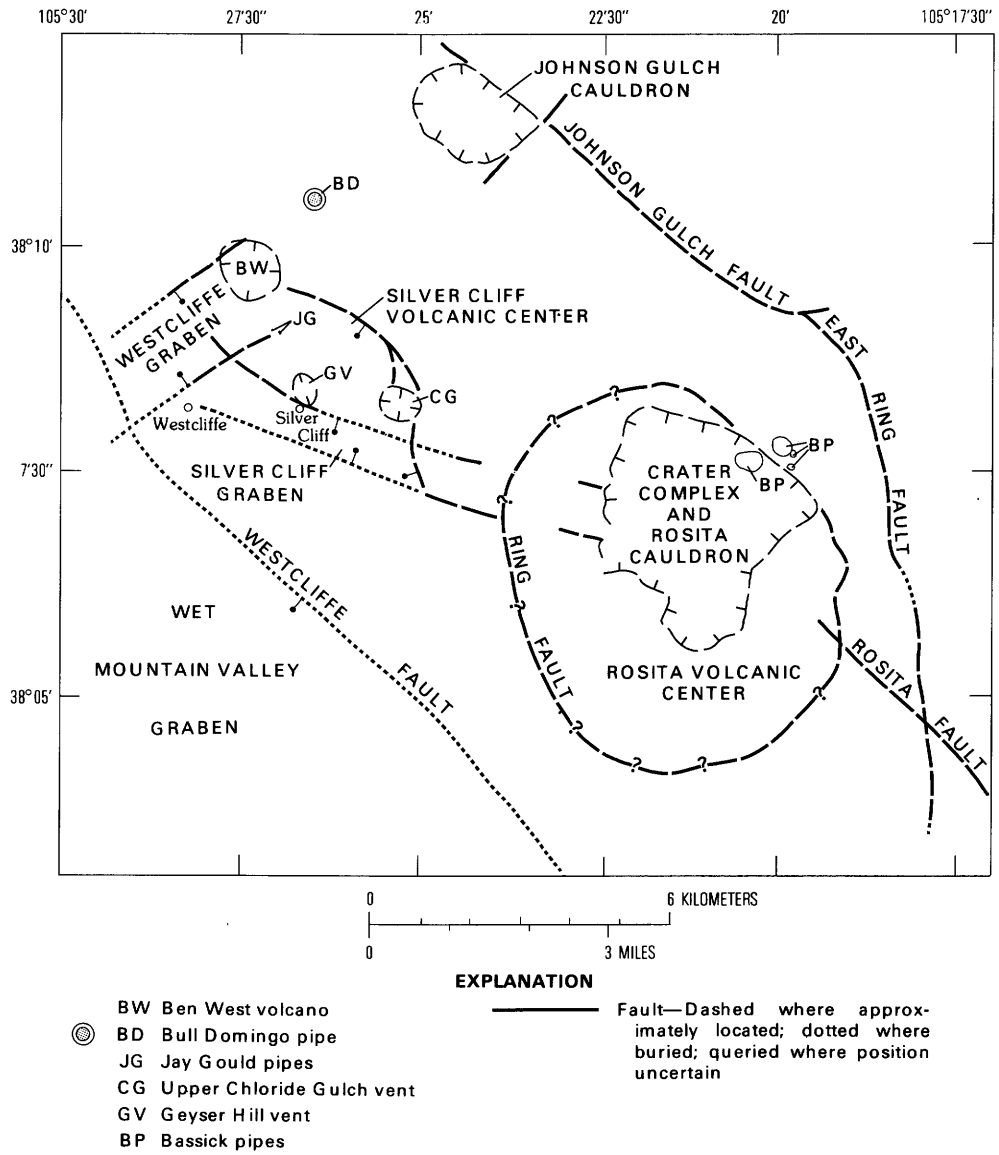

Figure H1. Index map of Silver Cliff and Rosita volcanic centers showing location of Bull Domingo pipe in relation to dominant volcanic and structural features. Custer County, Colo.

Table H1. Apatite fission-track ages and analytical data for apatites from the Bull Domingo mineralized boulder pipe, Custer County, Colo.

[cm^2, square centimters; $\lambda F = 7.03 \times 10^{-17} yr^{-1}$; *R*, correlation coefficient; ppm, parts per million. Number of tracks counted are shown in parentheses]

Sample No.	Lab. No.	Fossil tracks $cm^2 x 10^6$	Induced tracks $cm^2 x 10^6$	Neutrons $cm^2 x 10^{15}$	Age (Ma)	$\pm 2\sigma$ (Ma)	No. of grains	R	U (ppm)
BD-1	DF-2185	0.403	3.39 (363)	4.59 (1527)	32.6	2.2	6	0.993	21
BD-3	DF-2186	0.411	4.04 (167)	4.65 (820)	28.3	2.8	6	0.97	25
BD-4	DF-2187	0.531	4.70 (378)	4.55 (1675)	30.7	2.3	6	0.93	30
BD-6	DF-2188	0.624	5.44 (238)	4.52 (1037)	31.0	2.7	5	0.91	35

H1). The pipe was discovered in 1878 during the silver rush and mining episode at Silver Cliff. Mining at Bull Domingo followed the breccia-boulder pipe down to a depth of 550 feet or more with total value produced of about $1 million in silver and lead. The best geologic description of this pipe—the composition, the shape, ore characteristics, and thoughts on formation—are in "The Mines of Custer County," by S. F. Emmons (1896). Emmons related formation of the Bull Domingo to volcanism at Silver Cliff and considered the structure to be a product of hot fluids passing up through a fractured zone. He developed this model even though all clasts in the pipe are fragments of granite, gneisses, and syenite of the surrounding Precambrian and Cambrian terrane, and no Tertiary eruptive rocks are present in the explored parts of the pipe.

An older Cambrian age for the Bull Domingo pipe is indicated not only by its position in Precambrian terrane and the character of the clasts, but also by a possible association with local alkalic and mafic-ultramafic intrusive complexes of Cambrian age and by lead isotopic data from galena in the pipe. A product of the alkalic to mafic-ultramafic intrusive episodes is a series of red syenite dikes that are widely spaced and distributed in the region (Parker and Hildebrand, 1963). The Bull Domingo pipe pierces the Precambrian terrane at the site of a red syenite dike. Fragments of these rocks are found in the pipe. The eruptive energy for the pipe could have come from this alkalic intrusive episode. The intrusive complexes and the associated red syenite dikes are dated by rubidium-strontium, potassium-argon and fission tracks at about 500 Ma (Olson and others, 1977).

During the late 1950's and through the 1960's, interest in isotopic variations in rock and ore leads resulted in determination of isotopic composition of lead in the Bull Domingo pipe. Two galena samples from the Bull Domingo pipe were analyzed for lead isotopic compositions and reported by Delevaux and others (1966). The lead analyses were used to indicate a model age of 600 Ma (J. C. Antweiler, R. S. Cannon, and A. P. Pierce, unpub. data). This model age and the geologic relations both supported an older age for the Bull Domingo as well as a possible genetic relationship to alkalic intrusive rocks within the Precambrian terrane close by. However, J. C. Antweiler and others (unpub. data) advanced an alternative interpretation of remobilization and redeposition of Precambrian lead during Tertiary time.

In an effort to define a proper association of the Bull Domingo breccia pipe, fission-track ages were determined on apatite separated from gneissic boulders in the pipe. The reasoning, simply stated, was that apatite fission-track ages in these granitic to intermediate rocks of Precambrian age might have been reset at the time of pipe formation and would show a maximum age for that intrusion. The results of the fission-track analyses are given in table H1. The calculated ages from four populations of apatites range from 28.3 ± 2.3 Ma to 32.6 ± 2.2 Ma and average 30.7 Ma; the ages are concordant within the limitations of analytical uncertainty. This age related nicely to the earliest eruptive action of the Ben West volcano at Silver Cliff (Sharp, 1978).

The Bull Domingo pipe is a product of early explosive activity at the Silver Cliff volcanic center and is related specifically to the eruption of the Ben West volcano. The earlier conclusion by J. C. Antweiler and others (unpub. data), that the galena of the Bull Domingo is composed of Precambrian lead is explained if the lead in the Precambrian host rocks was remobilized by the local volcanic activity during the late Oligocene time.

REFERENCES CITED

Delevaux, M. H., Pierce, A. P., and Antweiler, J. C., 1966, New isotopic measurements of Colorado ore-leads, *in* Geological Survey research 1966: U.S. Geological Survey Professional Paper 550–C, p. C178–C186.

Emmons, S. F., 1896, The mines of Custer County, Colorado: U.S. Geological Survey 17th Annual Report, p. 405–472.

Olson, J. C., Marvin, R. F., Parker, R. L., and Mehnert, H. H., 1977, Age and tectonic setting of lower Paleozoic alkalic and mafic rocks, carbonatites, and thorium veins in south-central Colorado: U.S. Geological Survey Journal of Research, v. 5, no. 6, p. 673–687.

Parker, R. L., and Hildebrand, F. A., 1963, Preliminary report on alkalic intrusive rocks in the northern Wet Mountains, Colorado, *in* Geological Survey research 1962: U.S. Geological Survey Professional Paper 450–E, p. E8–E10.

Sharp, W. N., 1978, Geologic map of the Silver Cliff and Rosita volcanic centers, Custer County, Colorado: U.S. Geological Survey Miscellaneous Investigations Map I–1081.

1986

U.S. GEOLOGICAL SURVEY BULLETIN 1622

SHORTER CONTRIBUTIONS TO ISOTOPE RESEARCH

URANIUM-LEAD SYSTEMATICS OF A MIXED ZIRCON POPULATION—THE GRANITE AT YALE FARM, BERKSHIRE MASSIF, CONNECTICUT

Chapter I

By ROBERT E. ZARTMAN, LORETTA M. KWAK, and RALPH P. CHRISTIAN

CONTENTS

FIGURES

TABLES

Abstract

Late- to post-deformational granitic bodies in the Berkshire massif of western Massachusetts and Connecticut place a minimum age on major westward-directed thrust faulting. A detailed uranium-lead dating study of one such body, the granite at Yale Farm, reveals the presence of both inherited xenocrystic zircon and newly crystallized zircon. Varying proportions of these two components in different zircon size fractions establish a remarkably linear mixing array on a concordia diagram with upper and lower intercepts of 1,050±40 Ma and 430±10 Ma, respectively. We associate the former age with the underlying Middle Proterozoic crystalline basement rocks of the massif, and the latter age—adjusted to 430–450 Ma when supplemented by uranium-lead sphene analyses—with the crystallization of the granite.

The electron microprobe was used to chemically characterize the two components of zircon. Their hafnium and uranium contents proved to be the best discriminants in this regard—allowing us to classify individual grains and to map the interface between core and overgrowth of composite grains. Interestingly, the chemical interface did not always precisely match the optical interface and sometimes the optical interface was imperceptible. This observation leads us to the conclusion that the optical interface is of secondary origin and results largely from stresses arising from accumulating radiation dosages.

INTRODUCTION

The common presence of zircon as an accessory mineral in granitic rocks and its ability to withstand subsequent high-grade metamorphism has earned this mineral an unequaled reputation in geochronology. Information about primary age commonly can be obtained even though the host rock has been recrystallized pervasively. Indeed, the survival of preexisting zircon can persist beyond conditions of sillimanite-grade metamorphism and into the pressure-temperature field of anatectic melting. Under such extreme metamorphic conditions, the antecedent crystals generally are resorbed, and a new generation of zircon can form. In this latter instance, the igneous event that we wish to date actually may be recorded in the secondary component of zircon, whereas the primary component carries information about the source of the magma. The task for the geochronologist thus becomes one of resolving a complicated set of isotopic data obtained for polygenetic zircon suites into its geologically meaningful end members.

A clue to a multiple-stage history sometimes is recorded morphologically in the zircon population either by a core and overgrowth relationship or by the mutual existence of two or more distinct varieties of the mineral. At other times, careful examination under the optical microscope fails to identify any trace of interfaces within individual grains or inhomogeneities among the population. In both situations, however, unequivocal evidence for two (or more) generations of zircon formation has been found in the U-Pb (uranium-lead) isotopic systematics, which demand a mixture of components that have distinguishably different ages. A number of investigations detailing the experimental and interpretative techniques for deciphering the ages of such polygenetic zircon have been published during the past decade (excellent examples of such studies include Pidgeon and others, 1970; Koppel and Grunenfelder, 1971; Grauert and others, 1974; Pidgeon and Aftalion, 1978; Chase and others, 1978). Our purpose here in presenting a description of the mixed zircon population in the granite at Yale Farm, North Canaan, Conn., is to document another particularly good example of this phenomenon. Unraveling the physical and chemical properties of this zircon permits the rather precise dating of a significant structural event in the Berkshire massif.

Our effort to date this granitic body (hereafter informally referred to as the granite at Yale Farm) represents only one of our attempts, albeit at present the most successful one, to provide structural control for the tectonic history of the Berkshire massif in Massachusetts and Connecticut. During the past several years we have accumulated a potpourri of zircon uranium-lead analyses from a variety of granitic rocks intruding the Middle Proterozoic basement rocks and the Late Proterozoic(?) to Cambrian(?) mantling metamorphic rocks of the Berkshire massif. Both the basement and mantling rocks are imbricately stacked and were transported westward over autochthonous quartzite and carbonate rock of Late Proterozoic(?) and early Paleozoic age of the North American shelf (fig. I1). Although later metamorphic isograds attributed to the Acadian orogeny are superimposed on all these rocks (Ratcliffe and Harwood, 1975), a long-standing question not completely resolved by field relationships is the timing of major kinematic deformation. Constrained by the age of the youngest stratigraphic unit (Middle Ordovician Walloomsac Formation) involved in the thrust faulting and by the regional Early to Middle Devonian Acadian metamorphic overprinting, this deformational event might be attributable either to the Late Ordovician Taconic orogeny or to an early phase of the Acadian orogeny. We believe that our dating of the late to post-deformational granite at Yale Farm as Late Ordovician or Early Silurian resolves this controversy in favor of the Taconic orogeny.

ACKNOWLEDGMENTS

We are indebted to N. M. Ratcliffe, D. S. Harwood, and the late R. W. Schnabel of the U.S. Geological Survey, and S. A. Norton of the University of Maine for providing the rock samples that yielded the mineral

Figure 11. Generalized structure map of the central Berkshire massif, Massachusetts and Connecticut. Modified from Ratcliffe and Hatch (1979).

Table I1. Uranium-thorium-lead isotopic ages of zircon from the Berkshire massif

[Decay constants: $^{238}U=1.55125\times10^{-10}$ yr^{-1}; $^{235}U=9.8485\times10^{-10}$ yr^{-1}; $^{232}Th=4.9475\times10^{-11}$ yr^{-1}; $^{238}U/^{235}U=137.88$ Isotopic composition of common lead assumed to be $^{204}Pb:^{206}Pb:^{207}Pb:^{208}Pb$ = 1:18.0:15.6:38.0 for all samples except 3 for which it is assumed to be 1:17.0:15.5:36.8]

Sample No.	Mesh size	Concentrations (parts per million)			Isotopic composition of lead (atom percent)				Age, in millions of years			
									^{206}Pb	^{207}Pb	^{207}Pb	^{208}Pb
		U	Th	Pb	^{204}Pb	^{206}Pb	^{207}Pb	^{208}Pb	^{238}U	^{235}U	^{206}Pb	^{232}Th
1	(-100+150)	2920	83.4	192.2	0.016	92.52	5.656	1.806	440	459	554	623
	(-200+250)	2446	97.1	147.5	.014	92.62	5.552	1.816	405	423	523	446
2	(-100+150)	211	25.4	19.4	.062	87.30	6.548	6.086	570	611	769	642
	(-200+250)	277	43.4	24.6	.028	88.44	6.093	5.442	560	600	754	560
3	(-100+150)	290	48.2	48.9	.128	82.38	7.939	9.556	941	975	1051	1093
	(-200+250)	351	55.0	53.5	.067	85.29	7.230	7.416	895	934	1029	1065
4	(-100+150)	323	27.2	32.4	.111	85.33	7.154	7.404	597	635	774	840
	(-150+200)	298	24.7	29.0	.108	85.62	7.072	7.198	582	619	757	813
	(-250+325)	276	21.6	24.6	.117	85.62	7.078	7.190	534	568	705	698
	(-400)	387	33.3	34.0	.130	85.00	7.169	7.705	522	553	683	635
5	(-100+150)	417	49.8	47.1	.011	88.91	6.272	4.804	711	756	891	923
	(-150+200)	372	39.2	36.1	.012	89.46	6.126	4.401	619	665	825	813
6	(-100+150)	1162	169.5	102.6	.004	90.61	5.887	3.498	573	611	754	457
	(-200+250)	1311	203.8	94.5	.006	91.59	5.558	2.844	477	498	597	276
	(-325+400)	1315	247.7	80.7	.006	92.03	5.257	2.708	410	418	460	184
7	(-100+150)	119	25.2	10.1	.024	85.96	6.011	8.004	557	608	802	638
	(-150+200)	153	18.9	12.3	.019	88.92	5.919	5.147	510	551	722	641
	(-200)	253	32.6	18.8	.068	87.83	6.018	6.088	467	473	503	457
8	(-50+150)	443	129.1	41.6	.016	88.00	5.804	6.180	590	618	720	405
	(-150+250)	662	375.8	59.9	.013	83.36	5.397	11.23	541	570	690	385
	(-250)	983	652.7	76.0	.012	82.40	4.888	12.70	459	466	501	322

DESCRIPTION OF SAMPLES

Sample localities shown on figure I1. Quadrangles listed are names of U.S. Geological Survey 7-1/2 minute topographic quadrangle maps.

1. Gray, medium-grained gneissic granite from the Hubbard River, Granville State Forest, West Granville quad.; lat 42°03'20" N., long 72°57'47" W.
2. Light-gray, medium-grained gneissic granite from roadcut on Route 8 overlooking Colebrook Reservoir, Tolland Center quad.; lat 42°02'10" N., long 73°03'26" W.
3. Tectonic sliver of Washington(?) Gneiss west of Babb Hill, West Granville quad.; lat 42°07'22" N., long 72°59'41" W.
4. White, cataclastic muscovite granite (Ratcliffe and Hatch, 1979) from small quarry east of Cushman Brook, Becket quad.; lat 43°15'10" N., long 73°00'31" W.
5. Light-gray, fine-grained, weakly foliated granite from the New Whiting quarry, Otis quad.; lat 42°14'03"N., long 73°04'15" W.
6. Gray, coarse-grained binary granite from the Winn quarry, Otis quad.; lat 42°14'42" N., long 73°00'59" W.
7. Gray, medium-grained, well-foliated biotite granite from the Williams quarry, Otis quad.; lat 42°13'55" N., long 73°01'22"W.
8. Gray, medium-grained, weakly-foliated binary granite from small quarry on Yale Farm, South Sandisfield quad.; lat 42°02'11" N., long 73°13'48" W.

separates analyzed in this study. Numerous helpful discussions and correspondences with these colleagues as the work progressed aided us substantially in understanding and interpreting the resultant data, and in bringing our ideas together into this paper.

Just prior to completion of our manuscript, we learned of the research efforts by J. F. Sutter, N. M. Ratcliffe, and S. B. Mukasa using the $^{40}Ar/^{39}Ar$ method to decipher the tectonic history of southwestern New England. Basically, their work points to a greater Taconic and diminished Acadian role in the metamorphism of the Berkshire massif. Although they now bring into question an Acadian assignment for the metamorphic isograds used to assign a minimum age to the major deformation, we otherwise find the conclusions of both studies to be in agreement and mutually supportive in emphasizing the Taconic orogeny.

We gratefully acknowledge the following persons for technical assistance. Many of the preliminary uranium-lead analyses were performed by Margarita Gallego. G. T. Cebula and J. W. Groen assisted in the zircon and sphene separations. Barbara Lockett prepared the polished grain mounts for the electron microprobe.

PRIOR URANIUM-LEAD ZIRCON DATING EFFORTS IN THE BERKSHIRES

The polygenetic nature of these zircons was first detected in a reconnaissance study of small granitic plutons intruding the southeastern flank of the Berkshire massif. The structural complexity of this terrane was not appreciated fully at the time, and the intimately associated "gneisses" and "schists", now recognized as tectonically imbricated Middle Proterozoic basement and Late Proterozoic(?) to Cambrian(?) mantling rocks, respectively, were conjectured to be a normal stratigraphic succession sandwiched between the more coherent basement core of the Berkshires on the west and the Proterozoic or Cambrian Hoosac Schist and its equivalent, the Waramaug Formation on the east. When the first zircon analyses yielded $^{207}Pb/^{206}Pb$ ages of 523 to 769 Ma (sample localities 1–2, Table I1), they seemed to lend credence to the hypothesis that a major volcanoclastic unit comprised of massive flows and tuffs, the "gneiss", interbedded with clastic sediments, the "schist", conformably underlay the Hoosac Schist. According to this interpretation, the granitic bodies represented contemporaneous epizonal plutons associated with the volcanic centers.

Some suspicion was aroused, however, by the tendency of the isotopic data to lie close to a reference chord drawn between 400 and 1,100 Ma on a concordia diagram (fig. I2). The upper intercept of that chord approximates the age of the Middle Proterozoic basement for the Berkshire massif (Ratcliffe and Zartman, 1976), whereas the lower intercept could represent either the Taconic or Acadian orogeny. Further doubt was raised by the analysis of a third sample (sample locality 3, table I1)—a gneissic unit interlayered with schist and hypothesized to be a volcanic flow rock. Contradictory evidence comes from its uranium-lead zircon ages, which are considerably older than those of samples 1 and 2. In fact, these determinations plot on the concordia diagram amid previously published data for two samples of Middle Proterozoic basement rocks (Tyringham and Washington Gneisses; Ratcliffe and Zartman, 1976). A revisit to locality 3 now convinces us that the dated rock is really a tectonic sliver of possible Washington Gneiss in fault contact with Hoosac Schist. With the demise of the "normal stratigraphic succession" theory and our inability to refine the ages of these granitic bodies, we turned our attention to the north and west where detailed mapping was recognizing the true magnitude of the structures in the Berkshire massif.

By carefully establishing and tracing out stratigraphic units within the basement and mantling rocks, as many as 12 separate tectonic slices were delineated across the massif. This westward-directed telescoping of the eastern margin on the North American continental crust produced an imbrication of stratigraphic units that made previous efforts to view the Berkshires as a regionally coherent anticlinal arch obsolete. The most conservative restoration of these stacked slices demand at least a 50-percent shortening across the structure. Late-stage granites can be shown to intrude along several of the fault surfaces, and they present an opportunity for placing a further minimum age on the time of deformation. Much of this field and petrographic work, which provides the geologic context for the present study, has been published elsewhere (Ratcliffe, 1975; Harwood, 1975, 1979a; Ratcliffe and Zartman, 1976).

Similar to the pattern we had observed to the southeast, our uranium-lead zircon data from the central and

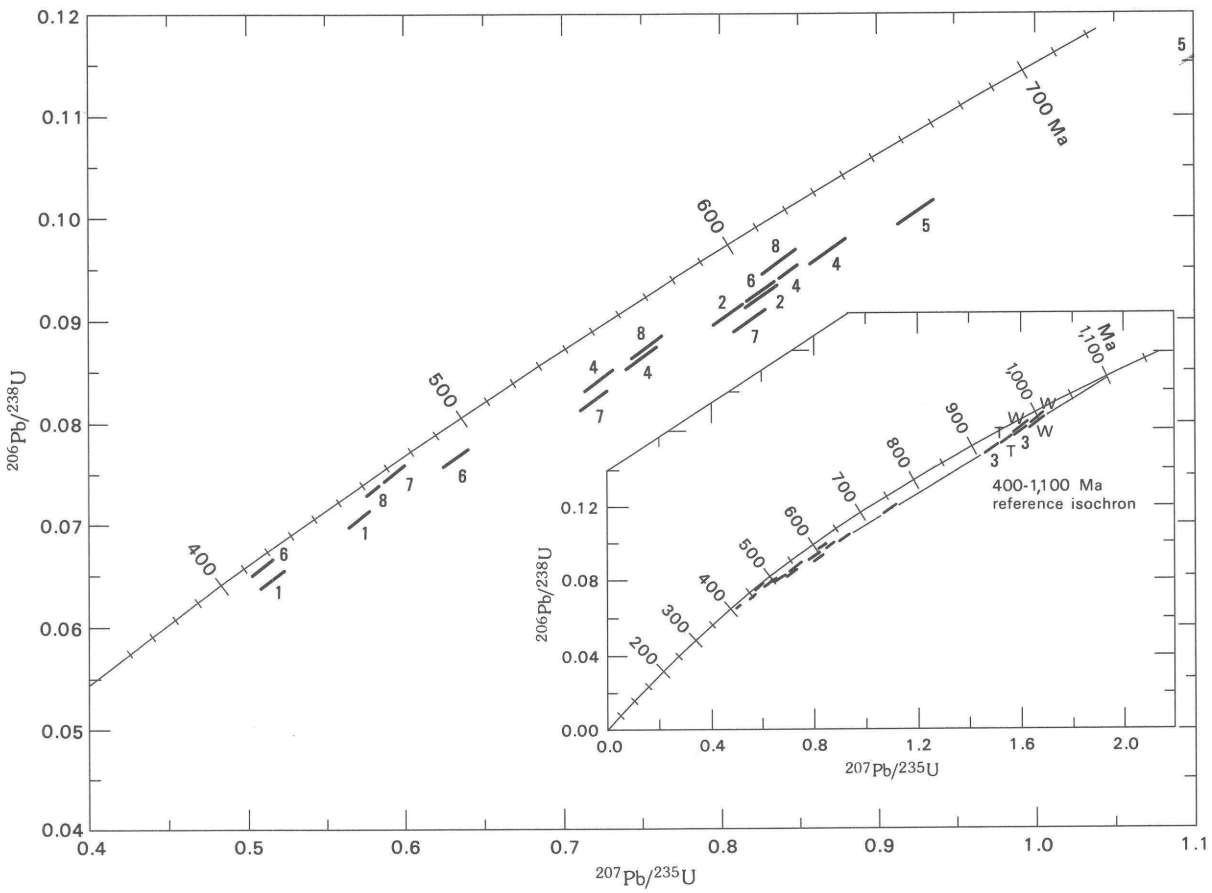

Figure I2. Concordia diagram for zircon from various localities in the Berkshire massif. (See figure I1 for sample localities and table I1 for sample descriptions.) Also shown are data from the Middle Proterozoic Tyringham (T) and Washington (W) Gneisses (Ratcliffe and Zartman, 1976).

southwestern Berkshires fell close to the 400- to 1,100-Ma reference line on the concordia diagram (see fig. I2, and sample localities 4–8; table I1). However, with our better understanding of the stratigraphy, the anomalous nature of these results was apparent immediately when $^{207}Pb/^{206}Pb$ ages in excess of 700 Ma were found for granites invading along faults, which themselves displaced strata no older than latest Late Proterozoic, and, more probably, Cambrian in age. The demonstrable time-equivalence of these faults hosting the granites to the main transport of the Berkshire terrane across the Cambrian to Middle Ordovician shelf-facies rocks served to clinch the argument. For at least some of the granites, a local, anatectic origin could be postulated from field evidence, and distinct zircon overgrowths could be seen to enclose ovoidal, partially resorbed cores. It is from these preliminary attempts to determine radiometric age control for the granites that we decided to re-collect a large sample of the granite at Yale Farm for detailed study. Otherwise, we do not propose to use our preliminary data given in table I1 to add to existing stratigraphic and structural interpretation of the Berkshires. Neither precise enough radiometric results to resolve between a Taconic or Acadian age nor a correlation of intrusive units beyond that established through independent field evidence is implied for any of the other granites.

GEOLOGIC SETTING OF THE GRANITE AT YALE FARM

The local geologic setting of the granite at Yale Farm is shown in figure I3. A brief description of field relationships is necessary to document the critical role this igneous rock plays in establishing the time of thrust faulting and metamorphism in adjacent strata. The granite at Yale Farm occupies the largest pluton—having an area of about 0.3 km^2 (square kilometers)—at the northwestern end of a linear trend of such bodies, which here cut across three of the stacked fault slices. Each of these slices contains a different lithologic assemblage, which, from lower to upper slice, consists of (1) Late Proterozoic or Cambrian Dalton Formation unconformably overlying Middle Proterozoic granitic gneiss, (2) Late Proterozoic and Cambrian Canaan Mountain Formation, and (3) Middle Proterozoic hornblende-biotite amphibolitic gneiss. Several kilometers to the west the lowermost of these slices overrides the Cambrian to Middle Ordovician autochthonous shelf carbonate rocks. Although by no means conclusively proved, stratigraphic and structural arguments can be made that successively higher slices have been transported from progressively further east during the period of major tectonic telescoping of the Berkshires.

The granite is gray, fine to medium grained, and varies in texture from massive to slightly foliated except where faulting and folding have imparted a stronger, local fabric on the rock. Compositionally, the bodies range from quartz monzonite to granite, contain two micas, and yield an accessory mineral suite of apatite, sphene, zircon, and opaque minerals.

For our re-collection, about 50 kg (kilograms) of especially fresh, weakly foliated granite at Yale Farm was obtained from the small quarry site near the west margin of the pluton that had provided the preliminary sample. A strong microscopic mortar structure associated with the Haystack Mountain thrust and presumably superimposed on the granite by the last movement of the fault, was avoided entirely in our sampling. Poor outcrop exposures do not permit precise location of the pluton's contact with its wall rock, but at the present level of erosion, Middle Proterozoic gneisses surround most of the body. If the magma was transported some distance either vertically or along the Haystack Mountain fault surface before final crystallization, country rock representative of two or all three of the fault slices, and even the underlying autochthon could have contributed to its production. The uranium-lead isotopic systematics reveal that a component of zircon inherited from the Middle Proterozoic crystalline rocks unquestionably is present in the granite. The analytical results obtained for zircon and sphene of the re-collected granite of Yale Farm form the basis of this report.

ANALYTICAL PROCEDURE

A brief account of our analytical procedure is given in this section with particular emphasis on documentation of precision and accuracy. The sensitivity of the concordia intercept ages to only slight shifts in the position of the data points demands that special care be taken in carrying out all aspects of the chemistry and mass spectrometry. We include the results obtained on an interlaboratory zircon standard, which defines our reproducibility prevailing for the duration of the study.

The sample size for individual analyses ranged from 1 to 20 mg (milligrams), and weighings were made on an appropriate semimicro or micro balance to achieve an accuracy of ± 0.4 percent or better. A HF-HNO_3 hydrothermal digestion procedure for the zircon closely followed that reported by Krogh (1973). ^{235}U and ^{230}Th tracer solution was added to the sample prior to its digestion in a 15–mL (milliliter) teflon bomb, and ^{208}Pb tracer solution was later added to an aliquot of the dissolved sample. Lead was purified by an anion-exchange column using an HBr elution technique as described by Manhes and others (1978), loaded with phosphoric acid and silica gel on a rhenium filament, and analyzed by a 12–inch, computer-controlled, solid-source mass spectrometer providing automated data reduction (Stacey and Hope, 1975). Uranium and thorium were purified by nitrate-form anion

columns from the HBr elutriant, and were analyzed using a triple filament configuration in a 6–inch mass spectrometer (Tatsumoto, 1966). The chemical procedure for the sphene differed only in the digestion step, in which HF, HCl, and $HClO_4$ were substituted as the reactant acids.

Total chemistry blanks range from 0.5 to 0.2 ng (nanograms) of lead depending mainly on the sample size,

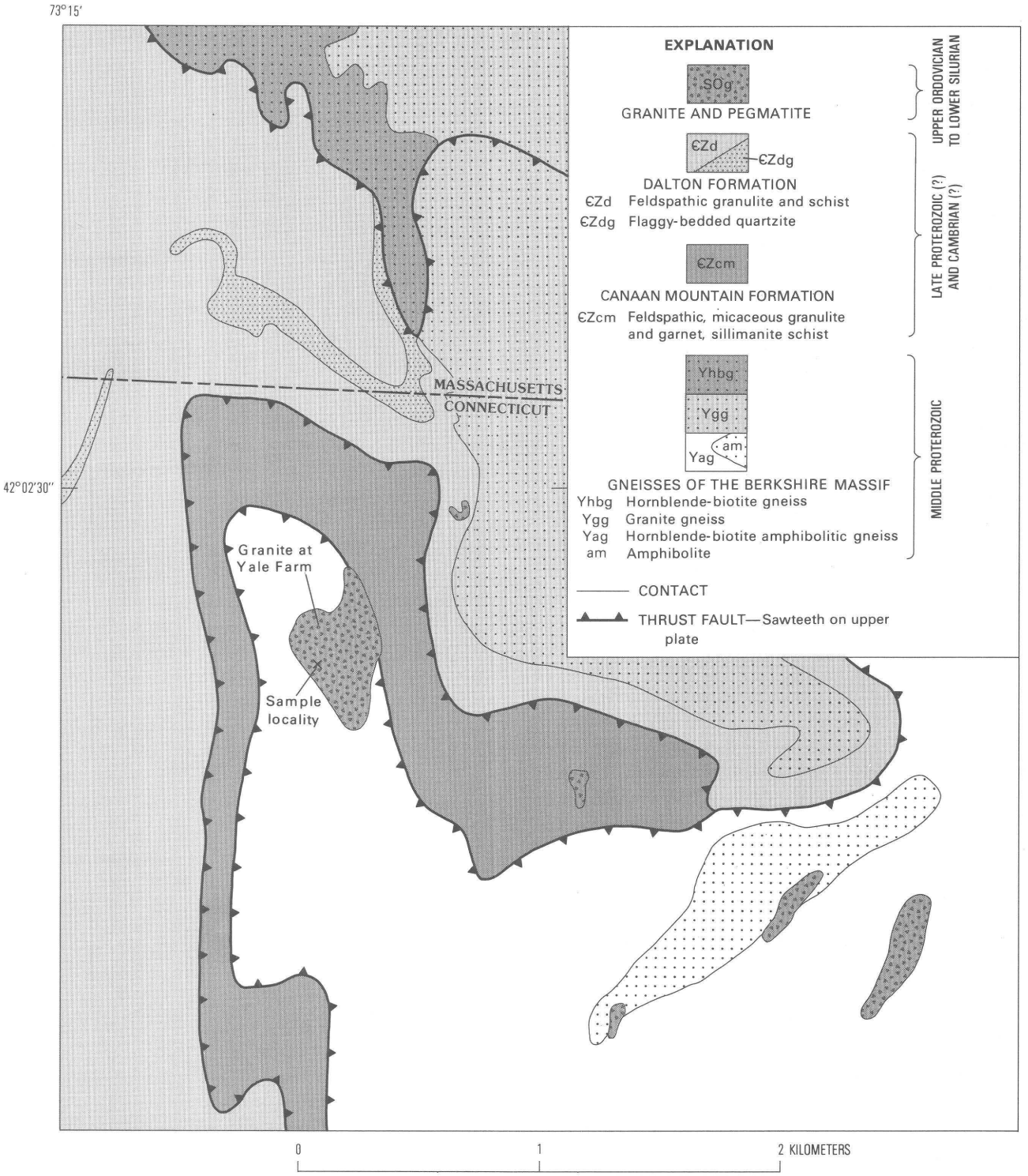

Figure 13. Geologic map of the granite at Yale Farm and vicinity. From Harwood (1979a).

Table I2. Uranium-thorium-lead isotopic ages of S-2–67 zircon standard

[Decay constants: $^{238}U=1.55125\times10^{-10}$ yr^{-1}; $^{235}U=9.8485\times10^{-10}$ yr^{-1}; $^{232}Th=4.9475\times10^{-11}$ yr^{-1}; $^{238}U/^{235}U=137.88$. Isotopic composition of common lead assumed to be $^{204}Pb:^{206}Pb:^{207}Pb:^{208}Pb=1:18.1:15.6:37.9$]

Date analyzed (mo./yr)	Approx. weight (milligrams)	Concentration (parts per million)			Isotopic composition of lead (atom percent)				Age, in millions of years			
		U	Th	Pb	^{204}Pb	^{206}Pb	^{207}Pb	^{208}Pb	$^{206}Pb/^{238}U$	$^{207}Pb/^{235}U$	$^{207}Pb/^{206}Pb$	$^{208}Pb/^{232}Th$
1/77	51.6	248.6	158.7	16.73	0.0295	78.02	4.664	17.29	379.2	379.5	381.5	383.9
10/77	42.9	245.6	161.6	16.61	0.0293	78.03	4.665	17.27	381.1	381.4	383.3	374.2
11/77	34.4	245.5	161.2	16.46	0.0287	78.05	4.652	17.27	378.0	378.4	380.5	372.2
2/78	32.4	247.6	162.9	17.03	0.0478	77.28	4.892	17.78	382.1	382.0	381.9	376.0
2/78	32.7	246.4	161.4	16.61	0.0194	78.39	4.542	17.05	382.4	382.7	384.5	378.2
12/79	34.5	253.1	163.6	16.76	0.0128	78.65	4.454	16.88	377.7	378.2	381.5	378.3
12/80	10.9	253.1	163.1	16.59	0.0101	78.76	4.425	16.80	374.7	376.0	383.9	376.2
12/80	14.2	249.3	162.3	16.56	0.0150	78.54	4.481	16.96	378.1	378.6	381.9	376.7
7/81	9.8	249.1	161.3	16.72	0.0155	78.52	4.490	16.98	381.8	382.0	383.4	382.7
5/82	11.9	250.1	163.5	16.82	0.0418	77.51	4.813	17.64	375.4	376.0	379.8	372.1
2/83	27.0	252.7	163.7	16.76	0.0213	78.36	4.557	17.07	376.1	376.5	378.6	375.0
6/83	9.1	251.9	159.5	16.59	0.0185	78.53	4.531	16.91	374.6	375.6	381.6	379.8
Average		249.4	161.9	16.69					378.4	378.9	381.8	377.1
Standard deviation		±2.6	±1.5	±0.15					±2.9	±2.6	±1.7	±3.7
Coefficient of variation (percent)		±1.0	±0.9	±0.9					±0.8	±0.7	±0.4	±0.9

and represent less than 0.5 percent of the sample lead. After removing a nominal blank from each analysis, the remaining ^{204}Pb was attributed to initial lead in the zircon that was assumed to have a model isotopic composition of $^{206}Pb/^{204}Pb=18.0$, $^{207}Pb/^{204}Pb=15.6$, and $^{208}Pb/^{204}Pb=38.0$. In no instance was the correction for either the chemistry blank or the initial lead a significant factor of uncertainty in the zircon age calculations. The initial lead isotopic composition is a critical consideration in determining the sphene ages, and, accordingly, the lead isotope ratios were measured in a coexisting microcline and were corrected for 430 Ma of in-place radioactive decay. We then used this feldspar lead isotopic composition ($^{206}Pb/^{204}Pb=18.46$, $^{207}Pb/^{204}Pb=15.61$, $^{208}Pb/^{204}Pb=38.14$), which differs slightly from the model isotopic composition, to compute the sphene ages.

All tracers were calibrated periodically against gravimetrically prepared shelf solutions, and over the lifetimes of individual tracers, concentrations of uranium and thorium remained constant to within ±0.3 percent, and of lead to within ±0.2 percent with no systematic drifts noted. Also, an analysis of the USGS BCR–1 rock standard was performed during the course of the study, and uranium, thorium, and lead contents were found to be within 0.2 percent of the published values (Tatsumoto and others, 1972). In order to establish the overall accuracy in element concentration for a sample, we need to add the effects of weighing errors, chemical and isotopic inhomogeneity, and mass spectrometer fractionation. From experience gained on replicate analyses and interlaboratory comparisons, we can demonstrate a short-term accuracy spanning the duration of this study of about ±0.4 percent (2σ) for uranium, thorium, and lead contents, although over a longer period of time (that is, the past 5 years) that value needs to be approximately doubled. A good indication of long-term reproducibility, which also should approximate accuracy, comes from a tabulation of results for our S–2–67 standard zircon (see table I2).

Based on replicate analyses of various lead isotope standards, the following uncertainties (2σ) are assigned to the measured ratios: $^{206}Pb/^{204}Pb$ ±0.4 percent (1000), ±2 percent (10,000), ±10 percent (100,000); $^{206}Pb/^{207}Pb$ ±0.09 percent; $^{206}Pb/^{208}Pb$ ±0.13 percent. Although at first glance the isotopic data for S–2–67 standard zircon suggests a much greater uncertainty in replicate isotope ratios, this variability is due almost entirely to different blank and (or) initial lead contents among the analyzed fractions. After this factor is removed, the calculated ages attest to a much greater precision in measurement of the radiogenic isotopes. Especially for the $^{207}Pb/^{206}Pb$ age with its precision of 0.3 percent can we recognize an uncertainty in this ratio commensurate with that just quoted. A more complete treatment of error assignment to uranium-thorium-lead isotopic data as used in this paper is given by Ludwig (1979).

GEOCHRONOLOGIC RESULTS

Standard heavy liquid and magnetic mineral separation techniques were used to obtain >99 percent pure zircon and sphene concentrates, which were additionally handpicked of any remaining impurities to provide the sample material for analysis. The zircon was sized through silk screens into −50+100, −100+150, −150+200, −200+250, −250+325, −325+400, and

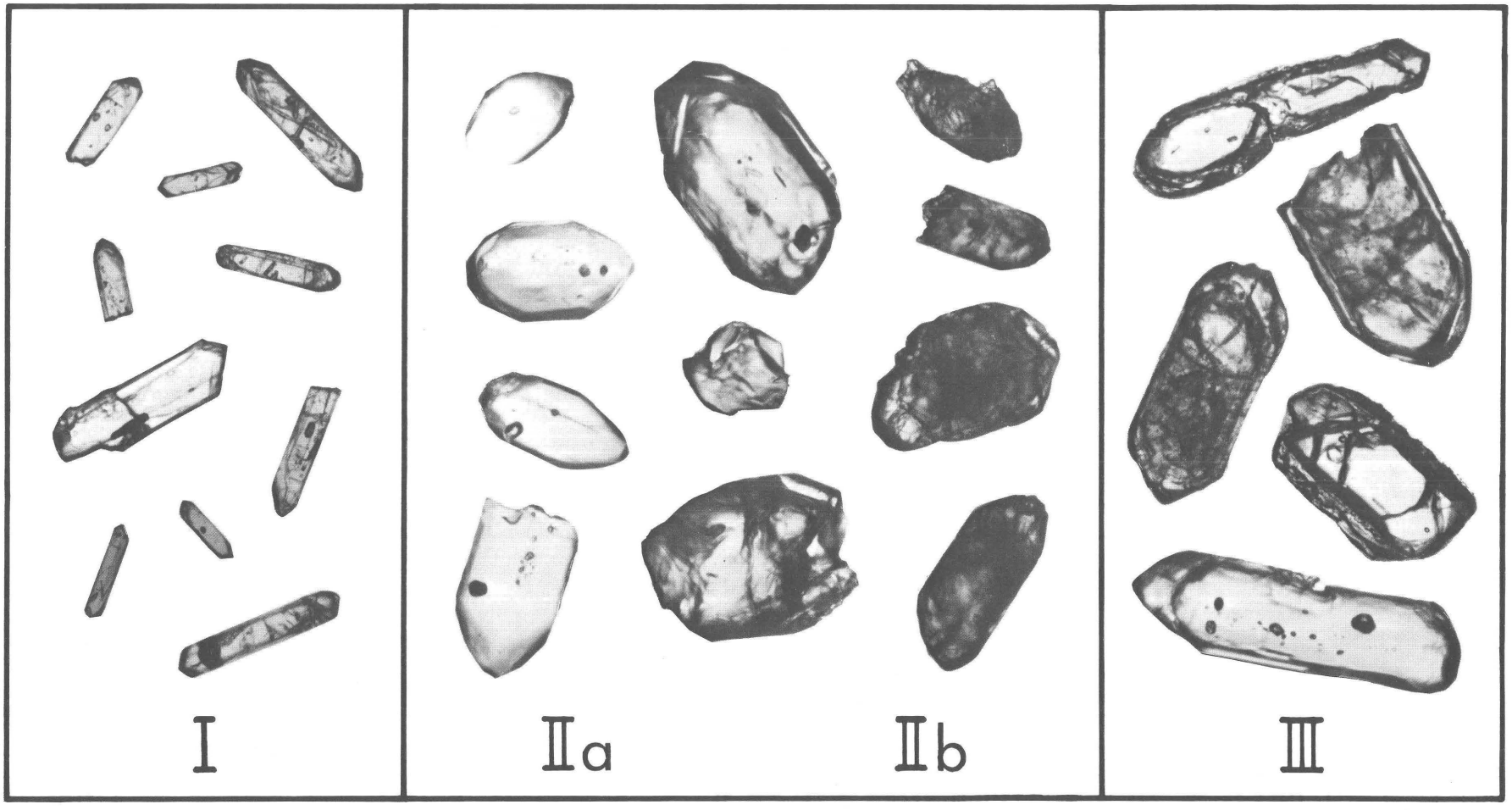

Figure 14. Photomicrographs of representative grains of the three varieties of zircon from the granite at Yale Farm. I, Colorless, acicular, euhedral grains; II, (a) Clear, brilliant, euhedral to (b) dark-brown, opaque, anhedral crystallographically complex grains; III, Composite grains with distinct rims and cores. Largest grains are about 700 micrometers in long dimension.

−400 mesh fractions, and each fraction was then weighed and examined under the binocular microscope. We were able to recognize three different morphological types of zircon: I, a colorless, euhedral variety comprised of simple, acicular crystals that increase in relative abundance with decreasing grain size; II, a crystallographically complex variety forming a continuum from clear, brilliant euhedral to dark-brown, opaque anhedral grains; and III, dominating all but the −400 mesh size fraction, composite grains with a distinct rim overgrowing a rounded and usually less turbid core. Initially, we thought that the extreme manifestations of variety II zircon represented two separate genetic groupings, but a more careful microscopic examination and subsequent electron microprobe analyses showed the morphological differences to be within a single population and to relate almost entirely to radioactivity. Apparently, the clarity of the zircon is a function of accumulated radiation dosage with the increased coloration and deteriorated crystallinity representing more advanced stages of metamictization. In order to facilitate discussion, the end-member components will be designated as follows: IIa, clear, low uranium, and IIb, brown, high uranium subvarieties. The division between them is defined arbitarily on the basis of perceived color, and the two subvarieties are differentiated mainly for the purpose of making rough estimates of abundance. Photomicrographs illustrating representative grains of the three varieties of zircon are presented in figure I4. The approximate proportion of morphological types among the seven size fractions has been determined by point-counting grain mounts (fig. I5), although a number of grains leave doubt as to their classification under this simplistic scheme. The greatest uncertainty arose in the assignment to variety II of grains containing virtually no hint of an internal interface until examined under the microprobe, where their true composite nature was revealed. Here, again, we came to recognize the visual contrast between overgrowth and core as due to differences in their uranium content and accumulated radiation damage.

Uranium-thorium-lead isotopic analyses were made on total splits of each of the seven size fractions of zircon, and the resultant data are given in table I3 and are plotted on a concordia diagram in figure I6. As we proceed with the discussion of the zircon isotopic systematics, a strong decoupling of the $^{238}U \rightarrow ^{206}Pb$ and $^{235}U \rightarrow ^{207}Pb$ and the $^{232}Th \rightarrow ^{208}Pb$ decay schemes soon will become apparent. Whereas the uranium and uranogenic lead isotopes give every indication of closed-system behavior, the thorium and thorogenic lead isotopes must have been affected by major postcrystallization open-system movement. We suspect that at least some of the thorium and resultant thorogenic lead is sited quite differently from the uranium and, thus, account for their independent migration. Attempts to identify such sites, either within the zircon lattice or in some separate, included phase, have not been successful yet, although, as is true of the −200+250 mesh fraction, there is reason to expect the presence of a discrete thorium mineral. Quite frankly, we are puzzled by the discrepancy in the thorium-lead system, which invites concern about a correlative uranium-lead effect. Nevertheless, evidence for such an effect was not seen in the remarkably regular behavior of the uranium-lead systematics.

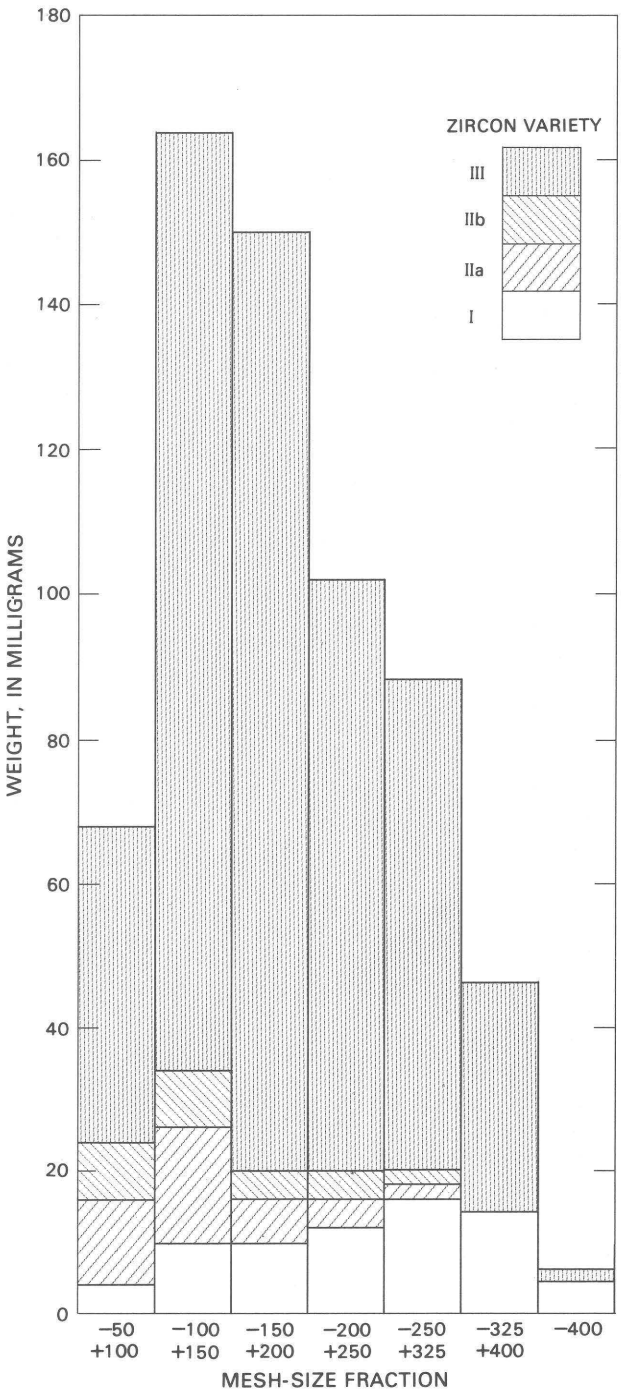

Figure I5. Abundances of the three varieties of zircon from the granite at Yale Farm as a function of mesh size.

Table 13. Uranium-thorium-lead isotopic ages of zircon and sphene from the granite at Yale Farm

[Decay constants: $^{238}U=1.55125\times10^{-10}$ yr $^{-1}$; $^{235}U=9.9585\times10^{-10}$ yr $^{-1}$; $^{232}Th=4.9475\times10^{-11}$ yr^{-1}; $^{238}U/^{235}U=137.88$ Isotopic composition of common lead assumed to be ^{204}Pb: ^{206}Pb: ^{207}Pb: $^{208}Pb=1:18.0:15,6:28.0$, except for sphene where ^{204}Pb:^{206}Pb: ^{207}Pb:$^{208}Pb=1:18.46:15.61:38.14$ as determined in coexisting microline]

Sample	Mesh size	Concentration (parts per million)			Isotopic composition of lead (atom percent)				Age, in millions of years			
		U	Th	Pb	^{204}Pb	^{206}Pb	^{207}Pb	^{208}Pb	$^{206}Pb/^{238}U$	$^{207}Pb/^{235}U$	$^{207}Pb/^{206}Pb$	$^{208}Pb/^{232}Th$
a	(-50+100)	561.3	146.6	48.00	0.0100	88.25	5.825	5.918	541	584	754	409
b	(-100+150)	708.0	299.4	65.47	.0051	86.64	5.595	7.763	574	607	733	373
c	(-150+200)	838.2	398.6	75.76	.0076	85.86	5.496	8.636	556	585	699	358
d	(-200+250)	895.4	762.4	83.43	.0054	81.08	5.115	13.80	542	569	678	336
e	(-250+325)	944.2	519.8	79.15	.0050	84.77	5.216	10.01	511	533	628	337
f	(-325+400)	958.4	653.6	76.72	.0056	82.80	4.943	12.25	478	492	557	319
g	(-400)	1087.4	867.2	83.20	.0154	80.81	4.795	14.38	446	451	474	299
h	(-50+150), variety IIa	236.7	74.4	21.09	.0392	85.10	5.790	9.071	540	562	652	484
i	(-50+150), variety IIb	1513.2	315.9	189.22	.0052	90.38	6.214	3.404	795	814	866	433
S-I	Sphene I	22.8	29.4	3.81	.629	48.31	11.88	39.18	443	445	459	442
S-II	Sphene II	17.9	20.4	3.96	.821	43.01	14.39	41.78	445	449	473	456

Most obvious in these total split data is the resemblance to a mixing array, which we were anticipating from the prior preliminary analyses of the granite at Yale Farm and elsewhere in the Berkshire massif. To a first approximation, the linear array can, in fact, be explained rather straightforwardly as a binary mixture of xenocrystic and igneous components. The uranium and thorium concentrations also support such two-component mixing with the less radioactive, xenocrystic zircon most abundant in the coarsest fractions, and the more radioactive, igneous zircon most abundant in the finest fractions. The high thorium content of the $-200+250$ mesh fraction is anomalous in this regard, but it might be explained by some undetected thorite or other high thorium phase included in that particular sample. In the coarser material, however, especially in the $-50+100$ and, probably, in the $-100+150$ mesh fractions, the presence of a third component that apparently was affected by some younger disturbance of its uranium-lead system rules out a completely binary behavior for the whole population. This third component appears to be related to rare but highly radioactive (>3000 ppm U; ppm, parts per million) domains in some of the large variety IIb zircon, which we have avoided in the later analyses.

The remarkably straight line defined by the $-150+200$, $-200+250$, $-250+325$, $-325+400$, and -400 mesh fractions does invite further consideration of those fractions as a true binary mixture. We see from figure I5 that the trend in apparent age for these five fractions correlates almost solely with the relative abundance of varieties I and III zircon. Such a correlation would be expected if—as seems reasonable—variety I is entirely related to the crystallization of the granite at Yale Farm and variety III records a polygenetic origin whereby the cores are partially resorbed zircon from the Middle Proterozoic crystalline basement and the overgrowths were added during granite crystallization. Barring any other complications in the isotopic systematics, the straight-line fit to the five data points will have a lower intercept with the concordia curve yielding the time of granite crystallization and an upper intercept representing the age of the xenocrystic component (Wetherill, 1956). Indeed, a least-squares regression of the data does indicate linearity to within experimental uncertainty with lower and upper in-

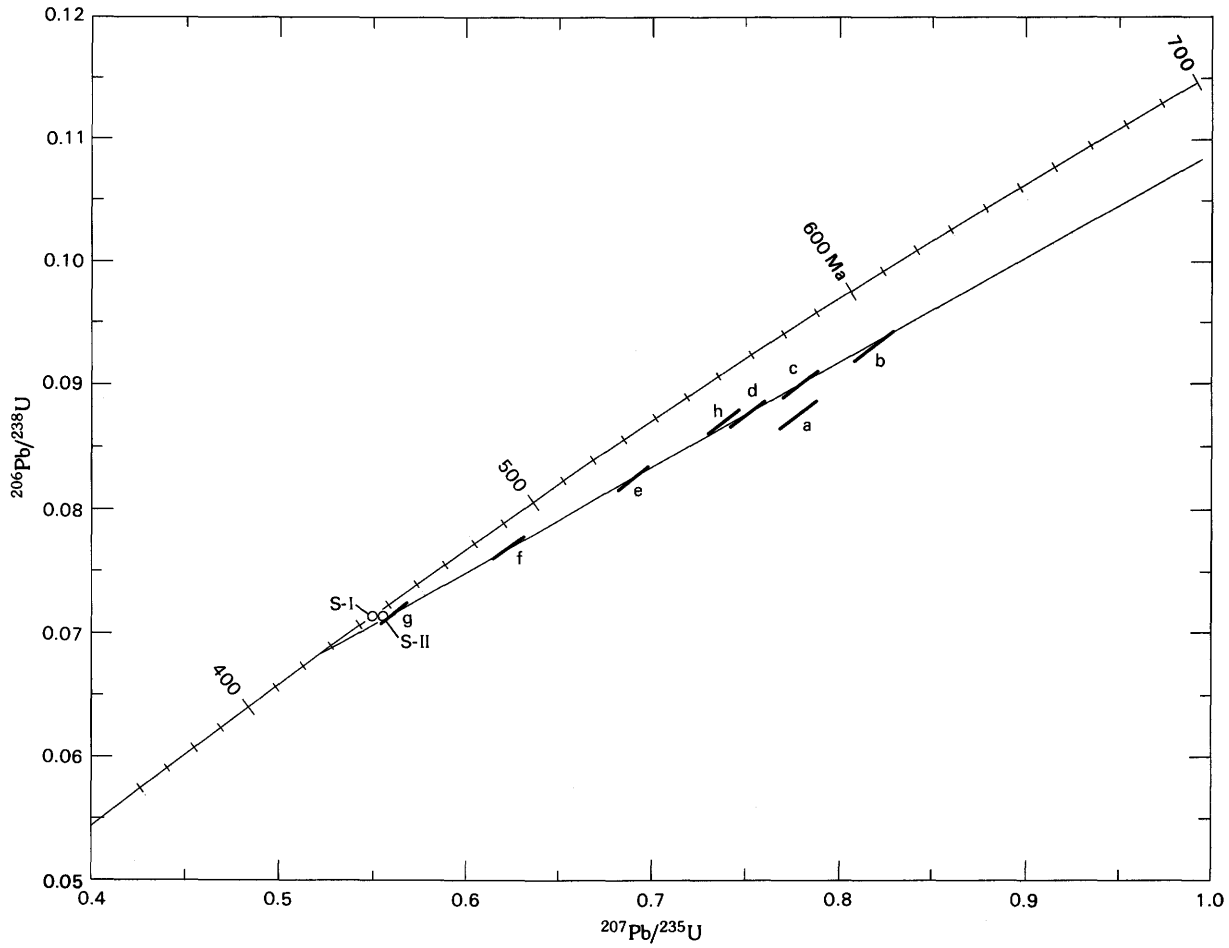

Figure 16. Concordia diagram for zircon and sphene from the granite at Yale Farm. Letters a-h are those of samples listed in table 13.

tercepts of 430 ± 10 Ma and 1,050 ± 40 Ma, respectively. These results certainly are within the time constraints established from geologic field relationships, and, when considered together with the sphene uranium-lead ages presented here, provide the best radiometric age we have for the emplacement of the granite at Yale Farm. Nevertheless, the extreme sensitivity of such a concordia intercept age to but a slight rotation of the determining data points prompts some cautionary comment.

Our experience has been that the most common complication to be superimposed on such a binary mixture of zircon arises from radiogenic lead loss accompanying near-surface dilatancy of the host rock. In New England this lead loss appears to take place quite recently—often indistinguishable from zero age at the resolution of concordia plots—and this phenomenon has the effect of moving data points toward the origin of the diagram. Furthermore, the amount of displacement usually correlates with the accumulated radiation damage in the zircon so that grains having the highest uranium content have the greatest percentage of lead loss. Accordingly, if any lead had been lost during recent rock dilatancy, we would predict it to result in a downward translation combined with a counterclockwise rotation of our Yale Farm trend. That is, because of the increasing uranium content with the decreasing grain size, the finer grained fractions should show proportionately more displacement. One might argue that the coarser fractions contain a higher percentage of the older, inherited component of zircon and, therefore, really have had greater total radiation dosages. However, any such preexisting damage certainly was annealed at the time of granite emplacement. Also, we feel confident that the contribution of the highly radioactive third component to the −150 + 200 and finer total splits is negligible. Most important to our discussion here is that *the consequence of a downward translation and (or) counterclockwise rotation of the array would be to reduce the lower intercept age*. Because an Early Silurian to Late Ordovician age for the granite at Yale Farm is near the Middle Ordovician upper limit of its allowable stratigraphic range; the data points do not appear to have been moved significantly. The good agreement of the upper

intercept age with that of the Middle Proterozoic basement further suggests that rotation of the linear array has not taken place.

Thus, from these zircon data alone we favor the conclusion that the granite at Yale Farm is of late Taconic rather than Acadian age. The calculated 430 ± 10 Ma age should, in fact, be regarded as a minimum if the zircons have lost even a minor amount of postcrystallization radiogenic lead. In a further effort to establish the age of this granite, two samples of sphene—a more magnetic (sphene I) and a less magnetic fraction (sphene II)—were analyzed (table I3). Our attempt to obtain a chemical distinction between the two samples by magnetically fractionating the abundant sphene was moderately successful, but the high common lead content of both fractions preclude a determination of precise $^{207}Pb/^{235}U$ and, consequently, precise $^{207}Pb/^{206}Pb$ ages. In order to reduce the uncertainty in making the common lead correction, we also analyzed the potassium feldspar from the granite as a means of ascertaining the isotopic composition of lead in the original magma. The resultant feldspar lead isotopic ratios ($^{206}Pb/^{204}Pb=18.46$; $^{207}Pb/^{204}Pb=15.61$; $^{208}Pb/^{204}Pb=38.14$; Pb=32 ppm, U=0.06 ppm, Th=0.04 ppm), corrected for almost negligible in place uranium and thorium decay is used in calculating the sphene ages given in table I3. Emphasis is placed on the closely agreeing $^{206}Pb/^{238}Pb$ and $^{208}Pb/^{232}Th$ ages, which are least susceptible to common lead correction, although no discrepancy not accommodated by analytical uncertainties exists even in the highly sensitive $^{207}Pb/^{206}Pb$ age.

We take these sphene data as confirmation of a Taconic age for the granite at Yale Farm, and propose that it was emplaced sometime within the 430–450 Ma range delineated by our combined zircon and sphene results. The fact that the sphene ages slightly exceed the concordia lower intercept age obtained for the zircon may be meaningful, but we would be extremely cautious about making so exact an interpretation of these limited data. Although an experimental precision with potential of resolving Paleozoic ages at the ± 3–Ma level has been demonstrated by repeated analysis of our interlaboratory zircon standard, it is now likely to be geologic factors that prevent us from generally reaching such a goal. When we acknowledge that sillimanite-grade metamorphism has been superimposed on these rocks, an opportunity for serious disturbance to the isotopic systems being investigated certainly is present. The result of such metamorphism upon zircon isotopic systematics can be complex, especially if a new generation of zircon is produced, but the overall effect is usually some lowering of the primary parent-daughter as well as $^{207}Pb/^{206}Pb$ ages toward that of the metamorphism. Either an increase or decrease in age might result from metamorphic recrystallization of sphene depending upon the relative losses or gains of uranium and radiogenic lead. In addition, newly grown zircon or sphene during a subsequent metamorphism would be expected to record the younger age of that event. Again, we stress that the rather tight clustering of ages for the granite argue against any drastic modification of the geochronologic systems in the case at hand. A small amount of disturbance cannot be ruled out, however, and, on the basis of our current data, we can assign no more precise an age than is implied by the 430- to 450-Ma range that we have quoted.

In an attempt to shed light on the nature of the variety II zircon found most abundantly in the coarser mesh fractions, typical grains of the clearest, euhedral subvariety IIa and of the darkest brown, anhedral subvariety IIb (hereafter simply called varieties IIa and IIb) were handpicked carefully from the combined −50 + 100 and −100 + 150 mesh fractions. Early in the study we anticipated that variety IIa formed predominantly when the granite crystallized, and that variety IIb was inherited from the source rock of the granite. As such, these two analyses were seen as holding promise of extending the chemical and isotopic characterization of the mixture in the directions of both "pure" components. Consequently, several surprises did arise from the analytical data (see table I2) obtained for them. In hindsight, we do note (1) that variety IIa zircon frequently does have a chemical interface between a core and overgrowth under the microprobe even though that interface is optically imperceptible, and (2) that variety IIb zircon is darker colored than the cores of most variety III zircon and itself shows few overgrowths. A further dilemma over our early interpretation arose when we realized that the two seemingly quite different morphologies were actually gradational into each other. We now know that both subvarieties entirely or in part derive from Middle Proterozoic source rock(s), although some questions about how their physical and chemical characters merge are left unanswered by these analyses.

Perhaps not so unexpectedly in view of its observed gradation into composite grains, the variety IIa zircon reveals a $^{207}Pb/^{206}Pb$ age demanding that a significant contribution by an old, inherited component is included in it. Indeed, the position of the analysis on the concordia diagram permits only a slightly larger proportion of the younger component than is contained by the −50 + 100 and −100 + 150 mesh total splits. If we allow for the contribution to the total splits by the old variety IIb zircon discussed below, no difference in relative abundance of end members can be demonstrated between varieties IIa and III zircon. What does serve to contrast them is their uranium and thorium concentrations, which are a factor of 2–3 lower in the handpicked clearest grains. Although this range in uranium and thorium content is geochemically interesting, we conclude that any genetic distinction between varieties IIa and III is more illusionary than real. Highly variable uranium content among individual grains

of otherwise homogeneous zircon populations is common in fission-track studies, and the concurrent effects of radiation dosage on crystal transparency, color, and morphology is well known. Thus, secondary rather than primary factors offer the best explanation of what, at their extreme development, appear to be profound varietal differences in zircon types.

At first glance, the analysis of the dark-brown anhedral variety IIb zircon seems to fit nicely with our anticipation that it was inherited largely from the source rock of the granite. The data point falls right on the 430- to 1,050-Ma mixing line as defined by the five finer grained total split samples, and indicates a much greater proportion of the older component than is contained by any other fraction. Assuming that its contact with the magma had caused some episodic lead loss, the variety IIb zircon might, in fact, qualify as the "pure" end member component to the mixing line if we ignored the uranium and thorium contents. However, judging from our isotopic and microprobe analyses, the variety IIb zircon is much too radioactive to represent the postulated old end member. Although apparently sharing a similar Middle Proterozoic age with the variety III cores, the brown zircon with its lack of overgrowths and color distinction records a somewhat unique history. We propose that the cores of variety III zircon were incorporated into the magma of the granite at Yale Farm at an early stage of melting so that they first were partially resorbed and then overgrown as the magma accumulated, migrated upward, and finally solidified. On the other hand, the variety IIb zircon was acquired as xenocrysts at a much later stage in the magmatic sequence and thereby almost completely escaped subsequent modification. The chemical and color distinctions between the zircon represent the different lithology but similar age of the country rock from which the two varieties were released. Of course, other interpretations that seek to reconcile the different uranium and thorium contents of the zircon wholly in terms of degree of reactivity with the magma are possible also.

ELECTRON MICROPROBE ANALYSIS OF ZIRCON

As a complement to the uranium-lead dating study, selected grains of different morphological types of zircon from the granite at Yale Farm were analyzed and characterized by the electron microprobe. Using this technique, we were able to identify distinct chemical domains, which correlate well with our interpretation of a polygenetic origin to the zircon population. In particular, the hypothesized Middle Proterozoic and the Lower Silurian or Upper Ordovician components can be recognized separately, whether present as individual or composite grains, based on their hafnium content. In this section we document the concentration and distribution of a few selected elements, but offer no further genetic modeling for these data beyond that put forward to explain the uranium-lead systematics.

Individual zircon grains representing each morphological type were probed to determine their chemical composition (table I4). The samples were analyzed at 20 kilovolts and 10 nanoamps sample current with a defocused beam of 10–μm (micrometer) diameter. Both natural minerals and synthetic glasses were used as standards, and data reduction was carried out by an atomic number, absorption, and fluorescence (ZAF) scheme. For varieties II and III composite grains, separate analyses made of cores and overgrowths show their different minor element concentrations. We note, first of all, that each analysis verifies a near approach to stoichiometric $(Zr,Hf)SiO_4$ for the zircon, and at the dimension of the probe beam, the absence of any other mineral species. The only elements in addition to Zr, Hf, and Si found were trace amounts of U, P, Ca, Th, and REE (rare-earth elements) sporadically indicated near their detection limits. These trace elements all could be crystallographically bound in the zircon lattice, and we tentatively make that assumption in the ensuing discussion.

The most useful aspect of these data in table I4 is in the systematic behavior of the two elements, hafnium and uranium. Almost certainly, the hafnium substitutes for zirconium in the basic mineral lattice, whereas the uranium is in some unknown but possibly correlative site to the hafnium. Immediately apparent is the higher average hafnium and uranium concentration in variety I grains and variety III overgrowths (1.73 ± 0.36 and 2.05 ± 0.32 percent Hf, and $1{,}100 \pm 500$ and $1{,}000 \pm 400$ ppm U, respectively) than in variety III cores (1.21 ± 0.24 percent Hf, and 400 ± 300 ppm U). Such a dichotomous chemical characterization of the zircon runs parallel with the previously proposed two-component mixing model whereby one component formed during crystallization of the granite and the other comprises the xenocrystic contribution to the magma. Although significant fluctuation exists in the hafnium and, particularly, the uranium contents of both components, we are convinced that a statistical distinction can be drawn between the two generations of zircon. Furthermore, such probe analyses of variety IIa grains first disclosed the true composite nature of the grains by showing a chemical interface between core and overgrowth not detectable under the microscope.

The intermediate hafnium and high uranium concentrations (1.60 ± 0.20 percent Hf, and $1{,}900 \pm 900$ ppm U) of variety IIb zircon do not fit so well into a dichotomous scheme, but this discrepancy could be taken as additional evidence of heterogeneity within the xenocrystic component. A possible scenario supporting such heterogeneity to explain the rarity of this high radiaoctivity species as the cores of variety III zircon has been given already. With regard to variety IIb zircon, we should mention also

Table I4. Average value (X), standard deviation (±), and range in element oxide concentration for representative grains of the different varieties of zircon

[All oxides in weight percent; microprobe beam size is about 10 micrometers in diameter]

	Variety I (27 analyses on 15 grains)		Variety IIa cores (12 analyses on 6 grains)		Variety IIa overgrowths (12 analyses on 6 grains)		Variety IIb (14 analyses on 6 grains)		Variety III cores (14 analyses on 6 grains)		Variety III overgrowths (10 analyses on 6 grains)	
	X±σ	Range	X±σ	Range	x±σ	Range	X±σ	Range	X±σ	Range	X±σ	Range
ZrO_2	65.80±0.89	(63.79–66.99)	65.69±0.97	(64.21–67.11)	64.78±1.03	(62.82–65.93)	66.01±0.67	(64.24–0.67)	65.57±1.13	(63.72–67.20)	64.50±1.24	(62.53–66.08)
HfO_2	1.73±0.36	(1.17–2.68)	1.13±0.19	(0.87–1.60)	1.82±0.26	(1.30–2.44)	1.60±0.20	(1.35–2.07)	1.21±0.24	(0.91–1.73)	2.05±0.32	(1.63–2.74)
SiO_2	32.33±1.08	(30.43–33.76)	32.20±0.75	(30.48–33.36)	31.49±0.74	(30.75–32.86)	31.40±0.46	(30.28–32.25)	31.98±0.63	(30.25–32.77)	31.69±0.48	(31.13–32.55)
CaO_2	0.02±0.02	(0.00–0.06)	0.02±0.02	(0.00–0.05)	0.02±0.02	(0.00–0.08)	0.01±0.01	(0.00–0.03)	0.01±0.01	(0.00–0.03)	0.03±0.03	(0.00–0.09)
Y_2O_3	0.17±0.12	(0.02–0.46)	0.05±0.03	(0.01–0.12)	0.07±0.05	(0.00–0.16)	0.12±0.07	(0.02–0.26)	0.04±0.03	(0.00–0.10)	0.06±0.05	(0.01–0.14)
Ce_2O_3	0.02±0.02	(0.00–0.07)	0.02±0.02	(0.00–0.07)	0.02±0.01	(0.00–0.04)	0.02±0.01	(0.00–0.04)	0.02±0.02	(0.00–0.06)	0.01±0.01	(0.00–0.02)
P_2O_5	0.03±0.03	(0.00–0.09)	0.02±0.01	(0.00–0.06)	0.03±0.02	(0.00–0.08)	0.01±0.01	(0.00–0.04)	0.01±0.02	(0.00–0.05)	0.02±0.02	(0.00–0.05)
UO_2	0.11±0.05	(0.04–0.24)	0.03±0.02	(0.00–0.10)	0.05±0.02	(0.01–0.10)	0.19±0.09	(0.11–0.31)	0.04±0.03	(0.00–0.16)	0.10±0.04	(0.04–0.16)
ThO_2	0.10±0.05	(0.03–0.32)	0.02±0.02	(0.00–0.07)	0.02±0.02	(0.00–0.08)	0.05±0.04	(0.00–0.12)	0.02±0.02	(0.00–0.08)	0.04±0.03	(0.00–0.10)

the presence of a few grains with almost black domains having 3,000–5,000 ppm U. A brief HF acid leach shows these domains to be especially soluble, and we speculate that they may be the sites of postcrystallization radiogenic lead loss implied by the uranium-lead isotopic data for the $-50+100$ and $-100+150$ total split analyses. Care was taken to exclude such grains with identifiable black domains from the handpicked sample of variety IIb zircon analyzed subsequently.

One final warning about the apparent correlative behavior of hafnium and uranium may be in order. Unlike the hafnium, which probably does represent rather straightforwardly the restricted Hf/Zr of the crystallization environment, uranium content is found to vary by at least an order of magnitude within a component and to have considerable overlap between components. Although noting that the overgrowths of variety III zircon generally do contain more hafnium and uranium than the cores, a direct coupling of the two elements need not exist. Thus, when we probed several unusual variety III grains that had a more turbid core than overgrowth, they did, in fact, have a higher uranium content in the core than the overgrowth while maintaining a normal hafnium relationship.

Perhaps the most interesting use of the microprobe comes from the detailed study of the interface between two generations of zircon within a single variety III grain. We chose to work on a zircon that had an especially well-developed core and overgrowth relationship so as to facilitate an optical comparison with the microprobe analyses. A photomicrograph of the subject grain, its electron backscatter electron image, and zirconium and hafnium scanning maps are shown in figure I7. Partial chemical analyses of nine selected 1-μm diameter spots of the core (1–5) and overgrowth (6–9) are presented in table I5. Again we note the essential stoichiometry of the zircon.

As we had come to expect from the reconnaissance survey, the contrast in hafnium and uranium content between the core and overgrowth are immediately apparent from the chemical data. Corresponding to the chemical distinction, an abrupt change in cathodoluminescence intensity of the probe spot also was observed at or near the interface between core and overgrowth. The core, depleted in hafnium, exhibited a bright luminescence, whereas the overgrowth, enriched in hafnium, had a faint cathodeluminescence. Luminescence spectra were measured with a grating monochrometer, and, except for the intensity, all spectra were identical with strong components at 465 and 505 nanometers. At one end of the crystal, the intensity boundary did depart appreciably from the interface as defined optically and by the crack pattern on the backscatter image (see fig. I7 for comparison). Our explanation of this disparity is that the actual crack as seen in the photomicrograph and backscatter image is a secondary, stress-induced feature, which only approximately follows the chemical boundary. Thus, although

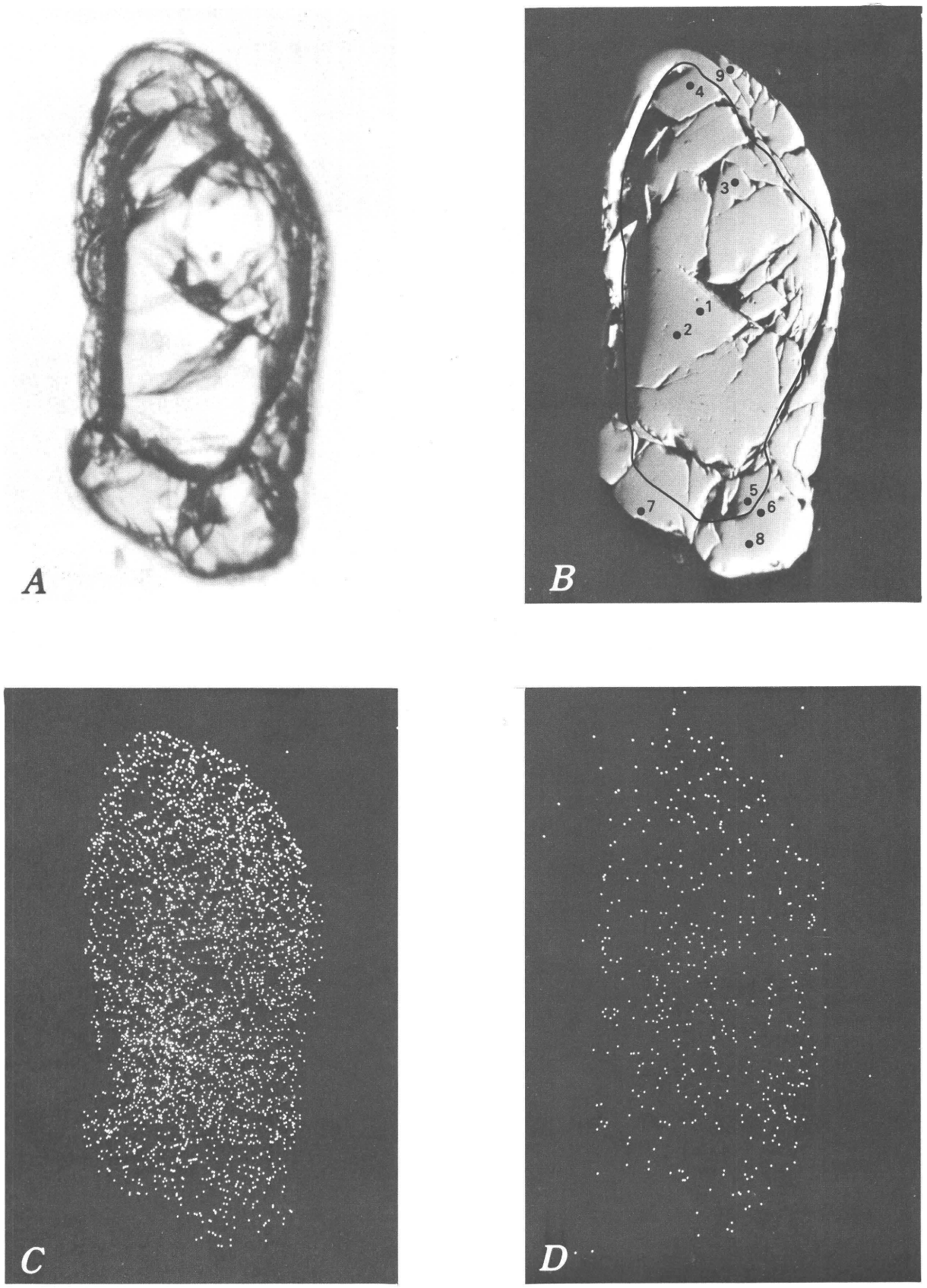

Figure 17. Photomicrograph (*A*), electron backscatter image (*B*), and zirconium (*C*) and hafnium (*D*) scanning maps of a select variety III zircon. Grain is about 550 micrometers in long dimension.

Table I5. Electron microprobe analyses of a selected variety III zircon

	Core					Overgrowth			
Analysis[1]	1	2	3	4	5	6	7	8	9
ZrO_2	66.65	66.46	66.11	67.05	64.92	66.16	65.62	65.34	66.02
HfO_2	1.06	1.03	.96	1.05	.99	1.92	1.79	2.19	1.88
SiO_2	32.88	32.25	32.31	32.56	31.98	31.64	31.64	31.62	32.31
CaO_2	.03	.01	.01	.00	.03	.05	.03	.00	.02
Y_2O_3	.03	.01	.00	.01	.02	.05	.05	.03	.03
Ce_2O_3	.01	.01	.00	.01	.00	.03	.00	.00	.00
P_2O_5	.01	.01	.01	.00	.01	.02	.01	.01	.00
UO_2	.04	.03	.01	.01	.02	.13	.02	.10	.03
ThO_2	.03	.00	.01	.01	.01	.05	.02	.00	.01
Sum----	100.24	99.81	99.42	100.70	97.98	99.05	99.18	99.29	100.30

[1]Numbered analyses are keyed to the indicated positions on the photomicrograph of the grain in figure I7.

stresses associated with the different chemistry and (or) accumulated radiation damage probably is greatest right along the interface of the core and the overgrowth, fracturing may locally jut irregularly into one or the other of the domains. The more fractured and turbid character of overgrowths relative to cores of many variety III zircons (see figs. I4 and I7) could be another manifestation of this phenomenon—suggesting that greater internal stresses do accompany the higher uranium content.

A corollary consideration in understanding the nature of the core to overgrowth relationship is the sharpness of the chemical gradient across the interface. In addition to the implications for stress concentration, the width of the chemical transition band holds information about diffusive distances during and after crystallization of the overgrowth. For example, if the transition is within the resolving capacity of the microprobe (2μm), an argument could be made for insignificant diffusive movement of hafnium and uranium during the superimposed Acadian orogeny. An equivalent immobility of radiogenic lead would then explain the apparent post-Taconic closed-system behavior of most of the zircon population. On the other hand, a broad diffusion band certainly might raise the issue of some episode of substantial ion migration. Although the crack pattern prevents a precise delineation of this chemical gradient along much of the perimeter of the core, an excellent opportunity exists to make the measurement where the crack does depart from the luminescence boundary. Analysis 5, table I5, of the core and analysis 6 of the overgrowth represent immediately adjacent probe spots on either side of the luminescence boundary separated by no more than 4 μm. These analyses do, in fact, bracket the full transition in hafnium and uranium contents, and thereby document an extremely abrupt gradient.

At this early stage in our use of the electron microprobe to supplement geochronologic studies, we find that almost every grain offers some new insight and surprise. However, the sensitivity of the technique severely limits its application in making quantitative measurements of trace elements below the 0.1 percent (1,000 ppm) level. We were fortunate to find so great a "hafnium effect" in this suite of zircons. The higher uranium concentration of the overgrowths compared with that of the cores, which was predicted by our binary mixing model, also can be seen in the microprobe data. However, analytical uncertainty and probable real heterogeneity within and among grains prohibit their quantitative use to define end-member compositions.

REFERENCES CITED

Chase, R. B., Bickford, M. E., and Tripp, S. E., 1978, Rb-Sr and U-Pb isotopic studies of the northeastern Idaho batholith and border zone: Geological Society of America Bulletin, v. 89, p. 1325–1334.

Grauert, B. W., Hanny, R., and Soptrajanova, G., 1974, Geochronology of a polymetamorphic and anatectic gneiss region—The Moldanubicum of area Lam-Degendorf, Eastern Bavaria, Germany: Contributions to Mineralogy and Petrology, v. 40, p. 105–130.

Harwood, D. S., 1975, Fold-thrust tectonism in the southern Berkshire massif, Connecticut and Massachusetts, *in* Ratcliffe, N. M., ed., Guidebook for field trips in western Massachusetts, northern Connecticut, and adjacent areas of New York, New England Intercollegiate Geological Conference, 67th annual meeting, New York City College, p. 122–143.

———1979a, Geologic map of the South Sandisfield quadrangle, Massachusetts and Connecticut: U.S. Geological Survey Geologic Quadrangle Map GQ–1519.

———1979b, Bedrock geologic map of the Norfolk Quadrangle, Connecticut: U.S. Geological Survey Geologic Quadrangle Map GQ–1518.

Koppel, V., and Grunenfelder, M., 1971, A study of inherited and newly formed zircons from paragneisses and granitised sediment of the Strona-Ceneri zone (Southern Alps): Schweizerische Mineralogische und Petrographische Mitteilungen, v. 51, p. 385–409.

Krogh, T. E., 1973, A low-contamination method for hydrothermal decomposition of zircon and extraction of U and Pb for isotopic age determination: Geochimica et Cosmochimica Acta, v. 37, p. 485–494.

Ludwig, K. R., 1979, Calculation of uncertainties of U-Pb isotope data: Earth and Planetary Science Letters, v. 46, p. 212–220.

Manhes, G., Minster, J. F., and Allegre, C. J., 1978, Comparative uranium-thorium-lead and rubidium-strontium study of the Saint Severin amphoterite; Consequences for early solar system chronology: Earth and Planetary Science Letters, v. 39, p. 14–24.

Pidgeon, R. T., and Aftalion, M., 1978, Cogenetic and inherited zircon U-Pb systems in granites; Paleozoic granites of Scotland and England: Geological Journal Special Issue 10, p. 183–220.

Pidgeon, R. T., Koppel, V., and Grunenfelder, M., 1970, U-Pb isotopic relationships in zircon suites from a para- and orthogneiss from the Ceneri zone, southern Switzerland: Contributions to Mineralogy and Petrology, v. 26, p. 1–11.

Ratcliffe, N. M., 1975, Cross section of the Berkshire massif at 42° N.; Profile of a basement reactivation zone, *in* Ratcliffe, N. M., ed., Guidebook for field trips in western Massachusetts, northern Connecticut, and adjacent areas of New York: New England Intercollegiate Geological Conference, 67th annual meeting, New York City College, p. 186–222.

Ratcliffe, N. M., and Harwood, D. S., 1975, Blastomylonites associated with recumbent folds and overthrusts at the western edge of the Berkshire massif, Connecticut and Massachusetts—A preliminary report, [chap.] A, *in* Tectonic studies of the Berkshire massif, western Massachusetts, Connecticut, and Vermont: U.S. Geological Survey Professional Paper 888, p. 1–19.

Ratcliffe, N. M., and Hatch, N. L., Jr., 1979, A traverse across the Taconide zone in the area of the Berkshire massif, western Massachusetts, *in* Skehan, J. W., S.J. and Osberg, P. H., eds., The Caledonides in the U.S.A., Geological excursions in the northeast Appalachians, Contributions to the International Geological Correlation Program, Project 27—Caledonide Orogen: Weston, Mass., Weston Observatory, p. 175–224.

Ratcliffe, N. M., and Zartman, R. E., 1976, Stratigraphy, isotopic age, and deformational history of basement and cover rocks of the Berkshire Massif, southwestern Massachusetts: Geological Society of America Memoir 148, p. 373–412.

Stacey, J. S., and Hope, J., 1975, A program for mass spectrometer control and data processing in isotope geology—Written in BASIC for an 8K Nova 1120 computer: U.S. Geological Survey Open-File Report 75–127, 48 p.

Tatsumoto, M., 1966, Isotopic composition of lead in volcanic rocks from Hawaii, Iwo Jima, and Japan: Journal of Geophysical Research, v. 71, no. 6, p. 1721–1733.

Tatsumoto, M., Knight, R. J., and Delevaux, M. H., 1972, Uranium, thorium, and lead concentrations in three silicate standards and a method of lead isotopic analysis, *in* Geological Survey research 1972: U.S. Geological Survey Professional Paper 800–D, p. D111–D115.

Wetherill, G. W., 1956, Discordant uranium-lead ages, 1: American Geophysical Union Transactions, v. 37, p. 320–326.

1986

U.S. GEOLOGICAL SURVEY BULLETIN 1622

SHORTER CONTRIBUTIONS TO ISOTOPE RESEARCH

FISSION-TRACK DATING OF SAMPLES OF THE ILLINOIS DRILL-HOLE CORE

Chapter J

By ROBERT A. ZIMMERMANN

CONTENTS

FIGURES

TABLES

Abstract

Drill holes UPH–1 and UPH–2 in Stephenson County, northern Illinois, penetrate to a depth of more than 1,640 meters, first through ~630 meters of Paleozoic sedimentary section and then into underlying Precambrian granitic basement. Samples of apatite (five) and zircon (one) from various depths in the recovered Precambrian basement core were dated by the fission-track method. Because of the instability of tracks in these minerals at high temperatures, the ages define points in the thermal history of the samples.

An apatite sample just beneath the basement unconformity (614 meters) presently at a temperature of ~20°C (Celsius) yielded an age of 132±16 Ma (million years) at the 95-percent confidence level. Apatite ages decrease linearly with depth to 50±8 Ma (95-percent confidence level) for the deepest sample (1,640 meters) at a temperature of ~46°C. The age of the sample closest to the unconformity has been totally reset (as evidenced by comparative track-length measurements) from an age expected to be older than the oldest overlying sediments. The observation that non-zero ages persist through the total depth of the hole demonstrates that the resetting or closure temperature is higher than the highest temperature in the hole. The fission-track age of the zircon sample from just below the unconformity is older than the age of the sediments, and thus, the temperature was never higher than ~160–180°C during the Phanerozoic.

The range of temperatures sampled suggests a minimum of 26°C cooling. The extrapolation of the least-squares regression line through the data to a zero age is at 56±2°C. This construction requires ~36°C cooling for the upper sample. However, a geologically accurate model of track fading predicts a closure temperature of 93±18°C, requiring 73±18°C of post-~130 Ma cooling, mostly after 50 Ma.

Consideration of a lower closure temperature (56°C) and a hypothetical large increase in geothermal gradient (to 36°C per kilometer at 130 Ma) requires the former existence and removal of >520 meters of cover. At the other extreme, a closure temperature of 93°C and the presently observed geothermal gradient of 23°C per kilometer require ~3,000 meters of cover, about 2,000 meters of which was removed post-50 Ma. These data suggest a history of sedimentation and uplift considerably different than that commonly proposed.

INTRODUCTION AND GEOLOGIC SETTING

The Illinois Deep Hole Project was an interdisciplinary study of the properties and characteristics of three deep holes (UPH–1,2,3) and their cores in Stephenson County, northern Illinois, near the town of Winslow, not far from the Wisconsin State line (see fig. E1, chap. E, for locations of drill holes). The geophysical, geochemical, and petrographic properties, as well as isotopic ages of the cored and the surrounding rocks, were studied by other investigators. With the objective of studying the cooling history of the cored basement rocks in the temperature range from ~180°C to ~100°C, apatite and zircon mineral separates were dated as part of the project. The results obtained in this study have broader significance to the former sedimentary and subsequent uplift history of the region in general.

The intrusion and crystallization of the granitic basement rocks between 1,430 Ma (rubidium-strontium) and 1,470 Ma (lead-lead) (Van Schmus and others, 1981) represent the earliest preserved geology in the region. The basement rocks show evidence of subsequent textural alteration and deformation (Lidiak and Denison, 1981). At some time prior to deposition of the Cambrian Mount Simon Sandstone, the Precambrian basement was uplifted and eroded, exposing a surface of moderate relief upon which Phanerozoic strata were later to be deposited. At the site of the drill holes, the sedimentary formations present start with the Mount Simon Sandstone, above the basement unconformity, and continue up to the Galena-Dolomite of Middle Ordovician age. The Middle Ordovician Kress Member of the St. Peter Sandstone is above an unconformity of regional extent. This unconformity is increasingly lower in the section to the north, and is related to the early phases of formation of the Wisconsin arch.

The drill holes are close to the axis of the Wisconsin arch near its bifurcation into the Mississippi River and the Kankakee arches, which bound the northern end of the Illinois structural basin. In its northern extension, the Wisconsin arch brings to the surface exposures of Precambrian basement in south-central Wisconsin. Within the Illinois and Michigan basins and along their flanks, rocks of Silurian through Pennsylvanian age are preserved. Isopach reconstructions suggest that previously some of these formations extended beyond the present structural basins. Paleocurrent measurements on basal-Pennsylvanian formations suggest continuity of sediment dispersal across interbasinal basement highs such as the Kankakee arch (Potter and Siever, 1956). Studies of coalification patterns in the Illinois Basin suggest the removal of ~970 meters of Pennsylvanian or younger sedimentary rock along the northern edge of the Illinois Basin, about 60 kilometers southeast of the drill sites (Damberger, 1971). It has been assumed that this is part of a general uplift of the Great Lakes region in post-Pennsylvanian time (Eardley, 1962). The presence of Cretaceous sediments, both to the west and to the south at the head of the Mississippi Embayment, represent the youngest pre-Pleistocene stratigraphy in the immediate region. Because of the thin and unconsolidated nature of these deposits, little burial or subsequent uplift can be implied where they occur and their presence suggests limits to allowable amounts of post-Cretaceous erosion in the region in general and at

the drill site in specific.

Zartman and others (1967) have dated a number of dikes and sills in southern Illinois that yield Permian ages. There is some suggestion of intermittent igneous activity into the Cretaceous and that this activity possibly was related to the subsequent formation of the Mississippi Embayment. McGinnis and others (1976), in discussing the regional increase in Bouguer gravity field from northern into southern Illinois, suggested that the gravity increase is caused by an increase in basement density due to deep level intrusions, possibly related to the evolution in the Cretaceous of the Mississippi Embayment structure. These igneous events are mentioned because of their relationship to a possible regional increase of heat flow and hence geothermal gradient during the Mesozoic. The effect of such an increase would be to alter significantly the interpretation of the cooling history made from the apatite fission-track ages presented here. If in the past the geothermal gradient was higher than the presently observed gradient of 23°C/km (degrees Celsius per kilometer) (Rahman and Roy, 1981), the cooling produced by the decrease in gradient must be taken into account in addition to that caused by erosion.

INTERPRETATION OF APATITE AND ZIRCON FISSION-TRACK AGES

Fission tracks are produced by the fissioning of uranium nuclei that leave a ~15-μm path of structurally damaged material in the path of the fission fragments. The ability to etch, optically observe, and count the damage tracks is reduced or eliminated by thermal energy. Geological observations such as studies of fission-track ages of apatites in boreholes in areas of known geothermal history, such as by Naeser (1979), or of the fission-track age of zircons relative to better defined isotopic age systems, such as presented in Harrison and others (1979), provide one means of determining the kinetics of fission-track "fading." Another approach taken is to interpret laboratory studies of track fading and to extrapolate these results to geologic conditions of time and temperature. The interpretation of laboratory data as representing a first-order rate law for track fading with unique singular values for the activation energy and preexponential factor describing the temperature dependence of this rate has been advocated by Zimmermann and Gaines (1978). This interpretation is the basis of a mathematical model of track accumulation that accurately predicts the observed age trends for the previously mentioned borehole studies of Naeser (1979) (R. A. Zimmermann, unpub. data). The geological appropriateness of this approach is the basis for using this as the method for the interpretation of the apatite data in the present report.

Apatite dates are here interpreted using the concept of effective closure temperature defined by Dodson (1973, p. 260) as "the temperature of the system at the time represented by its apparent age." The closure temperature is dependent upon the rate of sample cooling and decreases with decreasing cooling rate. Values for closure temperatures applicable to the present study were calculated from the relationships given by Dodson (1973) using the values of the kinetic constants given by Zimmermann (1977). Uncertainties in this closure temperature were calculated from equations derived from Dodson (1973). As an example, the closure temperature of apatite for a rate of cooling of 1°C/m.y., is about 100°C. The closure temperatures for zircon are known only relative to other isotopic age systems and probably fall in the range of 150°-180°C (Harrison and others, 1979).

EXPERIMENTAL PROCEDURES AND RESULTS

For this study, samples were obtained from the cores retrieved from the UPH–1 and UPH–2 drill holes. These holes penetrated 605 m (1,955 ft) and 660 m (2,179 ft), respectively, of lower Paleozoic sedimentary rock before entering the granitic basement. The temperature at the basement contact was about 20°C. The temperature at the bottom of the UPH–2 hole was about 46°C. The last four digits of the sample numbers in table J1 correspond to the depth, in feet, of the sample.

Sufficient apatite and zircon for dating were obtained from ~500 grams of cored basement rock. Each sample was separated by crushing to finer than 60 mesh and separating apatite and zircon from the -60 + 200 mesh (246–74 micrometers) fraction by heavy liquid and magnetic separation.

All samples were prepared for age determination by the external detector technique using procedures similar to those of Naeser (1976). Apatite samples were etched in 7-percent HNO_3 at 20°C for 30 or 40 seconds. Muscovite detectors were etched in 48-percent HF at 20°C for ~15 minutes. Zircons were etched in an eutectic NaOH-KOH mixture at 220°C for 2–8 hours. Only two grains in one of eight zircon samples were suitable for counting because of extremely high track densities and extreme grain corrosion.

For thermal neutron irradiation, the samples were placed in an aluminum tube with the NBS (National Bureau of Standards) reference glass 963, covered with muscovite detectors, at the top and bottom of the irradiation package. The irradiation was carried out in the U.S. Geological Survey Triga reactor (Denver) in the lazy susan ring at a power level of 200 kW (kilowatts). The thermal neutron fluence for the standard glasses was calculated using the values reported for the NBS glass irradiated in the RT-3 site with copper foils as the primary standard (Carpenter and Reimer, 1974). The fluence for each sample was calculated by interpolation between values determined for the standards.

Table J1. Fission-track age data for the Illinois drill-core samples

[ρs and ρi represent the observed fossil and induced track densitites, respectively. To correct for the 2π geometry of the external detector configuration, the induced track densities (or raw counts) are multiplied by a factor of 2 in calculating the age. tr, tracks; cm^2, square centimeter; ϕ, thermal neutron fluence (calibrated by NBS-SRM 963, copper value); n, neutrons, thermal; Ma, million years; ppm, parts per million. Quoted uncertainty in the age represents the 95-percent confidence limits (95 pct CL). Ages were calculated using the following constants: $\lambda_d = 1.55 \times 10^{-10} yr^{-1}$; $_f = 7.03 \times 10^{-17} yr^{-1}$; U-235/U-238=0.00725; λ_f=580.2 barns]

Sample No.	Depth (meters)	Mineral dated	Number counted: Fossil tracks	Number counted: Induced tracks	Number counted: Grains	ρs (10^6tr/cm^2)	ρi (10^6tr/cm^2)	Φ (10^{15}n/cm^2)	Time: Ma	Time: Δ Ma (95 pct CL)	Uranium (ppm)
UPH-1-2025	614	Apatite---	543	602	10	1.18	1.31	4.96	132	16	16
UPH-2-2185	662	--do------	584	660	10	1.54	1.74	4.96	130	15	22
UPH-2-2779	842	--do------	611	740	10	1.66	2.02	4.80	118	14	26
UPH-2-3194	968	--do------	173	271	7	.606	.949	4.80	91	18	12
UPH-2-4773	1446	--do------	236	545	12	.413	.954	4.80	62	10	12
UPH-2-5411	1640	--do------	232	688	11	.414	1.23	4.96	50	8	15
UPH-1-2004	607	Zircon----	153	22	2	15.0	2.16	3.92	768	325	36

Samples were counted at ~2,500× in transmitted light. For age calculations the following constants were used: $\lambda_d = 1.55 \times 10_{yr}{}^{-1}$; $\lambda_f = 7.03 \times 10^{-17}\ yr^{-1}$; U–235/U–238=0.00725; σ_f=580.2 barns. Systematic differences exist in commonly used methods to calibrate neutron fluences and in values of λ_f. The combination of values used here provides an accurate value for the fission-track age of the Oligocene Fish Canyon Tuff (Naeser and others, 1981) that has been well dated by various K-Ar (potassium-argon) mineral systems. Ages were calculated ultimately by pooling counts from individual grains in a sample. The age uncertainties were calculated taking into account the uncertainties in the fossil and induced track counts, as well as the uncertainty of the neutron fluence, by combining these in the manner described by Johnson and others (1979, appendix 1). The uncertainties in the fossil and induced track counts were evaluated by using the Poisson uncertainties of the individually pooled data. The inclusion of a term involving the correlation of individual grain counts, as suggested by McGee and Johnson (1979), is inappropriate in this situation and was not used. The uncertainties given in table J1 and shown as error bars in figure J1 represent 95-percent confidence intervals.

In order to measure the projected track-length distribution of sample UPH–2–2185, a separate mount of grains annealed at 550°C for one hour was prepared and irradiated. Fossil and induced track lengths were measured at ~2,500× using an electronic digitizer in conjunction with a drawing tube attached to the microscope. Five hundred and thirteen fossil tracks and 531 induced tracks were measured to produce the distributions shown in figure J2.

Before discussing the dating results, note that the average uranium concentration of all apatite grains measured was 17 ppm (parts per million). Other experimenters, working on these drill core samples, have observed extremely high concentrations of uranium in the whole-rock chemistry. The concentrations found in these apatites suggest that the whole-rock values are not due to higher than normal concentrations in the apatite phase. Although the observed concentration can be biased by selection criteria, I believe that the grains counted are representative of the samples in general. The uranium concentration shown for the zircon sample is biased, in the extreme, to low concentrations.

The dates of the five apatite samples range from 132 ± 16 Ma for the sample closest to the basement unconformity at a depth of 614 m (at a temperature of ~20°C) to 50 ± 8 Ma at a depth of 1,640 meters (at a temperature of ~46°C). The ages appear to decrease linearly with depth. A least-squares linear regression yields a slope for the present thermal gradient of 0.27°C/Ma with a "zero age" intercept at a depth of 2,174 meters and present temperature 56 ± 2°C. The dating of zircon from sample UPH–1–2004, just below the unconformity, yielding an age of 768 ± 325 Ma (95-percent confidence level), is subjectively of marginal worth as shown by the large uncertainty associated with the age. It nonetheless has some merit in the general interpretation of the geothermal history at the drill site and therefore is included for discussion.

A comparison of the projected track-length distribution for fossil and induced tracks in the apatite sample UPH–2–2185 reveals that the fossil distribution shows a shorter maximum and mean projected length than the induced distribution. Dakowski (1978) has shown that the projected track-length distribution for thermally unaffected (that is, unshortened) tracks is a sawtooth distribution with a linearly decreasing right shoulder; least-squares regression of this part of the distribution should produce the same maximum length intercept for both fossil and induced tracks. Sample UPH–2–2185 has maximum length

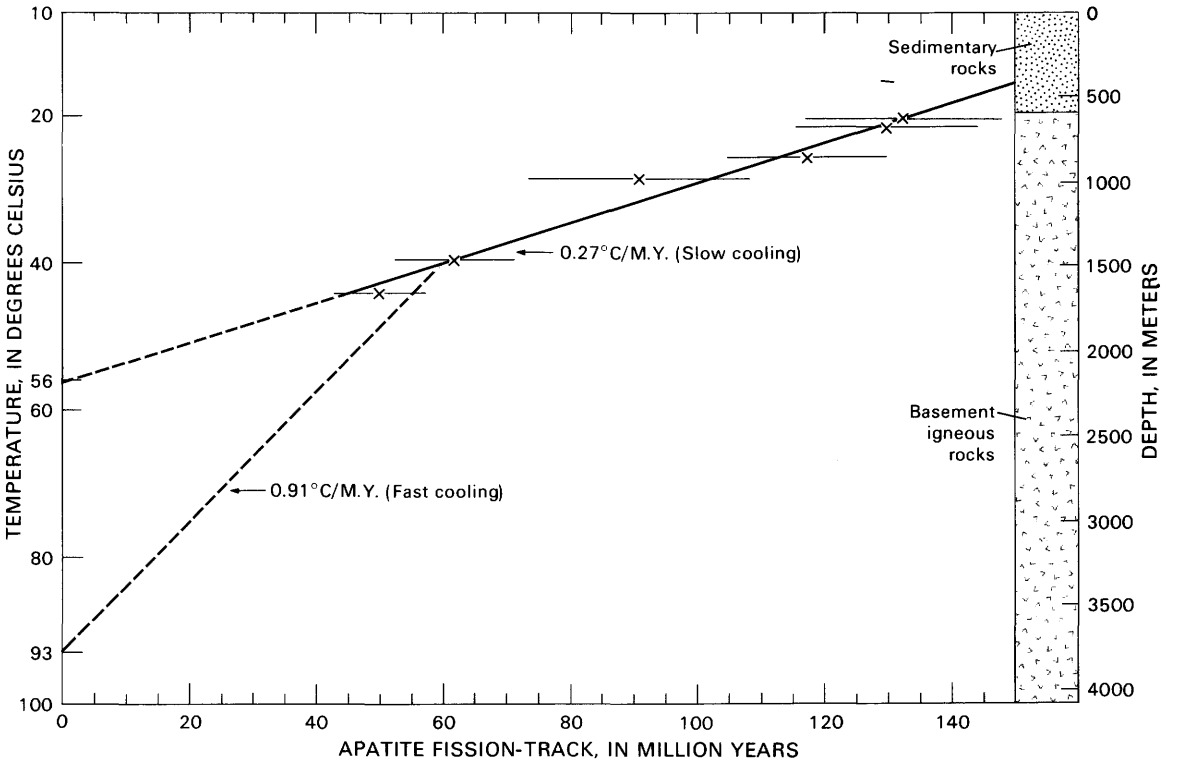

Figure J1. Apatite fission-track ages as a function of depth and present temperature in the Illinois drill holes UPH–1 and UPH–2. Error bars (centered on X) enclose the 95-percent confidence intervals. Regression line through the data indicates cooling of 0.27°C/m.y. (with present geothermal gradient) and "zero" age at a depth of 2,174 m (7,174 ft). Dashed line suggests most recent cooling rate if the closure temperature is 93°C.

intercepts of 12.6μm for the fossil and 14.6μm for the induced distribution suggesting some track shortening for the fossil tracks.

Although a relationship exists between track shortening and track fading, various studies of this relationship have no general agreement (for example, Märk and others, 1973; Wagner, 1979; Green, 1981). Partial annealing of a large track population at some time in the past could have produced a double peaked or bimodal distribution (Wagner, 1979). A more likely effect would be a break in slope, with a steepening of the distribution at shorter length, on the right side of the sawtooth distribution. In the present example, although the fossil length statistics (mean and maximum projected length) all are smaller than those of the induced population, there is no evidence of bimodality or of a significant nonlinearity on the right shoulder in the fossil distribution. This is interpreted as an argument against a mixed age (that is, the sample temperature was significantly higher than its closure temperature, completely removing pre-existing tracks) and for slow cooling through the temperature region of significant track fading such as to provide for the observed shortening of fossil versus induced tracks.

DISCUSSION

The unexpectedly young ages and additionally the presence of non-zero ages down the hole are significant. On the basis of the present geology, much different ages would be expected. The igneous nature and intrusive age of the basement rocks and the erosional surface developed at the basement unconformity clearly indicate that the basement was significantly uplifted and eroded before deposition of the Phanerozoic sedimentary sequence. Without subsequent reheating of that surface higher than the closure temperature for apatite, a pre-Mount Simon age for the apatite should be expected, reflecting that early uplift and cooling history. The observed apatite ages, therefore, require a reheating of the basement during the Paleozoic or Mesozoic and cooling during the Cenozoic. Two mechanisms for this reheating—formerly deeper burial and formerly higher geothermal gradients—will be discussed.

The observation that the samples deeper into the basement have non-zero ages means that the temperatures of these samples also are less than the apatite closure temperature. Thus, the presence of tracks in a sample at ~46°C (sample UPH–2–5411) means that sample UPH–

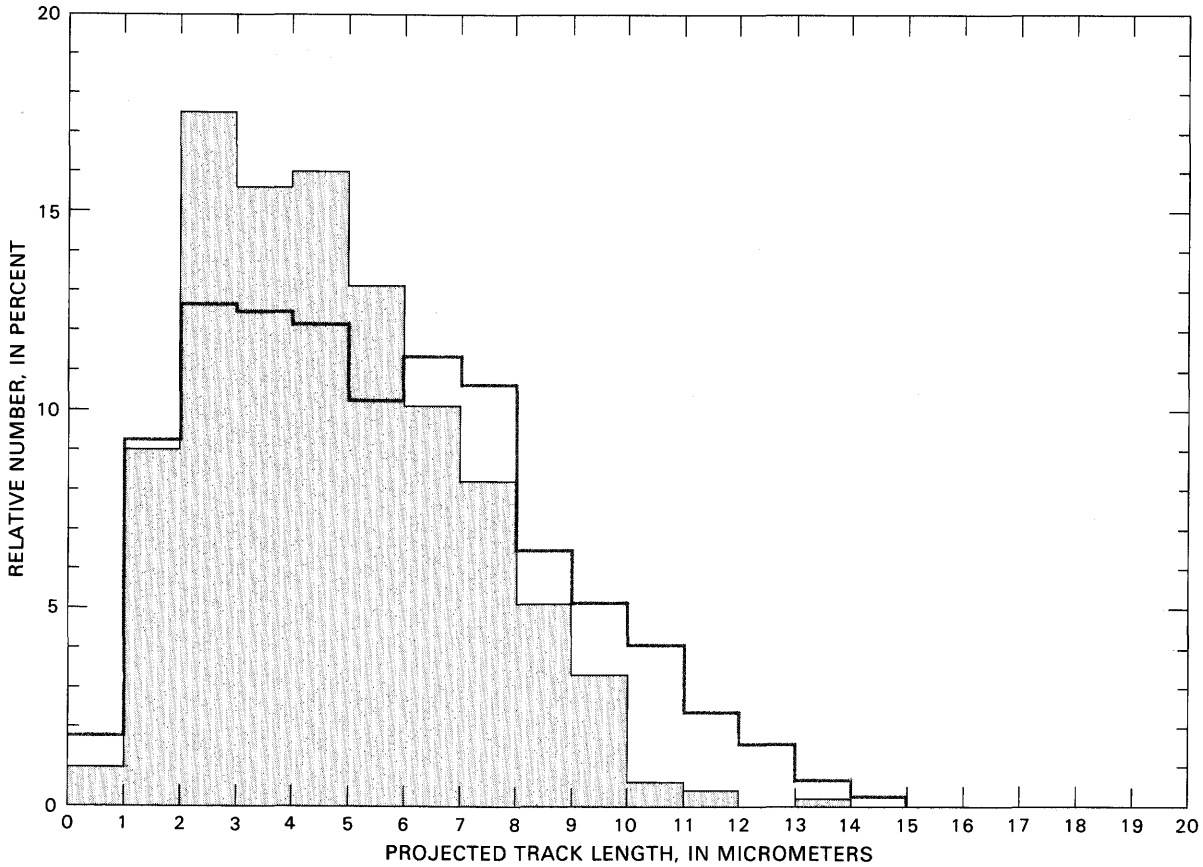

Figure J2. Projected track-length distribution of fossil (boundary of shaded area) and induced (light-grey) tracks in sample UPH–2–2185. The relative shapes and the regression-defined, right-shoulder intercept best show the shortening of the fossil tracks due, most likely, to slow cooling through the closure temperature rather than to partial resetting at lower temperatures.

1–2025 at ~20°C can have been cooled an absolute minimum of ~26°C during the last 132 Ma. Assuming that the geothermal gradient has been constant over time, the slope of the line through the data suggests cooling at a rate of 0.27°C/Ma. The extrapolation of this decreasing age trend to "zero age" is at the depth of 2,174 m (7,174 ft) and a temperature of 56°C. Under the condition of a constant cooling rate, this extrapolation provides the geometric construction of the closure temperature. Therefore, if the cooling rate remained the same and the geothermal gradient has remained constant, a closure temperature of 56 ± 2°C would be indicated. This construct requires a revised estimate of ~36°C for the minimum post-Jurassic cooling. However, application of the first-order loss model for track accumulation in apatite leads to the prediction of a closure temperature of 93 ± 18°C, thereby implying cooling on the order of 73 ± 18°C since the Jurassic. In addition, an increase in cooling rate after ~50 Ma (dashed line of fig. J1) is required.

Two mechanisms can be invoked to account for pre-Cretaceous heating and post-Jurassic cooling of the basement rocks. The first of these is burial by post-Ordovician sedimentary rocks later removed, possibly before but mostly after ~130 Ma. The second is the heating effect of a significantly higher geothermal gradient in the past, allowing for subsequent cooling as the gradient decreased to its present value and the closure temperature isotherm once again moved down deeper into the basement.

What evidence is there for the following:

1. Independently determined higher temperatures than presently exist in the basement or overlying sedimentary rocks,
2. Formerly existent sedimentary units possibly still present elsewhere but missing in northern Illinois, and
3. A higher geothermal gradient in the early Cenozoic?

No independent and direct evidence is known to exist for formerly higher temperatures in the rocks at the drill site. However, in the upper Mississippi Valley lead-zinc district, about 100 km west of the drill sites, McLimans (1977) has reported fluid-inclusion homogenization temperatures of 75°-220°C in the ores. The age of these deposits is unknown relative to the thermal history at the drill sites. Cobb (1981) has determined homogenization temperatures of fluid inclusions in sphalerite in coal from the western shelf of the Illinois Basin, about 100 km

southwest of the drill site, of from 75°C to 113°C. He also noted that there is no perceptible difference between the vitrinite reflectance of coals adjacent to or removed from the sphalerite veins, indicating thermal equilibrium between the sphalerite-forming solutions and the country rock. Cobb (1981) also calculated maximum temperatures of coalification on the western shelf for the Herrin (no. 6) Coal, assuming burial at maximum temperature for 50–75 m.y. of 70°C–80°C, on the basis of vitrinite reflectance values.

Options are extremely limited in this region for attempting to attribute higher temperatures to formerly deeper burial. Because the youngest sedimentary unit (neglecting Pleistocene deposits) at the drill sites is the Middle Ordovician Galena Dolomite and Plattville Formation and the apatite ages suggest that the basement was cooling by ~130 Ma, the time of deposition of the "missing strata" would have had to have been in the Late Ordovician-130 Ma interval. Within the Illinois Basin, Pennsylvanian strata are unconformable on the underlying formations, which range progressively from Mississippian through Ordovician age from south to north (Willman and others, 1967). If this uplift and erosion in Late Mississippian time increased in magnitude north to the drill sites, burial as the cause of pre-130 Ma reheating could be attributed only to Pennsylvanian through ~130-Ma-old sedimentation. The Sandwich fault zone is between the northernmost Pennsylvanian sedimentary rocks and the drill sites. The cumulative displacement within the zone is ~242 m (800 ft), with a sense of movement down to the north. Movement apparently was major between post-Middle Silurian and pre-Pleistocene time (Kolata and others, 1978). This structure might have caused a delay in the uplift and erosion of pre-Pennsylvanian units to the north until well after their removal to the south. If so, additional burial depth could have been maintained into the Early Cretaceous making a simple uplift- and erosion-induced cooling model more viable. On the basis of coal rank in the northern Illinois Basin (~60 km southeast of the drill sites), Damberger (1971) suggested about 970 m of former burial. His estimate was, however, dependent upon the geothermal gradients at the time the coal attained maximum rank. Although no Upper Pennsylvanian or Permian strata generally have been recognized in the Illinois Basin or to the north, Kehn and others (1981) reported the presence of Permian strata preserved in a graben in western Kentucky. This late sedimentation, although presently localized, might suggest the possibility of more widespread post-Pennsylvanian sedimentation in the region than is preserved.

On direct evidence, a case for an increased geothermal gradient in the region is difficult to make. This difficulty arises primarily because of the cryptic nature of the observable effects of such an increase and the inability to project back in time from present observations of geothermal gradients. However, an indirect case for this possibility can be made.

McGinnis and others (1976) interpreted the increasingly positive regional Bouguer anomaly in southern Illinois as due to midcrustal level intrusives that increased crustal density there and that resulted in the subsidence of the Mississippi Embayment. The small Permian-age intrusions isotopically dated by Zartman and others (1967) in southern Illinois might be the surface expressions of these larger deep-seated parent bodies, closely dating them as well.

If in the Permian, and perhaps through the Mesozoic, extra thermal energy was being transferred into and was heating the entire lithosphere along and extending beyond the axis of the Mississippi Embayment, the effect on the present observations of heat flow would be only minimal. Sleep (1971) showed that following a heating event of lithospheric dimensions, temperatures decrease exponentially with a time constant of about 50 Ma. The anomalous part of an increased geothermal gradient, therefore, would decay with a half-life of about 70 Ma. The measured geothermal gradient at the drill sites is 23°C/km. If a slightly lower geothermal gradient, say 18°C/km, actually would result from equilibrium heat flow, then a gradient of 36°C/km could have existed at 130 Ma and would have decayed to about 23°C/km by the present if the input of extra heat had ceased at or before 130 Ma. The value of 36°C/km in the following hypotheses is used as a maximum estimate of geothermal gradient in the Embayment rift environment because of its ability to decay to the present value in the time allowed while maintaining a regionally reasonable equilibrium value.

Four hypotheses involving two sets of assumptions are suggested for the interpretation of the fission-track data. The first set involves the contradictory assumptions that the geothermal gradient has remained constant and that it has been decreasing exponentially since Early Cretaceous time. The second set of assumptions deals with the interpretation made for the closure temperature of apatite. Independent estimates of maximum temperatures, such as fluid-inclusion homogenization and vitrinite-reflectance temperatures in adjacent areas, are, in general, supportive of temperatures in the past close to the theoretically derived apatite closure temperature. These temperatures are somewhat lower than the theoretical closure temperature and are observed in areas where plentiful evidence of sedimentary accumulation exists. For these reasons, in addition to the moderate uncertainty associated with the estimate of the apatite closure temperature (that is, 93 ± 18°C) and the apparent extrapolation of the age trend to the present temperature of 56°C, the possibility of a lower closure temperature is considered also.

The assumptions and their ramifications have been tabulated and are shown in table J2. The assumptions in

Table J2. Hypotheses presenting the range of possible cooling and burial over time

[Assumptions regarding the geothermal gradient over time and the closure temperature affect the interpretation of the apatite ages in terms of required amounts of former burial. The "temperatures at present burial depths" were calculated assuming a 15°C surface temperature and the appropriate geothermal gradient. °C/km, degrees Celsius per kilometer; Ma, million years]

Hypothesis	Assumptions		Temperature UPH-1-2025 At 130 Ma for present depth T_{130}	Additional cooling to the present T_c-T_{130}	Additional burial required at 130 Ma (meters)	Temperature UPH-2-5411 at ~50 Ma for present depth T_{50}	Additional cooling to the present T_c-T_{50}	Additional burial required at 50 Ma (meters)
	Geothermal gradient (°/C/km)	Closure temperature (T_c)						
1	Constant, 23	93°C	20°C	73°	3,174	46°C	47°	2,043
2	Constant, 23	56°C	20°C	36°	1,565	46°C	10°	435
3	Decreasing from 36 at 150 Ma to 23 at present	93°C	37°C	56°	1,556	58°C	35°	1,346
4		$56°<T_c<93°$	37°C	19°-56°	528-1,556	58°C	0-35°	0-1,346

the four hypotheses result in calculation of different amounts of cooling, in addition to that caused by a decrease in the geothermal gradient where this is assumed. Differences in the timing of that cooling are observed also. Once cooling due to changes in geothermal gradient has been subtracted from the total cooling, the residual cooling can be explained only by the removal of overlying sedimentary rocks. The amount of removal can be calculated by dividing the residual cooling by the value of the geothermal gradient in effect at the time of passage through the closure temperature. In addition to changes brought about by the assumed decreasing gradients over time, assumptions must be made about the thermal conductivity of the now-removed sedimentary rocks. For simplicity rather than insight, the conductivity in any removed sedimentary formations is assumed to have sustained a 23°C/km gradient under the present heat flow regime. Lower conductivity in the removed section would result in the calculation of smaller amounts of removal and vice versa.

In calculating hypothetical sample temperatures at the time of closure on the basis of present depths, a surface temperature of 15°C is assumed. The difference between these temperatures and the assumed closure temperature is then used to calculate the required additional burial. At 50 Ma, the exponentially decreasing gradient of hypotheses 3 and 4 would be ~26°C/km. This is the value used in the calculation of temperatures and additional burial for the bottom-hole sample, UPH–2–5411.

Apparent in all four hypotheses is a significant amount of post-~130 Ma. erosion. This erosion ranges from a low of 528 m (hypotheses 4) to a high of 3,174 (hypothesis 1). The effect of choosing a lower closure temperature with constant gradient (hypothesis 2) or the theoretically calculated closure temperature with an increased gradient (hypothesis 3) is to require approximately the same net erosion. However, the effect of choosing the higher closure temperature (hypothesis 1 and hypothesis 3) is to require significantly more erosion post-~50 Ma than with the minimum closure temperature of 56°C which may require none at all (hypothesis 4). Any increased geothermal gradient, although not changing the depth at which the projected "zero age" occurs, would increase the temperature at that depth and hence the value assigned for the closure temperature in this construction. Therefore, the closure temperature of 56°C is inconsistent with the assumption of decreasing gradient and some post-50-Ma erosion still would be indicated.

The fission track age found for the zircon sample of 768 ± 325 (95–percent confidence level) suggests that its age is greater than 500 Ma, the age of the Mount Simon Sandstone. This age is taken as qualified support for a conclusion that this sample was not reheated to higher than 150°-180°C during the Phanerozoic.

The younger than expected apatite fission-track ages at the Illinois drill sites are not unique in this region. Numerous apatite samples from the exposed Precambrian basement in central and northern Wisconsin and in northern Michigan also yield "young" fission-track ages, ranging from ~500 to 220 Ma (R. A. Zimmermann and C. W. Naeser, unpub. data). The general trend in these ages is for a decrease in age toward the present surface expression of the basement unconformity; the youngest ages are in southern Wisconsin. The Illinois drill hole results can, therefore, be viewed in the regional context of a progressive southward uplift and exposure of the Precambrian basement, which apparently has taken place at least since Permian time.

CONCLUSIONS

An inescapable conclusion of this apatite fission-track age study seems to be that there has been significant

post-~130 Ma erosion around the site of the Illinois drill holes. Even under the assumptions of hypothesis 4 discussed earlier, which are the most difficult to justify geologically, the amount of burial required to reset the apatite ages is comparable to the burial implied by Damberger (1971) from coal rank in the northernmost exposures of Pennsylvanian rocks of the Illinois Basin. The time of regional erosion is not until post-~130 Ma and possibly pre-~50 Ma. If the post-Upper Ordovician through Mississippian sedimentary sequence had been removed in pre-Pennsylvanian time in northern Illinois, the implication is that Pennsylvanian rocks of considerable thickness (>500 m) extended 100 km or more north of their present limit.

No compelling evidence exists from these data that requires a closure temperature as low as 56°C. An additional 2,000 ft of core, in retrospect, would have been conclusive in this respect. Independent geological calibration of the closure temperature and the apparent accuracy of the analytical approach used to calculate the closure temperature for these data suggest a closure temperature of 93 ± 18°C. Although the actual value may be somewhat lower, (toward the lower end of the calculated confidence interval), the amount of burial required with the constant or decreasing geothermal gradient is considerable. Additionally, a large amount of the uplift and erosion (maximum 1,346–2,043 m) would have taken place in the last 50 Ma. Maximum temperatures of 75°-110°C in the Pennsylvanian coals and sphalerite veins suggest similar former burial depths where Pennsylvanian rocks are preserved. Whereas these occurrences allow only for the removal of overlying Pennsylvanian and younger rocks in the area of the drill holes, rocks of Ordovician age to as young as Jurassic (pre-130 Ma) could have been removed. The thickness of the post-St. Peters Sandstone through Mississippian section preserved in the Illinois Basin is a minimum of about 800 m. These formations are truncated progressively downsection, however, and then are overlain by Pennsylvanian rocks farther northward out of the Basin. The only way of retaining this thickness of Paleozoic rocks until ~130 Ma, so as to provide the greatest depth of burial in northern Illinois, is to require a reversal or cessation of this northerly uplift just north of the structural basin—perhaps the role played by the Sandwich Fault zone. Uplift and erosion after ~130 Ma was then regional in extent, eroding and cooling the Pennsylvanian rocks in the Illinois basin, for which there is evidence, as well as the region to the north.

This study suggests a burial history involving greater thicknesses or temperatures than generally is accepted for this region. Awareness of this revised burial history could be significant in understanding the conditions of genesis of lead-zinc mineralization in the region. Furthermore, resetting of the apatites in the basement raises the possibility that minimum temperatures for hydrocarbon generation could have been reached in the lower sedimentary units.

REFERENCES CITED

Carpenter, B. S., and Reimer, G. M., 1974, Calibrated glass standards for fission track use: National Bureau of Standards Special Publication 260–49, p. 16.

Cobb, J. C., 1981, Geology and geochemistry of sphalerite in coal: Champaign, Ill., Illinois State Geological Survey, 187 p.

Dakowski, M., 1978, Length distribution of fission tracks in thick crystals: Nuclear Track Detection, v. 2, p. 181–189.

Damberger, H. H., 1971, Coalification pattern of the Illinois Basin: Economic Geology, v. 66, p. 488–494.

Dodson, M. H., 1973, Closure temperature in cooling geochronological and petrological systems: Contributions to Mineralogy and Petrology, v. 40, p. 259–274.

Eardley, A. J., 1962, Structural geology of North America (2d ed.): New York, Harper and Row, 743 p.

Green, P. F., 1981, "Track-in-track" length measurements in annealed apatites: Nuclear Tracks, v. 5, p. 121–128.

Harrison, T. M., Armstrong, R. E., Naeser, C. W., and Harakal, J. E., 1979, Geochronology and thermal history of the Coast Plutonic Complex, near Prince Rupert, British Columbia: Canadian Journal of Earth Sciences, v. 16, p. 400–410.

Johnson, N. M., McGee, V. E., and Naeser, C. W., 1979, A practical method of estimating standard error of age in the fission track dating method: Nuclear Tracks, v. 3, p. 93–99.

Kehn, T. M., Beard, J. G., and Williamson, A. D., 1981, The Manzy Formation; A new stratigraphic unit of Permian age in western Kentucky: U.S. Geological Survey Open-File Report 81–790, 15 p.

Kolata, D. R., Buschbach, T. C., and Treworgy, J. D., 1978, The Sandwich fault zone of northern Illinois: Illinois State Geological Survey Circular 505, 26 p.

Lidiak, E. G., and Denison, R. E., 1981, Petrography, chemistry, specific gravity and magnetic properties of silicic rocks, Illinois Deep Hole Project: EOS, v. 62, p. 388.

Märk, E., Pahl, M., Purtscheller, F., and Märk, T. D., 1973, Thermische Auscheilung von Uranspaltspuren in Apatiten, Alterskorrekturen und Beitäge zür Geothermochronologie: Tschermaks Mineralogische und Petrologische Mitteilungen, v. 20, p. 131–154.

McGee, V. E., and Johnson, N. M., 1979, Statistical treatment of experimental errors in the fission track dating method: Mathematical Geology, v. 11, p. 255–268.

McGinnis, L. D., Heigold, P. C., Ervin, C. P., and Heidari, M., 1976, The gravity field and tectonics of Illinois: Illinois State Geological Survey Circular 494, 28 p.

McLimans, R. K., 1977, Geological fluid inclusions and stable isotope studies of the upper Mississippi Valley zinc-lead district, southwest Wisconsin: College Station, Pa., The Pennsylvania State University Ph.D. thesis, 175 p.

Naeser, C. W., 1976, Fission track dating: U.S. Geological Survey Open-File Report 76–190, 65 p.

Naeser, C. W., 1979, Fission track dating and geologic annealing of fission tracks, *in* Jäger, E., and Hunziker, J. C., eds., Lectures in isotope geology: New York, Springer-Verlag, 329 p.

Naeser, C. W., Zimmermann, R. A., and Cebula, G. T., 1981, Fission track dating of apatite and zircon; An interlaboratory comparison: Nuclear Tracks, v. 5, p. 65–72.

Potter, P. E., and Siever, R., 1956, Source of basal Pennsylvanian sediments in the eastern interior basin: Journal of Geology, v. 64, p. 225–244.

Rahman, J. L., and Roy, R. F., 1981, Preliminary heat-flow measurement at the Illinois deep drill hole: EOS, v. 62, p. 388.

Sleep, N. H., 1971, Thermal effects of the formation of Atlantic continental margins by continental break-up: Geophysical Journal of the Royal Astronomical Society, v. 24, p. 325–350.

Van Schmus, W. R., Peterman, Z. E., and Doe, B. R., 1981, U-Pb and Rb-Sr geochronology of Precambrian granite from northern Illinois deep drill holes: EOS, v. 62, p. 389.

Wagner, G. A., 1979, Correction and interpretation of fission track age, *in* Jäger, E., and Hunziker, J. C., eds., Lectures in isotope geology: New York, Springer-Verlag, 329 p.

Willman, H. B., and others, 1967, Geologic map of Illinois; Urbana, Ill.: Illinois State Geological Survey, scale 1:500,000.

Zartman, R. E., Brock, M. R., Heyl, A. V., and Thomas, H. H., 1967, K-Ar and Rb-Sr ages of some alkalic intrusive rocks from central and eastern United States: American Journal of Science, v. 265, p. 848–870.

Zimmermann, R. A., 1977, The interpretation of apatite fission track ages with an application to the study of uplift since the Cretaceous in eastern North America: Philadelphia, Pa., University of Pennsylvania Ph.D. thesis, 126 p.

Zimmermann, R. A., and Gaines, A. M., 1978, A new approach to the study of fission track fading: U.S. Geological Survey Open-File Report 78–701, p. 467–468.

1986

U.S. GEOLOGICAL SURVEY BULLETIN 1622

SHORTER CONTRIBUTIONS TO ISOTOPE RESEARCH

OXYGEN ISOTOPIC CONSTRAINTS ON THE ORIGIN OF THE PRECAMBRIAN GRANITES FROM THE SOUTHERN WIND RIVER RANGE AND THE GRANITE MOUNTAINS, CENTRAL WYOMING

Chapter K

By K. K. CHEANG[1], D. B. WENNER[1], and J. S. STUCKLESS

CONTENTS

FIGURES

[1]Department of Geology, University of Georgia, Athens, GA 30602

TABLES

Abstract

Two contrasting types of approximately contemporaneous (~2.6 billion years old) granite batholiths from Wyoming were studied in order to elucidate their origins and to provide a general understanding of why one is significantly more enriched in uranium and thorium than the other. The first, from the Granite Mountains, central Wyoming, comprises the granite of Long Creek Mountain and the volumetrically dominant granite of Lankin Dome. The granite of Lankin Dome consists of two major phases, a biotite granite and a leucocratic granite, both of which contain garnet, primary muscovite, and a few metasedimentary xenoliths. The second, the Louis Lake batholith is at the southern end of the Wind River Range, and comprises a hornblende-biotite granodiorite and a leucocratic biotite granite, both bearing sphene, hornblende, epidote and magnetite, and abundant hornblende-enriched rounded clots.

An average of 32 analyses of the granite of Lankin Dome shows that it is peraluminous, with molar $Al_2O_3/(Na_2O+K_2O+CaO)=1.1$, and high CIPW normative corundum=1.4. An average of 14 analyses of the Louis Lake batholith shows that it is metaluminous with $Al_2O_3/(Na_2O+K_2O+CaO)=0.96$ and low normative corundum=0.4. The two granites also differ in radioelement content with uranium, thorium, potassium and thorium-uranium ratios all higher in the granite of Lankin Dome.

Average $\delta^{18}O$ values in parts per thousand (per mil) of the granite of Long Creek Mountain is 8.2 ± 0.3 per mil (N=4), and average $\delta^{18}O$ values of the two phases from the granite of Lankin Dome are as follows: biotite granite=8.5 ± 0.5 per mil (N=37), and leucocratic granite=8.4 ± 0.3 per mil (N=12). The average $\delta^{18}O$ values for the Louis Lake batholith are: hornblende-biotite granodiorite=7.3 ± 0.3 per mil (N=13), and leucocratic biotite granite=7.7 ± 0.1 per mil (N=6). Average $\delta^{18}O$ quartz and $\delta^{18}O$ feldspar for the Granite Mountains are 9.8 (N=15) and 7.8 per mil (N=8), respectively, whereas for the Louis Lake batholith, the average $\delta^{18}O$ quartz and $\delta^{18}O$ feldspar values are 9.5 (N=6) and 7.5 per mil (N=5), respectively. Quartz-feldspar fractionation of pristine granites from both units in the Granite Mountains (7 samples) and Louis Lake batholith (5 samples) give average values of 2.0, reflecting a close approach to high-temperature equilibrium.

Three types of hydrothermally altered granites have been identified in the Granite Mountains. These, as well as their mean $\delta^{18}O$ values, include the progressively altered rock types: sericitized-chloritized-saussuritized granites (whole rock=7.1, N=17; quartz=8.9, N=6; feldspar=6.4, N=6); albitized granites (whole-rock=6.3, N=6; quartz=8.1, N=3; and feldspar=5.6, N=3); silicified-epidotized granites (whole rock=4.7, N=26; quartz=5.6, N=4; feldspar=3.2, N=4). These rock types are all ^{18}O-depleted compared with the unaltered granites, which indicates an interaction between the granite and a low ^{18}O-fluid, probably meteoric water.

The whole-rock, oxygen isotopic, mineralogical, chemical, and strontium isotopic data from the unaltered granites indicate that the magmas that formed the granites in the Granite Mountains probably were derived from a uranium-enriched source that had some peraluminous metasedimentary component, whereas the Louis Lake batholith was formed by partial melting of igneous source materials that are not strongly enriched in uranium. Thus, for the Granite Mountains, this metasedimentary protolith may be important in allowing the preconcentration of uranium and thorium. This difference in protolith and the possible presence of hydrothermally altered units may explain why granites from the Granite Mountains are spatially related to three major uranium districts, but the Louis Lake batholith is not.

INTRODUCTION

Oxygen isotopic studies combined with existing and new major- and trace-element chemical investigations were made of two contrasting types of approximately contemporaneous (~2.6 Ga (billion years)) granite batholiths from Wyoming: the granitic rocks of the Granite Mountains, and the Louis Lake batholith of the southern Wind River Range (fig. K1).

Both the Granite Mountains and Louis Lake batholith lie within the southern extension of the Middle Rocky Mountain Province and form part of several Precambrian basement blocks uplifted during the Laramide orogeny. Most of the Precambrian blocks, including the Louis Lake batholith, trend north to northwest, but the Granite Mountains are exposed as a series of partly buried, discontinuous knobs and ridges forming an east-west trending band of outcrops about 20 km (kilometers) wide and 110 km long, with an exposed area of roughly 2,200 km^2 (square kilometers). The Louis Lake batholith, which lies at the southern end of the Wind River Range, is about 50 km long and 40 km wide with an exposed area of 2,000 km^2 (Bayley, 1965a, b).

The granites of Granite Mountains are of interest because they have been proposed as the source for the uranium in the sandstone-hosted Tertiary deposits at the Gas Hills, Crooks Gap, and Shirley Basin uranium districts (Rosholt and Bartel, 1969). These three areas represent some of the largest uranium-producing districts in the United States. Each contains reserves plus production of ore (at 0.1 percent U_3O_8) of more than 1 million tons (Butler, 1972).

The granite of Lankin Dome that forms most of the Granite Mountains (Stuckless and Peterman, 1977) initially was enriched in uranium when it formed, but present-day values are lowered to slightly above world average as a result of an average 20–percent loss between 1,400–1,700 Ma (million years) and a more extensive loss (generally more than 70 percent) in the Cenozoic (Stuckless and Nkomo, 1978). The timing of uranium minerali-

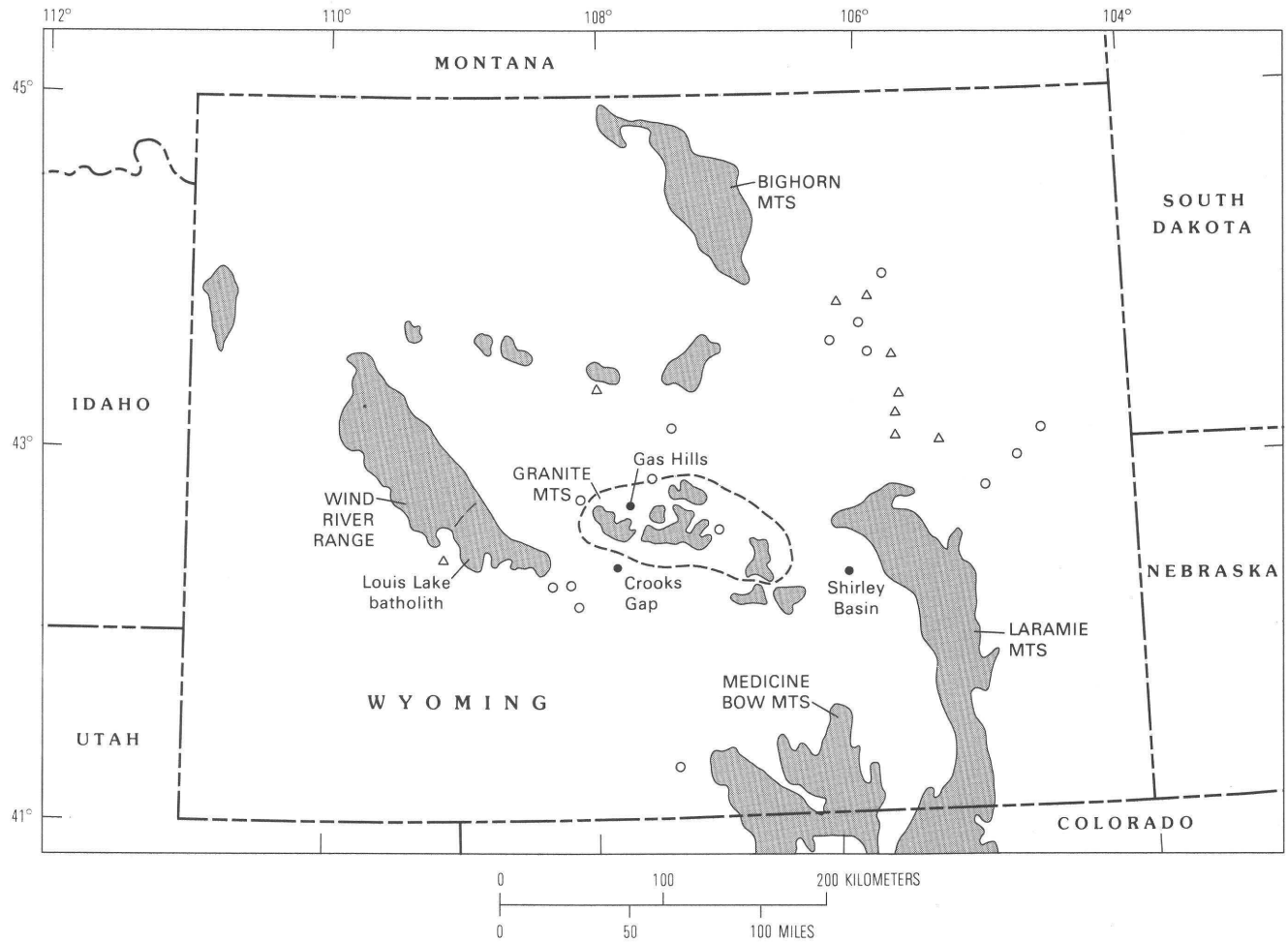

Figure K1. Index map of the principal Precambrian exposures (stippled areas) in Wyoming (from Stuckless and Nkomo, 1978) and the location of uranium deposits in Tertiary rocks. Solid circles, three producing districts with reserves plus production of ore (U_3O_8>0.1 percent) of more than 1 million tons; triangles, deposits with ore reserves plus production between 1,000 and 1,000,000 tons; open circles, deposits with reserves plus production between 1 and 1,000 tons (Uranium data from Butler, 1972.) Dashed line encloses area of the Granite Mountains.

zation in the sandstones (Ludwig, 1978, 1979) coincides with the period of Cenozoic uranium loss. The Granite Mountains were also the provenance for the sandstones that host the uranium ore (Seeland, 1976, 1978).

The Louis Lake batholith represents a contrasting granite body in terms of mineralogy, major- and trace-element chemistry, and oxygen and strontium isotopic composition. It is provenance for Tertiary sandstones of central Wyoming (Seeland, 1978), but it is not associated with large uranium deposits (fig. K1). We have made a study of these two contrasting batholiths principally in order to elucidate the nature of the source rocks for these two granitic terranes. Such a comparison ultimately should lead to a better understanding of the kinds of protoliths that are responsible for producing uranium-enriched granites.

Laboratory Procedures

Oxygen isotope analyses were performed for 213 whole-rock and mineral separates. This large number of analyses was necessary in order to provide adequate coverage of the exposed outcrop area, to elucidate the subtle differences among the different granitic units and phases, and to adequately define the various types of hydrothermally altered units. The number of samples of each unit analyzed was in proportion to the size of the unit, the degree of variability within each unit, and the availability of samples. Geologic relations pertinent to the interpretation of oxygen isotope and other data were noted in the field.

Prior to analyses, all samples were checked for "freshness", and only unweathered samples were selected.

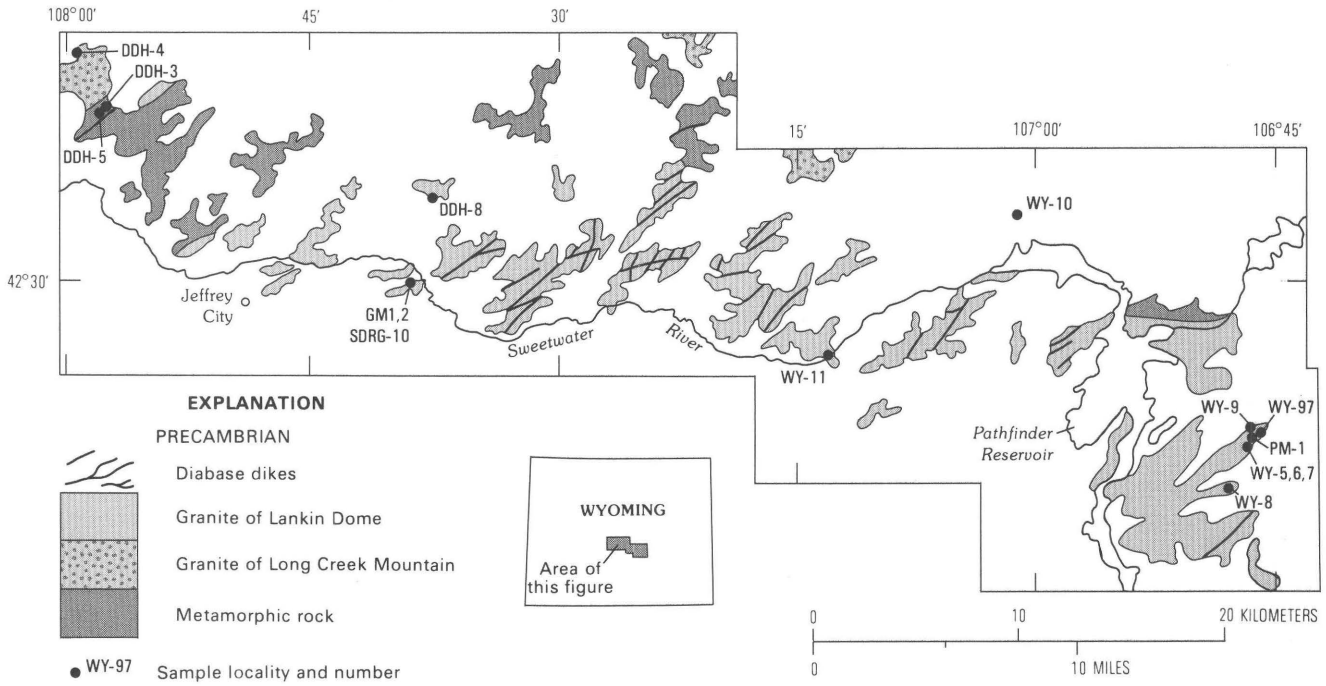

Figure K2. Generalized Precambrian geology of the Granite Mountains region. Geology from Peterman and Hildreth (1978) and Stuckless and Nkomo (1978).

All outer parts of whole-rock specimens were removed, and thin sections were made for each sample and checked under the polarizing microscope. The sample localities from the Granite Mountains are shown in figure K2; many of the samples are the same as those studied by Stuckless, Bunker, VanTrump, and Bush (1978, p. 6–13) and Peterman and Hildreth (1978, p. 4). Sample localities for the Louis Lake batholith are shown in figure K3.

The relatively coarse-grained nature of the granites facilitated separation by handpicking. No attempt was made to separate potassium-feldspar and sodic plagioclase because their oxygen isotopic behavior is similar (O'Neil and Taylor, 1967) and their resistance to oxygen exchange is nearly equal. Quartz separates were purified by treating with cold hydrofluoric acid to remove any feldspar impurities.

Extraction of oxygen from powdered whole-rock samples and mineral separates of quartz, feldspar, and biotite was achieved by reaction with fluorine in nickel vessels using the method described by Taylor and Epstein (1962). The oxygen liberated was converted to CO_2 gas by combustion with a resistance-heated graphite rod in the presence of a platinum catalyst. Oxygen analyses were performed on the CO_2 using a 90°-sector, magnetic-deflection isotope ratio mass spectrometer (McKinney type).

The experimental data are reported in the standard δ notation, with all data reported relative to SMOW (Standard Mean Ocean Water). In our laboratory, National Bureau of Standards standard reference material 28 is defined as 9.61 per mil. Replicate analyses of 41 samples indicate a precision of ± 0.2 per mil. Partitioning of ^{18}O between coexisting minerals A and B is reported as $\Delta A\text{–}B = \delta A - \delta B$.

Magnetic susceptibility measurements were made by Dr. B. B. Ellwood of the University of Georgia, on weighed samples using a susceptibility bridge. Data are reported as the initial susceptibility, χ in G/Oe (gauss per oersted) calculated from:

$$\chi_{sample} = \frac{\text{scale reading of sample} \times \text{mass of standard} \times \chi_{standard}}{\text{scale reading of standard} \times \text{mass of sample}}$$

where the mass and scale reading of the standard are known.

GEOLOGICAL SETTING

The Precambrian geology of the Granite Mountains (fig. K2), has been described by Love (1970), Peterman and Hildreth (1978), Stuckless and Peterman (1977), Stuckless, Bunker, Bush, and others (1977), Stuckless, Bunker, VanTrump, and Bush (1978), and Stuckless, Bunker, Bush, and VanTrump (1981), Stuckless and Nkomo (1978), and Ludwig and Stuckless (1978). In brief, the three major Precambrian lithologies that are recognized among the rocks within the Granite Mountains area include:

1. Amphibolite-grade metamorphic rocks (2860 ± 80 Ma; Peterman and Hildreth, 1978),

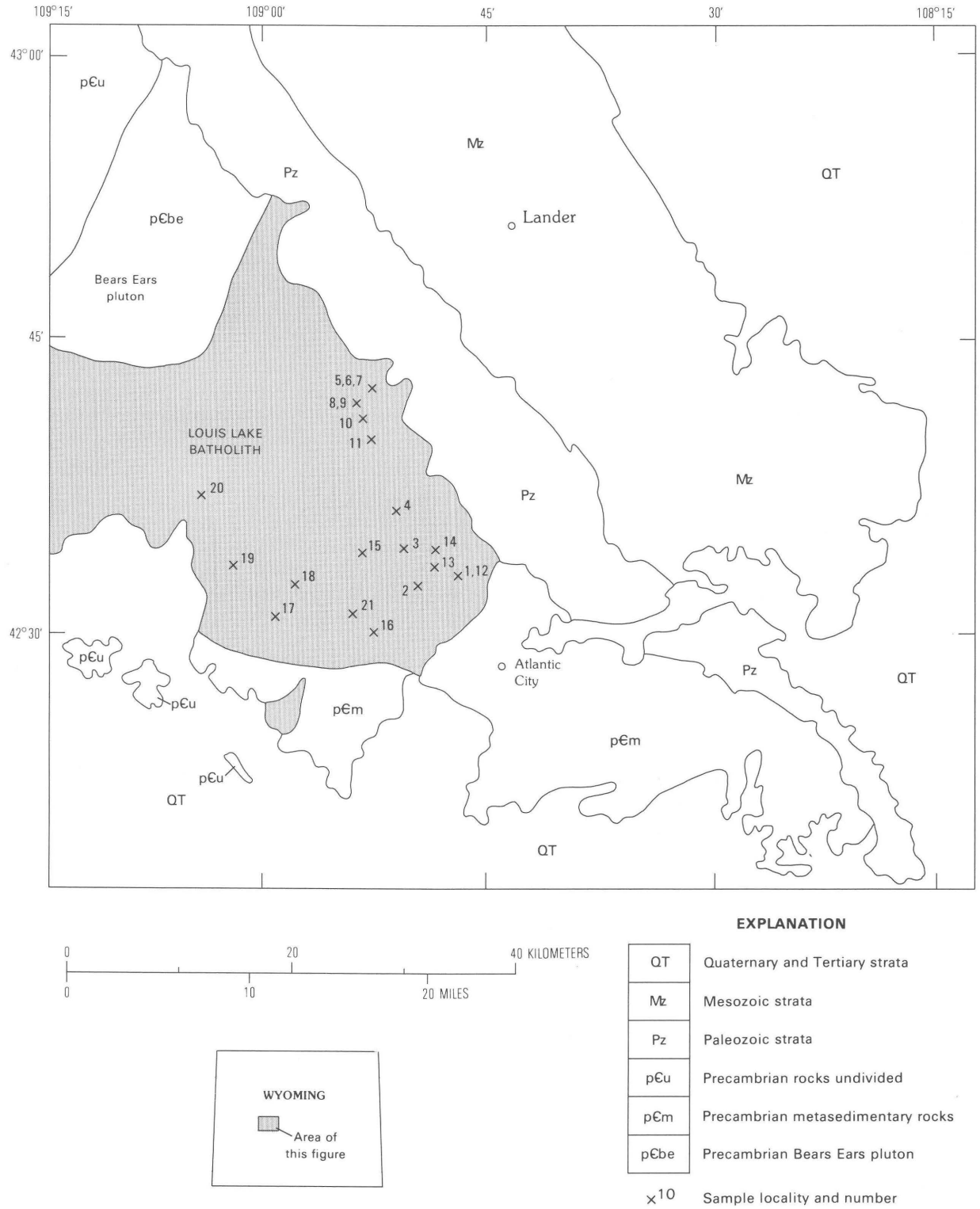

Figure K3. Generalized geologic map of the southern Wind River Range, Wyo. (from Naylor and others, 1970) showing the location of the Precambrian Louis Lake batholith (stippled) and sample localities.

2. Intrusive peraluminous biotite granitic units (2640 ± 20 Ma, for the granite of Long Creek Mountain and 2595 ± 40 Ma for the granite of Lankin Dome, Ludwig and Stuckless, 1978), and

3. Crosscutting diabase dikes ranging from less than 1 m wide to as much as several tens of meters wide (2650 ± 260 Ma; Peterman and Hildreth, 1978).

The metamorphic rocks (about 10 percent of the total exposed outcrop) are schists and tonalitic to granitic or granodioritic gneisses. Present in lesser amounts are amphibolite gneisses intercalated with minor epidote- and biotite-rich horizons.

The granite of Long Creek Mountain (10 percent of granite exposure) and the granite of Lankin Dome (90 percent of granite outcrop) intrude the metamorphic units. The granite of Lankin Dome consists of a leucocratic phase (8 percent) and a biotitic phase (92 percent) and is transected by several aplites and pegmatites. Hydrothermally altered rocks include albitized granites, recognized only in drill cores (Stuckless and Peterman, 1977), and silicified-epidotized granites (2,325–2,560 Ma; Stuckless, Nkomo, and Doe, 1981) that form dikelike or tabular zones that crosscut the unaltered granites.

The Louis Lake batholith (fig. K3), which intrudes Precambrian metagreywackes, schists and iron-formations, consists predominantly of a hornblende-biotite granodiorite (2,642 ± 9 Ma; Naylor and others, 1970)[2] with a volumetrically minor amount of leucocratic biotite granite (2562 ± 75 Ma; Naylor and others, 1970)[2]. The presence of xenoliths of hornblende-biotite granodiorite within the leucocratic biotite granite, combined with radiometric ages, suggests that the latter is slightly younger. Although aplite and pegmatite veins are common in the northern section of the Louis Lake batholith, no distinct hydrothermally altered zones have been recognized.

OXYGEN ISOTOPE DATA—GRANITE MOUNTAINS

Granitic Rocks

Oxygen isotope data for the various granitic units in the Granite Mountains are presented in table K1 and plotted on figure K4. These values are considered representative of the initial $\delta^{18}O$ signature of the primary magma because of the relatively little-altered nature of the rocks as shown in thin-section studies and the lack of isotopic reversals for quartz, feldspar, and biotite values in representative samples. The narrow range of $\delta^{18}O$ values (table K2) for quartz (9.3–10.8 per mil; N=15) and feldspar (7.2–8.2 per mil; N=8), and the mean Δquartz-feldspar of 2.0 suggest a close approach to high-temperature isotopic equilibrium. The latter mean quartz-feldspar value is within the limit of 1.5–2.0 for "normal" igneous plutonic rocks (Taylor and Epstein, 1962; O'Neil and Taylor, 1967).

[2]Ages as recalculated by Ludwig and Stuckless (1978).

Table K1. Whole-rock $\delta^{18}O$ data for samples from the Granite Mountains, Wyo.

[Values in per mil relative to Standard Mean Ocean Water; see text. For details of sample localities, see Stuckless, Bunker, VanTrump, and Bush (1978), and Peterman and Hildreth (1978). gdg, granodioritic gneiss; gg, granitic gneiss; tg, tonalitic gneiss; amqg, amphibolite intercalated with quartzofeldspathic gneiss]

Sample No.	$\delta^{18}O$	Sample No.	$\delta^{18}O$
Biotite granite of Lankin Dome			
BBSW-1	9.2	IR-13	8.4±0.03
BR-3	8.1	L-4	9.1
BRQ-1	8.6	L-5	8.8±0.2
DDH-3	10.2±0.2	LD-14	7.9
DDH-5	9.0	LM-4	9.1±0.3
DDH-8	8.6	LM-9	8.8
GM-1-8.8	8.2	MS-20	8.7
GM-1-67.0	8.2±0.3	PD-5	8.8
GM-1-86.3	8.3	PD-16	8.0
GM-1-125.8	8.0	PM-1-459	8.0
GM-1-228.9	8.5	PM-1-491	8.5
GM-1-266.7	8.6	PRSW-10	8.6
GM-1-285.0	8.8	PRSW-11	8.3±0.3
GM-1-374.0	8.4	SM-4	8.6
GM-1-1195.8	8.3	SM-8	8.2
GM-1-1278.5	8.9	SP-3	7.8
GM-1-1342.5	8.9	W2-CR-1-134.5	8.1
GM-2-1413.0	8.5	WY-11	7.8
IR-6	8.6		
Leucocratic granite of Lankin Dome			
BBL-9	8.7	GM-1-851.9	8.0
GM-1-581.9	8.6	GM-1-1022.2	8.3
GM-1-739.0	8.6	GM-1-1325.0	8.4
GM-1-773.5	8.6	IR-12	8.4±0.03
GM-1-814.5	8.3	PM-1-295.0	8.0
GM-1-850.1	8.5	SP-6	7.9
Granite of Long Creek Mountain			
BBL-13	8.1	DDH-4	7.8
TCM-2	8.2	MS-31	8.5
Metamorphic units			
GM-35-68(gdg)	7.1	GM-78-68(gg)	7.4
GM-38-68(tg)	7.8	GM-98-68(tg)	4.8±0.3
GM-76-68(tg)	7.5±0.03	GM-103A-69(amqg)	6.0
GM-77-68(gdg)	7.0	GM-104-69(gdg)	5.3±0.3
GM-76-68(quartz)	8.7		
Diabase dikes			
IR-10	5.0	SD-5	5.5
MS-8	4.7	SD-14	5.3
PM-1-1210.3	4.2	SRQ-2	3.8
PM-1-1350.7	4.4	WY-9 (PD-5)	2.1±0.1
PRSW-8	2.8		

Table K2. $\delta^{18}O$ values of coexisting minerals from the Granite Mountains and Louis Lake batholith, central Wyoming

[Values in per mil relative to Standard Mean Ocean Water, see text. Leaders (---) indicate not analyzed]

Sample No.	Quartz	Feldspar	Biotite	Rock
Biotite granite of Lankin Dome				
GM-1-266.7	10.8	8.2	5.6	8.6
L-5	10.0	7.9	---	8.8
LM-9	10.0±0.15	7.9±0.13	---	8.8
MS-20	10.0	8.1	---	8.7
PM-1-459	9.4±0.02	7.2	---	8.0
WY-11	9.4	7.5	3.3	7.8
GM-2-1413	9.7	---	---	8.5
IR-27	9.3	---	---	7.9
LD-14	9.8	---	---	---
SP-6	9.7	---	---	---
SP-10	10.0	---	---	---
Leucocratic granite of Lankin Dome				
GM-1-773.5	9.9	8.1	---	8.6
GM-1-850.1	10.0	7.9	---	8.5
Average-----	9.8	7.8	---	---
Hornblende-biotite granodiorite of Louis Lake				
LLB-2	9.5	7.0	3.0	7.4
LLB-4	9.3	7.1	---	7.3
LLB-5	9.5	7.7	3.7	8.0
LLB-17	9.3	7.8±0.2	3.4	7.3
LLB-16	9.8	7.9	---	7.6
LLB-19	9.8	---	---	6.7
Average-----	9.5	7.5	---	---

Relatively fresh samples from the volumetrically dominant granite of Lankin Dome are characterized by a biotite granite that has a mean $\delta^{18}O=8.5\pm0.5$ per mil (N=37) and a leucocratic granite with mean $\delta^{18}O=8.4\pm0.3$ per mil (N=12). The granite of Long Creek Mountain has a mean isotopic value of $\delta^{18}O=8.2\pm0.3$ per mil (N=4) that is nearly identical to that of the granite of Lankin Dome.

Whole-rock $\delta^{18}O$ values for the various granitic units fall within relatively narrow ranges (table K1). Typically, $\delta^{18}O$ values for the biotite granites are within 7.8–9.1 per mil or within a 1.3 per mil range, with the exception of sample DDH–3, which has a value of 10.2 per mil. The leucocratic granites have values ranging from 7.9–8.7 per mil or within a 0.8 per mil range. Hence, practically all the samples from the granite of Lankin Dome fall within 7.8–9.1 per mil. The granite of Long Creek Mountain also falls within a narrow limit between 7.8 and 8.5 per mil or 0.7 per mil. Among unaltered samples, the whole-rock $\delta^{18}O$ and quartz-feldspar values show no obvious variation with either geographic distribution or depth as reflected in one 426.7-m (1400-ft) drill core (GM–1; see fig. K6). Thus, the Granite Mountains appear to be quite isotopically uniform both in vertical and areal extent.

Metamorphic Rocks

The rocks intruded by the granite consist of amphibolite-grade granodioritic gneisses, tonalitic gneisses, epidote-rich gneisses, and amphibolites. These rocks have a $\delta^{18}O$ range of 4.8 to 7.8 per mil with an average of 6.6 per mil (N=8). (See table K1 and fig. K5.) The $\delta^{18}O$ value of a quartz separate from sample GM–76–68 has a value of 8.7 per mil and a whole-rock $\delta^{18}O$ value of 7.4 per mil, indicating a close approach to high temperature isotopic equilibrium.

These Precambrian metamorphic units appear to have lower $\delta^{18}O$ values than do equivalent lithologies from the Canadian Shield (Longstaffe and Schwarcz,

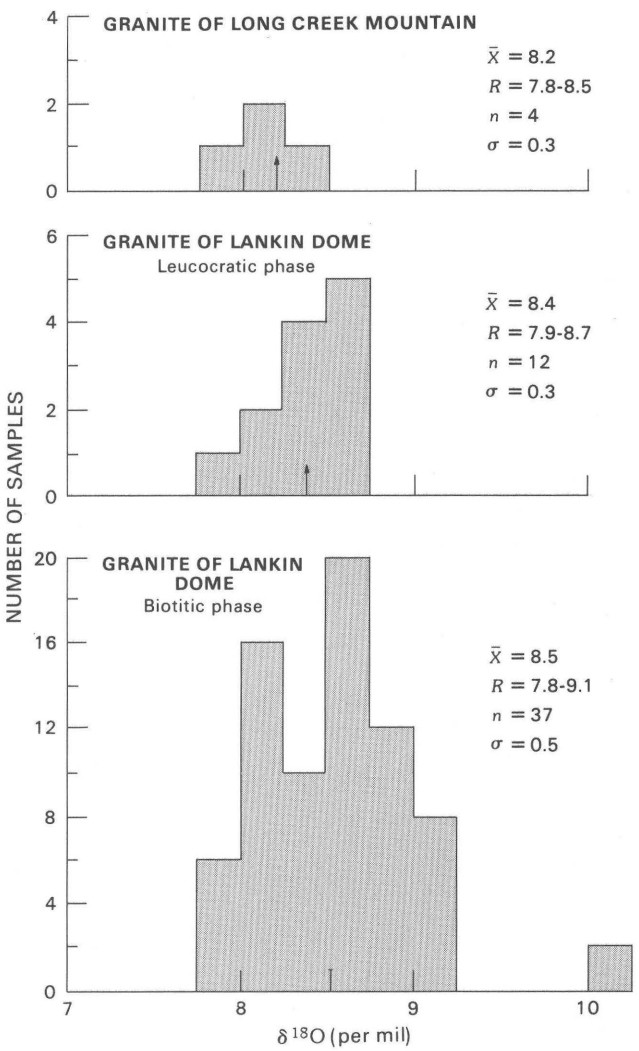

Figure K4. Histogram showing ^{18}O values of various granitic units within the Granite Mountains. Vertical arrow positioned on the horizontal axis shows the mean oxygen isotopic composition. $\bar{X}$, mean value, R, range of values; n, number of samples; σ, standard deviation.

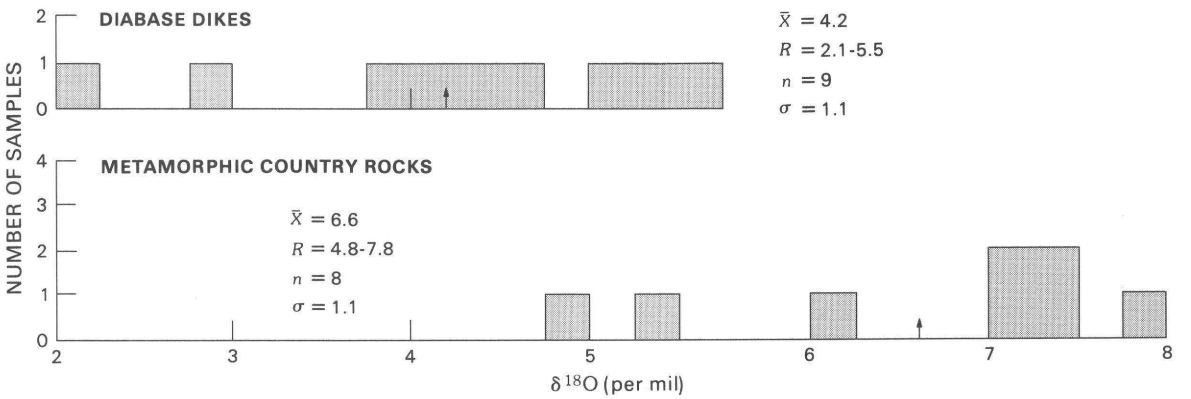

Figure K5. Histogram showing $\delta^{18}O$ values of diabase dikes and metamorphic rocks from the Granite Mountains. Vertical arrow positioned on horizontal axis shows the mean oxygen isotopic composition. $\bar{X}$, mean value; R, range of values; n, total number of samples; and σ, standard deviation.

1977), possibly reflecting a more primitive protolith. Alternatively, these lower $\delta^{18}O$ values also may reflect the higher grade of regional metamorphism, which in many studies has been observed to produce a systematic lowering of the $^{18}O/^{16}O$ of whole rocks (Hoefs, 1980).

Examination of the oxygen isotope data also suggests that the granites of the Granite Mountains were not derived directly from the metamorphic country rock through an anatectic process. All the metamorphic rock types have distinctly lower $\delta^{18}O$ values (4.8–7.8 per mil; mean of 6.6 per mil) than the granite (mean=8.5 per mil). Because of the high temperatures involved in anatectic processes, the $^{18}O/^{16}O$ partitioning between a protolith and granitic melt should be small (O'Neil and others, 1977), implying that the source rocks for the granites of the Granite Mountains must themselves have been ^{18}O-enriched compared to the country rocks.

Contacts between the metamorphic rocks and granites are fairly sharp and do not show any merging or intermingling boundaries. Locally, foliations in the metamorphic units parallel the granite contacts and generally wrap around the intrusives. All this evidence suggests forceful intrusion rather than in-situ derivation from the metamorphic rocks. Because the metamorphic complex is intruded by the granite, the source of the granite would appear to be from deeper levels in the crust, perhaps from different lithologies than those exposed at the surface.

Diabase Dikes

Diabase dikes from the Granite Mountains have a large variation in $\delta^{18}O$ values ranging from 2.1 to 5.5 per mil, with an average of 4.2 per mil (table K1 and fig. K5). "Normal" basaltic or diabasic dikes have $\delta^{18}O$ values of about 5.5–6.0 per mil (Taylor, 1974; Longstaffe, McNutt, and Schwarcz, 1980). The lowered $\delta^{18}O$ values of the diabase dikes demonstrate that varying degrees of exchange with low $\delta^{18}O$ waters have taken place in the dikes. These fluids may have been channeled along the same fracture zones that localized the hydrothermally altered granites. Chemical analyses of the mafic dikes (for three samples), show the presence of water ranging from 0.2 to 0.8 to 1.8 percent by weight (Stuckless and Peterman, 1977). Mineralogical studies show that intense saussuritization of calcium plagioclases, chloritization of biotites, and uralitization of augites, are present in most samples.

HYDROTHERMALLY ALTERED ROCKS

Stuckless, Bunker, Bush, Doering, and Scott (1977) and Stuckless, Nkomo, and Doe (1981) recognized two types of hydrothermally-altered units in the Granite Mountains. These units include the albitized granite, which was observed only in those parts of drill cores that appear to be associated with fracture zones (fig. K6), and the silicified-epidotized granite, which is exposed as long, narrow, resistant ridges that cut across the granite along fracture planes and zones of weakness. A rock type not previously reported, the sericitized-chloritized-saussuritized granites, have a more subtle type of hydrothermal alteration. These altered granites have been recognized principally through the oxygen isotope studies. Petrographically, they are similar in mineralogy to the biotite and leucocratic granites, but have a higher, and more variable degree of sericitization and saussuritization of the feldspars and an intense chloritization of the biotites. These samples are also in many places restricted to highly fractured parts of drill cores (fig. K6).

All the hydrothermally altered rocks have low $\delta^{18}O$ whole-rock values (table K3 and fig. K7), slightly de-

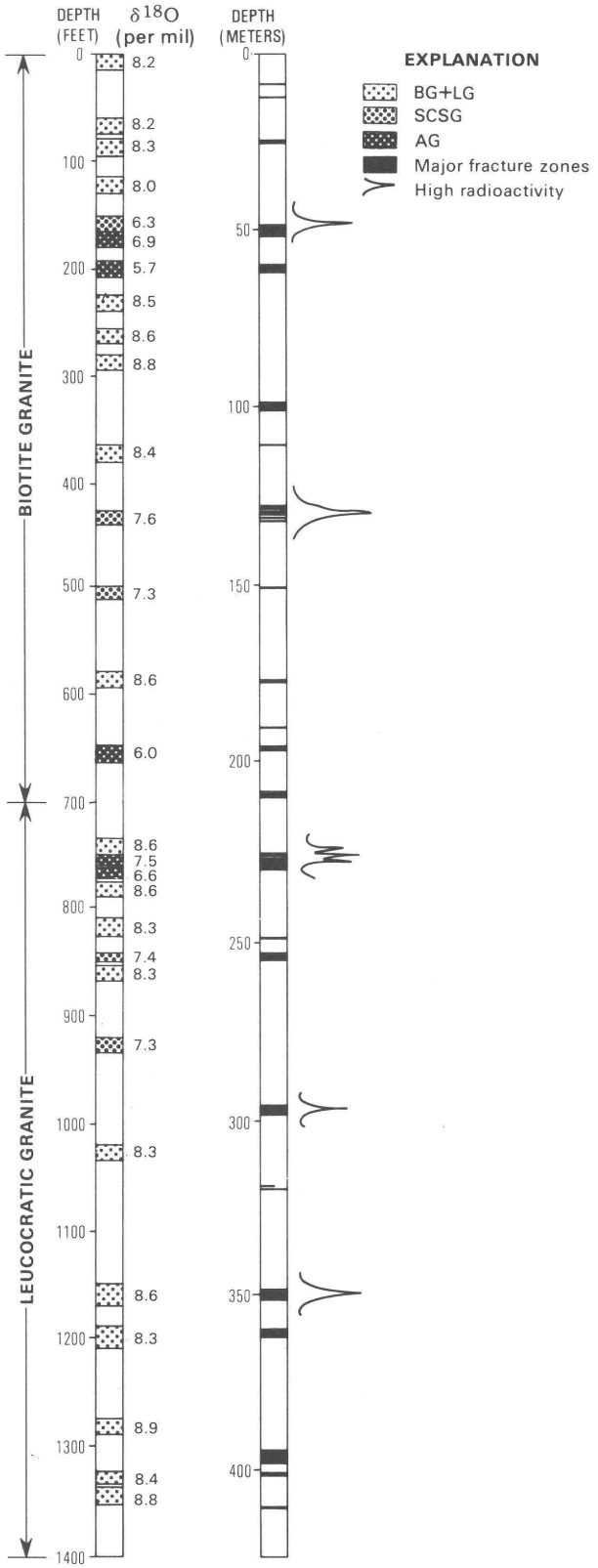

pleted $\delta^{18}O$ quartz values, and significantly lower $\delta^{18}O$ feldspar and $\delta^{18}O$ biotite values; all Δquartz-feldspar and Δquartz-biotite values deviate severely from normal (table K4). The water content (Stuckless and Peterman, 1977, appendix 1) also is higher for the sericitized-chloritized granites. The oxygen isotopic data for the hydrothermally altered rocks can be summarized from table K3 as follows:

1. The sericitized-chloritized-saussuritized granite has a mean $\delta^{18}O$ whole-rock value of 7.1 per mil (N=17), a mean $\delta^{18}O$ quartz of 8.9 per mil (N=6), and a mean $\delta^{18}O$ of feldspar of 6.4 per mil (N=6).
2. The albitized granite has a mean $\delta^{18}O$ whole-rock value of 6.3 per mil (N=6), a mean $\delta^{18}O$ quartz of 8.1 per mil (N=3), and a mean $\delta^{18}O$ of feldspar of 5.6 per mil (N=3).
3. The silicified-epidotized granite has a mean whole-rock value of 4.7 (N=26), a mean $\delta^{18}O$ of quartz of 5.6 per mil (N=4), and a mean $\delta^{18}O$ of feldspar of 3.2 per mil (N=4).

In contrast, mean $\delta^{18}O$ values for the whole-rock, quartz, and feldspar samples from the Granite Mountains (8.5, 9.85, and 7.85 per mil, respectively) and Louis Lake batholith (7.4, 9.53, 7.52 per mil, respectively) are relatively ^{18}O-enriched. Thus, the $\delta^{18}O$ values for the whole-rock, quartz, and feldspar become progressively lowered in the sequence from unaltered granites to chloritized granites to albitized and finally, silicified-epidotized granites (tables K1, K2, K3, and K4, and figs. K4, K6, and K7) indicating an increasing degree of interaction between the granite and a low ^{18}O fluid, probably meteoric water, as a function of time and (or) water to rock ratio. The ^{18}O-depleted, hydrothermally altered zones appear to have acted as ancient channelways for these low ^{18}O fluids. These same sites also are associated with fracture zones that have a high radioactivity and anomalous uranium concentrations at depth as observed in drill core GM–1 (fig. K6), and thus may serve as sites where uranium become concentrated during the period of major uranium loss in the Cenozoic.

OXYGEN ISOTOPE DATA—LOUIS LAKE BATHOLITH

As is true for the Granite Mountains, whole-rock (table K5) and quartz $\delta^{18}O$ data (table K2) from the Louis Lake batholith are considered to represent the primary $^{18}O/^{16}O$ of the magma for the following reasons:

Figure K6. Vertical profile of drill-core GM–1 described by Stuckless, Bunker, Bush, Doering, and Scott (1977) showing the relationship between the $\delta^{18}O$ values of the various granitic types, the major fracture zones and sections with high γ activity and uranium values. BG, biotite granite; LG, leucocratic granite; SCSG, sericitized-chloritized-saussuritized granite; AG, albitized granite.

Table K3. Whole-rock $\delta^{18}O$ data for the hydrothermally altered rocks within the Granite Mountains

[± reported for samples analyzed in duplicate except sample GM–1–1156.6 which was analyzed 5 times]

Sample No.	$\delta^{18}O$ (per mil)	Sample No.	$\delta^{18}O$ (per mil)
Sericitized-chloritized-saussuritized granites			
BR-4	6.8±0.1	PD-22	7.1±0.1
GM-1-164.4	6.3	PM-1 2197.0	6.6
GM-1-431.9	7.6	SR-10	6.6±0.4
GM-1-502.2	7.3	SRQ-3	7.6±0.2
GM-1-651.7	6.0	WY-5	6.9
GM-1-842.2	7.4	WY-7	7.3
GM-1-922.7	7.3	WY-8	6.9
L-26	7.4±0.4	WY-12	7.1
PD-21	7.7±0.3		
Albitized granites			
GM-1-166.0	6.9±0.2	GM-1-1156.6	8.7±0.3
GM-1-202.2	5.7	GM-2-934.4	4.6
GM-1-755.0	7.5±0.1	WY-6	6.8
GM-1-757.0	6.6±0.3		
Silicified-epidotized granites			
BBL-3	6.5	MS-6	4.9
FR-3	6.4	MS-15	6.1
GR-3	6.2	PRNW-5	5.2
GR-4	5.6	PRNW-12	4.0
GR-5	4.1	PRSW-5	7.2±0.1
JC-2	3.9	SD-8	3.3
L-12	5.2	SDRG-1a	4.8
L-18	6.1	SDNE-11	3.3
L-38	5.1	SM-5	7.3
LD-1	4.0	SM-11	4.7
LD-17	3.3	SRQ-7	2.4
LM-2	2.6	WY-10	3.6
MS-1	2.6±0.2	WY-13	4.8
Episyenite			
WY-97	6.8		

Table K4. $\delta^{18}O$ values of minerals from hydrothermally altered zones within the Granite Mountains

[Leaders (---) indicate not analyzed]

Sample No.	$\delta^{18}O$ per mil (Standard Mean Ocean Water)			
	Quartz	Feldspar	Biotite	Rock
Sericitized-chloritized-saussuritized granites				
BR-4	9.7	6.6	---	6.8
GM-1-164	8.4	5.8	3.9	6.3
PM-1-2197	8.8	6.5	---	6.6
WY-7	8.7	6.4	---	7.3
WY-8	9.0±0.3	6.4	1.3	6.9
WY-12	8.9	6.7	2.0	7.1
Albitized granites				
GM-1-166	7.8	5.8	---	6.9
GM-1-755	9.7±0.05	6.8±0.06	---	7.5
GM-2-934.4	6.7	4.1	---	4.6
Silicified-epidotized granites				
JC-2	5.2	3.1	---	3.9
MS-1	5.3±0.2	3.0	---	2.6
PRNW-12	5.9	3.5	---	4.0
SM-11	5.9±0.2	3.2±0.1	---	4.7
Episyenite				
WY-97	8.3	5.9	---	6.8

1. Petrographic examination reveals little alteration. Although a few samples do show minor incipient sericitization in the cores of plagioclase, their $\delta^{18}O$ values are not significantly different from the fresh, unaltered samples.
2. $\delta^{18}O$ of quartz (9.3–9.8 per mil, N=6) and feldspar (7.0–7.9 per mil, N=5) show relatively restricted ranges of isotopic compositions.
3. $\delta^{18}O$ relations among coexisting minerals for six samples have mean $\delta^{18}O$ values of quartz=9.5 per mil (N=6) and feldspar=7.5 per mil (N=5) with average Δquartz-feldspar=2.0 (N=6). The lack of Δ quartz-feldspar isotopic reversals and the approximation of Δquartz-feldspar to "normal" values of 1.5–2.0 per mil (O'Neil and Taylor, 1967) would appear to indicate close approach to isotopic equilibrium.

Oxygen isotope data for relatively fresh whole-rock samples from the Louis Lake batholith average 7.3±0.3 per mil (N=13) for the hornblende-biotite granodiorite and 7.7±0.1 per mil (N=5) for the leucocratic granitic phase (table K5). The leucocratic granite may represent a differentiate of the hornblende-biotite granodiorite because of its slightly higher $\delta^{18}O$ value, more felsic composition, mineralogy, and the presence of granodioritic xenoliths within this unit.

A mafic xenolith within the hornblende-biotite granodiorite, interpreted to be a restite (sample LLB–7), has a $\delta^{18}O$ value of 7.1 per mil, close to that of the hornblende-biotite granodiorite (mean=7.3 per mil).

RELATIONSHIPS BETWEEN $^{18}O/^{16}O$ AND MAGNETIC SUSCEPTIBILITY

Another parameter that may be used to characterize and elucidate the contrasting nature of granites is the magnetite content. Ishihara (1977), for example, suggested that the magnetite content of granites serves as a key constituent that defined the nature of the source rock. In particular, he noted that the presence or near absence of this mineral reflects the oxygen fugacity of the magma, which in turn is controlled fundamentally by the protolith; thus, granites forming from lower crustal sources have quite different oxygen fugacity conditions than those from metasedimentary protoliths.

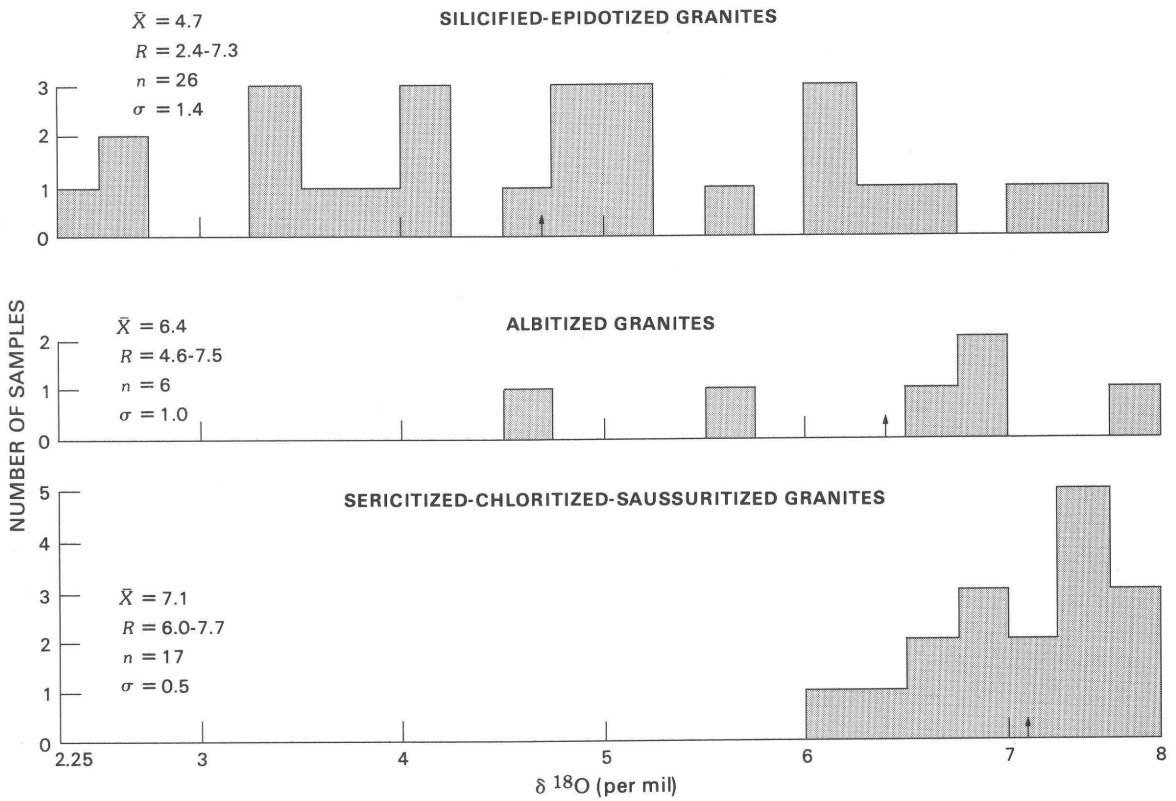

Figure K7. Histogram showing $\delta^{18}O$ values of hydrothermally-altered units from the Granite Mountains. Vertical arrow positioned on the horizontal axis shows mean oxygen isotopic composition. $\bar{X}$, mean value; R, range of values; n, total number of samples; and σ, standard deviation.

Table K5. $\delta^{18}O$ whole-rock data for the Louis Lake batholith

Sample No.	$\delta^{18}O$ (per mil)	Sample No.	$\delta^{18}O$ (per mil)
Hornblende-biotite granodiorite			
LLB-2	7.4	LLB-15	7.5
LLB-3	7.5	PRM-10	7.6
LLB-4	7.3	PRM-11	7.3±0.2
LLB-5	8.0±0.1	PRM-12	7.5
LLB-8	7.4	PRM-13	6.7±0.1
LLB-9	7.4	PRM-14	6.8
LLB-10	7.4	LLB-7 (xenolith)	7.1
LLB-11	6.9		
Leucocratic biotite granite			
LLB-1	7.6	LLB-13	7.9±0.1
LLB-6	7.6	LLB-14	7.8
LLB-12	7.8	PRM-9 (dike)	7.1

Magnetic susceptibility measurements provide an ideal method of determining the relative amounts of magnetite in a rock where quantitative volumetric determinations by optical means are difficult, as for example because of the small size and disseminated nature of magnetite grains, the general problem of identification of opaque minerals and the commonly observed intergrowth of magnetite with other mafic minerals.

The relative amounts of magnetite for the granites of the Granite Mountains and Louis Lake batholith are expressed by the initial magnetic susceptibility, χ. These data are compared with the results of Ellwood and Wenner (1981), who have demonstrated that the low ^{18}O granites of the southern Appalachian Piedmont, (5.5–8.2 per mil) have higher ($>1\times10^{-4}$ G/Oe) magnetic susceptibilities than do the ^{18}O-enriched ones (7.9–11.4 per mil).

The initial magnetic susceptibility of 10 samples from the Granite Mountains and 8 from the Louis Lake batholith are reported in table K6 and are plotted on figure K8. The magnetic susceptibility measurements shown in figure K8 clearly indicate that the Louis Lake batholith has higher mean χ values (4.5×10^{-4} G/Oe) than the Granite Mountain (1.5×10^{-5} G/Oe). Petrographically, the Louis Lake batholith may be estimated to contain much more magnetite (~2 percent) than the Granite Mountains (~0.3 percent). Ishihara's (1977) work suggested that the

Table K6. Initial magnetic susceptibility (χ) and $\delta^{18}0$ data for the Granite Mountains and the Louis Lake batholith

Sample No.	Scale-reading	Mass (grams)	χ (gauss/oersted)[1]	δ^{18} per mil
Granite Mountains				
GM-1-773.5	13	25.5	$1.12X10^{-5}$	8.6
GM-1-1278.0	10	22.6	$9.69X10^{-6}$	8.9
GM-1-1342.1	11	28.1	$8.57X10^{-6}$	8.8
GM-2-1413.0	10	32.8	$6.68X10^{-6}$	8.5
LD-14	6	28.9	$4.55X10^{-6}$	7.9
LM-4	15	31.4	$1.05X10^{-5}$	9.1
LM-9	58, 58	29.7	$4.28X10^{-5}$	8.8
MS-20	32	35.7	$1.96X10^{-5}$	8.7
PRSW-10	35	40.9	$1.87X10^{-5}$	8.6
WY-11	7	15.9	$9.64X10^{-6}$	7.8
		Average--	$1.42X10^{-5}$	
		Standard deviation--	$1.11X10^{-5}$	
Louis Lake batholith				
LLB-6	256	24.6	$2.28X10^{-4}$	7.6
LLB-8	1210	27.0	$9.81X10^{-4}$	7.4
LLB-9	330	23.6	$3.06X10^{-4}$	7.4
LLB-11	1290	29.3	$9.64X10^{-4}$	6.9
LLB-13	54	26.3	$4.50X10^{-5}$	7.9
LLB-14	130	27.3	$1.04X10^{-4}$	7.8
PRM-11	820	27.4	$6.55X10^{-4}$	7.3
PRM-13	1130	31.7	$7.81X10^{-4}$	6.7
		Average--	$5.08X10^{-4}$	
		Standard deviation--	$3.83X10^{-4}$	

[1]All magnetic data courtesy of B. B. Ellwood of the University of Georgia.

higher magnetic susceptibility and magnetite content in the Louis Lake batholith can be ascribed to a higher oxygen fugacity during solidification of the magma. In such instances, most of the iron probably is consumed in the formation of iron oxides rather than being available for the formation of ferromagnesian minerals. In the Granite Mountains, the relatively low bulk magnetic susceptibility and magnetite content imply a low oxygen fugacity in the source region. However, near the end of crystallization, high oxygen fugacities may have occurred locally, resulting in the formation of some of the magnetite segregates observed in the granites (Stuckless and Peterman, 1977). Thus, the combined higher magnetic susceptibility and lower $\delta^{18}O$ values of the Louis Lake batholith relative to the Granite Mountains imply that these two granites were formed from different sources that had different oxygen fugacities.

CHEMICAL AND MINERALOGICAL FEATURES

Granites of the Granite Mountains

Detailed whole-rock chemical analyses, petrographic studies, and uranium and thorium data are reported by Stuckless, Bunker, Bush, Doering, and Scott (1977), Stuckless, Bunker, VanTrump, and Bush (1978), Stuckless and Miesch (1981), and Stuckless and Peterman (1977) for a large number of samples from the Granite Mountains. The bulk of the Granite Mountains pluton contains subequal amounts of quartz, plagioclase, and microcline; biotite (1–10 percent) is the dominant minor constituent. Magnetite and primary epidote are minor to trace constituents in all samples. Zircon and apatite are the only ubiquitous trace minerals. Muscovite is present in all leucocratic variants, and is locally abundant.

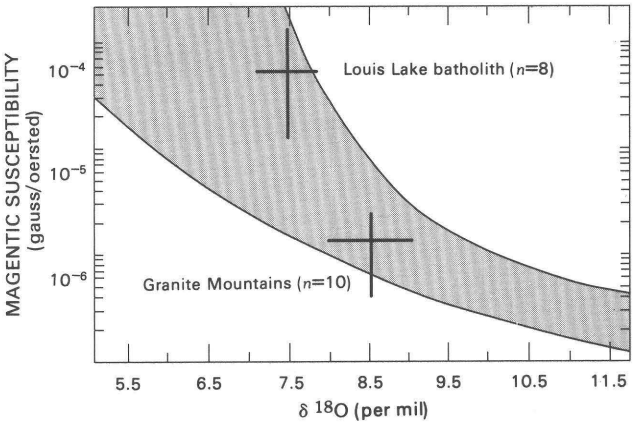

Figure K8. Three-cycle semilog plot of initial magnetic susceptibility versus $\delta^{18}O$ for the Granite Mountains and Louis Lake batholith. These data are contrasted with similar data (stippled area) for the Paleozoic age, late orogenic granites of the southern Appalachians studied by Ellwood and Wenner (1981). n, number of samples.

Whole-rock chemical analyses reveal that the granites of the Granite Mountains are rich in normative corundum (1.0–1.9 percent), with a moderately high mean molecular $Al_2O_3/(Na_2O+K_2O+CaO)$ value of 1.1, high SiO_2 content of 74–75 percent, high K_2O content of 5.1 percent, and a moderate Na_2O content of 3.4–3.8 percent. The granite of Lankin Dome has an average uranium concentration of 8.1 ppm (parts per million), an extremely high average thorium concentration of 40.8 ppm and a very high mean thorium-to-uranium ratio of 14.6 (Stuckless and others, 1978) compared with the world averages for these elements in granites (Rogers and Adams, 1969a, b). However, Stuckless and Nkomo (1978), have shown that the granite of Lankin Dome lost most of its uranium (as much as 80 percent from even apparently fresh samples and from depths as great as 400 m) principally during the Cenozoic. Assuming that the thorium-lead system was closed, they calculated that the initial uranium content of the granite had to have once been 20–50 ppm. Although such high uranium contents are 5–12 times higher than are typical for granites (Rogers and Adams, 1969b), granites with 50 ppm uranium have been recovered from deep drill holes (Rosholt and Huestis, 1981).

Table K7. Chemical and CIPW normative data for samples from the Louis Lake batholith, Wyoming

[Leaders(---) indicate not determined. Where FeO is not determined, total iron is reported as Fe_2O_3. Samples LLB–1,6, and 12 are leucocratic biotite granite. All other samples are hornblende-biotite granodiorite]

Sample No.	LLB-1	LLB-2	LLB-3	LLB-4	LLB-5	LLB-6	LLB-7	LLB-8	LLB-9	LLB11	LLB12	LLB14	LLB15	PRM12
						Chemical composition (percent)								
SiO_2	76.1	65.8	65.2	63.5	65.4	75.3	58.8	65.1	72.6	64.6	71.6	75.0	64.8	56.8
Al_2O_3	13.9	16.1	16.1	16.0	15.9	13.8	16.7	14.8	14.2	16.1	14.6	13.4	16.2	12.3
Fe_2O_3	0.52	2.30	1.90	5.43	5.59	1.47	7.08	5.89	2.31	5.38	2.26	0.93	5.56	8.47
FeO	0.20	1.70	2.20	---	---	---	---	---	---	---	---	---	---	---
MgO	0.06	1.50	1.70	1.90	1.60	0.30	3.50	1.10	0.05	1.80	0.77	0.20	1.80	7.67
CaO	0.83	3.30	3.80	4.22	3.92	0.90	5.56	2.90	1.83	4.22	2.26	0.95	4.35	8.14
Na_2O	3.90	4.30	4.40	3.80	4.30	3.40	4.10	3.20	3.00	4.20	3.60	4.20	4.30	2.80
K_2O	4.70	2.80	2.40	2.40	1.99	5.45	2.09	4.52	5.00	2.24	3.74	3.66	1.96	1.61
H_2O	0.50	0.65	0.63	0.10	0.29	0.24	0.49	0.18	0.10	0.32	0.22	0.22	0.29	0.55
TiO_2	0.03	0.60	0.66	0.71	0.65	0.06	1.01	0.91	0.29	0.60	0.22	0.06	0.71	0.86
P_2O_5	0.05	0.26	0.31	0.30	0.40	0.05	0.40	0.30	0.10	0.30	0.10	0.05	0.30	0.40
MnO	0.04	0.05	0.05	0.06	0.06	0.01	0.11	0.04	0.01	0.06	0.03	0.01	0.06	0.17
CO_2	0.01	0.01	0.03	---	---	---	---	---	---	---	---	---	---	---
Total(-0)	100.84	99.37	99.38	98.42	100.10	100.98	99.84	98.94	99.49	99.82	99.40	98.68	100.33	99.77
						Normative composition (weight percent)								
Q	33.45	21.52	20.16	21.52	23.09	32.12	11.83	22.42	32.47	20.87	30.82	34.83	21.17	11.28
C	1.02	0.65	0.17	0.20	0.50	0.78	0.0	0.09	0.77	0.0	0.77	0.93	0.0	0.0
OR	27.54	16.65	14.27	14.41	11.75	31.89	12.37	27.00	29.70	13.26	22.23	21.92	11.54	9.54
AB	32.73	36.62	37.46	32.67	36.35	28.49	34.75	27.37	25.52	35.60	30.65	36.02	36.27	23.75
AN	3.70	14.70	16.74	19.28	16.82	4.10	21.03	12.56	8.47	18.59	10.62	4.45	19.05	16.28
WO	0.0	0.0	0.0	0.0	0.0	0.0	0.37	0.0	0.0	0.0	0.0	0.0	0.0	8.04
EN	0.15	3.76	4.26	4.81	3.98	0.74	8.73	2.77	0.13	4.49	1.93	0.51	4.47	19.15
FS	0.0	0.33	1.48	0.0	0.0	0.0	0.0	0.0	0.0	0.0	0.0	0.0	0.0	0.0
MT	0.68	3.36	2.77	0.0	0.0	0.0	0.0	0.0	0.0	0.0	0.0	0.0	0.0	0.0
HM	0.05	0.0	0.0	5.52	5.58	1.46	7.09	5.95	2.32	5.39	2.27	0.94	5.54	8.49
IL	0.06	1.15	1.26	0.13	0.13	0.02	0.24	0.08	0.02	0.13	0.07	0.02	0.13	0.36
TN	0.0	0.0	0.0	0.0	0.0	0.0	2.18	0.0	0.0	0.36	0.0	0.0	0.36	1.64
RU	0.0	0.0	0.0	0.65	0.58	0.05	0.0	0.87	0.28	0.39	0.19	0.05	0.50	0.0
AP	0.12	0.62	0.74	0.72	0.95	0.12	0.95	0.72	0.24	0.71	0.24	0.12	0.71	0.95
CC	0.02	0.02	0.07	0.0	0.0	0.0	0.0	0.0	0.0	0.0	0.0	0.0	0.0	0.0
Total-----	99.360	99.36	99.38	99.92	99.73	99.77	99.53	99.83	99.90	99.70	99.78	99.78	99.73	99.47

Table K8. Radium equivalent uranium, thorium, and potassium content of the Louis Lake batholith (Stuckless, Bunker, Bush, and VanTrump, 1981)

Sample No.	Concentration (parts per million) RaeU	Th	K (weight percent)	Th/RaeU
LLB-1	3.10	11.70	3.91	3.77
LLB-2	2.80	15.60	2.27	5.57
LLB-3	2.70	8.80	1.83	3.26
LLB-4	2.87	14.70	1.86	5.12
LLB-5	5.72	12.60	1.64	2.20
LLB-6	6.55	23.5	4.43	3.59
LLB-7	3.50	21.3	1.76	6.09
LLB-8	8.38	63.7	3.73	7.60
LLB-9	3.70	44.9	4.09	12.1
LLB-10	4.59	45.7	3.95	9.96
LLB-11	5.57	14.1	1.89	2.53
LLB-12	1.90	15.2	3.11	8.00
LLB-13	8.21	22.0	3.51	2.68
LLB-14	1.78	11.4	3.06	6.40
LLB-15	3.01	9.8	1.67	3.26
PRM-9 (LLB-21)	1.00	7.8	3.44	7.80
PRM-10(LLB-16)	1.94	19.4	1.76	10.0
PRM-11(LLB-17)	2.63	15.1	2.19	5.74
PRM-12(LLB-18)	2.23	4.2	2.19	1.88
PRM-13(LLB-19)	2.21	7.9	1.86	3.57
PRM-14(LLB-20)	1.82	12.3	1.28	6.76
Average----------	3.63	19.1	2.64	5.61
Range----------	1.0-8.4	4.2-63.7	1.3-4.4	1.9-12.1
Standard deviation	2.1	14.8	1.0	2.9

Louis Lake Batholith

The bulk of the Louis Lake batholith typically contains hornblende, sphene, trace apatite as inclusions, abundant biotite (1–16 percent), epidote (3.7 percent), and magnetite (2 percent).

Whole-rock chemistry shows that the Louis Lake batholith (table K7) is rich in normative diopside (0.2–1.0 percent), has low $Al_2O_3/(Na_2O+K_2O+CaO)$ ratio (0.58–1.07), moderate SiO_2 values (57–76 percent), low K_2O values (3.2 percent), and high Na_2O (3.8 percent). The uranium content is slightly less than is typical of granite (3.6 versus 4.0 ppm), but about normal thorium content (19 ppm) and a mean Th/U of 5.6 (table K8). Preliminary evaluation of lead-isotope ratio (J. S. Stuckless and I. T. Nkomo, unpub. data) does not indicate any pronounced, post-crystallization loss of uranium for the Louis Lake batholith.

Table K9. Comparison between diagnostic features of the granite of the Granite Mountains and the Louis Lake batholith

[Leaders (---) indicate not present. Modal mineralogy in volume percent. Normative corundum, SiO_2, Na_2O, and K_2O in weight percent. Uranium and thorium in parts per million. G/Oe, gauss per oersted]

	Granite of the Granite Mountains	Louis Lake batholith
Modal mineralogy		
Muscovite	0.3	---
Garnet	0.4	---
Magnetite	0.3	2.0
Epidote	0.6	3.7
Biotite	1-5	1-16
Hornblende	---	4-6
Sphene	---	2.0
Plagioclase composition	An_{14-19}	An_{28}
Apatite occurrence	sparse discrete crystals.	Small poikilitic inclusions.
Chemistry		
Normative corundum	1-1.9	0.0-1.0
Al_2O_3/Na_2O+K_2O+CaO (molar)	1.1	0.96
SiO_2	74-75	57-76
Na_2O	3.5-3.8	2.8-4.4
K_2O	5.1	3.2
Uranium	8.1	3.6±2.0
Thorium	40.8	19±15
Uranium (initially)	20-50	4.8
Isotopic and other features		
Age (million years)	2600	2642
Hydrothermally-altered zones.	Three major types	None recognized.
Inclusions	Few xenoliths (metasedimentary).	Many hornblende-bearing clots.
$\delta^{18}O$ permil	8.5±0.5	7.4±0.4
$^{87}Sr/^{86}Sr$ (initial)	0.7053	0.7020
χ, G/Oe	$1.5X10^{-5}$	$4.5X10^{-4}$
Inferred source characteristics		
Alumina saturation	Peraluminous	Metaluminous.
Protolith	Metasedimentary U-enriched.	Metaigneous, not highly U-enriched.

DISCUSSION

Comparison Between the Granite Mountains and Louis Lake Batholith

The various isotopic, mineralogical, field, and chemical characteristics of both the Granite Mountains and Louis Lake batholith are summarized in table K9. The most noticeable contrasting features include the following.

1. The Granite Mountains consist of two mappable granitic units of peraluminous biotite granite, the granite of Long Creek Mountain and the granite of Lankin Dome. Mean $\delta^{18}O$ values for these units are 8.2±0.3 per mil (N=4) for the former and 8.5±0.3 per mil (N=12) for a leucocratic phase of the latter, respectively. The Louis Lake batholith is a metaluminous hornblende-biotite granodiorite with minor quantitites of a leucocratic biotite granitic phase. Mean $\delta^{18}O$ values for these two units are 7.3±0.3 per mil (N=13) and 7.7±0.1 per mil (N=5), respectively. Thus, based on estimates of the areal expo-

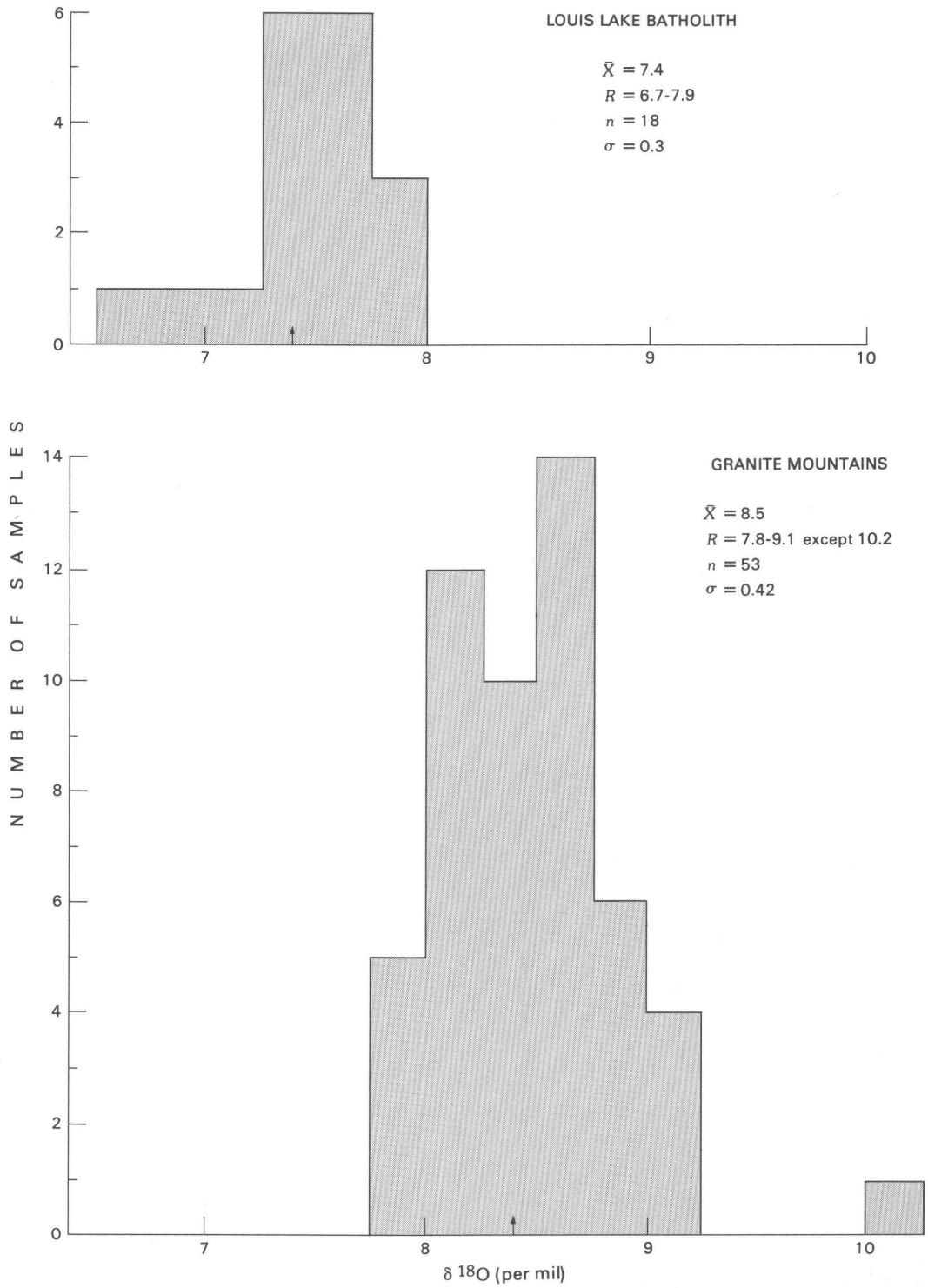

Figure K9 Histogram showing a comparison between the $\delta^{18}O$ values of unaltered whole rocks of the Louis Lake batholith and granites from the Granite Mountains. Vertical arrow positioned on the horizontal axis shows the mean oxygen isotopic composition.

sure of each granitic phase, the Granite Mountains have a distinctly higher weighted mean $\delta^{18}0$ of 8.5 ± 0.5 per mil compared with that of the Louis Lake batholith of 7.4 ± 0.4 per mil (fig. K9).

2. Oxygen isotopic analyses made of feldspar and quartz from representative unaltered samples from both bodies (7 samples from the Granite Mountains and 5 from the Louis Lake batholith) give average Δquartz-feldspar val-

ues (2.0) that reflect a close approach to equilibrium, indicating that the whole-rock data essentially reflect the $^{18}O/^{16}O$ of the primary magmas.

3. The Granite Mountains have a higher initial $^{87}Sr/^{86}Sr$ ($0.7053 \pm .0056$, Peterman and Hildreth, 1978) than the Louis Lake batholith (0.7020 ± 0.001, Naylor and others, 1970).

4. The mean magnetic susceptibility of the Granite Mountains is distinctly lower (1.5×10^{-5} G/Oe) than that of the Louis Lake batholith (4.5×10^{-4} G/Oe), which is consistent with the observed, greater magnetite content of the batholith.

5. There are obvious differences in whole-rock chemistry, reflected principally by the high normative corundum and peraluminous nature of the granites of the Granite Mountains compared with the low normative corundum and metaluminous nature of the Louis Lake batholith.

6. The granite of Lankin Dome was enriched initially in thorium (mean of 40.8 ppm) and uranium (calculated range of from 20 to 50 ppm) compared with rocks of the Louis Lake batholith, which has more nearly normal thorium (mean of 19 ppm) and uranium (mean of 3.6 ppm) contents.

7. The leucocratic phase of the granite of Lankin Dome is uniquely characterized by certain accessory minerals (muscovite, garnet) that are not observed in the Louis Lake batholith. In contrast, the mafic and accessory assemblage of the Louis Lake batholith is hornblende, biotite, sphene, and magnetite.

8. The Granite Mountains contain only rare xenoliths (possibly of metasedimentary origin), whereas the Louis Lake batholith typically contains many rounded, mafic-rich hornblende-sphene-magnetite-epidote-biotite bearing xenoliths (possibly of metaigneous origin).

9. The granites from the Granite Mountains preserve distinct oxygen isotopic evidence of hydrothermal alteration involving waters of probable meteoric origin. This alteration is manifested as pervasive, narrow lenticular zones of silicified-epidotized granite, and the more subtle albitized granite and sericitized-chloritized-saussuritized granite observed in drill cores. From least to most intensely altered these include: the sericitized-chloritized-saussuritized granite (mean whole-rock $\delta^{18}O = 7.1$ per mil ($N = 17$)), the albitized granite (mean whole-rock $\delta^{18}O = 6.3$ per mil ($N = 6$)), and the silicified-epidotized granite (mean whole-rock $\delta^{18}O = 4.7$ per mil ($N = 26$)). Isotopically depleted diabase dikes also have been identified in the Granite Mountains. No such altered rock types have been recognized in the Louis Lake batholith.

Comparison With Phanerozoic Granites

In recent years, considerable oxygen isotope data have been obtained for granitic rocks of different ages from different tectonic settings. Most detailed studies exist for the large Phanerozoic granitoid batholiths, including for example those from southeastern Australia (O'Neil and Chappell, 1977; and O'Neil and others, 1977), the southern Appalachian Piedmont (Wenner and Whitney, 1979; Wenner, 1981), the British Caledonian granitic suites (Harmon and Halliday, 1980), southwestern Nova Scotia (Longstaffe, Smith, and Muehlenbachs, 1980), the Peninsular Range of southern and Baja California (Taylor and Silver, 1978), and the Sierra Nevada of California (Masi and others, 1981). Among these, the most complete and detailed information comparable to what exists for the Granite Mountains and Louis Lake batholith is that from the southeastern Australian granitoids.

For the southeastern Australian granites, O'Neil and Chappell (1977) and O'Neil and others (1977) have demonstrated that oxygen isotope data can provide one of the best criteria for characterizing granite protoliths. In particular, Chappell and White (1974), O'Neil and Chappell (1977), and O'Neil and others (1977) noted that granites that formed from source rocks of metaigneous origin (I-type granites) had differing isotopic, petrologic, chemical, and field characteristics compared with those of metasedimentary origin (S-type granites). These differences are summarized in table K10.

Postulated Source Rocks

The summary of contrasting features of the Granite Mountains and the Louis Lake batholith listed in table K9, and the criteria used for differentiating between the S- and I-type granitoids of southeastern Australia shown in table K10 suggest that a number of geologic, mineralogic, and chemical features are similar. These features strongly imply that the Granite Mountains body was derived by partial melting of a peraluminous, uranium-enriched source material of sedimentary origin, whereas the Louis Lake batholith formed from a metaluminous, less uranium-enriched protolith that is probably of a deep-seated igneous origin.

However, a direct comparison of all of the various features serving to distinguish between the S- and I-origin of granites in the Paleozoic is not entirely applicable to the Archean granites of Wyoming, because certain fundamental differences do exist, primarily with the initial strontium and the oxygen isotopic data. Although differences between the initial strontium isotopic ratios of the Paleozoic and Archean granites may reflect their widely contrasting ages, the $^{18}O/^{16}O$ discrepancies remain an enigma.

The most obvious feature of the oxygen isotopic data is the absence of any significant ^{18}O-enrichment of the Granite Mountains, a body whose geologic setting, mineralogy, chemistry, and relatively radiogenic initial strontium isotopic composition all point to an origin from metasedimentary source rocks. This same feature has been

Table K10. Criteria used for distinguishing between I- and S-type Paleozoic granites in southeastern Australia (Chappell and White; 1974, O'Neil and Chappell, 1977; O'Neil and others, 1977)

Properties	Granites	
	S-type	I-type
Na_2O for felsic varieties with K_2O >5 percent.	<3.2 weight percent.	>3.2 weight percent.
Molar $Al_2O_3/(Na_2O+K_2O+CaO)$---	>1.1 percent.	<1.1 percent.
Normative corundum----------	>1 weight percent.	<1 weight percent.
SiO_2----------	High percentage, narrow range of values.	Broad spectrum of felsic to mafic.
Mineral assemblage----------	Garnet, muscovite, apatite (discrete)	Hornblende, sphene, epidote magnetite, apatite (inclusions)
$^{87}Sr/^{86}Sr_i$ (Berridale) batholith.	>0.708	0.704-0.706
Xenoliths----------	Rare, metasedimentary blocks.	Many, hornblende-bearing clots with igneous texture.
$\delta^{18}O$ values (per mil):		
New England batholith------	10.4-12.5	7.7-9.9
Berridale batholith--------	9.9-10.5	7.9-9.4

noted for many other large Archean granite bodies (Shieh and Schwarcz, 1977; Taylor, 1977; Longstaffe and others, 1978). From limited studies made to date, virtually all large Archean granitic bodies appear to have $\delta^{18}O$ values that are no more ^{18}O-enriched than the Granite Mountains. This oxygen isotopic difference between the Paleozoic and Archean peraluminous granites of metasedimentary origin points to fundamental differences between the source rocks involved in granite genesis during these two different periods.

The most likely explanation for the relatively lower $\delta^{18}O$ values of the Granite Mountains compared with Phanerozoic granites of metasedimentary origin is that more detritus may have been present in the peraluminous, clay-rich metasediments of the Archean protolith. Such source rocks would be expected to have a lower overall $\delta^{18}O$ value and thus be capable of generating a granite through anatexis whose $^{18}O/^{16}O$ signature is similar to that of the protolith. These source rocks still would be capable of producing a granitic batholith with the mineralogy, chemistry, and initial stronitum isotopic composition of the Granite Mountains. In such a model, the metasedimentary source rocks may be peraluminous, but the relative proportion of the detrital component to authigenic clay or metapelitic materials is important.

This idea is supported by the observations of Longstaffe and Schwarcz (1977) and Shieh and Schwarcz (1978). They pointed out that Archean clastic sediments have distinctly lower mean $\delta^{18}O$ values (as much as 4 per mil) than those of Phanerozoic age. They also noted that a similar systematic difference is mirrored by Archean granites, and suggested that the lower $\delta^{18}O$ values of the metasedimentary protolith of Archean granites is due to higher proportions of unaltered felsic volcanic rock fragments or granitic detritus in the metagreywackes, and to lesser amounts of a weathered clay component. Likewise, Stuckless, Bunting, and Nkomo (1981) noted that Archean metasedimentary rocks typically may be less matured, in terms of chemical weathering and element separation, than their Phanerozoic equivalents.

Similarly, the Louis Lake batholith has oxygen isotopic compositions (7.4 ± 0.4 per mil) that are distinctly lower than those of the southeast Australian I-type granites (7.7–9.9 per mil; O'Neil and others, 1977), with virtually little overlap in the $\delta^{18}O$ data. This relatively light oxygen again may reflect a fundamental difference in source-rock characteristics between igneous-protolith granites in the Archean and those in the Paleozoic of Australia. Alternatively, different processes may have brought about a difference in oxygen isotopic composition while leaving the mineralogy, chemistry, and magnetic and field data virtually identical. Differences in the initial strontium isotopic ratio between the Louis Lake batholith and Australian I-type granites again can be attributed to their contrasting ages.

Another important fundamental difference between the $^{18}O/^{16}O$ data of the Australian and Wyoming granites is the relatively extreme oxygen isotopic homogeneity of

the latter. In fact, the range of oxygen isotopic compositions for such large granite bodies as the Granite Mountains and the Louis Lake batholith appears to be relatively limited compared with that of many of the Phanerozoic composite batholiths of comparable dimensions. These extremely uniform oxygen isotopic compositions for the two Wyoming granite batholiths may indicate that the source rocks were quite homogeneous in their $^{18}O/^{16}O$. In contrast, for example, the granitoids that comprise the Sierra Nevada (Masi and others, 1981) and Peninsular Range batholiths (Taylor and Silver, 1978) have a wide range of $\delta^{18}O$ values, initial strontium isotopic compositions, and mineralogical and chemical characteristics that have been attributed to a variety of source rocks.

Alternatively, the extreme oxygen isotopic uniformity of the Granite Mountains and Louis Lake batholith could have been caused by convective processes operating in granite bodies of such large dimensions. For example, in the Fish Canyon magma system (J. A. Whitney, oral commun., 1981) the extreme homogeneity of this large magma body (at least 30,000 km^3) may be due to complete mixing by thermal convection. If such convective processes had operated in the granites of the Granite Mountains, then an isotopically heterogeneous source cannot be ruled out.

CONCLUSIONS

The contrasting primary features indicate two differing protoliths. From the data, the Granite Mountains are inferred to have formed from a peraluminous, metasedimentary source rock that previously was enriched in uranium and throium. Such a source rock is believed to have contained a greater detrital to authigenic component compared with most Phanerozoic sediments, because the $^{18}O/^{16}O$ of the Granite Mountains is notably isotopically depleted compared with many chemically and mineralogically similar Phanerozoic granites thought to have formed from metasedimentary protoliths. Such a metasedimentary protolith thus may have been important in preconcentrating uranium and thorium. In contrast, interpretation of the data obtained from the Louis Lake batholith suggests that this magma formed from a metaigneous protolith that was not highly enriched in uranium or thorium.

Uncertain is what, if any, significance the hydrothermal alteration event identified in the Granite Mountains may have had. The $^{18}O/^{16}O$ lowering of progressively altered granite clearly points to interaction with waters of possible meteoric origin at an elevated temperature. Conceivably, such effects may have been responsible for preconditioning the granite for subsequent uranium loss, as this process appears to be restricted to the Archean granite body that clearly has lost much of its uranium at a subsequent time. However, the absence of any systematic $^{18}O/^{16}O$ correlation in either whole-rock or Δquartz-feldspar values with samples that have had differing degrees of uranium loss, as for example was observed in drill-core GM–1 (Stuckless and Nkomo, 1978), strongly implies that uranium loss must have taken place at extremely low temperatures. By way of comparison, Wenner and Taylor (1976) estimated that temperatures as low as 50°–100°C produced systematic changes in both whole-rock $\delta^{18}O$ and Δquartz-feldspar values within the Proterozoic-age volcanic and plutonic rocks of southeastern Missouri. Temperatures lower than this range conceivably may have existed in the Granite Mountains during the major uranium-loss event in the Cenozoic.

ACKNOWLEDGMENTS

This work was supported by a U.S. National Science Foundation Grant No. EAR–7818127 to D. B. Wenner, J. A. Whitney, and J. C. Stormer, Jr., and a USGS Grant No. 14–08–0001–G–590 to Wenner and a Georgia Tech USDI Mining Fellowship No. 10–11–RH176–099 to Cheang. We especially wish to thank J. A. Whitney for guidance, encouragement and constructive comments during the course of this work.

REFERENCES CITED

Bayley, R. W., 1965a, Geologic map of the Miners Delight quadrangle, Fremont County, Wyoming: U.S. Geological Survey Geologic Quadrangle Map GQ–460.

———1965b, Geologic map of the Louis Lake quadrangle, Fremont County, Wyoming: U.S. Geological Survey Geologic Quadrangle Map GQ–461.

Butler, A. P., Jr., 1972, Uranium, *in* Mallory, W. W., ed., Geologic atlas of the Rocky Mountain region: Denver, Colo., Rocky Mountain Association of Geologists, p. 315–317.

Chappell, B. W., and White, A.J.R., 1974, Two contrasting granite types: Pacific Geology, v. 8, p. 173–174.

Ellwood, B. B., and Wenner, D. B., 1981, Correlation of magnetic susceptibility with $^{18}O/^{16}O$ data in late orogenic granites of the southern Appalachian Piedmont: Earth and Planetary Science Letters, v. 54, p. 200–202.

Harmon, R. S., and Halliday, A. N., 1980, Oxygen and strontium isotope relationships in the British late Caledonian granites: Nature, v. 283, p. 21–25.

Hoefs, J., 1980, Stable isotope geochemistry: Heidelberg, Berlin, Springer-Verlag, p. 73.

Ishihara, S., 1977, The magnetite-series and ilmenite-series: Mining Geology, v. 27, p. 293–305.

Longstaffe, F. J., McNutt, R. H., and Schwarcz, H. P., 1980, Geochemistry of Archean meta-igneous rocks, Lake Despair area, Wabigoon subprovince, northwestern Ontario: Canadian Journal of Earth Sciences, v. 17, p. 1046–1063.

Longstaffe, F. J., and Schwarcz, H. P., 1977, $^{18}O/^{16}O$ of Archean clastic metasedimentary rocks; a petrogenetic indi-

cator for Archean gneisses?: Geochimica et Cosmochimica Acta, v. 41, p. 1303–1312.

Longstaffe, F. J., Schwarcz, H. P., and McNutt, R. H., 1978, The oxygen isotope geochemistry of Archean rocks from the Superior province, *in* Zartman, R. E., ed., Short papers of the 4th International Conference, geochronology, cosmochronology, isotope geology: U.S. Geological Survey Open-File Report 78–701, p. 255–256.

Longstaffe, F. J., Smith, T. E., and Muehlenbachs, K., 1980, Oxygen isotope evidence for the genesis of Upper Paleozoic granitoids from southwestern Nova Scotia: Canadian Journal of Earth Sciences, v. 17, p. 132–141.

Love, J. D., 1970, Cenozoic geology of the Granite Mountains area, central Wyoming: U.S. Geological Survey Professional Paper 495–C, 154 p.

Ludwig, K. R., 1978, Uranium daughter migration and U/Pb isotope apparent ages of uranium ores, Shirley Basin, Wyoming: Economic Geology, v. 73, p. 29–49.

———1979, Age of uranium mineralization in the Gas Hills and Crooks Gap Districts, Wyoming as indicated by U-Pb isotope apparent ages: Economic Geology, v. 74, p. 1654–1668.

Ludwig, K. R., and Stuckless, J. S., 1978, Uranium-lead isotope systematics and apparent ages of zircons and other minerals in Precambrian granitic rocks, Granite Mountains, Wyoming: Contributions to Mineralogy and Petrology, v. 62, p. 243–254.

Masi, U., O'Neil, J. R., and Kistler, R. W., 1981, Stable isotope systematics in Mesozoic granites of central and northern California and southwestern Oregon: Contributions to Mineralogy and Petrology, v. 76, p. 116–126.

Naylor, R. S., Steiger, R. H., and Wasserburg, G. J., 1970, U-Th-Pb and Rb-Sr systematics in 2700×10^6 year old plutons from the southern Wind River Range, Wyoming: Geochimica et Cosmochimica Acta, v. 34, p. 1133–1150.

O'Neil, J. R., and Chappell, B. W., 1977, Oxygen and hydrogen isotope relations in the Berridale batholith: Journal of the Geological Society of London, v. 133, p. 559–571.

O'Neil, J. R., Shaw, S. E., and Flood, R. H., 1977, Oxygen and hydrogen isotope compositions as indicators of granite genesis in the New England batholith, Australia: Contributions to Mineralogy and Petrology, v. 62, p. 313–328.

O'Neil, J. R., and Taylor, H. P., Jr., 1967, The oxygen isotope and cation exchange chemistry of feldspars: American Mineralogist, v. 52, p. 1414–1437.

Peterman, Z. E., and Hildreth, R. A., 1978, Reconnaissance geology and geochronology of the Precambrian of the Granite Mountains, Wyoming: U.S. Geological Survey Professional Paper 1055, 22 p.

Rogers, J.J.W., and Adams, J.A.S., 1969a, Thorium, *in* Wedepohl, K. H., ed., Handbook of geochemistry, v.2, no. 4: Berlin, Springer-Verlag, p. 90–1 to 90–0.

———1969b, Uranium, *in* Wedepohl, K. H., ed., Handbook of geochemistry, v. 2, no. 4: Berlin, Springer-Verlag, p. 92–B to 92–O.

Rosholt, J. N., and Bartel, A. J., 1969, Uranium, thorium, and lead systematics in the Granite Mountains, Wyoming: Earth and Planetary Science Letters, v. 7, p. 141–147.

Rosholt, J. N., and Huestis, G. M., 1981, Uranium-series disequilibrium in granite from core samples of drill hole UPH–3, Stephenson County, Illinois [abs.]: Geological Society of America Abstracts with Programs, v. 13, p. 541.

Seeland, D. A., 1976, Relationship between early Tertiary sedimentation patterns and uranium mineralization in the Powder River Basin, Wyoming: Wyoming Geological Association 28th Annual Field Conference Guidebook, p. 53–64.

———1978, Sedimentology and stratigraphy of the lower Eocene Wind River Formation, central Wyoming: Wyoming Geological Society 30th Annual Field Conference Guidebook, p. 181–198.

Shieh, Y. N., and Schwarcz, H. P., 1977, An estimate of the oxygen isotope composition of a large segment of the Canadian Shield in northwestern Ontario: Canadian Journal of Earth Sciences, v. 14, p. 927–931.

———1978, The oxygen isotope composition of the surface crystalline rocks of the Canadian Shield: Canadian Journal of Earth Sciences, v. 15, p. 1773–1782.

Stuckless, J. S., Bunker, C. M., Bush, C. A., Doering, W. P., and Scott, J. H., 1977, Geochemical and petrologic studies of a uraniferous granite from the Granite Mountains, Wyoming: U.S. Geological Survey Journal of Research, v. 5, p. 61–81.

Stuckless, J. S., Bunker, C. M., Bush, C. A., and VanTrump, G., Jr., 1981, Radioelement concentrations in Archean granites of central Wyoming: U.S. Geological Survey Open-File Report 81–948, 40 p.

Stuckless, J. S., Bunker, C. M., VanTrump, G., Jr., and Bush, C. A., 1978, Radiometric results and areal distribution for granitic samples from the Granite Mountains, Wyoming: U.S. Geological Survey Open-File Report 78–803, 51 p.

Stuckless, J. S., Bunting, J. A., and Nkomo, I. T., 1981, U-Th-Pb systematics of some granitoids from the northeastern Yilgarn Block, Western Australia and implications for uranium source rock potential: Journal of the Geological Society of Australia, v. 28, p. 365–375.

Stuckless, J. S., and Miesch, A. T., 1981, Petrogenetic modeling of a potential uranium source rock, Granite Mountains, Wyoming: U.S. Geological Survey Professional Paper 1225, 39 p.

Stuckless, J. S., and Nkomo, I. T., 1978, Uranium-lead isotope systematics in uraniferous alkali-rich granites from the Granite Mountains, Wyoming; implications for uranium source rocks: Economic Geology, v. 73, p. 427–441.

Stuckless, J. S., Nkomo, I. T., and Doe, B. R., 1981, U-Th-Pb systematics in hydrothermally-altered granites from the Granite Mountains, Wyoming: Geochimica et Cosmochimica Acta, v. 45, p. 635–645.

Stuckless, J. S., and Peterman, Z. E., 1977, A summary of the geology, geochronology and geochemistry of Archean rocks of the Granite Mountains, Wyoming: Earth Science Bulletin, v. 10, p. 3–20D.

Taylor, H. P., Jr., 1974, The application of oxygen and hydrogen isotope studies to problems of hydrothermal alteration and ore deposition: Economic Geology, v. 69, p. 843–883.

———1977, Water/rock interactions and the origin of H_2O in granitic batholiths: Journal of the Geological Society of London, v. 133, p. 509–558.

Taylor, H. P., Jr., and Epstein, S., 1962, Relationships between $^{18}O/^{16}O$ ratios in coexisting minerals of igneous and metamorphic rocks. Pt. 1; Principles and experimental results: Geological Society of America Bulletin, v. 73, p. 461–480.

Taylor, H. P., Jr., and Silver, L. T., 1978, Oxygen isotope relationships in plutonic igneous rocks of the Peninsular Ranges batholith, southern and Baja California, *in* Zartman, R. E., ed., Short papers of the 4th International Conference, geochronology, cosmochronology, isotope geology: U.S. Geological Survey Open-File Report 78–701, p. 423–426.

Wenner, D. B., 1981, Oxygen isotopic compositions of the late orogenic granites in the southern Piedmont of the Appalachian Mountains, and their relationship to subcrustal structures and lithologies: Earth and Planetary Science Letters, v. 54, p. 186–199.

Wenner, D. B., and Taylor, H. P., Jr., 1976, Oxygen and hydrogen isotope studies of a Precambrian granite-rhyolite terrane, St. Francois Mountains, southeastern Missouri: Geological Society of America Bulletin v. 87, p. 1587–198.

Wenner, D. B., and Whitney, J. A., 1979, Oxygen isotope compositions of Hercynian age granites in the Southern Piedmont and their relationship to subcrustal lithologies structures [abs.]: Geological Society of America Abstracts with Programs, v. 11, p. 538.

1986

U.S. GEOLOGICAL SURVEY BULLETIN 1622

SHORTER CONTRIBUTIONS TO ISOTOPE RESEARCH

ORIGIN OF THE LITHIUM-RICH BRINE, CLAYTON VALLEY, NEVADA

Chapter L

By JOSEPH R. DAVIS[1], IRVING FRIEDMAN, and J. D. GLEASON

CONTENTS

FIGURES

TABLE

[1]Present address: ARCO, P. O. Box 2819, Dallas, TX 75221

Abstract

The lithium-rich brines pumped from beneath Clayton Valley, Nevada, provide about one-third of the present United States requirements for lithium. Although the pre-Tertiary rocks in the vicinity do not contain anomalous amounts of lithium, the Tertiary volcanics that abound in the area could have been the origin of the lithium. Extensive diagenetic alteration of vitric material has taken place, and high lithium concentrations are associated with smectite in the Miocene Esmeralda Formation exposed east of the playa. The brines contain about 20 percent sodium chloride and as much as about 320 parts per million of lithium. The deuterium contents of two samples of the brine are –97 and –113 per mil Vienna Standard Mean Ocean Water. The deuterium content of the brine is close to that of the recharge to the aquifers beneath the playa. Springs in the recharge area range in δD from –106 to –114. The brine results from solution by ground water of halite beds that are high in lithium. These salt beds probably were formed during the desiccation of a small saline lake that occupied the position of the present playa.

INTRODUCTION

In the first part of this century, demand for sodium and chloride, sodium carbonate, borates, and potash salts led to an extensive reconnaissance of playa lakes throughout the western United States. The playa in Clayton Valley near Silverpeak, Nev., was first studied by Dole (1912), who found high concentrations of sodium chloride in near-surface brines but made no mention of lithium. The lithium deposit at Silverpeak remained undiscovered until the late 1950's, when the Leprechaun Mining Company[2] of Las Vegas, Nev., while searching for potassium brines, discovered high concentrations of lithium in the subsurface brines of the playa. In 1964, Foote Mineral Company acquired the property to develop the brine as a primary source of lithium.

Foote Mineral Company pumps brine from depths of about 100–250 m (meters) into a series of evaporating ponds (Barrett and O'Neil, 1970). Solar evaporation results in the precipitation of sodium chloride and the concentration of lithium. Brines that initially contain about 300 ppm (parts per million) lithium thus are concentrated to as much as 5,000 ppm lithium. After precipitation of the sodium chloride, lithium carbonate is precipitated in a processing plant. Production of Li_2CO_3 from the Clayton Valley brine field began in 1967 and has continued to the present. The reported annual capacity of about 6,500 metric tons of Li_2CO_3 represents about one-third of the present United States requirements and is about 90 percent of all nonpegmatite lithium production in the United States.

GEOGRAPHIC SETTING

Clayton Valley is one of a group of intermediate-size valleys in west-central Nevada. It has a playa floor of about 100 km^2 (square kilometers) that receives surface drainage from an area of about 1300 km^2. Figure L1 shows the location of the important physiographic features in the vicinity. The playa floor is surrounded by alluvial fan slopes and these, in turn, by mountain ranges, including the Silver Peak Range on the west and the Palmetto Mountains and Montezuma Range on the south and southeast. The Weepah Hills and Paymaster Ridge form mountain barriers on the north and the east, respectively. Altitudes range from 1,300 m on the playa floor to 2,880 m at Piper Peak in the Silver Peak Range.

There is no evidence of anomalous amounts of lithium in pre-Tertiary rocks. The Tertiary volcanic rocks, however, are considered likely to be involved in the origin of the lithium deposit because volcanism could have provided the heat energy and hydrothermal activity required to mobilize lithium from volcanic glass and other relatively unstable minerals. About 100 km^3 (cubic kilometers) of lava erupted from the Silver Peak volcanic center in the western part of Clayton Valley about 6 million years ago (Robinson, 1972).

East of Clayton Valley, more than 100 km^3 of Tertiary ash-flow and air-fall tuff is exposed at Clayton Ridge and as far east as Montezuma Peak. These predominantly flat-lying, pumiceous rocks are interbedded with tuffaceous sediments between Clayton Ridge and Montezuma Peak; but at Montezuma Peak these rocks are altered considerably and dip at angles of as much as 30°. In the Montezuma Range, they are unconformably overlain by rhyolitic agglomerates. The source of these tuff sheets may have been a volcanic center to the east near Montezuma Peak, or to the south in the Montezuma Range, or the Palmetto Mountains, or Mount Jackson, or perhaps even the Silver Peak center to the west.

Tertiary sedimentary rocks are exposed in the Silver Peak Range, in the Weepah Hills, and in the low hills east of the Clayton Valley playa. These rocks all are included in the Esmeralda Formation (Turner, 1900). The Esmeralda Formation consists of sandstone, shale, marl, breccia, and conglomerate, and is intercalated with volcanic rocks, although Turner (1900) excluded the major ash-flow units and other volcanic rocks in defining the formation. The rocks of the Esmeralda Formation in and around Clayton Valley apparently represent sedimentation in several discrete Miocene basins. The age of the lower part of the Esmeralda Formation in Clayton Valley is not

[2]Use of company names is for descriptive purposes only and does not imply endorsement by the U.S. Geological Survey.

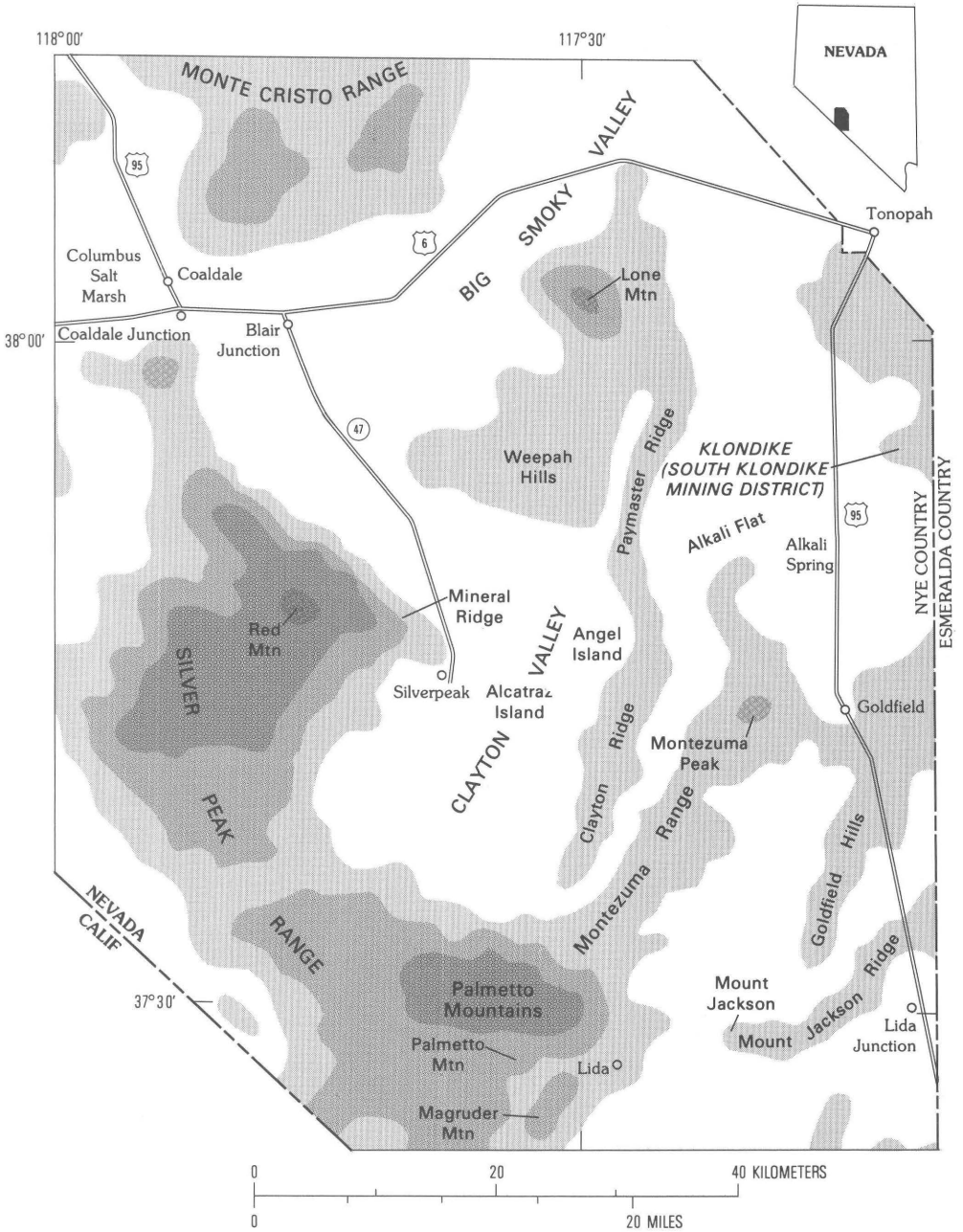

Figure L1. Major physiographic features in area of Clayton Valley, Nev. Modified from Albers and Stewart (1972).

known, but an air-fall tuff in the uppermost unit of the Esmeralda Formation has a K-Ar (potassium-argon) age of 6.9 ± 0.3 Ma (million years) (Robinson and others, 1968).

Extensive diagenetic alteration of vitric material to zeolites and clay minerals has taken place in the tuffaceous sandstone and shale of the Esmeralda Formation, and anomalously high lithium concentrations (as much as 120 ppm lithium) accompany the alteration. However, lithium concentrations in these rocks generally are less than 200 ppm except where smectite is present, and the high lithium concentration associated with smectite is confined to the Esmeralda Formation exposed east of the playa. High lithium concentrations in these rocks is in hectorite, a lithium clay mineral thought to have been precipitated from alkaline lake waters (J. R. Davis, unpub. data).

GEOLOGY OF THE BASIN FILL

In mapping the Quaternary deposits of Clayton Valley, the playa surface, the surrounding alluvial fans and slopes, and the sand dunes are easily distinguished. A

large part of the playa surface has been changed by the construction of roads and evaporating ponds, but prior to this construction the northeastern part of the playa was characterized by a central zone of soft, moist silt and salt, an intermediate zone of silt and sand, and a marginal zone of either travertine or vegetated mounds of soft, puffy silt (Motts and Matz, 1970). The southwestern part of the playa is higher and dryer than the central zone of the northeastern part, and is similar to the marginal vegetated zone there. Alluvial fans are highly dissected and deeply entrenched in the southeastern part of the valley and less dissected elsewhere. Fan surfaces of at least two different ages can be distinguished in many parts of the valley. Sand dunes are in the southern part of the valley and are partially stabilized by vegetation.

The subsurface stratigraphy of the basin fill is known from numerous wells drilled in the playa and adjacent alluvial slopes drilled by Foote Mineral Company between 1964 and 1978, and by the U.S. Geological Survey in 1912 and 1977. Poor sample recovery, contamination of cuttings, and the highly faulted nature of the playa sediments inhibited a clear understanding of the stratigraphy until Foote Mineral Company initiated an exploratory drilling program in 1976 using rotary drilling with reverse circulation and careful logging of the cuttings by well-site geologists. Much of the data collected since that time is still proprietary, but data from several wells are available (Davis and Vine, 1979), making the following summary possible.

Essential to understanding the subsurface data is the concept of fluctuating pluvial and interpluvial climates throughout the Pleistocene. During pluvial periods, which were cooler or wetter than today, shallow-water lacustrine conditions favored deposition of mud in the central part of the valley, merging laterally with fluvial and deltaic sands and muds and with well-sorted beach sands and gravels. During interpluvial periods, like the present, ephemeral lacustrine conditions favored deposition of muds, silt, sand, and evaporite minerals in the central part, grading laterally to alluvial deposits. The gravity data (Wilson, 1975) and subsurface stratigraphic correlations (fig. L2) suggest that the center of deposition and subsidence in Clayton Valley was in the northeastern arm of the playa throughout late Quaternary time. This center of deposition is bounded on the south and east by steeply dipping normal faults that parallel the two fault-scarp trends in alluvial gravels of late Quaternary age. The thickest clastic and chemical sedimentation was confined to the downdropped area north and west of these faults.

The lacustrine sediment that was deposited near the center of pluvial lakes in Clayton Valley is generally green to black calcareous mud. About half of the mud, by weight, is smectite and illite, which are present in nearly equal amounts. Calcium carbonate generally makes up 10–20 percent of the mud, and koalinite, chlorite, sand- and silt-size volcaniclastic detritus, traces of woody organic material, and diatoms compose the rest. In the northeastern arm of the playa, thick layers of evaporite minerals are interbedded with lacustrine muds. These evaporite minerals probably were precipitated as the lake dried up during interpluvial periods. The correlation between the only radiometric date from the subsurface of

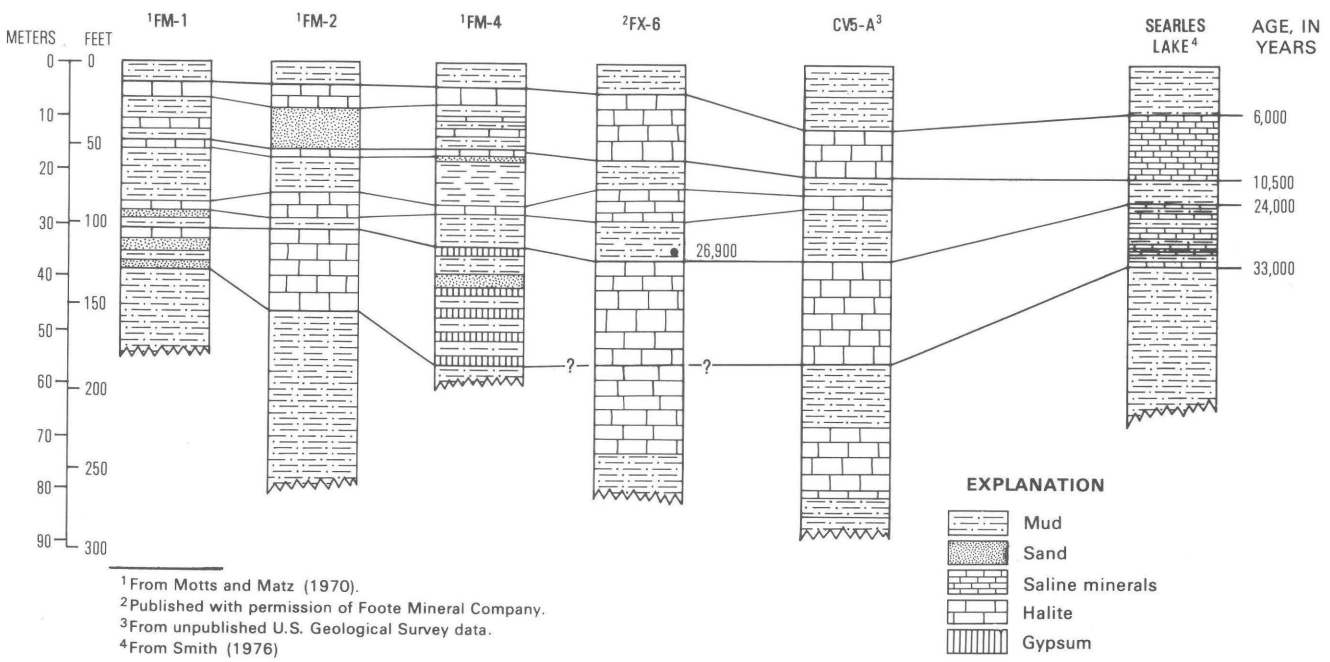

Figure L2. Well logs from Clayton Valley, Nev., and correlation with Searles Lake, Calif.

Clayton Valley (fig. L2) to nearby wells suggests that the pluvial stratigraphy in Clayton Valley possibly can be correlated with that in Searles Lake, Calif. (Smith, 1979) and Lake Lahontan, Nev. (Benson, 1978). If the correlation of these salt and mud cycles is correct, the upper salt bed in well CV5–A was deposited since the last pluvial period ended about 10,500 years B.P. The underlying mud and salt sequence was deposited during the last pluvial period from 24,000 to 10,500 years B.P. (fig. L2).

Subsurface Hydrology

The structural and stratigraphic setting of Clayton Valley has contributed to a complex hydrologic system. The Paleozoic rocks in Clayton Valley contain much thinner sequences of carbonate rocks and probably do not form the effective fractured aquifers that they do 150 km to the southeast at the Nevada Test Site (Winograd and Thordarson, 1975). However, the upper Cenozoic rocks include alluvial sediments, bedded tuffs, and welded tuffs that act as aquifers. The chemical character of the ground water varies considerably within the basin, and three basic types can be identified: (1) cold, dilute ground water in the bedrock highlands; (2) thermal, saline ground water near the playa margin; and (3) cold, saline brines of the playa zone.

The cold, dilute ground-water reservoir of the bedrock highlands is recharged by infiltration through the soil zones, alluvial channel bottoms, and bedrock fractures, but the thin alluvial cover and the low porosity and permeability of the clastic Paleozoic bedrock impedes deep circulation and large reservoir size.

The thermal ground-water system obtains its heat from deep circulation or from contact with a shallow magma chamber. Circulation to at least 1-km-depth would be necessary to acquire this heat from contact with rocks heated due to the geothermal gradient, and the basin structure would require at least 500 m of this circulation into bedrock that is relatively impermeable except where fractured. However, the Quaternary cinder cone and Pliocene volcanics north of the playa suggest the presence of a magma chamber that could create a heat flux in excess of the normal geothermal gradient.

The aquifers of the central playa zone contain cold, saline ground water. The recharge of these economically important aquifers is central to the topic of brine evolution and will be discussed.

Groundwater Geochemistry

The subsurface brines used for lithium production in Clayton Valley are sodium chloride brines of about 20 percent salinity when they are first pumped from the playa (table L1). More dilute ground waters from the playa zone have similar proportions of major constituents, with salinities as low as 1 percent. Lithium seems to correlate well with concentration of these waters and shows no correlation to temperature; the thermal ground water has major-ion composition nearly identical to cold ground waters of similar concentration.

All the ground waters from the vicinity of the playa are supersaturated with respect to calcite, the clay mineral hectorite, and the zeolite phillipsite. The brines also are supersaturated with respect to cristobalite and analcime, whereas some of the more dilute waters are saturated with respect to sepiolite. No natural brines analyzed from Clayton Valley are saturated with respect to gypsum or halite.

The solute chemistry of the ground waters in Clayton Valley and the adjacent basins does not support the concept of subsurface drainage into Clayton Valley from the adjacent basins (Rush, 1968; Motts and Matz, 1970). There certainly appears to be no lithium-enriched source waters in any of the other basins, which makes the possibility of inflow unimportant in considering the chemical evolution of the brines.

Brine Evolution

The most lithium-enriched brines are in the downfaulted northeastern arm of the playa. Brine is produced primarily from the southeast-dipping air-fall tuff bed or "ash aquifer." Although some brine previously was produced from the permeable salt beds overlying the ash aquifer, the practice was abandoned due to dissolution of the salt and collapse around the wells. The highest lithium concentrations are found in brines produced from the tuff where it abuts the faults and forms a structural trap for the dense brines (fig. L3).

The lithium-enriched, sodium-chloride brines in Clayton Valley are typical of the sodium-sulfate-chloride brines that evolve during evaporation of inflow waters having approximately equal bicarbonate and calcium plus magnesium contents (Eugster and Jones, 1979). The halite and gypsum beds in the surface give direct evidence of high salinity levels during the interpluvial periods, but the isotopic composition of the brine suggests that it was not formed by evaporative concentration, and therefore the brine cannot be a residual pore water.

Deuterium composition in a brine increases during evaporation due to differential fractionation of the lighter hydrogen isotope in the vapor phase. A careful study of this process has been made at Owens Lake, Calif., which is about 100 km to the southwest of Clayton Valley. At Owens Lake, the fractionation mechanism was shown to increase the deuterium values from about $\delta D = -115$ per mil on the inflow to $\delta D = +3$ per mil in evaporated brines of similar composition to those in Clayton Valley (Fried-

Table L1. Partial solute chemistry of selected ground waters from Clayton Valley

[Leaders (---) indicate no data; temp. (°C), temperature in degrees Celsius; SMOW, Standard Mean Ocean Water]

Sample source	Depth (meters)	Temp. (°C)	Concentration (parts per million) Na	Cl	Li	Molar Na/Cl	Molar Li/Cl	δD (per mil SMOW)
Wells								
CV1----------	96	22.0	7,073	11,788	27	0.923	0.012	---
CV2----------	53	21.0	7,094	10,837	29	1.0097	0.014	---
CV3----------	127	33	9,775	15,640	42	0.952	0.014	---
CV4----------	242	36	12,700	20,500	58	0.954	0.014	---
CV5----------	72	22	5,900	9,850	26	0.9255	0.013	---
CV5A---------	218	19.5	82,375	132,860	283	0.9435	0.011	---
FM116--------	---	19.5	63,750	100,000	230	0.9083	0.013	-97
FM133--------	---	19.5	46,930	69,400	180	0.9826	0.012	-113
Springs								
Minneosta-----	---	---	60	100	.05	0.8966	---	-109
Coyote--------	---	---	57	75	.05	1.1905	---	-109
Tarantula-----	---	---	105	120	.05	1.3529	---	-111
Big-----------	---	---	52	55	.05	1.4375	---	-114
McNamara------	---	---	31	65	.05	0.6842	---	-106
Waterworks----	---	---	350	740	0.69	0.7204	---	---

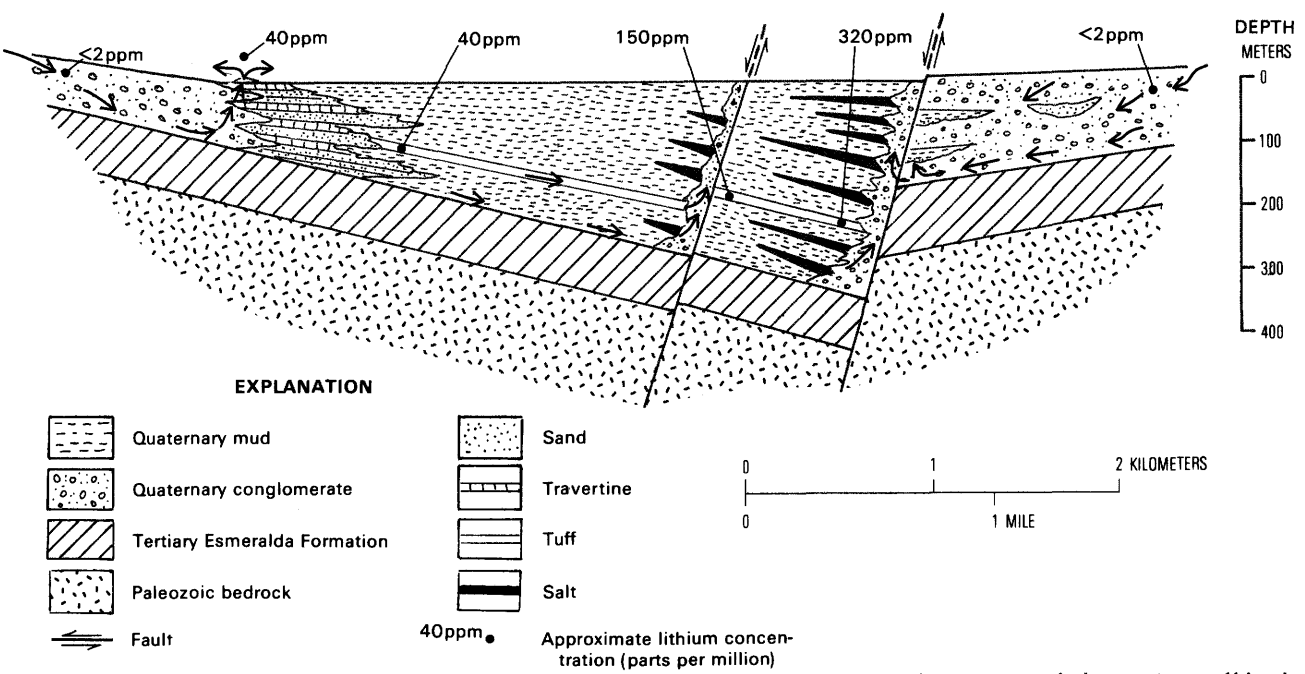

Figure L3. Generalized cross section of Clayton Valley playa, showing structural position of the major tuff-bed aquifer and inferred directions of ground-water movement.

man and others, 1976). However, in Clayton Valley, the brines have deuterium compositions approximately equal to the inflow (table L1), indicating that the brine was not produced by evaporative concentration of the inflow waters. Furthermore, the isotopic compositions of the two brine samples from Clayton Valley show considerable variation ($\delta D = -97$ per mil and $\delta D = -113$ per mil). This variation probably is due to seepage of small amounts of the isotopically heavy waters in the evaporating ponds into the aquifer near well FM 116. Well FM 113 is located away from the ponds, and the deuterium concentration from that well ($\delta D = -115$ per mil) is similar to that of potential ground-water recharge emanating in the Silver Peak Range to the west or in the Palmetto Mountains to the south.

Further study of the geochemistry of the hydrologic system also suggests that the brine is produced primarily from dissolution of halite. Dilute inflow in the basin varies in sodium and chloride concentrations, having molar Na:Cl that range from 0.6 to 1.4 (table L1), whereas ground waters and brine from the playa have molar Na:Cl near unity regardless of concentration. Given the large amount of variation in the Na:Cl of the inflow waters, it is difficult to conceive of any process other than dissolution of halite that always would produce an Na:Cl so near unity.

Plots of molar chloride concentrations against various cation concentrations (figs. L4–L6) give added insight to the problem of brine evolution. Figure L4 demonstrates how the Clayton Valley brines and more dilute ground waters from the playa plot on a trend of equal molar proportions of sodium and chloride. Figures L5 and L6 show

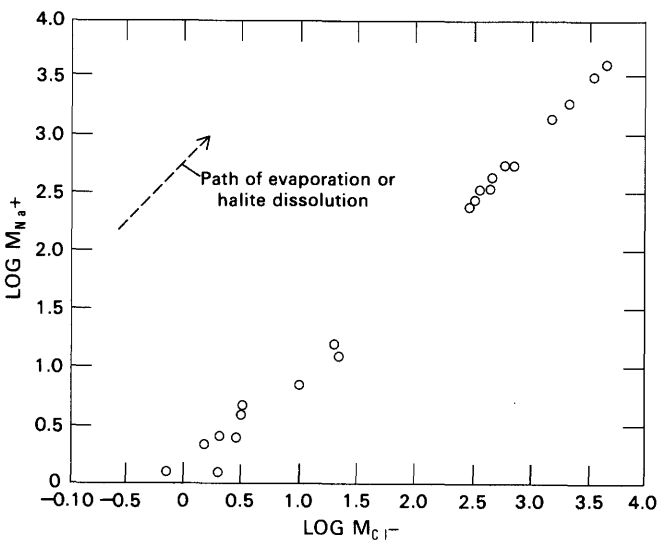

Figure L4. Plot of molar (M) chloride (Cl) and sodium (Na) concentration in water samples from Clayton Valley.

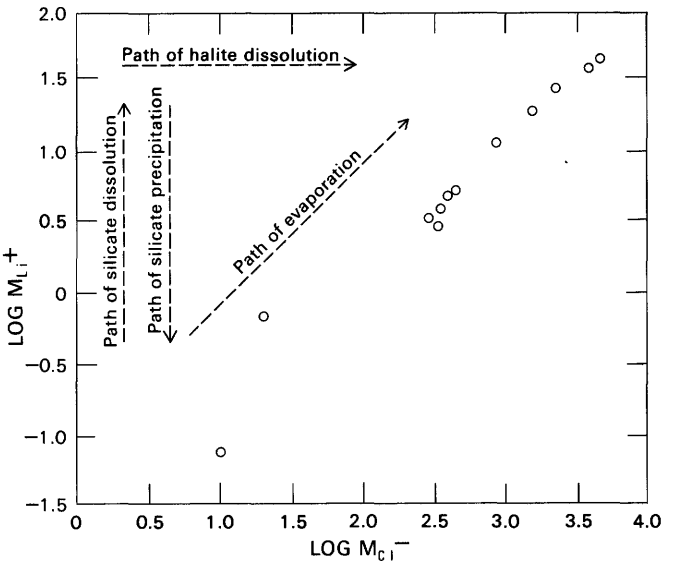

Figure L5. Plot of molar (M) chloride (Cl) and lithium (Li) concentrations in water samples from Clayton Valley.

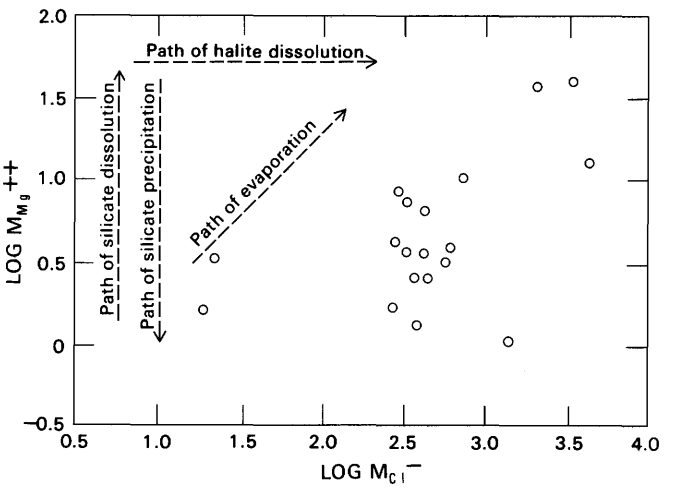

Figure L6. Plot of molar (M) chloride (Cl) and magnesium (Mg) concentrations in water samples from Clayton Valley.

that the lithium and magnesium increase in proportion to chloride concentration, although magnesium shows much more variation than lithium. These trends indicate that the lithium, and to a lesser extent magnesium, were concentrated with chloride by the same evaporative processes that led to halite precipitation.

Microscopic examination of halite and gypsum crystals reveals fluid inclusions as well as fine-grained detrital material incorporated in many crystals. Roedder and Bassett (1981) reported that bedded halite may contain several

weight percent water or brine in the form of fluid inclusions, intergranular fluids, and hydrous minerals. Fluid in the inclusions or intergranular pores would be a lithium-enriched bittern, and release of this fluid during halite dissolution could be modeled as a closed system. The linear trend of the lithium-chloride plot (fig. L5) supports the closed-system model, whereas the deviation from the linear trend in the magnesium-chloride plot (fig. L6) suggests that the magnesium concentration in the brine has been altered, probably by interaction with hydrous minerals or by cation-exchange with clays.

CONCLUSIONS

The playa sediments in Clayton Valley were deposited in a lithium-enriched environment. The lack of evidence for large pluvial lakes in Clayton Valley and the general character of the subsurface sediments suggests that the depositional environment probably was a playa or shallow lake that evaporated to total or near dryness in some seasons or years. This process concentrated dilute inflow with low lithium concentrations many times. The mechanism that we propose for the formation of the present lithium brine is that dilute, lithium-containing, sodium-chloride waters were concentrated by evaporation on a playa during interpluvial periods. Halite was deposited with a bittern fluid enriched in lithium. During the last 10,000 years, meteroric water has penetrated the playa sediments, dissolving halite, and producing a brine similar in concentration and chemistry to an evaporative brine.

REFERENCES CITED

Albers, J. P., and Stewart, J. H., 1972, Geology and mineral deposits of Esmeralda County, Nevada: Nevada Bureau of Mines and Geology Bulletin 78, 80 p.

Barrett, W. T., and O'Neill, B. J., Jr., 1970, Recovery of lithium from saline brines using solar evaporation, *in* Rau, J. L., and Dellwig, L. E., eds., Third symposium on salt: Northern Ohio Geological Society, v. 2, p. 47–50.

Benson, L. V., 1978, Fluctuation in the level of pluvial Lake Lahontan during the last 40,000 years: Quaternary Research, v. 9, p. 300–318.

Davis, J. R., and Vine, J. D., 1979, Stratigraphic and tectonic setting of the lithium brine field, Clayton Valley, Nevada, *in* Newman, G. W., and Goode, H. D., eds., 1979 Basin and range symposium: Denver, Colo., Rocky Mountain Association of Geologists, p. 421–430.

Dole, R. B., 1912, Exploration of salines in Silver Peak Marsh, Nevada: U.S. Geological Survey Bulletin 530–R, p. 1–18.

Eugster, H. P., and Jones, B. F., 1979, Behavior of major solutes during closed-basin brine evolution: American Journal of Science, v. 279, p. 609–631.

Friedman, Irving, Smith, G.I., and Hardcastle, K. G., 1976, Studies of Quaternary saline lakes—II; Isotopic and compositional changes during desiccation of brines in Owens Lake, California, 1969–1971: Geochimica et Cosmochimica Acta, v. 40, p. 501–511.

Motts, W. S., and Matz, D. B., 1970, Reconnaissance geology of Clayton Playa, Nevada, Chapter 6, *in* Motts, W. S., ed., Geology and hydrology of selected playas in the western United States: U.S. Air Force Cambridge Research Laboratories, Hauscom Field, Bedford, Mass., Final report, Contract No. AFL 19 (628)–2486, p. 214–236.

Robinson, P. T., 1972, Petrology of the potassic Silver Peak Volcanic center, Western Nevada: Geological Society of America Bulletin, v. 83, p. 1693–1708.

Robinson, P. T., McKee, E. H., and Moiola, R. J., 1968, Cenozoic volcanism and sedimentation, Silver Peak region, western Nevada and adjacent California: Geological Society of America Memoir 116, p. 577–611.

Roedder, Edwin, and Bassett, R. L., 1981, Problems in determination of the water content of rock-salt samples and its significance in nuclear-waste storage siting: Geology, v. 9, p. 525–530.

Rush, F. E., 1968, Water-resources appraisal of Clayton Valley, Stonewall Flat area, Nevada and California: Nevada Department of Conservation and Natural Resources Water Resources Reconnaissance Series Report 45, 54 p.

Smith, G. I., 1979, Subsurface stratigraphy and geochemistry of late Quaternary evaporites, Searles Lake, California: U.S. Geological Survey Professional Paper 1043, 130 p.

Turner, H. W., 1900, The Esmeralda Formation, a fresh water lake deposit: U.S. Geological Survey Annual Report 21, part 2, p. 191–208.

Wilson, C. W., 1975, Bouguer gravity map of Clayton Valley, Nevada: U.S. Geological Survey Open-File report 75–333.

Winograd, I. J., and Thordarson, W., 1975, Hydrogeologic and hydrochemical framework, south-central Great Basin, Nevada–California, with special reference to the Nevada Test Site: U.S. Geological Survey Professional Paper 712–C, 120 p.

1986

U.S. GEOLOGICAL SURVEY BULLETIN 1622

SHORTER CONTRIBUTIONS TO ISOTOPE RESEARCH

CHEMICAL AND STABLE ISOTOPE COMPOSITIONS OF ANOROGENIC GRANITE FROM STEPHENSON COUNTY, ILLINOIS

Chapter M

By T. KURTIS KYSER

CONTENTS

FIGURES

TABLES

Abstract

Oxygen isotope and chemical compositions were measured in samples of granite from the Precambrian basement of Illinois. Samples were selected from three cores, each of which penetrated an unconformity between Paleozoic sedimentary rocks and the granitic basement at a depth of 2,000–2,200 feet. The chemical and isotopic compositions indicate that granite near the unconformity is altered and is enriched in ^{18}O and in many incompatible elements relative to deeper samples. The variable $\delta^{18}O$ values of feldspars and biotites and δD values of the biotites suggest that samples near the unconformity may have interacted at temperatures greater than 300°C with formation waters typical of the Illinois basin. Chemical compositions and $\delta^{18}O$ values of 7.0 per mil for unaltered samples suggest that the Illinois granites may have differentiated from magmas that formed from melting of the upper mantle or primitive lower crust.

INTRODUCTION

Samples of granite from three drill holes in Stephenson County, Ill., yield whole-rock Rb-Sr (rubidium-strontium) and U-Pb (uranium-lead) ages of 1,400–1,500 Ma (chap. E, this volume). Although rubidium-strontium mineral ages (chap. E, this volume) and Pb-Th-U (lead-thorium-uranium) systematics (Doe and others, 1983) suggest that there have been younger disturbances in some samples, the emplacement age indicates that these samples probably are part of a 1,500–Ma event that produced anorogenic granites over large areas of North America (Hoppe and others, 1983). The core samples are enriched in light rare-earth elements (Schulz, 1981), uranium, thorium (Schulz, 1981; Doe and others, 1983), fluorine, and other incompatible elements (chap. E, this volume; present report) but their low $\delta^{18}O$ values of 7.0–8.3 per mil (Shieh, 1983; Kombrink and Clayton, 1983) indicate that the granites probably did not form from the anatexis of typical sedimentary or metasedimentary rocks (for example, O'Neil and Chappell, 1977; O'Neil and others, 1977). A whole-rock $^{87}Sr/^{86}Sr$ initial value of 0.7026 ± 0.0041 for the granite and a calculated initial Rb/Sr of 0.029–0.25 for the source suggest that the Illinois granite could have been derived from the partial melting of the mantle or lower crust (chap. E, this volume).

The Precambrian granitic basement in Stephenson County, Ill., is unconformably overlain by 2,000–2,200 ft (feet) of lower Paleozoic sedimentary rocks (Hinze and others, 1981). Uranium, lead, and thorium isotope systematics of the granite (Doe and others, 1983) suggest that there may have been an interaction between the granite near the unconformity and a chloride brine about 200–800 Ma. This study uses petrographic observations and chemical and stable isotopic compositions of samples from the three drill holes UPH–1, UPH–2, and UPH–3 (see figure E1, chap. E, this volume) to characterize the alteration of the granite and to place constraints on the history and origin of the granite.

ACKNOWLEDGMENTS

The author is indebted to Z. E. Peterman and S. S. Goldich for their encouragement and advice and to T. Bell for the petrographic and modal analyses. The analytical expertise of J. Gleason and M. Huebner is greatly appreciated as is the scientific advice of I. Friedman. The author benefited greatly from the reviews of J. L. Hannah, J. F. Whelan, and J. R. O'Neil.

ANALYTICAL TECHNIQUES

Several samples from each core were selected to determine the range in the chemical and stable isotopic compositions of the granites. The abundances of most of the elements were determined using standard X-ray fluorescence spectroscopy. Fluorine contents were measured with an ion selective electrode, sulfur concentrations were determined with an IR analyzer, CO_2 quantities were measured coulometrically, and water and Fe^{+2} were analyzed by standard techniques. The average 2σ error for all elements is ± 2 percent of the amount present.

Oxygen was extracted from whole-rock powders and mineral separates using the BrF_5 technique of Clayton and Mayeda (1963). Mineral separates were purified by use of heavy liquids and handpicking, and X-ray diffraction analysis indicates that the separates were more than 95 percent pure. $\delta^{18}O$ values are expressed in units of per mil relative to the SMOW (Standard Mean Ocean Water) standard:

$$\delta^{18}O = \left[\frac{(^{18}O/^{16}O)\ \text{sample} - 1}{(^{18}O/^{16}O)\ \text{SMOW} - 1}\right] \times 1000$$

The value of NBS–28 (National Bureau of Standards) is +9.6 in the Denver laboratory. Hydrogen isotopic compositions were determined by fusing the mineral in vacuum and converting the water to hydrogen (Friedman, 1953; Godfrey, 1962). δD values also are reported in units of per mil relative to SMOW. $\delta^{18}O$ values are precise to ± 0.2 (2σ) whereas the reproducibility of the δD values is ± 2.0 (2σ).

PETROGRAPHIC DESCRIPTIONS

The samples in this study are holocrystalline and have xenomorphic or hypidomorphic textures. Samples closest to the unconformity tend to be finer grained than those from deeper parts of the cores. Biotite, fluorite, and zircon are accessory minerals present in most of the samples. The late-stage appearance of biotite in most samples suggests that the original water content of the magma may have been less than than 1.2 weight percent (Maaloe and Wyllie, 1975). Microcline is perthitic and the plagioclase is usually an_9 to an_{12}. Most of the samples contain a few short hairline fractures.

Samples from core of drill hole UPH–1, all of which are near the unconformity, contain highly sericitized plagioclase and iron-oxide stain. Calcite veins cut through many of the samples from UPH–1 and twinned biotites and plagioclases commonly are bent. The edges of some biotites are altered slightly to chlorite. The preponderance of altered plagioclase and the presence of calcite veins indicate that these samples have interacted with an aqueous fluid.

Only a few of the samples from cores of drill holes of UPH–2 and UPH–3 but the plagioclases from deeper parts usually are less altered. Muscovite and chlorite are common accessory and alteration minerals, and calcite veins usually are absent. With the exception of the moderately altered samples close to the unconformity, most of the granite in cores of UPH–2 and UPH–3 has been affected by only minor alteration events.

CHEMICAL COMPOSITION

Chemical analyses of samples from cores of UPH–1, UPH–2 and UPH–3 are given in table M1. Variations in the composition of samples from UPH–3 are small relative to those measured in samples from UPH–2 despite the close proximity of these two holes (less than 1 kilometer apart). Hole UPH–1, which is 8 km (kilometers) north of holes UPH–2 and UPH–3, had a short core and many of the samples of the core were taken from nearly the same depth (sample 2064C is only 3 inches deeper than sample 2064B; 2071F and 2071G are only 6 inches apart). Differences among the compositions of those samples from UPH–1 that are separated by only a few inches commonly are as large as differences among samples from UPH–3 that are separated by several thousand feet. The range in the chemical compositions of samples from UPH–1 may reflect local differences in the degree of alteration.

There are subtle differences between the chemical compositions of samples from UPH–1 and UPH–3. For example, the content of P_2O_5, TiO_2, F, CO_2 and H_2O^+ in samples from UPH–1 are consistently higher than those of samples from UPH–3 (table M1). Samples from UPH–1 also have higher concentrations of MgO but lower concentrations of Na_2O than do samples from UPH–3 (fig. M1). The enrichment of incompatible elements in samples from core of hole UPH–1 relative to those from core of hole UPH–3 probably is the result of the pervasive alteration in UPH–1.

Calculated norms, $Al_2O_3/(Na_2O+K_2O+CaO)$, and modal anlayses are given in table M2. The presence of only small amounts of modal muscovite and calculated $Al_2O_3/(Na_2O+K_2O+CaO)$ of about 1.0 indicate that the samples are only mildly peraluminous. Most of the samples plot to the orthoclase-rich side of the minimum melting compositions in the quartz-albite-orthoclase system (fig. M2). Comparison of the normative compositions of the Illinois granites with the minimum melting compositions and with the results of experimental work in the granite system compiled by Anderson and Cullers (1978) indicates that the Illinois granites probably crystallized at a low pressure (for example <2 kilobars).

The normative compositions of the Illinois granites are comparable with those of Archean granites from Finland (Salvolahti, 1960; Harme, 1965) and with the 1,400- to 1,500-Ma granites from the Wolf River batholith, Wisconsin (Anderson and Cullers, 1978). The compositions of most of the samples from the Illinois cores plot within the field of the differentiated plutons from Wisconsin (fig. M2). Anderson and Cullers (1978) estimated that the differentiated granites from the Wolf River batholith crystallized at a pressure of 0.5–1.0 kilobars. Anderson (1980) calculated from the compositions of coexisting iron-titanium oxides that granites from the Wolf River batholith equilibrated slightly below the QFM buffer curve at subsolidus temperatures between 500° and 635°C. Plagioclase-liquid and coexisting feldspar geothermometers yielded solidus temperatures of about 700°C for granites of the Wolf River batholith. Inasmuch as the ages and chemical compositions of the granites from the Illinois cores are comparable with those of the differentiated batholiths from Wisconsin, the equilibration temperatures and pressures of the two probably were similar.

OXYGEN ISOTOPE COMPOSITIONS

$\delta^{18}O$ values of whole-rock powders and mineral separates are given in table M3. The oxygen isotopic composition of quartz is constant relative to that of the other minerals because quartz is the mineral most resistant to alteration. The $\delta^{18}O$ values of sodium-plagioclase and

Table M1. Chemical compositions of Illinois drill core samples

[Sample number comprises drill-hole number (UPH–1, –2, or –3) and the depth (in feet) of core at which sample was taken; letter suffix indicates

Sample No.-------	UPH-1 2004B	UPH-1 2025B	UPH-1 2064B	UPH-1 2064C	UPH-1 2071F	UPH-1 2071G	UPH-2 2185D	UPH-2 2358D	UPH-2 2779D	UPH-2 3194D	UPH-2 3678D	UPH-2 4204D	UPH-2 4405
SiO_2	70.6	71.8	73.0	71.3	69.9	73.1	70.3	71.7	71.5	73.9	76.5	75.7	70.4
Al_2O_3	13.6	13.3	12.4	14.0	13.1	12.9	13.8	12.9	14.7	13.1	12.1	12.6	14.6
Fe_2O_3	0.81	0.69	0.98	0.91	0.92	0.75	0.84	0.98	0.50	0.49	0.13	0.29	0.03
FeO	1.87	1.93	2.03	1.33	2.60	1.80	2.26	2.23	0.90	1.49	0.72	1.18	1.71
MgO	0.90	0.78	0.82	0.78	0.79	0.62	0.90	0.62	0.30	0.38	0.15	0.12	0.17
CaO	1.46	1.23	1.17	0.92	1.75	1.45	1.43	1.63	0.85	1.17	0.63	0.70	0.93
Na_2O	2.30	2.29	2.27	2.53	2.56	2.77	2.65	2.49	2.70	3.34	2.38	2.76	2.95
K_2O	6.43	6.35	5.45	7.44	5.49	5.75	5.76	5.66	7.26	4.60	6.33	6.15	7.28
H_2O^+	0.56	0.63	0.70	0.62	0.55	0.46	0.72	0.44	0.37	0.47	0.22	0.33	0.42
H_2O^-	0.09	0.04	0.06	0.07	0.07	0.05	0.05	0.04	0.05	0.03	0.03	0.03	0.07
TiO_2	0.57	0.42	0.48	0.30	0.59	0.44	0.54	0.57	0.20	0.27	0.08	0.13	0.21
P_2O_5	0.13	0.11	0.13	0.08	0.17	0.11	0.14	0.14	0.04	0.05	0.04	0.04	0.04
MnO	0.02	0.02	0.01	0.02	0.05	0.03	0.03	0.05	0.01	0.01	0.01	0.01	0.03
ZrO_2	0.04	0.04	0.04	0.03	0.05	0.03	0.04	0.04	0.02	0.03	0.01	0.01	0.03
CO_2	0.50	0.25	0.07	0.15	0.12	0.11	0.10	0.07	0.14	0.14	0.09	0.06	0.07
F	0.20	0.23	0.23	0.16	0.31	0.21	0.35	0.28	0.12	0.30	0.12	0.32	0.45
S	0.00	0.04	0.03	0.29	0.18	0.02	0.03	0.05	0.00	0.01	0.02	0.00	0.14
BaO	0.10	0.08	0.06	0.10	0.06	0.08	0.07	0.07	0.10	0.04	0.01	0.03	0.06
Total---- (less O)	100.10	100.13	99.88	100.96	99.13	100.59	99.86	99.84	99.71	99.69	99.62	100.33	99.40

Table M2. CIPW norms, $Al_2O_3/(Na_2O + K_2O + CaO)$, and modal analyses of samples from the Illinois deep hole cores

[nd, not detected; tr, trace; leaders (---) indicate not present. Trace hornblende present in samples UPH–1 2064C and UPH–1 2071F; trace monazite

Sample No.-------	UPH-1 2004B	UPH-1 2025B	UPH-1 2064B	UPH-1 2064C	UPH-1 2071F	UPH-1 2071G	UPH-2 2185D	UPH-2 2358D	UPH-2 2779D	UPH-2 3194D	UPH-2 3678D	UPH-2 4204D	UPH-2 4405
											Normative composition (weight		
Q	29.5	30.9	35.5	25.5	29.8	31.1	29.0	31.5	26.2	34.5	37.2	34.8	23.8
or	38.0	37.5	32.3	43.6	32.8	33.8	34.1	33.5	43.0	27.3	37.6	36.2	43.3
ab	19.5	19.4	19.2	21.2	21.9	23.3	22.5	21.1	22.9	28.3	20.2	23.3	25.1
an	2.04	2.33	3.03	2.14	4.81	4.44	3.21	4.91	2.41	2.51	1.47	0.57	0.76
hy	4.10	4.17	4.22	2.56	4.78	3.50	4.80	3.89	1.68	2.84	1.44	2.02	2.98
mt	1.17	1.00	1.42	1.31	1.35	1.09	1.22	1.42	0.73	0.71	0.19	0.42	0.04
il	1.08	0.80	0.91	0.57	1.13	0.83	1.03	1.09	0.38	0.52	0.15	0.25	0.40
ap	0.31	0.26	0.31	0.19	0.41	0.26	0.33	0.33	0.10	0.12	0.10	0.09	0.09
C	2.11	1.80	1.66	0.99	1.21	0.48	2.04	0.88	1.53	1.72	0.90	1.19	1.60
Z	0.06	0.06	0.06	0.04	0.08	0.04	0.06	0.06	0.03	0.05	0.02	0.02	0.05
fr	0.39	0.45	0.45	0.31	0.61	0.41	0.70	0.55	0.24	0.61	0.24	0.65	0.92
pr	---	0.08	0.06	0.54	0.34	0.04	0.06	0.09	---	0.02	0.04	---	0.26
cc	1.14	0.57	0.16	0.34	0.28	0.25	0.23	0.16	0.32	0.32	0.21	0.14	0.16
mg	---	---	---	---	---	---	---	---	---	---	---	---	---
													$Al_2O_3/(Na_2O+K_2O+CaO)$
	1.02	1.03	1.05	1.01	0.98	0.96	1.05	0.98	1.06	1.04	1.02	1.04	1.01
											Modal analyses (modes determined		
Quartz------	24.0	19.0	41.2	31.7	18.0	27.7	28.2	19.8	35.3	45.7	29.7	39.8	30.2
Microcline--	38.2	61.5	16.0	40.5	28.5	29.8	28.8	43.0	33.0	17.7	50.3	32.2	32.7
Plagioclase-	19.0	12.2	21.0	14.8	34.5	19.3	28.3	18.2	19.0	23.0	16.7	24.3	28.7
Biotite------	9.66	2.50	3.50	6.66	4.00	7.66	3.83	7.33	0.50	2.66	0.50	1.00	4.50
Muscovite----	nd	nd	nd	nd	nd	0.32	0.84	nd	1.50	1.33	0.33	1.66	3.33
Opaque minerals---	1.66	0.65	0.98	0.65	0.16	1.33	1.00	1.16	0.50	1.50	0.50	tr	tr
Apatite------	0.16	tr	0.32	0.16	nd	0.32	nd	nd	nd	nd	nd	nd	nd
Zircon-------	0.16	tr	0.48	0.00	0.16	0.48	tr	tr	0.33	0.16	tr	0.16	0.33
Fluorite-----	1.00	0.32	0.16	0.85	0.16	tr	0.66	0.50	nd	0.16	nd	0.32	tr
Chlorite-----	0.16	0.32	0.64	1.00	1.16	0.83	0.16	0.50	1.66	2.33	tr	0.50	nd
Sericite-----	5.66	3.50	15.50	2.66	12.16	11.83	8.16	9.00	7.66	5.16	1.83	tr	0.33
Carbonate----	0.32	tr	0.32	nd	nd	tr	nd	nd	0.50	nd	tr	nd	nd

exact split of core; totals include correction for excess oxygen. Analysts: J. S. Wahlberg, J. Taggert, J. Baker]

Sample No.--------	UPH-2 4773D	UPH-2 5411D	UPH-3 2209H	UPH-3 2290C	UPH-3 2397E	UPH-3 2422E	UPH-3 3333E	UPH-3 3514F	UPH-3 3880E	UPH-3 4059C	UPH-3 4609E	UPH-3 4689G	UPH-3 5056E
SiO_2	69.9	72.9	74.4	75.0	74.5	73.8	75.2	75.5	72.4	74.1	74.1	75.6	72.9
Al_2O_3	14.3	13.4	13.1	12.7	12.7	13.1	12.5	12.5	13.5	12.6	13.1	12.1	13.4
Fe_2O_3	0.99	0.43	0.33	0.46	1.35	0.44	0.42	0.43	0.46	0.61	0.44	0.40	0.40
FeO	2.37	1.69	1.25	1.13	1.23	1.08	1.38	1.16	1.44	1.90	1.62	1.62	1.60
MgO	0.60	0.28	0.13	0.19	0.14	0.15	0.19	0.15	0.35	0.36	0.23	0.22	0.26
CaO	2.01	1.28	0.90	0.92	0.95	0.90	1.08	0.99	1.24	1.39	1.08	1.11	1.13
Na_2O	3.43	2.80	2.75	2.75	2.81	3.10	2.64	3.02	2.86	2.67	2.72	2.76	2.76
K_2O	4.90	5.80	6.28	5.90	5.93	5.47	5.62	5.40	5.88	5.26	6.07	4.92	6.32
H_2O^+	0.52	0.41	0.47	0.50	0.40	0.35	0.47	0.49	0.39	0.36	0.39	0.45	0.43
H_2O^-	0.02	0.00	0.01	0.00	0.08	0.09	0.00	0.00	0.08	0.03	0.04	0.03	0.03
TiO_2	0.63	0.29	0.12	0.14	0.15	0.12	0.22	0.15	0.28	0.39	0.24	0.23	0.26
P_2O_5	0.15	0.05	0.04	0.04	0.04	0.04	0.04	0.04	0.08	0.08	0.04	0.04	0.04
MnO	0.06	0.03	0.03	0.01	0.01	0.01	0.02	0.01	0.01	0.04	0.03	0.03	0.03
ZrO_2	0.04	0.04	0.03	0.04	0.03	0.02	0.03	0.04	0.03	0.04	0.04	0.03	0.04
CO_2	0.10	0.06	0.13	0.02	0.04	0.04	0.05	0.12	0.11	0.07	0.06	0.06	0.06
F	0.49	0.42	0.66	0.62	0.57	0.55	0.44	0.43	0.32	0.39	0.45	0.48	0.36
S	0.11	0.03	0.07	0.02	0.08	0.01	0.01	0.02	0.02	0.00	0.01	0.02	0.05
BaO	0.06	0.05	0.01	0.01	0.01	0.02	0.03	0.02	0.06	0.06	0.04	0.03	0.06
Total---- (less O)	100.37	99.78	100.43	100.19	100.78	100.08	100.16	100.29	99.39	100.19	100.51	99.93	99.98

present in samples UPH–2 2358D, UPH–2 5411D, UPH–3 2209H, UPH–3 3333E, and UPH–3 4609]

Sample No.--------	UPH-2 4773D	UPH-2 5411D	UPH-3 2209H	UPH-3 2290C	UPH-3 2397E	UPH-3 2422E	UPH-3 3333E	UPH-3 3514F	UPH-3 3880E	UPH-3 4059C	UPH-3 4609E	UPH-3 4689G	UPH-3 5056E
percent)													
Q	26.9	31.9	33.4	35.4	34.6	35.0	36.4	35.9	31.0	35.3	32.9	38.7	30.2
or	28.9	34.3	36.9	34.8	34.8	32.3	33.2	31.8	35.0	31.0	35.7	29.1	37.4
ab	28.9	23.7	23.2	23.2	23.6	26.2	22.3	25.5	24.4	22.6	22.9	23.4	23.4
an	4.96	2.70	---	---	0.07	---	1.64	0.80	2.77	3.23	1.51	1.43	2.47
hy	4.02	2.97	1.76	1.87	1.09	1.79	2.31	1.87	1.65	3.31	2.81	2.83	2.78
mt	1.43	0.63	0.48	0.67	1.94	0.64	0.61	0.62	0.67	0.88	0.64	0.58	0.58
il	1.00	0.55	0.23	0.27	0.28	0.23	0.42	0.28	0.54	0.74	0.45	0.44	0.49
ap	1.35	0.12	0.09	0.10	0.09	0.10	0.10	0.09	0.19	0.19	0.09	0.10	0.10
C	1.52	1.53	1.77	1.79	1.62	2.08	1.47	1.39	1.43	1.33	1.49	1.71	1.12
Z	0.06	0.06	0.04	0.04	0.06	0.03	0.05	0.06	0.05	0.06	0.06	0.05	0.06
fr	0.98	0.86	1.18	1.21	1.16	1.12	0.90	0.87	0.65	0.79	0.91	0.98	0.73
pr	0.21	0.06	0.13	0.04	0.15	0.02	0.02	0.04	0.06	---	0.02	0.04	0.09
cc	0.23	0.14	---	---	0.09	0.09	0.11	0.27	0.25	0.16	0.14	0.14	0.14
mg	---	---	0.25	0.04	---	---	---	---	---	---	---	---	---
	0.98	1.01	1.01	1.01	1.00	1.04	1.01	0.99	1.01	1.00	1.01	1.02	1.00
by point counting)													
Quartz------	26.2	30.2	39.8	38.5	32.0	42.7	29.8	35.2	30.8	32.0	32.2	30.6	28.8
Microcline--	40.3	33.9	30.0	29.7	39.3	32.2	32.3	35.3	43.2	38.3	39.5	43.6	36.1
Plagioclase-	23.1	25.3	21.0	21.5	27.8	21.8	26.2	23.7	16.5	23.3	16.0	14.6	20.8
Biotite------	1.83	2.50	1.16	3.16	2.50	1.00	nd	1.00	6.83	3.33	8.16	7.16	7.00
Muscovite----	0.65	0.63	6.16	5.16	1.00	1.50	1.66	2.16	0.16	tr	0.83	0.64	0.16
Opaque minerals---	tr	0.50	nd	0.16	1.00	nd	0.66	0.16	tr	1.50	1.50	0.50	1.00
Apatite------	nd	0.16	nd	nd	nd	nd	nd	nd	nd	tr	nd	tr	tr
Zircon-------	tr	0.16	tr	0.50	tr	tr	0.33	tr	tr	tr	0.32	0.16	tr
Fluorite-----	0.32	0.16	0.16	1.00	0.50	0.16	1.33	0.66	tr	0.16	0.32	0.64	0.32
Chlorite-----	0.16	0.16	1.50	0.33	0.83	0.66	0.66	1.33	tr	tr	0.32	tr	0.16
Sericite-----	7.00	5.83	nd	nd	nd	tr	0.83	0.48	tr	1.34	0.64	1.60	5.33
Carbonate----	nd	nd	nd	nd	nd	nd	0.33	nd	nd	nd	tr	nd	nd

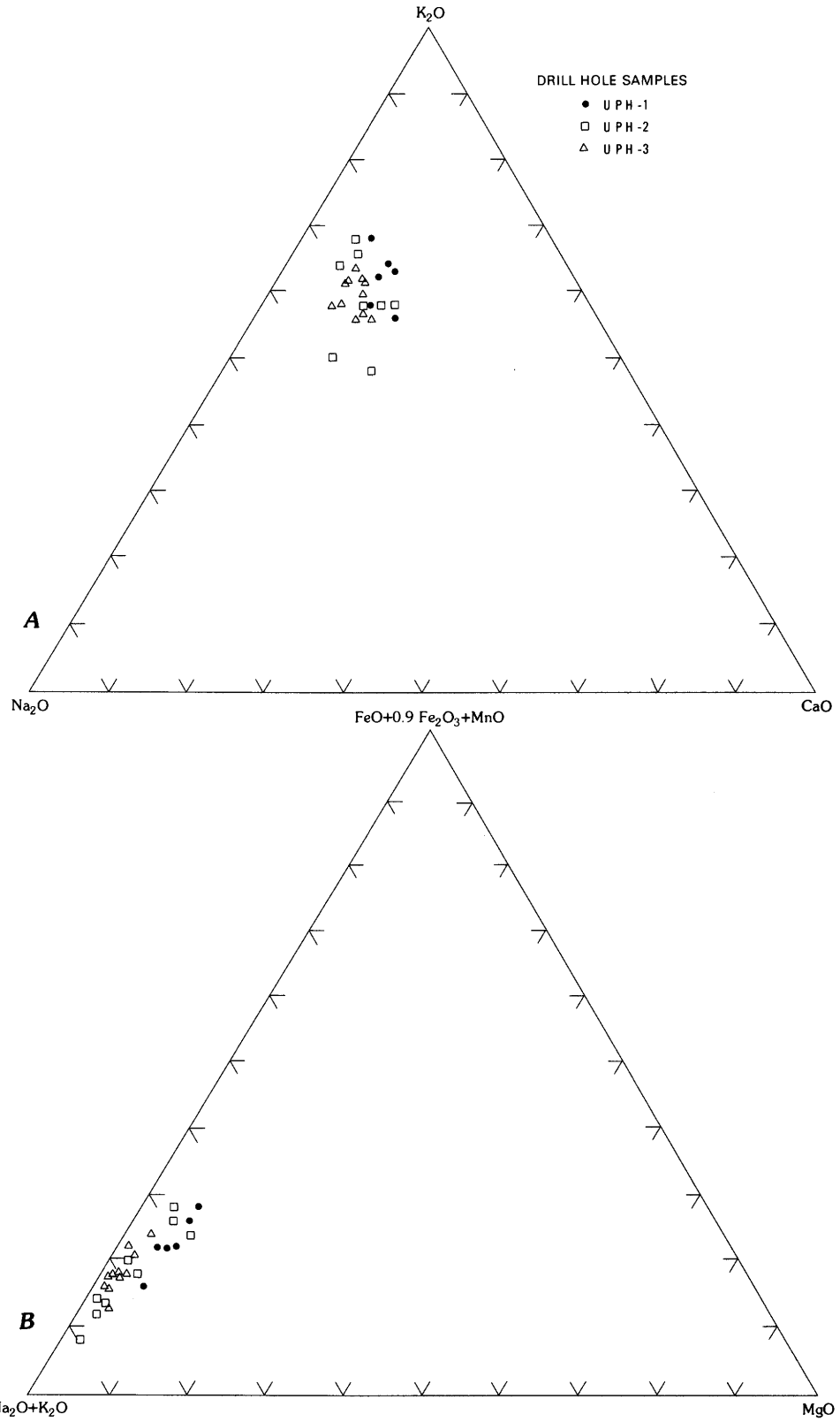

Figure M1. Ternary diagram showing composition of various constituents in samples of core from drill holes UPH–1, UPH–2, and UPH–3. *A*, Relationship of contents of Na_2O, K_2O, and CaO. Note that samples from UPH–1 are depleted in Na_2O relative to those from UPH–3. *B*, Relationship of Na_2O+K_2O, $FeO+0.9Fe_2O_3+MnO$, and MgO. Note that samples from UPH–1 are enriched in MgO but are depleted in alkalis relative to samples from UPH–3.

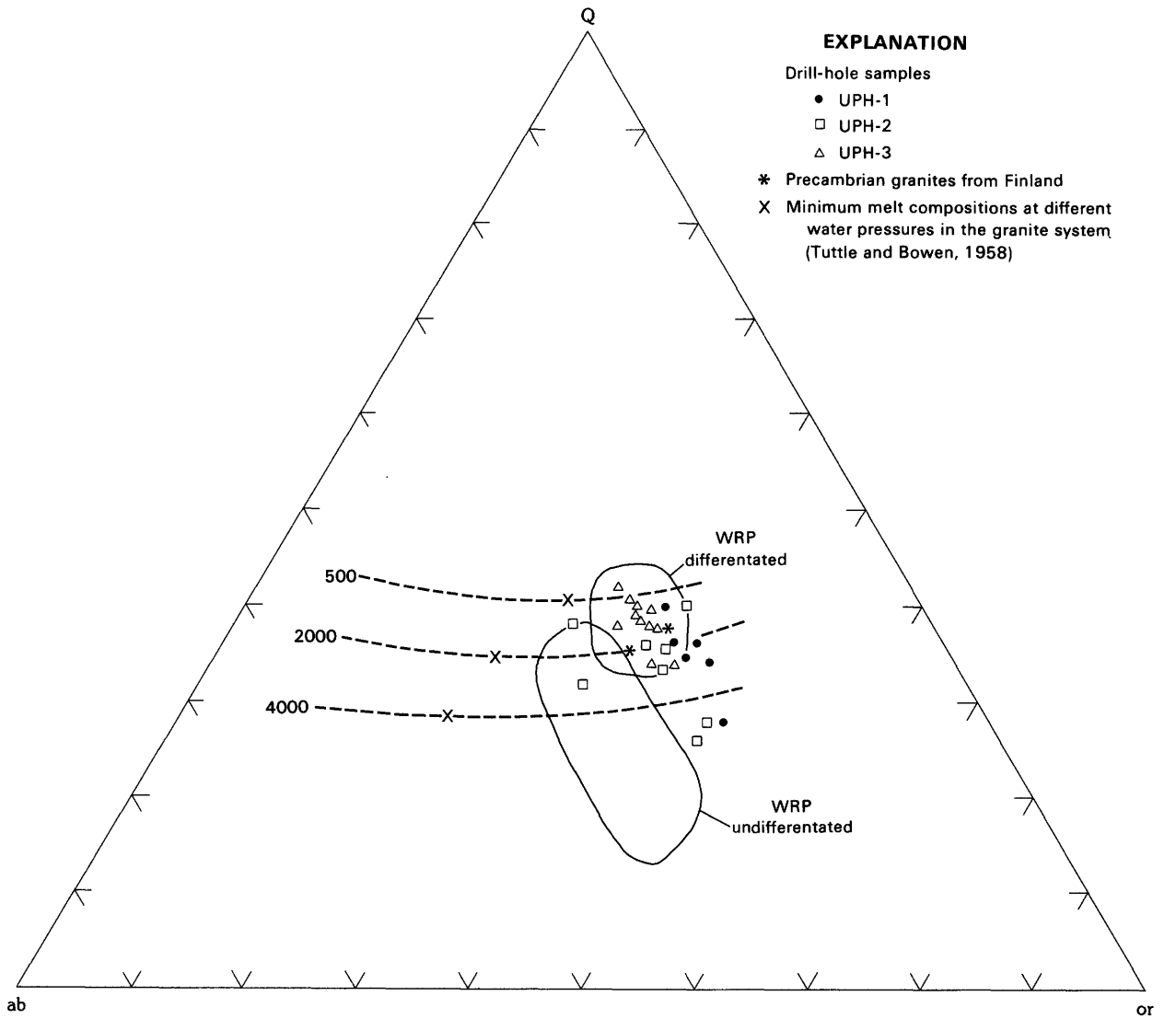

Figure M2. Comparison of the normative compositions of samples from present study with field of differentiated and undifferentiated plutons (WRP) from the Wolf River batholith, Wisconsin (Anderson and Cullers, 1978), and Precambrian granites from Finland (Savolahti, 1960; Harme, 1965). Dashed lines indicate water pressure, in bars, for minimum melt compositions in the granite system (Tuttle and Bowen, 1958).

microcline usually are identical, indicating that they are in isotopic equilibrium (O'Neil and Taylor, 1967). Samples closest to the unconformity are more ^{18}O-rich than are those from deeper parts of the cores which have a constant $\delta^{18}O$ value of 7.0 (fig. M3).

The low $\delta^{18}O$ values of the deeper samples indicate that the source of the granites cannot be sediments, metasediments, or altered continental crust. The relatively high $\delta^{18}O$ value of the samples nearest to the unconformity can be attributed to the same alteration events as those suggested by the petrographic and chemical analyses.

The fractionation of oxygen isotopes between quartz and any other mineral phase can be expressed as: $1000\ln\alpha(\text{Q-min}) = A + B/T^2$ (Bigeleisen and Mayer, 1947). A and B are constants for each quartz-mineral pair and are determined by combining experimental results with measurements of the ^{18}O fractionations in natural systems (Bottinga and Javoy, 1975). $1000\ \ln\alpha$(Q-min) is approximately equal to the difference between the $\delta^{18}O$ value of quartz and another mineral (that is, $\Delta^{18}O$ Q-min). A graphical method for evaluating the concordancy of equilibration temperatures of several coexisting minerals involves a plot of $1000\ln\alpha$(Q-min)-A against B (Javoy and others, 1970). Achievement of isotopic equilibrium is represented by a straight line of slope $1/T^2$ that passes through the origin and $\Delta^{18}O$ for every quartz-mineral pair.

Quartz-mineral fractionations of samples from the Illinois cores are plotted against B in figure M4. The values of A and B for each quartz-mineral pair are those

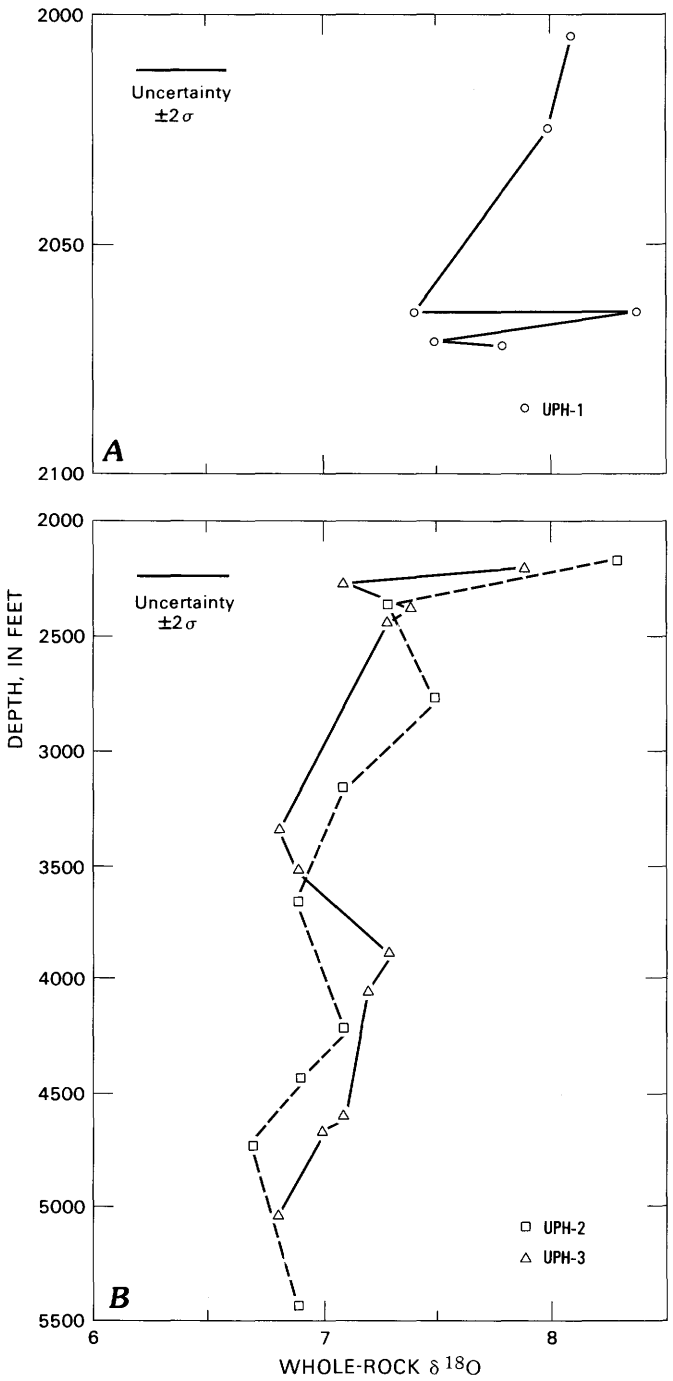

Figure M3. Whole-rock $\delta^{18}O$ values plotted as a function of depth for each core. *A*, Data for drill hole UPH–1; *B*, data for drill holes UPH–2 (dashed line) and UPH–3 (solid line). Depth (in feet) to the unconformity in each core is as follows: UPH–1=1,975; UPH–2=2,172; and UPH–3=2,172. Note that core from UPH–1 is much shorter than core from UPH–2 and UPH–3.

determined by Bottinga and Javoy (1975). Shown for comparison are concordant slopes for equilibration temperatures of 500°, 600°, and 700°C.

The quartz-feldspar fractionations in some of the samples from UPH–1 are too small for reasonable equilibration temperatures (table M3; fig. M4). Small quartz-feldspar fractionations are probably the result of changes in the $\delta^{18}O$ value of the feldspar rather than of the quartz because feldspar exchanges oxygen more readily with most aqueous fluids than does quartz (O'Neil and Taylor, 1967; Clayton and others, 1968; Forester and Taylor, 1972). The enrichment of the feldspars in ^{18}O probably is related to the alteration events that produced the pervasive sericite. Quartz-biotite fractionations in UPH–1 correspond to equilibration temperatures of between 500° and 600°C. Comparison of the $\delta^{18}O$ value of the biotites in samples from UPH–1 with those from the deeper, less altered samples from UPH–3 (fig. M4) suggests that the biotites in samples from UPH–1 have become enriched in ^{18}O as a result of the alteration events so that the original quartz-biotite fractionations were larger. Magnetite from a sample from UPH–1 also is enriched in ^{18}O relative to magnetite from deeper samples so that even the magnetite near the unconformity has become slightly enriched in ^{18}O as a result of the alteration.

The ^{18}O fractionations among the minerals of the sample from core of UPH–2 and the samples from core of UPH–3 (fig. M4) yield nearly concordant quartz-feldspar-magnetite equilibration temperatures of 500 ± 60°C but lower quartz-biotite and quartz-muscovite equilibration temperatures. The concordant quartz-feldspar-magnetite equilibration temperatures compare favorably with the iron-titanium oxide subsolidus temperatures of samples from the Wolf River batholith (Anderson, 1980). The large fractionations between biotite or muscovite and the other minerals from deep samples may be the result of the continued exchange of oxygen isotopes between hydrous phases and other minerals at low temperatures. Local equilibrium between hydrous phases and adjacent minerals such as feldspar may be achieved at low temperature but the overall $\delta^{18}O$ of the feldspar will not be affected because the percentage of the total amount of feldspar that has exchanged with the biotite is small. Therefore, the ^{18}O fractionation between biotite and feldspar will approach that appropriate for the "closure" temperature for biotite. The lowest equilibration temperature of the oxygen isotopes in biotite and feldspar in the unaltered samples from cores of holes UPH–2 and UPH–3 is 395°C.

SIGNIFICANCE OF $\delta^{18}O$ VALUES OF ALTERED SAMPLES

The range in the $\delta^{18}O$ values of feldspars and biotites from samples near the unconformity (table M3) could have resulted from (1) variable degrees of exchange of oxygen isotopes between these minerals and the same

Table M3. $\delta^{18}O$ values of samples from the Illinois deep hole cores
[Leaders (---) indicate not measured]

Sample No.	Whole rock	Quartz	Plagioclase	Potassium feldspar	Biotite	Muscovite	Magnetite
			Drill hole UPH-1				
2004B	8.1	8.2	8.1	8.0	3.6	---	2.0
2025B	8.0	8.0	7.2	7.3	---	---	---
2064B	7.4	7.9	8.3	8.1	2.8	---	---
2064C	8.4	8.5	---	7.4	---	---	---
2071F	7.5	8.2	7.1	7.7	3.1	---	---
2071G	7.8	---	---	---	---	---	---
			Drill hole UPH-2				
2185D	8.3	---	---	---	---	---	---
2358D	7.3	---	---	---	---	---	---
2779D	7.5	---	---	---	---	---	---
3194D	7.1	---	---	---	---	---	---
3678D	6.9	---	---	---	---	---	---
4204D	7.1	---	---	---	---	---	---
4405	6.9	---	---	---	---	---	---
4773D	6.7	---	---	---	---	---	---
5411D	6.9	8.5	---	6.9	1.4	---	0.5
			Drill hole UPH-3				
2209H	7.9	8.4	---	7.2	4.6	---	---
2290C	7.1	---	---	---	---	---	---
2397E	7.4	8.5	---	7.4	---	4.3	---
2422E	7.3	---	---	---	---	---	---
3333E	6.8	8.5	---	6.5	1.5	---	0.6
3514F	6.9	8.6	---	6.7	1.4	---	---
3880E	7.3	---	---	---	---	---	---
4059C	7.2	---	---	---	---	---	---
4609E	7.1	8.0	---	6.3	1.6	---	0.2
4689G	7.0	8.6	7.2	7.2	1.8	4.8	-0.3
5056E	6.8	8.5	---	7.2	1.8	---	-0.9

aqueous fluid, (2) exchange with the same fluid but at different temperatures, (3) interaction with fluids having a range of $\delta^{18}O$ values, or (4) exchange with fluids having variable chemical compositions that produce different rates of exchange by altering the mechanism of the exchange reaction (Cole and Ohmoto, 1976). The rate of diffusion of oxygen in feldspar usually is faster than that in micas (Giletti and Anderson, 1975; Giletti and others, 1978) so that partial exchange should affect the $\delta^{18}O$ value of feldspar more than that of biotite. Inasmuch as the most ^{18}O-rich feldspar is not from the same sample as the most ^{18}O-rich biotite, the $\delta^{18}O$ variations in the feldspars and biotites are not likely to be only a consequence of different degrees of exchange with the same fluid. Variations in the differences between the $\delta^{18}O$ values of coexisting feldspar and biotite from samples near the unconformity are more likely the result of different rates of exchange of these minerals with fluids having variable chemical and isotopic compositions.

Doe and others (1983) suggested that granite near the unconformity may have reacted with a chloride brine 200–800 Ma ago. Clayton and others (1966) measured $\delta^{18}O$ values of from –4 to +5 for chloride-rich formation waters from deep wells in the Paleozoic sedimentary rocks of the Illinois basin. The formation waters have the appropriate age and location to be the aqueous fluids that may have interacted with the granite. Temperatures of 150°–400°C are inferred to produce feldspars of 8.3–7.1 per mil from the Illinois formation waters (O'Neil and Taylor, 1967).

HYDROGEN ISOTOPIC COMPOSITION OF BIOTITES

δD values and water contents of biotites from deep samples and from samples near the unconformity are given in table M4. The δD values of the granite are similar to those measured in unaltered basic lavas (T. K. Kyser and J. R. O'Neil, 1984), phlogopites from ultramafic xenoliths (Boettcher and O'Neil, 1980), and younger granites (for example, Baur and others, 1978).

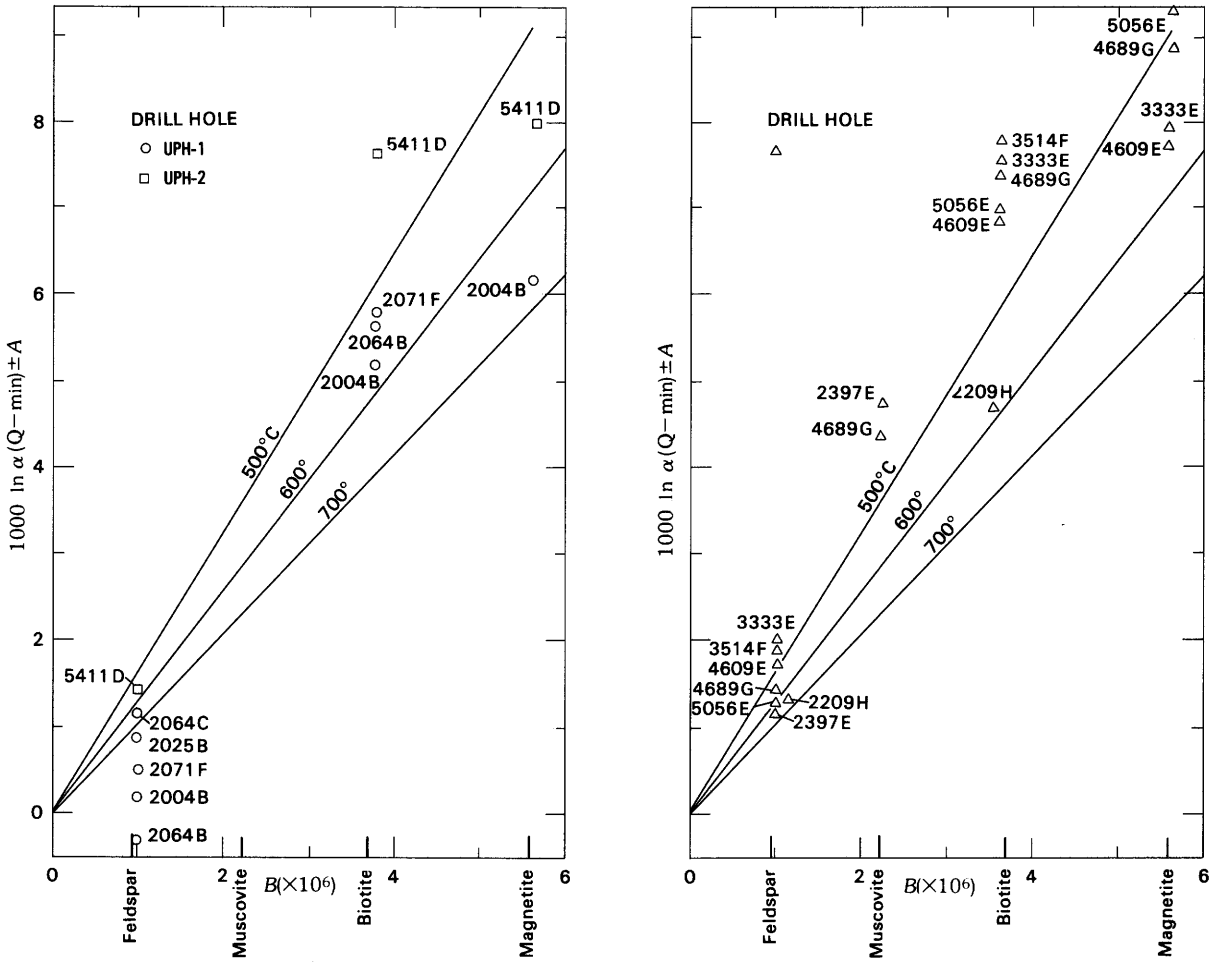

Figure M4. Oxygen isotope fractionations between quartz and other minerals in each core as a function of the constant *B* (see text for discussion). Concordant equilibrium fractionations for 500°, 600°, and 700°C are shown for comparison.

Table M4 δD values and water contents of selected biotites from the Illinois deep hole cores

Drill hole No.	Sample No.	Water (weight percent)	δD (per mil)
UPH-1	2004B	2.6	-71
UPH-2	5411D	2.2	-73
UPH-3	2209H	2.1	-71
UPH-3	5056E	2.5	-74

These similarities suggest that the Illinois granites may have been derived from deep sources that have maintained a constant hydrogen isotopic composition.

The hydrogen isotopic compositions of these samples are the same despite the large variations in their $\delta^{18}O$ values (table M3). The rate of exchange of hydrogen isotopes between minerals and water is much faster than the rate of exchange of oxygen isotopes (O'Neil and Kharaka, 1976), so that biotites that are enriched in ^{18}O because of alteration events probably will have δD values that reflect equilibration with the fluid. Extrapolated fractionation factors for biotite and water (Suzuoki and Epstein, 1976) suggest that biotite is depleted in deuterium by about 50 per mil relative to water at 400°C. Assuming that the δD value of biotite from samples near the unconformity equilibrated with a fluid at temperatures of about 400°C, the δD value of the fluid would have been about −20. If the fluid equilibrated with the biotite at 150°C, the δD value of the fluid would have been about +30. The δD values of formation waters from deep wells in the Illinois basin range between −46 and +7 (Clayton and others, 1966) suggesting that the biotites and formation waters could have equilibrated only at temperatures higher than about 300°C.

CONCLUSIONS

Chemical and normative compositions of the Precambrian granites from the Illinois Deep Hole Project suggest that the granites are differentiated batholiths that crystallized at pressures less than about 2 kilobars. Differences in the chemical compositions between shallow samples near the unconformity and deep samples can be attributed to the interaction of the shallow samples with aqueous fluids. Alteration of samples near the unconformity has resulted in enrichments of K_2O, P_2O_5, H_2O+, CO_2, F, and ^{18}O in addition to increases in the modal amounts of sericite and calcite. The $\delta^{18}O$ values of quartz are nearly identical in every sample, but feldspar and biotites from altered samples are more ^{18}O-rich than are these minerals in unaltered samples. Oxygen and hydrogen isotopic compositions of biotites and $\delta^{18}O$ values of feldspars from altered samples suggest that formation waters in the Illinois basin are likely candidates for the aqueous fluids that produced the alteration. Moreover, the chemical and isotopic compositions and temperatures of these fluids probably were quite variable.

Oxygen isotope compositions of quartz, feldspar, and magnetite from unaltered samples yield concordant equilibration temperatures of 500 ± 60°C. Quartz-biotite and quartz-muscovite equilibration temperatures are substantially lower at 380°C, probably because hydrous minerals continued to exchange oxygen with quartz and feldspar at lower temperatures. The $\delta^{18}O$ values of most of the unaltered samples are about 7.0, which indicates that the source for these anorogenic granites must be the upper mantle or unaltered primitive crustal material. Initial $^{87}Sr/^{86}Sr$ of 0.7029 ± 0.0041 do not eliminate these possibilities (chap. E, this volume).

REFERENCES CITED

Anderson, J. L., 1980, Mineral equilibria and crystallization conditions in the late Precambrian Wolf River rapakivi massif, Wisconsin: American Journal of Science, v. 280, p. 289–332.

Anderson, J. L., and Cullers, R. L., 1978, Geochemistry and evolution of the Wolf River batholith, a late Precambrian rapakivi massif in northern Wisconsin, USA: Precambrian Research, v. 7, p. 287–324.

Baur, W. H., Friedman, I., and O'Neil, J. R., 1978, Hydrogen, *in* Wedepohl, K. H., ed., Handbook of geochemistry: New York, Springer-Verlag, v. 2, p. 1B1–1L4.

Bigeleisen, J., and Mayer, M. G., 1947, Calculation of equilibrium constants for isotopic exchange reactions: Journal of Chemical Physics, v. 15, p. 261–267.

Boettcher, A. L., and O'Neil, J. R., 1980, Stable isotope, chemical, and petrographic studies of high-pressure amphiboles and micas; evidence for metasomatism in the mantle source regions of alkali basalts and kimberlites: American Journal of Science, v. 280A, p. 594–621.

Bottinga, Y., and Javoy, M., 1975, Oxygen isotope partitioning among the minerals in igneous and metamorphic rocks: Review of Geophysics and Space Physics, v. 13, no. 2, p. 403–418.

Clayton, R. N., and Mayeda, T. K., 1963, The use of bromine pentafluoride in the extraction of oxygen from oxides and silicates for isotopic analysis: Geochimica et Cosmochimica Acta, v. 27, p. 43–52.

Clayton, R. N., Muffler, L.J.P., and White, D. E., 1968, Oxygen isotope study of calcite and silicates of the River Ranch no. 1 well, Salton Sea geothermal field, California: American Journal of Science, v. 266, p. 968–979.

Clayton, R. N., Friedman, I., Graf, D. L., Mayeda, T. K., Meents, W. F., and Shimp, N. F., 1966, The origin of saline formation waters—[pt.] 1. Isotopic composition: Journal of Geophysical Research, v. 71, p. 3869–3882.

Cole, D. R., and Ohmoto, H., 1976, Effect of NaCl on the rate of oxygen isotopic exchange reactions between rocks and water [abs]: Geological Society of America Abstracts with Programs, v. 8, p. 817.

Doe, B. R., Stuckless, J. S., and Delevaux, M. H., 1983, The possible bearing of the granite of the UPH Deep Drill Holes, Northern Illinois, on the origin of Mississippi Valley ore deposits: Journal of Geophysical Research, v. 88, p. 7335–7345.

Forester, R. W., and Taylor, H. P., Jr., 1972, Oxygen and hydrogen isotope data on the interaction of meteoric ground waters with a gabbro-diorite stock, San Juan Mountains, Colorado: International Geological Congress, 24th, Montreal, Proceedings, sec. 10, p. 254–263.

Friedman, I., 1953, Deuterium content of natural waters and other substances: Geochimica et Cosmochimica Acta, v. 4, p. 89–103.

Giletti, B. J., and Anderson, T. F., 1975, Studies in diffusion; II, Oxygen in phlogopite mica: Earth and Planetary Science Letters, v. 28, p. 225–233.

Giletti, B. J., Semet, M. P., and Yund, R. A., 1978, Studies in diffusion; III, Oxygen in feldspars—An ion microprobe determination: Geochimica et Cosmochimica Acta, v. 42, p. 45–58.

Godfrey, J. D., 1962, The deuterium content of hydrous minerals from the east-central Sierra Nevada and Yosemite National Park: Geochimica et Cosmochimica Acta, v. 26, p. 1215–1245.

Harme, M., 1965, On the potassic migmatites of Southern Finland: Bulletin de la Commission Géologique de Finlande, no. 219, 43 p.

Hinze, W. J., Haimso, B. C., and Van Schmus, W. R., 1981, The Illinois deep hole project—An overview [abs.]: EOS, v. 62, no. 17, p. 387.

Hoppe, W. J., Montgomery, C. W., and Van Schmus, W. R., 1983, Age and significance of Precambrian basement samples from northern Illinois and adjacent states: Journal of Geophysical Research, v. 88, p. 7276–7286.

Javoy, M., Fourcade, S., and Allegre, C. J., 1970, Graphical method for examination of $^{18}O/^{16}O$ fractionations in silicate rocks: Earth and Planetary Science Letters, v. 10, p. 12–16.

Kombrink, M., and Clayton, R. N., 1983, Oxygen isotopic compositions of minerals from Illinois Deep Drill Hole granites: Journal of Geophysical Research, v. 88, p. 7305–7306.

Kyser, T. K., and O'Neil, J. R., 1984, Hydrogen isotope systematics of submarine basalts: Geochimica et Cosmochimica Acta, v. 48, p. 2123–2133.

Maaloe, S., and Wyllie, P. J., 1975, Water content of a granite magma deduced from the sequence of crystallization determined experimentally with water-undersaturated conditions: Contributions to Mineralogy and Petrology, v. 52, p. 175–191.

O'Neil, J. R., and Chappell, B. W., 1977, Oxygen and hydrogen isotope relations in the Berridale batholith: Journal of the Geological Society of London, v. 133, p. 559–571.

O'Neil, J. R., and Kharaka, Y. K., 1976, Hydrogen and oxygen isotope exchange reactions between clay minerals and water: Geochimica et Cosmochimica Acta, v. 40, p. 241–246.

O'Neil, J. R., Shaw, S. E., and Flood, R. H., 1977, Oxygen and hydrogen isotope compositions as indicators of granite genesis in the New England batholith: Contributions to Mineralogy and Petrology, v. 62, p. 313–328.

O'Neil, J. R., and Taylor, H. P., Jr., 1967, The oxygen isotope and cation exchange chemistry of feldspars: American Mineralogist, v. 52, p. 1414–1437.

Savolahti, A., 1960, The Ahvenisto massif in Finland: Bulletin de la Commission Géologique de Finlande, no. 174, 96 p.

Schulz, K. J., 1981, Trace element geochemistry of Precambrian granite from northern Illinois deep drill hole UPH–3 [abs.]: Geological Society of America Abstracts with Programs, v. 13, p. 549.

Shieh, Y., 1983, Oxygen isotope study of Precambrian granites from the Illinois Deep Drill Hole project: Journal of Geophysical Research, v. 88, p. 7300–7304

Stuckless, J. S., Doe, B. R., and Delevaux, M., 1981, U-Th-Pb isotope systematics and uranium distribution within granite recovered from drill-hole UPH–3, northern Illinois [abs.]: Geological Society of America Abstracts with Programs, v. 13, p. 562.

Suzuoki, T., and Epstein, S., 1976, Hydrogen isotope fractionation between OH-bearing minerals and water: Geochimica et Cosmochimica Acta, v. 40, p. 1229–1240.

Tuttle, O. F., and Bowen, N. L., 1958, Origin of granite in the light of experimental studies in the system $NaAlSi_3O_8$–$KAlSi_3O_8$–SiO_2–H_2O: Geological Society of America Memoir 74, 153 p.

1986

U.S. GEOLOGICAL SURVEY BULLETIN 1622

SHORTER CONTRIBUTIONS TO ISOTOPE RESEARCH

NEGATIVE $\delta^{18}O$ VALUES FOUND FOR EASTERN NEVADA PLUTONIC ROCKS DEFORMED BY STRESSES RESULTING FROM POST-CRYSTALLIZATION MOVEMENT ALONG SPATIALLY RELATED THRUST FAULTS

Chapter N

By DONALD E. LEE, IRVING FRIEDMAN, and JIM D. GLEASON

CONTENTS

Abstract

Four plutons tens of kilometers apart in eastern White Pine County, Nevada, have been deformed or even cataclasized by post-crystallization movement along spatially related thrust faults. This deformation has resulted in the reduction of both the $^{18}O/^{16}O$ and the apparent potassium-argon ages of the affected rocks. In each case there apparently was oxygen isotope exchange between the rock and meteoric waters at about the same time as the constituent micas were degassed by stresses resulting from movement along the thrust faults.

Modification of the oxygen isotope composition of these deformed or cataclasized intrusive rocks was more spotty than pervasive. Also, in the Young Canyon-Kious basin area of the southern Snake Range (the "type" area), cataclasis did not change the rubidium-strontium systematics of the intrusive. Quartzites in the study area have "normal" $\delta^{18}O$ values, even though collected just beneath the sole of the Snake Range décollement. However, metamorphic micas recovered from such quartzites were degassed at the time of latest movement along the overlying thrust fault.

We attempt to explain how the oxygen isotope exchange between meteoric waters and the deformed or cataclasized plutons may have been effected.

INTRODUCTION

Oligocene (32 ± 1.5 Ma; chap. P, this volume) plutonic rocks of the Young Canyon-Kious basin area, southern Snake Range, Nevada (fig. N1) have been cataclasized by post-crystallization movement along the overlying Snake Range décollement (Lee and Van Loenen, 1971, p. 6, 40). A small amount of secondary muscovite formed during cataclasis was dated (17–18 Ma) by the K-Ar (potassium-argon) method to fix the time of deformation (Lee and others, 1970). These same writers also described spuriously young K-Ar age results for micas present in relatively undeformed Cretaceous (chap. P, this volume) and Jurassic (Lee and others, 1968) intrusive rocks of the southern Snake Range and concluded that the modified K-Ar ages are a result of partial degassing of the micas by stresses related to late movement on the overlying Snake Range décollement.

These same deformed igneous rocks of the Young Canyon-Kious basin area have quite low $\delta^{18}O$ values (to –2.6 per mil), apparently resulting from oxygen isotope exchange between the plutonic rock and meteoric waters at the time of cataclasis (Lee and others, 1982). The undeformed plutonic rocks of the southern Snake Range were found to have $\delta^{18}O$ values in the "normal" range of +9 to +13, even though, as just noted, some of the constituent micas gave spuriously low K-Ar age results.

In other words, micas recovered from the cataclasized rocks of the Young Canyon-Kious basin area, southern Snake Range, Nev., give spuriously low (17–18 Ma) age results, and the rocks themselves have extremely low (to –2.6 per mil) $\delta^{18}O$ values. The K-Ar ages and the $\delta^{18}O$ values apparently were modified at the same time; that is, when the rock was cataclasized as a result of post-crystallization movement on the overlying Snake Range décollement. The purpose of this paper is to present negative $\delta^{18}O$ values for three other deformed plutons in eastern White Pine County, Nev. At each locality there apparently was oxygen isotope exchange between plutonic rocks and meteoric waters during post-crystallization movement along a spatially related thrust fault.

RECENT DATA

Nelson (1966, p. 938) stated: "The rocks in the easternmost part of the Kern Mountain pluton have been subjected to cataclasis and shearing which, as determined from the orientation of the shear planes, is believed to be related to the eastward-directed décollement thrusting * * *." Although in the eastern part of the Kern Mountains the main décollement has been completely eroded away (R. K. Hose, written commun., 1978; also, see map of Hose and Blake, 1976), the cataclasis described by Nelson is practically identical to that described by Lee and Van Loenen (1971, p. 6, 40) for the Young Canyon-Kious basin area of the southern Snake Range, about 83 km (kilometers) south of the Kern Mountains (fig. N1).

The main intrusive in the Kern Mountains crystallized about 75 Ma ago (chap. D, this volume). Muscovite recovered from a sample (no. 564) of the cataclasized intrusive of Kern Mountains gave a K-Ar age of 24.7 ± 1.1 Ma (Lee and others, 1980), appreciably younger even than an Oligocene (31 m.y.) event postulated by Best and others (1974). Rock sample 564 has a $\delta^{18}O$ value of –5.4 per mil. Thus in the Kern Mountains, as in the Young Canyon-Kious basin area of the southern Snake Range, post-crystallization movement on an overlying thrust fault has reduced both the apparent K-Ar age and the $^{18}O/^{16}O$ of the resulting cataclasized pluton.

Samples 383 and 384 were collected from a quartz-monzonite pluton in the Warm Springs area of the northern Egan Range, Nev. (fig. N1). This pluton has been sheared and deformed where these samples were collected, and Lee and others (1980, p. 26) attributed the shearing and deformation to stresses related to movement on an overlying (eroded) thrust fault shown on the map and cross section E–E′ of Fritz (1968). We have determined $\delta^{18}O$ values of –0.9 and –3.0 per mil for rock samples 383 and 384, respectively, and values of –7.2 and –7.1 per mil for muscovites 383 and 384, respectively. Splits of these same muscovite fractions gave K-Ar ages of 25.2 ± 0.7 and 36.2 ± 1.0 Ma, respectively, but

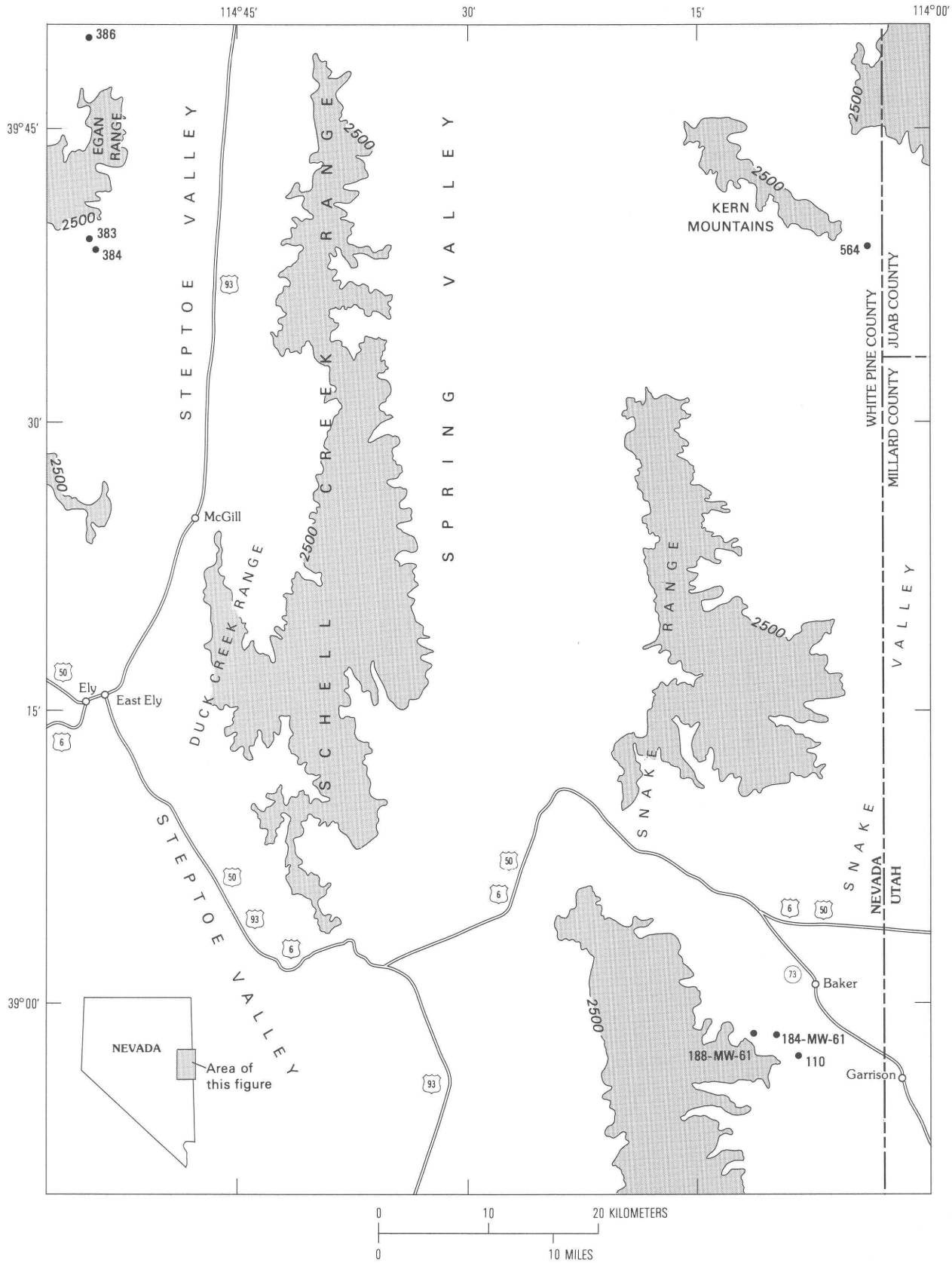

Figure N1. Map of part of eastern Nevada and western Utah, showing sample localities. The 2500–m contour lines are not shown in the southwestern part of the map area. Samples 184–MW–61 and 188–MW–61 are from the Young Canyon-Kious basin area.

Table N1. Summary of $\delta^{18}O$ values and potassium-argon age data for selected plutonic rocks and minerals of eastern White Pine County, Nev.

[Latitude and longitude are given in degrees (°), minutes (′), and seconds (″)]

Sample Number	Latitude, north	Longitude, west	$\delta^{18}O$ value, per mil	Muscovite K-Ar age (Ma)
Intrusive (Oligocene, 32 Ma) Young Canyon-Kious basin area, southern Snake Range				
184-MW-61	38°57′58″	114°10′50″	-2.6 (rock); -6.6 (microcline)---	17.0±0.8
[1]188-MW-61	38°57′50″	114°09′32″	-0.9 (rock)----------	18.5±1.0
110	38°57′02″	114°08′16″	-1.1 (rock)----------	Not determined.
Intrusive (Cretaceous, 70 Ma), Kern Mountains				
564	39°38′05″	114°03′35″	-5.4 (rock)	24.7±1.1
Intrusive (age unknown), Warm Springs area northern Egan Range				
383	39°38′05″	114°53′20″	-0.9 (rock); -7.2 (muscovite)----	25.2±0.7
384	39°37′40″	114°52′55″	-3.0 (rock); -7.1 (muscovite)----	36.2±1.0
Intrusive (age unknown), Big Rock area, Cherry Creek district, northern Egan Range				
386	39°48′20″	114°53′25″	-0.4 (rock)----------	34.9±1.0

[1]Sample 188-MW-61 is the same as number 105 in Lee and others (1982, table 1).

Lee and others (1980, p. 26) regarded these ages as spuriously young, and suggested that the intrusive may have crystallized at a much earlier time. To our knowledge this pluton has not yet been dated by either Rb-Sr (rubidium-strontium) or U-Th-Pb (uranium-thorium-lead) isotope age work.

The intrusive at Warm Springs clearly seems to have been deformed no earlier than 36 Ma ago in the area of sample sites 383 and 384 as a result of movement on the overlying thrust fault, and the $^{18}O/^{16}O$ of the rock seems to have been modified at the time of deformation. The age of this pluton has yet to be determined.

Sample 386 is from the "Big Rock" area of intrusive outcrop in the southern part of the Cherry Creek district of the northern Egan Range. The intrusive is cut by shears in the area of the sample site, which is about 100 m (meters) east of a fault within the intrusive that dips about 30° east-northeast (see the map of Adair, 1961). The alteration and deformation of parts of this intrusive were recognized clearly by Adair (1961, p. 43), who stated: "The fact that thrust faults exist in and around this igneous body can hardly be questioned." Rock sample 386 has a $\delta^{18}O$ value of –0.4, and the muscovite recovered from this rock gave a K-Ar age of 34.9 ± 1.0 Ma, regarded as spuriously young by Lee and others (1980, p. 26). The $^{18}O/^{16}O$ of this intrusive rock appears to have been modified during a deformation that took place within the last 34.9 Ma, but the time of crystallization of this pluton is as yet undetermined.

From the data discussed here and summarized in table N1, we conclude that the $^{18}O/^{16}O$ of each of these rocks and minerals was modified during deformation or even cataclasis resulting from post-crystallization movement along a spatially related thrust fault. The times of cataclasis are indicated by the K-Ar results listed. Where the rocks are only sheared and deformed but not cataclasized, as in the northern Egan Range (samples 383, 384, and 386), degassing of the dated muscovites may not have been complete, and the K-Ar results indicate a maximum age for the time of deformation.

Beyond our conclusion that there was oxygen isotope exchange between plutonic rocks and meteoric waters in the tectonic environments described, any explanation of the exact process that produced these low $\delta^{18}O$ values must be reconciled with three additional lines of evidence. First, in the Young Canyon-Kious basin area, the "type" area, where relations are best exemplified and most intensively studied, masses of relatively undeformed intrusive are suspended in the more contorted rock, as described in detail by Lee and Van Loenen (1971, p. 6, 40). In general, the most cataclasized samples tend to have the lowest $\delta^{18}O$ values (Lee and others, 1982). In other words, the modification of the oxygen isotope composition of these rocks was more spotty than pervasive.

The cataclasis of the intrusive in Young Canyon-Kious basin intrusive did not change the Rb-Sr systematics of that rock. Three points based on $^{87}Sr/^{86}Sr$ and $^{87}Rb/^{86}Sr$ data for one sample of the undeformed intrusive

and two samples of its cataclasized equivalents fall near a straight line that indicates an initial $^{87}Sr/^{86}Sr$ of 0.71215 at an age of 32 ± 1.5 Ma (chap. P, this volume).

A final line of evidence is provided by our unpublished oxygen isotope data for 23 quartzite samples of late Precambrian-Early Cambrian age collected within the area of figure N1. The field settings are described and petrographic and K-Ar age data for all these quartzites are included in a study by Lee and others (1980). Some of these quartzites, collected just beneath the sole of the Snake Range décollement have a strong directional element obviously formed during late movement on the décollement. Micas recovered from these schistose quartzites gave K-Ar ages similar to those listed in table N1, and were interpreted by Lee and others (1980) to represent a maximum age for the most recent movement on the décollement. However, none of these 23 quartzite samples has a $\delta^{18}O$ value of less than 9.7 per mil, and the $\delta^{18}O$ values determined for these rocks and their constituent micas are not related to distance below the décollement in any obvious way.

We note that three samples of Cambrian Pole Canyon Limestone exposed in contact with the cataclasized intrusive in the Young Canyon-Kious basin area have relatively low $\delta^{18}O$ values (Lee and others, 1982). These low $\delta^{18}O$ values may be due to some kind of contact action, or they might result from isotopic exchange between the limestone and either the cataclasized intrusive or meteoric waters during movement on the overlying thrust fault. We have not yet investigated limestone exposed beneath the sole of a thrust fault but remote from any intrusive rock.

SUMMARY AND CONCLUSIONS

In the area of figure N1 the constituent micas of various plutonic rocks and of upper Precambrian-Lower Cambrian quartzites were degassed by stresses resulting from movement along spatially related thrust faults. At or about the same time the $^{18}O/^{16}O$ ratios of these plutonic rocks were lowered, apparently as a result of oxygen isotope exchange with meteoric waters. However, there was no obvious change in the $^{18}O/^{16}O$ ratio of any of the quartzites, even those exposed just beneath the sole of the Snake Range décollement, which have a pronounced metamorphic fabric obviously formed during movement on the overlying thrust. Thus in the rocks discussed here the process leading to lowered $\delta^{18}O$ values would seem to have been operative only within the deformed plutons.

Such low $\delta^{18}O$ values as those listed in table N1 were reported by Taylor (1968) for a few granophyres or shallow granites from the Scottish Hebrides, the Skaergaard intrusion, and the Seychelles Islands. Taylor (1968, p. 39) stated, "The only obvious manner in which such low δ-values could arise is by mixing or exchange between the magmas and low-^{18}O meteoric ground waters." Later such isotopic exchange between *magma* and ground water low in ^{18}O was shown for the rhyolites of the Yellowstone Plateau (Friedman and others, 1974), and for the ash-flow sheets of southern Nevada (Lipman and Friedman, 1975).

The plutonic rocks described in the present study (table N1), however, were crystallized before deformation, and their undeformed equivalents have "normal" $\delta^{18}O$ values. Thus mixing of meteoric water with *magma* cannot have produced the low $\delta^{18}O$ values listed. Inasmuch as the process leading to lowered ^{18}O values was operative only within the deformed plutons, either meteoric waters were selectively commingled with the affected intrusive rocks, or meteoric waters already in the intrusive environment were activated, by stresses resulting from movement on the thrust fault.

In the Young Canyon-Kious basin pluton, at least, the system does not appear to have been open to large amounts of meteoric waters. Modification of the oxygen isotope composition of the cataclasized rocks apparently was more spotty than pervasive, and the cataclasis had no apparent effect on the Rb-Sr systematics of this intrusive.

If the quartzites were well cemented with silica before metamorphism, porosities may have been reduced to the point at which little meteoric pore water was available for isotopic exchange. On the other hand, the polymineralic granitoid rocks contained many grain surfaces that might have held low-^{18}O water. Activation of such water during the heating associated with cataclasis may have been enough to cause the spotty reduction of $\delta^{18}O$ values best exposed in the Young Canyon-Kious basin area.

REFERENCES CITED

Adair, D. H., 1961, Geology of the Cherry Creek district, Nevada: Utah University M.S. thesis, 125 p.

Best, M. G., Armstrong, R. L., Graustein, W. C., Embree, G. F., and Ahlborn, R. C., 1974, Mica granite of the Kern Mountains pluton, eastern White Pine County, Nevada—Mobilized basement of the Cordilleran miogeosyncline?: Geological Society of America Bulletin, v. 85, no. 8, p. 1277–1286.

Friedman, I., Lipman, P. W., Obradovich, J. D., Gleason, J. M., and Christiansen, R. L., 1974, Meteoric water in magmas: Science, v. 184, p. 1069–1072.

Fritz, W. H., 1968, Geologic map and sections of the southern Cherry Creek and northern Egan Ranges, White Pine County, Nevada: Nevada Bureau of Mines Map 35, scale 1:62,500.

Hose, R. K., Blake, M. C., 1976, Geology of White Pine County, Nevada: Nevada Bureau of Mines and Geology Bulletin 85, pt. 1, p. 1–35.

Lee, D. E., Friedman, I., and Gleason, J. D., 1982, Oxygen isotope composition of granitoid and sedimentary rocks of the southern Snake Range, White Pine county, Nevada: Contributions to Mineralogy and Petrology, v. 79, p. 150–158.

Lee, D. E., Marvin, R. F., and Mehnert, H. H., 1980, A radiometric age study of Mesozoic-Cenozoic metamorphism in eastern White Pine County, Nevada, and nearby Utah: U.S. Geological Survey Professional Paper 1158–C, p. 17–28.

Lee, D. E., Marvin, R. F., Stern, T. W., and Peterman, Z. E., 1970, Modification of potassium-argon ages by Tertiary thrusting in the Snake Range, White Pine County, Nevada, *in* Geological Survey research 1970: U.S. Geological Survey Professional Paper 700–D, p. D92–D102.

Lee, D. E., Stern, T. W., Mays, R. E., and Van Loenen, R. E., 1968, Accessory zircon from granitoid rocks of the Mount Wheeler mine area, Nevada, *in* Geological Survey research, 1968: U.S. Geological Survey Professional Paper 600–D, p. D197–D203.

Lee, D. E., and Van Loenen, R. E., 1971, Hybrid granitoid rocks of the southern Snake Range, Nevada: U.S. Geological Survey Professional Paper 668, 48 p.

Lipman, P. W., and Friedman, I., 1975, Interaction of meteoric water with magma—An oxygen-isotope study of ash-flow sheets from southern Nevada: Geological Society of America Bulletin, v. 86, p. 695–702.

Nelson, R. B., 1966, Structural development of northernmost Snake Range, Kern Mountains, and Deep Creek Range, Nevada and Utah: American Association of Petroleum Geologists Bulletin, v. 50, no. 5, p. 921–951.

Taylor, H. P., Jr., 1968, The oxygen isotope geochemistry of igneous rocks: contributions to Mineralogy and Petrology, v. 19, p. 1–71.

1986

U.S. GEOLOGICAL SURVEY BULLETIN 1622

SHORTER CONTRIBUTIONS TO ISOTOPE RESEARCH

PRELIMINARY HYDROGEN, OXYGEN AND SULFUR ISOTOPIC STUDY OF THE XIHUASHAN QUARTZ-WOLFRAMITE DEPOSIT, CHINA

Chapter O

By ROBERT O. RYE, T. P. DING[1], JOSEPH F. WHELAN, and GARY P. LANDIS

CONTENTS

FIGURES

TABLES

[1]Institute of Geology of Mineral Deposits, Chinese Academy of Geological Sciences, Peking, People's Republic of China.

Abstract

The Xihuashan quartz-wolframite deposit in southeastern China consists of more than 600 steeply dipping quartz veins in the upper margins of a complex Mesozoic biotite granite stock that intrudes Cambrian pelitic rocks. Mineralization is confined to veins in the stock and individual veins show a pronounced zoning in both vein and alteration assemblages.

The $\delta^{18}O$ data on the stock indicate postcrystallization exchange with ^{18}O-depleted meteoric water. Whole-rock and quartz $\delta^{18}O$ values suggest that the biotite granite may have some S-type characteristics, although alteration of the stock in the mine area makes determination of primary compositions difficult. The $\delta^{18}O$ data on quartz, wolframite, sericitized potassium-feldspar, and muscovite from the veins and associated greisen envelopes indicate deposition from fluids that had a remarkably narrow range of $\delta^{18}O_{H_2O}$ and temperature throughout vein formation and greisenization.

Preliminary measurements of filling temperature of fluid inclusions in quartz indicate that depositional temperatures were $250 \pm 50°C$ and that at times the fluids boiled; at 250°C, the $\delta^{18}O_{H_2O}$ of the hydrothermal fluids can be calculated to have been 1.0 ± 1.6 per mil. These values are low enough to imply that the fluids contained a substantial component of highly exchanged meteoric water. Most of the δD_{H_2O} values of the fluids are in the range typical of magmatic fluids and therefore cannot be used to distinguish magmatic- and meteoric-water components without a more detailed study. Sulfur isotopic data on sulfides, however, indicate that sulfide sulfur was derived from a deep-seated igneous source. Many features of the geology, the mineralogy, the paragenesis, and the geochemical environment of ore deposition of the Xihuashan deposit appear to be similar to those of other quartz-wolframite deposits that have been studied in greater detail and imply fundamental processes common to the origin of such deposits.

INTRODUCTION

Recent studies of vein-type quartz-wolframite deposits ranging in age from late Precambrian to Tertiary indicate many similarities in geologic environment, mineralogy, paragenesis, alteration assemblages and environment of ore deposition (see summary by Casadevall and Rye, 1980). Such deposits are typically tungsten ore bodies, with only minor sulfides and possibly some tin mineralization, and are present in quartz veins that are spatially associated with granites that have intruded pelitic rocks. Their sulfur invariably is derived from deep-seated sources even though meteoric waters often compose a substantial component of their hydrothermal fluids. The similarity of these different quartz-wolframite deposits indicates that fundamental to their origin is the history of a meteoric $\pm$ magmatic water hydrothermal system associated with a granite magma that intrudes certain pelitic rock suites.

The purpose of this study is to provide preliminary stable isotope data on the famous Xihuashan deposit of China for comparison with other quartz-wolframite deposits that have been studied in detail, as well as to constrain discussions about the origin of the deposit. Most of this study was conducted while T. P. Ding was a guest at the U.S. Geological Survey (USGS) laboratories in Denver, Colo., and is part of an ongoing investigation by the USGS to define the environment of quartz-wolframite deposition. Acknowledgements are made to C. H. Wang and Y. Z. Zhou for their help to T. P. Ding in field observations and sample collections at Xihuashan.

GENERAL GEOLOGIC FRAMEWORK

The Xihuashan tungsten deposit is about 9 km (kilometers) northwest of Dayu in the southern part of Jiangxi province in southeastern China. Tin was discovered in the area as early as the Song dynasty (A.D. 960–1279). The discovery of tungsten dates from 1908. The deposit has been one of the great wolframite producers of the world, having a daily production of as much as 3,000 tons of ore containing more than 1 percent WO_3. In addition to tungsten, the deposit contains tin, molybdenum, bismuth, and rare-earth elements. The following description of the district is based on reports of many geologists who have contributed to an understanding of the area and which are summarized by Xu and Ding (1941, 1943); Wang and Zhou (in press), and Wu and Mei (in press).

The Xihuashan deposit is in the Nanling tungsten metallogenic province (fig. O1). The deposits in this province are closely associated with Mesozoic granitic rocks that intrude folded and faulted Cambrian to Silurian clastic metasedimentary rocks and Devonian limestones. There are three types of tungsten deposits in the province: tungsten-molybdenum-beryllium bearing porphyries, scheelite-sulfide skarns, and quartz-wolframite veins. The quartz-wolframite deposits are economically the most important and Xihuashan is one of the most important examples of these in the province.

The Xihuashan deposit is in the southwestern part of the Xihuashan biotite-granite stock that has biotite K-Ar (potassium argon) ages of 138–155 Ma (Li and others, 1964), is exposed over an area of 20 km^2 (square kilometers) and is composed of five sequentially intruded phases, all of which have been mineralized (Wu and Mei, in press). The stock intrudes slightly metamorphosed arenaceous and argillaceous Cambrian rocks that have been metamorphosed to hornfels in contact zones adjacent to the stock.

Figure O1. Index map showing location of Nanling tungsten province and Xihuashan, China.

GEOLOGY OF THE XIHUASHAN DEPOSIT

The Xihuashan deposit is the most significant of six deposits that are defined on the basis of groups of vertical veins within the stock. The deposit consists of subparallel, en-echelon veins with an east-west trend. The veins are related to a well-defined joint pattern in the upper part of the stock. A diagrammatic cross section showing the relationship of the veins to the stock is shown in figure O3.

The veins range in thickness from a few centimeters to nearly 4 m (meters), with an average interval of about 4 m between the margins of major veins. The length of individual veins ranges from less than l00 m to more than 1,000 m and the average vertical extent is 200–300 m.

Mineralization was by fracture filling. The major mineral is quartz with wolframite, potassium-feldspar, beryl, calcite, muscovite, and fluorite. Minor amounts of topaz, molybdenite, cassiterite, arsenopyrite, and base-metal sulfides are present also. Quartz, comprising more than 90 percent of vein material, usually is massive; vugs are rare. Wolframite (Fe0–Mn0 mole ratio of 1.1 to 1.6), however, is present as individual black crystals that may

Figure O2 (above and facing page). Simplified geologic map of the Xihuashan deposit (modified from a map in the "Guidebook for field excursions," Symposium on Tungsten Geology, Jiangxi, China, (October 12–21, 1981) showing veins and projected sampling sites). Letter prefixes have been omitted from sample numbers to save space.

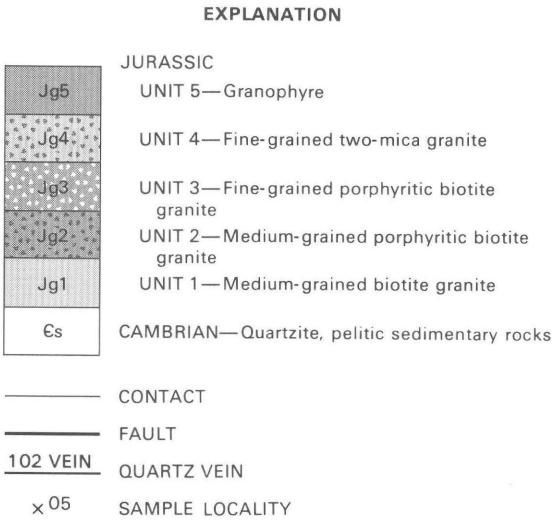

be as large as several centimeters. Potassium-feldspar is present as irregularly shaped masses that usually are partially sericitized.

The veins are characterized by a striking vertical zonation that extends from the deeper and inner levels of the veins toward their upper and outer margins. From the deeper levels, barren quartz veins grade into a quartz potassium-feldspar-sulfide assemblage, followed by a quartz-wolframite assemblage, and then to a quartz-wolframite-beryl assemblage that caps the veins. This zoning in the veins is accompanied by a zoning in wall-rock alteration. The deepest levels contain a sodium-rich feldspar alteration zone that grades into a zone of intense potassium-feldspar alteration, then into a zone of silification, and, finally, into a zone of greisen which involves intense development of muscovite and coincides with the richest ore in veins. Wolframite mineralization is closely related to the zones of greisen and silicification and is absent in the potassium-feldspar zone. Wolframite mineralization also is limited usually to veins in the stock and rarely

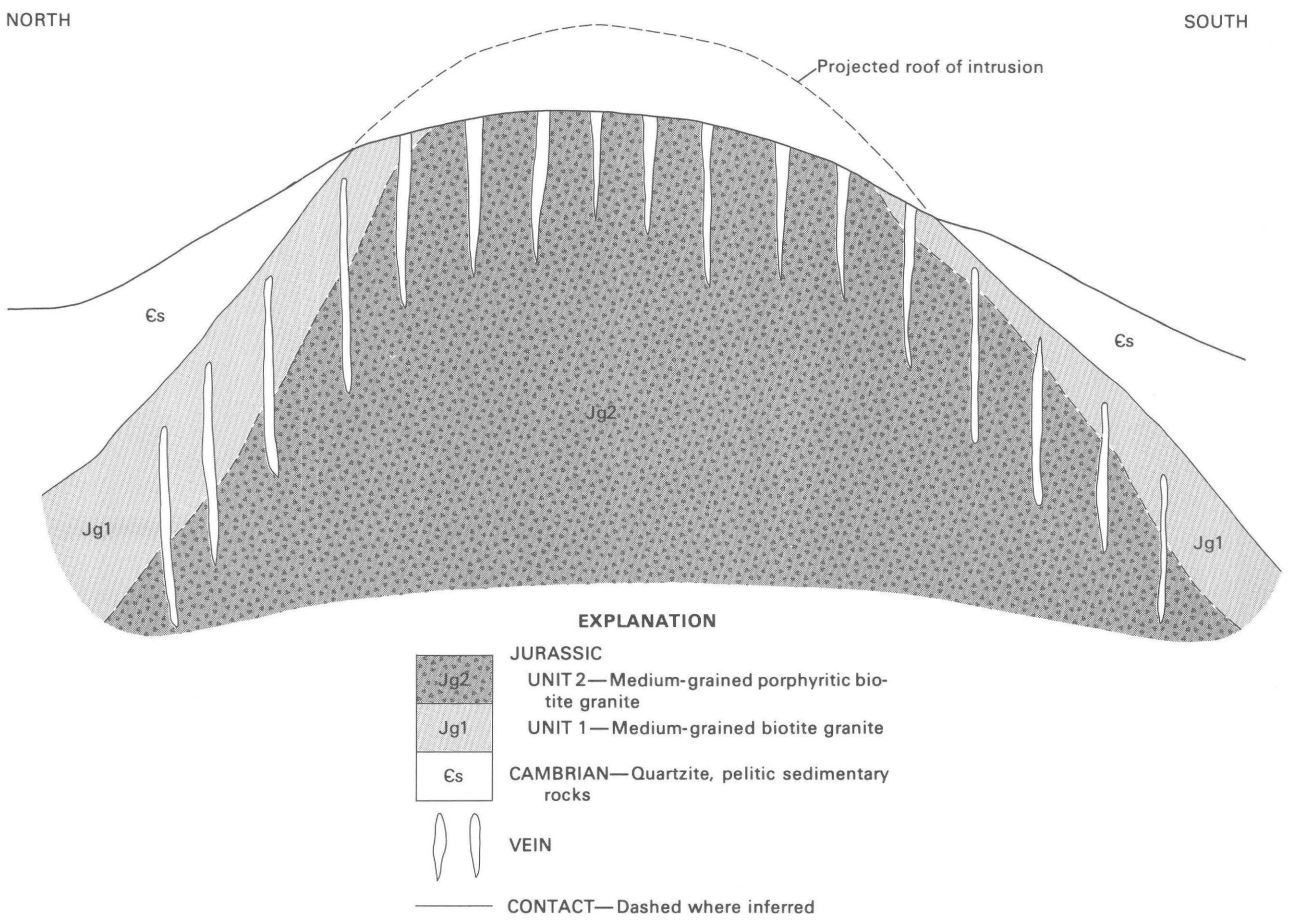

Figure O3. Diagrammatic north-south cross section of the Xihuashan deposit showing first and second phases of granite and relationship of quartz-wolframite veins to the margin of the stock.

extends into veins in the country rock. The formation of wolframite may be closely related to wall-rock alteration, and this association should be studied in future investigations of the area. Wolframite mineralization is limited to a 200- to 300-m zone that extends to about 200 m below the roof of the granite. (See fig. O5.)

The zoning and the general lack of vugs coupled with the complex nature of individual veins makes detailed paragenetic studies difficult. However, quartz mineralization clearly spans the major part of the paragenetic sequence and brackets wolframite mineralization.

STABLE ISOTOPE STUDIES

Most vein and greisen samples were collected from the 299 vein, which is one of the major veins in the northern part of the deposit. Samples also were collected from the 247 vein in the southern part of the deposit and from a few other places in the central part of the deposit, as indicated in the tables. Samples of the granite were taken from numerous underground and surface sites throughout the deposit. Although sample coverage of the 299 vein is fairly representative of temporal and spatial variations in that vein, it is only one of more than 600 veins in the deposit. To what extent the samples are representative of the entire deposit is not certain. The isotope results are summarized in tables O1–O3 and those from vein 299 are plotted in figures O4 and O5. Samples were analyzed by conventional techniques and are reported according to conventional standards as summarized by Rye and Sawkins (1974) and Thode and others (1961).

Sulfur Isotope Studies

Sulfide minerals are not abundant in the Xihuashan deposit and are confined to the deeper levels of the veins; only six samples were analyzed for sulfur isotopic composition. Sulfate minerals have not been described in the deposit and the hydrothermal system appears to have been sulfide-dominant. The $\delta^{34}S$ values of molybdenite, pyrite, and chalcopyrite range from only 1.0 to –0.7 per mil. Although no mineral pairs were analyzed, the narrow range of values and the trend of the ^{34}S enrichment among molybdenite, pyrite, and chalcopyrite suggest that the sulfides precipitated under equilibrium conditions that were extremely uniform over the sampled area.

The $\delta^{34}S$ values of the sulfides are typical of vein deposits associated with felsic intrusions in which the hydrothermal fluids are H_2S-dominant (Ohmoto, 1972). Under such conditions the $\delta^{34}S_{\Sigma S}$ of the hydrothermal fluid is slightly less than that of pyrite or about zero per mil (Ohmoto and Rye, 1979). The sulfur isotope geochemistry of the main-stage sulfides in the deposit is typical of all quartz-wolframite deposits studied to date. (See Landis and Rye, 1974; Kelly and Rye, 1979; Casadevall and Rye, 1980.) The sulfur involved in the Xihuashan deposit probably is of deep-seated igneous origin, either directly from a magma or by leaching of sulfur from igneous sulfides by meteoric-water hydrothermal fluids.

Oxygen Isotope Studies

More than 125 analyses were made on representative samples of granite, hornfels, veins, and greisen (tables O2 and O3). The following $\delta^{18}O$ values were found in the granite: quartz, from 11.3 to 13.2 per mil; plagioclase, from 6.8 to 9.7 per mil; potassium-feldspar, from 5.8 to 8.8 per mil; muscovite, 7.7 permil; biotite, 6.5 per mil; and whole rock from 7.7 to 10.7 per mil.

Temperatures calculated from the quartz-plagioclase, quartz-potassium-feldspar, quartz-muscovite, and quartz-biotite ^{18}O fractionations in the granite are too low to represent primary magmatic crystallization temperatures (table O4). Thus, post-crystallization exchange with

Table O1. The $\delta^{34}S$ values (in per mil) of sulfide minerals in samples from quartz-wolframite veins from the Xihuashan ore deposit

[Samples were analyzed by T. P. Ding while a guest at the laboratory of Dr. A. G. Thode, McMaster University, Hamilton, Ontario, Canada. Leaders (---) indicate not present or not analyzed. CDT, Canon Diablo troilite]

Sample number	$\delta^{34}S$ (CDT) Molyb-denite	Pyrite	Chalco-pyrite	Sampling site location
Xi 007	0.7	---	---	620 level, 299 vein, north wall.
Xi 022	0.4	---	---	538 level, 299 vein.
Xi 020	---	---	-0.7	Do.
Xi 037	---	-0.3	---	431 level, 71 vein.
Xi 038	1.0	---	---	Do.
Xi 062	---	0.3	---	270 level, 247 vein.

Table O2. $\delta^{18}O$ and δD values (in per mil) of minerals and whole rocks from granite and hornfels

[Q, quartz; Mus, muscovite; Pl, plagioclase, 20 percent anorthite; Kf, potassium feldspar; Bio, biotite; SMOW, Standard Mean Ocean Water. Leaders (---) indicate not present or not analyzed]

Sample No.	$\delta^{18}O$ (SMOW)						δD (SMOW)		Sampling site and granite phase
	Q	Pl	Kf	Mus	Bio	Whole rock	Mus	Bio	
					Granite				
Xi 018	11.8	7.3	---	---	---	8.9	---	---	538 level, 1.5 m from 299 vein; Jg2.
Xi 025	11.8	---	7.3	---	---	9.1	---	---	670 level, 1 m from 299 vein; Jg2.
Xi 033	12.2	---	6.7	---	---	8.6	---	---	431 level, on contact; Jg2.
Xi 034	12.3	---	6.6	---	---	7.7	---	---	431 level, 1 m from contact; Jg2.
Xi 044	12.0	---	6.1	---	---	8.0	---	---	431 level, on contact; Jg2.
Xi 045	13.2	---	6.3	---	---		---	---	431 level, 2 m from 134 vein; Jg2.
Xi 065	11.5	7.8	---	7.7	---	10.7	-79	---	270 level, 1 m from 247 vein; Jg2.
Xir 01	12.0	9.7	---	---	6.5	10.3	---	-96	594 level, 5 m from 62 vein; Jg2.
Xir 02	11.5	---	6.2	---	---	8.1	---	---	Surface; Jg3.
Xir 03	11.9	---	8.8	---	---	---	---	---	Surface; Jg4.
Xir 04	12.0	---	5.8	---	---	---	---	---	Surface; Jg5.
Xir 05	11.7	7.0	---	---	---	8.8	---	---	431 level, 3 m from 62 vein; Jg2.
Xir 06	11.3	6.8	---	---	---	8.6	---	---	632 level, 3 m from 61 vein; Jg2.
					Hornfels				
Xi 032	---	---	---	---	---	9.8	---	---	431 level, on contact with Jg2.
Xi 043	---	---	---	---	---	9.0	---	---	431 level, 0.5 m from contact.
Xi 031	---	---	---	---	---	8.5	---	---	431 level, 1 m from contact.
Xi 042	---	---	---	---	---	12.3	---	---	431 level, 5 m from contact.
Xi 041	---	---	---	---	---	9.4	---	---	431 level, 15 m from contact.
Xi 040	---	---	---	---	---	11.2	---	---	431 level, 25 m from contact.
Xi 039	---	---	---	---	---	10.3	---	---	431 level, 30 m from contact.

^{18}O-depleted waters has taken place among the biotite, muscovite, and feldspars in the granite. This fact is substantiated by petrographic evidence of incipient sericitization of feldspars in the granite.

In view of these ^{18}O depletions, the whole-rock $\delta^{18}O$ values must be considered minimum indicators of the initial magmatic values. A better indication of the primary magmatic values is given by the $\delta^{18}O$ of quartz, which is least susceptible to postmagmatic exchange. These values of 11.3–13.2 per mil are slightly greater than those of "normal" igneous granites (Taylor, 1968) and are in the lower part of the range recorded for S-type granites (O'Neil and Chappell, 1977).

S-type granites usually are highly silicic, two-mica granites that are characterized by normative corundum, high initial strontium ratios, and by $\delta^{18}O$ values of greater than 9 per mil. These granites presumably are derived from the anatexsis of shallow sedimentary rocks. There appears to be a strong positive correlation between tin or tin-tungsten mineralization and S-type granites (Chappell and White, 1974; Kelly and Rye, 1979). This relationship, however, does not appear to hold for deposits that contain only tungsten (Casadevall and Rye, 1980). The various phases of the Xihuashan granites are highly siliceous, biotite ± muscovite granites with some excess aluminum (Wang and Zhou, in press). However, because the Xihuashan granites have been so altered, whether or not they are S-type is unclear.

The hornfels adjacent to the granite stock has whole-rock $\delta^{18}O$ values of 8.5 to 12.3 per mil (table O2). A traverse across the granite-hornfels contact at the 431 level near the west end of the 71 vein indicates that the hornfels were not noticeably affected by exchange with ^{18}O-depleted fluids, except possibly within 1 m from the contact (table O2).

The range of $\delta^{18}O$ values for most minerals in the veins generally is less than 3 per mil: quartz ranges from 9.7 to 12.9 per mil; potassium-feldspar from 4.9 to 7.3

Table O3 $\delta^{18}O$ and δD values of minerals and inclusion fluids of veins and greisen from the Xihuashan deposit

[Q, quartz; Kf, potassium-feldspar; W, wolframite; Mus, muscovite; SMOW, Standard Mean Ocean Water. Leaders (---) indicate not present or not analyzed]

Sample No.	$\delta^{18}O$(SMOW)				δD(SMOW)			Sampling site
	Q	Kf	W	Mus	Musc	Kf alteration	Fluid inclusions in Q	
Xi 001	11.6	4.9	5.1	---	---	---	---	299 vein, 538 level.
002	11.5	---	6.0	---	---	---	---	299 vein, 620 level.
003	11.2	---	5.4	---	---	---	---	Do
004	11.2	---	5.9	---	---	---	-59	Do.
005	11.0	---	5.8	---	---	---	---	Do.
006	11.7	---	---	---	---	---	-61	Do.
008	12.9	7.3	5.9	---	---	---	---	Do.
009	11.8	---	5.7	---	---	---	---	Do.
010	12.2	5.7	5.6	---	---	-73	---	Do.
011	11.7	6.2	6.2	---	---	---	---	Do.
012	9.7	5.7	5.5	---	---	---	---	Do.
013	12.2	---	5.4	---	---	---	-56	299 vein, 594 level.
014	12.3	---	5.8	---	---	---	---	Do.
015	11.4	5.7	---	---	---	---	---	299 vein, 538 level.
016	11.4	---	---	---	---	---	---	Greisen near 015.
017	10.5	---	---	---	---	---	---	Do.
019	9.9	6.3	---	5.8	-84	-73	---	299 vein, 538 level.
020	10.4	4.8	---	---	---	---	---	Do.
021	11.4	---	5.5	---	---	---	-60	Do.
022	11.2	---	---	---	---	---	-67	Do.
023	10.5	6.1	5.0	---	---	---	-74	299 vein, 670 level.
024	4.2	---	---	---	---	---	---	Greisen near 023.
026	12.0	---	---	---	---	---	-78	299 vein, 632 level.
027	11.2	---	5.8	---	---	---	---	Do.
028	12.1	---	5.1	---	---	---	---	Do.
029	10.0	---	---	---	---	---	---	Do.
030	11.0	---	---	7.0	---	---	---	Greisen near Xi 029, 102 vein.
049	---	---	---	---	-79	---	---	Do.
051	11.4	5.4		6.7	-111		-62	Do.
054	11.9	---	6.2	8.4	---	---	---	247 vein, 270 level.
055	12.0	---	5.8	---	---	---	---	Do.
056	11.9	---	4.8	---	---	---	---	Do.
057	12.2	---	5.0	---	---	---	---	Do.
058	12.2	---	4.9	---	---	---	---	Do.
059	12.4	5.4	5.3	---	---	---	---	Do.
060	12.4	---	5.1	---	---	---	-75	Do.
061	12.4	---	5.5	---	---	---	---	Do.
062	12.4	---	---	---	---	---	---	Do.
063	11.8	---	---	8.1	-75	---	---	Greisen near 054.
064	11.8	---	---	7.9	-71	---	---	Do.
066	12.0	7.2	---	---	---	-62	---	247 vein, 270 level.

per mil; muscovite from 5.8 to 8.4 per mil; and wolframite from 4.8 to 6.2 per mil (table O3). The veins are dense and, because of the absence of vugs and crosscutting relationships, do not lend themselves readily to detailed paragenetic studies. However, an attempt was made to get some impression of the time-space variation of $\delta^{18}O$ in quartz and wolframite in the 299 and 247 veins that could be related to variations in temperature and (or) $\delta^{18}O_{H_2O}$ of the fluids. The results of traverses across different levels of the veins which range in thickness from

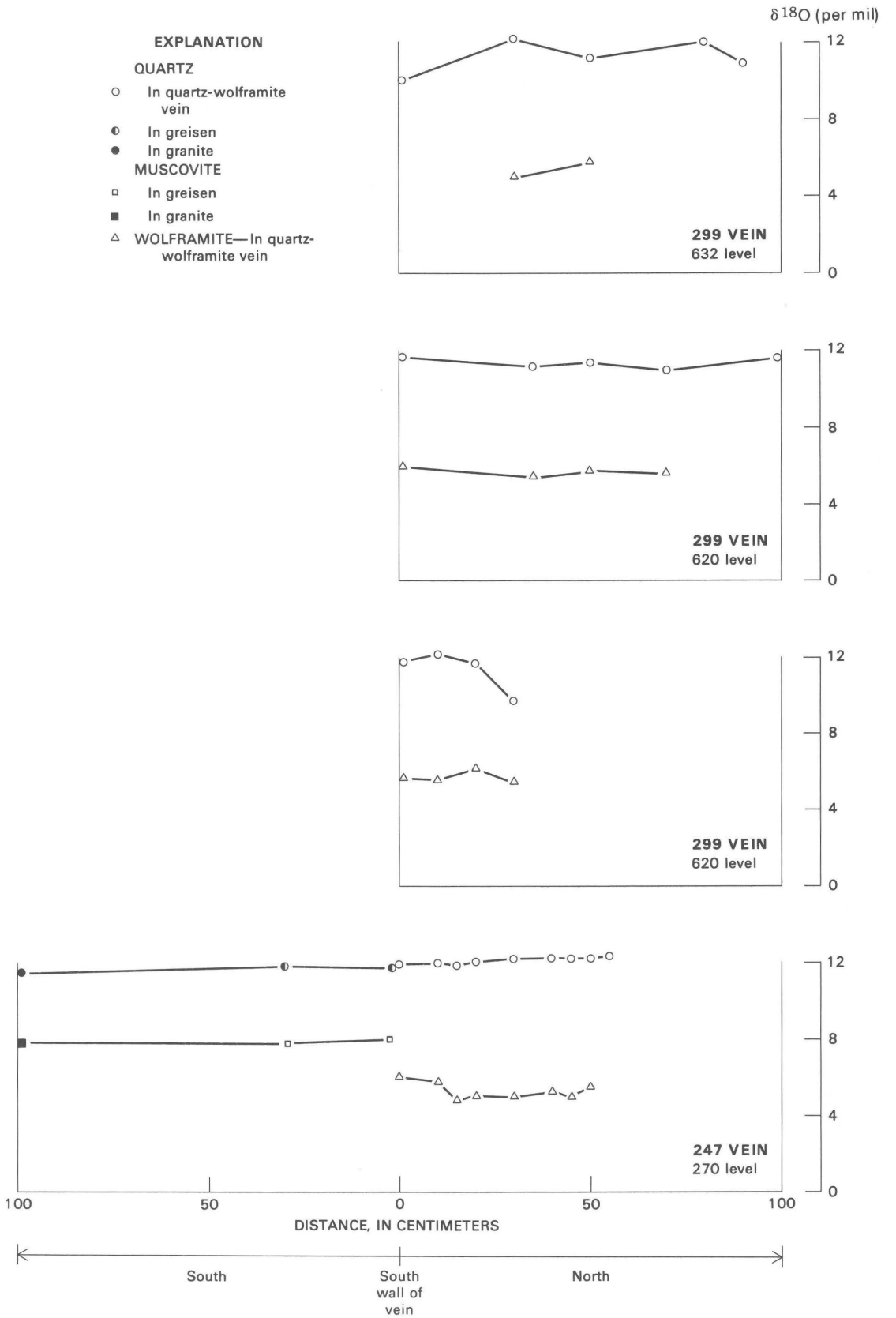

Figure O4. $\delta^{18}O$ values of samples collected from traverse across the 247 vein at the 270 level and across the 299 vein at the 620 and 632 levels. Data plotted at distances north and south from a plane representing the south wall of each vein.

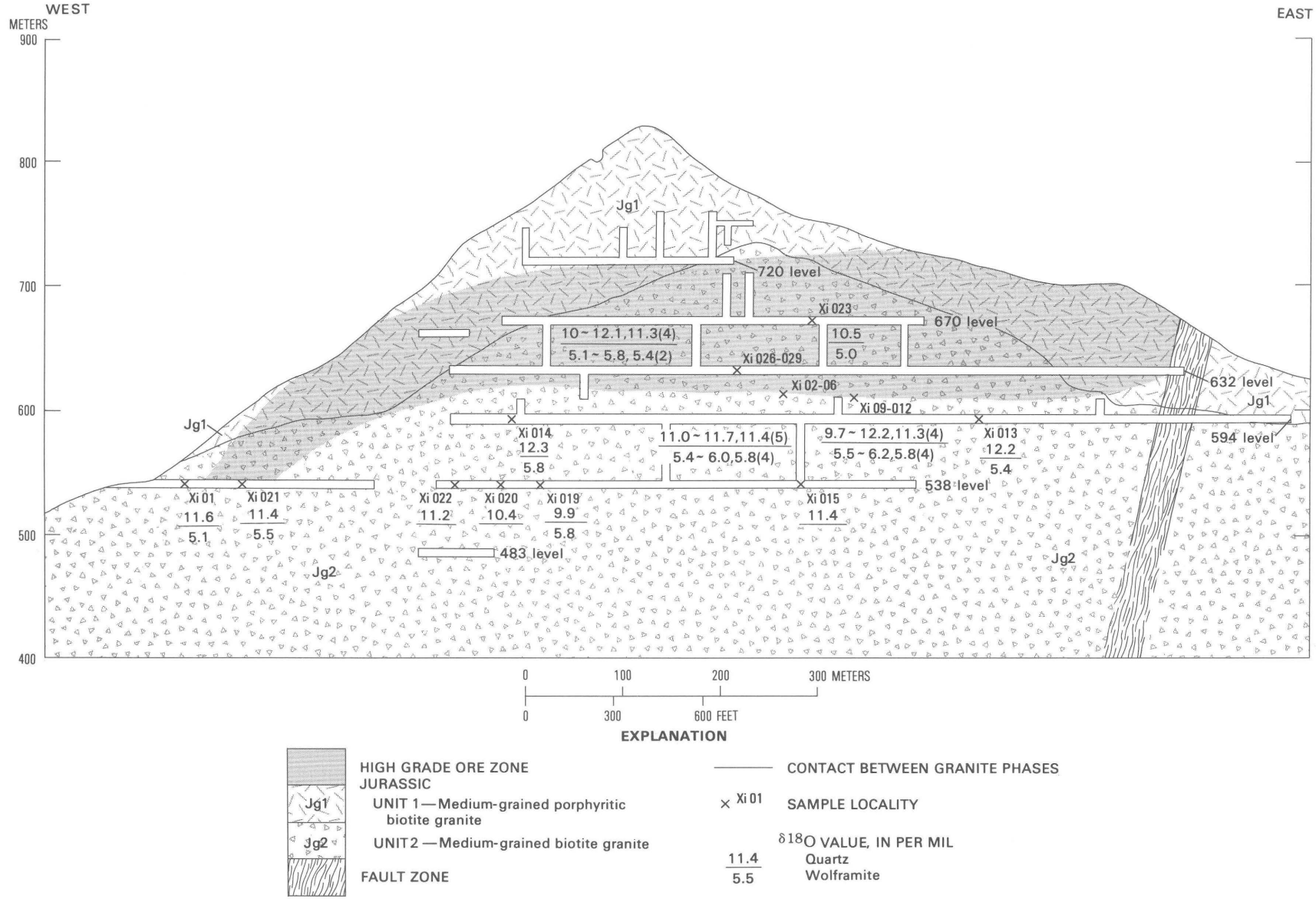

Figure 05. Cross section of the 299 vein showing sample localities and spatial distribution of $\delta^{18}O$ values for quartz and wolframite.

about 30 cm to 2 m are shown in figure O4. There are no consistent variations in either $\delta^{18}O$ values or quartz-wolframite ^{18}O fractionations.

In order to get some impression of possible spatial variations in the $\delta^{18}O$ of the quartz and wolframite, the data for the 299 vein are plotted in figure O5. Only the $\delta^{18}O$ values of wolframite show evidence of a spatial variation in that they tend to decrease toward the top, sides, and outer margins of the vein. This spatial variation in ^{18}O leads to a slight increase in quartz-wolframite fractionation toward the margins of the veins, suggesting a possible spatial decrease in temperature. The narrow range of $\delta^{18}O$ values for wolframite seems to be a characteristic feature of quartz-wolframite deposits and indicates that wolframite deposition takes place under restricted geochemical conditions in a low water-rock hydrothermal system during a specific phase in the evolution of an igneous body at individual deposits (Landis and Rye, 1974; Kelly and Rye, 1979; Casadevall and Rye, 1980).

The interpretation of the $\delta^{18}O$ data on the vein minerals is hampered by lack of detailed temperature information that can be related to specific $\delta^{18}O$ analyses, and by uncertainty in the ^{18}O quartz-water fractionation curves. The 3.2 per mil range in $\delta^{18}O$ quartz could be accounted for by a 60°–100°C temperature variation in the 200°- to 400°C-temperature interval. Because some of the range in ^{18}O quartz must have been due to at least minor variations in the $\delta^{18}O_{H_2O}$ of the fluid, the actual temperature variation during quartz mineralization probably was less than 60°–100°C.

Initial filling temperature measurements of fluid inclusions in quartz samples Xi 006, Xi 021, and Xi 060 range from about 200° to 300°C. Filling-temperature studies on these samples were hampered by the presence of a large number of secondary inclusions, by necking-down of inclusions, and by variable liquid to vapor ratios in the primary inclusions that give higher temperatures and indicate that, at times, the fluids were boiling. These results are consistent with those obtained by Lu and others (1977, 1982). If we assume that the fluid temperature was 250°C, the calculated $\delta^{18}O_{H_2O}$ of the fluids was 1.0 ± 1.6 per mil using the curve of Taylor (1974). The extrapolated curve of Bottinga and Javoy (1973) results in values about 1 per mil smaller; the curves of Clayton and others (1972) and Matsuhisa and others (1979) result in values about 1 per mil larger. Fluids derived from magmas have $\delta^{18}O_{H_2O}$ values determined by the composition of the magma, usually about 6–8 per mil (Taylor, 1974). These initial $\delta^{18}O$ values could be decreased by lower temperature exchange with previously crystallized igneous rock. At Xihuashan, the $\delta^{18}O$ values for the quartz in the granite, greisen, and veins are similar, suggesting that the hydrothermal fluids were in equilibrium with the host rocks at the temperatures prevailing during ore deposition. A similar situation was observed at Panasqueira (Kelly and Rye, 1979). One could argue that the fluids were magmatic in origin, and the low $\delta^{18}O_{H_2O}$ resulted from low-temperature exchange with the granite. This argument, however, would require nearly complete exchange between the magmatic fluids and the granite at the site of deposition—a condition that is unlikely to have existed in an open vein system. The calculated $\delta^{18}O_{H_2O}$ values seem likely to have been sufficiently low to indicate a significant component of highly exchanged meteoric water in the hydrothermal system. Only if the temperatures of mineralization were near 400°C could the fluids have had $\delta^{18}O_{H_2O}$ values large enough to argue for a predominantly magmatic origin.

An attempt was made to determine depositional temperatures from coexisting quartz and muscovite, and quartz and wolframite in the veins and greisen. There is no certainty that these minerals were deposited contemporaneously or in isotopic equilibrium. Furthermore, calculated temperatures can vary by as much as 160°C depending upon which fractionation curve is used. The quartz-muscovite curves derived from the experimental muscovite-water curve of O'Neil and Taylor (1969) and the quartz-water curve of Clayton and others (1972) and Matsuhisa and others (1979) give temperatures ranging from 246° to 356°C and 210° to 296°C, respectively (table O4), whereas the extrapolated curve of Bottinga and Javoy (1973) gives temperatures ranging from 371° to 459°C. Quartz-wolframite fractionations range from 4.2 to 7.2 per mil, but unfortunately the empirical equation for quartz-wolframite ^{18}O fractionations quoted in Landis and Rye (1974) is strongly dependent upon composition of the wolframites and needs to be calibrated experimentally (G. P. Landis and R. O. Rye, unpub. data).

The question of temperature needs to be resolved by detailed fluid-inclusion studies. The impression that we have at this stage is that depositional temperatures averaged $\sim 250 \pm 50$°C. If these are the depositional temperatures, the Xihuashan hydrothermal fluids probably had a significant component of highly exchanged meteoric water. This conclusion is consistent with the $\delta^{18}O$ data from the granite that require postcrystallization exchange with ^{18}O-depleted waters, although the fact that postcrystallization exchange with meteoric water took place with the granite does not necessarily require that hydrothermal fluids were of meteoric-water origin.

The $\delta^{18}O$ values of quartz and muscovite from the greisen adjacent to the veins are 4.2–11.9 per mil and 7.0–8.1 per mil (table O3), respectively. These values, with the exception of the 4.2 per mil for sample Xi 24, are consistent with those in the veins. The anomalously low value for Xi 24 indicates deposition from or exchange with relatively unexchanged meteoric waters in the upper part of the vein system.

Table O4 Temperatures (in degrees Celsius) calculated from $\delta^{18}O$ data of coexisting minerals in granite, griesen, and veins

[Leaders (---) indicate mineral pairs not present or not analyzed]

Sample No.	ΔQ-Pl[1]	ΔQ-Kf[1]	ΔQuartz-muscovite (1)	(2)	(3)	ΔQ-Bio
			Granite			
Xi 018	239	---	---	---	---	---
Xi 025	---	191	---	---	---	---
Xi 033	---	147	---	---	---	---
Xi 034	---	139	---	---	---	---
Xi 044	---	132	---	---	---	---
Xi 045	---	>102	---	---	---	---
Xi 065	291	---	435	---	---	---
Xir 01	443	---	---	---	---	305
Xir 02	---	155	---	---	---	---
Xir 03	---	285	---	---	---	---
Xir 04	---	122	---	---	---	---
Xir 05	228	---	---	---	---	---
Xir 06	239	---	---	---	---	---
			Veins			
Xi 019	---	(4)	410	294	248	---
Xi 051	---	(4)	370	246	210	---
Xi 054	---	(4)	455	358	296	---
			Greisen			
Xi 030	---	---	418	301	262	---
Xi 063	---	---	449	334	288	---
Xi 064	---	---	426	314	264	---

[1]Temperatures based on extrapolated curve of Bottinga and Javoy (1973).

[2]Temperatures based on experimental quartz-water curves of Clayton and others (1972), and muscovite-water curve of O'Neil and Taylor (1967).

[3]Temperatures based on curves of Matsuhisa and others (1979), and O'Neil and Taylor (1969).

[4]Quartz-potassium feldspar temperatures in veins were not determined because feldspar clearly is sericitized.

Hydrogen Isotope Studies

Hydrogen isotope analyses were made on hydrous minerals from granite, greisen, and veins and on inclusion fluids from vein quartz. Suitable samples of wolframite were not available for fluid-inclusion analyses.

One sample each of muscovite and biotite from the granite have δD values of –79 and –96 per mil, respectively. Using the equations of Suzuoki and Epstein (1976), these values correspond to δD_{H_2O} values of about –65 and –69 per mil, respectively, at magmatic conditions and are consistent with those for magmatic fluids (Taylor, 1974). However, because the $\delta^{18}O$ data suggest that some postcrystallization exchange with ^{18}O-depleted waters has taken place in the primary hydrous minerals in the granite, the δD values also should reflect exchange with these later waters.

Muscovite in the greisen and the veins has δD values ranging from –71 to –111 per mil (table O3) corresponding to δD_{H_2O} values of from –33 to –73 per mil at 250°C. These values agree reasonably well with the δD_{H_2O} values of inclusion fluids in quartz that range from –56 to –78 per mil, considering that there is great deal of uncertainty in the low temperature extrapolation of the muscovite-water D fractionation curve of Suzuoki and Epstein (1976).

The potassium-feldspars in the veins typically show incipient alteration to sericite. The δD values of four of these samples range from –62 to –74 per mil. These values overlap the lower range of values for muscovite in the veins and greisen, suggesting that the presumably later feldspar alteration was produced by fluids that had a less negative δD_{H_2O} or lower temperatures than the vein-greisen muscovite fluids. More detailed paragenetic information and analyses of additional minerals might allow recognition of variations in δD_{H_2O} among different generations of fluids that could be used to sort out the detailed water history of the deposit.

CONCLUSIONS

Perhaps the most significant result of this study is the extremely narrow range of $\delta^{18}O$ values for various minerals in the Xihuashan deposit indicating that mineralization took place from fluids that had a limited temperature and $\delta^{18}O_{H_2O}$ range. The calculated $\delta^{18}O_{H_2O}$ values are low enough to suggest a highly exchanged meteoric-water component in the hydrothermal fluids. This conclusion is consistent with the $\delta^{18}O$ data on the stock which indicate that the stock underwent exchange with ^{18}O-depleted fluids after crystallization. The fact that the $\delta^{18}O$ values of the vein minerals are so uniform indicates that the the hydrothermal fluids, regardless of their origin, had a remarkably uniform exchange history with the silicate wall rocks. The sulfide sulfur from the lower part of the veins was derived from deep-seated sources.

Initial fluid-inclusion data, when combined with $\delta^{18}O$ data on the minerals, suggest that the temperature of mineralization of quartz that obtained during most of the paragenesis probably was between about 200° and 300°C. At times the fluids were boiling.

Many aspects of the stable isotope geochemistry of the Xihuashan deposit appear similar to those of other quartz-wolframite deposits that have been studied in detail. The results of this study provide evidence that the Xihuashan deposit, like many other quartz-wolframite deposits, formed under a narrow range of conditions when a rock-dominated hydrothermal system formed during a specific phase in the evolution of a composite granite that intruded a pelitic sedimentary rock suite.

REFERENCES CITED

Bottinga, Y., and Javoy, M., 1973, Comments on oxygen isotope geothermometry: Earth and Planetary Science Letters, v. 20, p. 250–265.

Casadevall, T., and Rye, R. O., 1980, The Tungsten Queen deposit, Hamme District, Vance County, North Carolina; A stable isotope study of a metamorphosed quartz-huebnerite vein: Economic Geology, v. 75, p. 523–537.

Chappell, B. W., and White, A.J.R., 1974, Two contrasting granite types: Pacific Geology, v. 8, p. 173–174.

Clayton, R. N., O'Neil, J. R., and Mayeda, T. K., 1972, Oxygen isotope exchange between quartz and water: Journal of Geophysical Research, v. 77, p. 3057–3967.

Kelly, W. C., and Rye, R. O., 1979, Geoloigc, fluid inclusion, and stable isotope studies of the tin-tungsten deposit of Panasqueira, Portugal: Economic Geology, v. 74, p. 1721–1822.

Landis, G. P., and Rye, R. O., 1974, Geologic, fluid inclusion, and stable isotope studies of the Pasto Bueno tungsten-base metal ore deposit, northern Peru: Economic Geology, v. 69, p. 1025–1059.

Li, P., Dai, T. M., Qiu, C. Y., and Wang, J. W., 1964, A report of absolute dating of rocks and minerals by K-Ar method: Scientica Geologica Sinica 1964, no. 1, p. 24–34.

Lu, H. Z., Shi, J. X., Yu, C. M., and Xu, S. J., 1977, A study on the characteristics and temperatures of formation of fluid inclusions from various types of tungsten deposits in the Nanling region: Geochimica et Cosmochimica, no. 3., p. 179–193.

———1982, Geologic and fluid inclusion studies of ten types of tungsten ore deposits in South China: Geochemistry, v. 1, p. 200–217.

Matsuhisa, Y., Goldsmith, J. R., and Clayton, R. N., 1979, Oxygen isotope fractionation in the system quartz-albite-anorthite-water: Geochimica et Cosmochimica Acta, v. 43, p. 1131–1140.

Ohmoto, H., and Rye, R. O., 1979, Isotopes of sulfur and carbon, *in* Barnes, H. L., ed., Geochemistry of hydrothermal ore deposits, 2d. ed.: New York, Wiley-Interscience, p. 509–567.

Ohmoto, H., 1972, Systematics of sulfur and carbon isotopic fractionation in hydrothermal ore deposits: Economic Geology, v. 67, p. 551–579.

O'Neil, J. R., and Chappell, B. W., 1977, Oxygen and hydrogen isotope relations in the Berridale batholith: Journal of the Geological Society of London, v. 33, p. 559–571.

O'Neil, J. R., and Taylor, H. P., 1969, Oxygen isotope equilibrium between muscovite and water: Journal of Geophysical Research, v. 74, p. 6012–6022.

Rye, R. O., and Sawkins, F. J., 1974, Fluid inclusion and stable isotope studies on the Casapalca Ag-Pb-Zn-Cu deposit, central Andes, Peru: Economic Geology, v. 69, p. 181–205.

Suzuoki, T., and Epstein, S., 1976, Hydrogen isotope fractionation between OH-bearing minerals and water: Geochimica et Cosmochimica Acta., v. 40, p. 1229–1242.

Taylor, H. P., Jr., 1968, The oxygen isotope geochemistry of igneous rocks: Contributions to Mineralogy and Petrology, v. 19, p. 1–71.

———1974, The application of oxygen and hydrogen isotope studies to problems of hydrothermal alteration and ore deposition: Economic Geology, v. 69, p. 843–883.

Thode, H. G., Monster, J., and Dunford, H. B., 1961, Sulfur isotope geochemistry: Geochimica et Cosmochimica Acta, v. 25, p. 159–174.

Wang, C. H. and Zhou, Y. Z., in press, Two floor mineralization character and mineralogenetic model of Xihuashan ore deposits: Proceedings of symposium on tungsten geology, Jiangxi, China, Oct. 12–21, 1981.

Wu, Y. L. and Mei, Y. W., in press, Multistage petromineralogenetic processes and evolution regulation of Xihuashan tungsten mineral field: Proceedings of symposium on tungsten geology, Jiangxi, China, Oct. 12–21, 1981.

Xu, K. Q. and Ding, Y., 1941, Xihuashan tungsten ore deposits, Dayu county, Jiangxi province [abs.]: Bulletin of Central Geological Survey, Department of Economy, [China], A, no. 60, p. 1–21.

———1943, Geological records of tungsten ore deposits in southern Jiangxi: Geological Report of Central Geological Survey, Department of Economy, [China], no. 17, p. 170–191.

1986

U.S. GEOLOGICAL SURVEY BULLETIN 1622

SHORTER CONTRIBUTIONS TO ISOTOPE RESEARCH

THE STRONTIUM ISOTOPE COMPOSITION OF GRANITOID ROCKS OF THE SOUTHERN SNAKE RANGE, NEVADA

Chapter P

By DONALD E. LEE, RONALD W. KISTLER, and ALLEN C. ROBINSON

CONTENTS

FIGURES

TABLE

Abstract

Six discrete granitoid plutons are exposed within a 900 square-kilometer area in the southern Snake Range of eastern White Pine County, Nev. These granitoid rocks range in age from Jurassic to Tertiary. Initial $^{87}Sr/^{86}Sr$ range from 0.70714 to about 0.71574, $\delta^{18}O$ values from –2.6 to 13.2 per mil, and SiO_2 contents from 63 to 76 weight percent. The petrologic types include calc-alkalic rocks and two different types of two-mica granite. The younger granitoids were emplaced at progressively more shallow depths, and generally crystallized from increasingly evolved magmas. All intrusive types present in the southern Snake Range are present elsewhere in the eastern Great Basin, but the southern Snake Range is distinguished by the grouping of all these intrusive types within a relatively small area. The chronology of the igneous events in the study area is remarkably similar to that found in the Ruby Mountains of Elko County, Nevada, about 200 km to the northwest.

INTRODUCTION

Several granitoid masses are exposed within an area of 900 km^2 (square kilometers) in the southern Snake Range, White Pine County, Nev. (fig. P1). Previous studies (Lee and Van Loenen, 1971, and references cited therein) have shown that these rocks range in age from Jurassic to Tertiary and in composition from granodiorite (63 percent SiO_2) to granite (76 percent SiO_2). A similarly large range of $\delta^{18}O$ values (–2.6 to 13.2 per mil) was found in these plutons (Lee and others, 1982). Among the intrusive types recognized are two different kinds of two-mica granites (Lee, Kistler, Friedman, and Van Loenen, 1981). The strontium isotope data presented here supplement previously published data in a way that greatly increases our understanding of the igneous history of this part of eastern Nevada.

Several works on the regional variations in strontium and oxygen isotopes of Cordilleran granitoids have been completed in the last several years (Masi and others, 1976, 1981; Taylor and Silver, 1978). In addition to studies of oxygen isotope variation in granitoids in the Great Basin (Lee, Friedman, and Gleason, 1981), and oxygen isotope variations in granitoids generated from diverse source materials (O'Neil and Chappell, 1977), these works provide a data base for further study of the source materials of granitoid rocks in general.

INTRUSIVE ROCK OF THE POLE CANYON-CAN YOUNG CANYON AREA

The intrusive rock of the Pole Canyon-Can Young Canyon area is an unusual two-mica granite that was described in detail by Lee and Van Loenen (1971, p. 5, 38, 39). This rock is distinguished in part by the presence

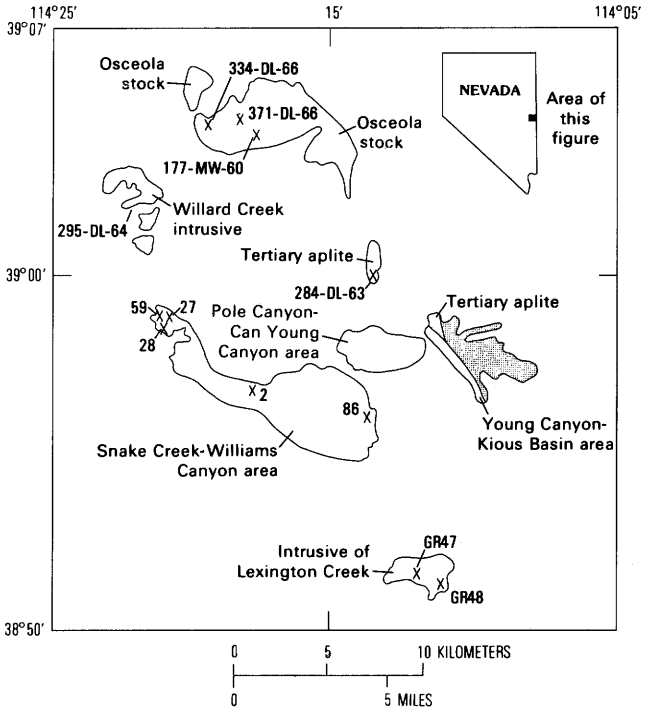

Figure P1. Map showing granitoid rocks of the southern Snake Range, Nevada. Outlines of intrusives modified from the map of Hose and Blake (1976). Shaded area shows intrusive that has been sheared and brecciated by the Snake Range décollement. Only selected sample localities are shown. Sampling sites 5, 12, 15, 31, 57, 61, 66, 79 and 83 (table P1) are present in sequence between sample localities 2 and 86.

of muscovite phenocrysts as large as 2 cm (centimeters) across that contain small inclusions of euhedral biotite. It is not unusual to find as many as 20 biotite euhedra within a single large grain of muscovite. Localities, chemical and modal analyses, and norms for samples 89, 92, 93, and 95 (table P1) and for five additional samples of this pluton (Lee and Van Loenen, 1971) show that these samples contain 2.8–3.4 percent normative corundum, and that each is strongly peraluminous (molecular $Al_2O_3 >> [CaO + Na_2O + K_2O]$).

The biotites in these intrusive rocks contain only about 6.0 percent MgO, leading Lee and Van Loenen (1970) to suggest that the magmas may have had relatively low oxygen fugacities. This inference is further substantiated by the complete absence of opaque oxides from these rocks. Indeed, the only accessory minerals present are monazite, an allanite-like mineral, and equant apatite containing many tiny inclusions of acicular zircon (see chap. D, fig. D2, this volume). Based mainly on field relations, Lee and Van Loenen (1971) concluded that this distinctive rock resulted from assimilation of the latest Precambrian Osceola Argillite of Misch and Hazzard (1962). More recently Lee Kistler, Friedman, and Van Loenen (1981) described two similar two-mica granite

Table P1. Rubidium-strontium data for intrusive and sedimentary rocks of the southern Snake Range, White Pine County, Nev.

Sample No.	Type	Concentration (parts per million) Rb	Sr	Rb/Sr	$^{87}Rb/^{86}Sr$	$^{87}Sr/^{86}Sr$
	Intrusive, Pole Canyon-Can Young Canyon					
89	Two-mica granite---------	185	327	0.566	1.64	0.71823
92	---do.-------------------	178	358	.497	1.44	.71841
93	---do.-------------------	164	358	.458	1.33	.71528
95	---do.-------------------	165	351	.470	1.36	.71753
[1]226-MW-61	Muscovite----------------	582	20.04	29.04	84.9	.8123
PCA-P1	Aplite-pegmatite---------	279	18.1	15.4	44.9	.76570
RK	Microcline megacryst-----	738	31.7	23.3	68.3	.79243
	Intrusive, Snake Creek-Williams Canyon					
2	Intrusive----------------	231	106	2.18	6.31	0.72115
5	---do.-------------------	219	119	1.84	5.33	.71875
12	---do.-------------------	153	224	.683	1.98	.71134
15	---do.-------------------	148	329	.450	1.30	.71017
27	---do.-------------------	136	421	.323	.935	.70991
28	---do.-------------------	144	415	.347	1.00	.70994
31	---do.-------------------	121	491	.246	.713	.70883
57	---do.-------------------	101	511	.198	.573	.70838
59	---do.-------------------	151	420	.360	1.040	.71025
61	---do.-------------------	83.8	713	.118	.340	.70781
66	---do.-------------------	86.2	676	.128	.370	.70786
79	---do.-------------------	82.3	716	.115	.333	.70775
83	---do.-------------------	100	678	.147	.427	.70832
	Intrusive, Young Canyon-Kious basin					
98	Intrusive----------------	238	68	3.49	10.12	0.71748
103	Cataclastic intrusive----	173	235	.786	2.13	.71307
110	---do.-------------------	109	409	.267	.772	.71251
	Tertiary aplite					
[1]284-DL-63	Aplite-------------------	529	8.88	59.6	173	0.7821
	Intrusive, Osceola					
177-MW-60	Intrusive----------------	92.3	482	0.192	0.554	0.70864
334-DL-66	---do.-------------------	200	87	2.3	6.66	.72119
371-DL-66	---do.-------------------	102	528	.193	.559	.70854
	Intrusive, Willard Creek					
295-DL-64	Two-mica granite---------	152	164	0.927	2.68	0.71432
	Intrusive, Lexington Creek					
GR47	Two-mica granite---------	101	610	0.165	0.479	0.71191
GR48	---do.-------------------	113	671	.168	.488	.71203
	[2]Sedimentary rocks					
Ar3	pCo----------------------	148	51.9	2.85	8.30	0.76454
Ar4	pCo----------------------	220	28.7	7.67	22.34	.80317
Q2	CpCm---------------------	113	28.9	3.91	11.41	.79620
S6	Cp-----------------------	338	28.4	11.9	34.75	.80272
S7	Cp-----------------------	217	45.9	4.72	13.77	.79023
P	Cpc----------------------					.70911

[1]Data from Lee and others (1970, table 3). Z. E. Peterman, R. A. Hildreth, and W. T. Henderson, analysts.

[2]pCo, Precambrian Osceola Argillite of Misch and Hazzard (1962); CpCm, Precambrian and Cambrian Prospect Mountain Quartzite; Cp, Cambrian Pioche Shale; Cpc, Cambrian Pole Canyon Limestone.

plutons in the Kern Mountains and the Toana Range of eastern Nevada and concluded that all three probably resulted from anatexis of upper Precambrian argillites under conditions of relatively low oxygen fugacity, along a line that coincides roughly with the westward disappearance of a continental basement as indicated by the lead isotope data of Stacey and Zartman (1978). However we should note that our unpublished strontium data indicate that the edge of the continental basement is farther to the west.

Granites have been classified according to source materials by Chappell and White (1974). In the scheme, granites inferred to be derived from predominantly sedimentary (weathered) protoliths are S-types, whereas those derived from igneous source materials are I-types. The chemical, mineralogical, and isotopic criteria used to distinguish between S- and I-type granites have been summarized by Chappell and White (1974), Beckinsale (1979), Furgeson and others (1980), and O'Neil and Chappell (1977). The peraluminous nature of the Pole Canyon-Can Young Canyon pluton, as well as its content of muscovite and monazite, are indicative of an S-type granite. The $\delta^{18}O$ values of nine samples of this rock (10.6–12.1 per mil) support the idea that this intrusion was derived from an evolved protolith such as the Osceola Argillite. Indeed, six samples of this argilllite gave $\delta^{18}O$ values that ranged from 11.6 to 12.5 per mil (Lee and others, 1982).

Rubidium-strontium data for four whole-rock samples, a muscovite, a microcline megacryst, and an aplite-pegmatite are listed in table P1. The scatter in the $^{87}Sr/^{86}Sr$ values for the four whole-rock specimens is not unusual for muscovite granites. We therefore averaged the $^{87}Rb/^{86}Sr$ and $^{87}Sr/^{86}Sr$ values for the whole rocks to 1.44 and 0.71736, respectively. A regression (York, 1969) of this value for the whole-rock specimens, the muscovite, the microcline, and the aplite-pegmatite yields an age of 79.1 ± 0.5 Ma with an initial $^{87}Sr/^{86}Sr$ of 0.71574 ± 0.00003. Other isotope data (chap. D, this volume) support these conclusions and reaffirm the great similarities between this two-mica granite and that of the Kern Mountains, about 83 km to the north. The initial $^{87}Sr/^{86}Sr$ determined (0.71574) is well within the range representative of S-type granites. For comparison, a two-point isochron diagram for the muscovite-phenocrystic two-mica granite of the Kern Mountains is included in figure P2.

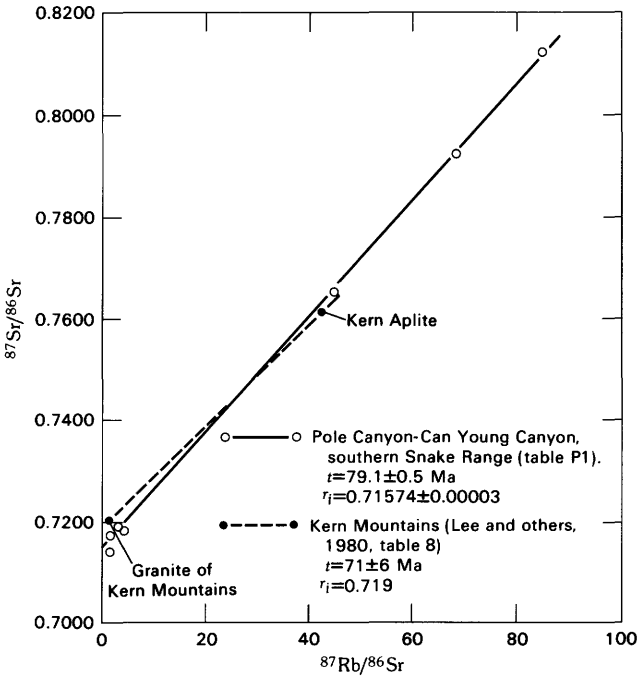

Figure P2. Strontium evolution diagram for the muscovite-phenocrystic two-mica granite of the Pole Canyon-Can Young Canyon area (fig. P1). The two-point isochron diagram for a practically identical muscovite-phenocrystic two-mica granite in the Kern Mountains is shown for comparison (Lee and others, 1980, fig. 11, table 8). t, time in millions of years; r_i, initial $^{87}Sr/^{86}Sr$.

INTRUSIVE ROCK OF THE SNAKE CREEK-WILLIAMS CANYON AREA

The Jurassic (Lee and others, 1968; Lee, Stern, and Marvin, 1981) intrusive of the Snake Creek-Williams Canyon area is separated from the just-described Upper Cretaceous two-mica granite of the Pole Canyon-Can Young Canyon area only by a septum of sedimentary rocks about 2 km long and 200 m (meters) wide (Lee and Van Loenen, 1971, p. 1). This Jurassic intrusive is undeformed, probably has not been eroded to a depth of much more than 300 m, and is well-exposed in contact with quartzite, shale, and limestone. Within a horizontal distance of 5 km, the intrusive grades from quartz monzonite (76 percent SiO_2, 0.5 percent CaO) where the host rock is quartzite to granodiorite (63 percent SiO_2, 4.5 percent CaO) where the host rock is limestone. Other major elements vary as would be expected in a normal differentiation sequence. Most minor elements show similar variations, the notable exceptions being the rare earths (Lee and Van Loenen, 1971, p. 24, 25). Cain (1974) showed that the distribution of rare-earth elements in this pluton can be attributed to their uptake in accessory minerals, which contain 80–98 percent of the rare earths (except europium) present in the rock.

Chemical analyses of this intrusive rock cluster within and near Bowen's (1937) thermal valley on the liquidus surface in the system $NaAlSi_3O_8$-$KAlSi_3O_8$-SiO_2 (Lee and Van Loenen, 1971, p. 32, 33). As emphasized by Tuttle and Bowen (1958), such a concentration of points is explained readily by liquid-crystal equilibria, but would be a remarkably fortuitous result of any mechanism not involving a magma. Based on a number of mineralogi-

cal and geochemical features summarized by Lee and Van Loenen (1971, p. 44, 45) we have concluded that the crystallizing magma was contaminated by reaction with country rock. In other words, the field and laboratory studies cited indicate that the intrusive rock of the Snake Creek-Williams Canyon area evolved through combined assimilation-fractional crystallization.

The results of recent oxygen isotope work (Lee, Friedman, and Gleason, 1982) also support the idea that both assimilation and fractional crystallization were involved in the development of the Snake Creek-Williams Canyon pluton. Whole-rock $\delta^{18}O$ values for 25 samples of this pluton range from 10.2 to 12.2 per mil, indicating that the magma was derived from an evolved (sedimentary) protolith. Moreover, there is a rather systematic increase in $\delta^{18}O$ values from the most mafic (63 percent SiO_2) to the most felsic (76 percent SiO_2) parts of the exposure. Enrichment of $\delta^{18}O$ in the felsic rock is consistent with a fractional crystallization model because most early crystallizing minerals (such as biotite, magnetite, epidote, and sphene) are ^{18}O-poor (Taylor, 1968).

Rubidium-strontium data for 13 samples of the Snake Creek-Williams Canyon pluton are listed in table P1. Ten samples fit an isochron with an indicated age of 155.2 ± 4 Ma and an initial $^{87}Sr/^{86}Sr$ of 0.70714 ± 0.00006 (fig. P3).

Samples 27, 28, and 59 (table P1, fig. P3) plot above the ten-point isochron just noted. They are displaced toward the "field" of the whole-rock samples from the two-mica granite of the Pole Canyon-Can Young Canyon area (table P1, fig. P2). This displacement is of particular interest because the Snake Creek-Williams Canyon pluton is in contact with the Osceola Argillite only in the area of samples 27, 28, and 59 (see Lee and Van Loenen, 1971, pl. 1), and as noted, there is ample evidence that the Pole Canyon-Can Young Canyon pluton formed through anatexis of this argillite and related sediments. The apatite-zircon relationship already noted is also of special interest here. In discussing the petrography and petrology of the Pole Canyon-Can Young Canyon pluton, Lee and Van Loenen (1971, p. 39) stated: "One of the most striking mineralogical distinctions of these rocks is the apatite-zircon relationship mentioned earlier. The apatite has a stubby habit, and almost all of the zircon in these rocks is present as tiny needlelike inclusions within this apatite. This is different from anything observed in the Snake Creek-Williams Canyon area, except in one small area north of Williams Canyon on the west side of the range, where (locs. 27, 28, and 59, pl. 1) the intrusive is exposed in contact with the Osceola Argillite. In this restricted area, the apatite carries a few grains of acicular zircon * * *."

Thus, rubidium-strontium results tend to confirm previous conclusions based on field, chemical, mineralogical and oxygen isotope data. Although the ten-point isochron supports a fractional crystallization model, the displacement of the points for samples 27, 28, and 59 is evidence that the country rock had some influence on the crystallizing intrusive in the area north of Williams Canyon, where the pluton is in contact with Osceola Argillite.

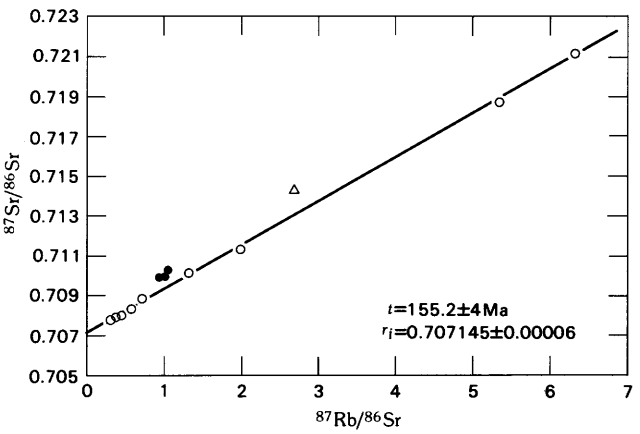

Figure P3. Strontium evolution diagram for the Snake Creek-Williams Canyon pluton (open circles). Samples 27, 28, 59 (solid circles) were collected from the extreme northwestern part of the pluton (fig. P1), where intrusive is in contact with the Osceola Argillite, and were not used in calculating the isochron. Sample 295–DL–64 (open triangle) is from the Willard Creek intrusive. t, time in millions of years; r_i, initial $^{87}Sr/^{86}Sr$.

The 155.2 ± 4 Ma rubidium-strontium age (fig. P3) for the Snake Creek-Williams Canyon pluton is in good agreement with the uranium-thorium-lead isotopic ages determined for zircon from this same pluton (Lee and others, 1968; Lee, Stern, and Marvin, 1981). The initial $^{87}Sr/^{86}Sr$ (0.70714 ± 0.00006) suggests a sialic protolith (Kistler and Peterman, 1973), in agreement with our $\delta^{18}O$ data. However, some of the chemical characteristics of this intrusion are ambiguous as indicators of the type of magma protolith. Thus, Na_2O is mostly >3.2 percent, and some of the larger xenoliths in the mafic parts of the intrusive contain hornblende (I-type granite). Normative corundum is both greater than 1 percent (S-type) and less than 1 percent (I-type). Perhaps the most striking ambiguity is apparent from study of the accessory minerals (Lee and Van Loenen, 1971, fig. 10). The most mafic parts of the intrusive (63 percent SiO_2) contain 2 weight-percent epidote, 1 percent sphene, 0.5 percent magnetite, and well-developed allanite, apatite, and zircon. As SiO_2 increases, the amounts and types of accessory minerals change gradually, until the most felsic parts of the intrusive (76 percent SiO_2) contain only ilmenite, garnet, monazite, and trace amounts of apatite and zircon. The entire suite of accessory minerals comprises only about 0.1 weight percent of the most felsic parts of the intrusion.

INTRUSIVE ROCK OF THE YOUNG CANYON-KIOUS BASIN AREA

Most of the granitoid rock exposed in the Young Canyon-Kious basin area (fig. P1) has been deformed cataclastically as a result of stresses related to late movement on the Snake Range décollement. The deformed and undeformed parts of this granitoid rock are separated by a fault. Concentrates of secondary muscovite recovered from the cataclastic part of the intrusion have K-Ar ages of 17–18 Ma, presumbably indicating the time of deformation and thus of the most recent movement on the Snake Range décollement (Lee and others, 1970).

The $\delta^{18}O$ values determined for three undeformed samples (8.7, 9.8, and 10.0 per mil) are relatively high compared with $\delta^{18}O$ values determined for 115 plutons from the Basin and Range Province (Lee and others, 1982). However, most samples of the cataclastic part of this intrusive have very low (to –2.6 per mil) $\delta^{18}O$ values. In general, the most intensely deformed samples usually have lowest $\delta^{18}O$ values, leading Lee, Friedman, and Gleason (chap. N, this volume) to conclude that this intrusive underwent oxygen isotope exchange with meteoric water during cataclasis.

Rubidium-strontium data for undeformed sample 98 ($\delta^{18}O$ of +10.0 per mil) and for cataclasized samples 103 and 110 ($\delta^{18}O$ of +0.1 and –1.1, respectively) are listed in table P1. These data gave an initial $^{87}Sr/^{86}Sr$ of 0.71203 ± 0.00010 at an age of 37.4 ± 1.5 Ma (fig. P4). The fact that both undeformed and deformed samples fit the isochron strongly suggests that cataclasis did not affect the rubidium-strontium systematics of this rock, even though it led to modification of both K-Ar ages and $^{18}O/^{16}O$.

Our results clearly show that there was Jurassic, Cretaceous, and Oligocene intrusive activity within the relatively restricted area of figure P1. The high initial $^{87}Sr/^{86}Sr$ of the Oligocene phase indicates derivation from sedimentary materials, an interpretation consistent with the relatively high $\delta^{18}O$ values found in the undeformed part of this intrusion.

TERTIARY APLITE

A wedge-shaped mass of Tertiary aplite separates cataclastic from undeformed intrusive rocks in the northwestern corner of Kious basin (fig. P1; Lee and Van Loenen, 1971). This aplite body is in fault contact with the adjacent Tertiary (37 Ma) intrusive rocks, possibly indicating that it represents late-stage felsic material that was squeezed into place by stresses resulting from movement on the Snake Range de'collement (Lee and Van Loenen, 1971). According to this interpretation, the aplite is related genetically to both the cataclastic and the undeformed intrusive with which it is in fault contact.

Rubidium-strontium data for sample 284–DL–63 (table P1), collected from an outcrop of aplite exposed about 5 km northwest of the wedge-shaped mass of Tertiary aplite just referred to, yields an apparent age of 28.5 Ma if it had the same initial strontium isotopic composition as did the intrusive in Young Canyon-Kious basin. This 28.5–Ma age indicates that the aplite phase is younger and is not related to the main intrusive mass of the Young Canyon-Kious basin area.

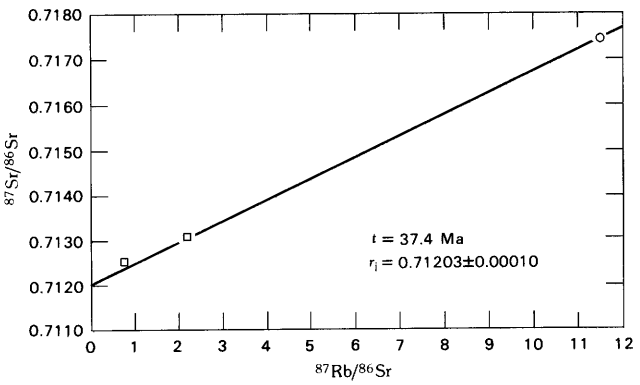

Figure P4. Strontium evolution diagram for the intrusive rock of the Young Canyon-Kious basin area (fig. P1), based on one sample of undeformed rock (open circle) and two samples of cataclasized rock (open squares). *t*, time in millions of years; r_i, initial $^{87}Sr/^{86}Sr$.

OSCEOLA STOCK

The area of intrusive rock referred to as the Osceola stock (fig. P1) by Armstrong (1966) has not been studied nearly as intensively as has the Snake Creek-Williams Canyon pluton, but preliminary work has indicated that the two intrusives are similar. Both plutons become more felsic from east to west, and both have relatively high $\delta^{18}O$ values (Lee and others, 1982). Rubidium-strontium results for the two plutons are similar (table P1), and the points for three samples of the Osceola stock would plot close to the Rb-Sr isochron for the Snake Creek-Williams Canyon pluton (fig. P3). However, taken alone, the data for the Osceola stock (fig. P5) give an age (145 Ma) slightly younger than the 155.4 ± 4 Ma determined (fig. P3) for the Snake Creek-Williams Canyon pluton. Data for the three samples of the Osceola stock give an initial $^{87}Sr/^{86}Sr$ of about 0.7075, slightly greater than the 0.70714 ± 0.00006 value obtained for the Snake Creek-Williams Canyon pluton. The results of U-Pb (uranium-lead) age work on a zircon fraction recovered from sample 177–MW–60 (chap. D, this volume) are in fair agreement with these Rb-Sr results for the Osceola stock.

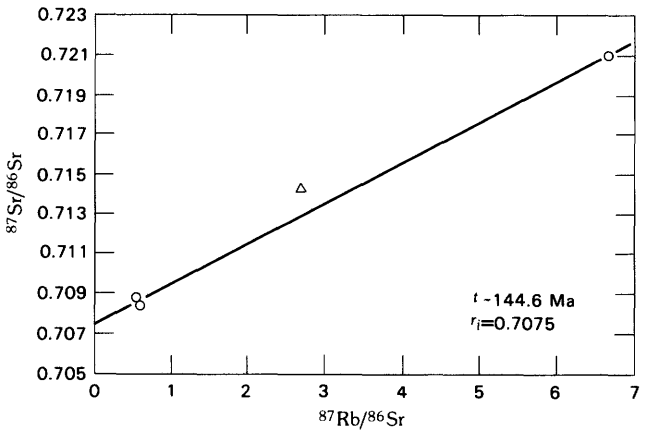

Figure P5. Strontium evolution diagram for the Osceola stock (fig P1). Sample 295–DL–64 (open triangle), from the Willard Creek mass, is not comagnatic with the Osceola stock (open circles). *t*, time in millions of years; r_i, initial $^{87}Sr/^{86}Sr$.

INTRUSIVE ROCKS OF WILLARD CREEK

The equigranular two-mica granite of the Willard Creek area (fig. P1) has been regarded as a felsic phase of the Osceola stock (Lee, Marvin, Stern, and Peterman, 1970; Lee, Kistler, Friedman, and Van Loenen, 1981; Lee, Friedman, and Gleason, 1982). However, Rb-Sr results for sample 295–DL–64 (table P1) show that the Willard Creek mass is not comagmatic with either the Osceola stock (fig. P5) or the intrusive rock of Snake Creek-Williams Canyon (fig. P3). Muscovite recovered from sample 295–DL–64 gave a K-Ar age of 151 ± 4 Ma. (Lee, Marvin, Stern, and Peterman, 1970, table 1), similar to the Rb-Sr ages determined for the Osceola stock (~145 Ma) and the Snake Creek-Williams Canyon pluton (155.4 ± 4 Ma). The data in table P1 gave an initial $^{87}Sr/^{86}Sr$ of 0.70857 for the Willard Creek mass at an age of 151 Ma. Although this value is somewhat higher than the initial ratios determined for the intrusive masses of the Osceola and Snake Creek-Williams Canyon areas, it is appreciably lower than the values (0.7111 to 0.7250) determined for four other two-mica granites in northeastern Nevada (Lee, Kistler, Friedman, and Van Loenen, 1981), which would indicate that the Willard Creek mass was generated from less radiogenic source materials than were the other two-mica granites in the area. On the other hand, the $\delta^{18}O$ value of sample 295–DL–64 was found to be 13.2 per mil (Lee, Friedman, and Gleason, 1981), and such a high value suggests that sedimentary materials were an important component in the source region of this two-mica granite.

INTRUSIVE ROCK OF LEXINGTON CREEK

The map of Whitebread (1969) shows the Lexington Creek pluton cut by a thrust fault; Lee, and others (1980) suggested that the foliation noted by Whitebread and by Drewes (1958) may have resulted from movement on the thrust before the pluton was crystallized completely. The original mineralogy of this pluton has been obscured somewhat by deuteric alteration that may have accompanied formation of the foliation. However, the unaltered intrusive apparently was a two-mica granite in which the biotite and muscovite were present as discrete crystals. This texture contrasts with that of the Pole Canyon-Can Young Canyon pluton, which has biotite euhedra present within muscovite phenocrysts.

Analysis of the zircon recovered from sample 378 suggests that Lexington Creek pluton is Cretaceous in age and was derived at least in part from a sedimentary source (chap. D, this volume). Muscovites recovered from three samples gave Late Cretaceous K-Ar ages ranging from 77.9 to 86.3 Ma (Lee and others, 1980). The 86.3–Ma age is assumed to be most nearly representative of the time of emplacement of this pluton because there may have been partial degassing of the analyzed micas as a result of heat stress related to late movement along the thrust fault that truncates the intrusive. Using 86 Ma as the emplacement age of this pluton results in a calculated ($^{87}Sr/^{86}Sr$) of 0.7114.

SEDIMENTARY ROCKS

Rubidium-strontium data are listed (table P1) for six samples of sedimentary rocks collected in the study area. Localities, $\delta^{18}O$ values, and chemical analyses of these rocks are given by Lee and Van Loenen (1971) and Lee and others (1982). Although the $^{87}Sr/^{86}Sr$ of these samples range from 0.70911 to 0.80317, most of the clastic rocks have ratios of about 0.8000. Some ratios may have been modified during the complex igneous and metamorphic history of this area (Lee and others, 1980).

SUMMARY AND CONCLUSIONS

Although a great deal of information has been accumulated on the intrusive rocks exposed in the area of figure P1 during the last 20 years, it has remained for the rubidium-strontium data presented here to resolve many of the questions regarding the complex history of these granitoid rocks. The magmatic activity of the area began with the emplacement of three plutons of Middle Jurassic age. These are the equigranular two-mica granite of the Willard Creek area and the calc-alkalic intrusives of the Osceola and Snake Creek-Williams Canyon areas. The calc-alkalic masses of the Osceola and Snake Creek areas had initial $^{87}Sr/^{86}Sr$ of 0.7075 and 0.707145 ± .00006, respectively. These are the lowest initial ratios determined for any of the intrusive rocks of the southern Snake Range, and they indicate source materials possibly in the lower continental crust (Kistler and Peterman, 1973). The initial ratio of the Willard Creek

pluton was somewhat higher at 0.70857, but this value is low compared with those of younger two-mica granites of the area.

After a period of quiescence lasting about 75 m. y. intrusive activity resumed with the emplacement of the Upper Cretaceous two-mica granites of the Pole Canyon-Can Young Canyon and the Lexington Creek areas. Although these two-mica granites are only 10 km apart and each crystallized from a relatively evolved magma, they are different rock types (Lee, Kistler, Friedman, and Van Loenen, 1981). For example, the Lexington Creek mass contains discrete grains of both muscovite and biotite, whereas all the biotite in the Pole Canyon-Can Young Canyon pluton is present as euhedra within large phenocrysts of muscovite.

The next period of quiescence lasted almost 50 m. y. and ended with the emplacement of the 37-Ma-old calc-alkalic mass of the Young Canyon-Kious basin area, and the penecontemporaneous formation of an aplite phase in the same general area. These intrusive phases had a relatively high initial ratio ($^{87}Sr/^{86}Sr=0.71203$).

Field studies indicate that none of the intrusive masses exposed in the southern Snake Range has been eroded to a depth of more than about 300 m. Thus, the tops of these intrusives are present at about the same level, even though they range in age from Jurassic to Oligocene. Furthermore, initial $^{87}Sr/^{86}Sr$ tend to increase with decreasing age. These observations suggest that the younger masses were emplaced at progressively more shallow depths, and crystallized from generally more evolved magmas. In addition, all the plutons of the southern Snake Range are exposed at or beneath the level of the Snake Range décollement. Indeed, the Young Canyon-Kious Basin and the Lexington Creek intrusive masses were affected by late movement on this structure (Lee, Marvin, Stern, and Peterman, 1970; Lee, Marvin, and Mehnert, 1980).

There is evidence to indicate that the spatial relationships between the intrusive rocks and the thrust faults is not unusual in the eastern Great Basin (chap. N, this volume). There also appears to be a confluence of regional igneous types in the southern Snake Range. We have noted the similarities between the distinctive muscovite-phenocrystic two-mica granite of the Pole Canyon-Can Young Canyon area and that of the Kern Mountains, about 83 km to the north. Another similar pluton is present farther north in the Toana Range of Elko County, Nev., and extends the north-south trend defined by these distinctive granites to about 225 km (Lee, Kistler, Friedman, and Van Loenen, 1981). The Middle Jurassic calc-alkalic plutons in the Osceola and the Snake Creek-Williams Canyon areas are similar in age and petrology to the Notch Peak intrusive mass (169 ± 3 Ma) of the House Range in western Utah (chap. D, this volume) and to the southern part of the intrusive (152 Ma) outcrop of the Gold Hill, Utah, area (Stacey and Zartman, 1978). The middle Tertiary igneous event apparent in the Young Canyon-Kious basin area is represented by the Oligocene (38 Ma) pluton that makes up the northern part of the intrusive outcrop of the Gold Hill, Utah, area (Stacey and Zartman, 1978).

Finally, we note that the sequence of igneous events described here is remarkably similar to that found in the Ruby Mountains of Elko County, about 200 km northwest of the area of figure P1. Jurassic (160 ± 2 Ma), Cretaceous (83 ± 1.3 Ma) and Tertiary (31.9 ± 1.2 Ma) intrusive rocks all are present in the Ruby Mountains (Kistler and others, 1981).

REFERENCES CITED

Armstrong, R. L., 1966, K-Ar dating using neutron activation for Ar analysis: Geochimica et Cosmochimica Acta, v. 30, no. 5, p. 565–600.

Beckinsale, R. D., 1979, Granite magmatism in the tin belt of southeast Asia, *in* Atherton, M. P., and Tarney, J., eds., Origin of granite batholiths; geochemical evidence: Kent, United Kingdom, Shiva Publishing, Ltd., 148 p.

Bowen, N. L., 1937, Recent high-temperature research on silicates and its significance in igneous geology: American Journal of Science, v. 33, no. 193, p. 1–21.

Cain, D., 1974, The determination and interpretation of rare earth abundances in hybrid granitoid rocks of the southern Snake Range, Nevada: Golden, Colo. Colorado School of Mines, M.S. thesis, 94 p.

Chappell, B. W., and White, A.J.R., 1974, Two contrasting granite types: Pacific Geology, v. 8, p. 173–174.

Drewes, H., 1958, Structural geology of the southern Snake Range, Nevada: Geological Society of America Bulletin, v. 69, no. 2, p. 221–239.

Furgeson, J., Chappell, B. W., and Goleby, A. B., 1980, Granitoids in the Pine Creek geosyncline: Vienna, International Atomic Energy Agency, p. 73–89.

Hose, R. K., and Blake, M. C., 1976, Geology of White Pine County, Nevada: Nevada Bureau of Mines and Geology Bulletin 85, pt. 1, p. 1–35.

Kistler, R. W., Ghent, E. D., and O'Neil, J. R., 1981, Petrogenesis of garnet two-mica granites in the Ruby Mountains, Nevada: Journal of Geophysical Research, v. 86, no. B11, p. 10591–10607.

Kistler, R. W., and Peterman, Z. E., 1973, Variations in Sr, Rb, K, Na and initial $^{87}Sr/^{86}Sr$ in Mesozoic granitic rocks and intruded wall rocks in central California: Geological Society of America Bulletin, v. 84, p. 3489–3512.

Lee, D. E., Friedman, I., and Gleason, J. D., 1981, Map showing the oxygen isotope composition of granitoid rocks of the Basin-Range Province: U.S. Geological Survey Miscellaneous Field Studies Map MF–1305, scale 1:3,168,000.

———1982, The oxygen isotope composition of granitoid and sedimentary rocks of the southern Snake Range, Nevada: Contributions to Mineralogy and Petrology, v. 79, p. 150–158.

Lee, D. E., Kistler, R. W., Friedman, I., and Van Loenen, R. E., 1981, Two-mica granites of northeastern Nevada: Journal of Geophysical Research, v. 86, no. B11, p. 10607–10616.

Lee, D. E., Marvin, R. F., and Mehnert, H. H., 1980, A radiometric age study of Mesozoic-Cenozoic metamorphism in eastern White Pine County, Nevada, and nearby Utah, *in* Geologic studies in White Pine County, Nevada: U.S. Geological Survey Professional Paper 1158–C, p. 17–28.

Lee, D. E., Marvin, R. F., Stern, T. W., and Peterman, Z. E., 1970, Modification of potassium-argon ages by Tertiary thrusting in the Snake Range, White Pine County, Nevada, *in* Geological Survey research 1970: U.S. Geological Survey Professional Paper 700–D, p. D92–D102.

Lee, D. E., Stern, T. W., and Marvin, R. F., 1981, Uranium-thorium-lead isotopic ages of zircon from the southern Snake Range, Nevada: Isochron/West, no. 31, p. 25.

Lee, D. E., Stern, T. W., Mays, R. E., and Van Loenen, R. E., 1968, Accessory zircon from granitoid rocks of the Mount Wheeler mine area, Nevada, *in* Geological Survey research 1968: U.S. Geological Survey Professional Paper 600–D, p. D197–D203.

Lee, D. E., and Van Loenen, R. E., 1970, Biotites from hybrid granitoid rocks of the southern Snake Range, Nevada, *in* Geological Survey research 1970: U.S. Geological Survey Professional Paper 700–D, p. D196–D206.

———1971, Hybrid granitoid rocks of the southern Snake Range, Nevada: U.S. Geological Survey Professional Paper 668, 48 p.

Masi, U., O'Neil, J. R., and Kistler, R. W., 1976, Stable isotope systematics in Mesozoic granites near the San Andreas and Garlock fault systems, California [abs.]: Geological Society of America, Abstracts with Programs, v. 8, p. 998.

———1981, Stable isotope systematics in Mesozoic granites of central and northern California and southwestern Oregon: Contributions to Mineralogy and Petrology, v. 76, p. 115–126.

Misch, P., and Hazzard, J. C., 1962, Stratigraphy and matamorphism of Late Precambrian rocks in central northeastern Nevada and adjacent Utah: American Association of Petroleum Geologists Bulletin, v. 46, no. 3., pt. 1, p. 289– 343.

O'Neil, J. R., and Chappell, B. C., 1977, Oxygen and hydrogen isotope relations in the Berridale batholith: Journal of the Geological Society of London, v. 133, p. 559–571.

Stacey, J. S., and Zartman, R. E., 1978, A lead and strontium isotopic study of igneous rocks and ores from the Gold Hill mining district: Utah Geology, v. 5, p. 1–15.

Taylor, H. P., Jr., 1968, The oxygen isotope geochemistry of igneous rocks: Contributions to Mineralogy and Petrology, v. 19, p. 1–71.

Taylor, H. P., and Silver, L. T., 1978, Oxygen isotope relationships in plutonic igneous rocks of the Peninsula Ranges batholith, southern and Baja, California, *in* Short papers of the Fourth International Conference, geochronology, cosmochronology and isotope geology: U.S. Geological Survey Open-File Report 78–701, p. 423–426.

Tuttle, O. F., and Bowen, N. L., 1958, Origin of granite in the light of experimental studies in the system $NaAlSi_3O_8$–$KA1Si_3O_8$–H_2O: Geological Society of America Memoir 74, 153 p.

Whitebread, D. H., 1969, Geologic map of the Wheeler Peak and Garrison quadrangles, White Pine County, Nevada, and Milford County, Utah: U.S. Geological Survey Miscellaneous Geologic Investigations Map I–578, scale 1:48,000.

York, D., 1969, Least-square fitting of a straight line with correlated errors: Earth and Planetary Science Letters, v. 5, p. 320–324.

1986

U.S. GEOLOGICAL SURVEY BULLETIN 1622

SHORTER CONTRIBUTIONS TO ISOTOPE RESEARCH

LEAD-ISOTOPE EVIDENCE FOR A PRE-GRENVILLE CRUST UNDER THE PIEDMONT OF GEORGIA

Chapter Q

By J. S. STUCKLESS, D. B. WENNER[1], and I. T. NKOMO

CONTENTS

FIGURES

[1]Department of Geology, University of Georgia, Athens, GA 30602

TABLES

Abstract

Isotopic data for the Elberton Granite batholith, Georgia, do not yield isochrons in the uranium-lead, thorium-lead, or lead-lead systems except for samples that have essentially identical $\delta^{18}O$ values. Three-point isochrons in the uranium-lead and thorium-lead systems yield ages that are compatible with those reported for zircons. Slopes of feldspar and whole-rock pairs in the lead-lead system also are compatible with a 320-million-year age for crystallization.

Data in the lead-lead system, corrected to the age of intrusion, yield an excellent linear array that is interpreted to be a secondary isochron that retained the age of the protolith. This age is interpreted to be $1{,}720 \pm 30$ million years. Although this age is much older than that obtained for Grenville-age basement rocks in the southeastern United States, at least three other studies have suggested that rocks of this age may exist.

The Elberton Granite batholith is different from many isotopically studied granites in that only one of 14 whole-rock samples has any evidence of recent uranium mobility in response to near-surface effects. Like many other granites, the granite from the Elberton batholith has a wide range and high mean for thorium-uranium values. However, the data strongly suggest that this feature developed at the time of intrusion rather than through recent uranium mobilization in the near-surface environment.

The protolith for the Elberton batholith is interpreted to be a complex mixture of two heterogenous sources consisting of rocks of mafic and intermediate composition with the latter having a significant pelitic component. Interpretation of the compositions of the protoliths presents an enigma in that the presumed mafic end member had a higher $^{206}Pb/^{204}Pb$ value at the time of granite formation than did the more intermediate end member. This anomalous feature may reflect a trace-element difference between the two sources or may suggest an early history of metamorphism of the two sources that more strongly affected the intermediate end-member protolith. These two end-member sources appear to be consistent with other geochemical and geophysical data that suggest that a mafic protolith underlies both the Charlotte belt and the Carolina slate belt and that an intermediate end member underlies the Inner Piedmont belt.

INTRODUCTION

The Elberton batholith consists uniformly of a fine-grained biotite granite that is exposed over an area of ~ 500 km^2 (square kilometers) in northeastern Georgia. This granite body represents one of a series of discrete late orogenic granitic plutons that are exposed throughout the southern Piedmont province.

The batholith is intruded along the eastern flank of older (the metamorphic age is estimated at ~380–420 Ma (million years) by Dallmeyer, 1978) high-grade, polydeformed metasedimentary and metavolcanic rocks comprising the Inner Piedmont belt (fig. Q1). Immediately to the southeast of the batholith, a major, regionally extensive pre-Elberton-age ductile shear zone called the Middleton-Lowndesville fault zone, separates the Inner Piedmont belt from other major lithotectonic belts, such as the Charlotte and Carolina slate belts (Whitney and Stormer, 1980). The latter two belts represent a series of variably metamorphosed and deformed volcanic, volcaniclastic, and volcanic sedimentary units that may in part constitute an ancient protoisland-arc system (Whitney and others, 1978).

The Elberton Granite magma was intruded at an estimated depth of from 12 to 15 km (Stormer and others, 1980) about 320 Ma (Ross and Bickford, 1980). Subsequently, rapid uplift produced argon retention ages of hornblende at ~270 Ma and of biotite at ~240 Ma (Dallmeyer and others, 1981). Uplift probably was completed during the Triassic when diabase dikes were intruded and quenched against existing units about 200 Ma.

The regional pattern of oxygen and strontium isotopic compositions of the late orogenic granitic plutons of the southern Piedmont (Wenner, 1981) combined with seismic (Cook and others, 1979) and gravity (Long, 1979) data have been interpreted as indicating that thinning older continental crustal material may underlie the Elberton batholith (see for example, the tectonic models by Whitney and others, 1980). Accordingly, the Elberton batholith essentially may be rooted to its protolith (Ellwood and Whitney, 1980), which, according to strontium- and oxygen-isotope data (Wenner, 1981), may consist of gradational subcrustal sequences of continental crustal to subcrustal mafic island-arc materials. This suggestion is consistent with the earlier reported zircon age of 450 Ma (Grunenfelder and Silver, 1958) from the Elberton Granite batholith, which may represent an inherited older component.

Detailed petrological and chemical studies (Ellwood and others, 1980; Stormer and others, 1980), as well as oxygen and strontium isotopic studies (Wenner, 1981) reveal that the Elberton batholith is essentially homogenous in its texture, major-mineral content, and major-element chemistry, but is extremely heterogeneous in certain dispersed trace elements (for example, Rb, Sr, Ba) and $^{18}O/^{16}O$ and initial $^{87}Sr/^{86}Sr$. These trace-element and isotopic heterogeneities observed throughout the batholith are interpreted as representing the preservation of magmatically produced stripes resulting from viscous laminar flowage.

Partial fusion of a lithologically variable protolith could produce a magma that would be essentially homogeneous in its major-element chemistry, yet would be heterogeneous in certain trace elements and isotopic ratios (Whitney and others, 1980).

The variability in initial strontium isotopic compositions noted for the Elberton batholith (Ellwood and others, 1980; Dallmeyer and others, 1981) has presented difficulties in obtaining accurate Rb-Sr (rubidium-strontium) whole-rock ages. Analysis of 13 whole-rock samples, in fact, reveals the presence of two generally parallel isochrons (Ellwood and others, 1980). One gives a generally consistent age of 350 ± 11 Ma, but this appears to be somewhat older than the U-Pb (uranium-lead) zircon intercept age of 320 ± 20 Ma (Ross and Bickford, 1980). Because of apparent problems in the Rb-Sr systematics, the zircon age is presumed to be a more accurate indication of the crystallization age of the Elberton granite batholith.

ANALYTICAL PROCEDURES

Uranium, thorium, and lead concentrations and the isotopic composition of lead were determined for 14 whole-rock and 5 potassium feldspar separates by isotope dilution and mass spectrometry (table Q1). Whole-rock analyses were made on about 1-g (gram) splits of finely pulverized material. Feldspar analyses utilized about 1-g of sample and were washed in warm HNO_3 prior to dissolution. Chemical procedures generally are those described by Tatsumoto and others (1972) except that final purification of lead was accomplished by electroplating (Barnes and others, 1973), and compositions and concentrations were determined on a single dissolution followed by liquid aliquoting.

Mass spectrometric analysis was done on an NBS-type (National Bureau of Standards) 12-inch radius-of-curvature machine. Lead compositions and concentrations were obtained by use of the silica gel-H_3PO_4 technique and a triple filament mode of ionization. Mass spectrometric results with more than 0.1 percent variation were rejected, and the sample was reanalyzed completely. Results reported in table Q1 are precise to ±0.1 percent (2σ) for compositions and ±0.2 percent (2σ) for concentrations.

Regression of best-fit lines was accomplished using the methods of York (1969). Age calculations for secondary isochrons were made with the equations of Rosholt and others (1973). Isotopic and decay constants used are those recommended by the International Union of Geological Sciences Subcommission on Geochronology (Steiger and Jäger, 1977).

Table Q1. Uranium, thorium, and lead concentrations (in parts per million) and the isotopic composition of lead for whole-rock and potassium-feldspar (Kf) samples from the Elberton Granite batholith, Georgia

	Concentration			Atomic ratio		
Sample No.	U	Th	Pb	$^{206}Pb/^{204}Pb$	$^{207}Pb/^{204}Pb$	$^{208}Pb/^{204}Pb$
EB-2	5.47	46.23	31.24	18.916	15.668	39.774
EB-2a	4.57	46.48	28.91	18.786	15.652	39.765
EB-8	6.96	42.92	29.02	18.896	15.667	39.700
EB-9	3.84	20.72	22.39	19.031	15.680	39.425
EB-12	1.95	36.63	27.67	18.543	15.651	39.454
EB-12Kf	0.33	0.74	58.03	18.425	15.645	38.265
EW-13	1.52	45.83	25.98	18.526	15.567	40.106
EW-17	1.91	45.84	25.78	18.570	15.649	40.090
EW-21	4.35	45.58	34.45	18.420	15.619	39.498
EW-21a	2.46	35.40	36.51	18.396	15.616	39.100
EW-21aKf	0.71	1.02	87.15	18.285	15.610	38.564
EW-23	1.17	50.16	24.69	18.488	15.650	40.273
EW-23a	2.73	39.91	25.01	18.510	15.636	39.661
EW-23aKf	0.12	0.42	59.58	18.333	15.627	38.314
EW-29	3.34	28.07	21.97	18.996	15.688	39.632
EW-29a	5.93	21.19	21.45	18.621	15.615	39.073
EW-29aKf	0.63	1.46	53.68	18.485	15.607	38.234
EW-42	6.12	34.85	33.35	18.802	15.651	39.391

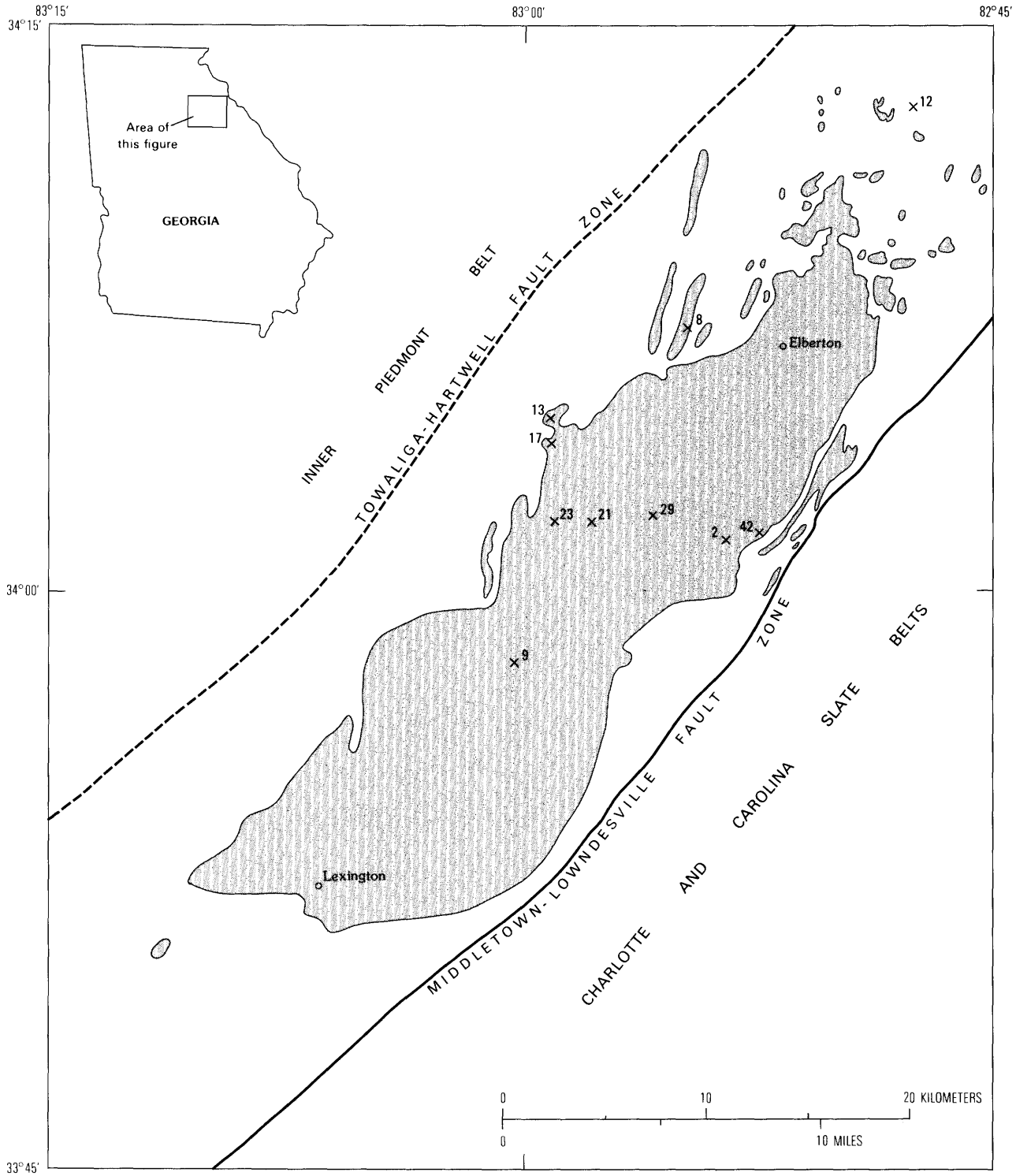

Figure Q1. Generalized geologic map (modified from Whitney and Stormer, 1980) showing location of the Elberton Granite batholith (stippled where exposed), Georgia, the relationship of the granite to the Inner Piedmont and Charlotte-Carolina slate belts, and sample localities. Contact dashed where uncertain.

Oxygen isotope data (table Q2) were obtained following the fluorine extraction procedure described by Taylor and Epstein (1962). Analyses were made on a VG Micromass[2] model 602C modified with a PSC data acquisition and control system, $^{18}O/^{16}O$ data are reported relative to SMOW (Standard Mean Ocean Water), and are calibrated relative to the NBS-28 standard that has a defined value of 9.61 per mil (parts per thousand).

[2]Use of trade names is for descriptive purposes only and does not imply endorsement by the U.S. Geological Survey.

RESULTS AND DISCUSSION

Geochronology

The Pb-Pb, Th-Pb, and U-Pb whole-rock systems do not yield isochrons within the limits of analytical error (figs. Q2, Q3, and Q4). These results are similar to the Rb-Sr whole-rock results for which scatter has been attributed to variations in the initial $^{87}Sr/^{86}Sr$ (Whitney and others, 1980). Four samples that have $\delta^{18}O$ values of 7.6–7.7 per mil, which apparently are free of contamination from the country rock, yield an Rb-Sr isochron of 319 ± 26 Ma which is in good agreement with the zircon

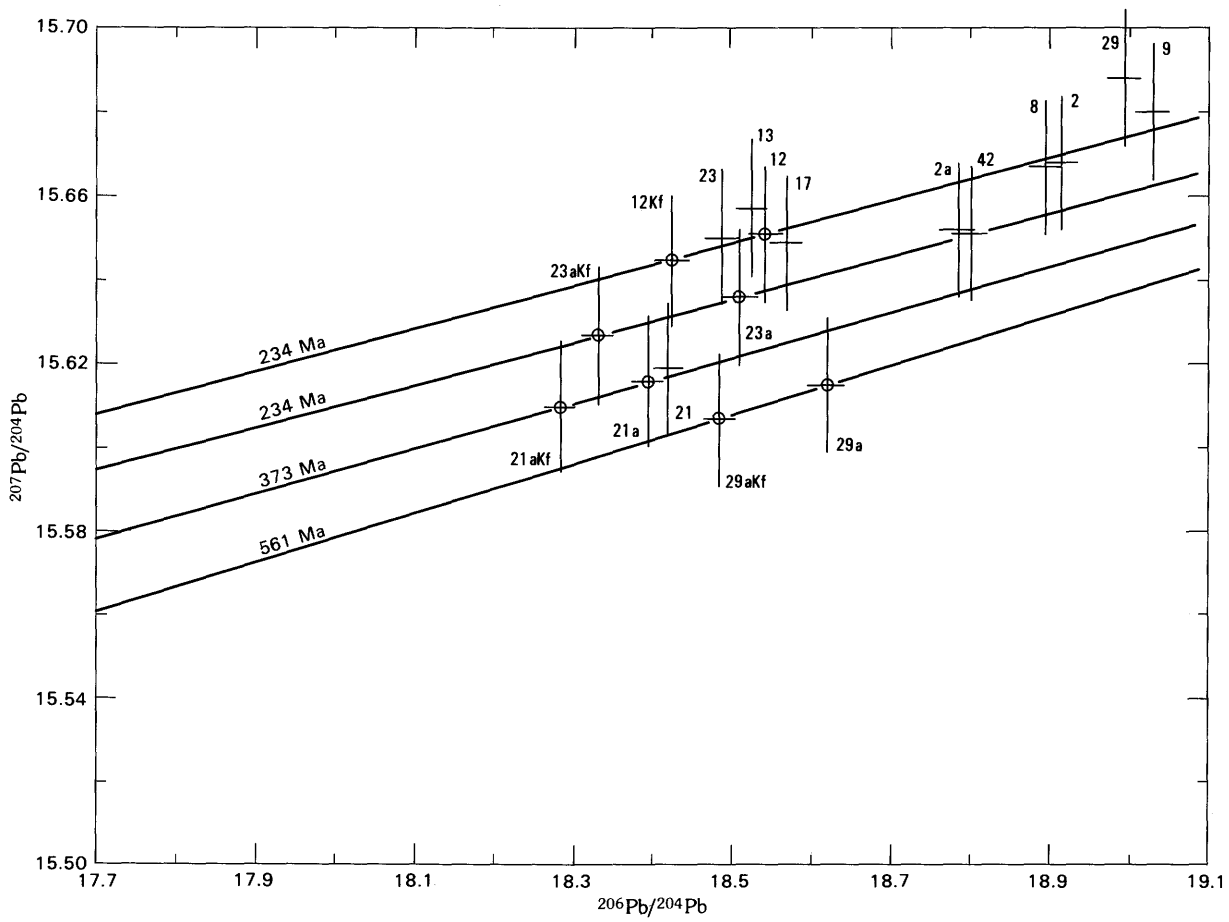

Figure Q2. Lead-lead diagram for whole-rock and feldspar samples (suffix Kf) from the Elberton Granite batholith, Georgia. Slopes for two-point isochrons (from top to bottom) correspond to ages of 234, 234, 373, and 561 Ma. Symbol size corresponds to $\pm 2\sigma$. Prefix letters EB and EW have been omitted from sample numbers to save space.

age of 320 ± 20 Ma (Ross and Bickford, 1980). Three samples that have similar $\delta^{18}O$ values of 7.3–7.4 per mil yield Th-Pb and U-Pb isochrons of 331 ± 46 Ma and 325 ± 19 Ma, respectively (figs. Q3 and Q4).

The correspondence of the U-Pb and Th-Pb ages is somewhat surprising in view of the well-documented mobility of uranium in many other whole-rock granite systems (Rosholt and others, 1973; Manton, 1973; Stuckless and Nkomo, 1978; Nkomo and others, 1978; and Stuckless, Bunting, and Nkomo, 1981; Stuckless, Nkomo, and Doe, 1981). If the U-Pb and Th-Pb whole-rock systems have been closed for all samples, then the lead compositions at the time of crystallization can be calculated.

Feldspar data (table Q1) are consistent with results reported for potassium feldspars from granites for which closed-system behavior for lead can be documented (Rosholt and others, 1973; Ludwig and Silver, 1977; Stuckless and Nkomo, 1978). Slopes of feldspar and whole-rock pairs in the Pb-Pb system (fig. Q2) approximate an age of 320 Ma, but all feldspars (corrected for the in-place accumulation of radiogenic lead) are much more radiogenic than the calculated initial leads for the whole-rock samples (table Q3). Furthermore, feldspar whole-rock pairs in the Th-Pb and U-Pb systems (figs. Q3 and Q4) do not yield lines whose slopes correspond to 320 Ma.

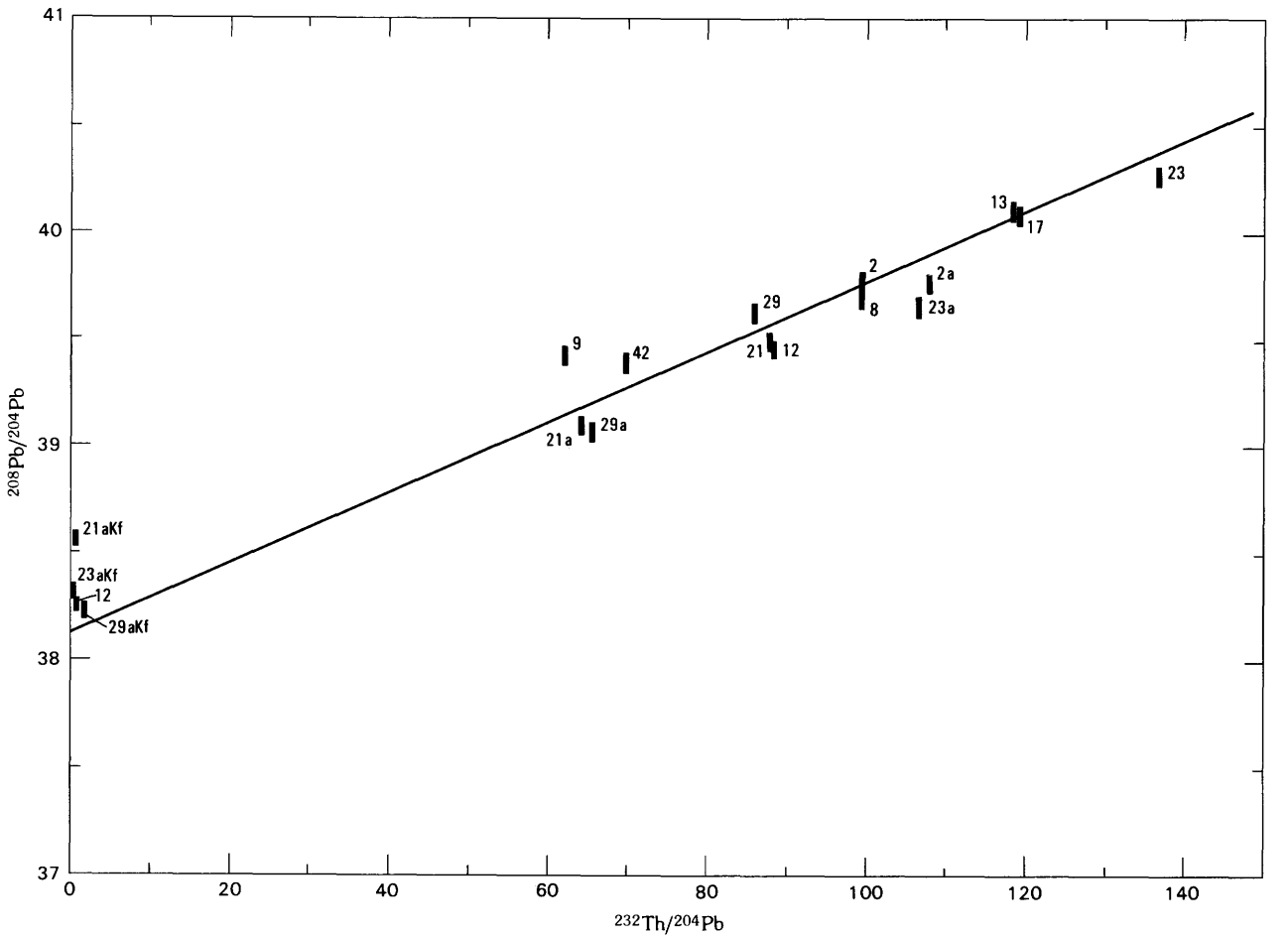

Figure Q3. Thorium-lead diagram for whole-rock and feldspar (suffix Kf) samples from the Elberton Granite batholith, Georgia. Regressed line (through points EB–2, EW–13, and W–17) has a slope of 0.01652 ± 0.0021 and an intercept of 38.129 ± 9,269 (at the 95–percent confidence level) that corresponds to an age of 331 ± 46 Ma. Symbol size corresponds to ±2σ. Prefix letters EB and EW have been omitted from sample numbers to save space.

Several studies (for example, Stuckless, Nkomo, and Doe, 1981) have suggested that whole-rock systems may remain closed with respect to lead because potassium feldspar serves as a trap for mobilized radiogenic lead. Feldspar from the Elberton Granite batholith is similar to other feldspars with a documented excess of radiogenic lead (Ludwig and Silver, 1977) in that it contains abundant microinclusions and alteration products. Thus feldspar data for four samples (EB–12, EW–21a, EW–23a, and EW–29a) seem to support the conclusion reached for three other samples (EB–2, EW–13, and EW–17) that lead at least has followed closed-system behavior, on a whole-rock scale, from the time of intrusion to the present. Calculation of initial lead compositions at the time of intrusion on the basis of present-day uranium and lead concentrations is therefore reasonable with the caveat that some scatter may result from gain or loss of either element.

Calculated initial $^{206}Pb/^{204}Pb$ and $^{207}Pb/^{204}Pb$ values are colinear within the limits of analytical error (fig. Q5) without consideration of errors caused by age assumptions, concentration errors, or open-system behavior by either uranium or lead. The resulting line can be interpreted as a mixing line or a secondary isochron. Several arguments suggest that even if the linear array is the result of mixing of two source regions, the source regions are related genetically and thus the slope of the line has age significance.

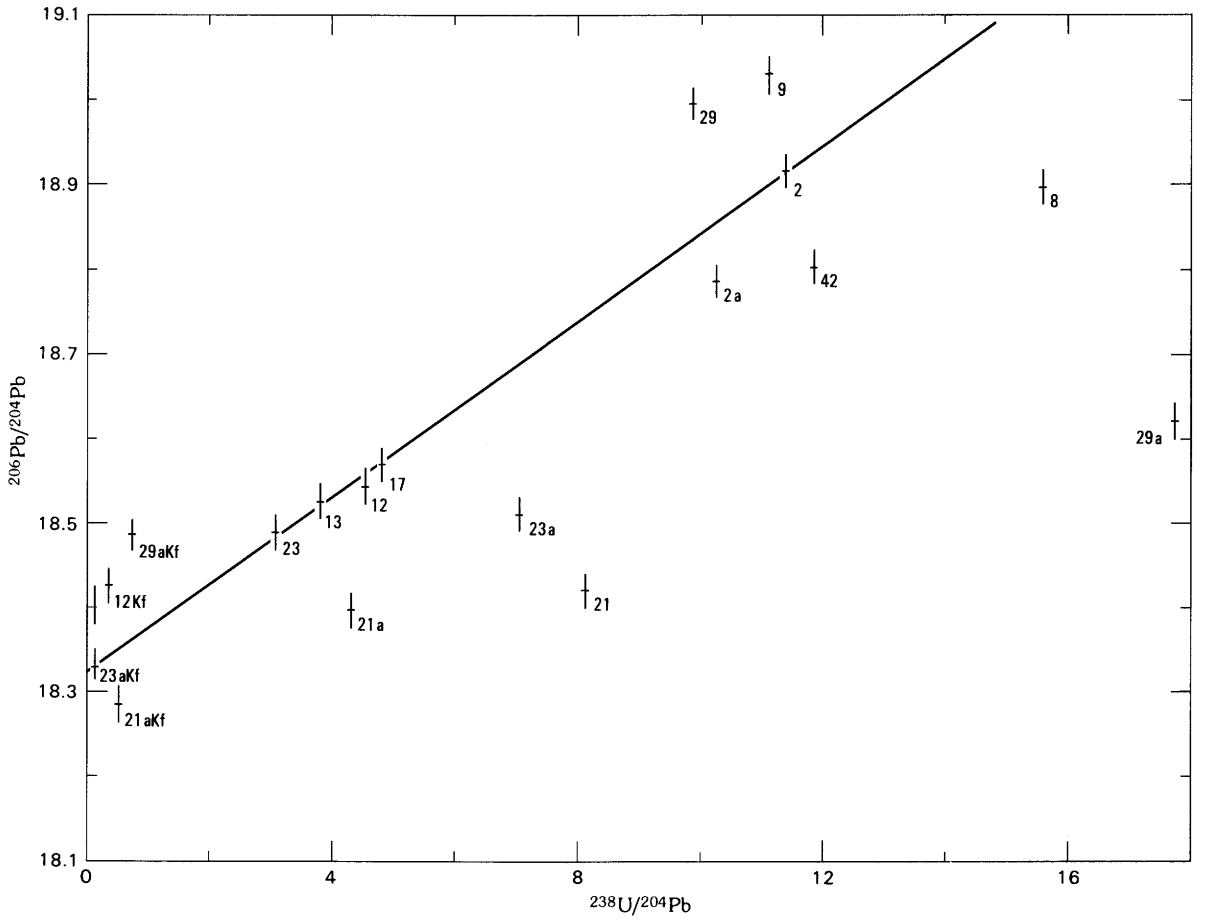

Figure Q4. Uranium-lead diagram for whole-rock and feldspar (suffix Kf) samples from the Elberton Granite batholith, Georgia. Regressed line (through points EW–13, EW–17, and EB–2) has a slope of 0.051788 ± 0.003054 and an intercept of 18.325 ± 0.023 at the 95–percent confidence level that corresponds to an age of 325 ± 19 Ma. Symbol size represents $\pm 2\sigma$ errors. Prefix letters EB and EW have been omitted from sample numnbers to save space.

Table Q2. Oxygen isotope compositions (in per mil) and lead isotope ratios corrected for the growth of radiogenic lead from 320 Ma to the present for for whole-rock and potassium feldspar (Kf) samples of the Elberton Granite batholith, Georgia

[Leaders (---) indicate not analyzed]

Sample No.	$\delta^{18}O$	$^{206}Pb/^{204}Pb$	$^{207}Pb/^{204}Pb$	$^{208}Pb/^{204}Pb$
EB-2	7.4	18.336	15.637	38.185
EB-2a	---	18.263	15.624	38.042
EB-8	7.8	18.102	15.625	38.114
EB-9	6.6	18.464	15.650	38.434
EB-12	8.7	18.312	15.639	38.046
EB-12Kf	---	18.407	15.644	38.252
EW-13	7.4	18.332	15.647	38.213
EW-17	7.3	18.325	15.636	38.182
EW-21	8.7	18.006	15.597	38.093
EW-21a	---	18.176	15.604	38.076
EW-21aKf	---	18.259	15.609	38.552
EW-23	7.1	18.331	15.642	38.090
EW-23a	---	18.151	15.617	37.960
EW-23aKf	---	18.327	15.627	38.307
EW-29	6.9	18.492	15.661	38.261
EW-29a	---	17.718	15.567	38.027
EW-29aKf	---	18.447	15.605	38.206
EW-42	7.7	18.178	15.619	38.276

Derivation of the Elberton Granite batholith through the mixing of magma from two geochemically distinct sources is highly probable because of its unique location along the boundary of two geologic provinces (fig. Q1). Whitney and Wenner (1980) and Wenner (1981) have summarized data that show chemical and isotopic differences between the post-metamorphic, late-orogenic granites of the Inner Piedmont region and those of the Charlotte-Carolina slate belts. The former yield characteristics typical of evolved granites derived from a crustal source. Some are strongly peraluminous, all have relatively high $\delta^{18}O$ values, and the few that have been examined have initial $^{87}Sr/^{86}Sr$ values greater than 0.710. Granites within the Charlotte-Carolina slate belts generally are metaluminous, have distinctly lower $\delta^{18}O$ values and have lower initial $^{87}Sr/^{86}Sr$ values. The Elberton batholith has characteristics between these extremes as shown for oxygen and strontium isotope data on figure Q6.

If the Elberton batholith formed by mixing of magma from two source regions that had a common heritage, the two source regions would have the same common lead. Granites derived from either or both of these source regions would retain characteristics of the lead common to both source regions. Thus, at the time of intrusion (assuming no contamination for extraneous leads) all lead compositions should plot along a line starting at the common or initial lead composition and extending to the lead from the domain of highest U/Pb.

Table Q3. Thorium-lead, uranium-lead, and thorium-uranium just prior to generation of the granite(initial) and at present, and percent change for whole-rock samples of the Elberton Granite batholith, Georgia

Sample No.	$^{232}Th/^{204}Pb$		Percent	$^{238}U/^{204}Pb$		Percent	Th/U		Percent
	Initial	Present	change	Initial	Present	change	Initial	Present	change
EB-2	39.36	99.59	153.0	10.53	11.40	8.26	3.67	8.45	130.3
EB-2a	37.41	108.0	188.7	10.24	10.27	0.29	3.58	10.17	184.1
EB-8	38.39	99.40	158.9	9.59	15.60	62.7	3.93	6.17	57.0
EB-9	42.76	62.09	45.2	11.03	11.14	1.0	3.81	5.40	41.7
EB-12	37.47	88.25	135.5	10.43	4.55	-56.4	3.53	18.78	432.0
EW-13	39.75	118.6	198.4	10.51	3.81	-63.8	3.71	10.14	173.3
EW-17	39.32	119.6	204.2	10.48	4.82	-54.0	3.69	24.00	552.2
EW-21	38.10	88.07	131.2	9.20	8.13	-22.5	4.07	10.48	157.5
EW-21a	37.38	64.17	69.4	9.89	4.32	-56.3	3.76	14.39	282.7
EW-23	38.06	136.8	259.4	10.51	3.09	-70.6	3.55	42.87	1108
EW23a	36.29	106.6	193.7	9.78	7.06	-27.8	3.64	14.62	301.7
EW-29	40.40	85.93	112.7	11.16	9.89	-11.38	3.55	8.40	136.6
EW-29a	37.20	65.55	76.2	8.04	17.76	120.9	4.55	3.57	-21.5
EW-42	40.61	69.84	72.0	9.97	11.86	19.0	4.00	5.69	42.3
Average	38.79	93.8	142.3	10.10	8.84	-10.8	3.79	13.08	255.5
1σ	±1.70	±23.1	±62.6	±0.80	±4.54	±53.4	±0.27	±10.24	±291.8
Stacey and Kramers (1975).	36.84			9.74			3.78		

A line formed by the mixing of two unrelated sources also would extend from an extreme low value to an extreme high value; however, if linearity for the leads is perfect, then linearity for other variables should be as good except under highly fortuitous circumstances. Correlation between initial thorogenic and uranogenic leads is good for the Elberton (fig. Q7) but not as good as that for the two uranogenic leads (fig. Q4), which implies more than two Th/U relative to Th/Pb or U/Pb in the source region. Similarly the correlation between initial uranogenic lead composition and oxygen isotope compositions (fig. Q8) or initial strontium composition and oxygen isotope compositions (fig. Q6) implies more than two end members in the source region. In fact, data in table Q3 show that five different samples represent extreme compositions in terms of initial U/Pb, Th/Pb, and Th/U compositions and only one of these represents the extreme in terms of oxygen isotope composition (table Q2). Furthermore, neither the lead isotope compositions or uranium or thorium concentrations yield geographic patterns similar to those observed for certain dispersed trace elements (Stormer and others, 1980).

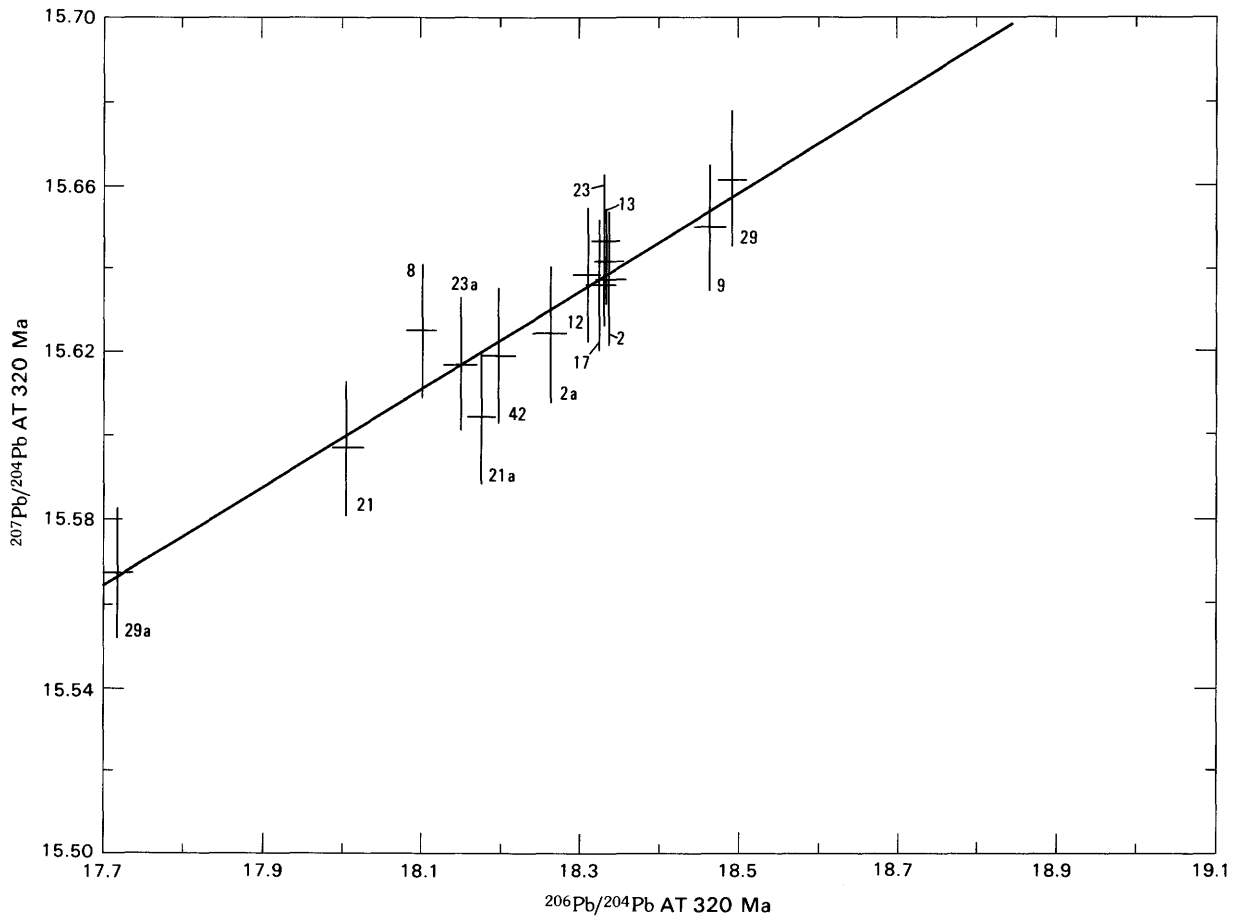

Figure Q5. Lead-lead isochron for whole-rock samples from the Elberton Granite batholith, Georgia, corrected for the growth of radiogenic lead from 320 Ma to the present. Regressed line yields a slope of 0.11734 ± 0.01951 at the 95–percent level of confidence which corresponds to an age of $1{,}750 \pm 280/350$ Ma. Symbol size corresponds to $\pm 2\sigma$ assuming analytical error only. Prefix letters EB and EW have been omitted from sample numbers to save space.

A final test of a mixing model can be made by plotting $^{206}Pb/^{204}Pb$ versus one over the concentrations of lead or $^{87}Sr/^{86}Sr$ versus one over the concentration of strontium (Lancelot and Allegre, 1974). Figure Q9 shows that neither of these plots is linear, although the lead plot yields a better correlation than the one for strontium. Thus there is no evidence that a simple mixing of two end members can explain the data.

Variations about trends such as those observed in figures Q6, Q7, Q8, and Q9 can be caused by mixing of two inhomogenous sources. Similar variations about a linear trend would also be expected in the initial lead-lead system except for the case where all composition evolved from a single common lead. An exact determination of the composition of the common lead is not possible, but a reasonable estimation can be made from the regressed line for the lead-lead system and the lead-evolution model of Stacey and Kramers (1975). This method requires that the approximate age of the common lead be known. This age can be estimated by assuming that the array on figure Q5 is that of a secondary isochron. The slope of this isochron corresponds to an age of 1,750 (within an error of either +280 or –350) Ma. The intersection of the secondary isochron with a chord that intersects the model growth curve of Stacey and Kramers (1975) at 3,700 Ma and 1,750 Ma yields the common lead composition.

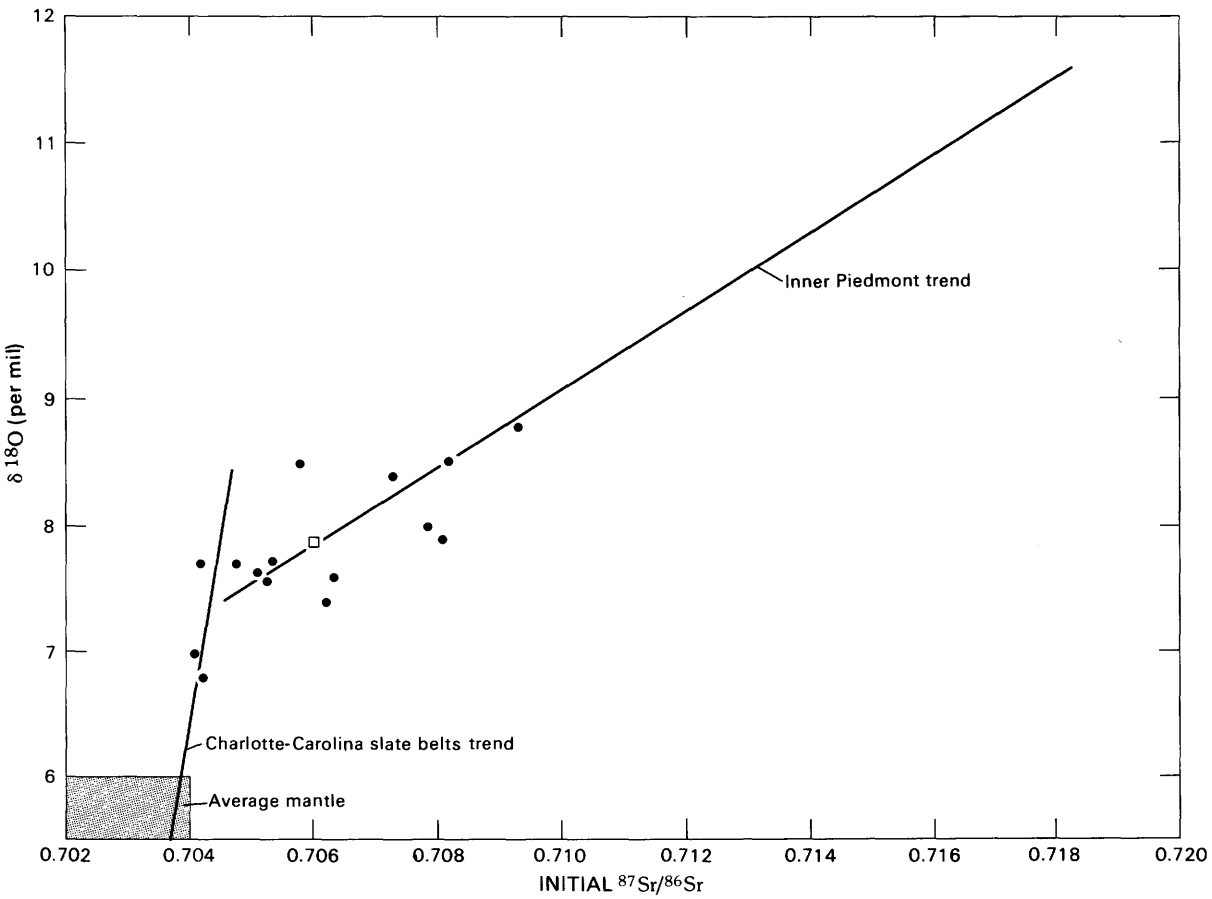

Figure Q6. Initial $^{87}Sr/^{86}Sr$ versus $\delta^{18}O$ values for the Elberton Granite batholith (Whitney and others, 1980) with trends for data from the Inner Piedmont and Charlotte-Carolina slate belts (Wenner, 1981). Square is the average for all Elberton Granite batholith data; solid circles are individual data points.

If the assumptions that yielded the secondary isochron and common lead composition are correct, the data can be reduced to a radiogenic component and a concordia diagram can be constructed. The resulting diagram should yield a linear array of points (within the limits of analytical error) with a lower intercept equal to the time of intrusion and an upper intercept equal to the time when the leads separated from a common source. The predicted linear array and lower intercept (290±90 Ma) are observed (fig. Q10), and we conclude that the internal consistencies of the model warrant interpretation of the upper intercept age (1,720±30 Ma) as the age of the source region. This age applies to either a single heterogeneous source region or two heterogeneous source regions that separated from a common source about 1,720 Ma ago and remained closed with respect to uranium and lead mobility until the formation of the granite.

The calculated age of the source region seems very old relative to reported ages for the Grenville-age basement rocks of the Appalachian and Piedmont regions; however, a few studies have suggested that older crustal rocks did exist in the area prior to the Grenville orogeny. Zircons from crystalline rocks of central Virginia suggest a precursor as old as 1,750 Ma (Davis, 1974), and detrital zircons from a lower Paleozoic sandstone in Florida yield a minimum age of 1,850 Ma (Odom and Brown, 1976). Because rocks of such antiquity were unknown in the southeastern United States, the authors concluded that the source for the zircons was the Guinean shield. Recent work on zircons by T. W. Stern (oral commun., 1981) suggests that the basement terrane within the Grandfather window of North Carolina also may have a precursor of Middle Proterozoic age.

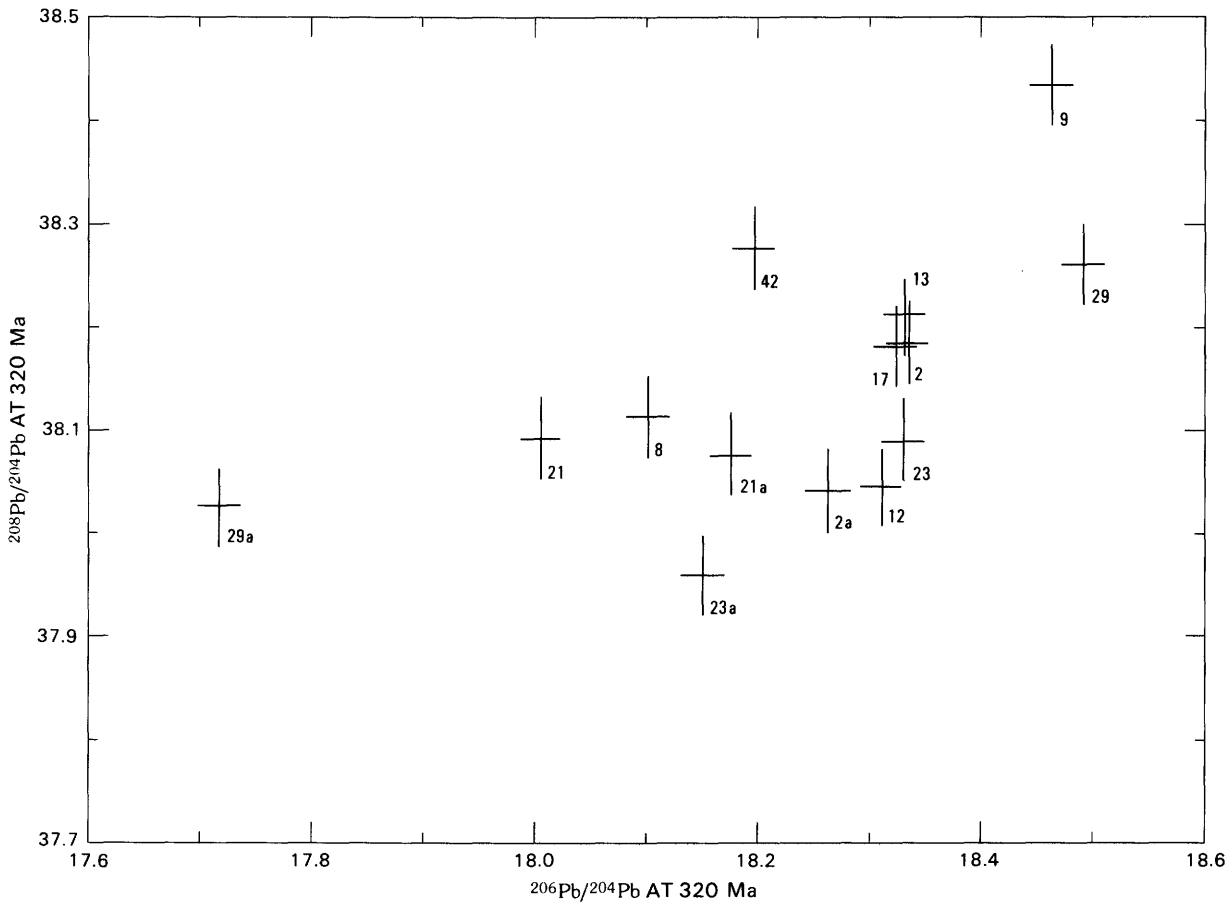

Figure Q7. Initial $^{206}Pb/^{204}Pb$ versus initial $^{208}Pb/^{204}Pb$ for whole-rock samples from the Elberton Granite batholith, Georgia. Symbol sizes correspond to $\pm 2\sigma$. Prefix letters EB and EW have been omitted from sample numbers to save space.

Concordia diagrams can be constructed by correcting the data for possible Grenville-age common leads. We evaluated the data using both a Grenville-age lead that would be colinear with the data array on figure Q5, and an average Grenville-age lead as calculated by the Stacey and Kramers (1975) orogene growth curve. Neither model provides consequences that are as attractive as those that result from the model based on a 1,750–Ma common lead.

A Grenville-age lead that is colinear with the initial lead-lead data can be calculated from the intersection of the lead-lead line (fig. Q5) and a line through the Stacey and Kramers (1975) values for average common leads at 3.7 and 1.0 Ga. This point yields slightly less radiogenic values ($^{206}Pb/^{204}Pb=17.001$ versus 17.066, and $^{206}Pb/^{204}Pb=15.481$ versus 15.509) than that reported for an average growth curve. If corrected for the less radiogenic Grenville-age lead, concordia intercepts correspond to ages of $1,705 \pm 60$ and 295 ± 75 Ma with a range in $^{238}U/^{204}Pb$ of from 6.45 to 13.4 for the source region of the granite. These intercept ages are not markedly different from those obtained by use of a 1,750 Ma common lead, but the upper intercept age contradicts the presumed age of the source-area common lead. Furthermore, this model requires that most samples gain considerable uranium relative to lead at the time of granite genesis, which makes interpretation of the high Th/U more difficult.

Correction of the data for an average Grenville-age common lead results in intercept ages of $1,430 \pm 140$ and 360 ± 200 Ma. These ages are in fair agreement with the known age of intrusion and assumed source age, but again the concordia plot shows that most samples would have gained a considerable amount of uranium relative to lead.

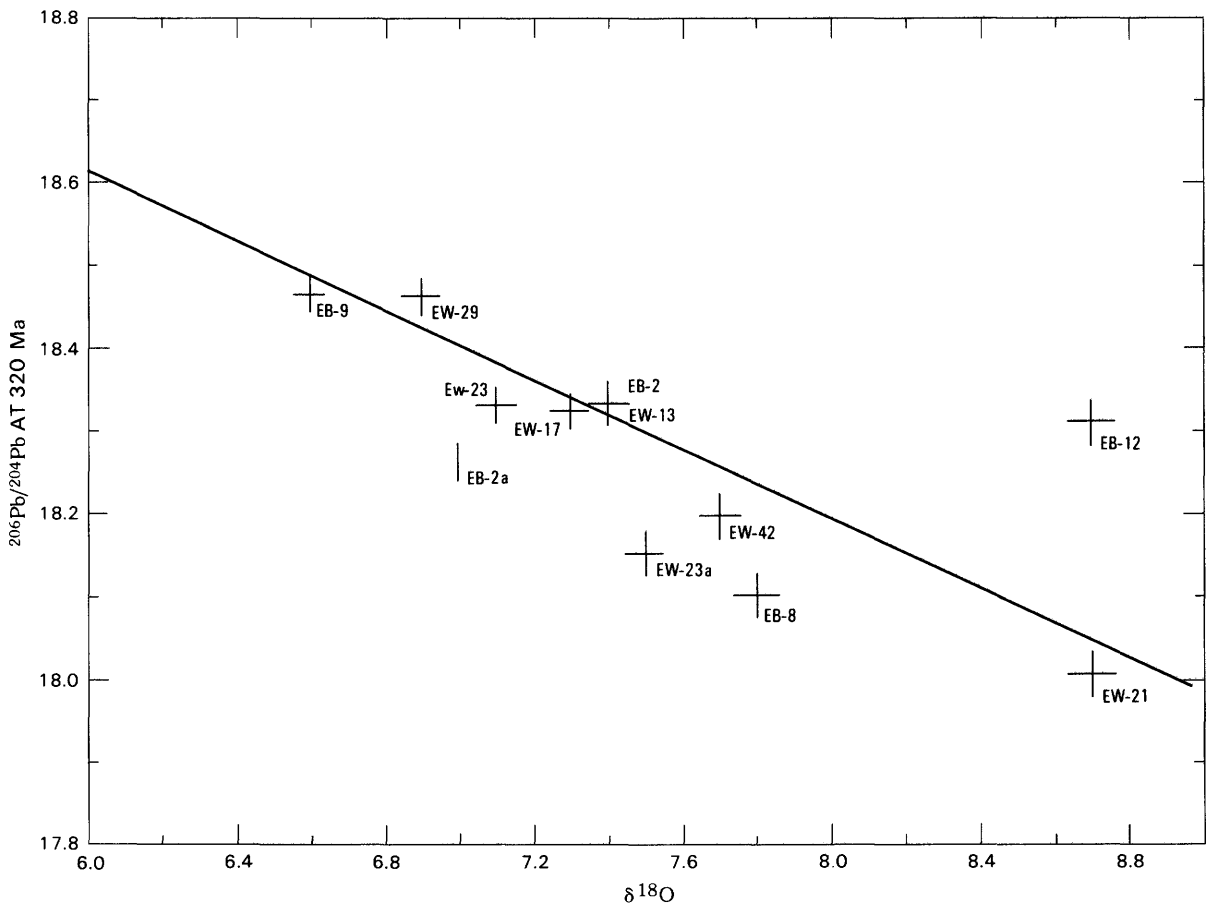

Figure Q8. Oxygen isotope composition versus initial $^{206}Pb/^{204}Pb$ for whole-rock samples from the Elberton Granite batholith, Georgia. Symbol sizes correspond to $\pm 2\sigma$.

Calculated $^{238}U/^{204}Pb$ for the source region range from 5.86 to 12.85 and correspond closely to lower and upper crustal values (5.89 and 12.24) of Doe and Zartman (1979), but this would require the lower crust to have high $\delta^{18}0$ and high $^{87}Sr/^{86}Sr$ values, and the upper crust to have low $\delta^{18}0$ and low $^{87}Sr/^{86}Sr$ values. We therefore conclude that a Grenville-age source region is inconsistent with the data.

Protolith and Magmatic Considerations

The Th/U observed for the Elberton Granite batholith range from 3.6 to 42.9 and average 13.1 (table Q3). Both the range and average are much larger than the range of 3 to 5 and average of about 4.5 cited as typical for granitic rocks (Rogers and Adams, 1969). In other granites, large and variable ratios have been interpreted to be the result of recent uranium loss in response to near-surface conditions (Stuckless and Nkomo, 1978). The data as modeled (fig. Q10 and table Q3) do not support a similar interpretation for the Elberton Granite batholith because open-system behavior such as gain or loss of uranium or lead for the whole-rock samples would prohibit generation of linear arrays on figures Q5 and Q10.

The data support the hypothesis of Wenner and Spaulding (1980) that the large and variable Th/U resulted in large part during the magmatic phase of the granite's history. These authors pointed out that the granite crystallized under conditions of high oxygen fugacity and in the presence of a free vapor phase such that separation of hexavalent uranium and tetravalent thorium could take place. They also reported that the presumed top of the batholith is the least depleted in uranium, and that late-stage pegmatites are strongly enriched in uranium relative to thorium.

Exact Th/U within the source region for the Elberton Granite batholith cannot be calculated because the common $^{208}Pb/^{204}Pb$ is not known. However, the calculated common $^{206}Pb/^{204}Pb$ and $^{207}Pb/^{204}Pb$ are very similar to the values reported by Stacey and Kramers (1975) for average terrestrial lead, and thus the average terrestrial $^{208}Pb/^{204}Pb$ at $1{,}720 \pm 20$ Ma ago probably provides a close estimate of that in the source region at 1,720 Ma ago. This assumption and preceding assumptions about closed-system behavior permit calculation of source-region Th/Pb and Th/U at the time of granite generation (table Q3). The calculations show that these ratios, as well as the U/Pb, were fairly constant and had mean values that are similar to terrestrial averages proposed by Stacey and Kramers (1975). The calculations also show a consistant and marked increase in Th/Pb between those in the source region and those currently observed in the granite, an increase in the Th/U for all but one sample, and a general decrease in the U/Pb.

Confirmation, within the limits of the modeled data, that the anomalous Th/U were generated at the time of magmatism can be seen on figure Q10. Displacement of data points by the preferential movement of uranium or lead will be along a chord that joins concordia at the age of disturbance and the position of the data point prior to disturbance. Lead gain or uranium loss will move data points away from the point on concordia that corresponds to the age of disturbance. The pattern on concordia for the Elberton Granite is best interpreted in terms of uranium movement because the points that plot above concordia are those with the largest Th/U (the sample with the largest Th/U, 42.87, plots furthest above concordia) and the points that plot below concordia are those with the smallest Th/U (the sample with the smallest Th/U, 3.57, plots furthest below concordia).

Figure Q10 also permits evaluation of the assumed immobility of uranium and lead in the recent, near-surface history of the granite. All but one data point lies on the chord that connects the age of the granite with the age of the source region. One data point (21a) lies slightly above this chord and may therefore reflect recent uranium loss (or lead gain, assuming an appropriate composition for the acquired lead). Projection of this point back towards a time of uranium loss of 0 Ma suggests that data point 21a should plot near point 21 (fig. Q10).

Figure Q9 (facing page). Initial isotopic ratios versus reciprocal of concentration for the systems $^{206}PB/^{204}Pb$ and $^{87}Sr/^{86}Sr$. Strontium data from Whitney and others (1980). Symbols correspond to $\pm 2\sigma$ assuming 1 percent for the strontium concentration error. Sample identification numbers for the strontium diagram are from table 1 of Whitney and others (1980). Prefix letters EB and EW have been omitted from sample numbers to save space.

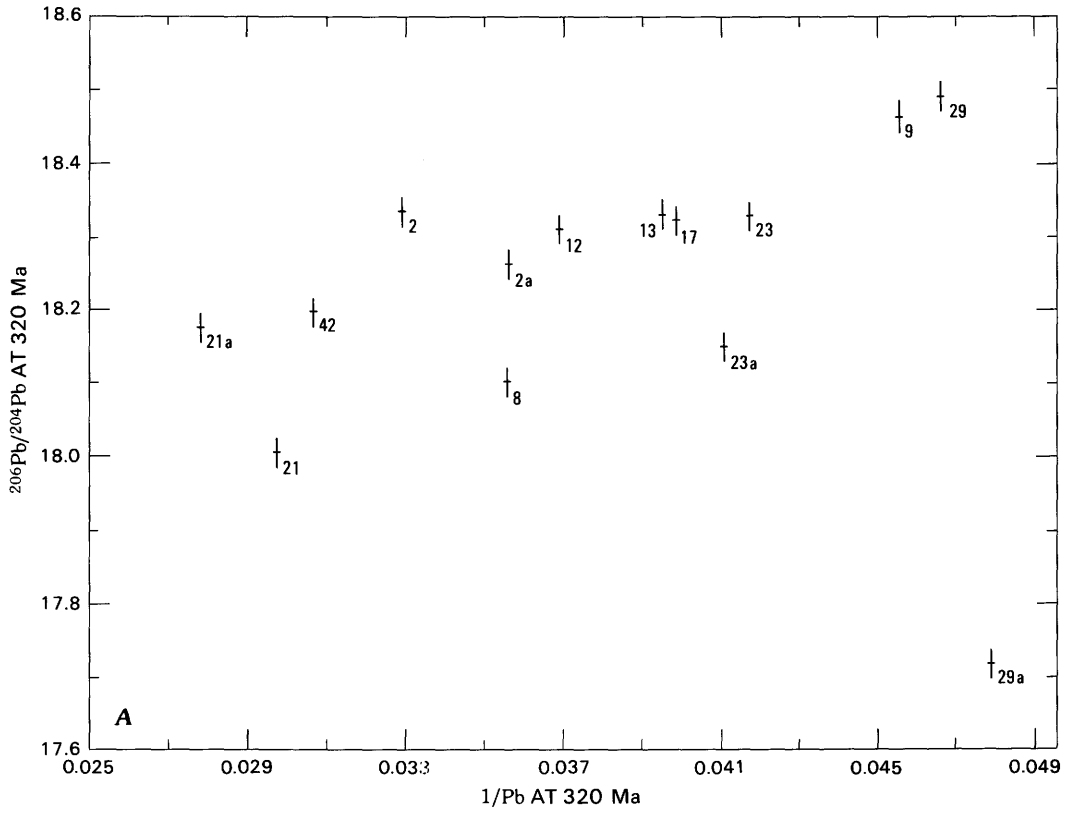
18.6
18.4
18.2
18.0
17.8
17.6
$^{206}Pb/^{204}Pb$ AT 320 Ma
0.025
0.029
0.033
0.037
0.041
0.045
0.049
1/Pb AT 320 Ma
A
29
9
2
12
13
17
23
2a
42
21a
23a
8
21
29a

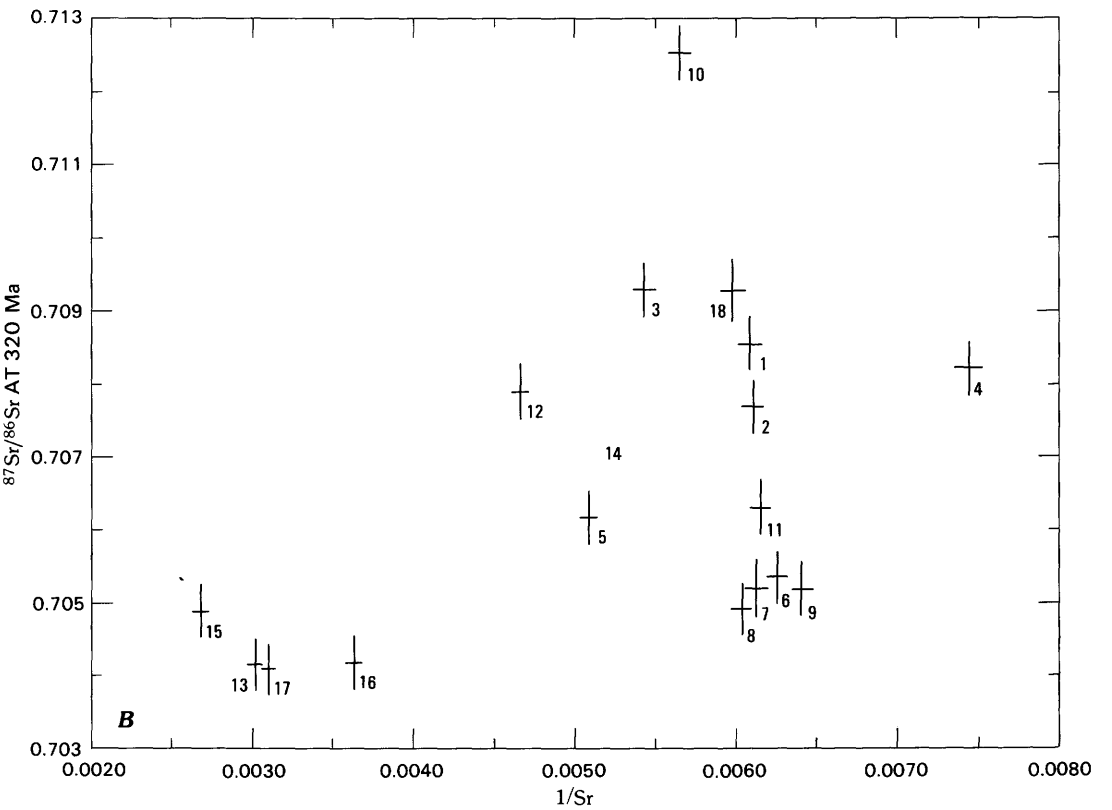
0.713
0.711
0.709
0.707
0.705
0.703
$^{87}Sr/^{86}Sr$ AT 320 Ma
0.0020
0.0030
0.0040
0.0050
0.0060
0.0070
0.0080
1/Sr
B
10
3
18
1
4
12
2
14
5
11
15
13
17
16
7
6
9
8

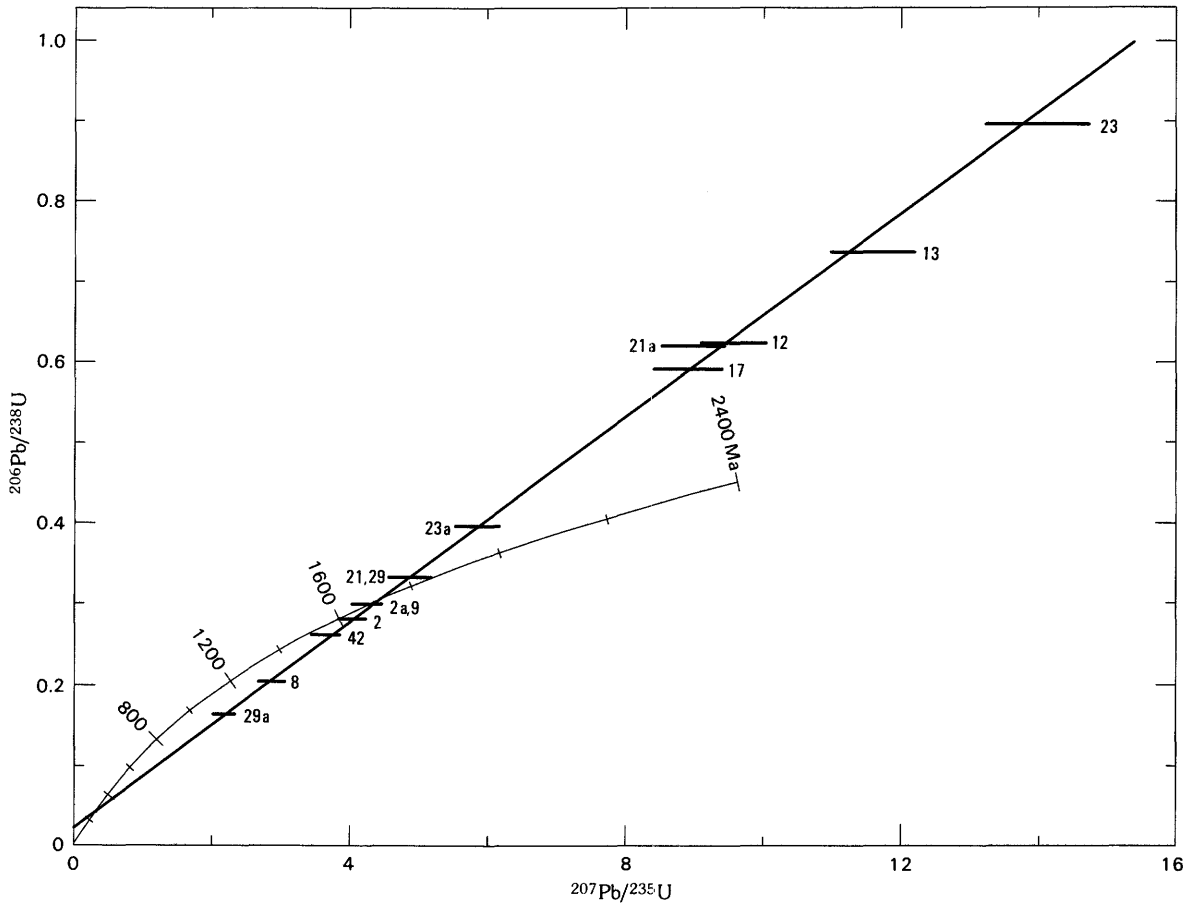

Figure Q10. Concordia diagram for whole-rock samples from the Elberton Granite, Georgia. Data are corrected for a common lead composition of $^{206}Pb/^{204}Pb=15.721$ and $^{207}Pb/^{204}Pb=15.332$. Regressed line intersects concordia at $1{,}720 \pm 30$ and 290 ± 90 Ma at the 95-percent confidence level. Symbol size corresponds to an estimated $\pm 2\sigma$, which includes an error magnification estimate for the choice of common-lead composition. Prefix letters EB and EW have been omitted from sample numbers to save space.

The isotopic data and the model age of the source region provide some constraints on the protolith of the Elberton Granite batholith. Table Q3 shows ranges in values for $^{238}U/^{204}Pb$, $^{232}Th/^{204}Pb$, and Th/U ratios that may have existed in the source region prior to generation of the granite. This range of values is at the low end of the range reported for the source region of other granites (table Q4) which is reasonable in that most of the granites listed in table Q4 are more evolved in terms of major-element chemistry than the Elberton Granite.

Published data for the Elberton batholith (Whitney and others, 1980) yield a range in initial $^{87}Sr/^{86}Sr$ ratios at 320 Ma from about 0.704 to almost 0.713. Assuming an age for the source region of 1750 Ma and an initial $^{87}Sr/^{86}Sr$ of 0.702, calculated $^{87}Rb/^{86}Sr$ range from 0.10 to 0.54 or Rb/Sr range from 0.29 to 1.53. These ratios, as well as those listed in table Q3, are reasonable for mafic to intermediate protolith materials.

Table Q5 lists features for the protoliths for granites in the Inner Piedmont and Charlotte-Carolina slate belts as they presumably correlate with the parameters measured for the Elberton Granite batholith.. The only anomalous feature of a mixed protolith for the Elberton is the negative correlation between initial $^{206}Pb/^{204}Pb$ or initial $^{208}Pb/^{204}Pb$ and $\delta^{18}O$ or initial $^{87}Sr/^{86}Sr$. At least two explanations are possible. The protolith beneath the Charlotte-Carolina slate belt has a component whose trace-element geochemistry is similar to that of alkali basalts such that uranium and thorium are enriched relative to lead, but that rubidium is not enriched relative to strontium. Alternatively, the protolith under the Inner Piedmont belt may have been more highly metamorphosed during its earliest history than that beneath the Charlotte-Carolina slate belt such that the U/Pb ratio was reduced greatly. A similar mechanism has been proposed to change the U/Pb ratio in the source region of other granites (Stacey and Zartman, 1978; Doe and Delevaux, 1980, table 4).

Table Q4. Calculated $^{238}U/^{204}Pb$ of the source regions of some granitic rocks

$^{238}U/^{204}Pb$	Granite age (Ma)	Source and (or) identification	Reference
8.04 to 11.16	320	Elberton granite batholith, eastern Georgia	This study.
7.4	2,600	Icarus pluton, northeastern Minnesota	Arth and Hanson (1975).
7.84 to 8.12	2,950	Granite gneiss of the Pilbara Block, western Australia	Oversby (1975).
11.64	2,670	Owl Creek Mountains, Wyoming	Nkomo and others (1978).
11.47	2,350	Mount Boreas type granite, western Australia	Stuckless, Bunting, and Nkomo (1981).
11.26	2,675	Syenitic granite, western Australia	Do.
12.01	2,600	Granite Mountains, Wyoming	Stuckless and Nkomo (1978).
[1]12.7, 7.4	38	Northern Gold Hill, Utah	Stacey and Zartman (1978).
[1]11.7, 12.1	152	Southern Gold Hill, Utah	Do.
[1]10.3, <9.0	1,850	Section 28 granite, Minnesota	Doe and Delevaux (1980).
[1]14.5, 4.5	2,600	Sacred Heart granite, Minnesota	Do.

[1]Reported as a two-stage ratio, value for earliest stage listed first.

Oxygen, strontium, and major-element data for the postmetamorphic granites strongly suggest that the protolith for the Inner Piedmont granites had a large pelitic component; therefore, an explanation for low U/Pb by uranium loss is attractive. Furthermore, the data for the Elberton Granite batholith have two features that have been observed in other areas for which a lowering of the U/Pb by metamorphism has been proposed. In the Gold Hill plutons, Utah, there is a negative correlation between initial $(^{87}Sr/^{86}Sr)_i$ and $(^{206}Pb/^{204}Pb)_i$ (Stacey and Zartman, 1978). For the Section 28 granite, Minnesota, Doe and Delevaux (1980) noted both a decrease in the U/Pb and an increase in the Th/U as a result of metamorphism. Data for the Elberton show a negative correlation between initial Th/U and initial $^{206}Pb/^{204}Pb$ (fig. Q11) that could be explained by a preferential loss of uranium from one source region shortly after it evolved.

Table Q5. Interpreted features of the protoliths for granites in the Inner Piedmont and Charlotte-Carolina Slate belts

Parameter	Inner Piedmont belt	Charlotte-Carolina slate belts
Molar Al/(Na+K+Ca)	High	Low.
Mafic content	Low	High.
$\delta^{18}O$	High	Low.
Initial $^{87}Sr/^{86}Sr$	High	Low.
Initial $^{206}Pb/^{204}Pb$	Low	High.
Initial $^{208}Pb/^{204}Pb$	Low	High.
Initial Th/U	High	Low.

SUMMARY AND CONCLUSIONS

Data presented in this study support the hypothesis that the Elberton Granite batholith formed by the partial melting of two distinct protoliths (Stormer and others, 1980; Wenner, 1981) and further suggest that these protoliths were at least heterogeneous with respect to several radioelements. Several isotopic parameters are correlated with each other, particularly if corrected to their values at the time of intrusion. This suggests mixing of two end members.

The Elberton magma did not mix isotopically at the time of intrusion. As a result of this unique magmatic history, the granite preserved the age of the source region. None of the correlated isotopic parameters, including isotopic ratios relative to the reciprocal of concentrations (such as $^{206}Pb/^{204}Pb$ versus 1/Pb, Lancelot and Allegre, 1974) are colinear within the limits of experimental error except for $^{206}Pb/^{204}Pb$ and $^{207}Pb/^{204}$ This fact can be explained by the mixing of two heterogeneous source regions that had the same common lead at the time the source regions formed. With this assumption, the lead data can be interpreted to yield an age for the protolith of $1,720 \pm 30$ Ma.

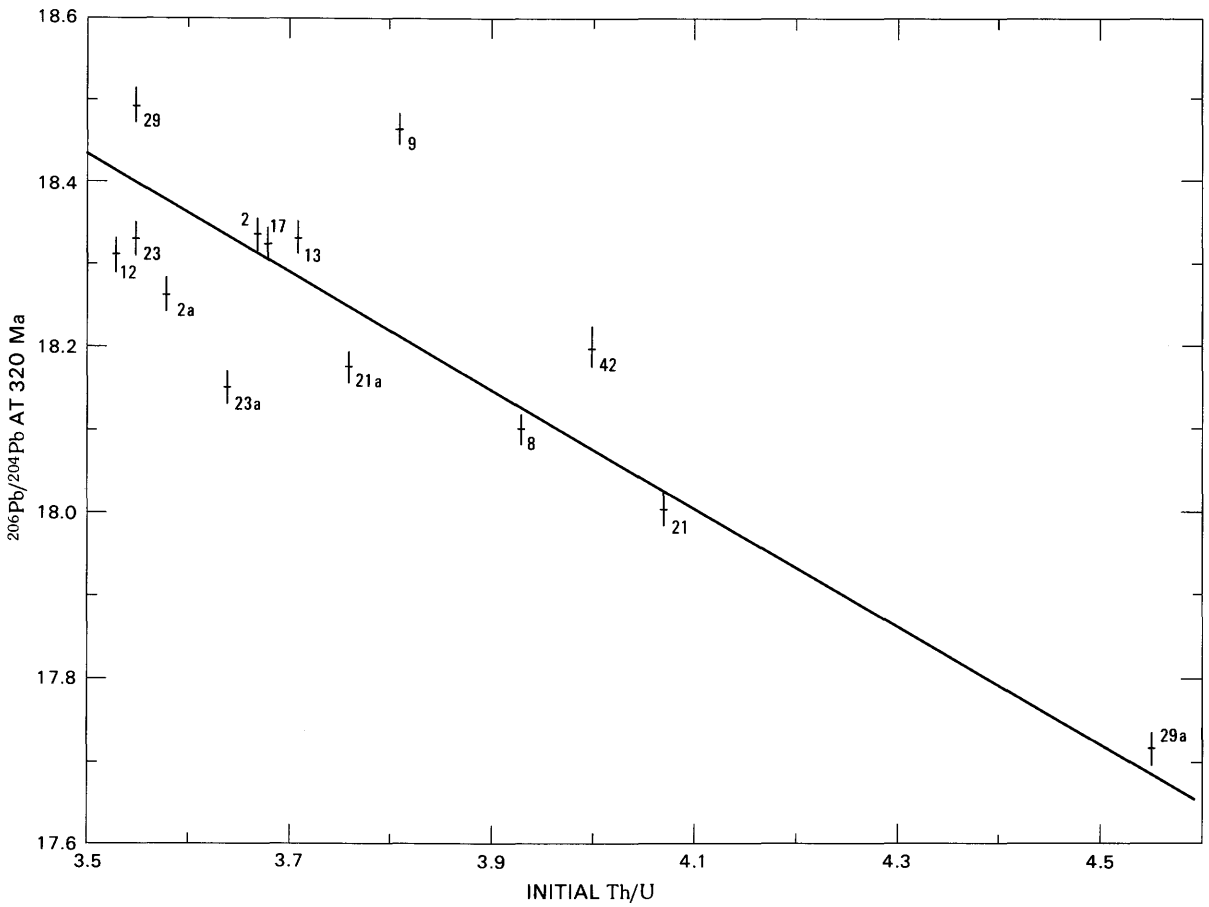

Figure Q11. Plot of $^{206}Pb/^{204}Pb$ versus Th/U for the protolith of the Elberton Granite batholith, Georgia at the time of granite formation. Symbol size corresponds to $\pm 2\sigma$. Prefix letters EB and EW have been omitted from sample numbers to save space.

The Elberton is similar to granites that have been identified as favorable source rocks for uranium (for example Stuckless and Nkomo, 1978) in that Th/U for the granite have a wide range of values and an anomolously large mean value. However, for granites that are associated with low-temperature uranium deposits, the large range and mean are thought to have originated by uranium loss in the near-surface environment. Isotopic data for the Elberton Granite indicate that the anomalous Th/U were generated as part of the magmatic process and that uranium has been remarkably immobile since the time of intrusion. This conclusion is supported by the enrichment of uranium in the upper parts of the intrusion and the existence of uraniferous pegmatites. Thus, the high Th/U probably are due to uranium loss, but this loss took place at the same time as the loss of volatiles from the magma.

REFERENCES CITED

Arth, J. G., and Hanson, G. N., 1975, Geochemistry and origin of the early Precambrian crust of northeastern Minnesota: Geochimica et Cosmochimica Acta, v. 39, p. 325–362.

Barnes, I. L., Murphy, T. J., Gramlich, J. W., and Shields, W. R., 1973, Lead separation by anodic deposition and isotope ratio mass spectrometry of microgram and smaller samples: Analytical Chemistry, v. 45, p. 1881–1884.

Cook, F. A., Albaugh, D. S., Brown, L. D., Kaufman, S., Oliver, J. E., and Hatcher, R. D., Jr., 1979, Thin skinned tectonics in the crystalline Southern Appalachians; COCORP seismic-reflection profiling of the Blue Ridge and Piedmont: Geology, v. 7, p. 563–567.

Davis, R. G., 1974, Pre-Grenville ages of basement rocks in central Virginia; A model for interpretation of zircon ages: Blacksburg, Va. Virginia Polytechnic Institute, M.A. thesis, 46 p.

Dallmeyer, R. D., 1978, $^{40}Ar/^{39}Ar$ incremental release ages of hornblende and biotite across the Georgia Inner Piedmont; Their bearing on late Paleozoic-early Mesozoic tectonothermal history: American Journal of Science, v. 278, p. 124–149.

Dallmeyer, R. D., Hess, J. R., and Whitney, J. A., 1981, Postmagmatic cooling of the Elberton Granite; Bearing on the late Paleozoic tectonothermal history of the Georgia Inner Piedmont: Journal of Geology, v. 89, p. 585–600.

Doe, B. R., and Zartman, R. E., 1979, Plumbotectonics I, The Phanerozoic, *in* H. Barnes, ed., Geochemistry of hydrothermal ore deposits: New York, John Wiley and Sons, p. 22–70

Doe, B. R., and Delevaux, M. H., 1980, Lead-isotope investigations in the Minnesota River Valley—Late-tectonic and post-tectonic granites: Geological Society of America Special Paper 182, p. 105–112.

Ellwood, B. B., Whitney, J. A., Wenner, D. B., Mose, D., and Amerigan, C., 1980, Age, paleomagnetism, and tectonic significance of the Elberton Granite, northeast Georgia Piedmont: Journal of Geophysical Research, v. 85, p. 6521–6533.

Ellwood, B. B., and Whitney, J. A., 1980, Magnetic fabric of the Elberton Granite: Journal of Geophysical Research, v. 85, p. 1481–1486.

Grunenfelder, M., and Silver, L. T., 1958, Radioactive age dating and its petrological implications for some Georgia granites [abs.]: Geological Society of America Bulletin, v. 69, p. 1574.

Lancelot, J. R., and Allegre, C. J., 1974, Origin of carbonatitic magma in the light of the Pb-U-Th isotope system: Earth and Planetary Science Letters, v. 22, p. 233–238.

Long, L. T., 1979, The Carolina slate belt—Evidence of a continental rift zone: Geology, v. 7, p. 180–184.

Ludwig, K. R., and Silver, L. T., 1977, Lead isotope inhomogeneities in Precambrian igneous K-feldspars: Geochimica et Cosmochimica Acta, v. 41, p. 1457–1471.

Manton, W. I., 1973, Whole rock Th-Pb age for the Masuke and Dembe-Dwula complexes, Rhodesia: Earth and Planetary Science Letters, v. 19, p. 83–89.

Nkomo, I. T., Stuckless, J. S., Thaden, R. E., and Rosholt, J. N., 1978, Petrology and uranium mobility of an early Precambrian granite from the Owl Creek Mountains: Wyoming Geological Association 30th Annual Field Conference Guidebook, p. 335–348.

Odom, A. L., and Brown, J. F., 1976, Detrital zircons from Ordovician sediments in Florida [abs.]: Geological Society of America Abstracts with Programs, v. 8, p. 237–238.

Oversby, V. M., 1975, Isotopic ages and geochemistry of Archean acid igneous rock for the Pilbara, Western Australia: Geochimica et Cosmochimica Acta, v. 40, p. 817–829.

Rogers, J.J.W., and Adams, J.A.S., 1969, Thorium, *in* Wedepohl, K. H., ed., Handbook of geochemistry, v. 12, no. 4: Berlin, Springer-Verlag, p. 90–1 to 90–0.

Rosholt, J. N., Zartman, R. E., and Nkomo, I. T., 1973, Lead isotope systematics and uranium depletion in the Granite Mountains, Wyoming: Geological Society of America Bulletin, v. 84, p. 989–1002.

Ross, C. R., II, and Bickford, M. E., 1980, The U-Pb age of zircons from the Elberton granite, Piedmont of Georgia, *in* Stormer, J. C., Jr., and Whitney, J. A., eds., Guidebook 19, Geological, geochemical, and geophysical studies of the Elberton batholith, eastern Georgia: A guidebook to accompany the 15th annual Georgia Geological Society field trip, p. 52–62.

Stacey, J. S., and Kramers, J. S., 1975, Approximation of terrestrial lead isotope evolution by a two-stage model: Earth and Planetary Science Letters, v. 26, p. 207–221.

Stacey, J. S., and Zartman, R. E., 1978, A lead and strontium isotopic study of igneous rocks and ores from the Gold Hill Mining District, Utah: Utah Geology, v. 5, p. 1–15.

Steiger, R. H., and Jäger, E., 1977, Subcommission on geochronology; Convention on the use of decay constants in geo- and cosmochronology: Earth and Planetary Science Letters, v. 36, p. 359–362.

Stormer, J. C., Jr., Whitney, J. A., and Hess, J. R., 1980, Petrology and geochemistry of the Elberton Granite, *in* Stormer, J. C., Jr., and Whitney, J. A. eds., Guidebook 19, Geological, geochemical and geophysical studies of the Elberton batholith, eastern Georgia: A guidebook to accompany the 15th annual Georgia Geological Society field trip, p. 10–30.

Stuckless, J. S., Bunting, J. A., and Nkomo, I. T., 1981, U-Th-Pb systematics of some granitoids from the northeastern Yilgarn Block, Western Australia and implications for uranium source rock potential: Journal of the Geological Society of Australia, v. 28, p. 365–375.

Stuckless, J. S., and Nkomo, I. T., 1978, Uranium-lead isotope systematics in uraniferous alkali-rich granites from the Granite Mountains, Wyoming; implications for uranium source rocks: Economic Geology, v. 43, no. 3, p. 427–441.

Stuckless, J. S., Nkomo, I. T., and Doe, B. R., 1981, U-Th-Pb systematics in hydrothermally altered granites from the Granite Mountains, Wyoming: Geochimica et Cosmochimica Acta, v. 45, p. 635–645.

Tatsumoto, M., Knight, R. J., and Delevaux, M. H., 1972, Uranium, thorium, and lead concentrations in three silicate standards and a method of lead isotopic analysis, *in* Geological Survey research 1972: U.S. Geological Survey Professional Paper 800–D, p. 111–115.

Taylor, H. P., Jr., and Epstein, S., 1962, Relationship between o^{16}/O^{16} ratios in coexisting minerals of igneous and metamorphic rocks part I; Principles and experimental results: Geological Society of America Bulletin, v. 73, p. 461–480.

Wenner, D. B., 1981, Oxygen isotopic compositions of the late orogenic granites in the southern Piedmont of the Appalachian Mountains, U.S.A., and their relationship to subcrustal structures and lithologies: Earth and Planetary Science Letters, v. 54, p. 186–199.

Wenner, D. B., and Spaulding, J. D., 1980, U-Th geochemistry of the Elberton pluton, *in* Stormer, J. C., Jr., and Whitney, J. A., eds., Guidebook 19, Geological, geochemical, and geophysical studies of the Elberton batholith, eastern Georgia: A guidebook to accompany the 15th annual Georgia Geological Society field trip, p. 44–51.

Whitney, J. A., Hess, J. R., and Mose, D., 1980, Geochronology and cooling history of the Elberton Granite, *in* Stormer, J. C., Jr., and Whitney, J. A., eds., Guidebook 19, Geological, geochemical, and geophysical studies of the Elberton batholith, eastern Georgia: A guidebook to accompany the 15th annual Georgia Geological Society field trip, p. 63–69.

Whitney, J. A., Paris, T. A., Carpenter, R. H., and Hartley, M. T., III, 1978, Volcanic evolution of the southern slate belt of Georgia and South Carolina; A primitive oceanic island arc: Journal of Geology, v. 86, p. 173–192.

Whitney, J. A., and Stormer, J. C., Jr., 1980, Road log for the 1980 Georgia Geological Society field trip, *in* Stormer, J. C., Jr., and Whitney, J. A., eds., Guidebook 19, Geological, geochemical, and geophysical studies of the Elberton batholith, eastern Georgia: A guidebook to accompany the 15th annual Georgia Geologial Society field trip, p. 108–134.

Whitney, J. A., and Wenner, D. B., 1980, Petrology and structural setting of post-metamorphic granites of Georgia, *in* Frey, R. W., ed., Excursions in southeastern geology: American Geological Institute, v. 2, p. 351–378.

York, Derek, 1969, Least-squares fitting of a straight line with correlated errors: Earth and Planetary Science Letters, v. 5, p. 320–324.

1986

U.S. GEOLOGICAL SURVEY BULLETIN 1622

SHORTER CONTRIBUTIONS TO ISOTOPE RESEARCH

SOIL-GAS HELIUM DISTRIBUTION AT THE SHADOW MOUNTAIN COLLAPSE, CAMERON URANIUM DISTRICT, ARIZONA

Chapter R

By C. G. BOWLES, G. M. REIMER, J. M. BEEN, and D. G. MURREY

CONTENTS

FIGURES

Abstract

Soil-gas helium at the Shadow Mountain collapse ranged from 9 to 288 ppb (parts per billion) helium (with respect to air) with a mean helium concentration of 90 ppb. High helium values (110–180 ppb He) are distributed in a circular or annular pattern around the margin of the collapse. The pattern suggests a structural control for helium and its uranium parent analogous to the ring-fracture control for uranium ore deposits in breccia pipes of the Grand Canyon. The soil-gas helium anomalies provide favorable targets for uranium exploration.

INTRODUCTION

A soil-gas helium survey of the Shadow Mountain collapse in the northern part of the Cameron uranium district of Arizona (fig. R1) was made on October 17, 1980. The purpose of the survey was to determine whether or not helium detection methods can contribute to the evaluation of uranium potential within the district's collapse structures.

Helium detection is a promising technique for the discovery of deeply buried uranium deposits; however, many factors can alter the concentration and distribution

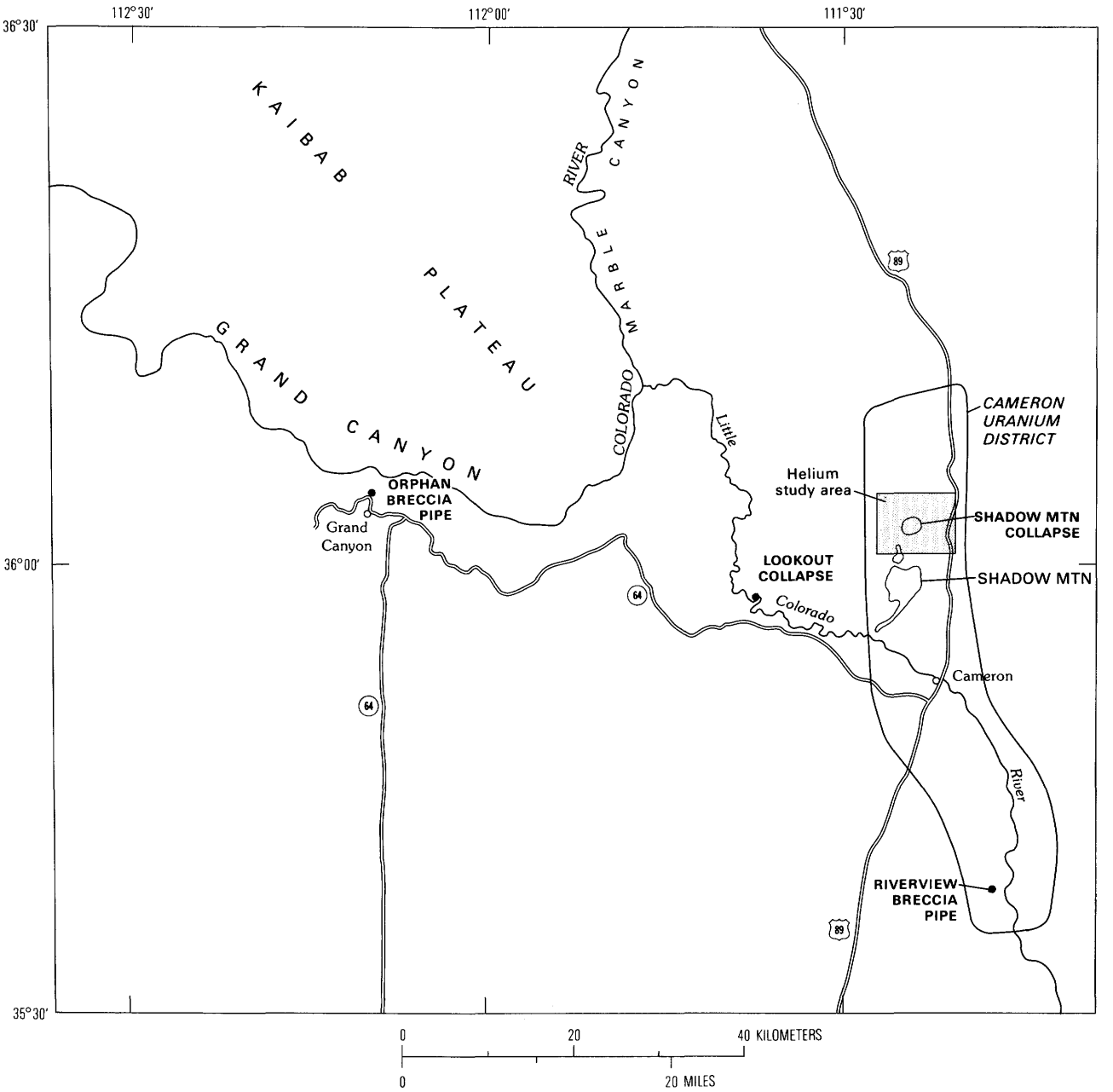

Figure R1. Index map showing location of helium study area, Cameron, Ariz.

of the helium. Helium is formed from alpha particles emitted during radioactive disintegration of the uranium and thorium decay series. Helium released by the rocks may be dissolved in the ground water, or it may migrate as a free gas. An upward leakage of free-gas helium to the soil zone is facilitated by the permeability of fractured and brecciated rock. For this reason a soil-gas helium survey may detect deeply buried uranium deposits within collapse structures.

Past speculation on the potential for economic vein-type uranium deposits within the Shadow Mountain collapse and other structures in the Cameron district was stimulated by the production of uranium and copper from the Riverview breccia pipe within the district. In addition, uranium and copper have been produced from the Orphan breccia pipe and other pipes of the Grand Canyon district to the west. Kerr (1958) called attention to uranium mineralization in the Shadow Mountain collapse, and later Barrington and Kerr (1963, p. 1254) reported that "outcrops within the collapse area display anomalous radioactivity, and [that] subeconomic uranium mineralization was found in drilling." A small uranium deposit in the Shinarump Member of the Chinle Formation of Triassic age is located near the north margin of the collapse. The deposit produced about 25 tons of "no pay ore" (D. N. Magleby, written commun., 1960). In addition, Barrington and Kerr (1963) reported radioactivity anomalies associated with the western fault of a graben that extends northward from Shadow Mountain toward the collapse.

GEOLOGIC SETTING

The Shadow Mountain collapse is in the outcrop of the lowermost Shinarump Member of the Chinle Formation of Triassic age (fig. R2). The overlying Petrified Forest Member crops out less than 1 km (kilometer) east of the collapse, and an outlier of this member forms the rim of the collapse structure and dips inward at 5°–18° (Cooley and others, 1969). Outside the collapse, the Chinle Formation dips 2°–4° eastward. The collapse forms a topographic bowl measuring 2.5 km across (fig. R3). The rim of the bowl rises as much as 35 m (meters) above the nearly flat inner floor. Intermittent streams flow eastward to southeastward across the structure through gaps incised into the west and north sides of the bowl and then merge to exit as a single stream at the southeast side. Alluvium of Quaternary age covers the bottom of the bowl as well as the drainages that dissect the rim. Horizontally bedded gravels of Quaternary(?) age rest unconformably upon a segment of the rim at the west side of the structure (Barrington and Kerr, 1963). These gravels were deposited in an earlier course of a stream that now flows through a gap in the rim, about 1,000 m to the south. During deposition of the gravels the topographic bowl of the collapse was occupied by strata of the Petrified Forest Member. The member is more resistant to erosion where it underlies the course of the ancestral stream. This fact and the abundance of fine-grained interstitial and veinlet calcite, described by Barrington and Kerr (1963), suggest that calcite cementation took place where bicarbonate- and carbon dioxide-bearing solutions may have ascended through the collapse structure to discharge into the drainage of the paleostream.

The vertical extent of the collapse structure is not known. Subsurface information within the collapse is limited to that obtained from a well drilled to a depth of 96 m. The drill hole penetrated conglomerate of the Shinarump Member at depths ranging from 76 to 91 m. The overlying Petrified Forest Member, which is draped into the collapse, may have subsided as much as 120 m at the center of the structure. A collapse of this magnitude requires that the structure extend at least into the Kaibab Limestone of Permian age, the highest stratigraphic unit (fig. R4) in which dissolution of rock could be on a scale necessary for the accommodation of the large volume of displaced rock. Within the buried 1,100–m-thick section of sedimentary rock underlying the Chinle are other carbonate strata, and they also may have been dissolved (fig. R4). These strata are present in the Muav Limestone of Cambrian age, the Temple Butte Limestone of Devonian age, the Redwall Limestone of Mississippian age, the Supai Group of Permian and Pennsylvanian age, and the Toroweap Formation of Permian age.

The Shadow Mountain collapse is at the north end of a graben, a structural relationship that suggests a genetic relationship. Within the Cameron district, faults and grabens are common in the vicinity of collapse structures and breccia pipes. The collapse structures are not present within the graben blocks; instead, the collapses are in adjacent fault blocks where solutions ascending along sympathetic tensional faults and fractures flow away from the graben, or the collapses are at the ends of the grabens. Both the breccia pipe at the Riverview uranium mine (Haines and Bowles, 1976) and the Shadow Mountain collapse are located where fractures in the monoclinal flexures at the ends of the grabens might readily transmit ascending solutions. The graben associated with the Shadow Mountain collapse extends southward 5 km to the Shadow Mountain volcanic cinder cone (fig. R2). This graben is as much as 390 m wide and its faults have a minimum throw of 20 m, as indicated by the topographic relief above the alluvium-covered downdropped block (Condit, 1974). The graben may have formed, at least in part, as a result of crustal dilation accompanying the development of a deep-seated magma chamber. According to Condit (1974), the graben formed before eruption of a lava flow that has been dated by Damon and others (1974) as Quaternary in age. Structural adjustments at the graben occurred penecontemporaneously with, or later than, this eruption. The northernmost basaltic cinder

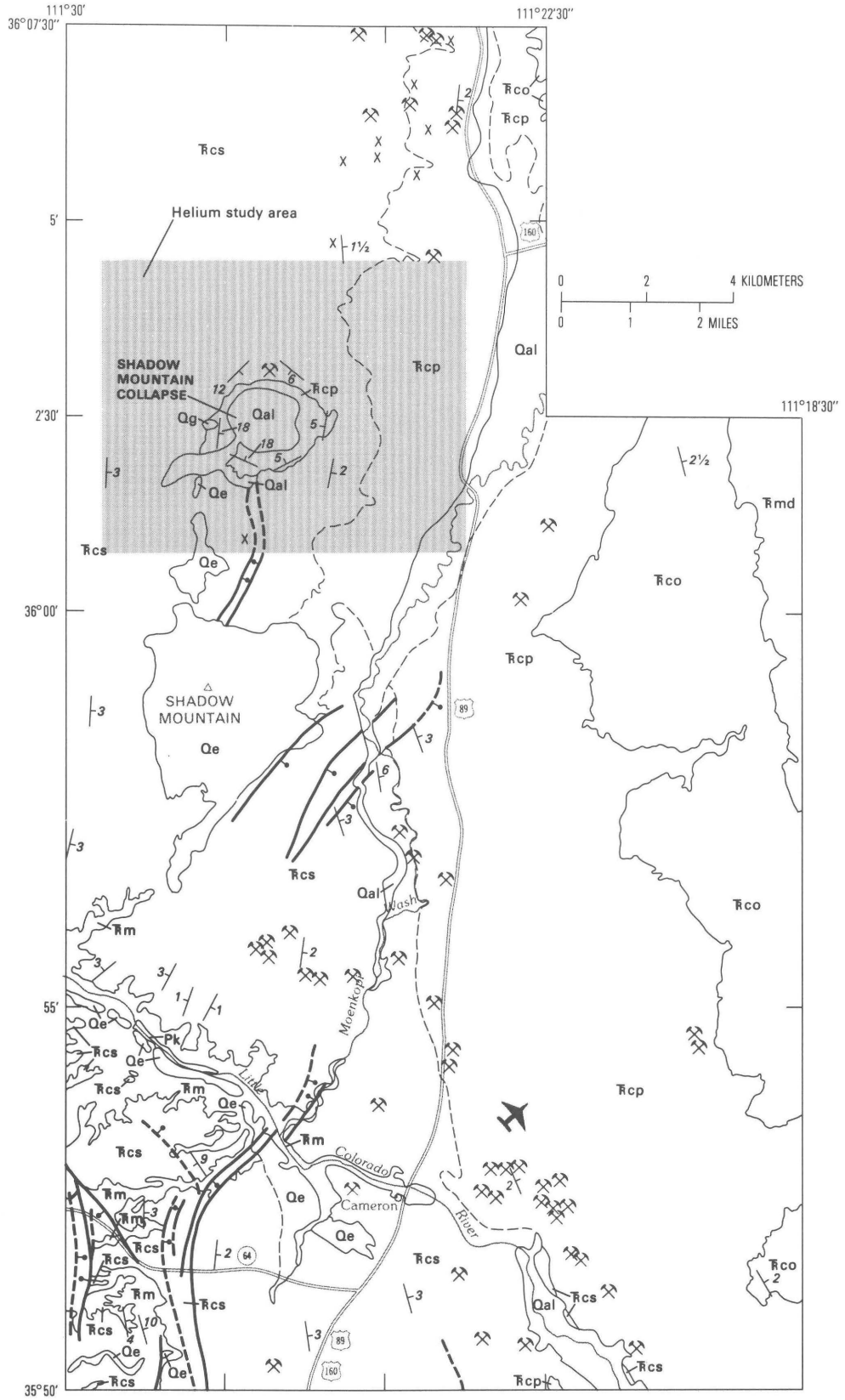

Figure R2 (above and facing page). Map showing geology of the Helium study area, Shadow Mountain collapse, Cameron uranium district. Geology modified from Chenoweth and Magleby (1960, revised 1971) and Haynes and Hackman (1978).

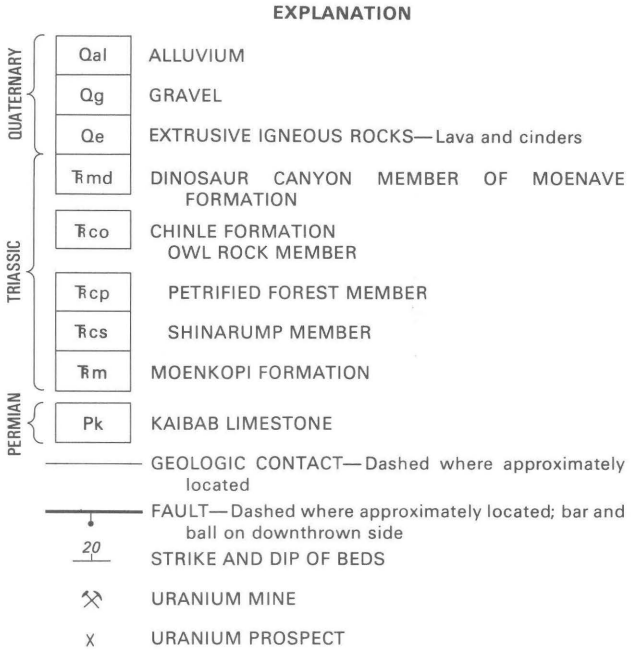

cones and associated dikes and flows of the Shadow Mountain volcanic field form a north-trending ridge that is less than 1 km south-southwest of the collapse and that is 750 m west of the graben. The proximity of the Shadow Mountain eruptive center to the collapse and the existence of an interconnective graben suggest that hydrothermal solutions probably have flowed within the collapse structure.

The Shadow Mountain collapse is considered to have formed as a result of the dissolution of carbonate rock by either hydrothermal or meteoric ground water, although at one time the collapse was thought to be a diatreme (Kerr, 1958). The diatreme hypothesis was replaced by a hydrothermal solution hypothesis by Barrington and Kerr (1963), who believed that all collapses in the Cameron district resulted from hydrothermal dissolution of carbonate rocks. As just discussed here, the hydrothermal solution origin for the Shadow Mountain collapse draws strong support from the proximity of the collapse to the Shadow Mountain eruptive center of late Tertiary(?) and Quaternary age. However, the possibility exists that the initial collapse at Shadow Mountain may have resulted from limestone dissolution by meteoric ground water before the commencement of volcanic activity in the area.

Hydrologic conditions favorable for the formation of solution collapse structures existed prior to volcanism at the Shadow Mountain eruptive center. By late Miocene(?) or early Pliocene time, renewed uplift of the Kaibab Plateau had blocked the flow of an ancestral river into the Grand Canyon (Hunt, 1969). Unpublished data by Bowles suggests that a lake formed in the upper part of Marble Canyon and recharged the Redwall Limestone and Coconino Sandstone aquifers. According to this hypothesis, the ground water migrated toward the Little Colorado River and, driven by artesian pressure, ascended along faults and fractures to discharge into the surface drainage system. In the Cameron uranium district, limestone dissolution by ground water ascending from the Coconino Sandstone through the Toroweap Formation and Kaibab Limestone probably was instrumental in the formation of many collapse structures, including the Shadow Mountain collapse. This stage of solution and collapse possibly overlapped the late Pliocene(?) to Pleistocene episodic volcanic and hydrothermal activity at Shadow Mountain.

Even though we favor our hypothesis for the origin of the Shadow Mountain collapse, we recognize a possibility that solution and collapse may have commenced in the more deeply buried Paleozoic rocks. The possible deeper origin for the Shadow Mountain collapse is supported by evidence from the Lookout collapse of the Cameron district (Barrington and Kerr, 1963). Ring fractures of the Lookout structure are present within the Coconino Sandstone; therefore the structure must bottom lower in the stratigraphic section, probably within the Redwall Limestone where dissolution and collapse is common (Bowles, 1977).

Even if the Shadow Mountain collapse is a deep-seated structure, uranium deposits comparable to those at the Orphan mine are not likely to be present at depth within the Supai Group. The proximity of the Shadow Mountain collapse to the graben suggests a structural control for dissolution and collapse, which also implies a late Cenozoic age for the collapse structure. If this implication is true, hydrologic and hydrochemical conditions at the Shadow Mountain structure differed from those present at the Orphan breccia pipe when Late Jurassic uranium mineralization took place in the pipe structure within the Supai Group (Gornitz and Kerr, 1970).

If uranium deposits are present at the Shadow Mountain collapse, their origin probably is related to the mineralization of the Cameron uranium district. The origin and age of primary uranium in the Chinle Formation is uncertain. Tetravalent uranium is present as uraninite associated with pyrite and marcasite in carbonaceous logs, indicating that a reducing environment effected mineralization and preservation of the deposits (Austin, 1964). According to Austin (1964, p. 89), acid and sulfate solutions formed by the oxidation of pyrite and marcasite were responsible "for the bleaching of the clay, the general yellowish tone of the ore zones, the alteration of montmorillonite to illite or kaolinite, and the solution of uranium from primary uraninite in fossil logs and its movement to disseminated secondary deposits." Uranium has been redistributed as recently as the Pleistocene.

The bleaching and alteration associated with the ore deposits of the Cameron district have effected color

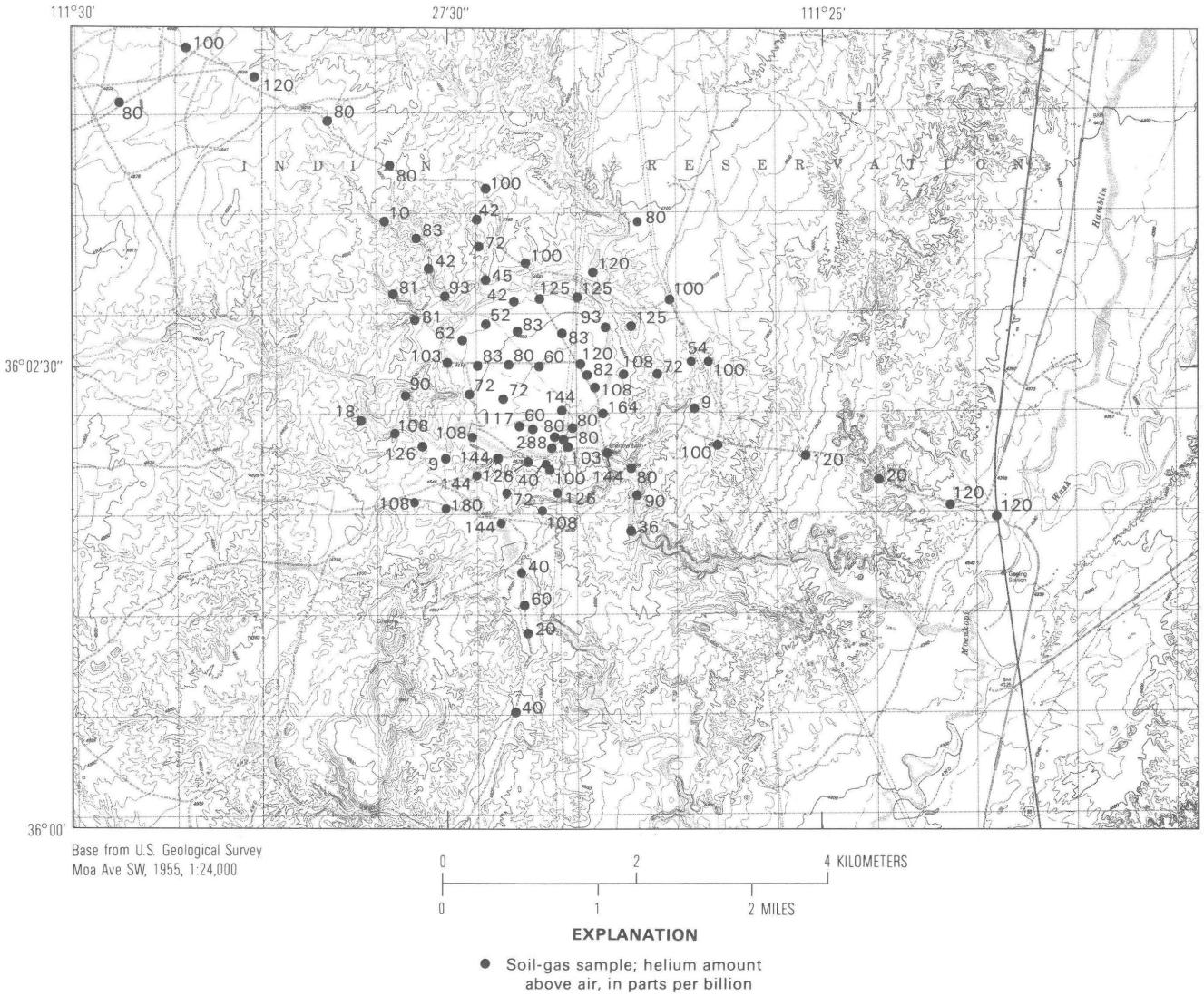

Figure R3. Map showing topography and location of sample sites at the Shadow Mountain collapse, Cameron uranium district, Arizona.

changes in a belt that trends north-south through the district. Landsat (ERTS–1) data prepared by Spirakis and Condit (1975) revealed significant differences in the reflectance of yellow-green light from the ground surface. Figure R5, derived from a stretch-ratioed false-color image (Spirakis and Condit, 1975), shows a zone characterized by relatively low reflectance of yellow-green light as compared with infrared (IR), and to the east a zone characterized by relatively high reflectance of yellow-green light. On the image, the Shadow Mountain collapse is within the zone of low yellow-green reflectance; however, the image shows some high yellow-green reflectance at the margin of the collapse. Uranium deposits generally are within the eastern zone of high yellow-green reflectance. This zonation is suggestive of alteration associated with the downdip migration of a redox front that has progressed eastward across the Shadow Mountain study area.

A transitory enrichment of uranium in the Chinle Formation would be expected during the advance of a redox front. Local retention of the uranium during the ensuing encroachment of oxygen-bearing ground water would be possible under favorable geologic and hydrologic conditions. The transmission of reducing gases and hydrothermal solutions of volcanic origin by the Shadow Mountain collapse structure could create a favorable site for the reduction, precipitation, and preservation of uranium in the Chinle Formation.

In summary, field evidence in the Cameron district suggests that solution collapse at many of the structures, including the Shadow Mountain collapse, is of mid- to

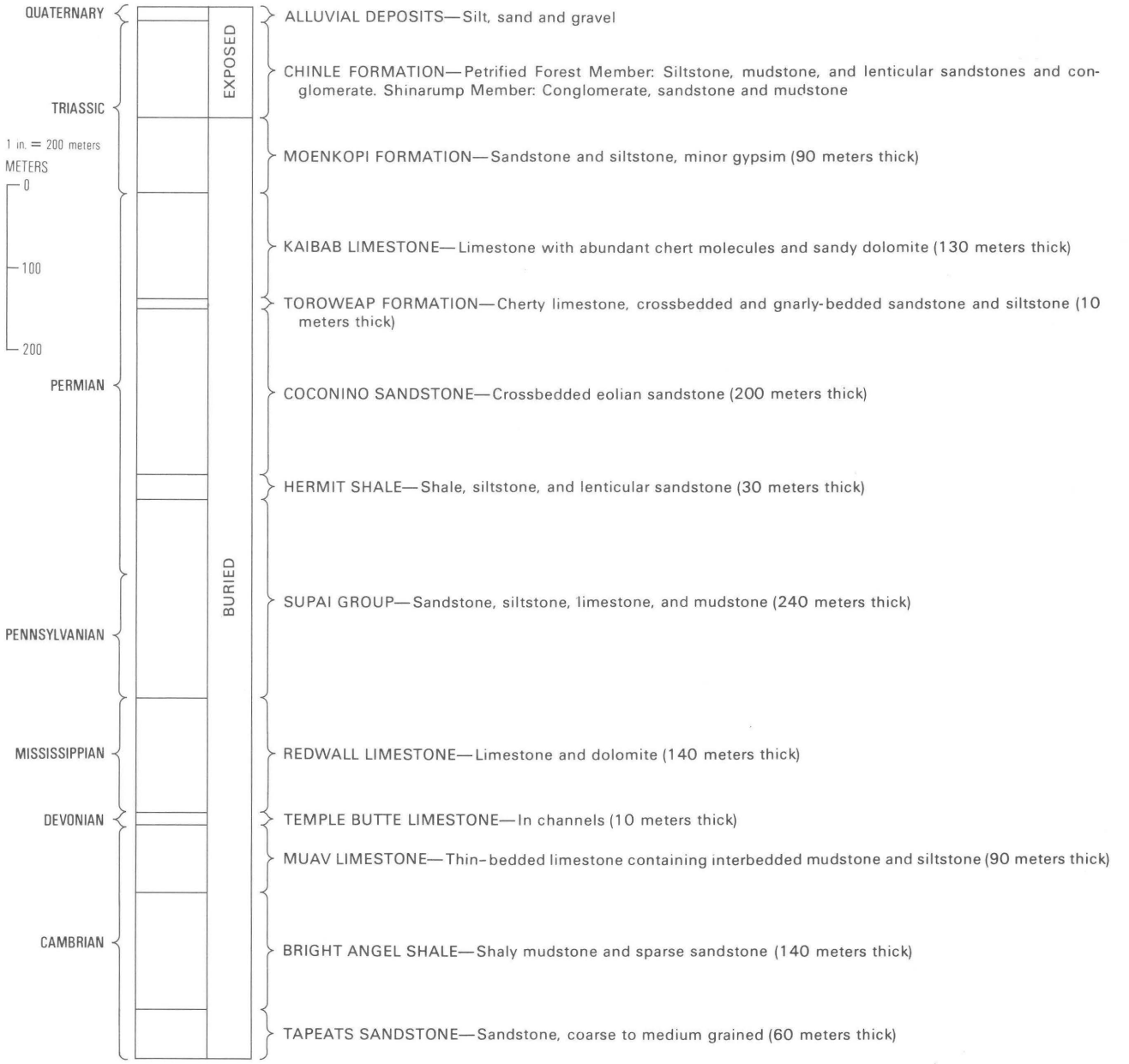

Figure R4. Diagrammatic section showing stratigraphy at the Shadow Mountain collapse, Arizona.

Soil gas at a 1-m depth was tapped by hollow late-Cenozoic age. Collapse in these structures probably is limited to formations above the Coconino Sandstone, but the structures may extend downward to the Redwall Limestone. Strata of the Shinarump and Petrified Forest Members of the Chinle Formation are the most favorable hosts for uranium deposits within the Shadow Mountain collapse, but a reducing environment favorable for uranium deposition may have existed throughout the vertical extent of the structure during volcanic eruptions at Shadow Mountain; therefore, uranium may be present in deeply buried rocks of Paleozoic age.

EQUIPMENT AND SAMPLING PROCEDURE

probes equipped with rubber septum holders, and the gas was collected in 10-cm^3 (cubic centimeters) hypodermic syringes. Soil-gas samples within the collapse and the nearby graben were taken at 0.2-mile (0.32-km) intervals from sites located by vehicle odometer distances and topographic control. Later the same day, seven additional samples were obtained from sites spaced at 0.1-mile (0.16-km) intervals. These additional samples were collected in the south part of the collapse in order to obtain greater sample control near one sampling site at which

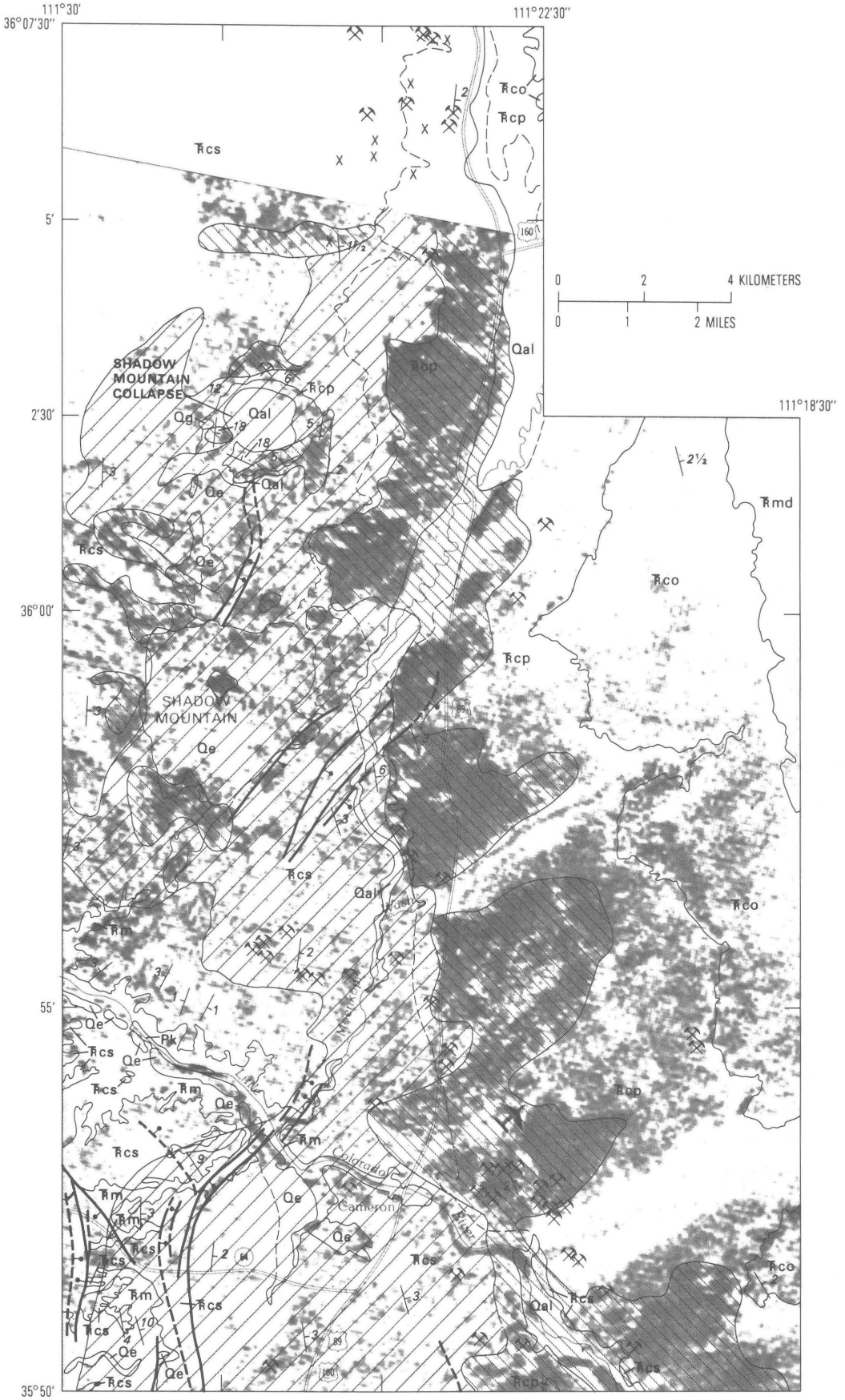
111°30'
111°22'30"
111°18'30"
36°07'30"
5'
2'30'
36°00'
55'
35°50'
Rcs
Rco
Rcp
Rmd
Rm
Rp
Qal
Qe
Qg
Pk
SHADOW MOUNTAIN COLLAPSE
SHADOW MOUNTAIN
Colorado
Cameron
0 2 4 KILOMETERS
0 1 2 MILES

a high concentration of soil-gas helium was detected. Samples also were collected outside the collapse to determine the regional helium background. The sampling sites for determination of the background helium concentration were located at 0.5-mile (0.8-km) intervals along two 2-mile-(3.2-km-) long traverses extending east and northwest of the collapse.

The dissolved-helium concentration in ground water within the alluvium was determined for one water sample obtained from a shallow well in the southeast part of the collapse structure. The water was collected in a 1-liter plastic bottle that had a rubber septum fitted into a needle guide that, in turn, was incorporated into the bottle cap. The bottle was filled three-fourths full with the sample water, leaving the remaining space occupied by air. The bottle was then capped and vigorously shaken for 30 seconds to degas the water. After allowing the bottle to stand for 2 minutes, 10 cm^3 of air was injected from a hypodermic syringe into the bottle to insure a positive pressure, thus enabling withdrawal of a gas sample into the syringe.

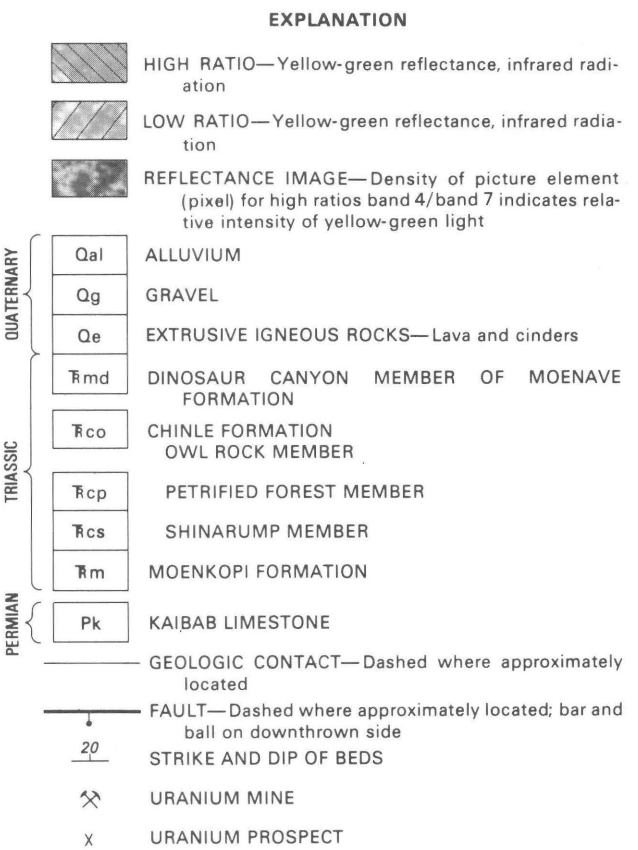

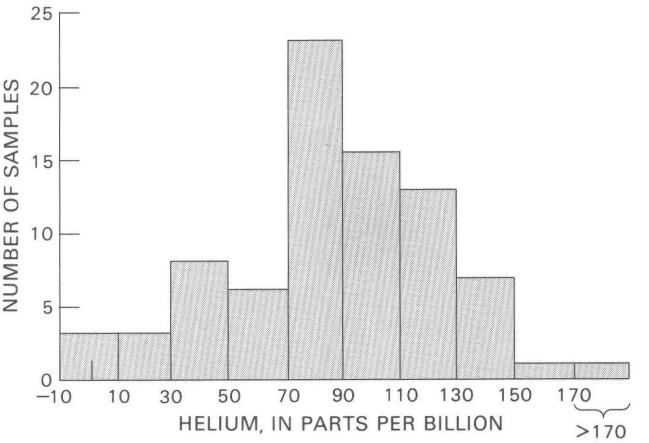

Figure R6. Frequency distribution of soil-gas helium in 82 samples from the Shadow Mountain collapse, Arizona. No samples contained less than 0 ppb helium with respect to ambient air.

The analytical equipment used for helium analysis was the mobile helium analyzer developed by the U.S. Geological Survey. This unit consists of a small mass spectrometer mounted in a four-wheel-drive, four-door pickup truck (Reimer, 1976). The equipment can make a helium analysis in the field with a sensitivity of 10 ppb (parts per billion) and with equal precision.

Helium analyses of the soil-gas samples are reported for convenience as parts per billion (ppb) of helium with respect to air that contains 5,240 ppb helium (Glueckauf, 1946). Helium analysis of the water sample is reported in cm^3 He/cm^3 H_2O. Water in equilibrium with air at standard temperature and pressure contains 45×10^{-9} cm^3 He/cm^3 H_2O.

HELIUM DISTRIBUTION

The helium concentration in 82 soil-gas samples collected at or near the Shadow Mountain collapse ranged from 9 to 288 ppb, and the mean helium concentration for all samples was 90 ppb. A frequency distribution (fig. R6) for the helium samples is positively skewed; however, about one-fourth of the samples are fairly uniformly distributed among the four class intervals that have less than 70 ppb He. The helium background for the area, as determined from the 14 samples collected away from the struc- from a reconnaissance study of helium in soil gas in the Powder River Basin (Reimer and others, 1980). The average helium soil-gas concentraion for ~838 samples collected for that study averaged 0 ppb.

Figure R5 (above and facing page). Map showing high and low ratios of yellow-green reflectance to infrared (IR) radiation in the northern part of the Cameron uranium district. Reflectance data modified from stretched-ratioed false-color images (L–1, formerly ERTS–1, band 4/band 7 and band 7/band 4) by Spirakis and Condit (1975, fig. R6). Geology modified from Chenoweth and Magleby (1960, revised 1971), and Haynes and Hackman (1978).

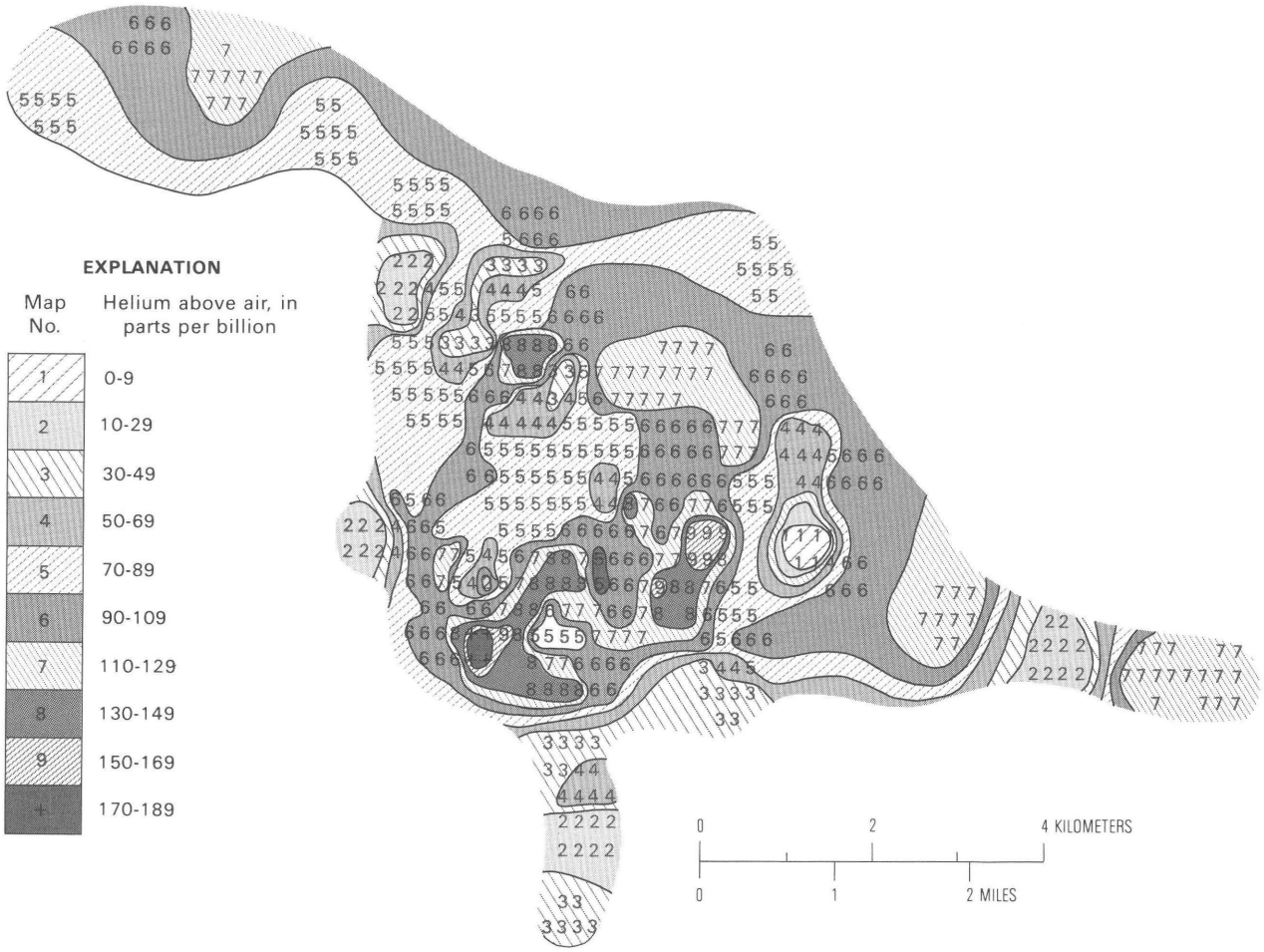

Figure R7. Map showing distribution of soil-gas helium at Shadow Mountain collapse, Arizona. Contours dashed where inferred.

Soil-gas helium is present in greater than average concentrations around the periphery of the structure and within its south half (fig. R7). The highest concentration of soil-gas helium (288 ppb He) was detected in a sample from the south part of the collapse, but similarly high helium concentrations were not present in seven additional samples collected on a grid pattern from nearby sites spaced 0.1 mile apart. A northeasterly trend appears on the helium distribution within the structure. Low concentrations of helium—less than 60 ppb He—are common just outside the structure, and similarly low helium concentrations also are present in four samples from within the graben that is south of the collapse. Ground water collected from a shallow well in the southeast part of the collapse contained $85 \times 10^{-9} cm^3 He/cm^3 H_2O$, which is not unusual. This weakly alkaline water (7.3 pH) had 9–10 ppb uranium in solution.

DISCUSSION

The high helium background in soil-gas samples collected away from the Shadow Mountain collapse probably is derived from uranium deposited during an episode of mineralization that took place in the Chinle Formation throughout the Cameron uranium district. This uranium may be present in the hexavalent state in secondary minerals formed within the oxidizing environment behind the advancing redox front.

At the Shadow Mountain collapse, the distribution of soil-gas helium suggests a structural control for uranium mineralization. High helium concentrations at the margin of the collapse form a ring-shaped pattern similar to that of the distribution of uranium minerals at the margin of breccia pipes in the Grand Canyon district. In addition, within the south half of the collapse is a northeast-

erly trending zone in which helium concentration in the soil is high. A computer-derived plot (fig. R7) (Reimer and Dean, 1979) of the soil-gas helium distribution in this zone resembles an irregular oval-shaped ring that shares a common segment with the helium anomalies at the south margin of the structure. This helium distribution suggests a possible analogy with the small secondary collapses that are present within the breccia pipe at the Orphan mine where ring fractures associated with the secondary structures commonly are mineralized with uranium. Solution collapse at the Shadow Mountain structure may have been more extensive and persistent at the south and southwest parts of the structure where steeper dips (18°) were mapped at the margin of the collapse by Cooley and others (1969). However, this suggestion should be considered only as a working hypothesis. The ring-shaped patterns for the high helium concentrations are suggestive of either direct or indirect fracture control for the helium distribution. Fractures may control the escape of gaseous helium, or the fractures may have controlled uranium mineralization that now generates the helium.

Extremely low concentrations of helium in soils sampled just outside the structure may reflect the leaching of uranium by an acidic solution. Such an acidic solution may have formed at the margin of the structure by the mixing of oxygenated ground water in the Chinle Formation with sulfurous hydrothermal waters transmitted through the collapse.

Helium values are low for samples of soil gas collected within the graben south of the collapse. The low values are not inconsistent with the uranium that is present along the west fault of the graben reported by Barrington and Kerr (1963). Parallel normal faults and fractures at the margins of the grabens form conduits to carry ascending solutions and gases away from the graben fault blocks. As a result, a favorable environment for uranium mineralization could have existed along faults and fractures along the west margin of the graben where a downdip flow of uranium-bearing ground water might have first come in contact with reductants in escaping gases or hydrothermal solutions and then precipitated uranium.

CONCLUSION

Geologic considerations, including the mineralization of the Chinle Formation throughout the Cameron district, suggest that the high concentrations of helium detected by the survey probably are derived from uranium deposits in the Chinle. The high concentrations of soil-gas helium at the south and west margin of the collapse and within the south half of the structure indicate the most favorable target areas for uranium exploration. The helium data alone resolve neither the question of the possible mineralization of rocks underlying the Kaibab Limestone, nor the question of the effectiveness of a soil-gas survey for detecting deeply buried deposits within a collapse structure. Deep exploratory drilling, preferably within the favorable target areas outlined by the helium survey, might resolve both questions. The helium survey does reveal the outline of the collapse structure and may be a useful technique in locating buried, eroded, or otherwise unrecognizable collapse structures.

REFERENCES CITED

Austin, S. R., 1964, Mineralogy of the Cameron area, Coconino County, Arizona: U.S. Atomic Energy Commission Report RME–99, 99 p.

Barrington, J., and Kerr, P. F., 1963, Collapse features and silica plugs near Cameron, Arizona: Geological Society of America Bulletin, v. 74, no. 10, p. 1237–1258.

Bowles, C. G., 1977, Economic implications of a new hypothesis of origin of uranium- and copper-bearing breccia pipes, Grand Canyon, Arizona, *in* Short papers of the U.S Geological Survey uranium-thorium symposium, 1977: U.S. Geological Survey Circular 753, p. 25–27.

Chenoweth, W. L., and Magleby, D. N., 1960, revised 1971, Mine location map, Cameron uranium area, Coconino County, Arizona: U.S. Atomic Energy Commission Preliminary Map 20.

Condit, C. D., 1974, Geology of Shadow Mountain, Arizona, *in* Geology of northern Arizona with notes on archaeology and paleoclimate; Part II—Area studies and field guides: Geological Society of America, Rocky Mountain section meeting, Flagstaff, Arizona, 1974, p. 454–463.

Cooley, M. E., Harshbarger, J. W., Akers, J. P., and Hardt, W. F., 1969, Regional hydrogeology of the Navajo and Hopi Indian Reservations, Arizona, New Mexico, and Utah: U.S. Geological Survey Professional Paper 521–A, 61 p.

Damon, P. E., Shafiqullah, M., and Leventhal, J. S., 1974, K-Ar chronology for the San Francisco volcanic field and rate of erosion of the Little Colorado River, *in* Geology of northern Arizona with notes on archaeology and paleoclimate; Part I—Regional studies: Geological Society of America, Rocky Mountain section meeting, Flagstaff, Arizona, 1974, p. 221–235.

Glueckauf, E., 1946, A microanalysis of helium and neon contents in air: London, Proceedings of the Royal Society, v. 185, p. 98–119.

Gornitz, V., and Kerr, P. F., 1970, Uranium mineralization and alteration, Orphan mine, Grand Canyon, Arizona: Economic Geology, v. 65, no. 7, p. 751–768.

Haines, D. V., and Bowles, C. G., 1976, Preliminary geologic map and sections of the Wupatki NE quadrangle, Coconino County, Arizona: U.S. Geological Survey Open-File Report 76–703.

Haynes, D. D., and Hackman, R. J., 1978, Geology, structure, and uranium deposits of the Marble Canyon 1°×2° quadrangle, Arizona: U.S. Geological Survey Miscellaneous Investigations Map I–1003.

Hunt, C. B., 1969, Geologic history of the Colorado River: U.S. Geological Survey Professional Paper 669–C, p. 59–130.

Kerr, P. F., 1958, Uranium emplacement in the Colorado Plateau: Geological Society of America Bulletin, v. 69, no. 9, p. 1075–1112.

Reimer, G. M., 1976, Design and assembly of a portable helium detector for evaluation as a uranium exploration instrument: U.S. Geological Survey Open-File Report 76–398, 18 p.

Reimer, G. M., and Dean, V. C., 1979, Computer program for the Hewlett–Packard–9825A to contour and plot data collected from helium surveys: U.S. Geological Survey Open-File Report 79–865, 15 p.

Reimer, G. M., Murrey, D. G., and Been, J. M., 1980, Helium soil-gas concentrations in the Torrington, Newcastle, Gillette, and Ekalaka 1°×2° quadrangles; Data from a reconnaissance survey: U.S. Geological Survey Open-File Report 80–452.

Spirakis, C. S., and Condit, C. D., 1975, Preliminary report on the use of LANDSAT–1 (ERTS–1) reflectance data in locating alteration zones associated with uranium mineralization near Cameron, Arizona: U.S. Geological Survey Open-File Report 75–416, 20 p.

1986

U.S. GEOLOGICAL SURVEY BULLETIN 1622

SHORTER CONTRIBUTIONS TO ISOTOPE RESEARCH

AN AUTOMATED HELIUM ANALYSIS STATION

Chapter S

By IRVING FRIEDMAN, JOE JURCEKA, WILLIS DOERING, WILLIAM LONG, and DON McNAIR

CONTENTS

FIGURES

Abstract

An automated device for the analysis of helium in well water has operated with minimum maintenance at a remote site for more than 5 years. This equipment makes an analysis once an hour and telemeters the data every 3 hours via satellite. A comparison of the telemetered data with data recorded onsite and with data secured by the analysis in Denver, Colo., of water samples collected daily from the well shows the three sets of data to be compatible.

INTRODUCTION

One of the objectives of the helium sniffer earthquake prediction program was to develop an automated station that could sample, analyze, and telemeter data, and that would operate with a minimum of supervision. The following description of the "automated Miller well" is of a system that successfully has extracted and analyzed helium from water for 5 years at a site remote from sophisticated facilities with infrequent (every 2–3 months) visits by technical personnel. Maintenance of components has been limited to occasional replacement of the mass spectrometer filament and replenishment of rotary pump oil by Mr. Miller and his family, the owner of the property, and by an annual cleanup of some of the valves that have become contaminated by the corrosive gases given off by the well waters. For the first year the data were recorded by a chart recorder at the site. At the beginning of the second year this recording mode was supplemented by telemetering of the data via GOES satellite to the receiving station in Wallops Island, Va. and then by phone line to Denver, Colo.

The 192-foot (58-meter) well is located on the Miller property 5.1 miles (8.2 kilometers) north of Gardiner, Mont. on highway 89. An enclosure was constructed over the well to protect the monitoring equipment (fig. S1).

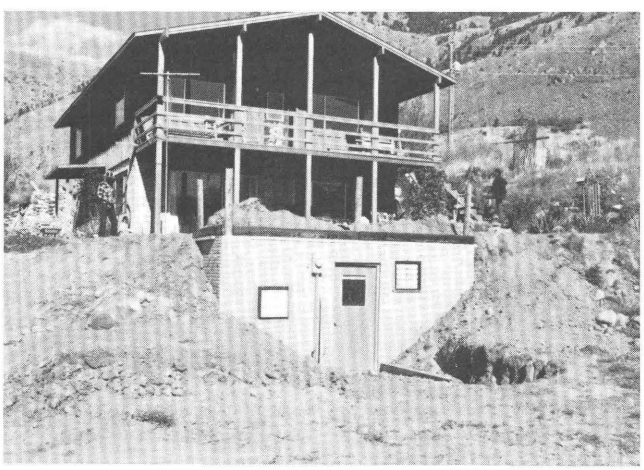

Figure S1. Underground enclosure on the Miller property.

ACKNOWLEDGMENTS

We are particularly indebted to Mr. and Mrs. Richard Miller for the use of their well, for their kind permission to construct an enclosure on their property, and for their continued help and hospitality. They, together with Mauray and Paul Miller were of great help in observing instrument performance, making repairs when necessary, collecting daily water samples for analysis in Denver, and, in general taking a continued interest in the success of the work.

The telemeter system, as well as the solid-state timing system, was constructed by Don McNair, aided by Willis Doering who also was responsible for the analysis of samples in Denver. The shower was constructed by William Long. Joe Jurceka was responsible for the construction of the sampling system.

Mr. Ted Denton was instrumental in first-model design and development and was the initiator of the constant-pressure device. His help in the initial stages of the project are gratefully acknowledged.

DESCRIPTION

Sampling Shower

The gas sample that is analyzed is secured by spraying the well water continuously into a small closed space. The gas in the water equilibrates with the air in the enclosure, and it is this equilibrated air that is sampled once an hour for its helium content. Figure S2 is a sketch of the sampling "shower"; figure S3 is a photograph of the shower.

The shower enclosure is vented to ambient air through a small opening. The well is pumped continuously at 1½ gallons/minute by a downhole pump located 180 ft from the ground surface, and about 170 ft from the water surface. The response time of the sampling shower was measured by changing the inflow water to a source quite low in helium, allowing the system to reach a steady state, and then changing the inflow again to water with a high helium content. Figure S4 is a plot of the response of the system and shows that the system will respond to a change in helium abundance of the input water with a response time (63 percent of the final value) of 3.6 hours.

Sampling System

The valving system for gas sampling shown in figures S5 and S6 uses inexpensive solenoid-operated stainless steel valves for switching gases. Once an hour a small

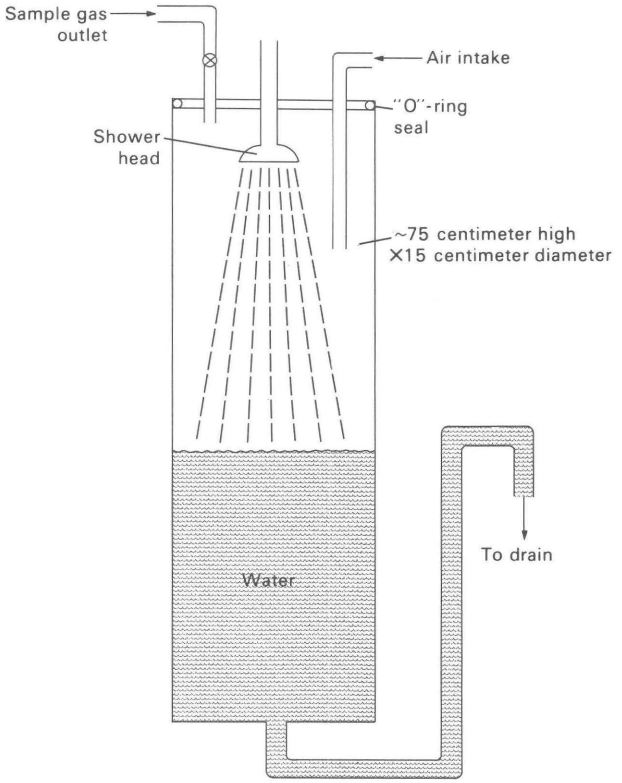

Figure S2. Diagram of sampling shower.

sample of the gas in the shower is pumped by a stainless steel bellows pump into a small volume. This volume is then opened to the mass-spectrometer inlet system through

Figure S3. Interior of enclosure showing shower (tall cylinder in center of photograph).

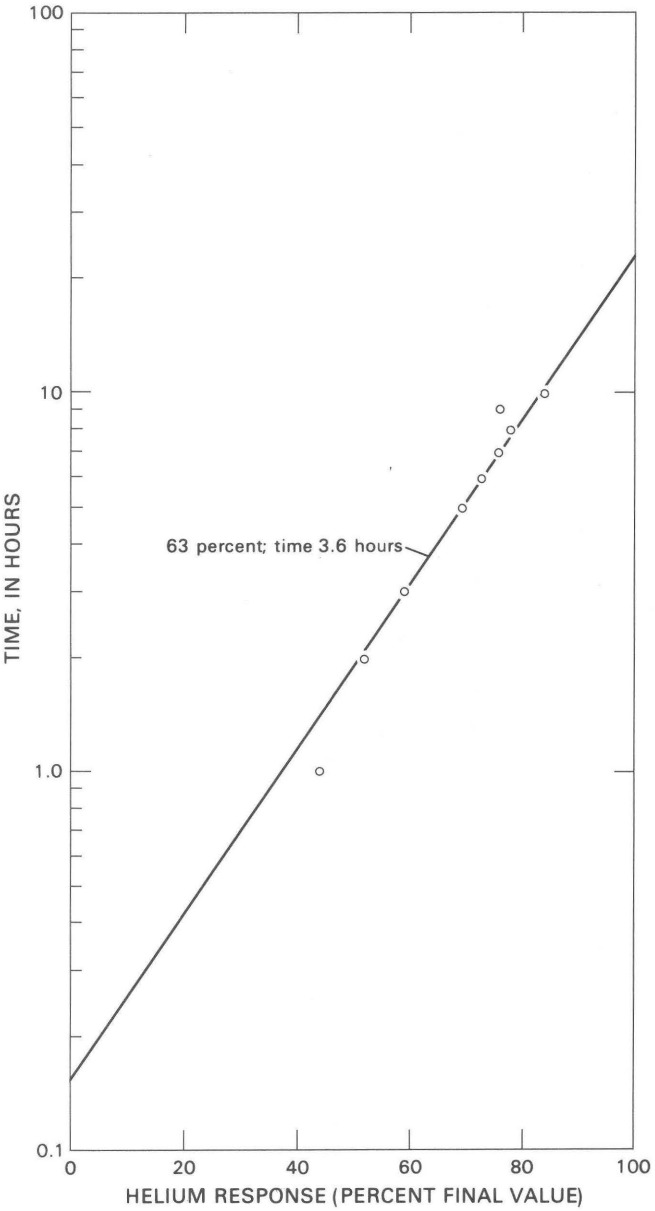

Figure S4. Plot of the helium reading versus time after an abrupt change in the helium abundance of water entering the sample shower.

an adjustable leak valve that allows a small amount of gas to flow into the mass spectrometer. In order to maintain a constant pressure of the gas flowing into the spectrometer, a vertically mounted glass hypodermic syringe is connected to the system. The gas pressure is sufficient to raise the plunger of the syringe, and the weight of the plunger in the almost frictionless barrel maintains a constant pressure on the gas flowing into the spectrometer. The ingenious glass-syringe constant-pressure device was suggested by Mr. Ted Denton. Gas leakage between the plunger and barrel of the unlubricated syringe is small and causes no problem.

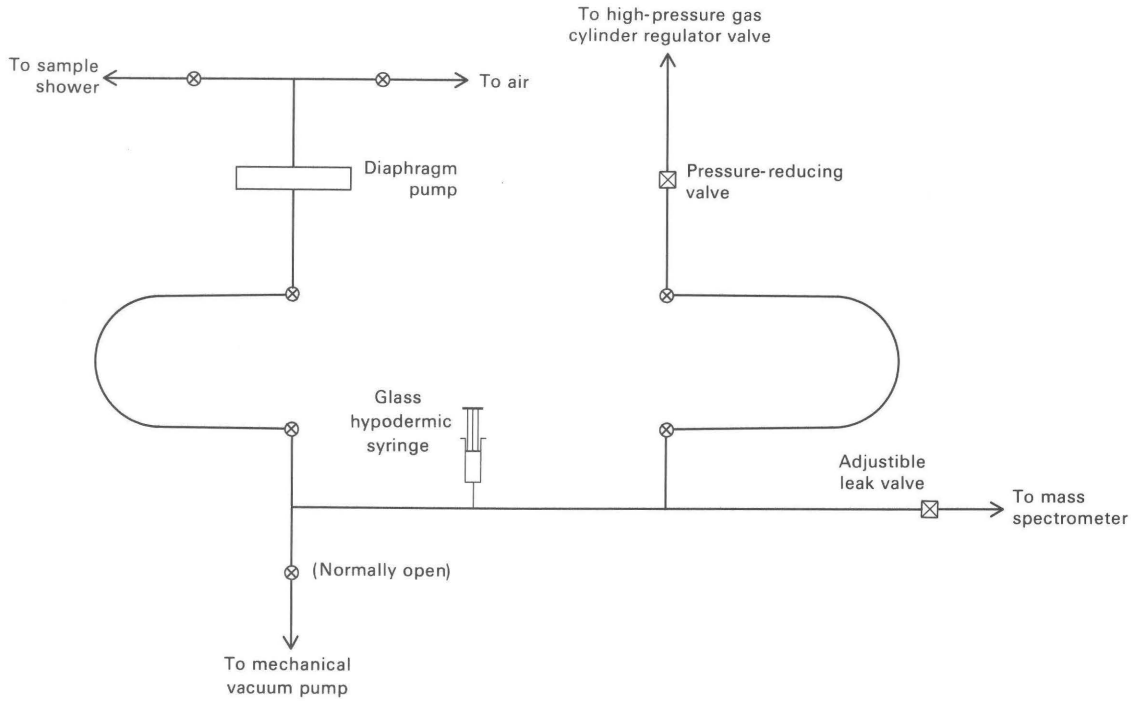

Figure S5. Diagram of automated sample inlet system. See figure S6 for approximate scale.

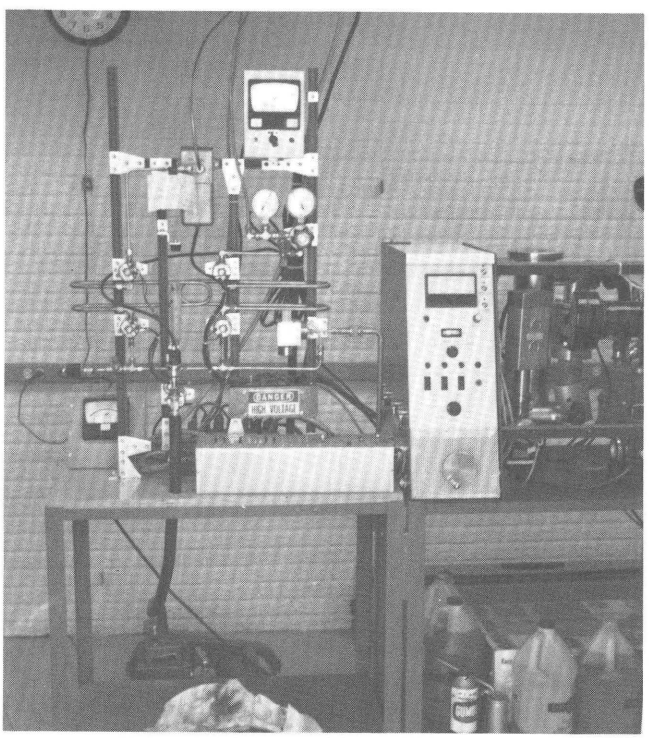

Figure S6. Automated sample inlet system.

Analytical System

The gas that flows past the variable leak valve (Granville Phillips, model 203) flows into a Dupont Instruments model 24–120B helium leak detector[1]. The only modifications that have been made to this instrument are (1) the installation of a fuse in the primary of the Penning gauge high-voltage transformer, and (2) the installation of a time-delay relay in the primary of the Penning gauge and the filament current circuits. The time-delay modification is necessary because power failures in the area are frequent, usually several per week and often as frequent as five per day. The power interruptions last from seconds to hours. When the power is off for more than a few minutes, the vacuum in the mass spectrometer is degraded by the gas continuously leaking by the glass syringe in the sample system, or by the fact that the power interruption may take place at a time when gas is being admitted into the spectrometer during a sample cycle. When the power is restored, normally the vacuum gauge and filament are actuated immediately, resulting in a burned-out filament and a high current flow in the vacuum gauge circuit and overheating of the Penning gauge transformer. The installation of a time-delay circuit of about 15 minutes between the time that power is restored (and the vacuum pumps restarted) and the time the Penning gauge and filament circuits are actuated has taken care of the problem.

The equipment is shown in figures S3, S6, and S7.

[1]Use of trade and company names is for descriptive purposes only and does not imply endorsement by the U. S. Geological Survey.

Figure S7. Inlet system, mass spectrometers and data recorder.

The output of the mass spectrometer amplifier is 40 volts above ground. We have introduced an isolation circuit so that the output from the instrument is referred to ground before it is fed into the telemetering platform for the GOES satellite transmitter.

The LeBarge convertible data-collection platform interrogates the spectrometer, and stores the data. It transmits the stored data to the satellite every 3 hours, during an assigned time slot. In order to keep alive the timing and other program functions during power interruptions, the platform is powered by a lead-acid storage battery that is charged continuously from the power line. Power interruptions of as many as several days can be accommodated by this system.

In order to calibrate the signal produced by the sample gas flowing into the mass spectrometer, we allow two reference gases (air and air spiked with helium) to flow into the spectrometer shortly before and after the sample gas. The sampling cycle takes 12 minutes and is as follows.

1. Sample system evacuated.
2. Sample system filled with reference gas from a cylinder (air spiked with helium).
3. Reference gas opened to spectrometer.
4. Reference gas pumped out of sample system.
5. Sample gas pumped into sample system from shower.
6. Sample gas opened to spectrometer and analyzed.
7. Sample gas pumped out of system.
8. Reference gas again admitted to system.
9. Reference gas again analyzed.
10. Reference gas pumped out.
11. Air pumped into sample system.
12. Air pumped opened to spectrometer and analyzed.
13. Air pumped out.
14. System evacuated and kept under vacuum until next cycle in 48 minutes.

The sample gas is bracketed by samples of the reference gas and the whole cycle completed by an analysis of air, (5.24 part per million helium). An example of the recorder chart is given in figure S8.

Figure S9 is a comparison of the data as read from the onsite recorder chart, the satellite telemetered data, and the data secured by the analysis of water samples collected daily by the Millers and mailed to the U.S. Geological Survey laboratory in Denver, Colo., for analysis. All three techniques yield comparable data.

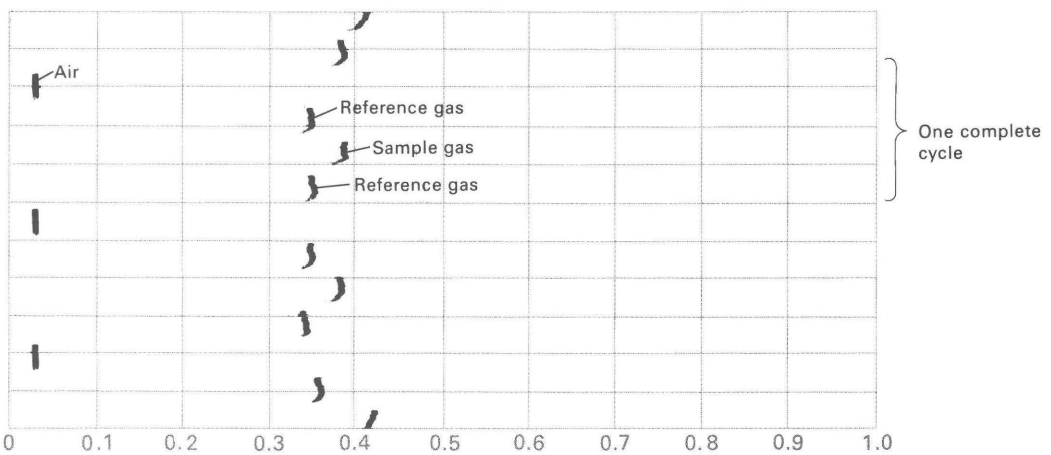

Figure S8. An example of a typical recorder chart.

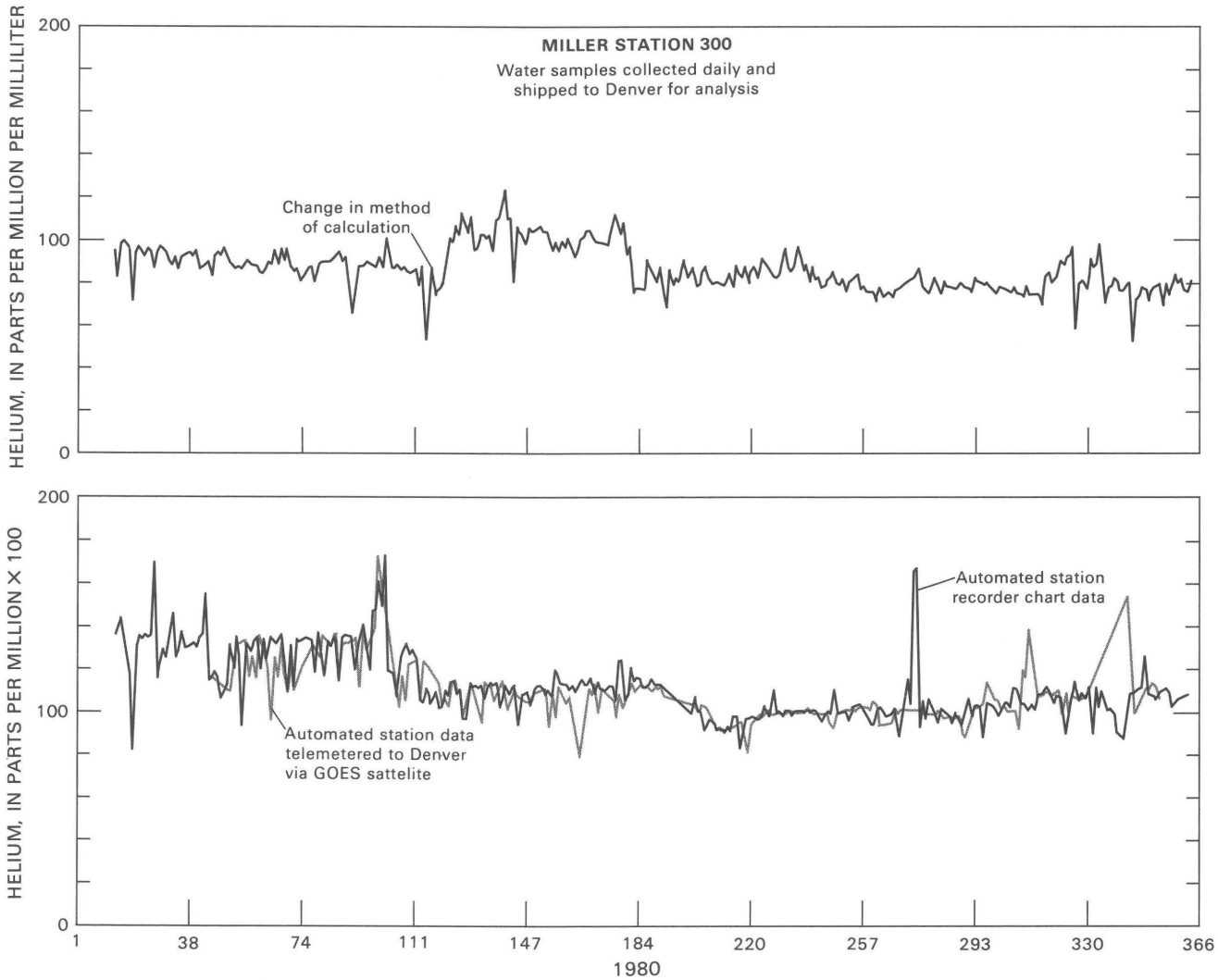

Figure S9. Comparison of the data plots secured by three different techniques.

1986

U.S. GEOLOGICAL SURVEY BULLETIN 1622

SHORTER CONTRIBUTIONS TO ISOTOPE RESEARCH

CONSTRAINTS ON TIME-EFFICIENT DATA-TAKING STRATEGIES FOR SINGLE-COLLECTOR, ISOTOPE-RATIO MASS SPECTROMETERS

Chapter T

By KENNETH R. LUDWIG

CONTENTS

Abstract

To a reasonable approximation, considerations of ion-counting statistics and dark noise lead to simple algorithms for calculating the most time-efficient allocation of peak-top and background integration times, where the goal is defined as obtaining the most precise data in a given amount of time.

INTRODUCTION

In single-collector, isotope-ratio mass spectrometry, decisions regarding the proper allocation of integration times for different isotopes, and for the ratio of background integration time to peak-top integration time, generally have been made either by a relatively inflexible computer algorithm or by the operator, using semi-intuitive decision procedures. Such procedures may not be unreasonable for relatively unstable ion-beams, but for the highly stable beams that are now attained by most laboratories for many elements, will not in general yield the most precise possible data for a given amount of data-taking time.

PRECISION OF ISOTOPE RATIOS

In the following discussion, I will assume a data-taking pattern where n cycles of peak switching and peak-top integration are performed over each of I isotopes, and the resulting background-corrected matrix is corrected in some interpolative manner to obtain estimates of the ratios of the I isotopes. Background data are assumed to be collected for each block of n peak-switching cycles, and taken either at independent positions in the mass spectrum for each isotope (background-type 1), or at one common position in the mass spectrum and applied to all peaks (background-type 2). Three types of ion-beam fluctuation will be considered.

Type 1.—Instability arising from the process of ionization itself; that is, an unstable beam due to factors intrinsic to the sample load. Accurately interpolable variations (for example, linear decay) do not concern us, however.

Type 2.—Noise that is independent of the ion-beam and constant in magnitude (that is, "dark noise"; for Faraday cup collectors, arising mainly from thermal noise in the feedback resistor).

Type 3.—Noise due to the finite number of ions arriving at the collector; thus giving counting-statistics limitations.

Uncertainty for perfectly stable beams:

The predicted uncertainty in the average intensity of a particular peak during a block of n cycles is then given by

$$\Sigma_i = 100\sqrt{A+B+C} \qquad (1)$$

where Σ_i=the uncertainty at one standard deviation, in percent, of the average peak intensity of peak i.

A=fractional variance[1] due to dark noise on the peak=

$$\frac{N^2}{nP_i^2T_i}$$

B=fractional variance[1] due to background uncertainty for i^{th} peak=

$$\frac{N^2}{P_i^2\ Z_i}$$

C=fractional variance[1] due to counting statistics=

$$\frac{1}{SnP_iT_i}$$

N=dark noise, in amperes/second
n=number of peak-switching cycles
P_i=ion-beam intensity for i^{th} peak, in amperes
T_i=integration time for i^{th} peak per peak-switching cycle
Z_i=background integration-time for background of i^{th} peak
S=number of singly charged ions per second per ampere=6.2×10^{18}

We assume here that no ions arrive at the collector at the background positions.

It follows that for perfectly stable beams, the percent uncertainty (Σ_R) in the ratio of any two isotopes (i,j) must be

$$\Sigma_{R_{ij}} = 100\sqrt{A'+B'+C'} \qquad (2)$$

where

$$\left[A' = \frac{N^2}{n}\right]\left(\frac{1}{P_i^2T_i} + \frac{1}{P_j^2T_j}\right)$$

$$\left[B' = N^2\right]\left(\frac{1}{P_i^2Z_i} + \frac{1}{P_j^2Z_j}\right) \quad \text{[background-type 1]}$$

[1]Variance divided by the square of the mean of the value measured; for example $\sigma^2_{\bar{X}}/\bar{X}^2$.

$$\text{or } B' = \frac{N^2}{Z_{ij}}\left(\frac{P_i - P_j}{P_i P_j}\right)^2 \qquad \text{[backgound-type 2]}$$

$$C' = \frac{1}{Sn}\left(\frac{1}{P_i T_j} + \frac{1}{P_j T_j}\right)$$

and A', B', and C' have significances similar to A, B, and C.

We are concerned here simply with finding the ratios of Z_i/nT_i and T_i/T_j that will yield the least uncertainty in the estimate of the mean of P_i/P_j, for a given total time spent taking data. In the first case, we constrain $Z_i + nT_i$ (background-type 1) or $Z_{ij} + n\ (T_i + T_j)$ (background-type 2) and differentiate the rearranged version of equation (1) to find

$$\beta_i = \sqrt{\frac{N^2}{N^2 + P_i/S}} \qquad \text{[background-type 1]} \quad (3)$$

where β_i is the ratio of Z_i/nT_i giving the lowest Σ_i; or

$$\beta_{ij} = \sqrt{\frac{(1 + 1/\rho_{ij})\left(\frac{P_i - P_j}{P_i P_j}\right)^2}{\left(\frac{1}{P_i^2} + \frac{\rho_{ij}}{P_j^2}\right) + \frac{1}{SN^2}\left(\frac{1}{P_i} + \frac{\rho_{ij}}{P_j}\right)}}$$

[background-type 2] (4)

where β_{ij} is the ratio of Z_{ij}/nT_i giving the lowest $\Sigma^2_{R_{ij}}$, and $\rho_{ij} = T_i/T_j$.

To find the optimum T_i/T_j, we constrain $T_i + T_j$ (sum of peak-top integration time for the two isotopes) and differentiate the rearranged version of equation (2) to find

$$\rho_{ij} = \sqrt{\frac{N^2/P^2 + 1/(SP_i)}{N^2/P_j^2 + 1/(SP_j)}} \qquad (5)$$

where ρ_{ij} is the ratio of T_i/T_j giving the lowest $\Sigma^2{}_{ij}$.

Equation (3) for βi approaches unity for small ion beams using a Faraday cup collector (relatively large dark noise), becomes somewhat less than one for large ion beams using a Faraday cup collector, and becomes much less than one for ion-counting techniques where N is insignificant. Equation (4) follows the same trend, except is reduced in all cases as the isotope ratios approach unity. Equation (5) for ρ_{ij} approaches P_i/P_j for small ion beams using a Faraday cup collector, and approaches $\sqrt{P_i/P_j}$ either for large ion beams using a Faraday cup collector or for ion-counting techniques where N is insignificant.

REAL-BEAM CONSIDERATIONS

Real ion beams may, of course, have a significant noninterpolable component of type-1 noise (although perhaps less often than is generally assumed), which in general will be proportional to the ion-beam intensity. Such noise will reduce the optimum ratio of background time to peak time, (β_i) but in most cases probably will not greatly affect ρ_{ij}. The exception is the case where the period of the major component of the noise is significantly less than the integration times on the peaks, and the magnitude of this noise is greater than the contribution of dark noise and ion-counting statistics. In this case, the optimum ρ_{ij} would tend towards unity. Actual examples of such noise, however, do not seem to be common for well- prepared samples.

The most effective strategy of dealing with most varieties of type-1 noise is probably the intuitively obvious one of reducing the cycle time ($=\Sigma[D_i + T_i]$, where D_i is the delay time after peak-switching and before integration begins), in order both to increase the accuracy of interpolation and to increase the number of calculated ratios. In practice, such a strategy implies that values of β_i and ρ_{ij} selected using equations (3) through (5) should be combined with cycle times just long enough that delay times (to allow magnet switching) do not become a major fraction of the cycle times, and thus constitute a limiting factor on the theoretical efficiency of the cycles. Personal experience indicates that with cycle times of as much as 20 seconds or so, linear interpolation of stable-appearing ion beams of less than about 10^{-12} amperes commonly gives isotope-ratio precisions limited only by type-2 plus type-3 noise, and that type-2 plus type-3 noise alone limits the precisions of ratios even from many runs with ion beams of greater than 10^{-11} amperes. Thus, the application of the simple concepts discussed here is of more than theoretical interest. The reader can calculate quickly the advantage of using equations (3) through (5) by substituting into equation (2) values from equations (3) through (5) and comparing the results to those using some standard set of P_i, T_i, and Z_i. A typical value of N for a 10^{11} Ω feedback resistor is 5×10^{-16} amperes/second.

☆U.S. GOVERNMENT PRINTING OFFICE: 1986-676-047:46001

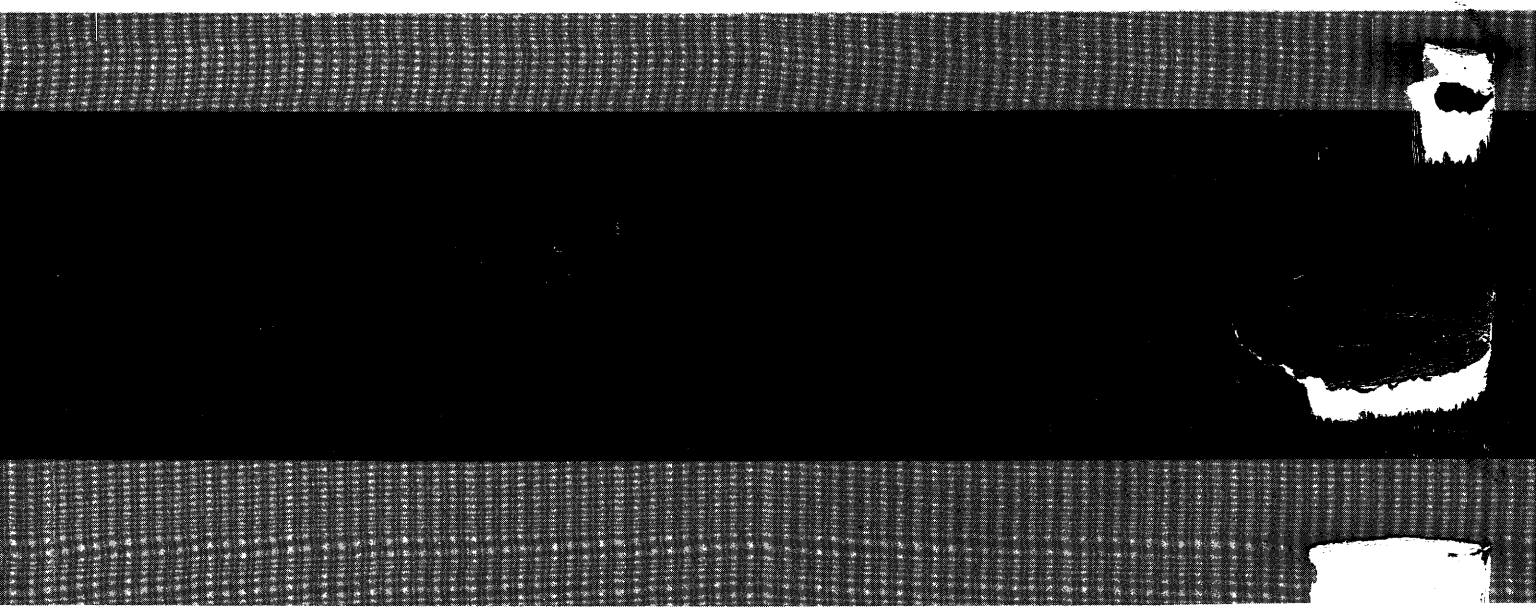


U.S. DEPARTMENT OF THE INTERIOR
March 3, 1849